GAS DISTRIBUTION IN SHALLOW PACKED BEDS.

IAN MILES PARSONS B.Sc.

Doctor of Philosophy

THE UNIVERSITY OF ASTON IN BIRMINGHAM

May 1991

The University Of Aston In Birmingham

GAS DISTRIBUTION IN SHALLOW PACKED BEDS.

Ian Miles Parsons

Doctor Of Philosophy, May 1991.

SUMMARY

Packed beds have many industrial applications and are increasingly used in the process industries due to their low pressure drop. With the introduction of more efficient packings, novel packing materials (e.g. adsorbents) and new applications (e.g. flue gas desulphurisation); the aspect ratio (height to diameter) of such beds is decreasing.

Obtaining uniform gas distribution in such beds is of crucial importance in minimising operating costs and optimising plant performance. Since to some extent a packed bed acts as its own distributor the importance of obtaining uniform gas distribution has increased as aspect ratios (bed height to diameter) decrease. There is no rigorous design method for distributors due to a limited understanding of the fluid flow phenomena and in particular of the effect of the bed base / free fluid interface.

This study is based on a combined theoretical and modelling approach. The starting point is the Ergun Equation which is used to determine the pressure drop over a bed where the flow is uni-directional. This equation has been used in a vectorial form so that it can be applied to maldistributed and multi-directional flows and has been realised in the Computational Fluid Dynamics code PHOENICS. The use of this equation and its application has been verified by modelling experimental measurements of maldistributed gas flows, where there is no free fluid / bed base interface.

A novel, two-dimensional experiment has been designed to investigate the fluid mechanics of maldistributed gas flows in shallow packed beds. The flow through the outlet of the duct below the bed can be controlled; permitting a rigorous investigation. The results from this apparatus provide useful insights into the fluid mechanics of flow in and around a shallow packed bed and show the critical effect of the bed base

The PHOENICS/vectorial Ergun Equation model has been adapted to model this situation. The model has been improved by the inclusion of spatial voidage variations in the bed and the prescription of a novel bed base boundary condition. This boundary condition is based on the logarithmic law for velocities near walls without restricting the velocity at the bed base to zero and is applied within a turbulence model.

The flow in a curved bed section, which is three-dimensional in nature, is examined experimentally. The effect of the walls and the changes in gas direction on the gas flow are shown to be particularly significant. As before, the relative amounts of gas flowing through the bed and duct outlet can be controlled.

The model and improved understanding of the underlying physical phenomena form the basis for the development of new distributors and rigorous design methods for them.

KEYWORDS: Packed Beds, Gas Distribution, Computational Fluid Dynamics, Base Of Bed Boundary Condition, Ergun Equation.

DEDICATION.

To My Father.

Although in most ways the exact manner in which water flows is difficult to perceive and still more difficult to define, as are also the forces attending such motion, certain general features both of the forces and the motions stand prominently forth, as if to invite or to defy theoretical treatment.

Osbourne Reynolds (1883)

ACKNOWLEDGEMENTS.

I would like to thank Professor K. E. Porter for his supervision, encouragement and enthusiasm throughout the course of this research.

Particular thanks are due to B.O.C. Cryoplants for their sponsorship of this research and particularly to the members of the Development Department for their ideas and encouragement.

Thanks are due to CHAM Ltd. for providing the Computational Fluid Dynamics code PHOENICS and for technical support.

I owe a great deal to my friends - thanks to them all, and to The Villa.

My heartfelt thanks go to my parents, who sacrificed so much for my education; and for so much else besides.

Last but definately not least, I would like to thank Helen (née Murray) my girlfriend, fiancée and wife during the course of this research. It wouldn't have happened otherwise.

CONTENTS.

LIST OF TABLES.

LIST OF PLATES.

LIST OF FIGURES.

LIST OF GRAPHS.

Page;

CHAPTER 1

INTRODUCTION

The applications of packed beds in the process industries are numerous and include such traditional separation processes as distillation and absorption as well as more modern processes such as adsorption. Recent years have seen a steady increase in the use of such beds. This has been due to:

i. The introduction of novel packings (e.g. the Norton Snowflake packing for distillation and novel adsorbents) which offer improved mass transfer performance and/or a lower resistance to gas flow.

ii. The lower pressure drops obtained in packed towers (in distillation and absorption) relative to trayed towers; this is of particular relevance when implementing energy saving schemes.

iii. The introduction of novel processes such as Flue Gas Desulphurisation.

This increase in the application of packed beds has been accompanied by the emergence of beds with a much lower aspect ratio (that is, the ratio of bed depth to bed width). This has also occured for the reasons discussed above, as well as because of the trend towards increased capacity plants (to exploit economies of scale).

A serious problem arises in the use of such shallow large diameter packed beds; this is the possibility of an uneven distribution of process fluids through the packing. A non-uniform distribution of gases and liquids (where both phases are encountered) has a much greater effect on the performance of large diameter columns than on smaller diameter columns. For maximum efficiency, both the gas and liquid should be uniformly distributed over the bed cross-section, and this uniformity should persist throughout the packing height.

Unsatisfactory gas distribution has led to expensive performance failures and in other case these problems have only been avoided by overdesign with attendant increases in capital and operating costs.

Although a considerable amount of work has been done on liquid distribution in packed columns, which is now well understood; far less has been done on gas distribution. Gas distribution is rarely a problem for small diameter columns where the packed height is very much larger than

the diameter of the column. Now that larger, shallower beds are being used the problem of gas distribution has become more significant. An example of such an "at risk" design is given in figure 1.1 which shows the pumparound section of a vacuum crude oil distillation column. The column has a diameter of 7m and a packed height of 2m; giving an aspect ratio of 1:3.5.

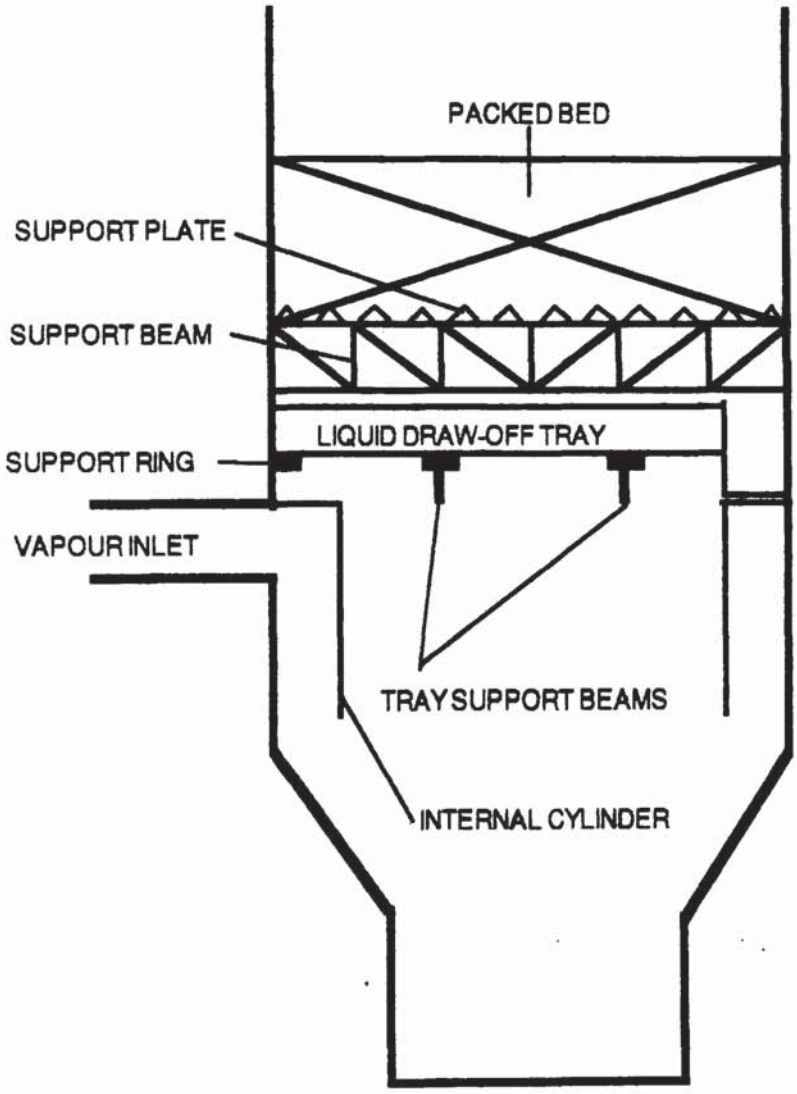

Figure 1.1. The Pumparound Section of a Vacuum Crude Oil Distillation Column. A Design "At Risk" from Gas Distribution Problems.

Ali (1984) performed the first thorough investigation of maldistributed gas flow in packed beds. Ali's work proposed a method of evaluating distributors that was subsequently used to empirically develop novel distributors. Also investigated were scale-up and the fluid mechanics of gas flow in packed beds. Ali's work was limited by the lack of

a comprehensive model to describe gas flow in packed beds and in particuar the effect of the bed base/free fluid interface.

This work has two basic and fundamental aims. The first of these is the creation of a model that fully describes the gas flow in a packed bed. This is achieved by expressing the well known Ergun Equation (which determines the pressure drop across a packed bed where the fluid flow is well distributed) in a vectorial form. This is subsequently implemented in the computational fluid dynamics code PHOENICS and verified by comparison with experimental results. The model is then extended to situations where the domain of study is not wholly packed and a novel base of bed boundary condition is presented.

The second aim is to further our understanding of the effect of the base of the bed on the flow of gases into and through a packed bed. Novel two- and three- dimensional experiments are realised, the measurements from which give greater insight into the effect of the bed base. In addition the two-dimensional experiment forms the basis of the final parts of the modelling work discussed above.

The development of the model and the conclusions drawn from the experimental program provide plant designers with useful insights on the optimal design of process equipment containing shallow packed beds. The models go some way to providing a rigorous design tool for such process equipment. Conclusions are also drawn on the implications for distributor design.

Initially however, the previous published work in this area is reviewed. This provides the basis for this work as discussed in Chapter Three where the approach to the problem is considered.

CHAPTER 2

LITERATURE SURVEY

2.1. INTRODUCTION.

This chapter presents the previously published work of relevance to this study. Initially, the effects of gas and liquid maldistribution on the performance of packed beds in various items of process equipment are shown and, the industrial significance of gas maldistribution problems established.

Thereafter, a brief review of gas distribution devices and their design and evaluation is presented. Experimental studies of gas distribution in packed beds are then discussed; this discussion covers voidage profiles, pressure and velocity distributions. Particular attention is drawn to the current understanding of the fluid mechanics of maldistributed gas flows.

A particular feature of this work is the recognition of the effect of the bed base on flow both in packed beds alone and in equipment containing such beds. The previous work on the effect of boundaries between free fluid areas and porous media is then reviewed.

The determination of pressure drop across packed beds is then discussed with particular reference to the Ergun Equation. Vectorial forms of this equation are then considered which are used when the definition of velocity is ambiguous (that is, when the gas flow is maldistributed).

Finally, various models of gas flow in and through packed beds are presented; the majority of these models are computational.

The subsequent chapter (Chapter 3) presents the approach to the problem (of maldistributed gas flows in packed beds) used in this work and, in so doing, more clearly illustrates why the subjects discussed here form the basis of this literature review.

2.2. THE EFFECT OF MALDISTRIBUTION ON THE PERFORMANCE OF PACKED BEDS.

2.2.1. Overview.

Maldistribution of gas (and liquid) flow in packed columns has three causes:

i. Small scale or 'natural' maldistribution occurs in all packed beds and is due to the heterogenous nature of the bed. It thus occurs on a scale equivalent to the packing size, cannot be avoided and, as is shown below, is not significant.

ii. A region of increased voidage occurs at the boundaries of packed beds (as discussed in section 2.4.1, below). This may cause a greater flow of fluid nearer the wall which will be particularly significant if heat transfer occurs across this wall.

iii. If the fluid flowing into the bed is not evenly distributed; maldistribution will occur in the bed. This is the most significant aspect of fluid maldistribution in packed beds.

This section shows how such maldistribution of fluids in packed beds contained in items of process equipment reduces the performance of such units.

2.2.2. The Effect on Performance of Maldistribution in Packed Columns.

The first study of the effect of fluid maldistribution on the performance of packed columns is that of Mullin (1957). He conceptually divided a distillation column longitudinally into two equal sections by an impermeable membrane. The two sections take an equal vapour load but, unequal liquid rates. McCabe-Thiele analysis was then performed and it was shown that as a result of the maldistribution the gradient of the operating line is decreased and therefore more closely approaches the equilibrium line (pinch) at one end of the tower. The number of theoretical stages required for the separation is therefore increased; or for a given design, performance is reduced.

Huber and Hiltbrunner (1966) introduced the idea of cross-mixing of liquid or vapour which acts to cancel out maldistribution. They predicted that in a small column only a small amount of cross-mixing is required to correct serious maldistribution. In a larger column, however, the cross-

mixing is less effective and so larger diameter, shallow beds are more likely to suffer from maldistribution than smaller diameter beds.

More recent studies on the effect on mass transfer of maldistribution in packed columns include those of Stichlmair and Stemmer (1987) who present a combined experimental and modelling approach. The model, although simple, enables decoupling of mass transfer and maldistribution effects. The theoretical treatment proves that up to 50% of mass transfer efficiency may be lost due to maldistribution even with good initial distribution. Zuiderweg and Hoek (1987) examined the effect on separating efficiency of the small scale or 'natural' maldistribution and concluded that this had only minor effects on the basic separation efficiency of the packing. A companion paper (Zuiderweg, Hoek & Lahm (1987), which considers the effects of large scale liquid maldistribution also examines the inter-relationship between gas and liquid maldistribution and shows that liquid maldistribution generates vapour maldistribution (since local vapour pressure drop is a function of liquid rate) although this aspect of vapour maldistribution has only a small effect on the column efficiency.

This work concentrates on gas distribution in packed beds. Ali (1984) has shown that such work is of use in understanding the flow pattern in beds containig both vapour and liquid. However, it is of greater applicability in understanding flow patterns in beds where only a gas phase exists, such as in packed catalytic reactors and adsorbers.

2.2.3. The Effect of Maldistributed Gas Flow on the Performance of Packed Catalytic Reactors.

The only study of the effect of flow maldistribution on performance in catalytic packed bed reactors where the width of the bed is very much greater than the particle size is that of Choudhary, Szekely and Weller (1986 a & b). In a combined experimental and modelling approach they examined the effect on conversion of flow maldistribution (in an isothermal reactor) caused by both the preferential flow near the wall (inherent in most systems) and by the deliberate arrangement of solid packing in the bed. The model is based on the vectorial Ergun Equation (see section 2.7.2 below) combined with a differential component balance and describes the velocity fields and reactant concentration profiles. The model shows that a

non-uniform flow field has a very strong effect in distorting the concentration isopleths, particularly at intermediate conversion levels. In an experimental study, based on the alumina catalyzed isomerisation of 1-butene to cis- and trans-2-butene; effluent gas composition monitored by gas chromatography was found to vary with radial position in a manner consistent with the modelling equations.

2.2.4. The Effect of Gas Maldistribution on Adsorber Performance.

Bushuyev, Kisarov & Fisher (1982) first considered the problem of gas maldistribution in adsorbers, and recognised that non-uniform gas distribution gives rise to a breakthrough over a period of time rather than as a sharp front. The same effect occurs if mass transfer in the front region is a significant effect. Hence, the gas maldistribution is modelled as a mass transfer coefficient. This coefficient is divided into two parts; one due to gas distribution which is independant of the amount of gas adsorbed and one due to the mass transfer resistance on adsorption which is dependant on the amount of gas already adsorbed onto the bed. A solution method for the resultant equations is given.

Krebs (1983) describes a model of mass transfer in a packed bed where maldistribution is modelled by dividing the bed into two regions; one with small passages and the other with large passages. This is used to construct a model predicting the number of transfer units in each region and its effect on the relative adsorption parameters of two different species. Experiments are then performed with water and Iso-propanol to investigate the predictions of the theory although no clear or useful conclusions are reached.

Vortmeyer & Michael (1985) numerically investigated the effect of non-uniform flow distribution on the performance of a tubular fixed bed adsorber for a linear adsoption isotherm and a constant total volume flow. Quite large effects on the radial dependance of breakthrough were found for a laboratory adsorber with a reactor: particle diameter of 21. Flow profiles depend on this ratio and, the effects will be smaller for larger values of the ratio. This, in turn, poses questions concerning similarity in small and large scale adsorbers in that they do not behave in the same way if the concept of a non-uniform flow distribution is introduced. These workers further conclude that, in larger beds and in accordance with the observations made in fixed bed chemical reactor theory, non-uniform flow

distribution brings about the major effects while the lower packed density near the wall is only of secondary importance.

Kagan et al. (1986) examined the effect of gross gas maldistribution on the performance of packed adsorbers. They used two distributors described as "a plane-parallel gas distribution device" and " a device narrowing in the direction of gas travel" which reduced experimentally determined adsorber performance (on a through put basis) by 39% and 6% relative to an ideally distributed flat velocity profile. Since isothermal conditions were used real beds would actually suffer further reductions in performance. The reactor: particle diameter ratio used was 207.3 with a bed diameter: height ratio of 13.7.

The literature thus shows that inadequate gas distribution to packed beds severely limits performance and is more signifcant than effects due to variations in local voidage near the wall. The subsequent section presents published gas distributor designs and methods for their evaluation.

2.3. GAS DISTRIBUTION DEVICES AND THEIR EVALUATION.

2.3.1. Methods for Distributor Evaluation.

The first work specifically aimed towards identifying gas maldistribution in packed beds and, evaluating distributors, was performed by Zaytoun (1981) who used a hot-wire anenometer to measure air velocities above a bed of 1.6 cm metal Intalox packing. A maldistribution factor Ø was defined:

$$\phi = \sum_{i=1}^{n} \left\{ 1 - \frac{v_i}{\bar{v}} \right\}^2 \qquad \text{Equation 2.1}$$

where v_i is a point velocity and $\bar{v}$ the average velocity above the bed. The lowest possible value of this maldistribution factor, ϕ_{min} which characterises the small scale maldistribution due to the randomness of the packing was determined, and further experiments performed to investigate the effect of bed height and inlet pipe diameter on Ø. This work also

demonstrates that the bed itself acts as a distributor (i.e. Ø reduces with an increase in packed height).

Zaytoun's work provided the basis for a subsequent investigation of gas distribution in shallow large diameter packed beds by Ali (1984). He found that Ø has a minimum value for well distributed flows and much larger values for maldistributed flows. By measuring the variation of Ø with packed height the performance of a distributor can be evaluated. A good distributor requires only a small packed height to achieve a uniform distribution.

The maldistribution factor, Ø, has been further characterised by Hassan (1986) who examined the effect of the inlet pipe: tower diameter and packing size on this factor. Bentham, Cavill & Turner (1985) also investigated the effect of packing size on the maldistribution factor and considered the use of an alternative measure of maldistribution, the coefficient of variation which is defined:

$$C_v = \frac{100}{n^{0.5}} \left[\sum_{i=1}^{n} \left\{ \frac{v_i - \bar{v}}{\bar{v}} \right\}^2 \right]^{0.5}$$

Equation 2.2.

therefore:

$$C_v = \frac{100}{n^{0.5}} \phi^{0.5}$$

Equation 2.3.

where n is the number of point velocities measured. This approach simplifies the evaluation of distributors and/or the quantification of maldistribution; since it allows for the number of point velocities measured.

Daraktschiev (1984) used a similar method, finding the minimum height of various packings above which a uniform velocity profile is observed.

Muir & Briens (1986) also determined the coefficient of variation of point velocity for various distributors in an unpacked column. This method fails to recognise the important 'one off' effect of the bed base and, in so doing, does not consider the interaction between the bed base and distributor.

Speiser, Muller & Barthel (1987) examined the velocity profile at the level of the bed base to distinguish between various distributor

designs. This approach, in addition to being quantitative suffers also from the limitation of the work of Muir & Briens (1986) discussed above.

As is shown below, these methods have all been used to evaluate distributor designs; however, these are not rigorous design methods or even reliable guidelines for designers. Individual designs must be constructed and then evaluated. There are however some heuristics for gas distributor design that may assist the designer:

i. Avoid radial inlets (Speiser, Muller & Barthel (1987)).

ii. Maximise column pressure drop (at the expense of increased operating costs, possible product degradation etc.).

iii. Minimise kinetic energy levels in the gas entering the column (i.e. maximise the inlet pipe diameter).

iv. Maximise distance between inlet pipe and bed base (ii. iii. & iv., Moore & Rukovena (1987)).

2.3.2. Description of Gas Distribution Devices.

In this sub-section various designs of gas distributors are presented.

Ali (1984) and Perry (1974) have both shown that a depth of packing acts to distribute the gas flow within it. Perforated plates can be used in a similair fashion (Liebson et al. (1957) gives design information).

Perforated or Sparge pipe distributors have frequently been used in packed process equipment. Their design has been discussed by Van Der Hegge Zijnen (1953), Senecal (1957), Perry (1974), Bailey (1975) and Moore & Rukovena (1987). These distributors are among the most reliable from a design point of view although they are expensive to fabricate and typically exhibit a high permanent pressure drop with consequent increases in operating costs. Slot distributors, modified slot distributors and turning vane distributors, illustrated in figures 2.1 to 2.3 are also used in packed columns.

Figure 2.1. The Slot Distributor.

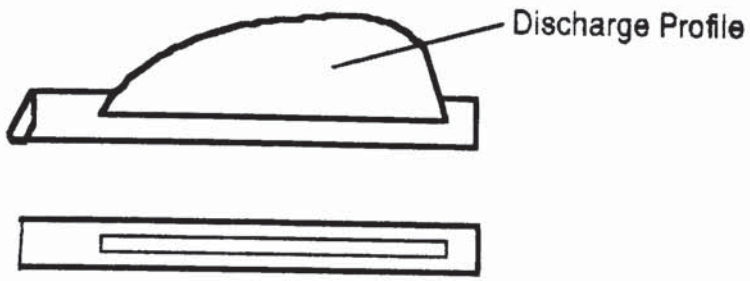

Figure 2.2. The Modified Slot Distributor. (in section).

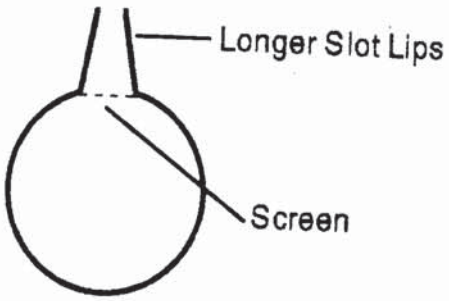

Figure 2.3. The Turning Vane Distributor.

Ali (1984) developed three modifications to the traditional internal cylinder (in a scale model of the apparatus illustrated in figure 1.1.) which are illustrated in figures 2.4 to 2.6. He concluded that distributor modification C is an excellent distributor. However, pressure drop across these distributors was not measured and hence this conclusion must be viewed with some reserve.

Figure 2.4. Distributor Modification A to the Internal Cylinder. Ali (1984).

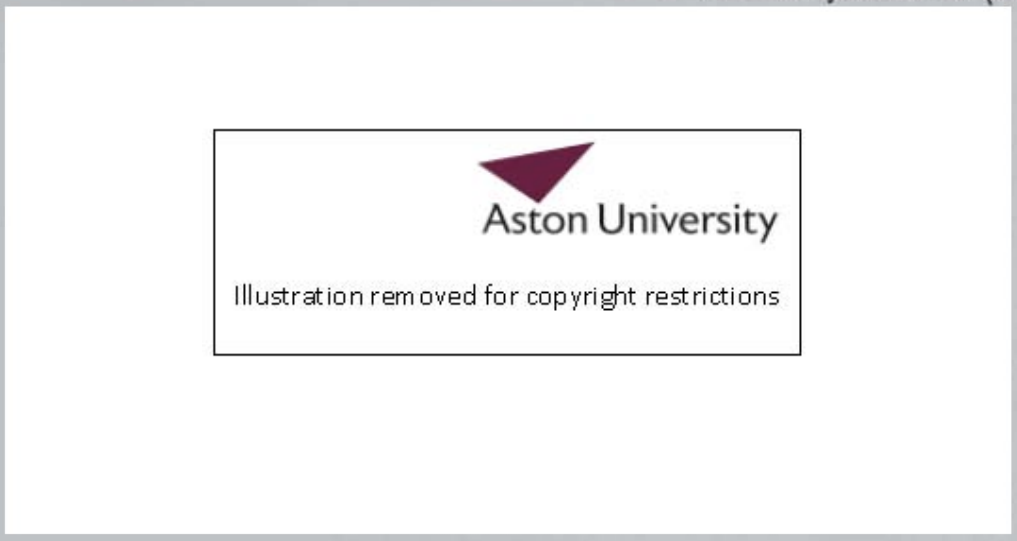

Figure 2.5. Distributor Modification B to the Internal Cylinder. Ali (1984).

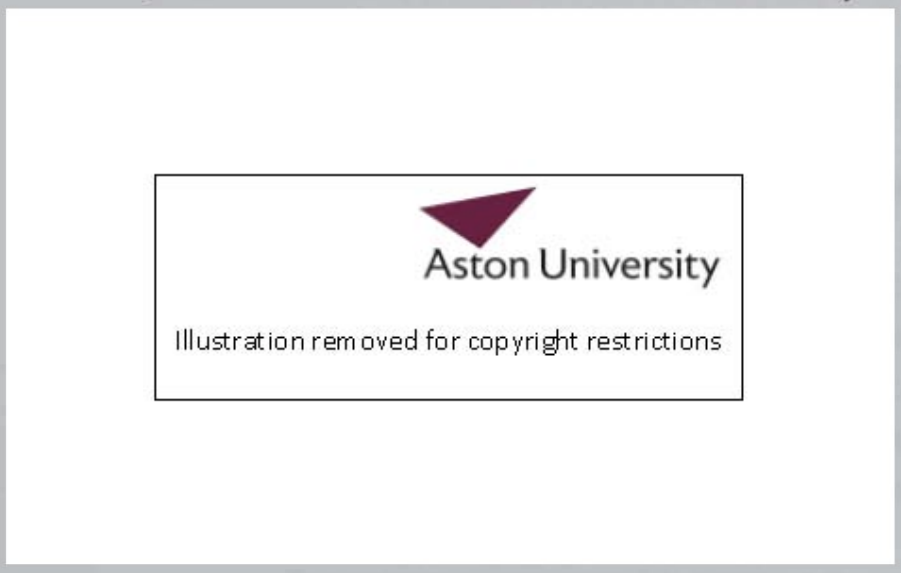

Figure 2.6. Distributor Modification C to the Internal Cylinder. Ali (1984).

Figure 2.7. Gas Distribution Devices Studied by Daraktschiev (1984).

Daraktschiev (1984) studied two distribution devices which are illustrated in figure 2.7. Again pressure drop was not measured although it was concluded that device 1 is a better distributor than device 2.

Speiser, Muller and Barthel (1987) compared seven distributor designs using the method described above. These devices are illustrated in figure 2.8.

The original paper gives full details of the performance of those disrtibutors and recommends particular designs for particular applications. In summary, it is concluded that device 6 is the best considering both the velocity distribution it gives and the pressure drop across it. Device 7 gives the best distribution at the expense of high pressure drop whereas device 1 which gives the lowest pressure drop is a very poor distributor.

Muir & Briens (1986) have examined the widest range of distributors and also present full pressure drop measurements. Initially they used the apparatus illustrated in figure 2.9; the various inlets and combinations of them, some with elbows, were examined. Figure 2.10 shows a modification of the original equipment which is an annular deflector ring. This was in turn modified by the addition of a ring above the annular deflector, this arrangement is similair to the internal cylinder used

Figure 2.8. Gas Distribution Devices Compared by Speiser, Muller & Barthel (1987).

by Ali (1984). In all 62 arrangements were examined. Full details are given in the original paper although the main conclusions of this work are that:

i. Two inlets are to be preferred to one.

ii. The annular deflector ring increases the pressure drop significantly but, substantially improves the velocity distribution.

iii. The addition of the ring above the deflector increases the pressure drop by a further 9% and gives still better gas distribution.

This section has reviewed existing knowledge of distributor designs, design methods and evaluation. It is apparent that empirical methods are used and that there are no rigorous design methods for efficient distributors and that the understanding of distributor function is extremely limited. Much of the work fails to recognise the interactions between the distributor and the bed (and particularly its base). The design of gas distributors is very much an art rather than a science and performance failiures are usually avoided by overdesign (i.e. additional

packed height, beyond that dictated by mass transfer requirements, which leads to excessive pressure drop).

Figure 2.9. The Original Apparatus of Muir & Briens (1986).

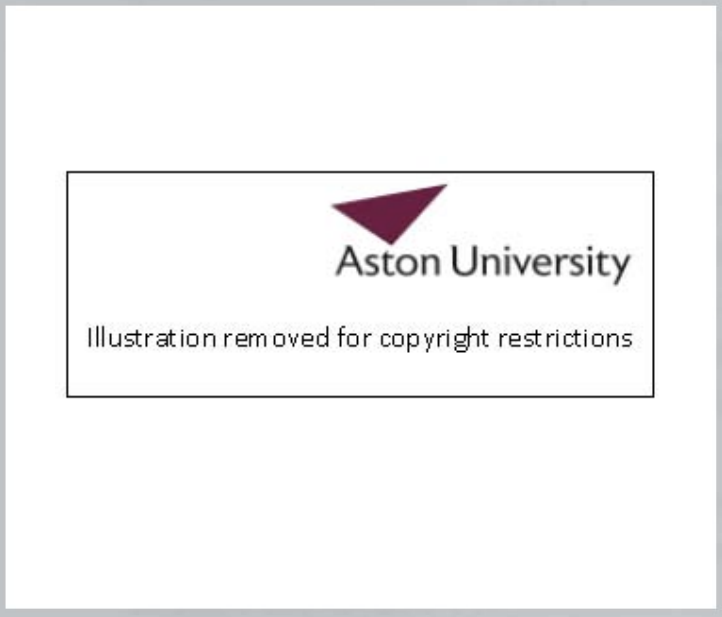

Figure 2.10. The Modified Apparatus of Muir & Briens (1986) with 2 New Inlets and an Annular Deflector Ring.

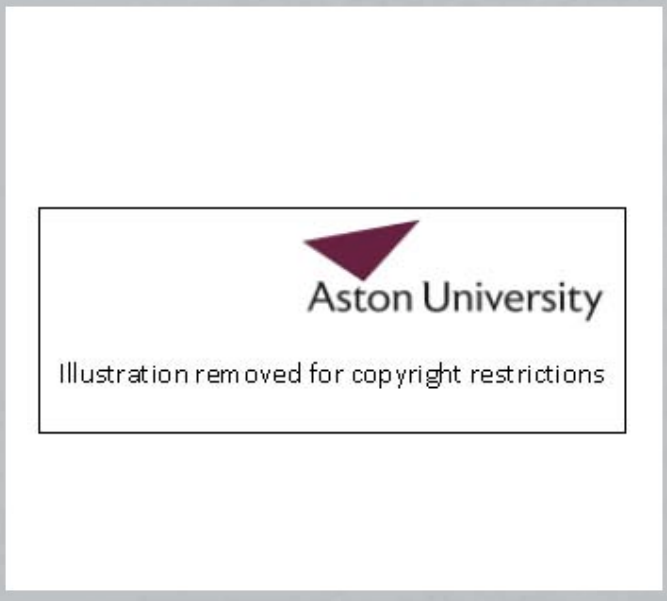

Ali (1984) has identified the following attributes of a good gas distributor:

i. Uniform gas distribution.
ii. Low (minimum) pressure drop.
iii. Sectional construction.

Two additional attributes may be added to this list:

iv. Low capital cost.

v. Satisfactory operation (viz. i. & ii.) over a wide range of flowrates (turndown).

2.4. EXPERIMENTAL STUDIES OF GAS FLOW IN PACKED BEDS.

This section presents experimental studies of gas flow in packed beds under headings of 'voidage variations', 'velocity measurements', 'turbulence and the laminar/turbulent transition in packed beds' and 'other studies'. The headings do not rigorously classify all the previous work, particularly where a study has examined more than one of these aspects. Nevertheless this description is a useful one in presenting this part of the literature.

Similarly, some experimental studies have been performed in close relation to modelling studies and are discussed with the relevant models in section 2.7.

2.4.1. Voidage Variations in Packed Beds.

As has already been indicated, voidage in packed beds varies due to the effect of the walls. This variation and the resultant variations in velocity above the bed (discussed in the next section) forms the basis of many of the earlier studies of packed bed fluid mechanics.

A number of methods have been used to measure localised voidage in packed beds:

i. Shaffer (1952) measured void space by rotating a horizontal packed column and introducing a known amount of liquid into the section, raising the liquid level in increments. By introducing imaginary annular sections of the same width as the height of the liquid level increments he was able to estimate void fraction as an average for an annular area. This method has also been used by Ridgway and Tarbuck (1966) and has been extended and improved by Griffiths (1988).

ii. After packing, beds are filled with wax, paraffin etc. which is then allowed to solidify. The bed is cut into sections (or, part of the cylindrical bed is removed with a lathe) and the volume of each section is determined. The section is then heated, the wax melts and is separated from the packing and the voidage is determined. This method has been

used by Kimura et al. (1955); Roblee, Baird & Tierney (1958) and Benanti & Brosilow (1962)

iii. Foumeny & Benhaya (1991) have extended this technique by examining sections cut from beds whose interstices have been filled with resin (of a different colour to the packing pieces) with an image analyser.

iv. Pillai (1977) has used an individual particle measurement technique whereby the number of packing pieces whose centre is within a given distance from the wall is counted. The method uses a two dimensional bed packed with one layer of packing pieces and may not, therefore represent accurately the voidage variation in a three dimensional bed. Govindaro & Froment (1986) have used a similar approach.

v. Photometric methods have been used by Thadani and Peebles (1966); Buchlin, Reithmuller & Ginoux (1977) and Schneider & Rippin (1988). These methods are based on the different adsorbtion of x-rays or γ-rays by the packing material and the matrix material. Stephenson & Stewart (1986) have used a marker tracking method to measure the radial distribution of porosity in packed beds.

The conclusions of these studies may be summarised as follows: at the wall the voidage of the bed of spheres is 1.0 it then decreases over approximately 5 particle diameters to the uniform bed value, going through a minimum value half a particle diameter into the bed. This decrease follows a damped sinusoidal form; as illustrated in figure 2.11. The exact nature of this decay is a function of particle to container size. The interpretation of this behaviour is well known: the wall is in contact with one well ordered layer of particles, that layer itself is less smooth than the wall and can only impose a weaker order on the adjacent layer, and so on (see for example, Marivoet et al. (1974)). Little data is available for non-spherical packings although it has been shown that more 'open', commercial packings such as Pall and Rashig rings achieve the bed voidage in fewer particle diameters from the wall.

Chandrasekhara and Vortmeyer (1979) have proposed a correlation for the variation in bed voidage with distance from the container wall. This correlation was obtained from the data of Benanti & Brosilow (1962) and is given as equation 2.4.

$$e = e_0 (1 + b\, e^{-c x / d_p})$$ Equation 2.4.

Figure 2.11. Radial Voidage Variations in Beds of Spheres (from Thadani & Peebles (1966)).

where e is the voidage at a distance x from the wall, e_o is the voidage at the centre of the bed, d_p is the particle diameter and b and c are constants dependant on the packing shape (b = 1 and c = 3 for spheres). This correlation satisfactorily predicts the overall decrease in voidage towards the centre of the bed but, does not predict the sinusoidal nature of this variation. Kalthoff & Vortmeyer (1980) and Hunt & Tien (1988) have presented a very similar correlation to that given in equation 2.4.

Benati & Brosilow (1962) have shown that the voidage profile around a tube, in the middle of the bed, is the same as that near a wall.

Furnas (1928) has performed experiments to measure the voidage of beds composed of various particles of different sizes. This work is discussed in further detail in Chapter 5.

2.4.2 Velocity Measurements.

Many of the studies of radial voidage variations in packed beds described in the previous section have also investigated the variation in fluid velocity in and leaving a packed bed. These studies include those of Marivoet et al (1974); Chandrasekhara & Vortmeyer (1979); Kalthoff &

Vortmeyer (1979) and Stephenson & Stewart (1986). Other studies of fluid velocity in and above a packed bed include those of Morales, Spinn & Smith (1951); Schwartz & Smith (1953); Calderbank & Pogorski (1957); Mickley, Smith & Korchak (1965), Price (1967 & 1968); Tikhonova (1970); Lerou & Froment (1977); Martin (1978); Drahos et al. (1982); McGreavy et al. (1984); Volkov et al. (1986); Bahnen & Stojanoff (1987) and Hunt & Tien (1990). Various methods are used to measure the gas velocity including anenometers, flow splitters and laser doppler velocometry. The majority of these studies are concerned with beds where the container diameter is, at most, 30 times that of the particle diameter and so are of peripheral interest to this study. The studies conclude, in accordance with the porosity results presented above, that velocity is much higher near the container walls (with significant consequent effect on heat transfer in, for example, packed catalytic reactors).

Various methods are used to allow for the variation in velocity due to the specific positioning of individual packing pieces. These include:

i. Repacking the bed many times and measuring point velocity.

ii. Circumferential averaging of velocities.

iii. Statistical analysis of velocities.

Fahien & Stankhovic (1979) present an expression for the velocity profile above the bed near the wall; caused by the local variations in voidage.

2.4.3. Turbulence and the Laminar/ Turbulent Transition in Packed Beds.

There is very little in the open literature on this subject. The majority of work in this area concerns pressure drag, boundary layer behaviour and separation etc. (e.g. Van Den Merwe and Gauvin (1971 a & b) and Karabelas, Wegner & Hanratty (1973)).

In determining the Reynolds Number for transition (which is based on the superficial fluid velocity and the particle diameter) four techniques are used:-

i. Mass transfer studies.

ii. Flow visualisation.

iii. Hot wire anenometry.

iv. Laser Doppler Velocimetry (L.D.V.).

For a random bed of spheres Jolls & Hanratty (1966) indicate the transition occurs when $150 < N_{Re} < 300$. The methods employed are reasonable. The remainder of the work is for regularly packed beds of spheres (i.e. cubic, rhombic, orthorhombic) (Kubo, Aratani, Mishima & Yano (1978)) which reveals a correlation between voidage and the transition Reynolds Numbers. For randomly packed spheres (voidage, $e = 0.41$) this gives the transition at $600 < N_{Re} < 1000$. The difference between this result and those of Jolls & Hanratty is due to the different contacts between the packing pieces (Karabelas, Wegner & Hanratty (1973)).

Dybbs & Edwards (1984) have used flow visualisation and laser anenometry within individual flow channels in beds of spheres and cylinders and have identified four distinct regimes. These regimes are characterised by a particle Reynolds Number defined thus:

$$N_{Re'} = \frac{\rho v d_p}{\mu (1 - e)} \qquad \text{Equation 2.5.}$$

where v is the superficial velocity. The four flow regimes are as follows:

i. The Darcy flow regime (also known as creeping flow) occurs where $N_{Re'} < 1$. Viscous forces dominate in this regime but, when $N_{Re'} = 1$ boundary layers start to develop.

ii. The inertial flow regime which occurs for $1 < N_{Re'} < 150$. Initially, the boundary layers become pronounced and an inertial core is developed; resulting in the non-linear dependance of pressure drop on bed velocity despite the fact that this is a laminar flow regime.

iii. The unsteady laminar regime occurs for $150 < N_{Re'} < 300$. At the lower particle Reynolds Numbers in this range, laminar wake oscillations are observed which become more pronounced as $N_{Re'}$ increases. Vortex formation initiates at $N_{Re'} \cong 250$.

iv. A turbulent regime is observed when $N_{Re'} > 300$.

This study has greatly clarified the fundamental nature of flow in porous media which had previously been viewed as undergoing a simple laminar - turbulent transition.

2.4.4. Other Studies.

As has already been shown, Ali (1984) has performed an extensive study of gas distribution in shallow large diameter packed beds.

In addition to examining point velocities above the bed (by the application of the Maldistribution Factor and the visual examination of response surfaces) he measured pressures in and below the bed, and velocities below the packed bed. The measurement techniques used to determine static pressure in the bed are subject to criticism, as is discussed in Chapter 6. Nevertheless, some of his results are presented as graphs 2.1 and 2.2, and were obtained on a scale model of the 7.3m diameter vacuum crude oil distillation column illustrated in figure 1.1.

Graph 2.1. Velocity Above and Below the Bed in a 1.22m Diameter Model of a Vacuum Pump-Around Section in a Crude Oil Distillation Column Determined by Ali (1984). Bed Depth 6cm, 16 mm Pall Rings. Tangential Inlet.

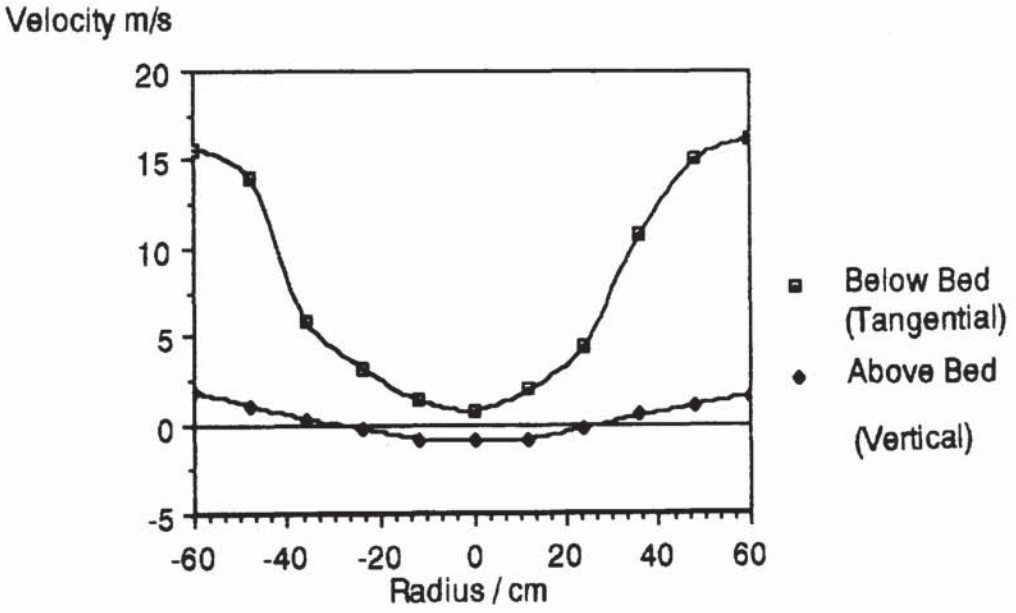

The pressure distribution was shown to be associated with the gas velocity in the feed pipe. From graphs 2.1 and 2.2 it can be concluded that:

i. The air below the bed has a high tangential velocity near the wall which decreases towards the centre.

ii. At low packed heights negative flow is observed in the middle of the bed. This phenomena has also been observed by Speiser, Muller & Barthel (1987) in a column with a radial inlet as is shown in figure 2.12.

Graph 2.2. Pressures in the Bed in a 1.22m Diameter Model of a Vacuum Pump-Around Section in a Crude Oil Distillation Column Determined by Ali (1984). Bed Depth 36 cm, 16 mm Pall Rings. Tangential Inlet.

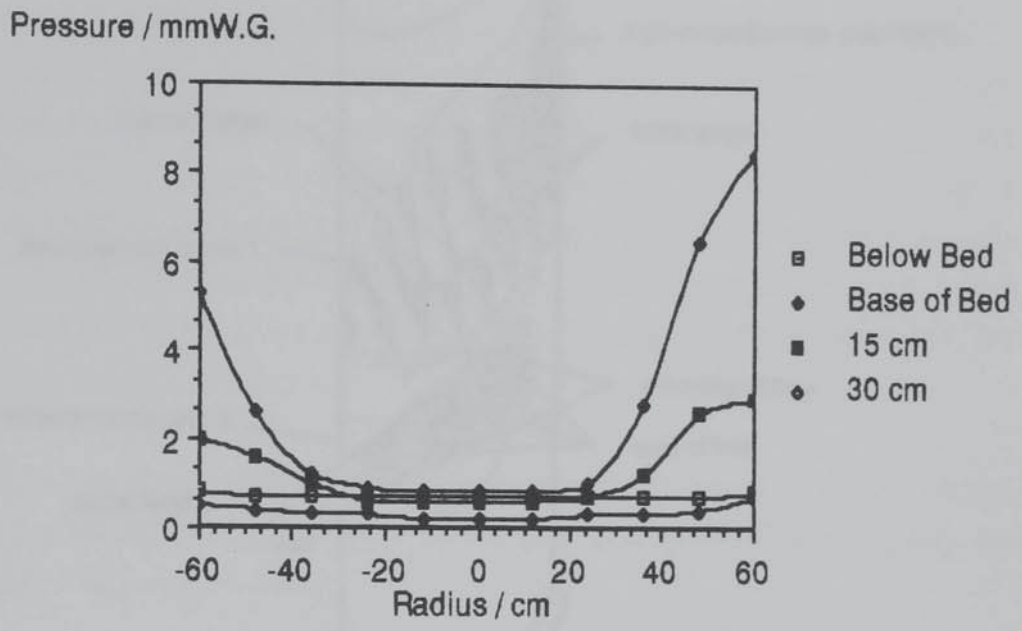

iii. The static pressure below the bed is constant.

iv. The static pressure profile flattens as it moves up the bed.

Other conclusions reached by Ali (1984) include:

i. The velocity generated static pressure (at the bed base) is independant of packed height but, increases with the inlet pipe velocity.

ii. The velocity generated static pressure at a point just within the bed, near its base, is proportional to the velocity of the swirling air below the bed at that point. Hence, the velocity generated static pressure is proportional to the square of the inlet pipe velocity.

iii. The pressure distribution below the bed is related to the velocity distribution above the bed.

Ali's measurements of gas maldistribution have also shown that the principle of dynamic similarity is satisfied if two geometrically similar beds are operated at the same N_{Re} providing that $N_{Ma} < 0.1$.

Figure 2.12. A Spatial Representation of the Velocity Profiles in a Column with a Radial Inlet. (Speiser, Muller & Barthel (1987)).

2.5. BASE OF BED FLUID MECHANICS.

The importance of this in understanding and describing maldistributed gas flow has already been shown in the Introduction (Chapter 1) and the previous section.

Early work in this area was performed by Beavers and Joseph (1967) who showed experimentally that when a viscous fluid flows past a porous solid; tangential stress moves the fluid just below the surface with a velocity U_B which is slightly greater than Q, the velocity of the fluid in the bulk of the porous medium. They measured this difference by confining the fluid above a porous surface in a narrow channel of height h and found a slightly greater flow than would have occurred if $U_B = Q$. This situation is illustrated in figure 2.13. To analyse their measurements they assumed (U_B-Q) is related to the surface drag $\mu\ (du/dy)_{y=0}$ by this equation:

$$\left\{\frac{du}{dy}\right\}_{y=0} = \frac{\alpha}{\sqrt{K}}(u_B - Q)$$

Equation 2.6.

where K is the Darcy constant ($K = \mu Q/(dP/dx)$) and Q is the volumetric flow rate per unit area perpendicular to x under the pressure gradient dP/dx. α is a constant dependant on the porous material and is assumed not to depend on h. Equation 2.6. thus describes a velocity profile across and through the free fluid/porous material boundary; this non-zero tangential velocity is usually known as the slip velocity, and is a considerable improvement on the prior assumption of a no-slip boundary condition. The presence of a boundary layer within the porous block is thus indicated; although equation 2.6. will only apply to porous media that are described by Darcy's Law.

Figure 2.13. Velocity Profile for the Flow in a Horizontal Channel formed by a Permeable Lower Wall (y = 0) and an Impermeable Upper Wall; after Beavers & Joseph (1967).

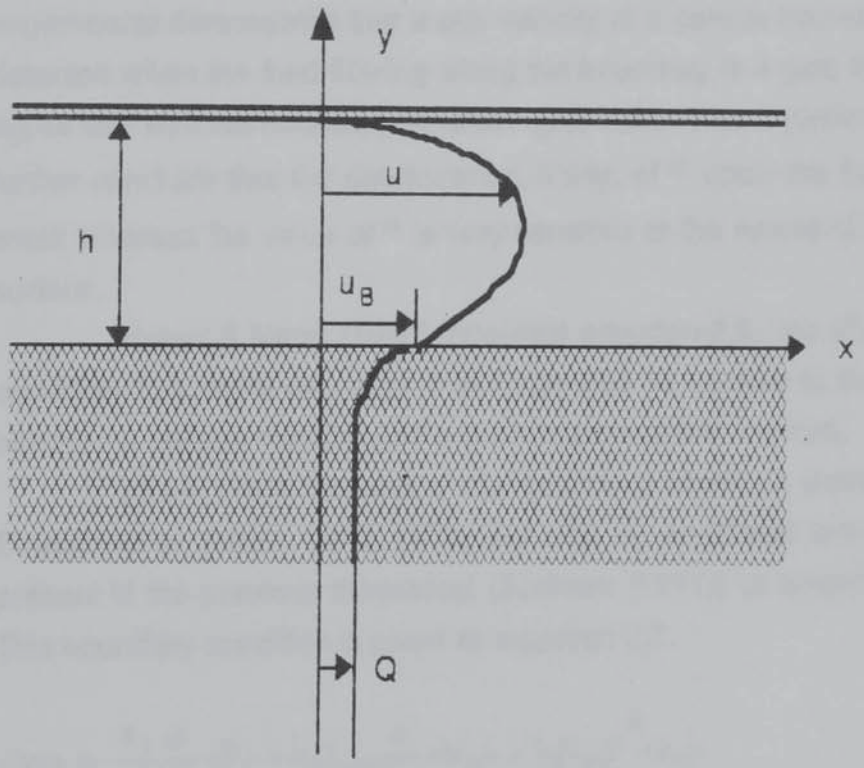

In a subsequent paper; Beavers, Sparrow & Magnusson (1970) performed further experiments, the results of which support the slip boundary condition described above. The agreement is particularly good

in the laminar flow regime. They conclude that the effect of the porous wall is to increase the mass flowrate and decrease the friction factor relative to the corresponding quantities for a solid-walled channel; they further indicate that the transition to turbulent flow occurs at a lower Reynolds Number because of the porous wall.

Taylor (1971) presents an artificial mathematical model of a porous medium which enables the flow inside and outside the porous medium to be calculated. The conceptual model was materialized and experimental results agree with the calculation. The calculated values of α are not quite independent of the external means of producing the external tangential stress.

Saffman (1971) presents a theoretical justification for the original, empirical 'slip' boundary condition of Beavers and Joseph (1967); the method is based on the use of a statistical approach to extend Darcy's Law to non-homogeneous porous media.

Beavers, Sparrow & Masha (1974) present results of an investigation of the slip boundary condition in gas flows. Their experiments demonstrate that a slip velocity at a porous boundary can be detected when the fluid flowing along the boundary is a gas; their results agree well with the boundary condition given above as equation 2.6. They further conclude that the dependence, if any, of α upon the fluid may be small whereas the value of α is very sensitive to the nature of the porous surface.

Haber & Mauri (1983) formulate equation 2.6., the slip boundary condition, in a novel way such that it can also be applied to the boundary between a porous medium and a solid, impermeable medium.

Ross (1983) presents a 'slip' boundary condition similar to that of Beavers et al. (1967, 1970, 1974) but with an additional term that is not present in the previous theoretical (Saffman (1971)) or empirical studies. This boundary condition is given as equation 2.7.

$$\langle v_i \rangle = -\frac{k_{ij}}{\mu}\frac{\partial}{\partial x_j}\langle P \rangle + k_{ij} L_{mk}\frac{\partial}{\partial x_k}\langle v_m \rangle + k_{ij} N_{jm} \nabla^2 \langle v_m \rangle \qquad \text{Equation 2.7.}$$

where $\langle\ \rangle$ denotes an average value, N is a tensor and L is the length scale of the boundary region. This equation is however difficult to apply in a practical situation since N and L must be determined. It is also shown how, in the special case of isotropic media α can be expressed in terms of

line and surface integrals of the linear map of average velocity into point velocity. This slip boundary condition reduces to the basic viscous flow of an incompressible Newtonian fluid above the boundary region and to the Darcy Equation for flow through a porous medium below the boundary region. The equation thus suggests that the effect of the bed base can be fully described by fluid dynamic equations that separately fully describe the free fluid and porous media flows.

The analyses discussed above have two serious limitations: firstly they are based on rigorously defined pressure fields, where the pressure is constant at any plane perpendicular to the nominal boundary between the porous media and the free fluid space. Thus, they shed little light on real situations such as those discussed by Ali (1984) (see below). Secondly, they will only apply to porous media that follow Darcy's Law and might better be described as permeable. The packings used in applications relevant to this study are, as shown below, best described by the Ergun Equation and can be considered as porous rather than permeable.

In addition to the analyses presented above, a number of workers (including Berman (1953); Yuan & Finklestein (1956); Yuan (1956); Berman (1958); Hirata & Ito (1981 & 1982); Hirato, Komatsu & Ito (1982); Brady (1984); Lessner & Newman (1984); Tichy & Bourgin (1986); Parnas & Cohen (1987); Sorour, Hassab & Estafanous (1987)) have discussed flow through porous pipes and annuli. These analyses involve rigorously defined flow fields, and porous media whose resistance to flow is so great that the only component of velocity within the media is that perpendicular to the media/free fluid boundary. This component of velocity is typically set as constant along the pipe/annulus length. These analyses are of peripheral interest to this study.

Ali (1984) has reported the existence of a velocity generated static pressure at the base of packed beds which occurs because of the porous media/free fluid interface. He comments qualitatively on this pressure distribution and concludes that the theoretical gas head below the bed is higher than the measured static pressure due to frictional losses. Thus, another way of describing the bed base would be as a frictional momentum sink in addition to that of the bed as a whole. Ali was unable to quantitatively describe this pressure distribution and this prevented him from fully modelling the maldistributed gas flow.

2.6. PRESSURE DROP ACROSS PACKED BEDS.

This work is concerned with beds whose overall size is much larger than the particle diameter. The flow in structures where the container size is closer to the particle diameter (e.g. catalyst particles packed in tubes) is fundamentally different because of wall effects (i.e. friction) and the increased effect of voidage fluctuations. Pressure drop across such beds is not discussed here; the reader is referred to the excellent study by Griffiths (1986).

PRESSURE DROP ACROSS LARGE BEDS OF SMALL PARTICLES.

2.6.1. Approaches.

Researchers have approached this problem in several ways; however the underlying physical models can be classified as considering the flow in and through the bed as analogous to:

i. The flow through a number of channels/capillaries.
ii. The flow through a series of orifices.
iii. The flow around a submerged object.

The first of these approaches is the most widely used, since the theoretical analysis is simple and the model is in itself physically appealing.

Early work on the subject by Forcheimer (1901) has provided the basis of the majority of subsequent efforts. Forcheimer suggested that the viscous and kinetic (sometimes referred to as inertial) resistances could be summed to give the beds overall resistance, thus:

$$\frac{(-\Delta P)}{L} = \alpha V + \beta V^2$$

Equation 2.8.

viscous losses | kinetic losses

2.6.2 The Ergun Equation.

Equation 2.8. forms the basis of many equations in the literature, of which the most widely used is the well known Ergun Equation (Ergun (1952)) which can be expressed:

$$\frac{(-\Delta P)}{L} = \frac{2\mu S_P^2 V}{e^3} + \frac{0.145\rho(1-e)V^2}{e^3}$$

Equation 2.9.

where S_P is the surface area of a particle per unit volume. This equation is derived assuming that the hypothetical channels in the porous media are straight and of uniform cross-sectional area. To allow for the effects of tortuosity and constriction the equation is modified to give this final form:

$$\frac{(-\Delta P)}{L} = \frac{a\mu(1-e)^2 V}{e^3 d^2} + \frac{b\rho(1-e)V^2}{e^3 d}$$

Equation 2.10.

which is based on flow through beds of spheres. The constants a=150 and b=1.75 were obtained by correlating the results of many workers including Burke & Plummer (1928), Oman & Watson (1944) and Morcom (1946) as is shown in graph 2.3.

Equation 2.10 can be expressed thus:

$$\frac{-\Delta P}{L} = f_1 V + f_2 V^2$$

Equation 2.11.

where:

$$f_1 = \frac{150\mu\,(1-e)^2}{e^3 d^2}$$

Equation 2.12.

$$f_2 = \frac{1.75\,\rho\,(1-e)^2}{e^3 d}$$

Equation 2.13.

Graph 2.3. A Comparison of the Pressure Drop in Packed Beds Determined by the Ergun Equation with Experimental Results.

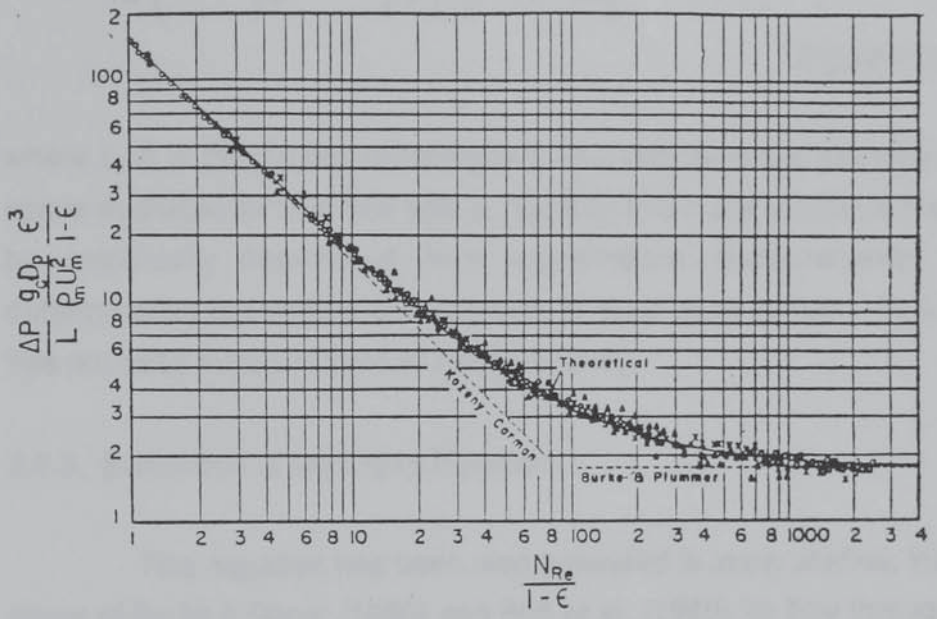

The relative importance of the viscous and kinetic terms can be determined from the particle Reynolds Number ($N_{Re'}$ as defined in equation 2.5) as follows:

$N_{Re'} < 10$	viscous term significant
$10 < N_{Re'} < 1000$	both terms significant
$1000 < N_{Re'}$	kinetic term significant.

in maldistributed flows both terms will be significant since $N_{Re'}$ will vary locally, possibly over the whole range indicated.

Molerus & Schweinzer (1989) have proposed a different correlation for particle $N_{Re'} < 10^4$. This is based on a dimensionless ratio that characterises the geometry of the space available for fluid flow. The Navier-Stokes Equations are used to discern the mutual interactions between pressure, inertia and viscosity for flow around a single sphere and combined with this dimensionless ratio. This is extended to a bed of particles and the following correlation results:

$$N_{Eu} = \frac{24}{N_{Re}}\left\{1 + k_1\left[\frac{r_o}{\delta} + 0.5\left\{\frac{r_o}{\delta}\right\}^2\right]\right\} + \frac{4}{\sqrt{N_{Re}}}\left[1 + k_2\left\{\frac{r_o}{\delta}\right\}^{1.5}\right] + 0.4 + \frac{k_3\left\{\frac{r_o}{\delta}\right\}}{\left[N_{Re}\right]^n}$$

Equation 2.14.

where r_o/δ is the dimensionless group characterising the geometry of the space available for fluid flow and k_1, k_2, & k_3 and n are constants that must be empirically determined from experimental measurements. This determination is complex and appears to yield good results. However it has not been tested or verified independantly.

2.6.3. Evaluation of the Ergun Equation.

This equation has been recommended in many studies, including those of Smith & Roper (1960) and Bird et al. (1960) for flow through beds of smooth spheres. It is also recommended in the literature review of Thomas (1962) and the critical analysis of MacDonald et al. (1979). Kler and Lavin (1987) used the Ergun Equation in a two dimensional computational fluid dynamics model of an adsorber and found the solution to compare well with experimental results. Its general applicability is confirmed by the well known Blake-Kozeny Equation (Blake (1922)) (also known as the Carman-Kozeny Equation) which is identical to the viscous flow term and by the equation of Burke & Plummer (1928) who produced an equation which is identical to the kinetic term. The Ergun Equation has been further verified by Ergun (1953). Ergun & Orning (1949) provide further explanation of the underlying theoretical basis and verification of the approach.

Foscolo, Gibilaro & Waldram (1983) criticise the Ergun Equation since, although it correctly predicts the smooth transition from fixed to fluidized behaviour, it does not correctly predict the minimum fluidising velocity. The transition is smooth because the differing channel sizes and shapes support different interstitial velocities, so the drag forces and hence the superficial velocity through the bed vary locally. In addition, the particle movement on fluidisation implies that the drag mechanisms are essentially different from those in a fixed bed, and hence, one would not expect the Ergun equation to apply at this transition. The alternative fixed bed pressure drop equation proposed by Foscolo et al. (1983) is:

$$\frac{(-\Delta P)}{L} = \frac{17.3\mu(1-e)V}{e^{4.8}d^2} + \frac{0.336\rho(1-e)V^2}{e^{4.8}d}$$

Equation 2.15.

This alternative form of the Ergun Equation is supposedly verified in a companion paper, Gibilaro et al. (1985) by comparison with the experimental results of Happel & Epstein (1954), Wentz & Thodos (1963) and Rumpf & Gupte (1971). However, the numerical accuracy of the results of the first two papers (concerned with artificially expanded beds of spheres) is dubious as the wires supporting the bed account for up to 50% of the measured pressure drop. Martin et al. (1951), Hendrie (1965) and Lyderson (1949) have shown that the resistance of regularly packed beds is different from comparable (in terms of voidage) random beds. In addition, Gunn & Malik (1966) and Susskind & Becker (1967) have observed that the resistance of expanded regular structures depends strongly on the particle spacing and orientation. These results imply that voidage alone is insufficient to describe the resistance of these beds. MacDonald et al. (1979) have analysed the results of Rumpf & Gupte (1971) and concluded that the data agrees well with the Ergun Equation. In their empirical analysis of the dependance on porosity of the viscous and kinetic parameters MacDonald et al. (1979) conclude that the Ergun Equation better represents experimental results if the power of voidage in the denominator is changed to 3.6. However, this change has no theoretical justification and an improved approach would be to modify the empirical constants a and b which allow for the tortuosity and constriction of the flow channels in the packed bed.

Puncochar, Drahos & Cermak (1990) have also examined the applicability of the Ergun Equation and conclude that it is 'very accepatable' until the velocity reaches the minimum bubbling limit.

The current acceptability of the Ergun Equation is not surprising given its firm theoretical basis. What is surprising is the lack of proposed new constants to allow for the tortuosity and constriction of the flow passages; the constants obtained by Ergun were based on experimental measurements. Many of these were made in small diameter columns where higher voidage and less tortuous flow channels near the walls would give a lower pressure drop than would otherwise be the case. Hence, the Ergun Equation might be expected to underpredict pressure drop.

2.6.4. Use of the Ergun Equation with Non-Spherical Particles.

Much of the previous work on gas distribution has been based on experimental work with non-spherical packings, such as Pall Rings (Ali (1984)). The Ergun Equation can be modified by the use of a Shape Factor (Ø) to describe the pressure drop across beds of commercial packing shapes (such as Pall Rings) and other regular shapes (cylinders, cubes etc.), thus:

$$\frac{(-\Delta P)_l}{L} = \frac{150\mu(1-\epsilon)^2 V_l}{\epsilon^3(\phi d_e)^2} + \frac{1.75\rho(1-\epsilon)V_l^2}{\epsilon^3 \phi d_e}$$

Equation 2.16.

where d_e is the equivalent particle diameter. The shape factor can be theoretically determined thus:

$$\phi = \frac{S_B}{\epsilon^3}$$

Equation 2.17.

where S_B is the surface area per unit volume of the bed. With open packings such as Pall Rings this differs from the experimentally determined values by a factor of between 2 and 5. For this type of packing further research is required on the determination of shape factors and, in the meantime, experimental results must be used to determine Ø.

An alternative approach has been used by Molerus & Schweinzer (1989) and is based on the simple consideration that it is always possible to find a spherical packing with a different particle diameter which has the same dimensionless pressure drop as the real packing. This allows the definition of a pressure drop shape factor which has been succesfully used with gravel and sand by Molerus and Schweinzer (1989). It might also be a more useful approach than that discussed above, for use with the Ergun Equation.

Many packing particles are not true spheres but have rough surfaces and beds of such particles may exhibit a size distribution (e.g. molecular sieves and adsorbents). In the latter case it is necessary to use a weighted average surface-to-volume ratio for the equivalent particle diameter (MacDonald et al. (1979)):

$$d_e = {}^{1}\Big/\sum_{1}\left({}^{Y_1}\Big/_{d_e}\right) = {}^{1}\Big/\sum_{1}\left({}^{Y_1}\Big/_{\phi_s d_{v1}}\right)$$

Equation 2.18.

where Y_i is the volume fraction of particles of size d_{ei} and, $\emptyset_s$ is the sphericity and d_v the diameter of a hypothetical sphere of the same volume as the particles. There is some evidence (Gupte (1970)) that for wide particle distributions this procedure is inadequate.

For rough particles MacDonald et al. (1979) propose that the coefficient a (in equation 2.10.) should be independent of particle roughness but that b, by analogy with pipe flow, should depend on the roughness. Further, there is evidence (Rumpf & Gupte (1971) and Kyan et al. (1970)) that the porosity dependence in equation 2.10. is not accurate over a wide range of porosity. Nevertheless, for engineering purposes, MacDonald et al. (1979) propose that $1.8 < b < 4.0$, the higher value applying to the roughest particles. Crawford & Plumb (1986) conclude, on the basis of experimental observations, that surface roughness does affect flow in the viscous regime. For both smooth and rough particles of spherical shape they propose the following correlation:

$$\frac{\rho(-\Delta P)\varepsilon^{5.5}(1-\varepsilon)^2}{G_O^2 SL} = \frac{5.6\mu S}{36G_O} + \frac{0.0471}{6} + \frac{0.5825}{6}\left(\frac{\theta}{D_1}\right)^{0.992}$$

Equation 2.19.

where G_o is the superficial mass flow rate, S the surface area per unit volume, θ the measured roughness height and D_1 the smooth sphere diameter.

This correlation has not been tested or verified by other workers; and in view of its lack of theoretical basis and the difficulties involved in measuring surface height is unlikely to be widely used.

2.6.5. The Ergun Equation in Multi-dimensional Flows (The Vectorial Ergun Equation).

The Ergun Equation has been used by many workers in a variety of modified forms to model non uni-directional fluid flows.

Early attempts to apply the Ergun Equation in this way include those of Radestock & Jeschar (1970), and Kuwabara & Muchi (1975 a, b & c), who used the uni-directional form thus:

$$-\frac{\partial P}{\partial x} = f_1 V_x + f_2 V_x^{\,2}$$

Equation 2.20.

This is clearly unsatisfactory since, if the velocity in a given direction is negative the kinetic pressure gradient (the V^2 term) will have the wrong sign and so, pressure will increase in the direction of the flow. This is only significant in situations where the flow direction may be reversed; that is, where the flow is severely maldistributed.

A 'differential' form has been used by Stanek & Szekeley (1972, 1973 & 1974), Cross & Gibson (1979) and Fenech et al. (1985) and is as follows:

$$-\frac{\partial P}{\partial x} = f_1 V_x + f_2 V_x |V_x|$$

Equation 2.21.

This formulation unlike that above is physically realistic. A full, vectorial form has been used by Shvydkii et al. (1974), Kitaev et al. (1975), Poveromo, Szekely & Propster (1975); Szekely & Poveromo (1975); Choudhary, Propster & Szekely (1976); Poveromo (1975), Choudhary, Szekely & Weller (1976 a & b); Fukatake & Okabe (1976); and Voller, Cross & Merrick (1983) and is as follows:

$$\text{grad } P + \underline{V}(f_1 + f_2 V) = 0$$

Equation 2.22.

where $\underline{V}$ is the velocity vector and V is the absolute magnitude of the velocity vector (given by the Pythagorous Theroem). In two dimensions (x & y):

$$V = \sqrt{v_x^2 + v_y^2}$$

Equation 2.23.

and in three dimensions (x, y & z):

$$V = \sqrt{v_x^2 + v_y^2 + V_z^2}$$

Equation 2.24.

For a given direction (x) and in three dimensions (x, y & z) equation 2.22. becomes:

$$-\frac{\partial P}{\partial x} = V_x\left[f_1 + f_2\sqrt{v_x^2+v_y^2+V_z^2}\right]$$

Equation 2.25.

and similarly for the y and z directions.

Apte et al. (1988) have used the Ergun Equation in this form (for the x direction):

$$-\frac{\partial P}{\partial x} = \left[f_1 V_x + f_2|V_x|\right]V$$

Equation 2.26.

which is a vectorial form which also features the improvements applied to the basic Ergun Equation. The formulation is clearly incorrect for maldistributed flows, V is always positive and hence; as when the basic Ergun Equation is applied, the formulation allows the pressure gradient to increase in the flow direction.

These formulations of the Ergun Equation have formed the basis of the vast majority of the theoretical and computer models of multi-directional flows in packed beds. These models are discussed in the following section.

2.7. MODELS OF GAS FLOW IN PACKED BEDS.

This section presents various models that describe gas flow in packed beds; particularly when the gas flow is maldistributed. The modelling of such flows is central to the approach used in this study.

2.7.1. Analytical Models.

Very few analytical models of maldistributed gas flows in packed beds have been presented in the literature. This is chiefly because of the difficulties encountered in obtaining solutions to the complex sets of equations that result; still fewer of these models are of practical use.

Nevertheless, Ali (1984) has presented such a model. The starting point in his analysis is an elemental volume in the bed for which

differential versions of the Ergun Equation are written. Unfortunately two fundamental mistakes are made at this stage:

i. The Ergun Equation constant designated f_1 in this work is incorrect (the denominator of f_1 is $e^3 (\phi d_p)^2$ and not $e^3 \phi d_p$).

ii. The form of the Ergun Equation used is that given as equation 2.20 which has already been shown to be incorrect since it can permit a velocity to increase along a pressure gradient.

He then considers these equations wholly or with only the f_1 or f_2 terms (which he incorrectly describes as laminar and turbulent). A steady state mass balance over the elemental volume is then made into which the Ergun Equation is inserted. Ali concludes that the resulting equations cannot be solved but considers simplified versions of the models.

This simplified model, the Two Areas Model is based on conceptually dividing the bed into two sections which support different fluid velocities (a similar approach to that of Mullin (1957)) initially this division is achieved by a conceptual impermeable membrane although this assumption is later relaxed.

The simplified model eventually results in an equation which identifies packed bed "designs at risk" from gas maldistribution, although; this equation must be considered in the light of the criticisms above.

Hassan (1985) and Aryan (1986) have developed a momentum balance model that permits the calculation of the swirl velocity below the bed for a tangential inlet. The velocity at the column wall (U_R) can be related to u_r, that at a radial position r below the bed using an equation of the form:

$$U_r = U_R (r/R)^n \qquad \text{Equation 2.27.}$$

Hassan takes n=1 and Aryan n=2. Momentum loss at the column wall and bed base is determined for the limiting case of column radius much greater than packed height and the following equation is obtained.

$$U_R^2 = \left(\frac{n+1}{S'}\right)^{1/2} V_T \left(\frac{D_T}{d_p}\right) \qquad \text{Equation 2.28.}$$

S' is the wall friction factor, V_T is the average velocity through the bed which has diameter D_T and contains packing of size d_p.

However, this analysis does not fully describe the bed base and does not allow the solution of Ali's model, as had been intended.

This example has illustrated the complexities of such analytical models and helps explain why numerical (or computational) methods are preffered.

2.7.2. Computational Models Based On The Vectorial Ergun Equation.

A number of forms of the Ergun Equation for use in modelling maldistributed gas flows were presented in 2.6.5. Some of these forms were shown to be incorrect and models based upon such formulations are not considered here.

Stanek & Szekely (1972) first applied a differential form of the Ergun Equation in a two-dimensional computational scheme with spatial voidage variations. The Ergun Equation is used as the equation of motion and combined with the equation of continuity in terms of the stream function; the resultant expression being solved by successive over relaxation. The computed results show that the presence of regions of higher or lower void fractions 'may appreciably modify the flow pattern through the system'. A subsequent study (Stanek & Szekely (1973)) extended this approach to non-isothermal systems. The results indicate that temperature profiles (resulting from heat transfer through the boundary walls) may lead to flow maldistribution even where porosity is uniform.

In Stanek & Szekely (1974) these workers first use a proper vectorial form of the Ergun Equation which is applied to three dimensions. This formulation of the Ergun Equation was found to be far more amenable to solution than the differential forms. Szekely & Poveromo (1975) (see also Poveromo (1975)) compared experimental measurements of maldistributed gas flow in a packed column (caused by the spatial variation of bed resistance and axisymmetric injection of gas) to computed profiles. The two dimensional model (numerically very similar to those discussed above) is supplied with the experimentally measured pressure drop and determines the velocity profile leaving the bed. At first sight the agreement between the two is very good but, there is a significant discrepancy in the presentation of this work which is discussed in greater detail in Chapter 5.

Kuwabara & Muchi (1975) used a similar model to examine flow patterns in blast furnaces; their conclusions confirm the results of the work discussed above albeit in a situation of greater practical interest.

Voller. Cross & Merrick (1983) present a similar model for gas flow in a coke oven charge. Although 'the model involves a number of simplfying assumptions, the predictions compare well, in a qualitative sense, with earlier descriptions of gas flow in coke ovens'. The results of this study are consistent with those discussed above; further details are given in Voller (1980).

Cross & Gibson (1979) uses a one term vectorial equation similar to the kinetic term of the Ergun Equation, and apply different resistances to the different velocity components to fully describe multi-layered porous media (encountered in, for instance, blast furnaces) and satisfactorily compare their results with those of Stanek & Szekekly (1972, 1973 & 1974) which are discussed above.

Poveromo, Szekely & Propster (1975) extend the three dimensional model, including the vectorial form of the Ergun Equation, discussed above to include the effects of heat transfer and spatial voidage variation. This model is set up for a blast furnace geometry and its results compared to experimentally determined velocity profiles from a cold model. These profiles agree reasonably well.

Fukutake & Okabi (1975) present a different numerical scheme (that also uses the vectorial Ergun Equation) that can determine the spatial variation in dimensionless pressure. This apart, their conclusions are similar to those of Szekely & Poveromo (1975). Calculated pressures are compared to experimental ones and while this comparison is poor; this work represents an important step towards the full and rigorous modelling of gas flow in packed beds.

2.7.3. Computational Models Based on Extended Versions of the Vectorial Ergun Equation.

The models descussed above have used the Ergun Equation as the equation of motion. Shvydkii et al. (1974) and Kitaev et al. (1975) have attempted to extend this approach by including inertial terms determined from an equation of motion proper, in a two dimensional scheme. The equations solved are:

for the x direction;

$$-\frac{\partial p}{\partial x} = f_1 V_x + f_2 V_x V + \rho V_x \frac{\partial V_x}{\partial x} + \rho V_x \frac{\partial V_y}{\partial y}$$

Equation 2.29.

and for the y direction;

$$-\frac{\partial p}{\partial y} = f_1 V_y + f_2 V_y V + \rho V_y \frac{\partial V_x}{\partial x} + \rho V_y \frac{\partial V_y}{\partial y}$$

Equation 2.30.

Disregarding, for the moment, the physical justification for this approach; conflicting results have been obtained using this formulation (relative to the normal vectorial Ergun Equation). Kitaev et al. (1975) and Shvydkii et al. (1974) both found that the inertial terms have a significant effect whereas Szekely, Propster & Choudhary (1975), Choudhary, Propster & Szekely (1976) and Buchlin (1986) all conclude that the inertial effects are negligible.

The fullest expression of this type (neglecting those discussed in section 2.7.4. below) is that of Hong, Tien & Kaviany (1985);

$$\rho\,(\underline{V}.\underline{\nabla}\,\underline{V}) = -\,\underline{\nabla}P - e\underline{V}(f_1 + ef_2 V) + \mu\underline{\nabla}^2\underline{V} + \rho\underline{g}$$

Equation 2.31.

mass x accel'n	pressure force	Ergun Equation	viscous force	gravitational force

So, the coupling of certain terms from the full equations of motion (the Navier-Stokes equations) with the semi-empirical Ergun Equation (in one of its forms) has become quite common. The justification for this is not clear in that the addition of any further terms to the Ergun Equation is physically doubtful due to the empirical nature of the Ergun Equation. The Ergun Equation is fitted to experimental results and will therefore include all contributions to the pressure drop. The addition of, for example, the inertial terms is therefore contra-indicated since their effect is already included. However the bed resistance is typically the dominant term and so the effects of the additional terms are likely to be small. The addition of these terms is however a useful first step towards modelling the flow both in and around a packed bed in an item of process equipment.

2.7.4. Computational Fluid Dynamics.

Recent versions of the C.F.D. code FLUENT (Creare Inc. (1990)) include a bed description option which is as follows:-

$$\underline{\nabla}P = C_1\underline{V} + C_2\underline{V}|\underline{V}| + \mu\nabla^2\underline{V} \qquad \text{Equation 2.32.}$$

Appropriate setting of the constants C_1 and C_2 will allow the description of a packed bed by the vectorial Ergun Equation. The addition of the viscous stress tensor (the 3rd term on the R.H.S. of equation 2.32.) may be questioned, following the argument outlined above. In addition, this formulation does not permit spatial variations in resistance (i.e. C_1 & C_2) as a result of local packing or fluid conditions, which is necessary to fully model maldistributed flows. However, the FLUENT package will permit the solution of equations describing both packed and unpacked areas. As will be seen, the addition of the vectorial Ergun Equation to a C.F.D. code and its subsequent application is a significant part of this study and, in this light it is appropriate to indicate that this work was underway some time before this option, in FLUENT, was introduced.

Kler and Lavin (1987) indicate that they have used the Ergun Equation with the C.F.D. code PHOENICS to investigate the flow patterns in a packed adsorber. No details are given of the exact formulation of the Ergun Equation used or, how it is applied. They compare their modelled results with experimental ones and find good agreement between them; however, the gas flow in the situation studied is well distributed.

2.8. CONCLUDING REMARKS.

This chapter has reviewed the published work on areas of interest to this study. The following conclusions are of particular relevance to this study.

i. The importance of obtaining uniform gas distribution in packed beds in items of process plant, particularly where the aspect ratios of such beds are low.

ii. The lack of understanding of the operating mechanisms of gas distributors and, the lack of design methods for them.

iii. The effect of walls on the voidage in packed beds and, the subsequent effect on local velocity.

iv. The effects of the bed base, which are not fully understood.

v. The robustness and accuracy of the Ergun Equation and, particuarly, the use of its vectorial form in describing maldistributed flows.

vi. The limitations of existing models of gas flow (particularly maldistributed flows) in packed beds.

CHAPTER 3

APPROACH TO THE PROBLEM

The literature survey has shown the importance of obtaining uniform gas distribution in packed beds. It has further shown that our understanding of the fluid mechanics of maldistributed gas flow in packed beds - and particularly the effects of the base of the bed - is limited to the extent that distributors can only be designed empirically. What is needed is a rigorous design tool for process equipment containing packed beds.

The computer models of gas flow in packed beds are also limited in that they are problem specific and only apply to situations where the domain of interest is wholly packed. That is, they cannot describe fluid flow outside the bed. More conventional mathematical models are constrained by a lack of understanding of the fluid mechanic effects of the bed base and the complexity of the equations obtained which cannot be solved analytically.

In order to resolve these dificulties, this work presents a combined theoretical and experimental study of gas flow in packed beds.

In theoretical terms the approach has been to implement the vectorial Ergun Equation within a computational fluid dynamics (C.F.D.) package. Such a model will not suffer from the limitations of the existing models discussed above and would form the basis of a useful design tool. The model is tested and verified (by comparison with independant experimental results) in situations where the domain of interest is wholly packed.

A novel, two-dimensional experiment has been designed and realised to examine in greater detail the effect of the bed base. As shown in figure 7.1, this consists of a shallow bed above a duct. The end of the duct below the bed can be blocked, partially obstructed or left open. This allows the relative amounts of gas leaving through the bed and the duct end to be controlled; resulting in different velocities at and below the bed base, and different static pressures in the duct. This permits a rigorous examination of the effects of the bed base. The experimental results from this investigation permit further qualitative understanding of the fluid mechanics of maldistributed gas flow in shallow packed beds and the

effect of the bed base. This investigation also features novel hardware to measure presure in, and at the base of, packed beds.

The experiment forms the basis of the final computer model which therefore describes a situation where the effects of the bed base are significant. The results from the model are compared to the experimental measurements and this comparison highlights the need for a novel description of the bed base beyond that of the vectorial Ergun Equation and the slip velocity. Two such descriptions are made, the first involves the representation of spatial voidage variations in the bed near its' base. The second is best described as a base of bed boundary condition and involves the application of the logarithmic law for velocities near the bed base within a turbulence model.

Finally, a novel three-dimensional experimental investigation of gas flow in packed beds is realised. This is a progression of the earlier experimental work and is particularly designed to emphasise the effects of changes in flow direction below the bed which are largely due to the effect of the vessel walls. As in the two-dimensional experiment, the relative amount of air leaving through the bed and the duct below the bed can be controlled so the effect of the bed base can be studied. The experimental results from this study can, in future, be used to verify a three-dimensional model of maldistributed gas flows in process equipment containing packed beds.

This combined programme is shown in flowchart form in figure 3.1. Initially the flowchart shows the current state of knowledge relative to this work. The development of, and inter-relationship between, the various aspects of this study is then shown. The final part of the flowchart shows how this work can be continued to give a full understanding of gas distribution in packed beds and develop a rigorous deign method for such equipment. The main part of the flowchart which shows the approach to, and structure of, the work in this thesis also details the relevant chapter numbers.

The main objectives of this work can be summarised as follows:

i. The identification of a suitable C.F.D. package which will allow the introduction of the vectorial Ergun Equation.

ii. The implementation of the vectorial Ergun Equation in this C.F.D. package.

iii. Basic testing of the resultant model.

iv. The verification of the model by comparison with the experimental results of Poveromo (1975).

v. The design and construction of of a two-dimensional experimental apparatus to investigate the fluid mechanics of gas flow in a shallow packed bed and, at the base of such a bed.

vi. The development of special pressure measurement hardware to measure pressure in, and at the base of packed beds.

vii. The experimental investigation of gas fluid mechanics in and at the base of shallow packed beds using the apparatus described above.

viii. The adaptation of the model described above to model the experimental situation described and subsequently to develop and improve this model.

ix. The investigation of the three-dimensional flow of gas in a shallow packed bed; highlighting the effects of the vessels containing walls.

Figure 3.1. A Flowchart Showing the Approach to Problem Adopted and the Basic Structure of the Thesis. Numbers are chapter numbers.

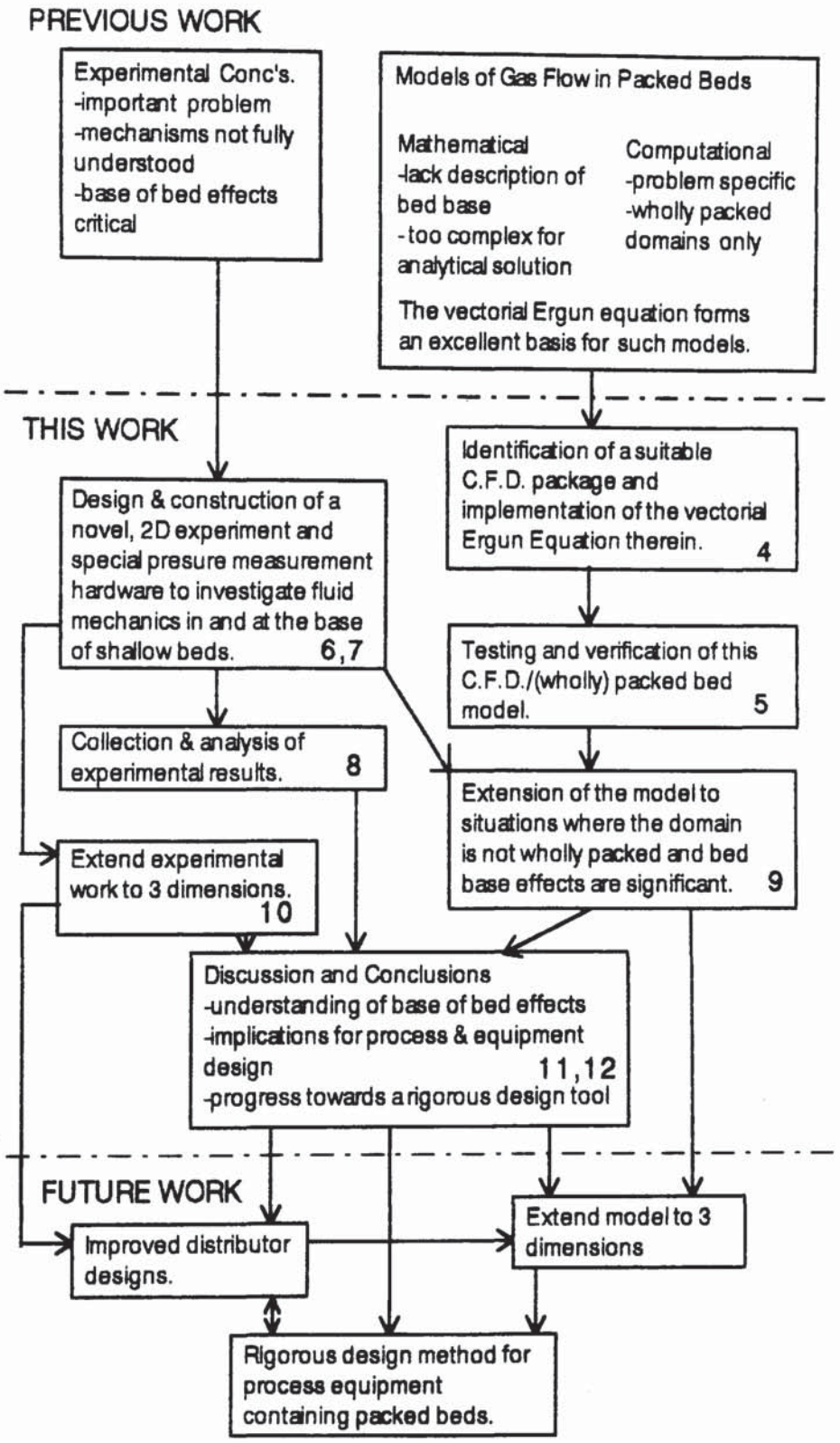

CHAPTER 4

A COMPUTER MODEL OF GAS FLOW IN PACKED BEDS PART ONE: DEVELOPMENT

4.1. INTRODUCTION.

As has already been shown in the literature survey the analytical solution of models of maldistributed gas flow is very difficult unless significant simplifications are made to such models.

An alternative method has been to use the vectorial Ergun Equation as the equation of motion in a specifically written computer model. This approach is only of limited value since the computer program is problem specific and the model is not easily extended to include the effects of wall friction etc. or, to situations where the area of study is not wholly packed and the bed base/free fluid interface may have a significant effect.

An alternative approach is to obtain a numerical solution using a Computational Fluid Dynamics (C.F.D.) package. C.F.D. packages are a modern engineering tool which solve the full equations of motion that describe a fluid flow in, for example, an item of process equipment. The effects of turbulence wall friction etc. can be included (Tayler (1989), Macilwain (1989)). This chapter presents the implementation of the vectorial Ergun Equation in such a package which is subsequently verified in Chapter 5. In Chapter 9 the model is extended to situations where the domain of study includes areas which are not wholly packed and, as such, of particular interest to this study. Such solutions are useful and may give a greater insight into the physics of maldistributed gas flows; they must however be rigorously checked within themselves (for grid independence, convergence etc.) as well as against experimental results wherever possible.

Initially, it is necessary to discuss the selection of one of the commercially available C.F.D. codes for this purpose.

4.2. SELECTION OF COMPUTATIONAL FLUID DYNAMICS CODE.

There are a large number of commercially available C.F.D. packages in a variety of code types including (Glynn et al. (1988)):

i. Finite-volume steady packages (such as: PHOENICS, FLUENT, HARWELL-FLOW3D)

ii. Finite-volume time marching (ESTET, FIRE).

iii. Finite-element (N3S, FIDAP, NISA).

iv. Marker and cell (NAGARE).

v. Panel based (VSAERO).

Of these types the finite-volume codes, and in particular; PHOENICS, FLUENT, and FLOW3D, are among the most highly developed and offer the highest level of features. PHOENICS (Spalding (1981)) was selected for use in this work particularly because it is designed to allow major changes of the type required to implement the vectorial Ergun Equation. Other significant factors in selecting PHOENICS included:

i. Its availability on the Aston University Cluster computer system.

ii. Kler and Lavin (1987) have reported using a two-dimensional Ergun Equation with the code (although, as discussed in Chapter 2, little detail is provided of its implementation and the situation modelled is such that the bed base/free fluid interface has no significant effect).

iii. The authors knowledge of and prior experience with the code.

It would, however, be informative to attempt to use the vectorial Ergun Equation with the other packages (particularly Fluent and Flow3D) and compare the results from the various packages.

The next section of this chapter describes the main features of PHOENICS. Subsequently the implementation of the vectorial Ergun Equation is described.

4.3. AN INTRODUCTION TO THE COMPUTATIONAL FLUID DYNAMICS CODE PHOENICS.

4.3.1. Introduction.

PHOENICS (Parabolic Hyperbolic Or Elliptic Numerical Integration Code Series) is a general purpose C.F.D. package, that is capable of simulating the flow in process equipment.

Built into PHOENICS are the major balance laws of physics (mass, momentum etc.) applied to a large number of contiguous sub-domains (often referred to as 'cells') into which the domain of interest is artificially divided.

When supplied with information on:

i. The physical properties of the fluid.

ii. Spatial information describing the boundaries, internal features etc. of the plant item being modelled.

iii. Inlet and outlet conditions (and initial conditions, if necessary).

in the appropriate form PHOENICS determines the solutions to the relevant differential equations returning them as tables of numbers of velocity, pressure etc. and as graphical representations of these numbers and derived values of particular interest to the user.

PHOENICS takes full account of the effects of viscosity, diffusion etc., it thus produces time averaged solutions of the full Navier-Stokes equations of motion, employing a finite-difference scheme to give approximate solutions to the exact equations. The software is described in detail in the manuals (Rosten & Spalding (1987 a & b)).

4.3.2. Structure.

The inter-relationship between the various PHOENICS routines and the files transferred between them is shown in Figure 4.1 and discussed below.

The basis of the software is two Fortran programs, EARTH & SATELLITE. The EARTH program is the main program of PHOENICS and contains all the equation solving coding: it cannot be altered by the user. The SATELLITE program is a Fortran pre-processor, which reads the Q1 file into which the user inserts coding that describes the flow simulation

required, the SATELLITE then writes a file EARDAT which describes the problem to EARTH. The rationale for this nomenclature is that there is only one EARTH, but, as many SATELLITES (or, more strictly Q1 files) as there are users and problems.

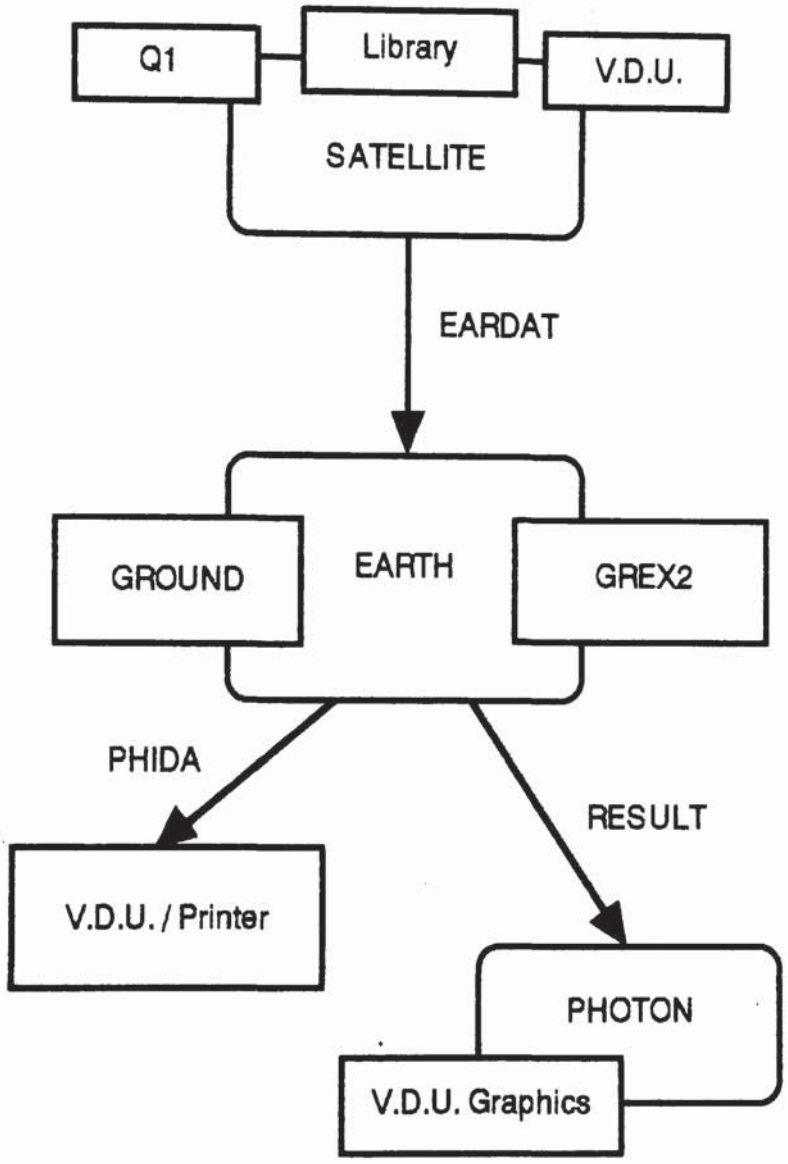

Figure 4.1. The Structure of Phoenics.

In the version of PHOENICS used in this study (Version 1.4), the SATELLITE can be used interactively. The QI file is used to store the users' commands which are written in PIL (Phoenics Instruction Language), which is later re-expressed in the appropriate form for the EARDAT file.

The GUIDE program is an instructional file that explains how

PHOENICS operates and how to run it. This, together with the HELP facility also forms the basis of the manuals (Rosten & Spalding (1987 a & b)).

When the EARTH run is completed, two files are written, RESULT which contains tables of values, line-printer plots etc. as defined by the Q1 files as well as error and warning messages and a listing of sources etc. The second file PHIDA is a data file for the PHOTON program. PHOTON is a PHOENICS specific graphics package which allows the user to construct plots which describe the flow field in terms of contours or velocity vectors. The grid can also be plotted, text added etc.

Finally, the GROUND routine allows the user to intervene in the solution procedure of EARTH. The use of GROUND (in particular to describe the pressure drop across packed beds) is discussed more fully in subsequent sections of this chapter. PHOENICS also provides GREX2 (Ground Example 2) which provides, for example; turbulence, wall friction etc. as switch-on options.

This chapter presents Fortran coding which is added to Ground to describe packed beds, it also introduces the Q1 commands necessary to implement this GROUND code. The subsequent chapter which concerns the verification of this coding also provides a detailed discussion of the Q1 coding, which describes the basic features of the fluid flow.

Both Ground and the Q1 file are arranged in 24 parts, known as Groups, each of which will contain related information on certain aspects of the flow simulation. The Group Numbers and Titles are presented below:

GROUP 1	Run title and other preliminaries
GROUP 2	Transience: time-step specification
GROUP 3	x-direction grid specification
GROUP 4	y-direction grid specification
GROUP 5	z-direction grid specification
GROUP 6	Body-fitted coordinates or grid distortion
GROUP 7	Variables stored, solved and named
GROUP 8	Terms (in differential equations) and devices
GROUP 9	Properties of the medium (or media)
GROUP 10	Interphase-transfer processes and properties
GROUP 11	Initialization of variable or porosity fields
GROUP 12	Convection and diffusion adjustments
GROUP 13	Boundary conditions and special sources
GROUP 14	Downsteam pressure for PARAB=T

GROUP 15 Termination of sweeps
GROUP 16 Termination of iterations
GROUP 17 Underrelaxation devices
GROUP 18 Limits on variables or increments to them
GROUP 19 Data communicated by SATELLITE to GROUND
GROUP 20 Preliminary printout
GROUP 21 Printout of variables
GROUP 22 Spot-value printout
GROUP 23 Field printout and plot control
GROUP 24 Dumps for restarts

4.3.3. Variables.

The 'conserved' dependent variables of interest in modelling flow in packed beds are: u, v & w the three components of velocity (in the x, y and z directions respectively) and the pressure (other possible variables include concentration, enthalpy per unit mass etc.). For turbulent flows two additional variables are required; K the turbulence energy and ε the turbulence dissipation rate. If the fluid is compressible or thermal effects are significant then density and temperature will also be dependent variables.

The independent variables are the components of the co-ordinate system: x, y and z for a Cartesian system and θ (designated x in PHOENICS), r (designated y) and z for a cylindrical-polar system.

4.3.4. Cell Geometry and Nomenclature.

As indicated above, in PHOENICS the domain of interest is artificially divided into contiguous sub-domains or 'cells'. For the reader to understand subsequent sections (particularly those involving the GROUND coding for the Ergun Equation) it is necessary to show how PHOENICS describes the cells.

Figure 4.2 is self-explanatory showing a typical domain and how the cell faces are named.

PHOENICS allows the use of Cartesian or cylindrical-polar co-ordinate systems. The version used also features Body-Fitted Co-ordinates (B.F.C.s) which allow the grid to be distorted to fit complex domain geometries; the grid is then non-orthogonal.

Where the domain boundaries are not specified (e.g. by the specification of wall friction, mass flow in or out etc.) PHOENICS treats them as fully-reflecting and impermeable to the transport of conserved variables.

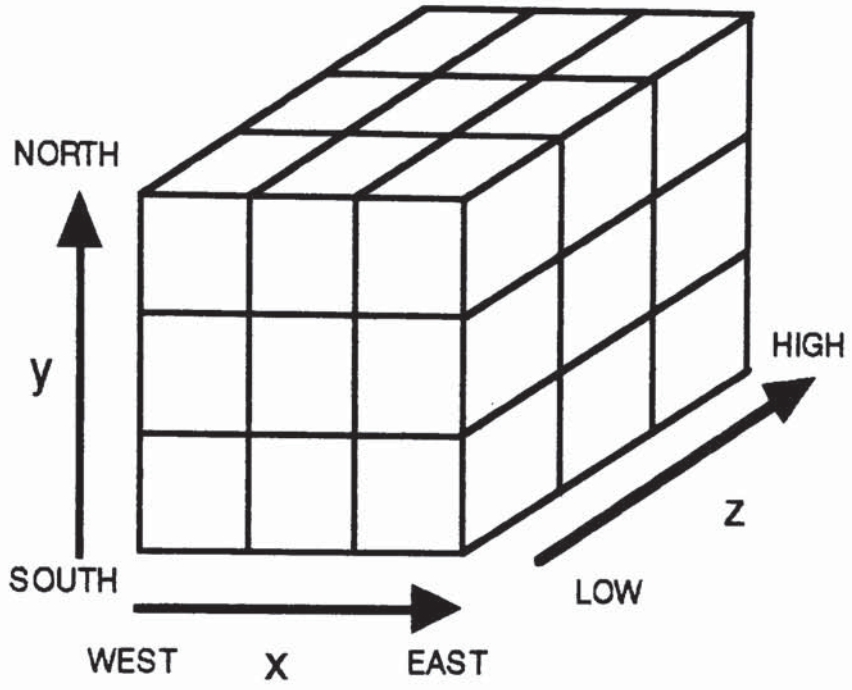

Figure 4.2. Cell Geometry & Nomenclature.

The equations solved by PHOENICS and the methods by which their solution is achieved are discussed below. However, because the discretized continuity equations consider velocities at alternate grid points (and not adjacent ones) velocity fields of the type shown in figure 4.3 may be generated. These fields are not realistic, but nevertheless satisfy the discretised continuity equations.

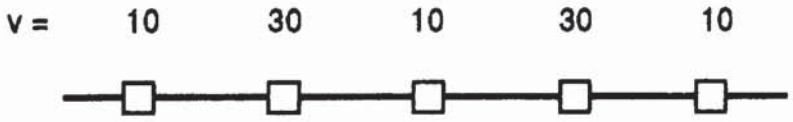

Figure 4.3. A Wavy Velocity Field that Satisfies the Discretised Continuity Equation.

This difficulty is resolved in PHOENICS by recognizing that all the variables do not have to be calculated at the same grid points. In the case of the velocity components if a displaced or 'staggered' grid is used the

difficulties described above disappear. A two-dimensional form of such a staggered grid is shown in figure 4.4; its use has a significant effect on the implementation of the vectorial Ergun Equation in PHOENICS, as is shown below.

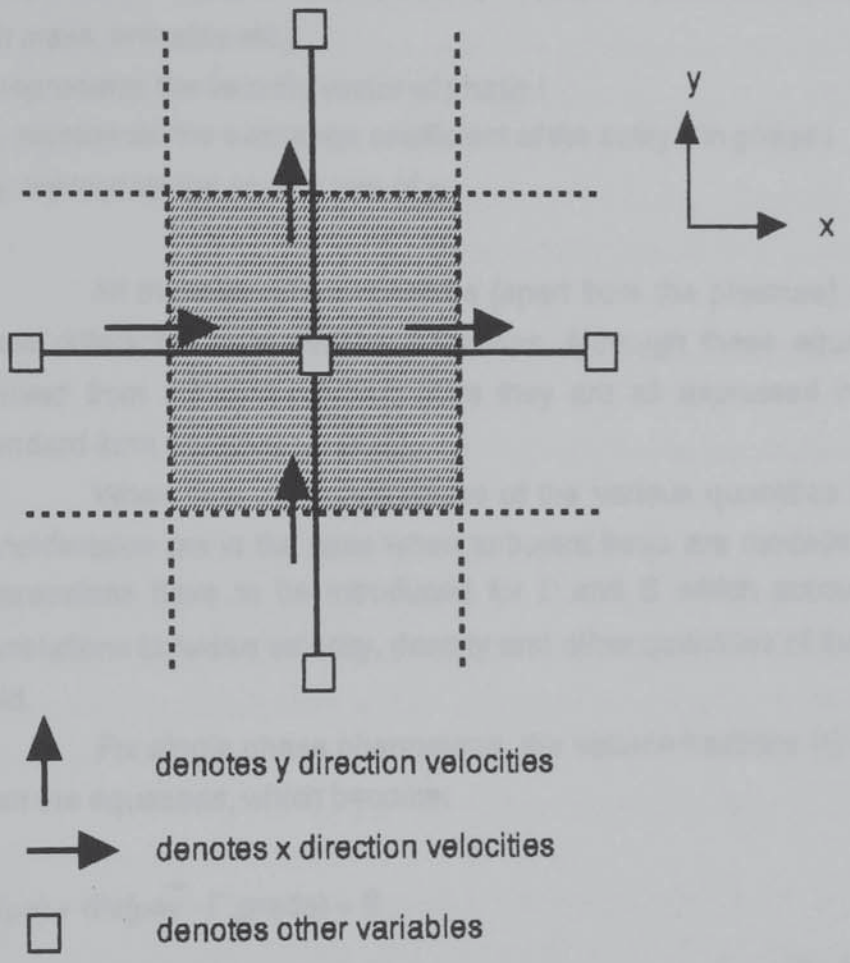

Figure 4.4. The Staggered Grid for Velocities.

4.3.5. Equations Applied.

PHOENICS provides solutions to the discretised versions of sets of differential equations having the general form:

$$\frac{\partial}{\partial t}(r_i \rho_i \phi_i) + \mathrm{div}(r_i \rho_i \phi_i \vec{v}_i - r_i \Gamma_\phi \mathrm{grad}\phi_i) = r_i S_i$$

transient convection diffusion source

Equation 4.1

where:

t represents time.

r_i represents the volume fraction of phase i

ρ_i represents the density of phase i

ϕ_i represents any conserved property of phase i (such as momentum per unit mass, enthalpy etc.)

V_i represents the velocity vector of phase i

$\Gamma\phi_i$ represents the exchange coefficient of the entity ϕ in phase i

$S\phi_i$ represents the source rate of ϕ_i

All the dependent variables (apart from the pressure) appear in these differential conservation equations. Although these equations are derived from different physical laws they are all expressed in the one standard form (Patanker (1980)).

When time averaged values of the various quantities are under consideration (as in the case when turbulent flows are modelled) special expressions have to be introduced for Γ and S which account for the correlations between velocity, density and other quantities of the flow and fluid.

For single phase phenomena, the volume fractions (r_i) disappear from the equations, which become:

$$\frac{\partial}{\partial t}(\rho\phi) + \text{div}(\rho\phi\vec{v} - \Gamma_\phi \text{grad}\phi) = S$$

Equation 4.2

The pressure variable is associated with the continuity equation:

$$\frac{\partial}{\partial t}P + \text{div}(\rho\vec{v}) = 0$$

Equation 4.3.

in anticipation of the so-called pressure correction equation which is deduced from the finite-difference form of the continuity equation.

The effective exchange coefficient of ϕ (Γ_ϕ) is determined from the turbulence parameters (k, ε) which, as discussed above are dependent variables of equation 4.1, if they are solved.

The specification of boundary conditions is described in section 4.4.1 below.

4.3.6. Solution Method.

Internally PHOENICS solves sets of algebraic equations which represent the consequences of integrating the differential equations (shown in the previous section) over the finite volume of a computational cell (and, for transient problems, over a finite time) and approximating the resulting volume, area and time averages by way of interpolation assumptions.

In PHOENICS the interpolation assumptions used are the 'fully-implicit upwind' set; selected because of their reliability. Essentially this implies that:

i. In time-dependent terms all fluid properties are taken as independent of position within a given cell.

ii. In convection terms all fluid properties are uniform over cell faces.

iii. In diffusion terms the property gradients and transport properties which they multiply are uniform over all cell faces; the gradients are based on the supposition that the properties vary linearly and the transport properties used are thus arithmetic averages of those on either side of the cell faces.

iv. In source terms the nodal values are taken as prevailing over the whole vell volume.

Many variants of these options can be used however, the result will be a set of algebraic equations of the form:

$$\phi_P = \frac{(a_E\phi_E + a_W\phi_W + a_N\phi_N + a_S\phi_S + a_H\phi_H + a_L\phi_L + a_t\phi_t + S)}{(a_E + a_W + a_N + a_S + a_H + a_L + a_t + a_P)}$$

Equation 4.4

Where Ø represents the dependent variable currently under consideration; the subscripts P,E,W,N,S,H,L denote the locations where the variable is determined (following the convention described in section 4.3.4), the subscript t denoting earlier time. The a's represent coefficients (temporarily taken as constants), those with subscripts express the interactions between neighbouring cells by diffusion and convection. S and a_p represent the source of the entity Ø, the specification of source terms is further discussed in the next section.

It is now necessary to describe how PHOENICS computes the distribution of dependent variables. The total number of algebraic equations to solve is NX * NY * NZ (= the total number of cells in the integration domain) times the total number of dependent variables. These equations are often stongly coupled.

PHOENICS therefore solves them in an iterative 'guess-and-correct' manner. This iterative process is a complicated one, involving a multi-stage, oft-repeated sequence of adjustment of values. Iteration is required because the equations although linear in appearance are generally non-linear; the non-linearities being exerted by the functional dependence of the coefficients and sources on the variables. During the iteration cycle the coefficients and sources are regarded as temporarily constant so that linear equation solvers can be employed.

For this disscussion, only the salient features of the iteration cycle are mentioned.

'Slabs' are arrays of cells having the same value of the co-ordinate z, as shown in figure 4.5. Many of PHOENICS' mathematical operations are performed over a single slab and many cycles of adjustments can be made for each slab. These cycles are known as 'slabwise solutions'.

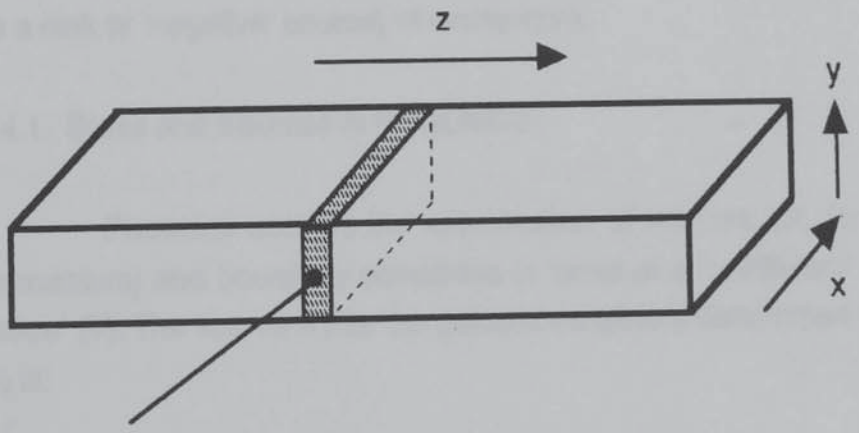

Figure 4.5. The 'Slab' of Cells.

A 'sweep' is a set of slabwise operations conducted, in order, from the lowest to the highest slab. Since the equations at a given slab make reference to values at other slabs, later adjustments at these slabs will, to a certain extent, invalidate the adjustments previously made.

Hence, many sweeps must be made until the equations are in balance and the solution given is a converged one.

4.3.7. Computer Software and Hardware Used.

Appendix 12 gives full details the hardware and software used in this work.

4.4. CODING OF THE ERGUN EQUATION IN PHOENICS.

Having described the main features of the C.F.D. package employed in this work; it is now possible to describe and explain how the vectorial Ergun Equation is applied within this package.

The basic version of the FORTRAN coding written for the GROUND sub-routine to describe packed beds by the vectorial Ergun Equation is presented as Appendix 1. This coding is heavily commented to assist the reader in relating the discussion below to its FORTRAN realisation.

Initially however, it is necessary to discuss the method used in PHOENICS to specify boundary conditions and other sources (and sinks). As is shown below, the vectorial Ergun Equation is described and coded as a sink (a 'negative' source) of momentum.

4.4.1. Sinks and Sources in PHOENICS.

Phoenics accepts the specification of sources (of, for example, momentum) and boundary conditions in terms of a 'coefficient' (C) and a 'value' (V). The source S_ϕ for the generic variable ϕ determined by C_ϕ and V_ϕ is:

$$S_\phi = C_\phi (V_\phi - \phi_P)$$

Equation 4.5.

where ϕ_P is the value of ϕ at node P (the in-cell value of ϕ).

S_ϕ is included in the full equations of motion as shown in equation 4.1 above.

This simple algebraic equation permits the full description of any source. For instance, if the coefficient is set to a very large number the equation reduces to:

$$\emptyset_p = (... + V \times C) / (... + C) = V$$

Equation 4.6

and hence $\emptyset_p$ is set to the desired value (V).

For a fixed-flux boundary condition; C is given a very small value so that it is negligible in comparison to the other terms in the denominator. V is then chosen so the product VxC equals the desired flux.

The PHOENICS satellite accepts the users' specification of the C and V quantities through a command named COVAL, applied over a sub-domain defined by the PATCH command.

When it is required to code such features as a packed bed, PHOENICS provides the GROUND sub-routine (where FORTRAN coding giving coefficients and values can be inserted). As discussed, this sub-routine is called throughout the solution procedure of EARTH and modifies the equations solved by EARTH.

4.4.2. The Vectorial Ergun Equation.

The vectorial Ergun Equation has been presented and extensively discussed in the literature survey (Chapter 2) where it was shown that this equation may be written:

$$\text{grad } P + v_l (f_1 + f_2 \overline{V}) = 0$$

Equation 4.7

where V is the magnitude of the velocity vector;

$$\overline{V} = (v_x^2 + v_y^2)^{1/2}$$

(in two spatial dimensions) Equation 4.8

and

$$\overline{V} = (v_x^2 + v_y^2 + v_z^2)^{1/2}$$

(in three spatial dimensions) Equation 4.9

For a given fluid and packing, f_1 and f_2 are constants and are as defined in Chapter 2. Equation 4.7 can be re-expressed for the three co-ordinate directions as follows:

for the x direction;

$$-\frac{\partial P}{dx} = v_x (f_1 + f_2 \overline{V})$$

Equation 4.10a

for the y direction;

$$-\frac{\partial P}{\partial y} = v_y (f_1 + f_2 \overline{V})$$

Equation 4.10b

for the z direction;

$$-\frac{\partial P}{\partial z} = v_z (f_1 + f_2 \overline{V})$$

Equation 4.10c.

The next section describes how the equation can be expressed as a coefficient; in which form it can be applied in PHOENICS.

4.4.3. The Ergun Equation as a Coefficient.

The vectorial Ergun Equation is expressed as a coefficient (rather than a value) since it is applied to the value of the appropriate variable(s) rather than defining this value.

It might be expected that the vectorial Ergun Equation would be coded as a coefficient on the pressure variable. This approach is not possible since the pressure variable is associated with the continuity equation (equation 4.3) which since it is subsequently expressed in a correction form does not have a source term. Furthermore, this approach would be inappropriate since it would not fully admit the vectorial nature of the equation.

Hence, the equation is applied as coefficients to the equations of motion for the velocity components. The coefficients of the velocity equations have (S.I.) units of kg m^{-3} s^{-1} (but, see section 4.4.4 below); and hence the coefficient is given (in the x direction);

$$C_{v_x} = -\frac{\partial P}{\partial x}\frac{1}{v_x}$$

Equation 4.11

Substituting in the vectorial Ergun Equation for the x direction gives:

$$C_{v_x} = v_x (f_1 + f_2\overline{V}) \frac{1}{v_x}$$

therefore;

$$C_{v_x} = f_1 + f_2\overline{V}$$

Equation 4.12a

and for the y and z directions:

$$C_{v_y} = f_1 + f_2\overline{V}$$

Equation 4.12b

$$C_{v_z} = f_1 + f_2\overline{V}$$

Equation 4.12c

The coefficients given as equations 4.12 will describe a packed bed by the vectorial Ergun Equation. The vectorial nature of the equation is clearly admitted when it is appreciated that the coefficients are applied to the equations of motion for the different velocity components. The reduction of the equations in this way means that the same coding can be used to determine the coefficients for all the velocity components (since the coefficients are all the same); thus reducing the programming and computational effort.

In simple terms, the mechanism by which the Ergun Equation is applied is that the coefficients are applied to the velocity equations and cause these equations to be out of balance (strictly more out of balance; since the process is iterative). The continuity (pressure correction) equation then seeks to balance the velocity equation and 'absorbs' the coefficient by increasing the pressure. The solution procedure is, as previously described, iterative and so this cycle is repeated many times with many adjustments to pressure made by the coefficients applied to the velocity components. The velocity components are, of course, also dependant on the pressure.

The coefficients include the magnitude of the velocity vector and so the velocity and pressures equations are particularly strongly coupled which may result in convergence problems.

The next two sections present, in detail, the coding written to apply the coefficients that describe the vectorial Ergun Equation in PHOENICS.

4.4.4. Q1 Coding Required To Activate Ergun Equation Coding.

The majority of coding for the vectorial Ergun Equation in PHOENICS is made in the GROUND sub-routine. As discussed above the Q1 file coding is explained in detail in the next chapter. Instructions must however be placed in the Q1 file so that the relevant part of the GROUND coding is used by the program; this section explains those commands.

It is necessary to first define the sub-domain over which the bed exists, this is achieved using the PATCH command which has the following form:

PATCH (name, type, lowest x cell, highest x cell, lowest y cell. etc.....)

any name can be used for the patch and its associated COVAL (Coefficient and Value) commands. The patch types appropriate to this example are VOLUME and PHASEM. The VOLUME type is used here and sets the sources as per unit volume. The units of the coefficients are strictly kg/Ds where D is a dimension specified by the patch type. In section 4.4.4 this dimension is given as m^3 and is thus consistent with the selection of the volume patch type. The PHASEM type dictates that the COVAL commands will be equal to:

coefficient * (value - variable value at grid node) * mass of the relevant phase in the cell.

and would be used with transient models, where the cells are partially blocked (to represent the packing volume) and so the quantity of gas in the bed is correct (such an adjustment of porosity in the Q1 file will have no effect on the resistance of the bed).(The Ergun Equation is based on superficial velocity through the bed). In many of the models presented as part of this work the voidage of the bed is not constant and if the PHASEM type were used this would have to be reflected in the setting of porosity in the Q1 file. The Phoenics Instruction Language used in the version of PHOENICS used in this study does not include commands that would make this straightforward and easily altered (this limitation has been removed in more recent versions). Hence, the VOLUME patch type is used and the model is limited to steady state. If the patch type were changed

from VOLUME to PHASEM the coefficients defined in section 4.4.3 should be divided by the fluid density (in addition to the full description of the bed voidage in the Q1 file).

Having defined the patch over which the bed exists the code is instructed to call Ground for the coefficients with this statement:
COVAL (name, variable, c,v).
One such statement will be required for each of the three components of velocity (the variables). Since the value is not to be altered v is set to zero, C is set to GRND which instructs the code to obtain the coefficients from section 1 of Group 13 of GROUND; where they are determined as explained in the subsequent section.

The command USEGRD=T must also be included in the Q1 file and informs the package that a GROUND file including user written coding is to be used.

4.4.5. Ground Coding for the Ergun Equation.

The FORTRAN GROUND coding which includes the vectorial Ergun Equation in a three-dimensional scheme is attached as Appendix 1. This section describes its operation.

PRELIMINARY CHANGES.

Two alterations are made to the GROUND sub-routine before the vectorial Ergun Equation is realised. These are:

i. PHOENICS stores all the numerical information used during the solution procedure in the so-called F-array. This is redimensioned to 10^6 since the simulation is extensive in terms of numbers of cells etc.. Increasing the size of the F-array prevents out of core operation and this reduces the computing time required to obtain the solution.

ii. The WRIT40 subroutine writes its argument to the VDU during the solution procedure and to the RESULT file. By editing the (text) argument of this subroutine the user can keep track of changes to his own coding.

OVERVIEW.

The basic steps in the realisation of the vectorial Ergun Equation in PHOENICS are shown in flow diagram form in figure 4.6. The coding is added to section 1 of Group 13 in accordance with the Q1 instructions discussed in section 4.4.4 above. The following description of the coding follows the structure of figure 4.6.

DESCRIPTION OF CODING.

i. Dimensioning of Arrays etc.

NXD & NYD, the number of cells in the x and y directions are specified and made parameters so that they can be subsequently used to define array sizes. It is not necessary to perform a similar operation for the number of z cells since PHOENICS employs a slabwise solution procedure (as described in section 4.3.6)

Various arrays are then defined and dimensioned, as described by the comments in the coding. Briefly, arrays are required for the velocities and the coefficients.

The real variables required are declared.

ii. Preliminary Checks.

Checks are made to ensure the correct patch has been called for the correct variables.

iii. Determination of The Ergun Constants etc.

The Ergun Equation constants (f_1 and f_2) are determined according to these basic definitions:

$$f_1 = \frac{150\mu(1-e)^2}{e^3(\phi d)^2}$$

Equation 4.13

$$f_2 = \frac{1.75\rho(1-e)}{e^3\phi d}$$

Equation 4.14

This is only performed once - at the lowest z slab of the bed, at the first sweep and for the variable solved first (the x component of velocity).

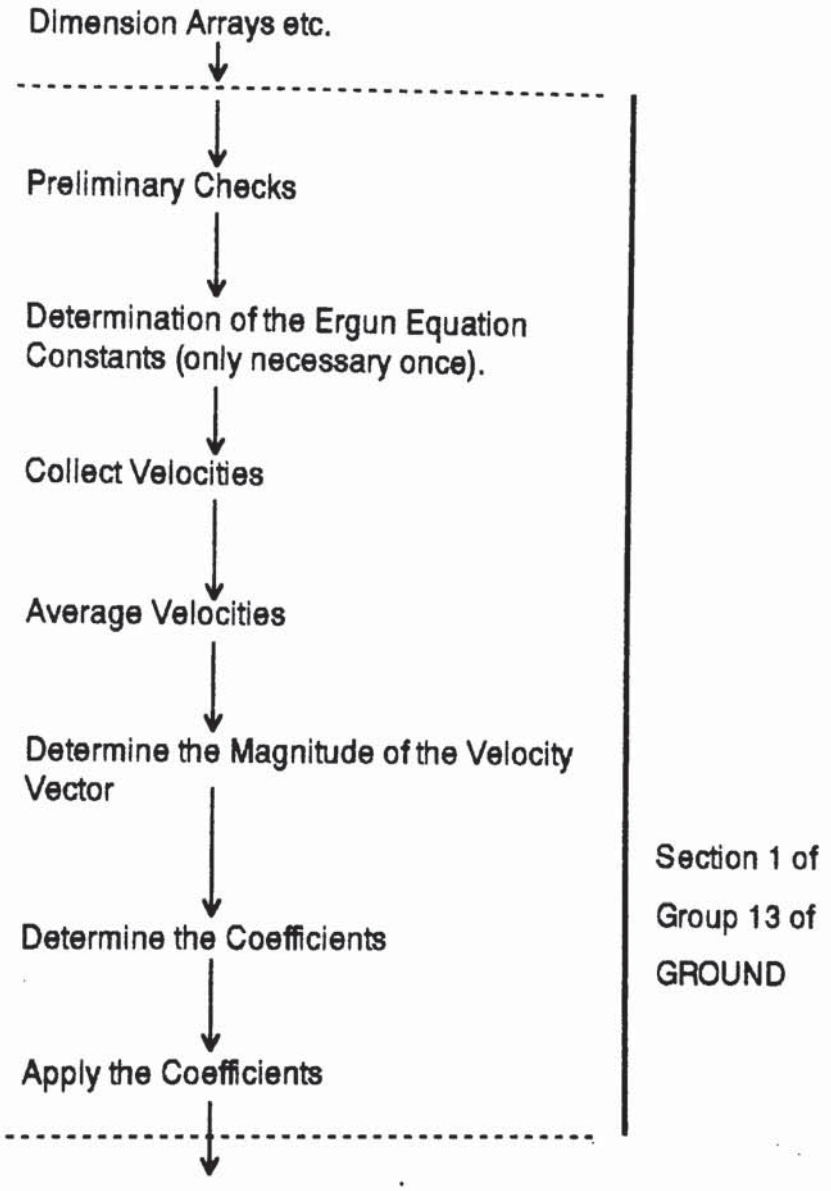

Figure 4.6. A Flow Diagram Showing the Basic Steps for the Implementation of the Vectorial Ergun Equation in the GROUND sub-routine of PHOENICS.

The voidage, particle diameter and shape factor are held in the RG(n) array which is defined in the Q1 file. This allows the packing type to be changed without altering the GROUND coding. Alternatively f_1 and f_2 could be defined alone.

Various warning messages are sent to the VDU to ensure the number of cells used by the Q1 and GROUND files are consistent and that the correct patch type has been specified.

iv. Collection of Velocities.

The velocities for the current slab are collected using the PHOENICS subroutine GETYX and read into the apppropriate arrays. The velocities for the previous (LOW) z-slab are also collected.

v. Averaging of Velocities.

The position of the bed within the domain is defined in the Q1 file using the IG(n) array which is automatically available to GROUND.Due to the staggered grid employed by PHOENICS the velocities for a given cell are the velocities leaving the 'high' side of each grid cell. It is therefore necessary, since the coefficient is applied to the middle of the cell (where the pressure is calculated) to obtain an average value of these velocities. This should improve the numerical accuracy of the converged solution and reduce the number of cells required to obtain a grid independent solution. This is illustrated in Figure 4.7.

The determination of these average velocities is complicated by the fact that where a boundary of the bed coincides with the 'low' boundary of the domain in which a solution is required there is no 'low' velocity and the average cell velocity must be taken as the 'high' face velocity multiplied by a suitable factor such as 0.5 (because the value of the velocity through the wall would be zero if it existed in PHOENICS). This factor (the variable GEVF) can be changed as its value does not affect the final solution; it will however affect the convergence of the model. The principle is illustrated in figure 4.8. Cells at the 'high' boundaries of the domain are treated in a similar fashion. 'New' bed boundaries are then created for the area in the bed where true averaging can be applied (eg. Jigone replaces IG(1) etc) and these averages are then determined.

vi. Determination of The Magnitude of The Velocity Vector.

The magnitude of the velocity vector is determined for each cell of the slab using equation 4.9.

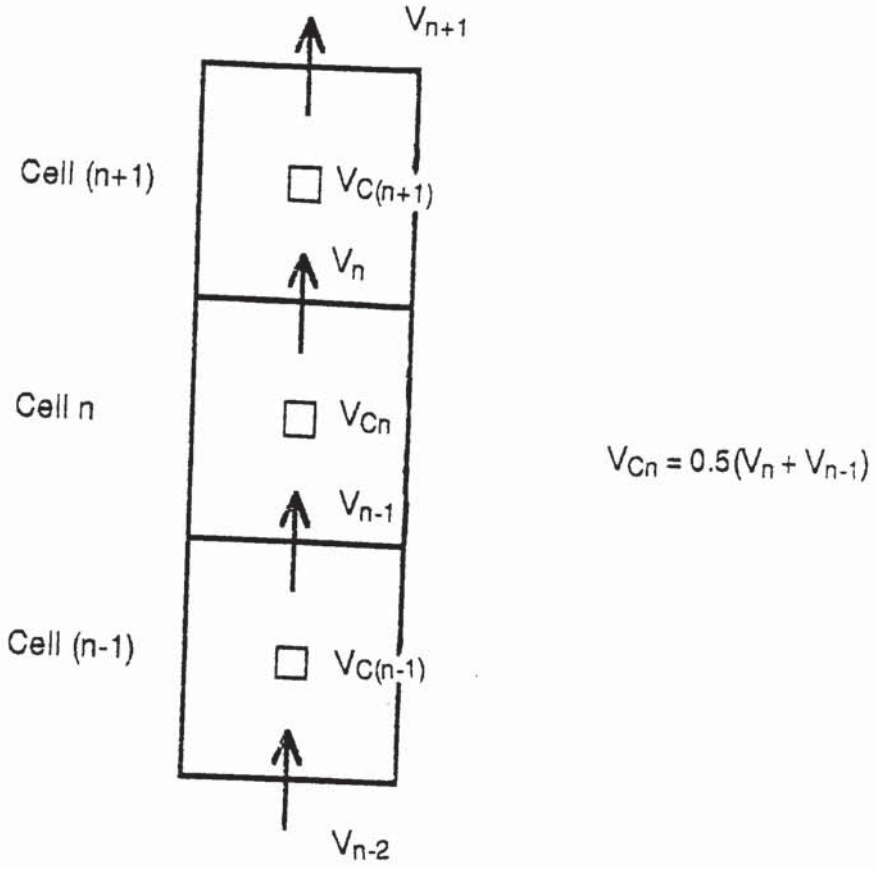

Figure 4.7. Cell Velocities

vii. Determination of the Coefficients.

The Ergun Constants and the Magnitude of the velocity Vector are used to determine the coefficients (according to equation 4.7) for each cell in the current slab.

viii. Application of the coefficients.

The coefficients are then placed in the F-array using the PHOENICS SETYX sub-routine; the coefficients are then available for use by the solver.

FINAL REMARKS.

This section has described the GROUND coding in Appendix 1 which realises the vectorial Ergun Equation in PHOENICS. This coding will be used by the solver for each of the three components of velocity at every slab of cells in the bed and at every sweep during the solution procedure.

Particular attention has been paid to the treatment of velocities which is necessitated by the staggered grid employed for velocities by PHOENICS.

The computational efficiency of the coding presented could be improved; however in its current form the coding is at its most straightforward and amenable to modification if required (for example as described in Chapters 5 and 9).

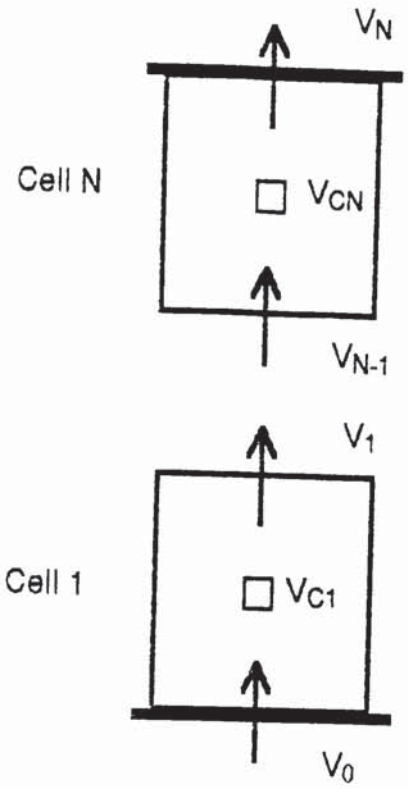

V_0 and V_N do not exist

therefore,

$V_{CN} = c * V_{N-1}$

$V_{C1} = c * V_1$

c = a constant

Figure 4.8. Cell Velocities At Domain Boundaries.

4.5. CONCLUSIONS.

i. PHOENICS, a commercially available C.F.D. code has been identified as one into which the vectorial Ergun Equation can be introduced.

ii. The PHOENICS package has been briefly described; in particular the basic equations and their method of solution have been identified.

iii. A strategy has been identified whereby the vectorial Ergun Equation can be applied in PHOENICS. The equation is re-arranged and expressed as a source term coefficient which is applied to the equations of motion for the velocity components.

iv. Fortran coding has been written in the GROUND subroutine of PHOENICS that implements the vectorial Ergun Equation in this form; and allows for the staggered grid used by PHOENICS.

The subsequent chapter tests and verifies this realisation of the vectoral Ergun Equation (and explains in some detail the commands used in the PHOENICS Q1 file).

CHAPTER 5

A COMPUTER MODEL OF GAS FLOW IN PACKED BEDS PART TWO:TESTING & VERIFICATION

5.1. INTRODUCTION.

The previous chapter presents the implementation of the vectorial form of the Ergun Equation in the GROUND routine of the C.F.D. code PHOENICS. Before this can be applied to cases of particular interest to this study (i.e. shallow packed beds and those where the free fluid/bed boundary interface will have a significant effect) the coding must be tested and verified.

This chapter presents such tests and the verification of the GROUND coding by the comparison of results from the model with the experimental results of Poveromo (1975) who studied maldistributed gas flows in a packed bed with no significant free fluid/bed boundaries.

As discussed in Chapter 4, in presenting these models the PHOENICS Q1 file commands are also explained.

5.2. APPROACH.

5.2.1. Methods of Verification.

Any verification of a solution of a gas flow field and its method of solution falls into three categories:

i. The comparison of the numerically predicted results with expected physical behaviour (see for example Stanek & Szekely (1972, 1974)),

ii. The comparison of predicted results with experimental results (Stanek & Szekely (1973), Szekely & Poveromo (1975), Poveromo, Szekely & Propster (1975) and Szekely & Propster (1977)),

iii. The comparison of predicted results with results obtained using alternative physical theories and/or solution methods (Cross & Gibson (1979)).

The first of these methods of validation although vague offers a simple first step to checking the theory as well as the solution method. Experimental measurements of gas flow in porous beds which have been used to test theoretical results include pressure drop, pressure distribution, and outlet velocity (method ii.). The majority of measurements are made on laboratory scale equipment and generally show some agreement with the theoretical predictions. The last of the above three methods of validation is used to check refinements to existing numerical methods or alternative approaches to the theory.

5.2.2. Verification Methods Used.

i. The basic facets of the theory and method outlined in chapter 4 will be checked (in Section 5.3) using a simple basic test problem and then considering the resulting predictions of flow patterns, pressure drop etc. for the expected physical behaviour.

ii. A further validation is made by comparing the predictions of the model with the experimental results of Poveromo (1975) (see also Szekely and Poveromo (1975)).

5.3. BASIC TESTS.

As discussed above this section seeks to make an initial test of the model, by considering results from it for expected physical behaviour.

It is not the purpose of this sub-section to verify the Ergun Equation in any of its forms (uni-directional, vectorial etc.) or its implemetation in Phoenics by comparison with experimental results which is the subject of the later parts of this chapter and chapter 9.

5.3.1. Explanation of The Test Problem.

Initially a simple test of the implementation of the vectorial Ergun Equation in PHOENICS is required. If a simple packed container is modelled so that inflow occurs across one face and the gas leaves through the opposite face the computed pressure drop can be compared to that calculated from the simple Ergun Equation. In the absence of wall friction the flow field within the cube should be uniform.

As discussed in section 5.3.4 (below) this basic test model can be extended to check that the model does not suffer from the limitations of many such computer realisations of the vectorial Ergun Equation discussed in the literature survey.

The Ground coding used in this basic test model is the same as that presented in the previous chapter and is included as Appendix 1. The Q1 file is attached as Appendix 2.

5.3.2. The Q1 File.

It is beyond the scope of this thesis to provide a complete explanation of all the commands used in the PHOENICS Q1 file. For such detailed information the reader is referred to the PHOENICS manuals (Rosten and Spalding (1987 a & b)). However, this section describes the Q1 file for the basic test model (presented as Appendix 2) and in explaining the features of this model the basic commands used in the PHOENICS Q1 file will become clear. The coding is described in order of the PHOENICS Groups.

Group 1. Run Title and Other Preliminaries.

The spatial boundaries of the bed and the physical details of the packing are defined. These details are defined as special variables in the IG(n) (for integers) and RG(n) (for real numbers) arrays so that they are also available to the GROUND routine.

Also defined are the height (HT) and width (WID) of the cube, in metres. WIN is the air velocity (in ms^{-1}) into the cube, which is such that the low z face is the inlet face and high z one the outlet one.

Group 2. Transience: Time-Step Specification.

The model is defined as a steady state one.

Groups 3, 4 & 5. Grid Specification.

The grid is defined as Cartesian. The GRDPWR command is used to define the grid and has four arguments: the first is the direction in which the command defines the grid (i.e. x,y or z) the second is the number of cells in this direction (equal to NX, NY and NZ respectively), the third is the physical size of the grid in this direction. The fourth argument is

used to define the discretisation of the domain into cells, when set to 1.0 the cells will be of equal size. The resulting grid is illustrated as figure 5.1.

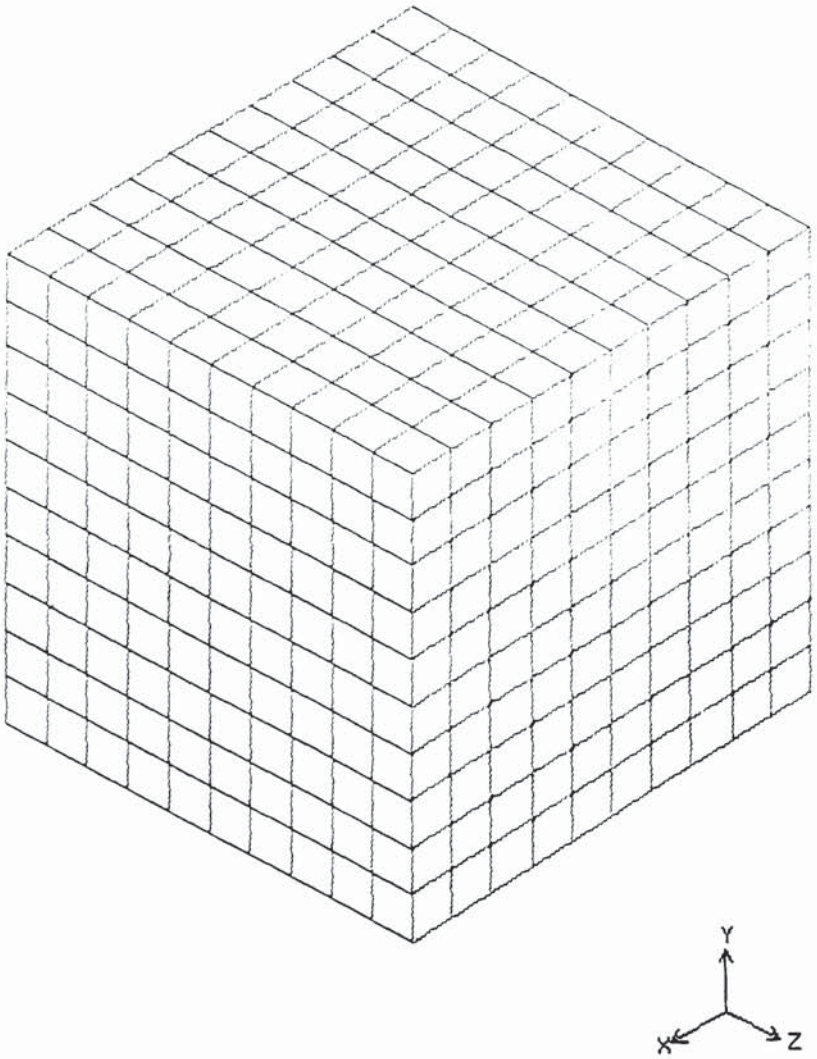

Figure 5.1. The PHOENICS Grid for the Basic Test Model.

Group 7. Variables Stored, Solved and Named.

This group is used to declare which variables are to be stored or solved for and, where appropriate, defines which solution method is to be used. The SOLUTN command is used to make this declaration and has seven arguments, as follows:

i. The name of the variable (P1 is the (first phase) pressure; U1, V1 & W1 are the velocities of the first phase in the x, y and z directions.

The remaining arguments are either Y's or N's; answering yes or no to these questions:

ii. Store the variable?

iii. Solve for the variable? (by the slab-by-slab method)

iv. Solve by the whole-field method?

v. Solve by the point-by-point method?

vi. Use explicit formulation if transient?

vii. Use harmonic averaging of exchange coefficients?

The four variables are stored; the velocity components are solved for using the point-by-point method (the preferred method for velocities, particularly when, as in this case, the effects of diffusion and convection are insignificant in comparison with source effects). Pressure is solved using the whole-field method particuarly since, in this case, the z direction links dominate (the z direction is the direction of flow).

Group 9. Properties of the Medium.

The physical properties of the fluid are defined here. The viscosity (ENUL) and density (RH01) are set to those of air. The turbulent viscosity (ENUT) is set to 100 times the laminar viscosity to promote numerical stability. The value chosen will not affect the final solution. The use of the turbulent viscosity and turbulence models in general are discussed further in chapter 9.

Group 13. Boundary Conditions and Special Sources.

This group is used to define boundary conditions and special sources. Boundary conditions are set using the Coefficient and Value approach described in Chapter 4. Two commands are used to define boundary conditions: PATCH and COVAL.

The PATCH command, as its name suggests, defines the region over which the boundary condition is active. It has 10 arguments. The first

argument is the patch name which is also used by the relevant COVAL command so the two are linked. The second argument is the patch type and indicates over which part of the patch the boundary condition is applied. Typically the patch name refers to a cell face, other special names may be used as discussed in chapter 4. The final arguments describe the sub-domain over which the boundary condition is applied in order: lowest x cell, highest x cell, lowest y, highest y, lowest z, highest z and earliest and latest time intervals (in transient flows).

The COVAL command is used to set the boundary condition using the COefficient and VALue approach described in Chapter 4. The command has four arguments: the COVAL name, the variable to which the boundary condition is applied and the Coefficient and Value applied to describe the boundary condition.

The inlet boundary is fully descibed by setting the velocity to WIN with the coefficient ONLYMS (which has a numerical value of 0.0) and specifying a fixed flux of WIN x RH01 using the coefficient FIXFLU (=1.E-10) on the pressure variable.

At the outlet boundary the pressure is set to zero using the coefficient FIXP (=1.0).

Group 13 also includes the commands activating the GROUND coding that includes the vectorial Ergun Equation. The call to GROUND is made for the three components of velocity, the values are set to zero (since no change to the values of the velocities is made here) and the coefficients are set to GRND. This has no numerical value but instructs the solver to obtain the coefficients from the relevant part of GROUND.

Group 15. Termination of Sweeps.

LSWEEP is the number of iterative sweeps through the integration domain required. A relatively low number is required in a simple case such as this.

Group 17. Under-Relaxation Devices.

As with many numerical methods, relaxation is used in PHOENICS to reliably procure speedy convergence. The RELAX command is used to specify relaxation and has three arguments. The first argument is the name of the variable to be relaxed, the second specifies the type of relaxation to be used: LINRLX specifies linear relaxation (used for pressure) and FALSDT false time step relaxation (used for velocities).

The final argument is the relaxation factor; the specification of which is a matter of experience. The factors given in Appendix Two will ensure convergence although not necessarily with the minimum of computer effort.

Group 19. Data Communicated by SATELLITE to GROUND.

In this group the computer is instructed to use the user defined GROUND routine (USEGRD=T). It is not necessary to use the PHOENICS example GROUND and hence USEGRX=F.

Group 21. Printout of Variables.

The OUTPUT command allows the user to specify in detail what output is required. The command has seven arguments the first being the name of the variable under consideration. The remaining arguments are either Y's or N's; answering yes or no to these questions:

ii. Field printout?
iii. Correction-equation monitor printout?
iv. Slabwise-residual printout?
v. Whole-field residual printout?
vi. Spot-value table and/or plot?
vii. Residual table or plot?

The setting of these arguments and those in Groups 22 and 23 shown in Appendix Two will give full tables of the variables at the end of the solution procedure as well as providing adequate monitoring during the solution procedure.

Group 22. Spot-Value Printout.

The residuals of the equation are printed every TSTSWP sweeps during the solution of the equations.

Group 23. Field Printout and Plot Control.

NPRINT sets the number of sweeps after which the tables of velocity and pressure are printed. By equating it to LSWEEP the tables are produced at the end of the solution procedure.

5.3.3. Running the Model.

The GROUND coding is first compiled and is then linked to the executable form of the EARTH program using the BLDEAR command file supplied with PHOENICS. The RUN_PRIVATE command file is then used to run the Fortran Pre-Processor (the satellite) and subsequently the EARTH program with the specially written GROUND.

5.3.4. Presentation and Discussion of Results.

The basic, simple test model was run for a wide range of test conditions: working fluid (density and viscosity), packing type (size, voidage and shape factor) , bed size (packed height), orientation (relative to the grid - x, y or z), and fluid flowrate which collectively result in resistances between 2.5 and 1.8×10^6 pascals.

As has been discussed, if correctly formulated and applied, the model should show an even, uni-directional flow. Figures 5.2 and 5.3 where produced on the PHOENICS graphics package PHOTON and show flat, equi-spaced pressure contours and parallel, equal sized velocity vectors. Such results were obtained for all the cases considered and are wholly satisfactory.

The pressure drop determined by the model was also compared to that calculated (by hand) from the basic Ergun Equation and agrees to within 0.06% which is equivalent to the round-off tolerence of the computer used; except for very low resistance beds (e.g. those with a resistance less than ten pascals where the difference may be as much as 1.8%).

When the pressure drop is determined from the model results, the effect of solving the equations over a grid must be allowed for. Figure 5.4 shows a typical grid section. The pressure drop determined by the PHOENICS model is actually the pressure drop between the centres of two cells i.e. the pressure drop determined for the example illustrated will be that between points P_1 and P_N. This must then be adjusted to allow for the half height of the top and bottom cells (distances x and y) to give the true pressure drop over the whole bed depth (distance z in figure 5. 4) which is then compared to that calculated from the simple Ergun Equation.

This problem could be avoided in two ways:

I. By adjusting the constants in the Ergun Equation, however this would typically make the model specific to one grid geometry and will

clearly not apply to maldistributed flows. This method is not used in subsequent models.

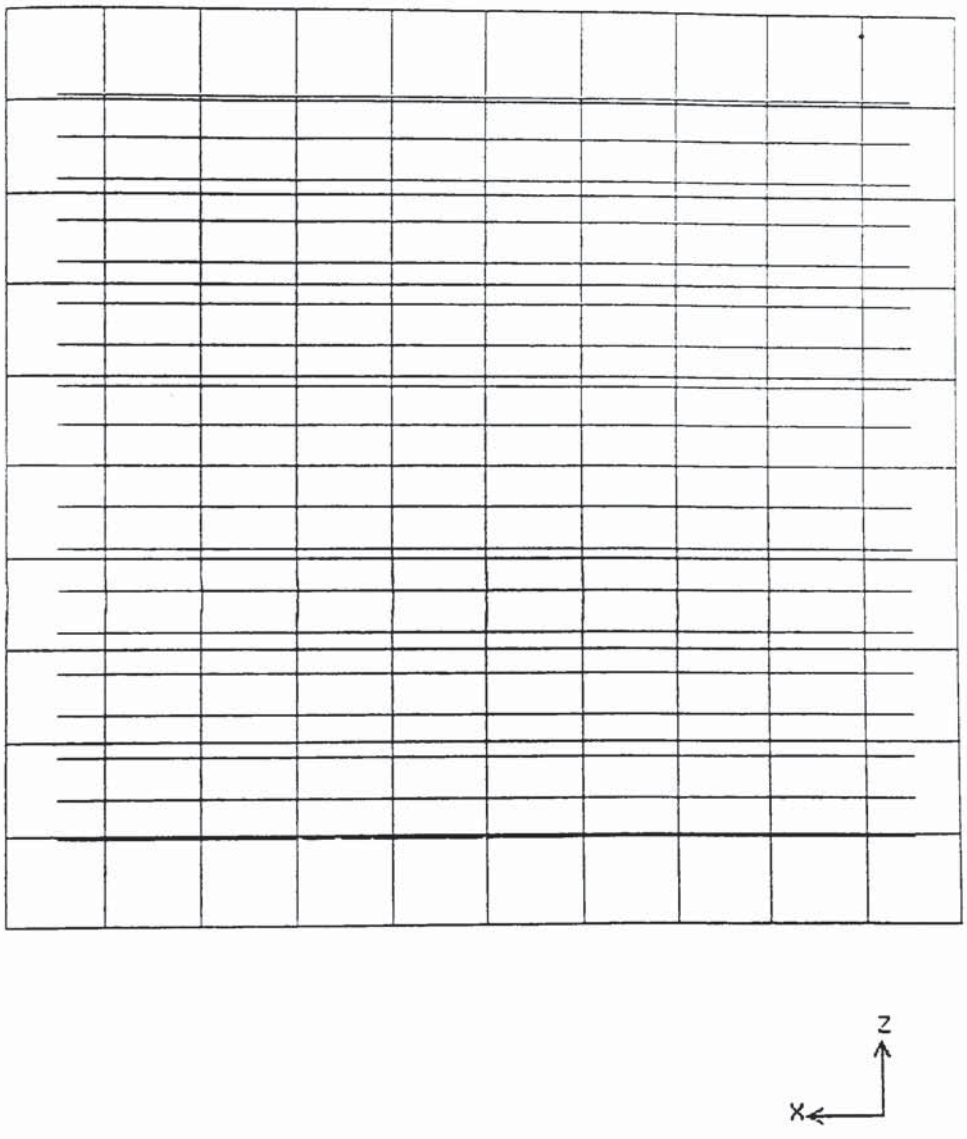

Figure 5.2. Typical Pressure Contours for the Basic Test Model.

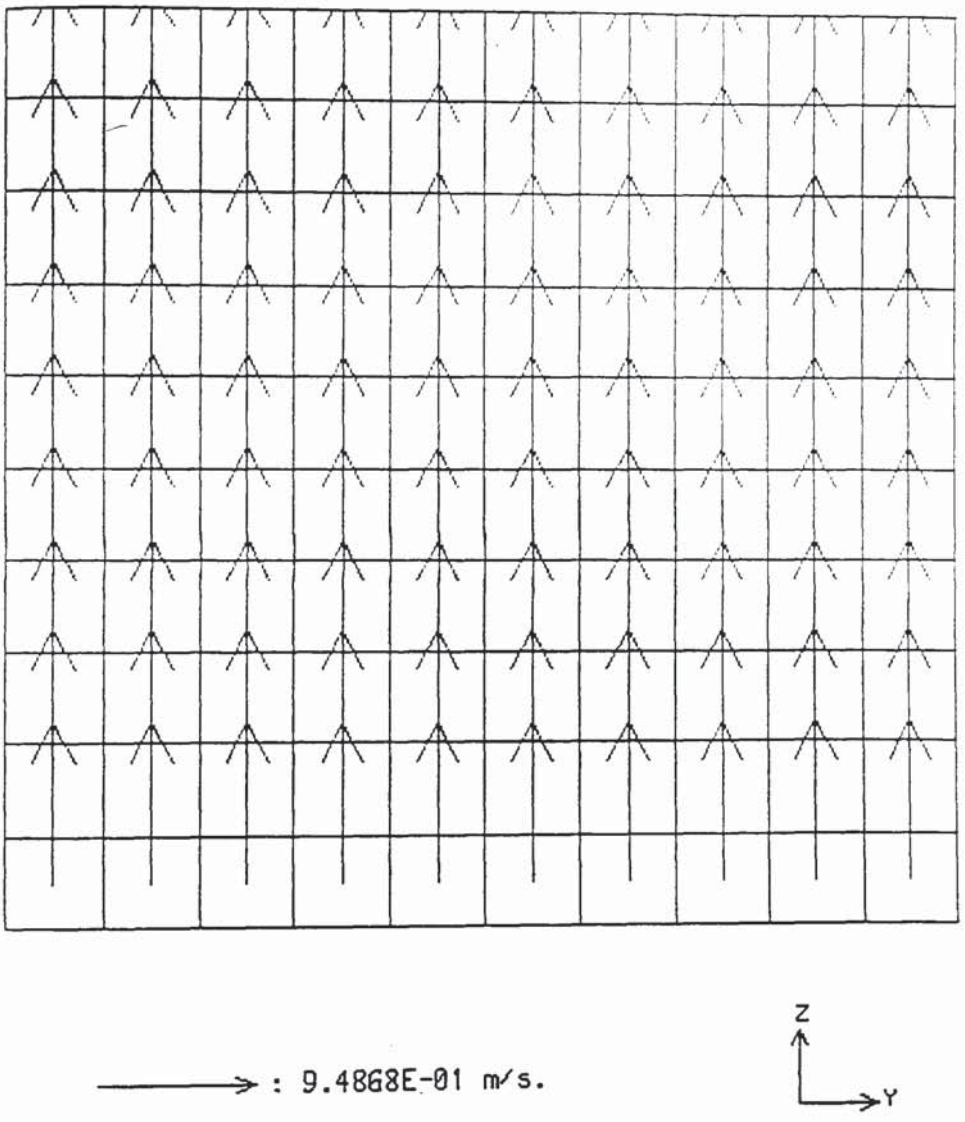

Figure 5.3. Typical Velocity Vectors for the Basic Test Model.

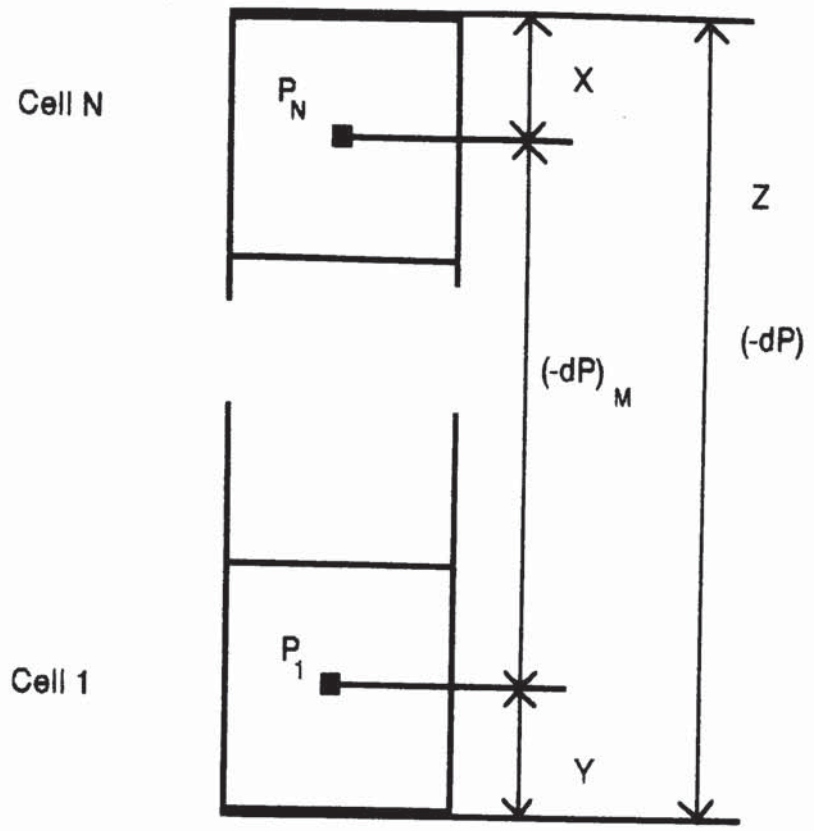

(-dP) = true pressure drop over bed

$(-dP)_M$ = modelled pressure drop

$$(-dP) = (-dP)_M \left[\frac{Z}{Z-X-Y} \right]$$

The grid used in the basic test model discussed here is regular, X =Y .

Figure 5.4. The Effect of Cell Size on the Modelled and Actual Pressure Drop.

ii. By minimising the sizes of the cells at the edge of the bed. As cell size is decreased so the accuracy of the model will improve at the expense of greater computational labour. The model cannot produce the exact solution to the equation but will tend towards this as cell size

decreases. This method is used subsequently due to its portability and physical realism.

As discussed in the literature survey, some computational realisations of the vectorial Ergun Equation give decreasing pressure drops in a direction opposite to that of the flow, when the flow direction is from high-numbered cells to low-numbered ones. The realisation of the Ergun Equation in this work has been designed so that it does not behave in this way, and the testing of this facet of its operation is now discussed.

If the basic test model is modified so that the inlet or outlet of the cube is positioned over a few, central cells of the relevant plane; the model will produce a symmetrical flow field if it does not suffer from these limitations. The complex, maldistributed nature of this flow necessitates the use of a finer grid as shown in figure 5.5. Figure 5.6 shows velocity vectors and pressure contours for such a case where a smaller inlet is used and figure 5.7 for a smaller outlet. The symmetrical nature of these profiles clearly show that this implementation of the Ergun Equation does not suffer from the problem discussed here. The profiles are not exactly symmetrical because of the algorithm used in the graphics package PHOTON and the low flowrates used to mobtain the results presented.

5.3.5. Conclusions.

The Ergun Equation as implemented functions correctly within the scope of the tests discussed above; it must now be verified against experimental measurements of a maldistributed flow in packed beds.

5.4. VERIFICATION OF THE MODEL BY COMPARISON WITH THE EXPERIMENTAL RESULTS OF POVEROMO (1975).

This section presents and discusses the verification of the PHOENICS/Ergun Equation Model for flow in packed beds. The verification is made by modelling the experimental results of Poveromo (1975) (see also Poveromo, Szekely & Propster (1975) and Szekely & Poveromo (1975)).

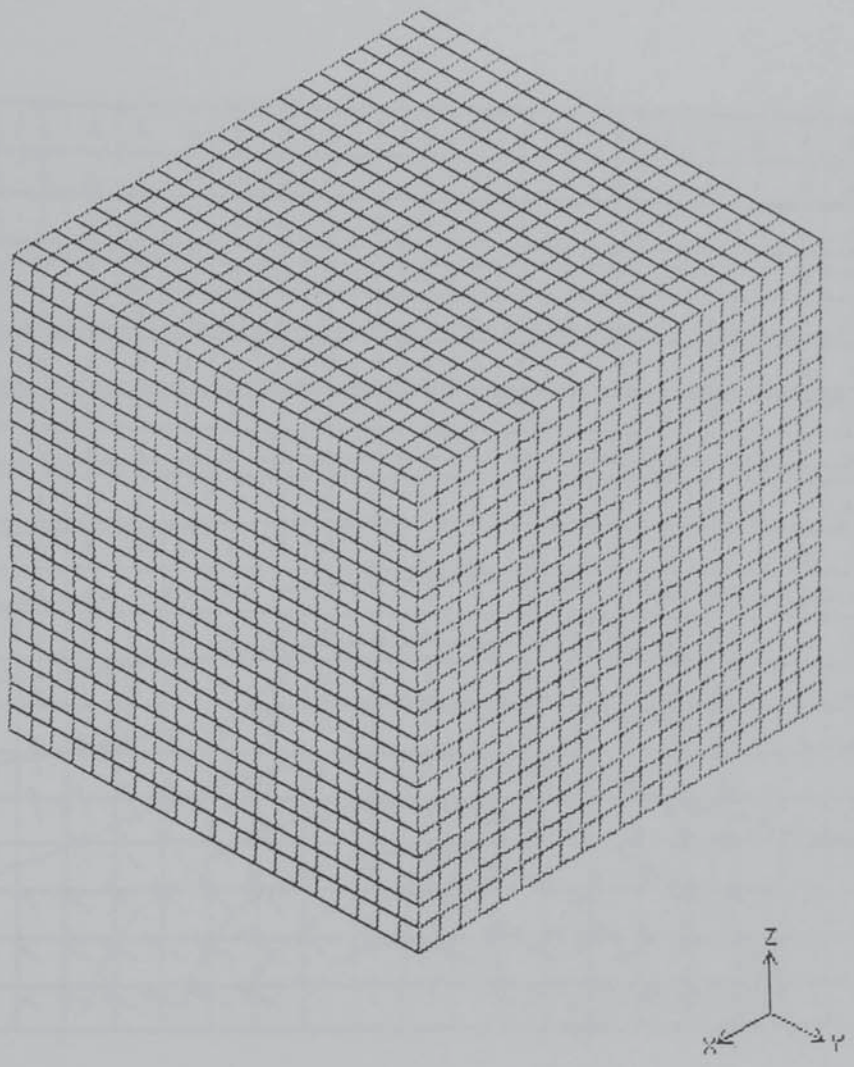

Figure 5.5. The Finer Grid used for Maldistributed Gas Flow Studies with the Basic Test Model.

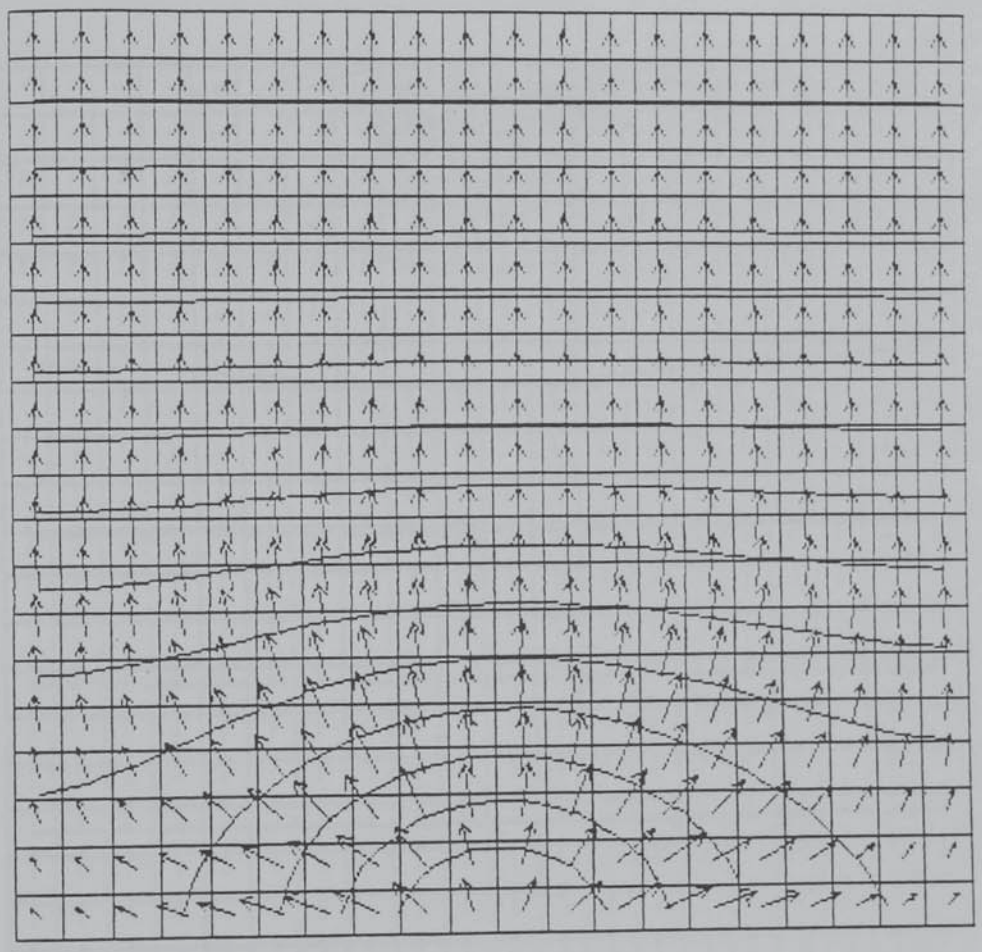

Figure 5.6. Velocity Vectors and Pressure Contours for the Basic Test Model with a Small Inlet.

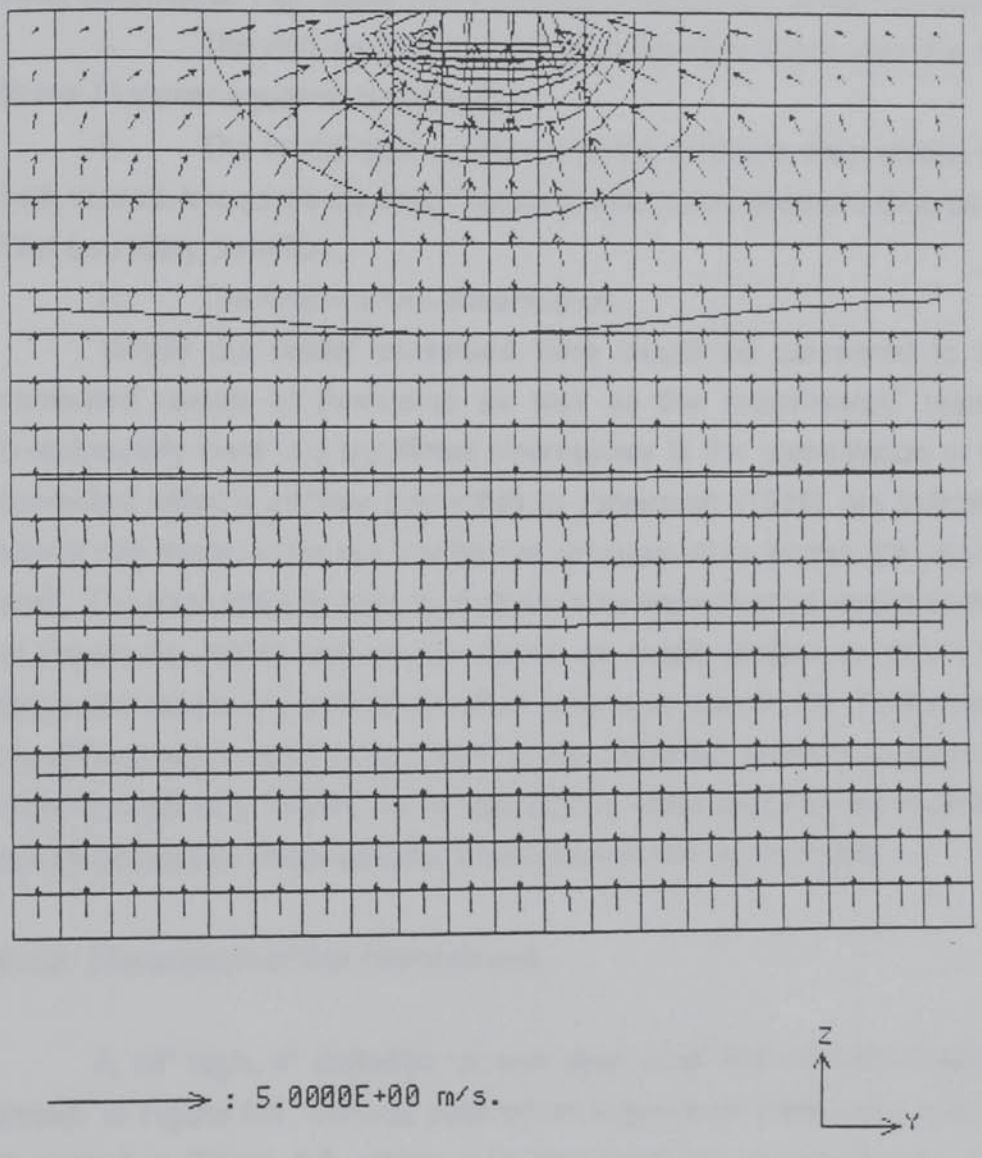

Figure 5.7. Velocity Vectors and Pressure Contours for the Basic Test Model with a Small Outlet.

This work seeks to obtain a satisfactory model of these experimental results and not to discuss the experimental results themselves: for such a discussion the reader is referred to the source text and, to a lesser extent, the literature survey.

5.4.1. Other Computer Models of Poveromo's Experiments.

Poveromo used the Ergun Equation (after some manipulation) as the equation of motion in a two-dimensional, Succesive Over-Relaxation (S.O.R.) scheme to solve for flow patterns in the packed bed arrangement described below. This model has a number of limitations, which include:

i. The viscous term of the Ergun Equation is not used (i.e. the Burke-Plummer equation is applied),

ii. The model cannot determine the pressure drop across the bed; indeed, it requires the experimentally determined pressure drop as an inlet boundary condition,

iii. The model is two-dimensional.

Ideally the model presented here would be compared to the computed results of Poveromo as well as the experimental results. Unfortunately there is a significant discrepancy in the presentation of the computed velocity profiles presented in Poveromo (1975) (as indicated above this model does not predict the pressure drop across the packed bed). The experimental velocity profiles in the experimental results section of Poveromo (1975) are not the same as those profiles to which the computed results are compared either in form or magnitude. Furthermore insufficient explanation is provided of the modelled cases (e.g. pressure drop, flowrate etc). Hence, no comparison is made between the modelled results presented below and the results from Poveromo's model.

5.4.2. Explanation of The Test Problem.

A 16" high, 4" diameter column was used with various inlets as shown in Figure 5.8. Various packing arrangements were used and are illustrated in Figure 5.9, which also describes the nomenclature used. These arrangements produce maldistributed gas flows in the bed by assymetric injection of gas and/or local variations in bed resistance. The

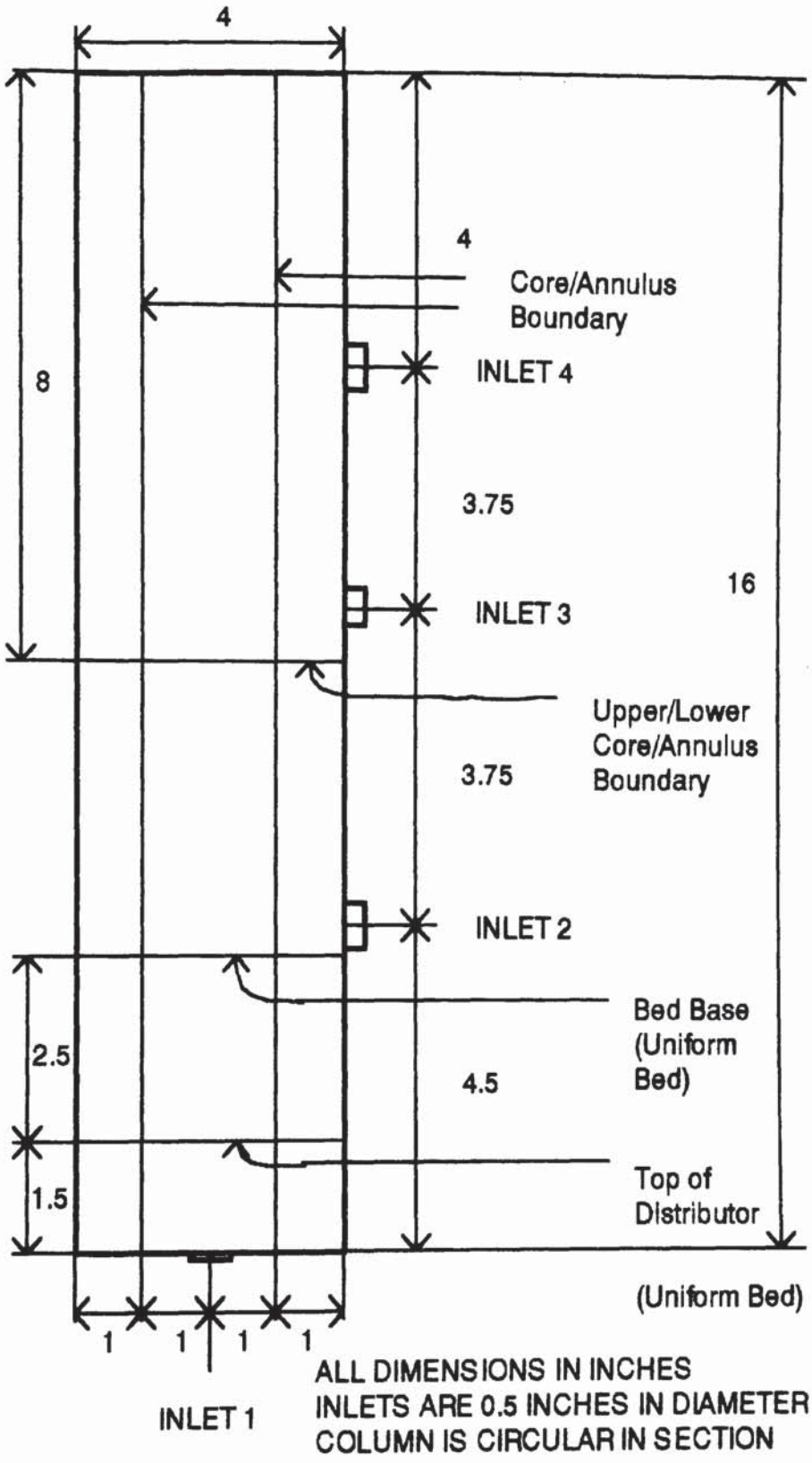

Figure 5.8. The Dimensions of the Packed Column used by Poveromo (1975).

Figure 5.9. Packing Patterns used by Poveromo (1975).

i). Uniform Bed.

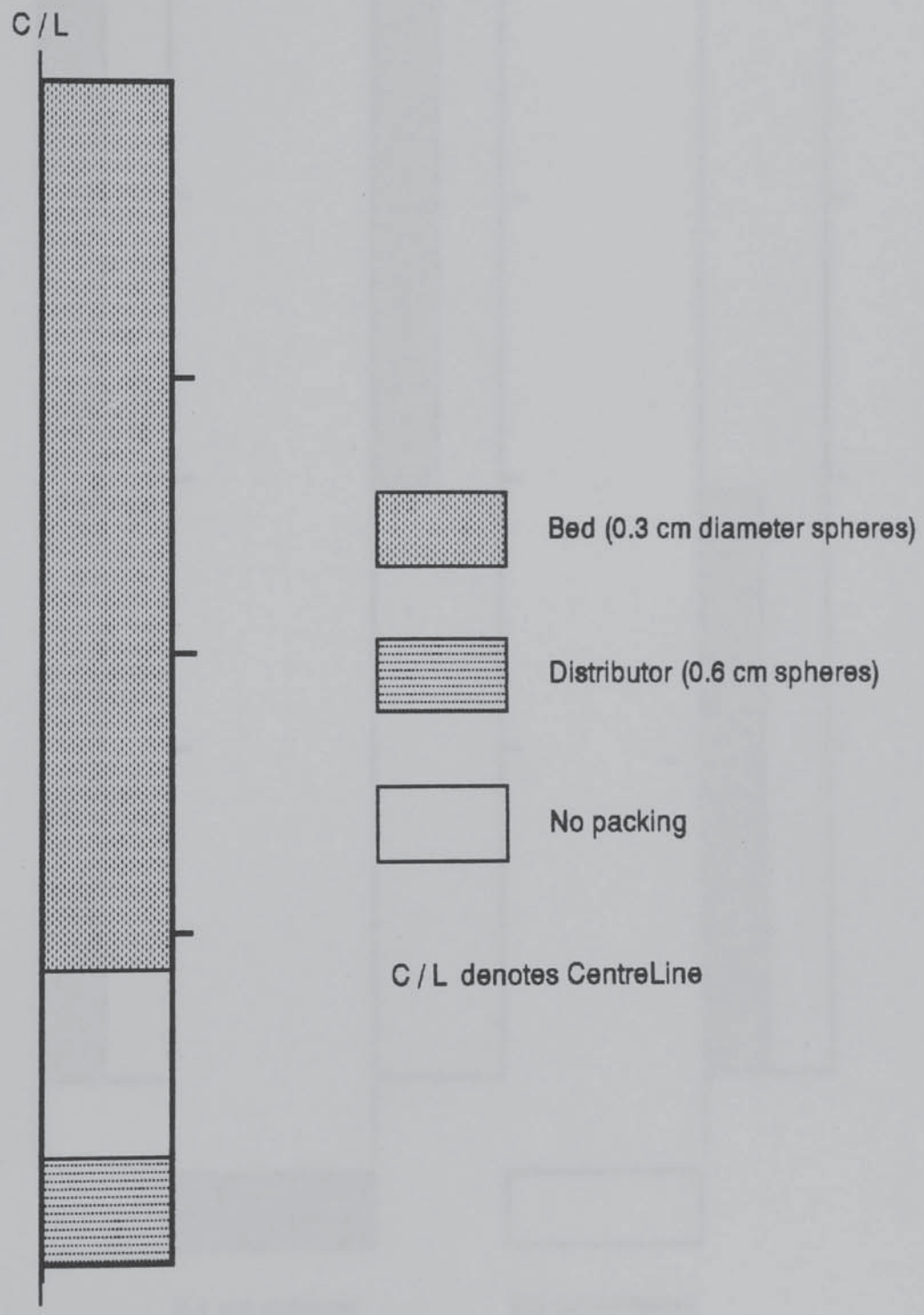

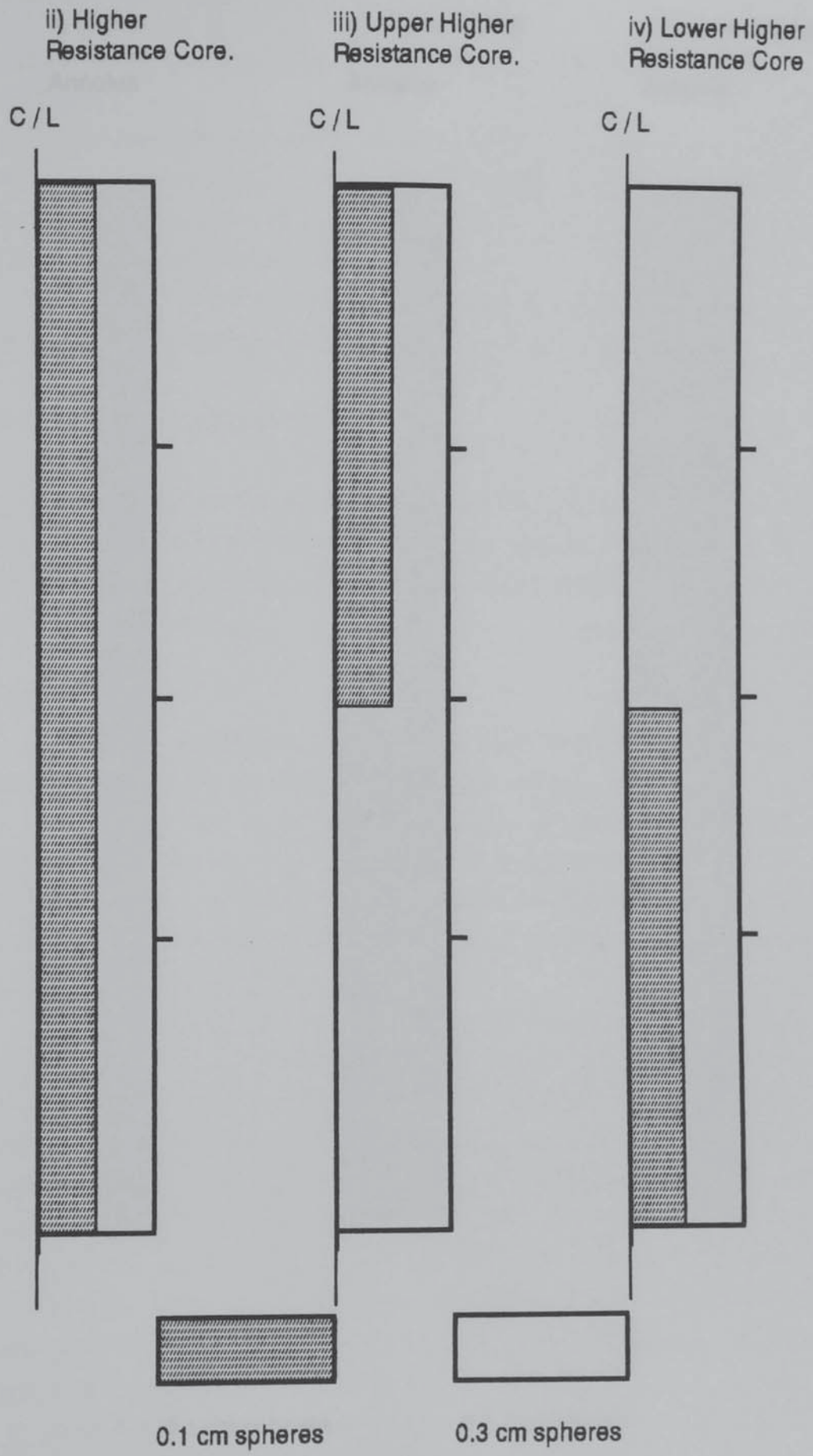
ii) Higher Resistance Core.
iii) Upper Higher Resistance Core.
iv) Lower Higher Resistance Core
C / L
C / L
C / L
0.1 cm spheres
0.3 cm spheres

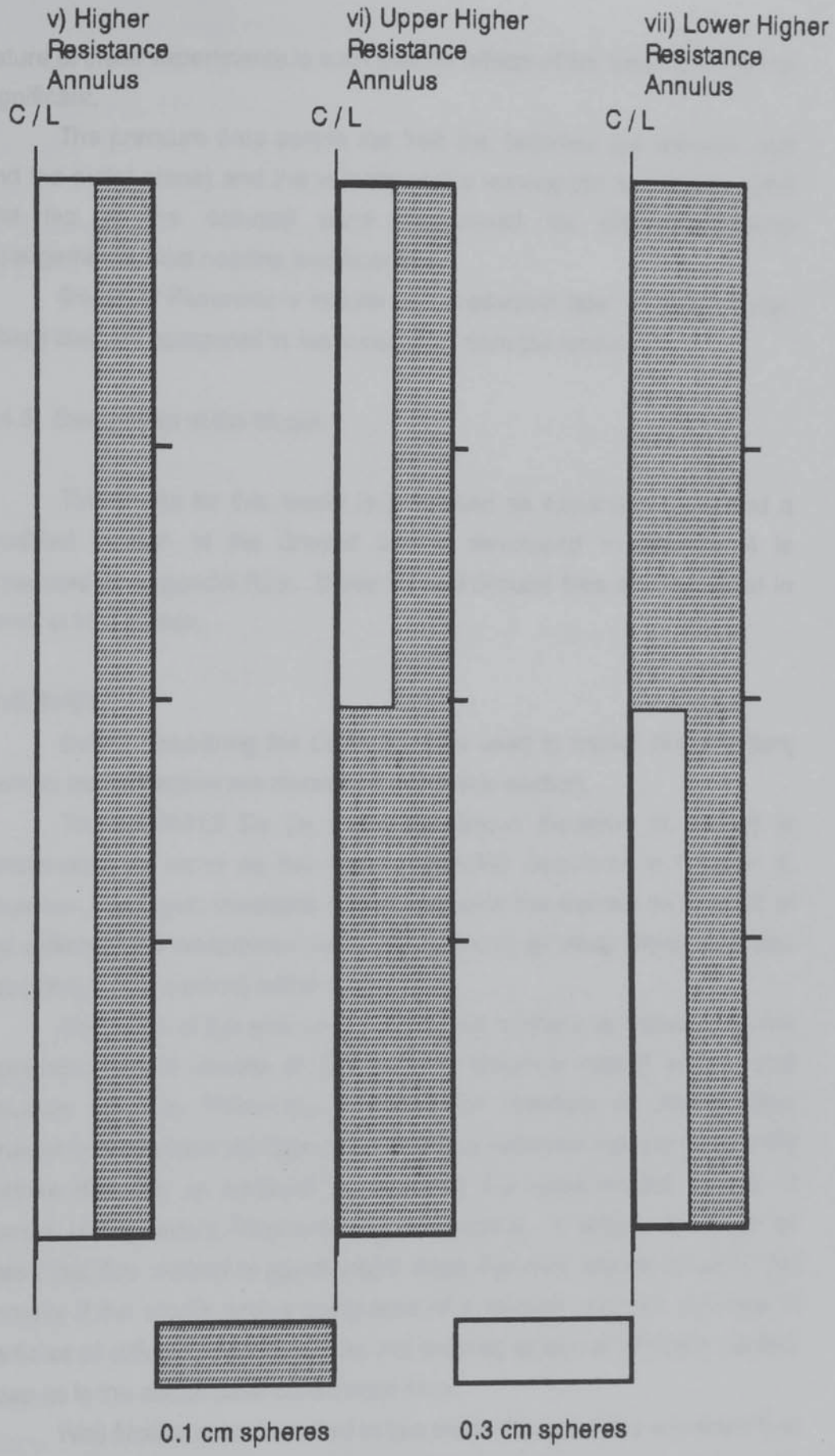
v) Higher Resistance Annulus
C / L
vi) Upper Higher Resistance Annulus
C / L
vii) Lower Higher Resistance Annulus
C / L
0.1 cm spheres
0.3 cm spheres

nature of these experiments is such that the effects of the bed base are not significant.

The pressure drop across the bed (i.e. between the relevant inlet and the outlet plane) and the velocity profile leaving the bed at the outlet (the top of the column) were determined for different packing arrangements, inlet nozzles and flowrates.

Some of Poveromo's results are presented later in this chapter, where they are compared to those obtained from the model.

5.4.3. Description of the Model.

The Q1 file for this model is presented as Appendix Three and a modified version of the Ground coding developed in Chapter 4 is presented as Appendix Four. These Q1 and Ground files are discussed in detail in this section.

OVERVIEW.

Before describing the computer files used to model this situation; various overall factors are discussed in this sub-section.

The GROUND file (in which the Ergun Equation is coded) is functionally the same as the 'basic' GROUND described in Chapter 4. However, the Ergun constants (which vary over the domain as a result of the different bed resistances used) are stored in an array which is written according to the packing pattern used.

The effect of the wall on the local bed voidage is included by the application of the results of Benanti and Brosilow (1962) on the grid structure used by Poveromo. Similarly the interface or mixing effect caused by decreased voidage at the interface between regions of different particle diameter is included by applying the experimental results of Furnas (1929) within Poveromo's grid structure. It should however be noted that this method is approximate since Furnas's results consider the porosity if the whole bed is composed of a mixture of given amounts of particles of different diameters and not ordered arrays of different particle sizes as is the actual case considered here.

Wall friction is not included in this model because it is expected that it is not a significant frictional factor relative to the resistance of the bed. Walls are represented as impermeable and reflecting.

The model does not represent gas compressibility. At the maximum pressure encountered experimentally (20" W.G) the gas density is (determined by the ideal gas law) is 5% more than that at atmospheric pressure. The omission of gas compressibility in this model will not then have a significant effect relative to the assumption made above but will considerably reduce the computational effort. This assumption will cause the model to underpredict the pressure drop slightly.

THE Q1 FILE.

This is presented as Appendix Three. The coding is only explained where it is significantly different compared to that discussed in section 5.3.2 above. As before, the discussion is made group by group.

Group 1. Run Title and Other Preliminaries.

The required variables are declared and specified; basic explanations of their purpose are given.

Group 3,4,& 5. Grid Specification.

The setting 'CARTES=F' indicates that the required grid is not cartesian but, by default, cylindrical polar. The x direction is the circumferential one and the y direction is the radial one. A different method is used to define the grid in this model than in the previous model; this is the so-called 'method of pairs', pairs of numbers are used to define individual sections of the grid: the first of the pair is the number of cells in that section and the second its total dimension. The grid being defined by the X-,Y- or Z-FRAC (n) command (n is an integer). The method of pairs is activated by setting X-,Y- or Z-FRAC(1) to a negative number. The coding is written so that the numbers of cells in each section can be varied although the heights of the sections are set by the physical size of the apparatus. Very thin cells are defined at the boundaries of the domain in accordance with the comments made in section 5.3.4 above. The final grid is illustrated in figures 5.10 and 5.11.

The grid is specifically designed to accomodate the regions of differing voidage caused by the walls and the interactions of areas of different sizes of packing.

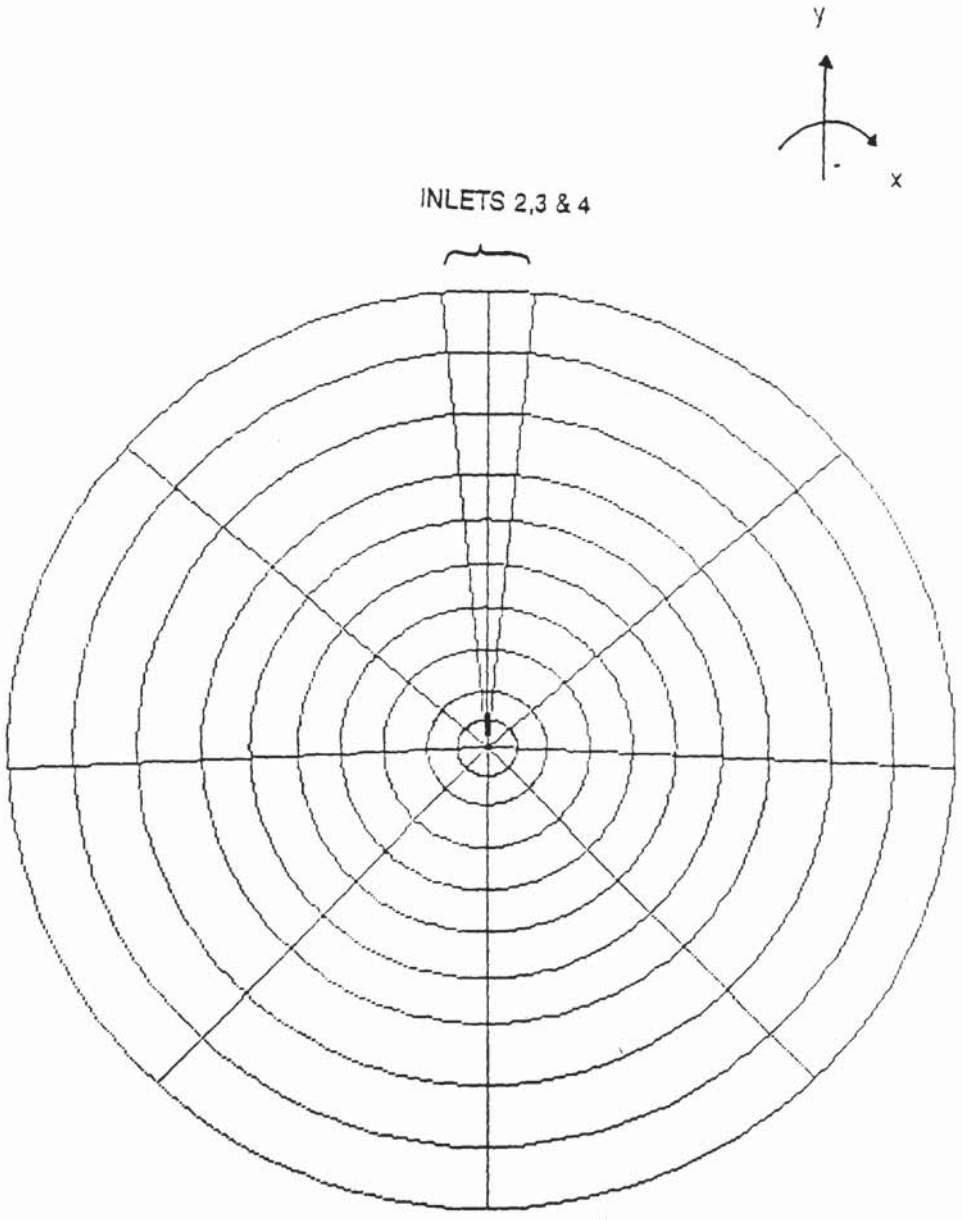

Figure 5.10. The Grid for the Poveromo Model - The Z-Plane.

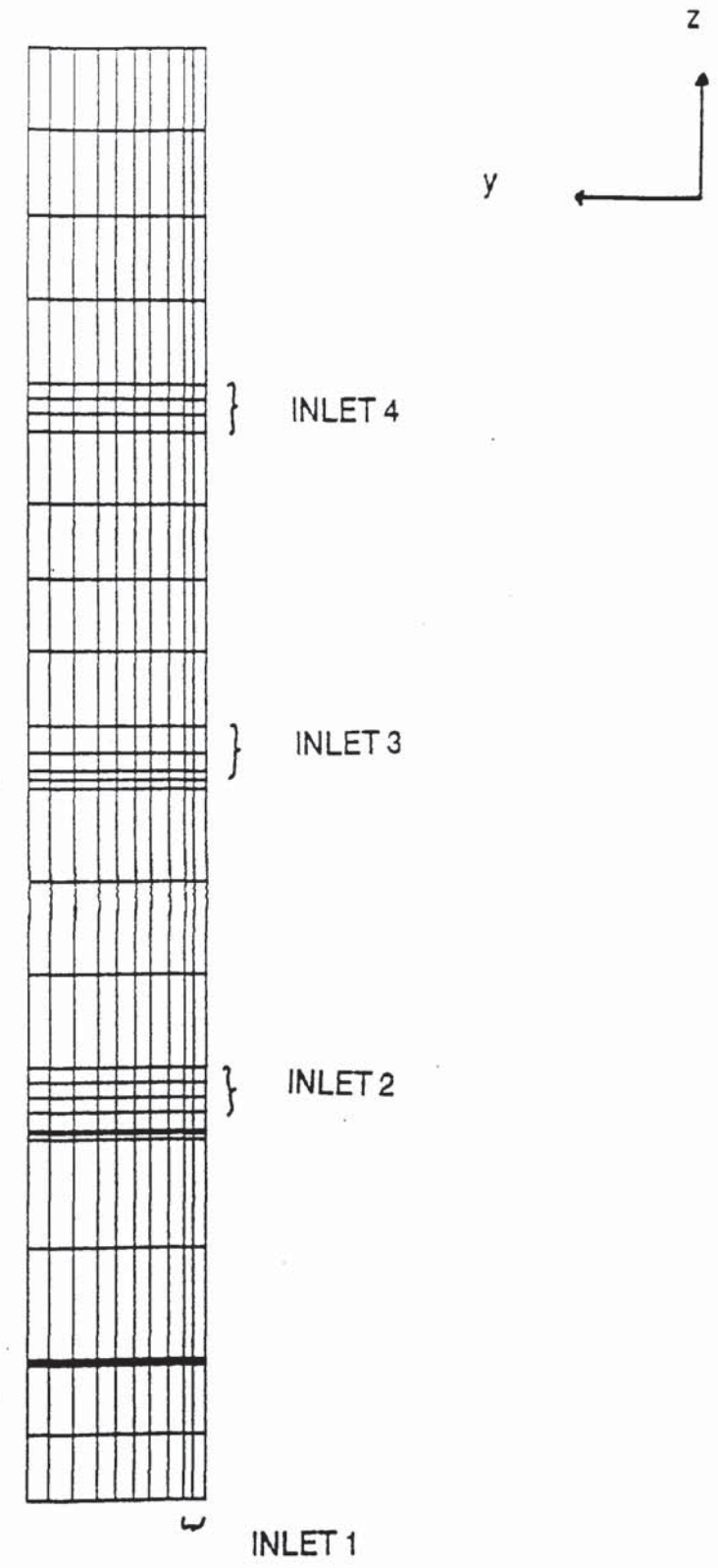

Figure 5.11. The Grid for the Poveromo Model - The X-Plane.

Group 13. Boundary Conditions and Special Sources.

Inlet boundary conditions are specified for all four inlets; the three which are not required are commented out.

Group 19. Data Communicated by SATELLITE to GROUND.

The packing pattern required is specified and transmitted to the GROUND routine using the special array LG (n) (for logical variables). The grid and packing information required by Ground is also defined and transmitted using the special arrays RG(n) and IG(n) (for real and integer variables).

THE GROUND FILE.

This is presented as Appendix Four. In terms of the basic algorithm employed it is identical to the GROUND coding presented as Appendix 1 and fully described in Chapter 4.

In addition to the use of different inlet nozzles to achieve maldistributed flows; areas of different size packings are also employed as shown in figure 5.9, above. It is clearly necessary to represent these local variations in resistance; which are a result of differing particle sizes and voidages (as discussed above). This is achieved by making the Ergun constants variable arrays; the local value of the Ergun Constant is then determined from the local voidage and particle diameter.

The array of Ergun Constants is determined at the beginning of the solution procedure according to the setting of the logical variables in the Q1 file. If more than one pattern is specified a warning message in printed.

The algorithm employed in determining the Ergun Constants is straightforward. The bed resistance is set for the main packing type over the whole domain (e.g. for upper/lower/whole height high resistance cores the whole bed is initially described as low resistance) the wall voidage and consequent Ergun Equation constants are then overwritten. Two markers are initialised which represent the top and bottom of the core the constants for which are then written. Finally, the constants for the boundary voidage areas are written.

This part of the code was tested and performs satisfactorialy if not particularly efficiently. It could for instance be improved if the calculation of the Ergun constants was performed in a subroutine.

As has been indicated the remaining coding is the same as that described in Chapter 4 except that the Ergun constants are held in arrays.

5.4.4. Running The Model.

The programs are run in the same way as the basic test model discussed above (see section 5.3.3). In many cases the Q1 file presented did not yield a satisfactorily converged solution. Depending on the particular situation being studied adjustments to the relaxation parameters, the use of a finer grid, control of the maximum and minimum increments to a variable at a given cell from sweep to sweep (VARMAX and VARMIN commands of Group 18) and/or the use of the results file from another run as initial guesses of the flow field enabled the achievement of satisfactory convergence which typically occured after about 50 sweeps (c.f. Poveromo's model typically requires 65 to 70 iterations). Satisfactory convergence was viewed as obtained when residuals (divided by 10^6) reached 10^1 or 10^2 (for a 30 x 10 x 10 grid and an inlet velocity of the order of 20 ms^{-1}); and the solution did not significantly change when more sweeps were performed. The convergence of this model is discussed further in Chapter 9.

5.4.5. Presentation and Discussion of Results.

VELOCITY PROFILE RESULTS.

Graphs 5.1 to 5.5 compare predicted and experimental velocity profiles leaving the bed for five experimental cases that fully encompass the alternative packing arrangements, inlet nozzles and flowrates. The agreement between the two sets of data is very good particularly in the uniform bed case where there are no voidage interface effects. The absence of wall friction and possibly the inadequacy of the description of voidage at the wall is also apparent.

The very good agreement between the measured and computed velocity profiles is in part due to the lack of dependence on the 'constants' (a & b) in the Ergun Equation; it is the ratio of these quantities that is signifcant. This is confirmed below where it is observed that the agreement between modelled and experimental pressure drops is not as

good as the agreement for the velocity profiles (clearly, the overall pressure drop does depend on the empirical constants).

Graph 5.1. Computed and Experimental Velocity Profiles at the Bed Outlet Uniform Bed, Inlet 1, Flowrate = 10.0 scfm.

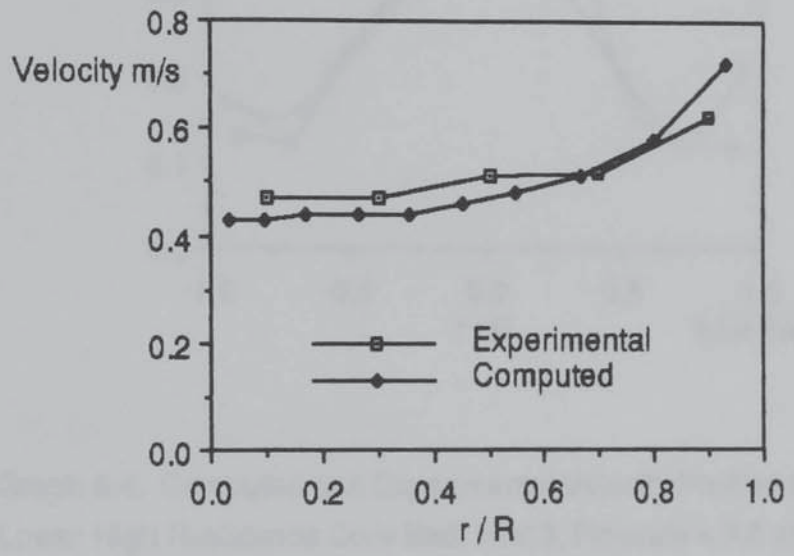

Graph 5.2. Computed and Experimental Velocity Profiles at the Bed Outlet Uniform Bed, Inlet 3, Flowrate = 7.5 scfm.

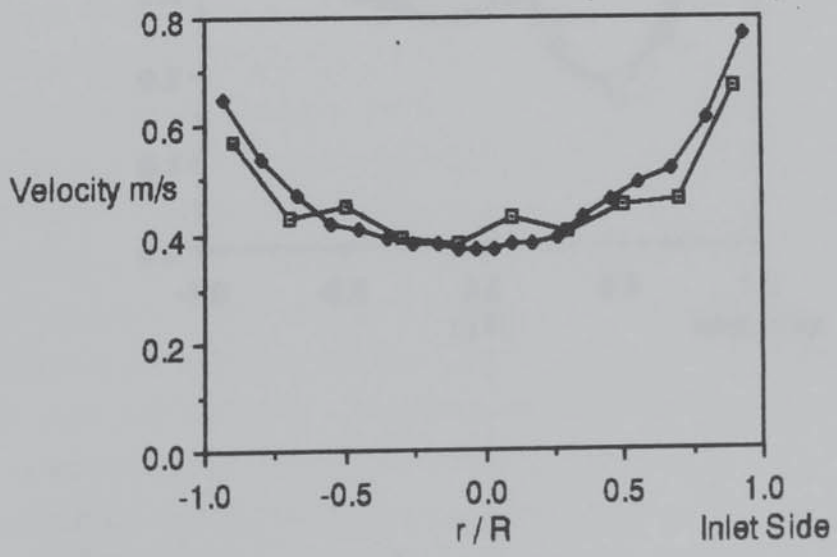

Graph 5.3. Computed and Experimental Velocity Profiles at the Bed Outlet
Higher Resistance Annulus Bed, Inlet 2, Flowrate = 3.8 scfm.

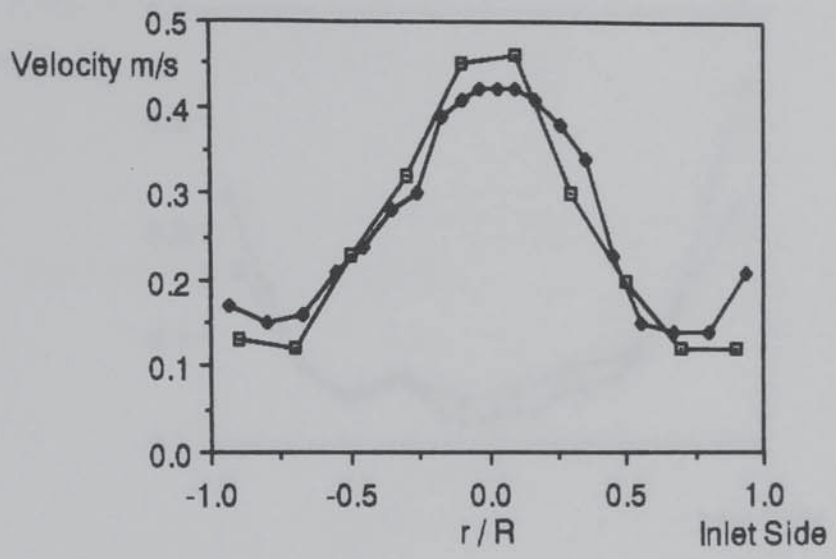

Graph 5.4. Computed and Experimental Velocity Profiles at the Bed Outlet
Lower High Resistance Core Bed, Inlet 3, Flowrate = 7.0 scfm.

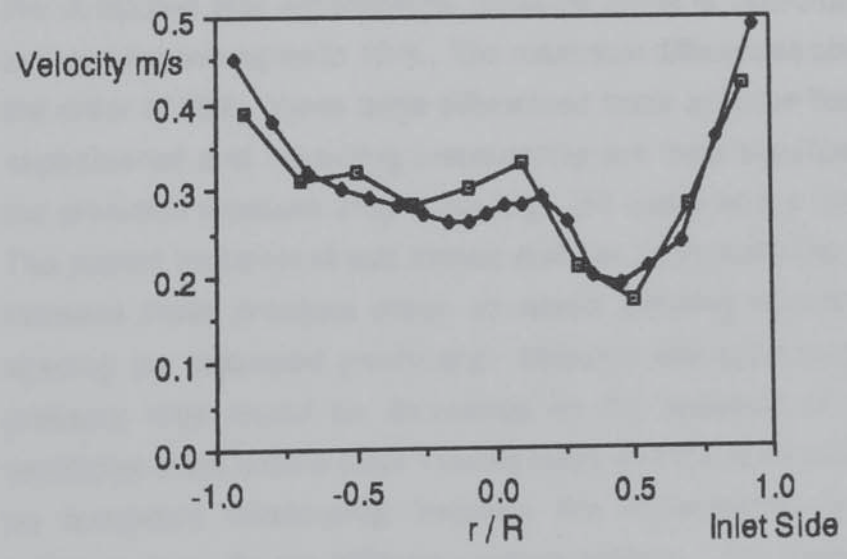

Graph 5.5. Computed and Experimental Velocity Profiles at the Bed Outlet Upper High Resistance Core Bed, Inlet 4, Flowrate = 3.0 scfm.

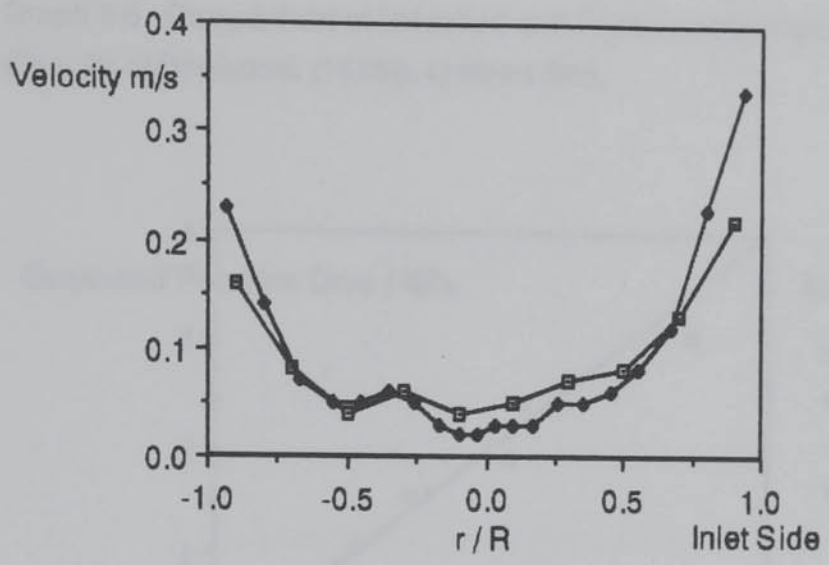

PRESSURE DROP RESULTS.

These are presented for all the experimental situations investigated by Poveromo (1975) as graphs 5.6 to 5.11. Each part considers the pressure drops for a given packing arrangement. The agreement between the computed and experimental pressure drops is reasonably good: on average the two agree to 13 %. The maximum differences observed are of the order of 25%, these large differences occur at lower flowrates where experimental and modelling inaccuracies are most significant. Typically the predicted pressure drop is too high (36 cases of the 56 considered). The correct inclusion of wall friction and gas compressibility would further increase these pressure drops as would allowing exactly for the grid spacing (as discussed previously) although fine grids were used. The pressure drop would be decreased by the inclusion of wall voidage variations at the bottom (inlet 1 cases only) and top of the column. There is no consistent relationship between the experimental and computed pressure drops for the different packing patterns. The agreement is best for inlet nozzles 2, 3 & 4. It is significantly worse for inlet nozzle 1 which can be explained both by the comments above and the lack of rigorous description of the free fluid space between the distributor and bed (see figure 5.9 part i.). Nevertheless the agreement between the predicted and

experimental pressures confirm the validity of the vectorial Ergun Equation and its implementation in Phoenics.

Graph 5.6. Comparison of Modelled and Experimental Pressure Drops (Results of Poveromo (1975)). Uniform Bed.

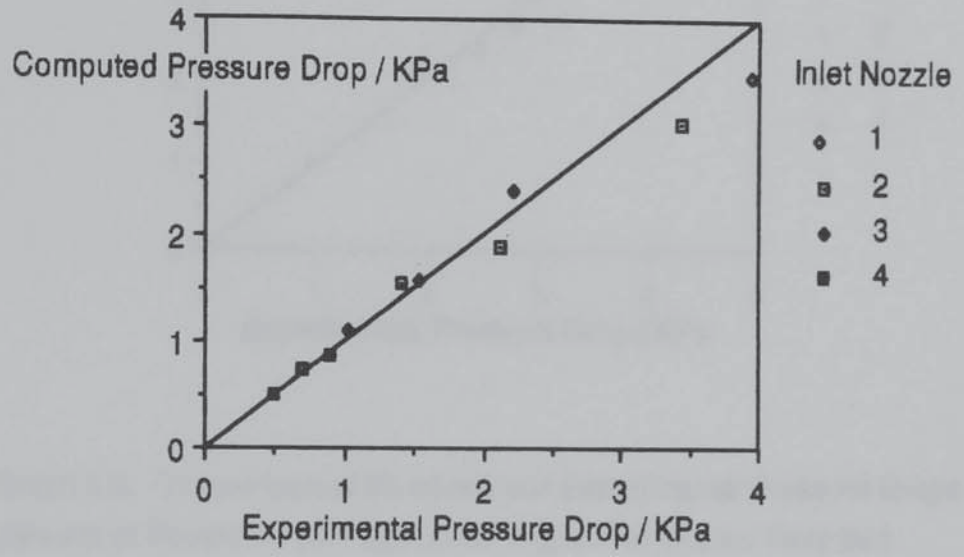

Graph 5.7. Comparison of Modelled and Experimental Pressure Drops (Results of Poveromo (1975)). Higher Resistance Core Bed.

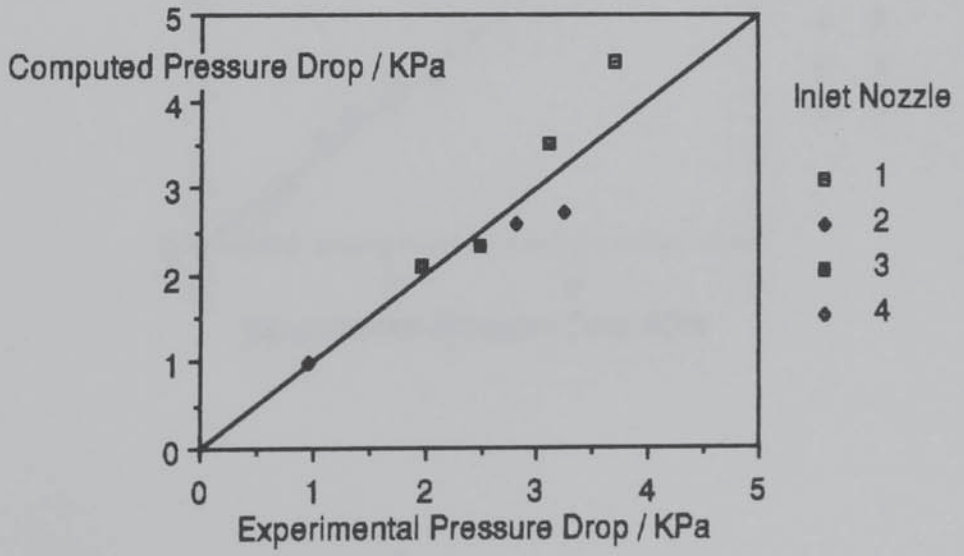

Graph 5.8. Comparison of Modelled and Experimental Pressure Drops (Results of Poveromo (1975)). Higher Resistance Annulus Bed.

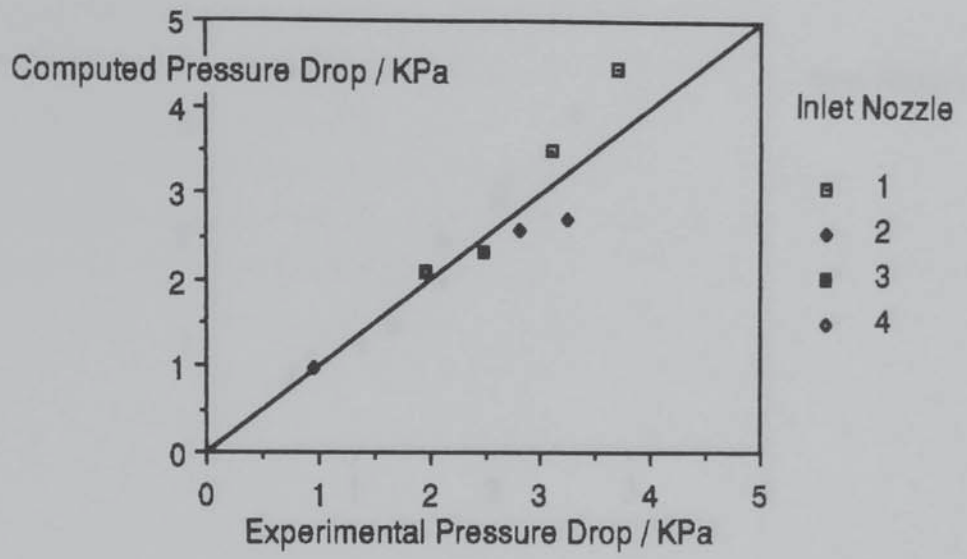

Graph 5.9. Comparison of Modelled and Experimental Pressure Drops (Results of Poveromo (1975)). Lower Higher Resistance Core Bed.

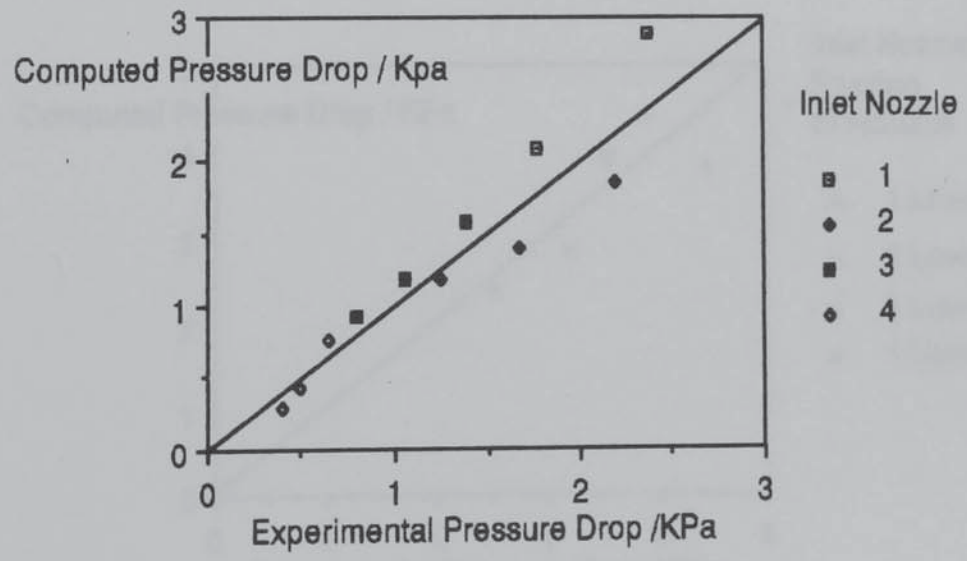

Graph 5.10. Comparison of Modelled and Experimental Pressure Drops (Results of Poveromo (1975)). Upper Higher Resistance Core Bed.

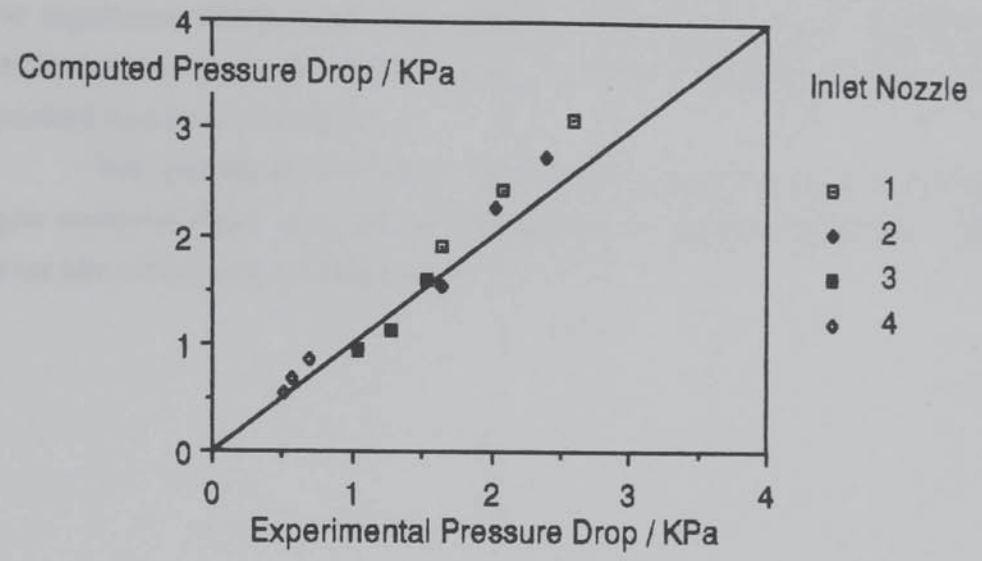

Graph 5.11. Comparison of Modelled and Experimental Pressure Drops (Results of Poveromo (1975)). Lower & Upper Higher Resistance Annuli Bed.

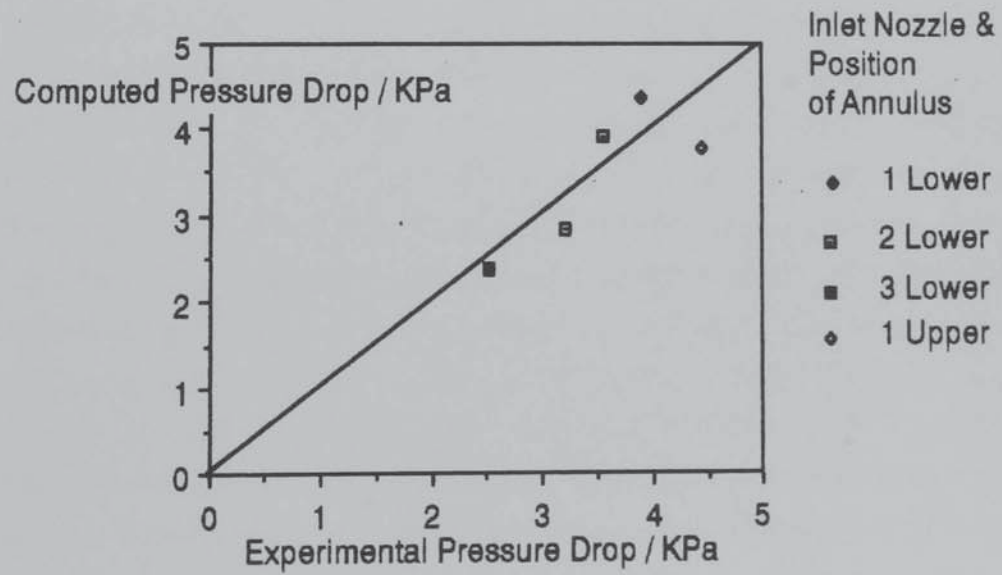

5.4.6. Conclusions.

The use of the vectorial Ergun Equation and its implementation in PHOENICS (in a situation where the bed boundary/free fluid interface has no significant effect) has been verified by comparison with independent experimental results for a wide range of three dimensional, maldistributed, packed bed flow conditions.

The assumptions made in this model (neglecting wall friction and gas compressibility and, concerning the local values of voidage) have thus been shown to be reasonable.

CHAPTER 6

AIR SUPPLY EQUIPMENT & INSTRUMENTATION

6.1. INTRODUCTION.

In all the experimental work performed in this study, a flow of air through a packed bed is required. This chapter describes the equipment used to supply and measure this air flow. Much of the apparatus described in this section (that constructed of glass) is substantially the same as that used by Ali (1984). Also described are the techniques used to measure air flowrate, point velocities and the various components of pressure.

6.2. AIR SUPPLY EQUIPMENT.

6.2.1. Overall Description.

Air is supplied to the experimental apparatus by a 11 horsepower fan with a maximum capacity (at the no load condition) of 2,500 scfm (1.18 standard $m^3 s^{-1}$) through a 6" n.b. (i.d. 152 mm) glass QVF. pipe. The fan is connected to the glassware by 180 mm i.d., 600 mm long flexible piping to absorb vibration and the start-up shock of the fan. The flow is regulated by two 'Audco Slimline' butterfly valves, one of which passes excess air through a silencer and to atmosphere. The glass tubing is supported on wooden cradles bolted to the bench and secured by straps. This part of the system is on the same level as the fan exit. A flexible tube connects the glass tubing to a 6"n.b. perspex pipe which is itself connected to a distribution device and terminates in a flanged duct 10 c.m. x 25 c.m. which can be connected to the packed bed sections described in chapters 7 and 10. The flowrate of the air passing to the apparatus is measured by a 'Dall Tube' flowmeter. A flow diagram of the air supply equipment is presented as Figure 6.1. The system is supported on a bench made of 38 mm x 38 mm Handy Angle steel bars.

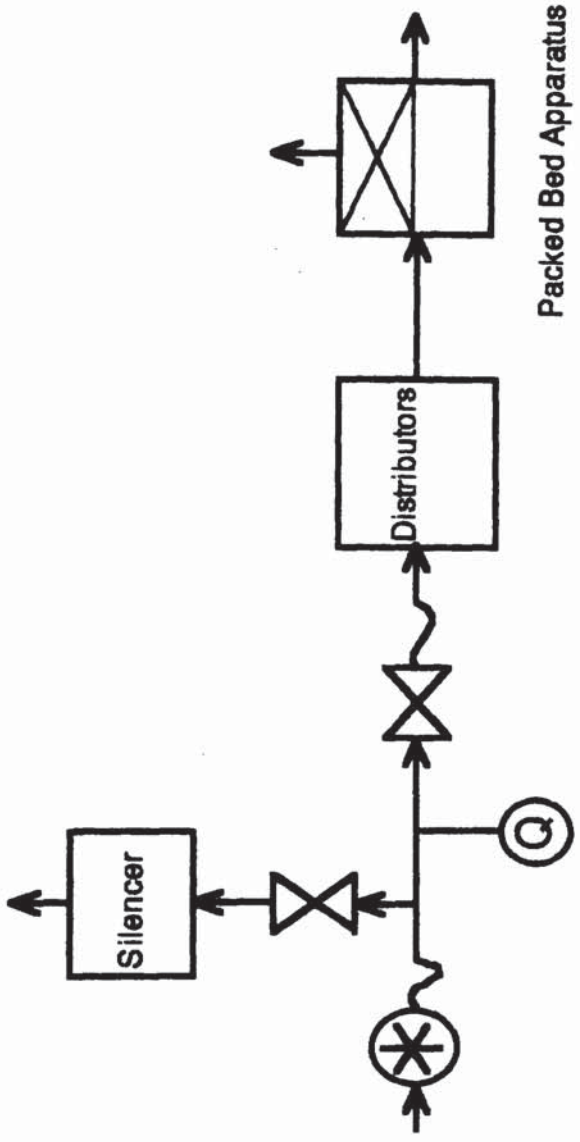

Figure 6.1. Flow Diagram of the Air Supply Equipment.

6.2.2. Flow Measurement.

The Dall Tube was selected for this duty due to its low permanent pressure loss. It is illustrated in Figure 6.2 and consists of a short length of parallel lead-in pipe, followed by short lengths of converging upstream cone and diverging downstream cone . A small gap between these two cones allows the fluid to fill the annular space between the liner and its case (the 'pipe' wall) . The throat pressure is transmitted to the annular chamber and then via pressure piping to the measuring instrument.

Figure 6.2. The Dall Tube (Cross-Section).

The Dall Tube has the desirable features of a high measured pressure drop (Perry R.H.(1984)) and a low permanent pressure drop, comparable to that of a Venturi meter; while also exhibiting a very short length. These apparently inconsistent advantages have been demonstrated experimentally but have yet to be fully explained theoretically.

The significant advantages of the Dall Tube over other forms of variable pressure drop flowmeter (including the flow-nozzle & Venturi meter) can be summarized as follows:

i. Lowest Head Loss; the permanent pressure loss of the Dall Tube is between 1/3 and 1/2 of that of the long-pattern Venturi Tube.

ii. Cheaper and simpler installation than a Venturi Tube. The Dall Tube is approximately half the length and weight of the Venturi Tube.

iii. Lower initial cost than the Venturi Tube due to economies in materials and machining.

The observed pressure drop across the Dall Tube was measured by a micromanometer (see 6.5.1 below) or a water-filled U-tube manometer. Its calibration is presented below in section 6.3.2.

6.2.3. Noise Reduction.

A major source of noise in process plant and experimental apparatus of this kind is from flowing fluids and in particular gases. Here, noise is generated by;

i. The venting of excess air (to prevent an unacceptably high level of back pressure on the fan and to improve the controllability of the air flow to the experimental apparatus).

ii. The fan.

iii. The fan motor.

The noise generated by air flowing in the fan inlet and the mechanical noise of the fan were reduced by the application of 2 cm thick rubber foam.

A simple silencer is used to;

i. Reduce the level of noise by orienting the discharge vertically to direct the noise away from the work area.

ii. To act as an attenuator to absorb fluctuations in the air flow (without the silencer the air velocity from the packed bed was observed to fluctuate with a frequency of about 0.5 Hz).

Air enters the silencer through one of the butterfly valves. The silencer is illustrated in Figure 6.3 and consists of the following parts;

i. Two 300 mm i.d. Q.V.F. pieces flanged together to form a vertical pipe 2 m high and closed at the base. This acts as a reservoir to absorb the flow fluctuations.

ii. A 12 mm thick P.V.C. plate perforated with 5 mm diameter holes and having 50 % free area, the total free area equals the silencer outlet area and double the inlet area to minimise the occurence of

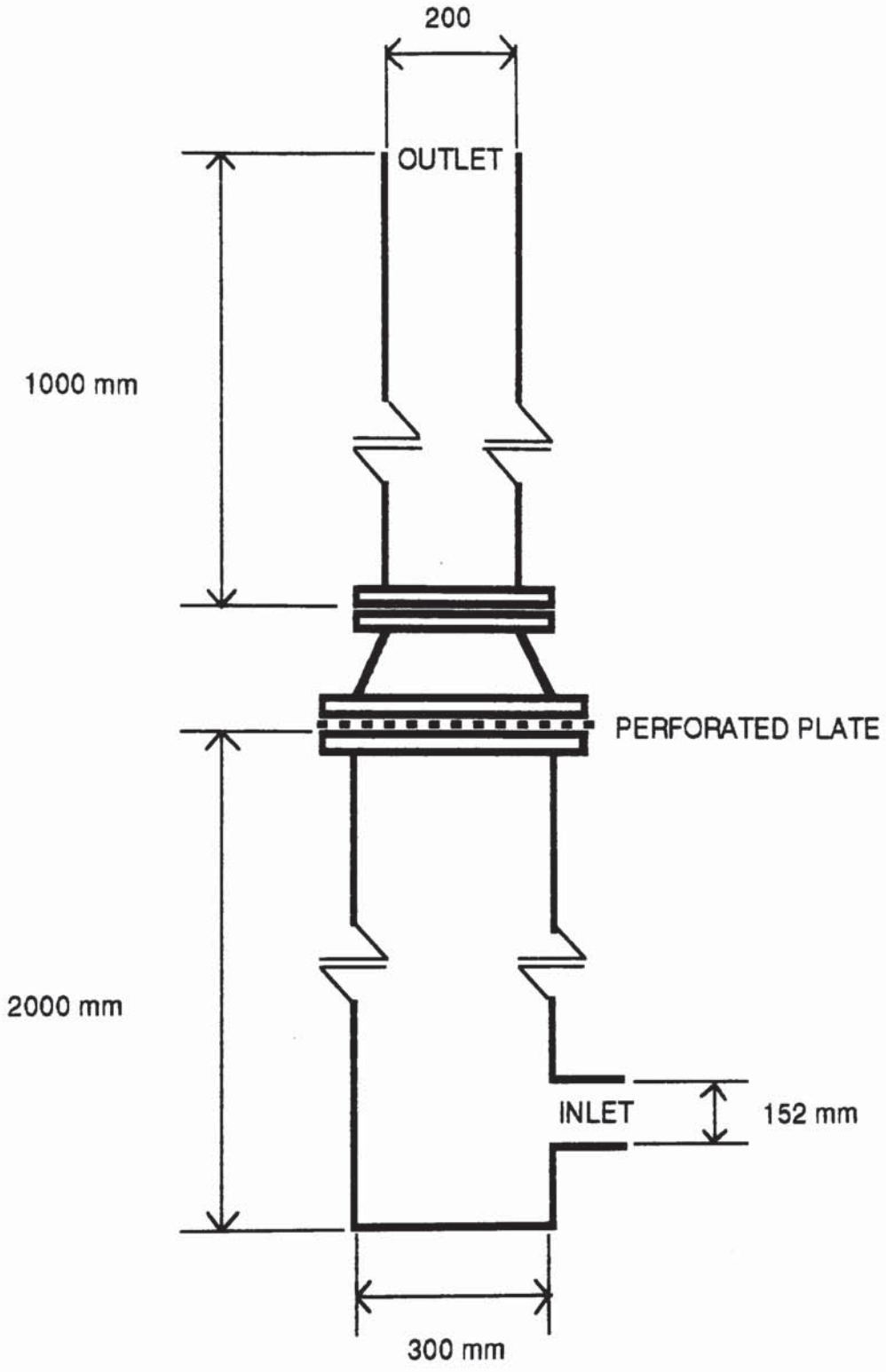

Figure 6.3. The Silencer.

regenerated noise. The pressure loss across the plate helps generate a uniform upstream flow.

iii. A QVF reduction piece flanged to the top of the part described in i. and holding the perforated plate in place. The top of the

reducing piece is flanged to a 200 mm diameter QVF pipe 1 m long, from which the air is discharged.

This design removes all the fluctuations in air flow observed above the bed and reduces the noise level to approximately half its level without the silencer, although ear protection is still necessary.

6.2.4. Ductwork and Distributors.

As is shown in the following chapter the air flow into the packed bed section is required in a duct 25 cm wide and of variable and adjustable height between 2 cm and 10 cm. This section describes a method of connecting the air supply to a duct of varying height. Furthermore, as explained in Chapter 7, the velocity across the duct should be constant. That is, a flat velocity profile is required.

A 6" n.b. perspex pipe is connected to the glass piping described above by a flexible pipe. This in turn is connected to a diverging/ converging duct made of 6mm perspex that is flanged and has an 10 cm by 25 cm outlet. This is connected to a feed section adjustable for duct height (a 'duct height adjuster') that is also made of 6 mm perspex sheet. The duct height adjuster has an inlet flange of fixed dimensions. The top and bottom walls are not attached to the sides and are made in three sections two of which are connected to the inlet and outlet flanges. The middle section is connected the outer ones by thick gasket rubber bolted to the perspex sheets. This allows a duct of constant height or smoothly decreasing height. The top and bottom plates are clamped in position and sealed against the side walls using a silicone sealant. The outlet flange is cut as shown in figure 6.4. so that the upper and lower faces can be moved independantly, and when positioned correctly bolted to the side walls through one of a number of appropriately positioned holes. A sectional plan of the duct height adjuster is presented as figure 6.5.

The air leaving the duct height adjuster will not have the desired flat velocity profile and hence a distributor is required. Three flanged sections of duct 10 cm long were made in each of two duct heights of 5 and 10 cm. This allows the middle section to be filled with packing (to act as a distributor) without having to strip down and re-assemble the remaining apparatus. This section of the apparatus is illustrated, unpacked in Plate 6.1; which also illustrates the height adjustable supports used. These are necessary since when the duct height is adjusted either the distributor

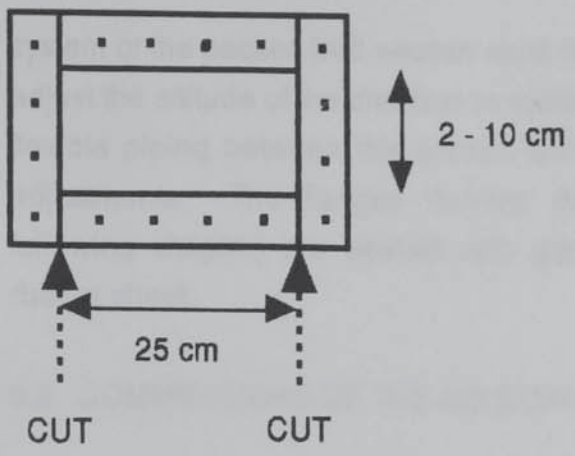

Figure 6.4. The Duct Height Adjuster Outlet Flange.

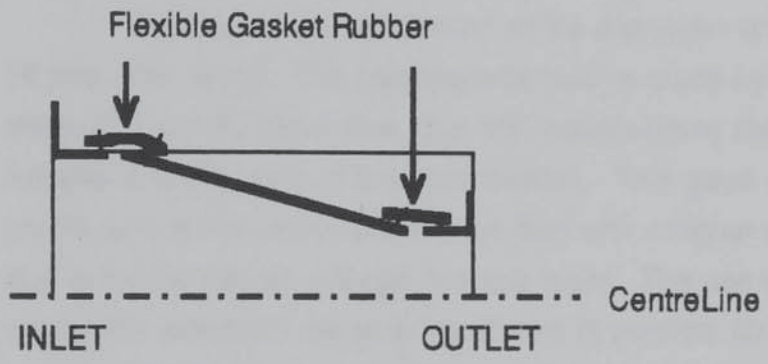

Figure 6.5. Sectional Plan of the Duct Height Adjuster.

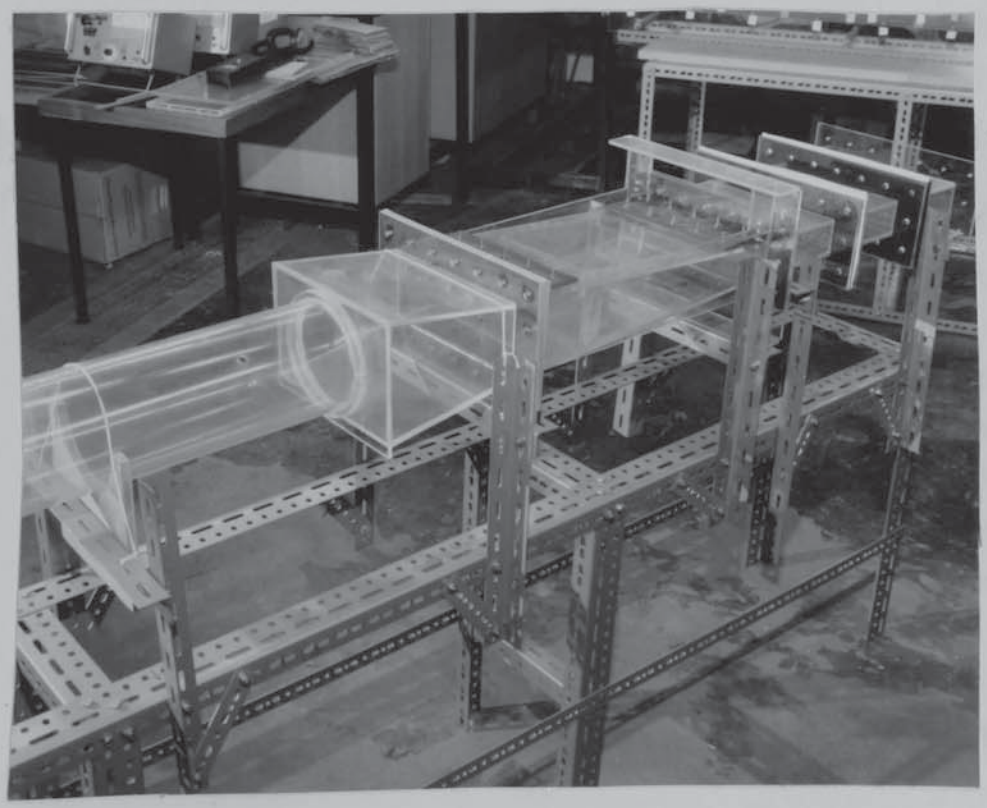

Plate 6.1. The Duct Height Adjuster.

system or the packed bed section must be vertically moved. It is easier to adjust the attitude of the distribution system as it is smaller and lighter. The flexible piping between this section and the glass section permits such adjustments. The flanges (whose dimensions are specified in the following chapter) are sealed with gaskets specially made from 1/16" rubber sheet.

6.3. COMMISIONING OF THE AIR SUPPLY EQUIPMENT.

6.3.1. Distributor Tests and Development.

Initially the central section of the distributor unit was packed with 16 mm. Pall Rings. The packing was held in place by two pieces of wire mesh (1.2 mm diameter wire on a 1/2" square pitch) clamped between the flanges at either end of the duct section. This gave a very flat velocity profile across the central parts of the duct with a higher velocity at the walls due to the increased voidage near the walls. The use of smaller packings where this effect will be less significant (it persists for approximately five particle diameters into the bed) is precluded since low resistance packings (such as Pall Rings) are not available in smaller sizes and packings such as spheres which are available in smaller sizes have a higher resistance which reduces the maximum flowrate that can be achieved in the duct to an unsatisfactory extent. Perforated plates and honeycombs of small tubes were also rejected due to their excessive permanent pressure losses.

A novel distributor was therefore realised. Knitmesh is a finely woven 'cloth' made up of wire 'threads'; it is usually encountered rolled in a bundle which can be inserted into a pipe to act as a distributor or de-mister. Two layers of this cloth were attached by wire ties to the mesh previously used to hold the packing in place. The outer parts of this distributor were sealed with PVC tape and clamped between the flanges, an air-tight fit is thus achieved. When two such distributors are used they provide sufficient resistance to give a uniform distribution without an excessive pressure drop. The distributors are shown in plates 6.2 and 6.3. The resultant velocity profiles (measured using the pitot static tube described in section 6.5.2) are shown in graphs 6.1 and 6.2 which show that a satisfactory flat profile has been achieved over the full range of operating flowrates.

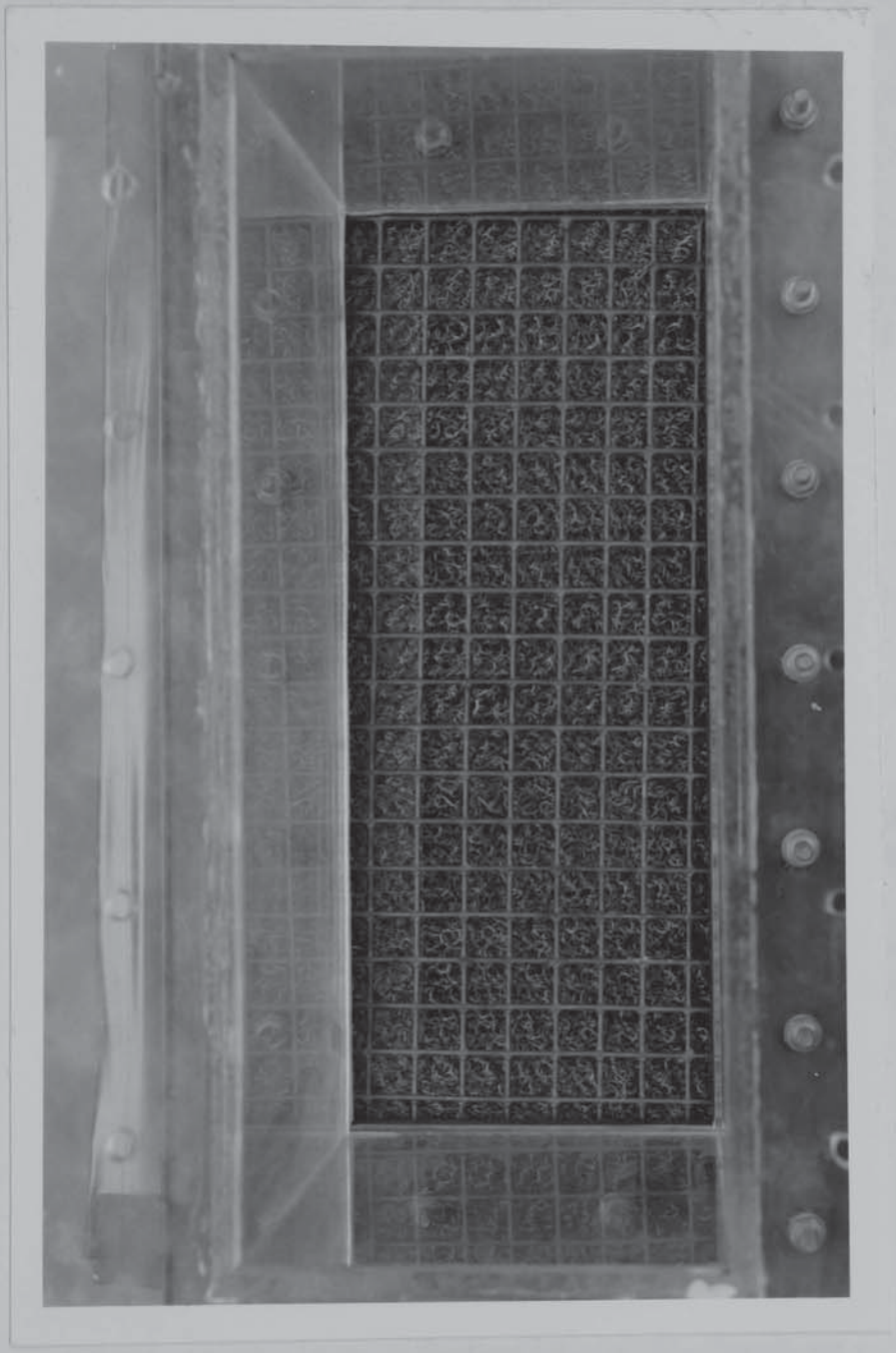

Plate 6.2. Detail of a Distributor.

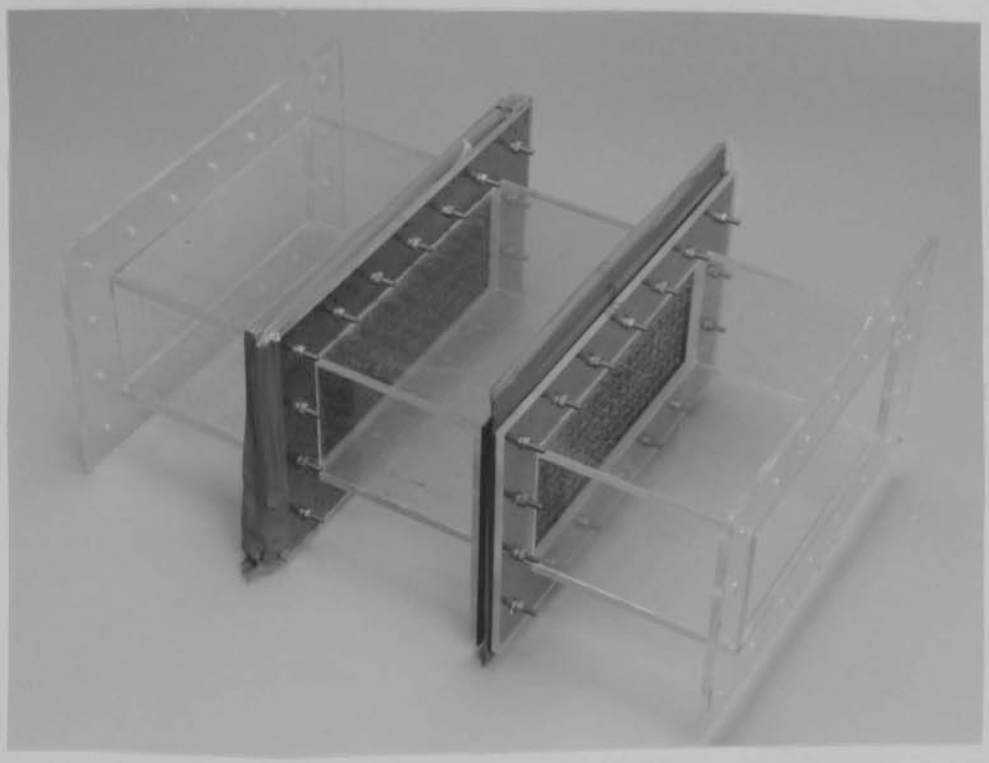

Plate 6.3. The Overall Distributor Arrangement.

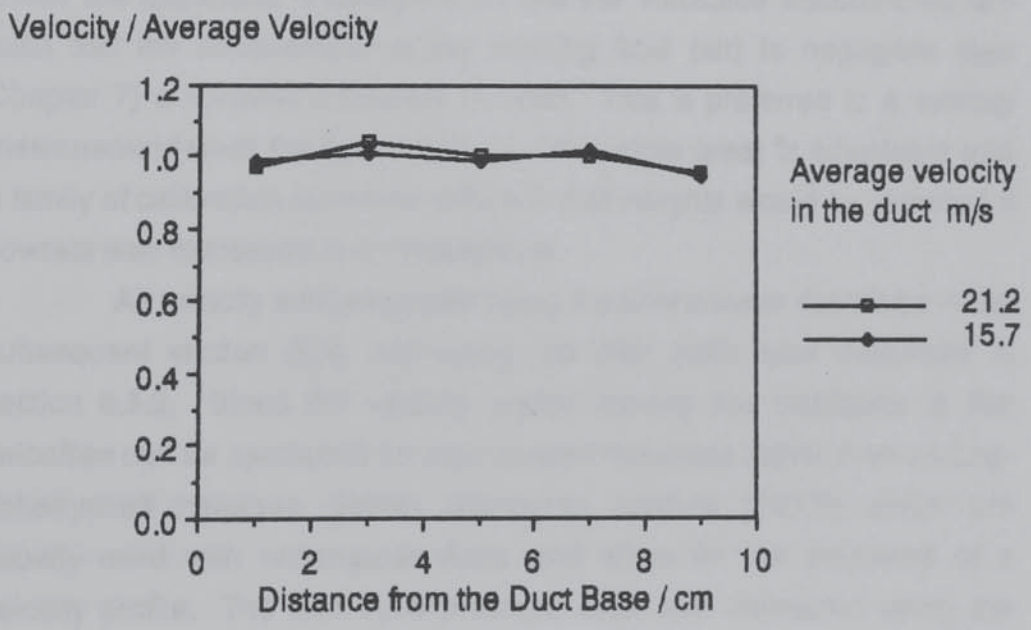

Graph 6.1. Vertical Velocity Profiles Leaving The Distributors.

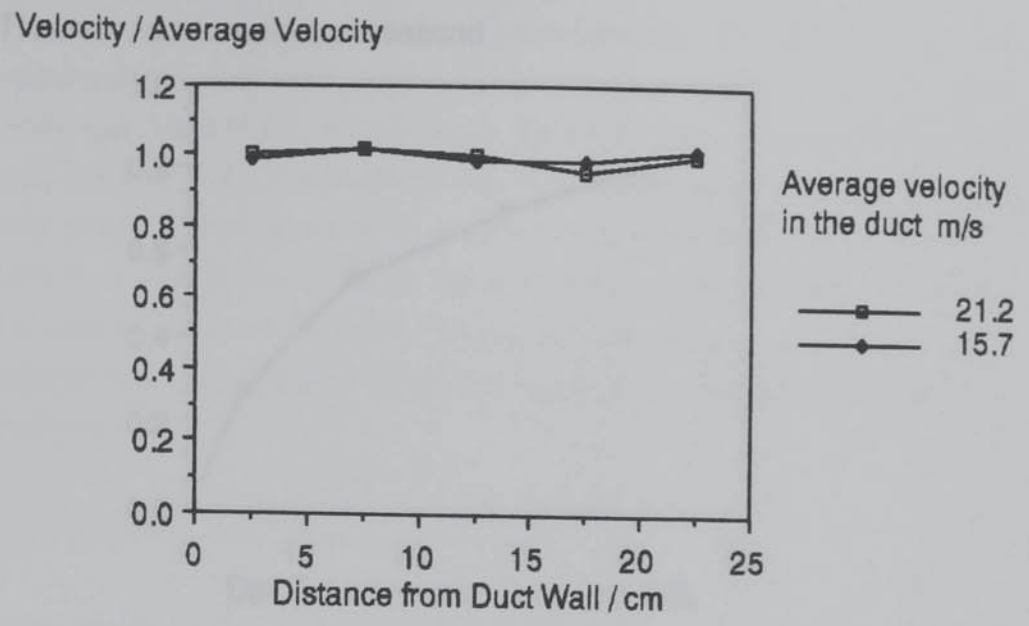

Graph 6.2. Horizontal Velocity Profiles Leaving The Distributors.

6.3.2. Dall Tube Calibration.

It is necessary to calibrate the Dall Tube so that the measured pressure difference across it can be directly expressed as an air flowrate. Since the apparatus is designed so that the velocities encountered are such that the compression of the working fluid (air) is negligible (see Chapter 7) a volumetric flowrate is used. This is preferred to a velocity measurement since the duct height (and therefore area) is adjustable and a family of calibration curves for different duct heights would be required if flowrate was expressed in a velocity form.

Air velocity was measured using the anenometer described in the subsequent section (6.4) and using the pitot static tube described in section 6.5.2. Since the velocity profile leaving the distributor is flat; velocities can be measured on equi-spaced traverses rather than on Log-Tchebycheff traverses (British Standards Institute (1977)) which are usually used with rectangular ducts and allow for the existence of a velocity profile. The Dall Tube pressure drop was measured using the micromanometer described in section 6.5.1. The resultant calibration is presented as graph 6.3. .It was found that the flowrates determined by the pitot tube and anenometer differed randomnly by a maximum of 5% (which is comparable to the resolution of these instruments at the lower flowrates).

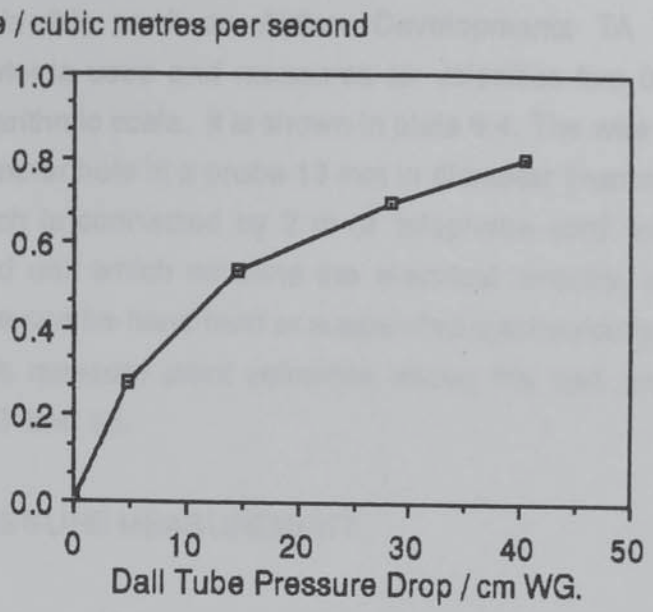

Graph 6.3. The Dall Tube Calibration Curve.

6.4. VELOCITY MEASUREMENT.

A hot-wire anenometer was selected to measure point air velocities (typically leaving a packed bed). These anenometers are made in two basic forms; the constant current type and the constant temperature type (Klapetsky (1970)), the difference between these types is primarily in the electrical circuitry.

The hot-wire anenometer essentially consists of a fine, electrically heated wire (usually platinum) exposed to the gas stream whose velocity is being measured. A change in fluid velocity alters the rate of heat transfer from the wire to the gas. thus changing the temperature of the wire and altering its electrical resistance. In the constant current type, gas velocity is determined by measuring the resistance of the wire; in the constant temperature type, gas velocity is determined from the current required to hold the wire temperature and therefore resistance constant. The constant temperature type is usually preferred for the measurement of steady velocities and is used in this work.

A further factor that affects the rate of heat transfer is the convection film coefficient of heat transfer which depends on the fluid in question . The anenometer must then be zeroed in a stationary sample of the relevant fluid.

In this work an Airflow Developments TA 3000 T hot-wire anenometer is used and measures air velocities fom 0 to 15 ms^{-1} on a semi-logarithmic scale. It is shown in plate 6.4. The wire is positioned in a 1 cm diameter hole in a probe 13 mm in diameter (maximum) and 15.3 cm long which is connected by 2 m of 'telephone cord' wire to a compact, hand-held unit which contains the electrical circuitry, battery and scale. The probe can be hand held or suspended mechanically, the latter method is used to measure point velocities above the bed and is explained in chapters 7 and 10.

6.5. PRESSURE MEASUREMENT.

6.5.1. Pressure Measurement Using A Micromanometer.

The micromanometer used to measure pressure was an Air Neotronics PDM 204 digital type shown in Plate 6.5 and chosen because it is a sensitive pressure measuring device capable of measuring gas pressures down to 0.01 "W.G. It displays pressures up to 20 "W.G. in these units or in KPa. Its accuracy as a percent of F.S.D. of the instrument is 0.1%, or one scale unit (whichever is greater). The micromanometer is designed to be connected in the same way as a U-Tube manometer and should be adjusted to read zero on the scale before any connection. The pressures to be measured are taken to the measuring head via two small hose entries on the top panel of the instrument, one hose entry for the low pressure side, the other for the high pressure side. For a straightforward pressure measurement the high pressure entry is used and the low pressure one is left open to the atmosphere in such a way that the local air velocity is zero, the pressure so obtained being a gauge presure. Differential pressures are measured by connecting both hose entries. The meter also features a 'slow reading' setting for use with turbulent flows where the meter automatically averages instantaneous velocity fluctuations.

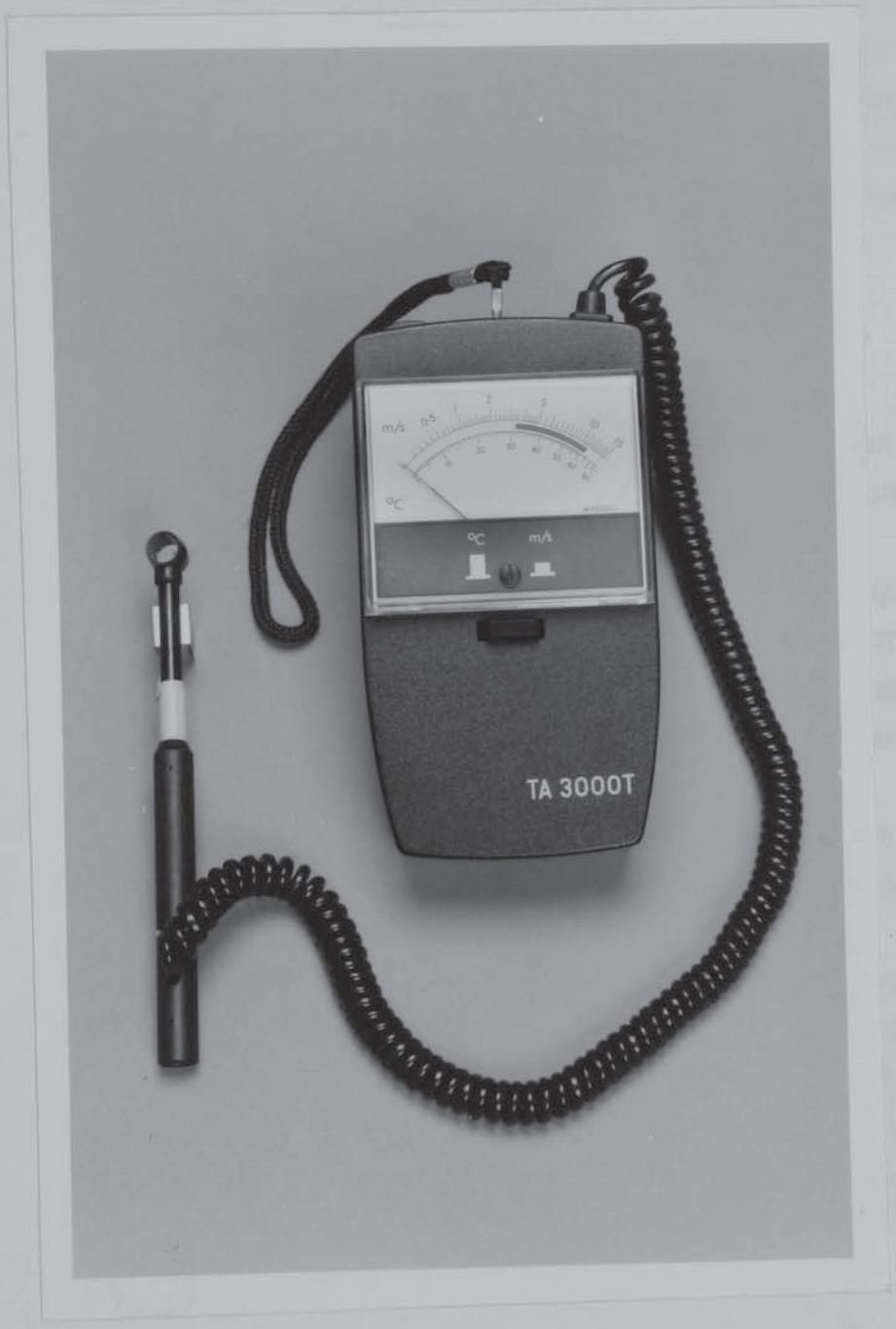

Plate 6.4. The Hot Wire Anenometer.

The measuring head (within the micromanometer) consists of two symmetrically arranged cavities separated by a metal diaphragm. The diaphragm, together with a fixed electrode on either side, forms two condensers. Movement of the diaphragm due to a pressure difference between the two cavities causes a variation in the capacitance between it and the adjacent electrode, thus unbalancing the voltage across the circuits. These voltages are compared by a differential voltmeter, and the difference is amplified and is shown on a digital display calibrated directly in pressure. The diaphragm in the measuring head will respond to sine wave pressure variations up to 200 Hz. However, the long length (3m) of the PVC tubes connected to the pressure probes attenuates the signal and hence the measured pressure is constant.

6.5.2 Pitot Static Tubes.

Pitot Static Tubes are used in conjunction with the micromanometer to determine the dynamic, static and total pressures at a point in a flowing air stream.

To measure static or total pressure the relevant tapping on the pitot tube is connected to the high pressure entry on the micromanometer as described above. The total pressure tapping communicates with the hole on the tip of the tube and the static pressure tapping communicates with the circumferential ring of holes on the tube.

To measure dynamic pressure the total pressure tapping is connected to the high pressure side of the micromanometer and the static pressure tapping to the low pressure side.

Where velocity changes rapidly over a short distance the total and static pressures must be measured at the same point. In this situation the tube must be inserted twice, at different points, so the total and static pressure holes are at the same point. The dynamic pressure is then given by the difference between the total and static pressures at the same point.

Plate 6.5. The Micromanometer.

The velocity is determined from the dynamic pressure thus (British Standards Institute (1977)).

$$V = 20.41 \left[\frac{760}{P_B} \frac{T}{293} \frac{407.5}{407.5 + P_S} P_D \right]^{1/2}$$

Equation 6.1

where:

V = velocity ms^{-1}

P_B = barometric pressure mm Hg

T = air temperature K

P_S = static pressure "WG

P_D = dynamic pressure "WG

It is very important that the pitot static tube is aligned parallel to the direction of the gas flow, as otherwise the static pressure measurement will 'include' part of the total pressure. This is discussed in more detail in chapter 8. The dimensions of the pitot static tube used in this work are given in table 6.1.

Table 6.1. The Dimensions of the Pitot Static Tube.

Tube Type:	small, curved
Tube Diameter / mm:	3.5
Length, tip to circumferential holes / mm:	30
Length, circumferential holes to bend / mm:	30
Total length / mm:	348

Various specially made pressure tubes were also used in this study to determine the static pressure in the bed and; the total and static pressures at the bed base. These are described, and their use discussed, in Chapters 7, 8 and 10.

6.6. FLOW VISUALISATION.

In addition to the classic pressure and velocity measurements that describe a fluid flow, flow visualisation is a useful technique since it allows a fuller understanding of fluid flow phenomena, particularly since 'parcels' of fluid can be followed through the apparatus.

The rig was constructed of perspex to permit this type of study and a Nutem 206 'smoke' machine (the smoke is actually oil vapour) used. The smoke machine is illustrated in Plate 6.6. The main unit contains an oil reservoir and pump, a thin, flexible oil tube connects this unit to the probe. It also contains the heater control, the heater itself is contained in the end of the probe. The oil is pumped to the probe where it is vapourised to produce a plume of grey 'smoke'. The quantity and density of the smoke can be controlled by adjusting the pump speed and heater voltage.

The shape of the probe permits easy insertion into a duct and is such that the attitude of the probe can be altered.

6.7. CONCLUSIONS.

The air supply equipment for the apparatus and experiments presented in Chapters 7, 8 and 10 has been described. In particular novel distributors have been made so that the velocity profile leaving the air supply equipment is flat.

The basic equipment used to measure air flowrate velocity and pressures has been described.

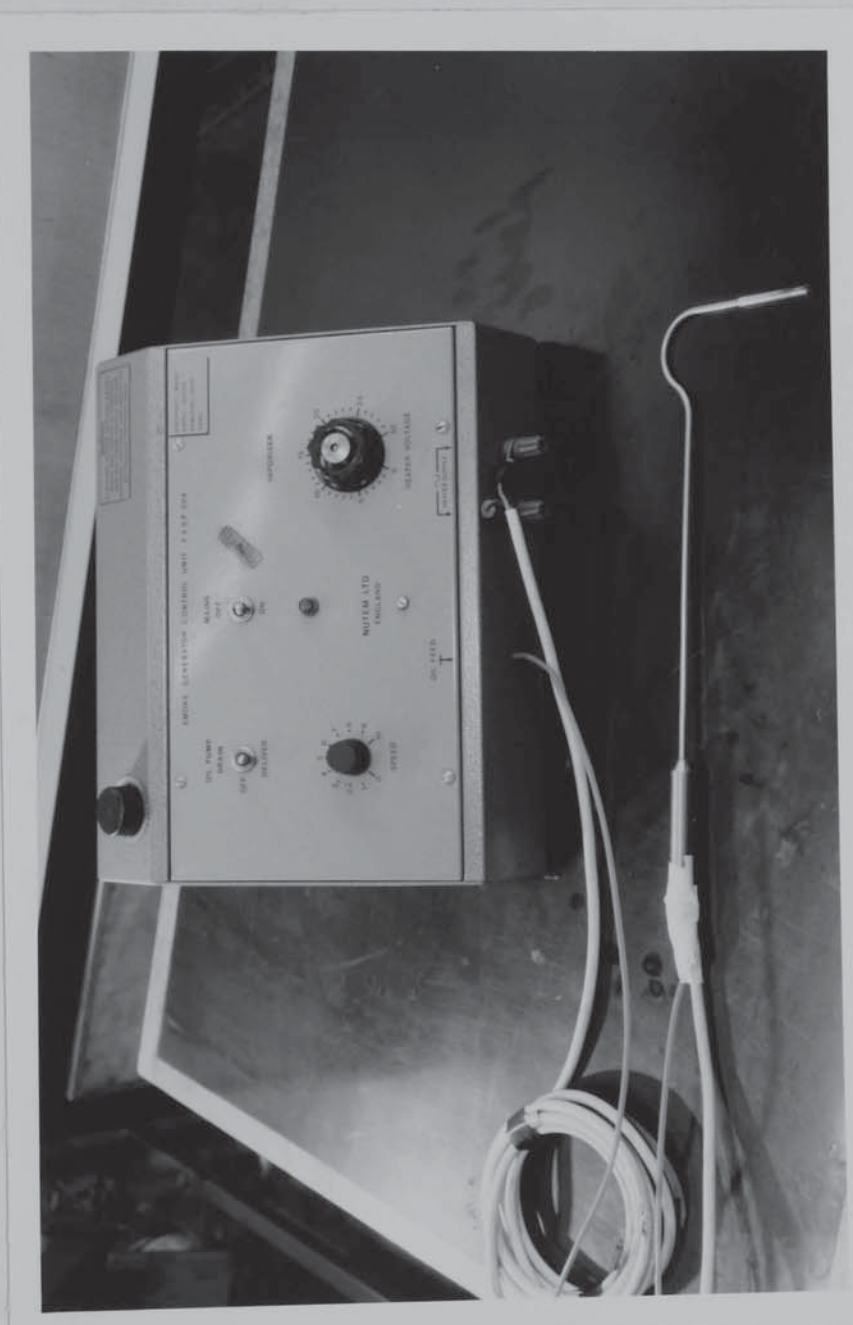

Plate 6.6. The Smoke Machine.

CHAPTER 7

EXPERIMENTAL EQUIPMENT FOR A TWO DIMENSIONAL INVESTIGATION OF PACKED BED FLUID MECHANICS

7.1. INTRODUCTION.

In Chapter 3 (Approach to the Problem) the need for an experimental investigation into the fluid mechanic behaviour of shallow packed beds and, particularly at the base of such beds, was shown.

This chapter describes the construction and commissioning of the experimental apparatus which was made to perform such an investigation. The experimental results obtained from the apparatus are presented in the subsequent chapter. The apparatus was constructed to satisfy three separate objectives.

i. The experimental measurements from the apparatus should further our understanding of shallow packed bed (and particularly base of bed) fluid mechanics.

ii. The experimental situation should be amenable to C.F.D. modelling; so that the models presented in Chapters 4 and 5 can be extended to the situation where the bed interacts with unpacked areas and base of bed mechanisms are important. An apparatus with a simple overall geometry will be of the greatest use in this context.

iii. Given the importance of the effect of the bed base, it is reasonable to suggest that novel distributor designs that are contained within the bed support would be an improvement on current designs. Therefore the apparatus was designed so that various bed supports/ distributors can be used.

Initially, it was decided to build an apparatus where the flow patterns are essentially two dimensional in nature. This will ease the interpretation and analysis of the experimental measurements of velocity and pressure and make the development of the C.F.D. model and analysis of its results easier. This chapter describes the two-dimensional apparatus used in this work. A three dimensional apparatus is described and experimental results from it are presented in Chapter 10.

This chapter also describes the traversing mechanism built for the anenometer probe which is used to measure point air velocities leaving the bed. Special pressure probes used to determine pressure within the bed and at the bed base are also described. Experimental results are presented that confirm that the flow pattern along the centre plane of the apparatus is representative of that in an infinitely wide apparatus; confirming that the results can be considered as two dimensional.

7.2. DESCRIPTION OF THE APPARATUS.

The apparatus is illustrated in plate 7.1 and an overall sectional view is given as figure 7.1. These illustrations show the desired long, shallow bed above a duct; an arrangement which emphasises the desired features of the investigation in accordance with the three objectives outlined above. This section of the chapter describes the apparatus in full and presents the reasons for the specific details of its design. Its design was aided by experience gained constructing and running a prototype apparatus that consisted of a packed bed contained within a four sided wooden box positioned over a slot cut in the side of a 6" n.b. pipe.

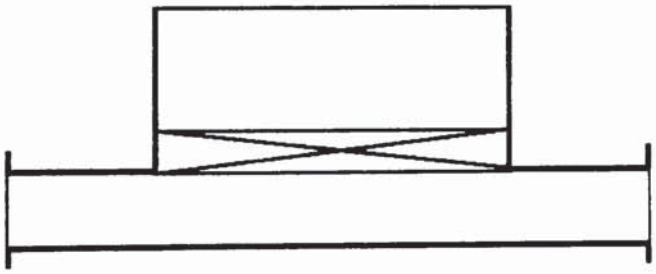

Figure 7.1. A Sectional, Side View of the Two Dimensional Apparatus.

7.2.1. Packing Material.

Section 2.6.4 of the literature survey discusses the required use of shape factors with the Ergun Equation in order to fully describe non-spherical packings. It further indicates that the theoretical determination of shape factors is not satisfactory and that empirical factors must be used. The use of such factors with the vectorial Ergun Equation has not been experimentally tested. Hence, this experimental investigation will be confined to the use of spherical packings where shape factors are not

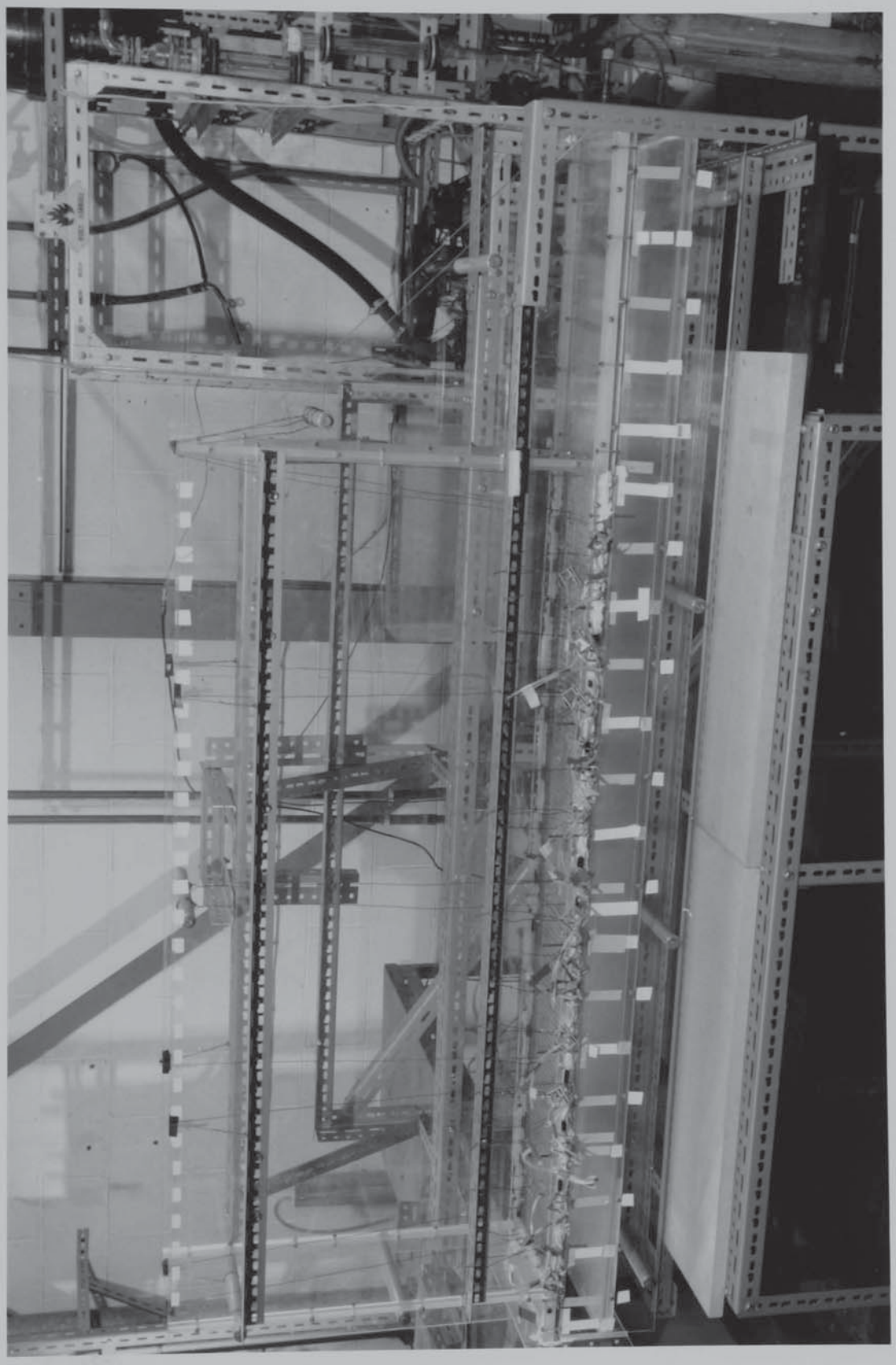

Plate 7.1. The Bed Section of the Two Dimensional Apparatus.

required and the use of the vectorial Ergun Equation has been verified. This choice is particularly appropriate given the excellent agreement between the experimental results of Poveromo (1975) and the C.F.D. model of packed bed flow presented in Chapter 5. The availability of a large quantity of 12mm diamenter glass spheres led to their selection as the packing material used in this study.

7.2.2. Determination of Duct and Bed Dimensions.

A maximum velocity in the duct of approximately 30 ms^{-1} is required for two reasons:

i. This is the highest velocity observed by Ali (1984) in his study of maldistributed gas flows in packed beds. This study was based on a geometrically and dynamically similar model of a pumparound section in a vaccuum crude oil distillation tower and is the highest velocity likely to be encountered in commercially sized process equipment. Investigation of higher velocities would be of limited practical interest.

ii. This velocity corresponds to a Mach Number of about 0.1; below which compressibility effects can be ignored. This simplifies the analysis of the results and significantly reduces the C.F.D. modelling effort.

The maximum flowrate leaving the distributors is approximately 0.75 m^3s^{-1} which gives the area of the duct below the bed for the maximum velocity required as 0.75/30= 0.025 m^2. The width of the duct must be such that velocity and pressure are constant across its central part so that measurements made in the central plane are representative of those in an infinitely wide duct. The minimum width will be set by the width of the boundary layer on the side walls of the duct, or, the distance from the side walls over which the bed voidage is not constant. Typically voidage variations in a bed of spheres caused by a wall persist for about five particle diameters into that bed (Benanti and Brosilov (1962)), which is equivalent to 5 cm for 12 mm diameter spheres. Both side walls will have this effect which gives a minimum width of 10 cm. Since the effects of this voidage variation on local fluid velocities and pressures may be apparent over a greater distance and so that larger packing sizes can be used in the equipment (e.g. 16mm Pall Rings) a duct width of 25 cm was selected which gives a duct height of 10 cm. However, the equipment is designed so that the duct height can be decreased below this (see section 6.2.4 of Chapter 6 and section 7.2.4 below).

Approximately 0.038 m^3 (1.35 cubic feet) of 12 mm glass spheres were available for use in this study. Taking the maximum bed depths as equal to the maximum duct height (10 cm) gives a maximum bed length of 1.5 m (for a bed width of 25 cm). This gives a bed aspect ratio (packed height : bed length (or diameter in a column)) of 1/15 which clearly satisfies the criteria of a shallow bed. This bed height is such that the voidage in the centre (vertically) of the bed will be the same as in the centre of a very large bed of spheres. These basic dimensions of the apparatus are shown in figure 7.2.

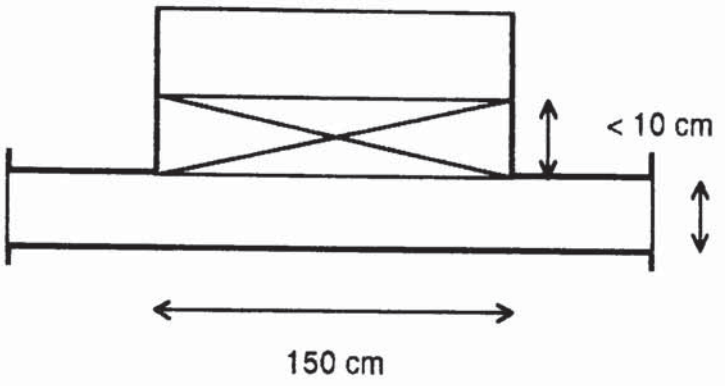

Figure 7.2. The Basic Dimensions of the Two Dimensional Apparatus.

7.2.3. Material of Construction.

In order to make full use of flow visualisation and so that, in future, Laser Doppler Velocimetry (L.D.V.) could be used to determine air velocites in the equipment a transparent material of construction is required. L.D.V. would give unambiguous velocity readings inside as well as outside the bed and will not suffer from the limitations of pitot static tubes encountered in this experimental study (which are discussed in the following chapter) but was, however, beyond the resources of this study.

Perspex (poly methyl methacrylate) was therefore selected as the main material of construction; despite its brittleness and high cost. The rig is largely constructed of 6mm thick perspex sheet.

7.2.4. Description of Apparatus.

The major dimensions of the bed and duct have been established in the previous section. This section describes the apparatus in full.

A length of ducting is necessary both up and downstream of the bed so that the connecting flanges can be attached. On the inlet end this length was selected as the minimum practical value which is 10 cm (since the beginning of the bed must be as close as possible to the distributor). The outlet duct length was then made the maximum length possible (given the size of the uncut perspex sheet) which is 55cm. This ducting will allow the examination of the change in velocity profile in the duct after the end of the bed.

The bed section was made in upper and lower sections: the division being made at the base of the bed.

The Lower Section.

The side walls are cut as shown in figure 7.3. The 'groove' is cut to accomodate the bed support as discussed in section 7..3.1. The duct

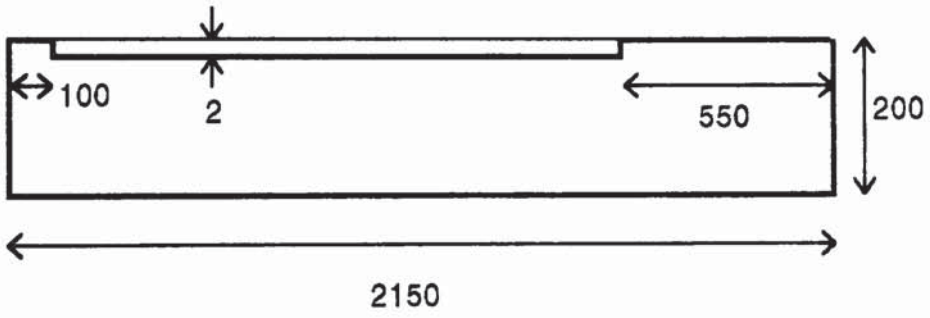

All Dimensions in mm. Not to Scale

Figure 7.3.The Lower Section Side Wall.

base is cut and attached to the duct sides as shown in figure 7.4; it is easily repositioned to give different duct heights. Three 25 cm long, 1" diameter steel bracing rods were made to give the arrangement greater strength and stability and are attached between the duct sides. This attachment is achieved by drilling and tapping holes in the end of the rods; these holes are then aligned with appropriately positioned holes in the duct side walls and the rods are bolted into place.

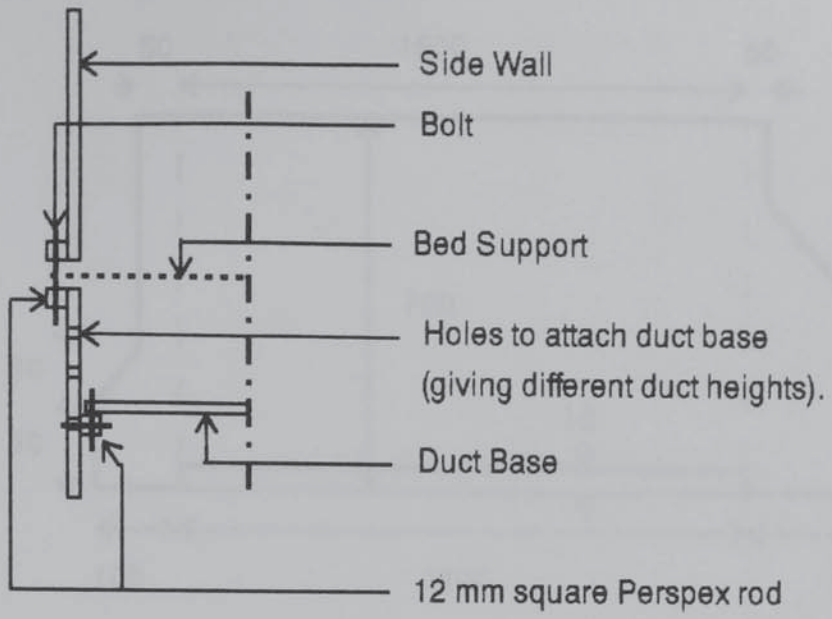

Figure 7.4. A Cross-Section Through the Apparatus.

The Upper Section.

The cut side wall sheets are as illustrated in figure 7.5, the method and details of construction being essentially the same as for the lower section. The various sheets (duct tops, bed ends, bed sides) are joined using 12 mm square perspex rod. Five steel bracing rods are used to strengthen the assembly.

12 mm rods are bolted to the sides of the top of the lower section and the bottom of the upper section so that they form two sides of a flange. The rods are drilled so the two sections can be connected. The flange faces have a 12 mm gap between them (below the bed) to accomodate bed supports/distributors whose method of attachment is detailed in section 7.3.1.

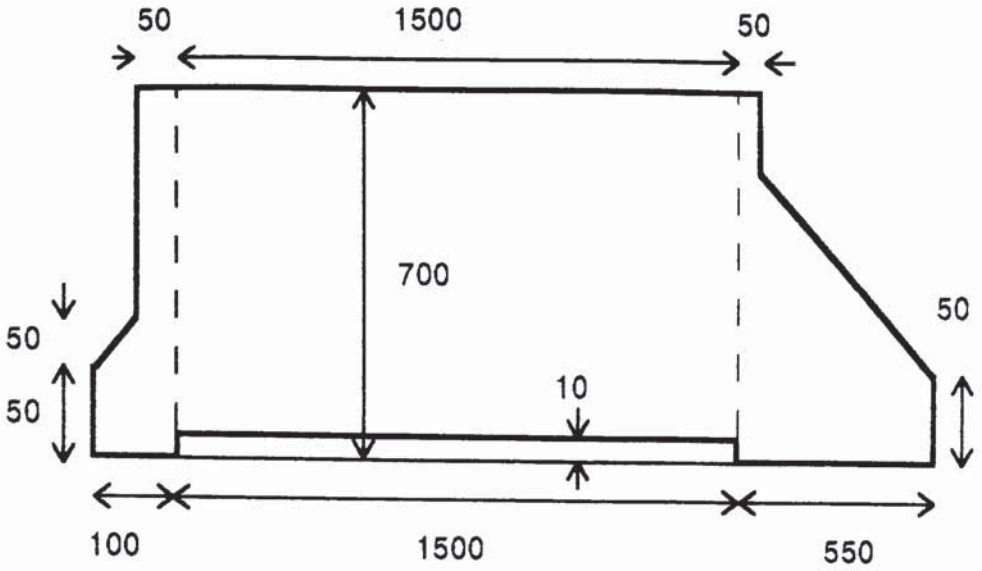

— — — — denotes position of end walls

All Dimensions in mm. Not to Scale.

Figure 7.5. The Upper Section Side Wall.

Perspex plates were also made that can be inserted in this flange so that the bed length can be reduced, these are used in conjunction with a false bed end wall. This allows bed lengths of 0.5 m, 1,0 m as well as the standard 1.5 m to be realised.

Standard flanges cut as shown in figure 6.4 to allow for duct height adjustments (as described in section 7.2.5) are attached to the duct ends to permit connection to the air supply equipment (Chapter 6) and the various duct end closures detailed in section 7.2.5.

7.2.5. Flanges and Duct Closures.

A standard flange design was used for the inlet and duct outlet of this apparatus as well as for the distributors described in the previous chapter and the apparatus for a three dimensional investigation of shallow packed bed fluid mechanisms described in Chapter 10.

Flanges were made of 6mm perspex sheet and cut and drilled for 2BA bolts as shown in figure 7.6. The standard spacing of the bolt holes allows the connection of the various duct heights to the air supply equipment.

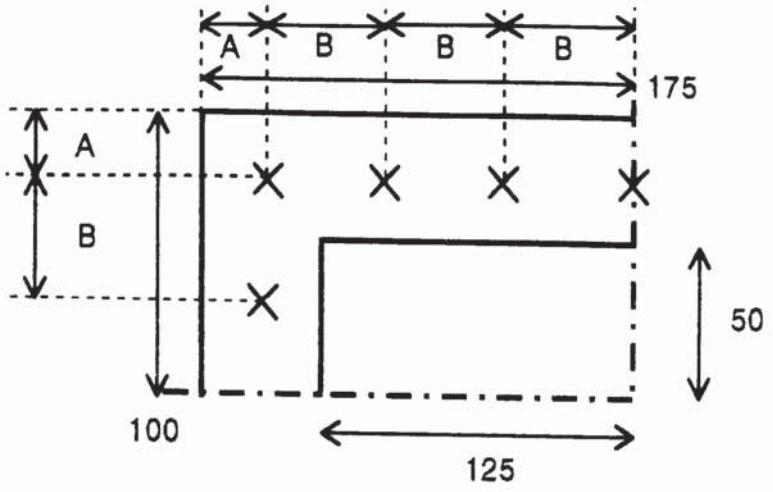

X denotes Bolt / Bolt Hole

Dimension A = 25 mm
Dimension B = 50 mm

All Dimensions in mm

Figure 7.6. Flange Dimensions (10 cm duct height).

The number of bolts used to connect these flanges is to ensure an air tight seal rather than through any consideration of mechanical strength. The flanges are sealed with specially made gaskets of 1/16" thick rubber sheet.

The apparatus as described in section 7.2.4 allows the air to leave the apparatus through the bed and the duct. Various plates were made so that the duct outlet is totally blocked either at the duct end or, at the end of the bed.

The plate closing the duct outlet is the same size as the flange and drilled appropriately. That closing the duct at the end of the bed is 10 c.m. x 25 c.m. and drilled so that 12mm square perspex rods can be attached to it. The rod has holes drilled in it that are coincident with holes drilled in the side walls of the duct to which walls the plate is attached.

Thus, as discussed in Chapter 3 (Approach to the Problem) the gas can be made either to flow wholly through the bed or allowed to find its own 'balance' between the bed and duct outlets. A perforated plate was made for the duct outlet which will increase the amount of gas leaving through the bed relative to that leaving through the duct (by increasing the static pressure in the duct). The use of this plate will allow an additional comparison between the two cases described above.

The plate was drilled (over the active area) with 10mm holes on a 15mm square pitch (giving a free area of 35%) which gives a plate pressure drop of 2.1 "W.G. at a duct velocity of 10 ms^{-1} using the expression and orifice coefficient of Liebson et al. (1957).

These duct closures are shown as plate 7.2 (for a 10 cm duct).

7.2.6. Probe Holes.

Holes were drilled in the side of the duct wall to allow the insertion of the pitot static tube or the smoke machine probe. Holes were drilled 2,4,6 and 8 cm. below the top of the duct (the bed base level) which permit access to any vertical point within the duct. These sets of holes were drilled every 10 cm. along the length of the duct, and taped over with insulating tape when not in use to prevent air leakage.

7.2.7. Support Frame.

The whole of this section of the experimental apparatus is supported on a frame made of 38mm x 38mm Handy Angle steel bars.

7.2.8. Hot Wire Anenometer Traverse Mechanism.

The hot wire anenometer (described in section 6.4 of Chapter 6) is used to measure point velocities above the bed. A traverse mechanism was built so that the anenometer can be easily and accurately positioned above the bed.

The traverse mechanism is shown in plate 7.3. It is made of Handy Angle; the long central part is bolted at right angles to two smaller pieces that run along the top of the sides of the packed bed section permitting movement of the anenometer along the length of the bed. The central bar has a groove cut in it (see plate 7.3) through which a threaded bar is inserted. The threaded bar is held in place by lock-nuts; the bar can

Plate 7.2. Duct Closures (10 cm duct height).

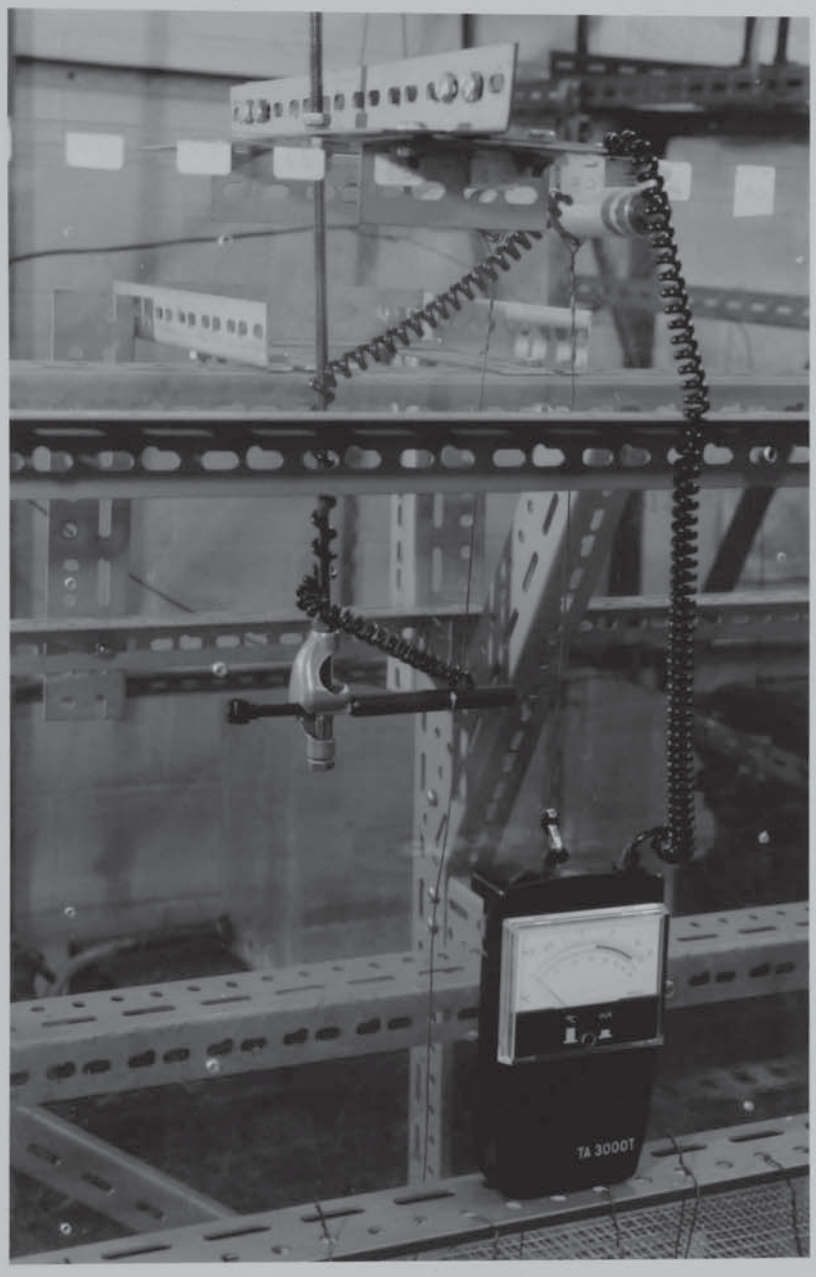

Plate 7.3. The Hot Wire Anenometer Traverse Mechanism.

be moved along the groove thus permitting the collection of velocities across the width of the bed if required (typically, velocities are only collected along the centre of the bed).

A retort clamp is screwed to the end of the bar and is used to hold the anenometer probe. The threaded bar can be moved vertically by adjusting the lock-nuts that hold it to the traverse mechanism.

This traverse mechanism allows the collection of point velocities above the bed at any position.

7.3. COMMISIONING OF THE APPARATUS.

7.3.1. The Bed Support.

Some form of bed support is clearly necessary; however, for the purpose of this investigation it should be such that it has no discernible effect on the fluid flow in the apparatus.

A simple wire mesh (1.2mm diameter wire on a 1/2" square pitch) was initially selected. However, the beads were found to lie neatly in the interstices of the mesh and as a result the bed packed regularly . A finer mesh (6.5mm wire on a 1/4" square pitch) was then tried but, buckled under the weight of the packing. Finally the two meshes were wired together, this arrangement was found to give a randomn packing arrangement and to have sufficient mechanical strength.

It was however observed that the support mesh sags (a 10 cm deep bed weighs approximately 56 kg) regardless of how it is clamped at the sides (see below). This problem is exacerbated by the design of the apparatus which is such that the mesh is only clamped along the side walls. The problem was overcome by attaching wires to the mesh which are then attached to the steel bracing bars or the support frame and tensioned appropriately. This will cause a variation in local voidage in the bed where the wires pass through it but is preferable to using a larger, stronger mesh which will have a greater effect on the fluid flow.

The support wires are clearly visible in plate 7.1 and their positions are shown in figure 7.7.

Various methods of clamping the mesh in place (between the side flanges of the apparatus described in section 7.2.4) were tried. This

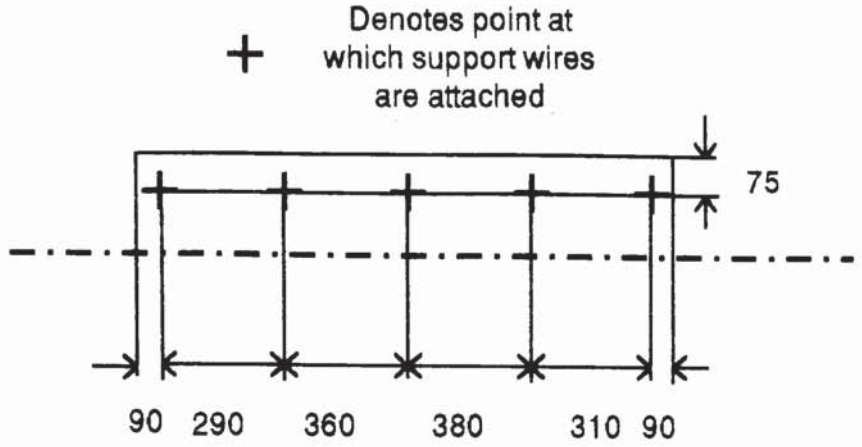

Figure 7.7. Position of the Support Wires.

attachment must be such that the bed support cannot move and yet fine adjustments to the support are easily made so that it lies flat and level. The final scheme used is to hold the mesh in place between the flanges with thin, rolled up strips of gasket rubber which are then clamped in place by tightening the flange bolts as shown in figure 7.8. Finally the gap between the flanges is sealed with a silicone sealant.

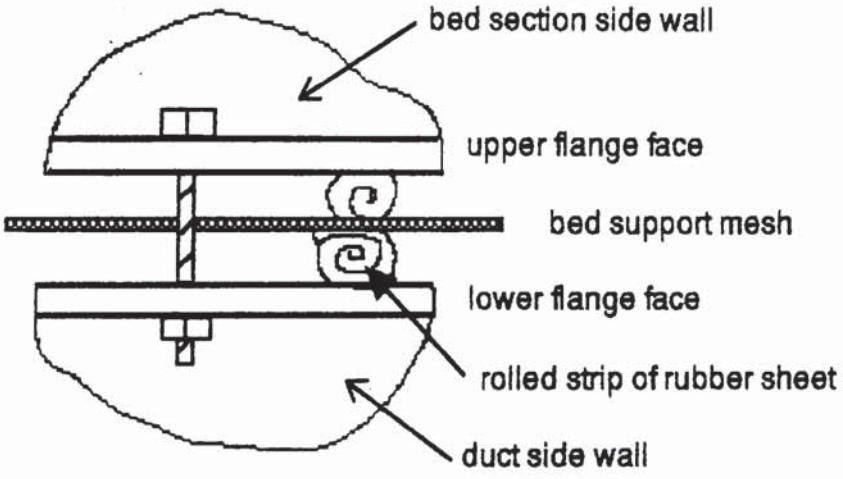

Figure 7.8.The Clamping Method used to hold the Support Mesh in Place.

7.3.2. Point Velocity Collection.

It was observed experimentally, for a wide range of gas flowrates, that a measured velocity of air at a specific point in the surface of the bed depends on the distance above that point that the anenometer probe is situated. This variation occurs because at the top of the bed the voidage ranges between zero and unity and correspondingly the velocity between its maximum value and zero according to the precise position of the packing pieces in the top layer of the bed. Subsequently, as the gas leaves the bed it mixes to give a locally representative velocity.

It is therefore necessary to determine the optimum height above the bed base at which point velocities are measured. Velocities were measured at various heights above the bed and, at various positions along the length of the bed. Some of these measurements are presented as graph 7.1.

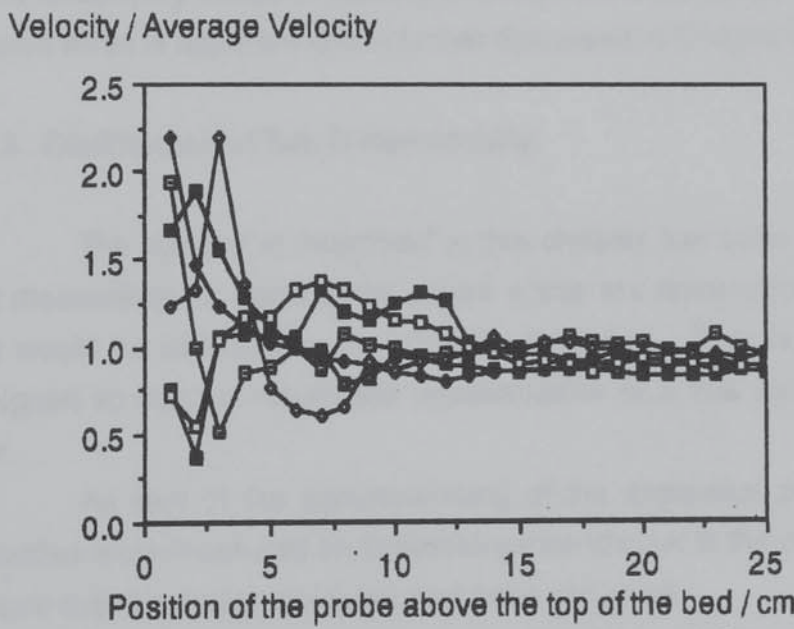

Graph 7.1. Typical Point Velocities above the Bed and Anenometer Probe Height.

This graph shows that over the initial 15 cm, velocity varies randomnly with probe position as a result of the non-homogenous nature of the bed. Thereafter a constant representative value is shown. Point velocity measurements were therefore made at a distance of 20 cm above the top of the bed.

It must be accepted that this will not give a particularly clear picture of the velocity profile leaving the bed. These measurements can, however, be compared to velocities given by the C.F.D. model (Chapter 9),

which, when verified will give an accurate indication of the velocity at a point at the top of the bed as though it were homogenous.

However, when the velocity profiles (above the bed) collected in this manner are viewed, the effect of randomn nature of the bed on the profile is still apparent. This can be minimised by measuring more point velocities above a given bed and by re-packing the bed (and thus changing the exact nature of the various pathways through which the gas flows in the bed). Extensive trials were performed to determine the optimum velocity measurement strategy which was found to be collecting velocities every 5 cm along the length of the bed for three different packs.

The velocities, at a given position are averaged over the three packs; the average velocity is then taken as representative of that point in the bed. The resulting profile is still jagged, but, is not improved by the collection of more velocities for a given pack or the collection of velocities from a greater number of packs. The overall profile gives a clear indication of the underlying trends in velocity although the effect of the bed support support wires is apparent and is further discussed in Chapter 8.

7.3.3. Confirmation of Two Dimensionality.

The apparatus described in this chapter has been designed so that measurements made at the centre plane are representative of those that would be obtained in an infinitely wide duct. That is, it has been designed so that the results are representative of a true two-dimensional flow.

As part of the commissioning of the apparatus pressures and velocities were measured on traverses perpendicular to the centre plane to ensure that this design objective had been achieved.

Graphs 7.2. to 7.4 present (horizontal) velocity measurements (determined from dynamic pressures) across the centre of the duct (vertically) at various positions along the duct. The flat nature of these profiles in the middle of the duct show that no gas is flowing in a direction perpendicular to the centre plane and that the two-dimensional objective has been realised.

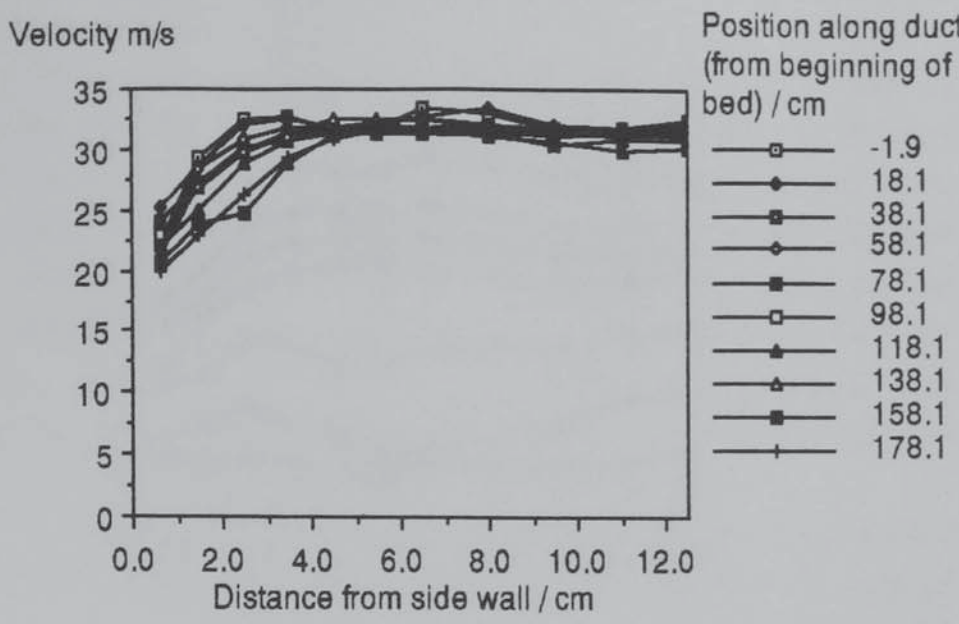

Graph 7.2. Horizontal Duct Velocity Profiles (Duct Outlet Open).

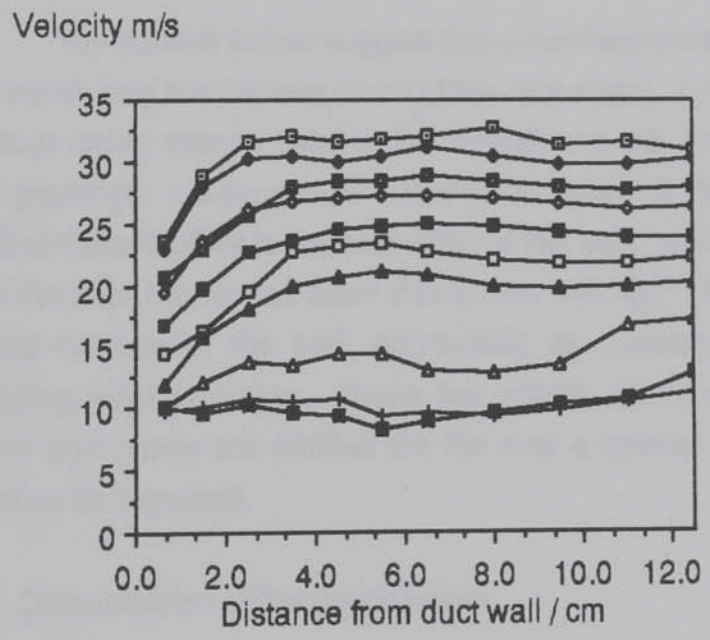

Graph 7.3. Horizontal Duct Velocity Profiles (Duct Outlet Partially Blocked with Perforated Plate).[Key as Graph 7.2].

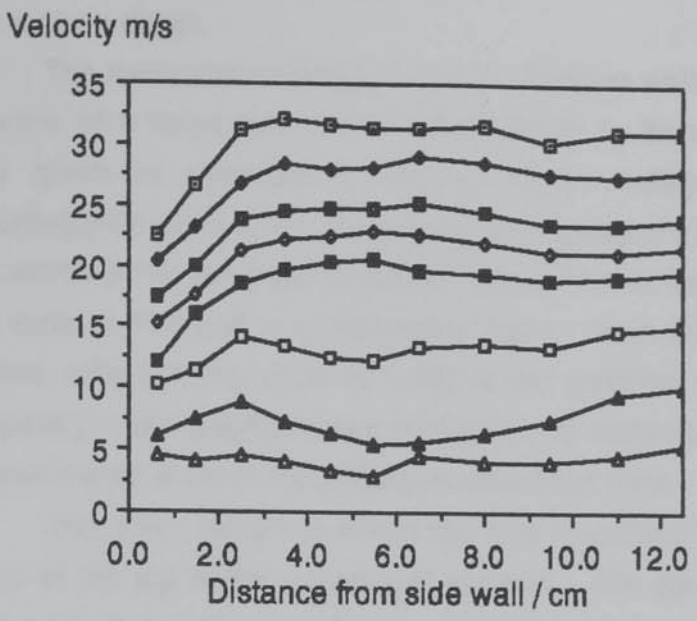

Graph 7.4 Horizontal Duct Velocity Profiles (Duct Outlet Blocked at the End of the Bed).[Key as Graph 7.2].

The profiles further suggest that a narrower duct could have been used (since they are flat over much of the duct width) this is a result of the generous safety margin used in the design and will allow for the use of larger packings. It is suggested that another reason for the particularly flat nature of these profiles is the dual effect of the wall: wall friction slows the gas in the duct, but, as has been shown, the wall also causes an increase in local voidage in the bed, decreasing its resistance and therefore increasing local flowrates. These two effects act in opposition to one another and hence the profiles are flat over a greater width than would otherwise be expected.

7.3.4. Determination of the Bed Voidage.

The bed voidage is easily determined. If the spheres making up the bed are weighed (55.78 kg for a 10 cm deep bed) and compared to the mass of a known number of spheres (219.1g for 100) the number of spheres in the bed can be found (25,460). The diameter of the spheres is known (12 mm) and their total volume can then be determined (0.02218 m^3). The overall dimensions of the bed (0.25 m wide x 1.5 m long x 0.10 m deep) give its volume (0.0375 m^3) and hence the voidage is found to

be 0.409. The main source of inaccuracy in this calculation is packing the bed to a given depth.

The measured voidage of 0.409 compares well to the voidage in the centre of a large bed of 0.39 determined by Benanti and Brosilov (1962) given the existence of areas of higher voidage near the walls. Contrastingly Coulson et al. (1978) give the voidage of a bed of spheres as 0.407, which is the generally accepted value. Due to the significant effect of the walls in this bed a considerably higher value than this would be expected, although the value of 0.407 is not qualified in any way. The discrepancy is explained in terms of this lack of detail in the literature and the experimental error in the procedure described here.

The given height to which the bed is packed is defined as the position of the top of the uppermost spheres. The top layer of spheres were 'brushed' into place so that a constant bed height is obtained. The exact position of the top of the bed is of particular importance to the modelling work (Chapter 9).

7.4. DEVELOPMENT OF SPECIAL PRESSURE MEASUREMENT HARDWARE.

This study concentrates particularly on the fluid flow mechanisms within and at the base of a packed bed. The basic pressure and velocity measurement hardware used in this work, described in Chapter 6, is designed to be used in free gas flows. Special hardware was therefore developed to measure pressure in and at the base of the bed, so that experimental measurements of pressure can be made of these points, which are of particular interest to this study.

7.4.1. Bed Static Pressure Probe.

Ali (1984) used a staight pitot static tube to determine static pressures in a bed. This method has three drawbacks:

i. Inserting a tube or rod into a packed bed will cause a higher local voidage around the tube as illustrated in graph 7.5. This increase in voidage will allow higher local velocities and hence the measured pressure will not be actual pressure if the tube was not there.

ii. Since the total pressure hole and static pressure holes are separated along the length of the pitot tube; when static pressures are

measured near the base of the bed the end of the tube will protrude through the base of the bed and into the free flowing gas below the bed. This will also result in the measured static pressure differing from the true static pressure.

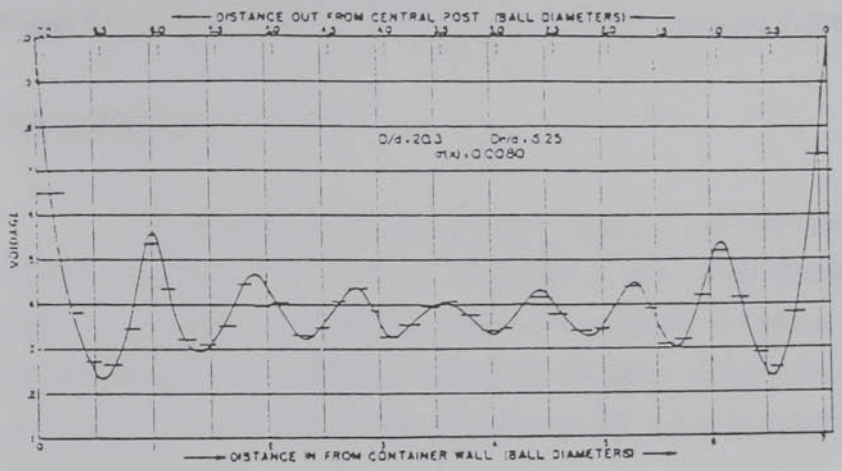

Graph 7.5. Voidage Profiles Caused by a Rod in a Packed Bed (taken from Benanti & Brosilov(1962)).

iii. Pitot static tubes have a ring of static pressure holes around their circumference. As has already been shown the definition of velocity in a packed bed is ambiguous (that is, it is not uni-directional). Hence, the ring of holes will detect elements of the dynamic pressure and will not indicate the true static pressure.

A special static pressure probe was therefore made which will not have the second and third limitations discussed. A 7 mm diameter, 35 cm long tube was blocked at one end (with a rubber bung). A single 2 mm diameter hole was drilled in the side of the tube near the blocked end. This static pressure tube is illustrated in plate 7.4. The other end of the tube can be attached to a PVC tube and manometer. By inserting the tube into the essentially two dimensional flow in the bed so that the hole is facing the side walls of the apparatus an indication of the true static pressure in the bed can be obtained.

The bed static pressure tube was tested against a pitot tube by inserting both into a pipe and measuring the differential pressure, which was equivalent to the resolution of the micromanometer over a range of flowrates up to 30 ms^{-1}.

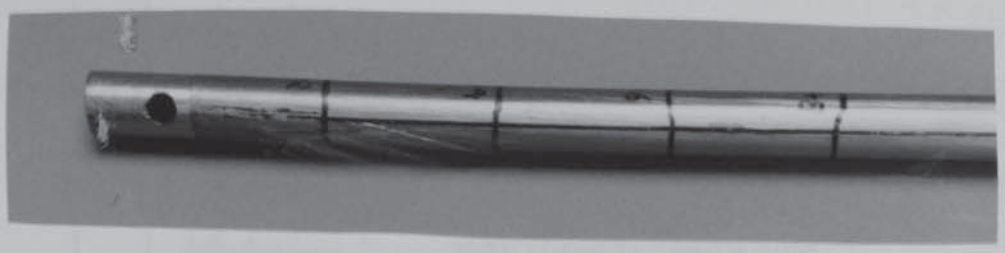

Plate 7.4 The (tip of the) Specially Made Static Pressure Tube.

7.4.2. Bed Base Pressure Probes.

In view of the difficulties encountered in commissioning the bed support (section 7.3.1) and the suggestion that novel distributors should be incorporated into the bed support; the need for pressure measurement hardware that will specifically measure pressure either side of the support is apparent. Such hardware also allows the measurement of pressure at the bed base.

This section describes special pressure probes developed specifically to meet these objectives. The probes are essentially lengths of 20 gauge hypodermic tube (and are therefore referred to as needle tubes). The hypodermic tubes are tied to both sides of the bed support (so that its effect can be quantified) with cotton thread. The tubes can be bent or left straight to measure total or static (and hence, by difference dynamic) pressure as shown in figure 7.9.

The other ends of the tubes extend beyond the sides of the bed support and hence outside the packed bed section. These tube ends must then be attached to a manometer. This is achieved by pushing the end of the tube through the wall of a P.V.C. tube which is then folded, sealed with tape and clamped with a Hoffman Clip to form an air-tight fit as shown in figure 7.10 and plate 7.5. The other end of the P.V.C tube can then be directly attached to the micromanometer.

14 total and 14 static pressure tubes were made; all were individually leak tested by attaching the P.V.C. tube to a compressed air supply, blocking the open end of the needle by pushing it into a bung and immersing the whole arrangement in a basin of water. When airtight the tubes were inserted into a pipe (through a wall in its side) next to a pitot tube and the differential pressure between the needle tube and the

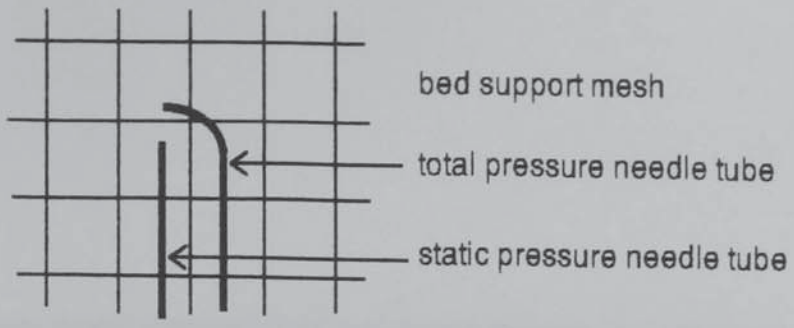

Figure 7.9. Arrangement of the Needle Tubes.

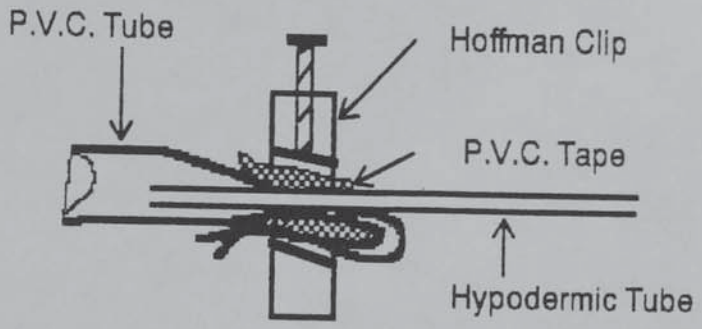

Figure 7.10. Sectional Detail of the Attachment of the Needle Tube and the P.V.C. Tube.

relevant pitot tube taping measured. Provided the ends of the needle tubes are not blocked the differential pressure (measured over a range of flowrates) is 0.01" W.G. or less which is comparable to the resolution of the micromanometer.

The needles are attached to the mesh in pairs (total and static) every 20 cm along the bed; from the beginning of the bed for the duct side of the support mesh and from 10 cm from the beginning of the bed on the bed side. They are attached so the pressure readings are made precisely at 10, 20, 30, etc. cm from the beginning of the bed.

7.5. CONCLUSIONS.

Apparatus has been designed, built and commisioned to investigate the two dimensional aspects of the fluid mechanics of shallow packed beds and particularly, the effect of the bed base.

The apparatus was specifically designed to facilitate the realisation of a C.F.D. model of it and, to allow the future evaluation of novel bed support distributors.

Plate 7.5. The attachment of the Needle Tube and the P.V.C. Tube.

Novel pressure probes have been designed and made. These measure the total and static pressures (and hence dynamic pressures and air velocities) either side of a bed support and, the static pressure in the bed.

CHAPTER 8

EXPERIMENTAL RESULTS FROM THE TWO DIMENSIONAL APPARATUS

8.1. INTRODUCTION.

This chapter describes and presents the experimental work performed on the two dimensional, shallow packed bed apparatus described in the preceding chapter.

This investigation was performed for two main reasons:

i. To further our understanding of the mechanisms of gas flow in shallow packed beds and, particularly at the base of such beds

ii. To provide experimental data with which results from the C.F.D. models presented in the subsequent chapter can be compared. This comparison directs futher developments to the original model.

A range of experimental measurements are presented, as follows (the numbers given in brackets are the section numbers in this chapter):

i. Flow visualisation using smoke tracers (8.2),

ii. Point velocity profiles above the bed (8.3),

iii. Duct pressures and velocity profiles (8.4),

iv. Pressures and velocities at the bed base (8.5),

v. Static pressures in the bed (8.6),

vi. Experimental measurements (i. to iv. above) made when the bed outlet is blocked (8.8).

The instrumentation etc. used to collect these measurements is as previously described in Chapter 6. As discussed in Chapter 7 a range of duct outlets are used to fully examine the fluid mechanics of the bed base. These are as follows:

i. Duct outlet end open,

ii. Duct outlet end partially blocked (with the perforated plate described in chapter 7)

iii. Duct outlet end blocked at the end of the bed.

In all cases the bed is 1.5 m long, bed heights of 5 and 10 cm. were used with duct heights of 5 and 10 cm. The majority of measurements were made with both bed and duct heights equal to 10 cm. In all cases the

bed is packed with 12 mm spheres and supported on wire mesh as described in section 7.3.1.

A range of flowrates were investigated corresponding approximately to average velocities in the duct before the beginning of the bed of; 11.5, 21.0, 27.5 & 33.5 ms^{-1} for the 10 cm high duct and 23.0 & 42.0 ms^{-1} for the 5 cm high duct. When the 5 cm high duct is used the maximum flowrate obtainable is equivalent to a Dall Tube pressure drop of 22 cm W.G. (due to the higher velocities in the smaller duct) and lower flowrates only can be investigated. The Dall Tube calibration is presented as graph 6.3 of Chapter 6.

8.2. FLOW VISUALISATION.

In addition to the classic pressure and velocity measurements that describe a fluid flow, flow visualisation is a useful technique since it allows a fuller understanding of fluid flow phenomena, particularly since 'parcels' of fluid can be followed through the apparatus.

The apparatus was constructed of perspex to permit this type of study and a Nutem 206 'smoke' machine used (as described in section 6.6). It was found that the smoke was best observed using a 100 watt directional spotlight mounted above the bed, the flow is observed from one side of the rig while the other side is 'masked' using a black, photographers' cloth. Smoke plumes can then be observed above and below the bed (but, due to the opacity of the glass beads used as packing not in the bed). Unfortunately the low smoke density of these plumes and the reflective nature of the perspex walls of the apparatus has prevented satisfactory photography of the flow visualisation experiments. The clearest smoke plumes were obtained with the smoke machine settings as follows:

Heater Voltage	18
Pump Speed	7

These experiments were only performed for duct and bed heights of 10 cm.

In section 8.3 (below) it is shown that the flow patterns in the apparatus are the same regardless of the flowrate studied. Hence, the smoke visualisation experiments were only performed at one flowrate. The flowrate selected was that where the smoke is most clearly visible and is equivalent to an average velocity in the duct before the bed of about 27.5 ms^{-1}. Three separate sets of experiments were performed as follows:

i. Smoke injected into the duct,

ii. Smoke injected into the base of the bed,

iii. Smoke injected so as to identify the location of a so-called separating streamline (these experiments are strictly a subset of i.).

In these experiments a clear form of smoke plume leaving the bed has been identified. This is first described and characterised.

8.2.1. The Smoke Plume.

The plume observed consists of a central, denser region with less dense regions on either side as illustrated in figure 8.1.

Figure 8.1. The Appearance of The General Smoke Plume.

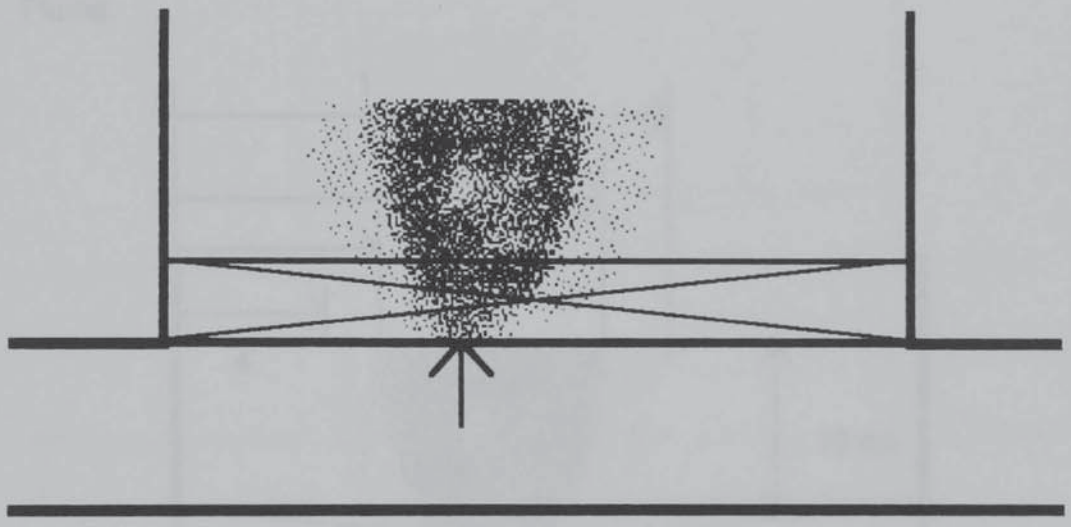

Typically the plume is slightly shifted in the direction of flow in the duct. The less dense outer plumes are not always observed; usually, they are only observed on the downstream side of the denser plume.

From these observations it can be concluded that the fluid flowing through the bed has a horizontal component of velocity as well as a vertical one. This is implied by the vectorial Ergun Equation and shows the need for a slip boundary condition for the bed base (rather than a 'no-slip' form). The existence of the outer plume may be due to the natural or small-scale flow maldistribution caused by the gross effects of the individual, randomnly positioned packing pieces. In addition, the observations that the outer plume is more frequently seen on the

downstream side of the denser inner plume, and that when the outer plume is observed on both sides of the inner plume the downstream part of the outer plume is typically larger; suggest that the existence of the outer plume is also due to smoke/air travelling horizontally along the bed base (i.e. above the support mesh and in the higher voidage area at the bed boundary). It is suggested that the positioning of the less dense plume up or downstream of the injection point indicates in which direction the gas at the bed base is flowing. Furthermore the width of this plume may give an indication of the air velocity in this area.

Various measurements can be made that describe the plume leaving the bed and are shown in figure 8.2.

Figure 8.2. The Experimental Measurements Describing the Smoke Plume.

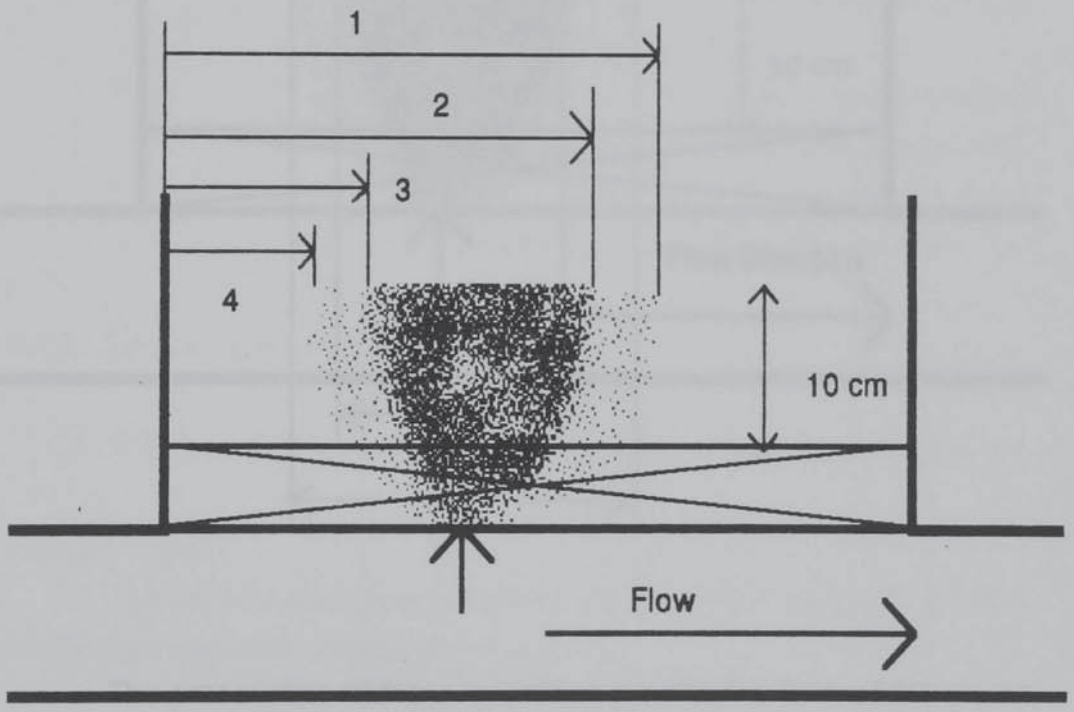

These measurements were made 10 cm above the bed because:

i. It is difficult to clearly and quantitatively observe the plume below this height because of the handy angle bracing attached to the apparatus,

ii. Between the top of the bed and this point the plume becomes wider whereas above this point it remains constant in size.

A number of derived quantities that describe the plume can be obtained from the experimental measurements (shown in figure 8.2), these derived quantities are illustrated in figure 8.3.

Figure 8.3. Derived Quantities Describing The Smoke Plume.

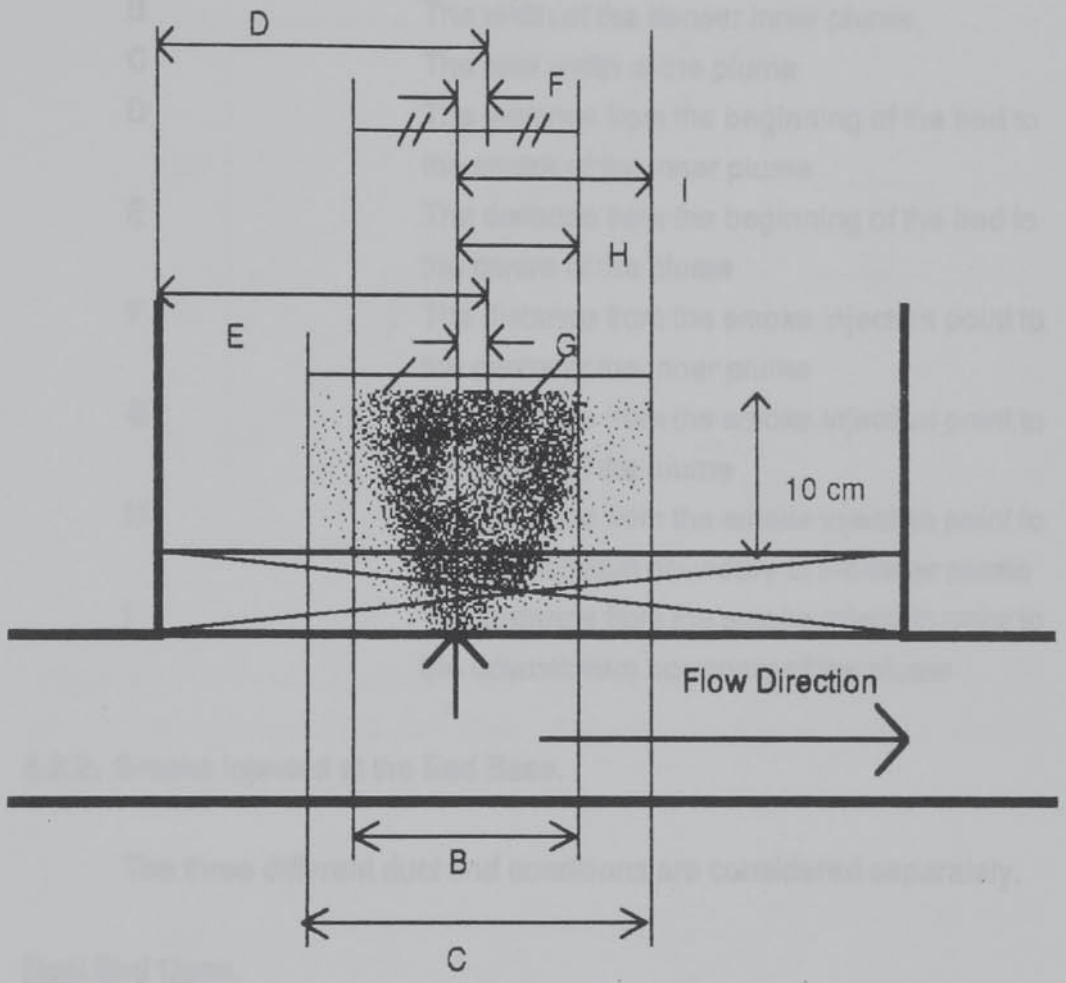

The prescription of these quantities permits the form of the plume and changes in it with position along the length of the bed to be rigorously examined in graphical form. Table 8.1 describes and defines these quantities:

Having described the generalised smoke plume, the results obtained for the three experimental situations above are now presented.

Table 8.1. Definition of the Derived Quantities Describing the Smoke Plume.

LETTER	DESCRIPTION;
B	The width of the denser inner plume
C	The total width of the plume
D	The distance from the beginning of the bed to the centre of the inner plume
E	The distance from the beginning of the bed to the centre of the plume
F	The distance from the smoke injection point to the centre of the inner plume
G	The distance from the smoke injection point to the centre of the plume
H	The distance from the smoke injection point to the downstream boundary of the inner plume
I	The distance from the smoke injection point to the downstream boundary of the plume

8.2.2. Smoke Injected at the Bed Base.

The three different duct end conditions are considered separately.

Duct End Open.

The experimental measurements are presented as graph 8.1 and the derived quantities as graphs 8.2 and 8.3.

Graph 8.1. Experimental Measurements of the Smoke Plume with Smoke Injected at the Bed Base. Average Velocity in the Duct Before the Bed = 27.3 ms^{-1}. Duct End Open.

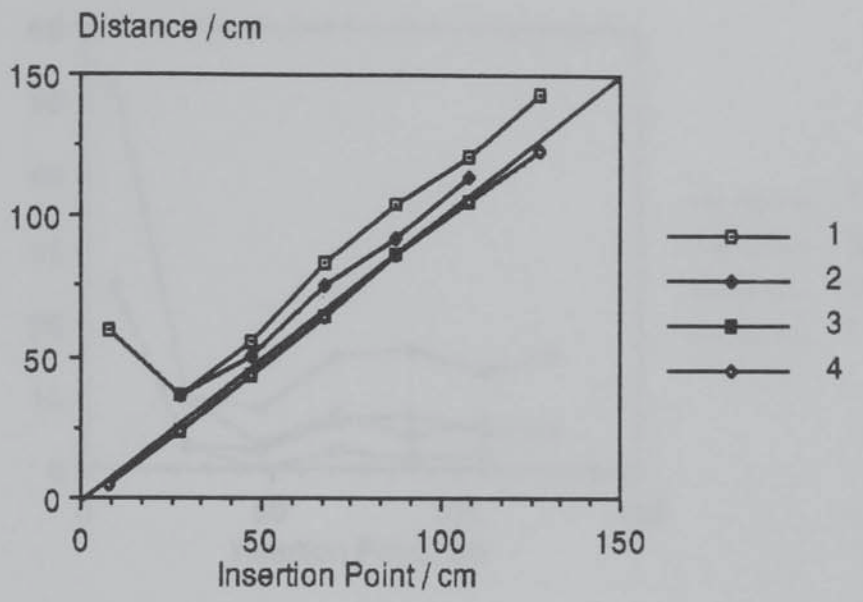

Graph 8.2. Derived Quantities from Measurements of the Smoke Plume with Smoke Injected at the Bed Base. Average Velocity in the Duct Before the Bed = 27.3 ms^{-1}. Duct End Open.

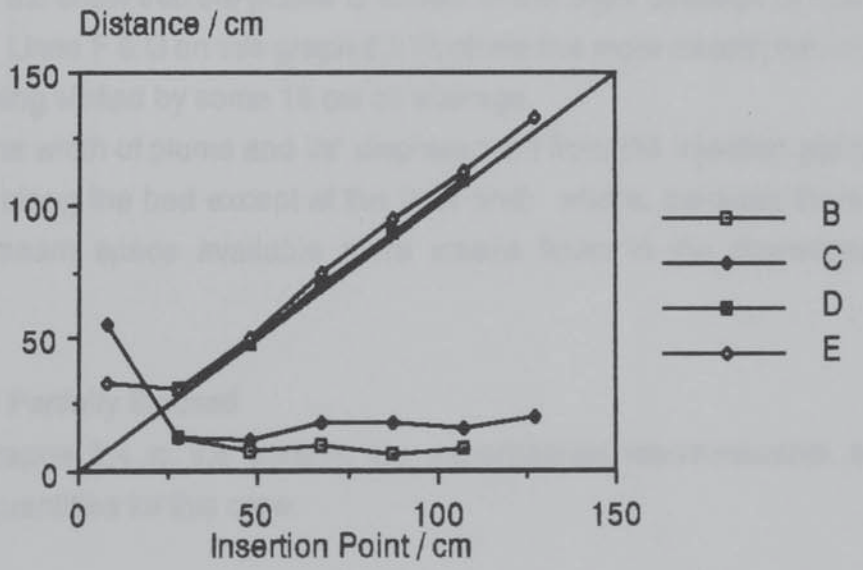

Graph 8.3. Derived Quantities from Measurements of the Smoke Plume with Smoke Injected at the Bed Base. Average Velocity in the Duct Before the Bed = 27.3 ms^{-1}. Duct End Open.

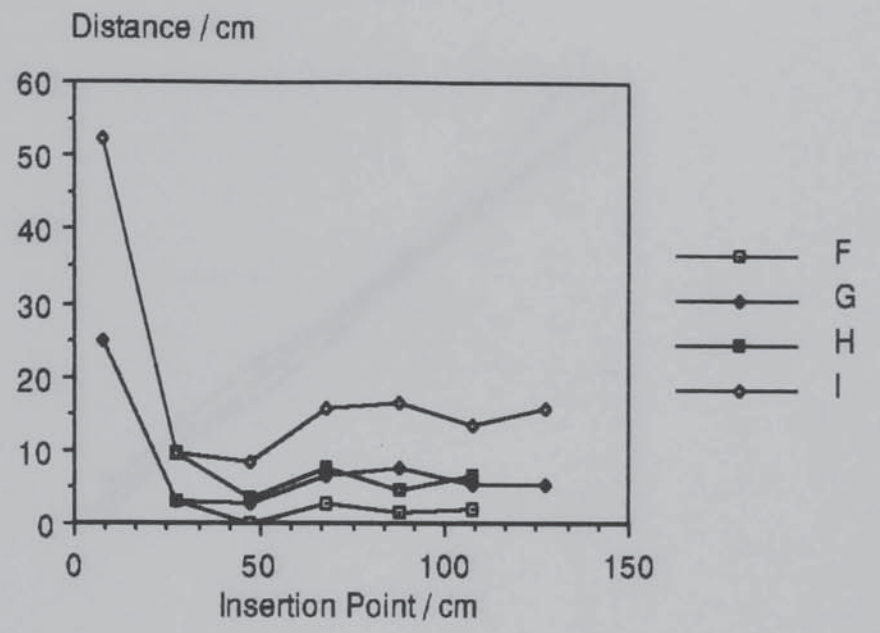

The coincidence of readings 3 and 4 shows the lack of the less dense plume upstream of the injection point. A less dense downstream plume is observed and this is approximately constant in width along the bed, as is the denser inner plume (lines B & C of graph 8.2). Lines D & E on graph 8.3 show that the plume is shifted in the main direction of flow in the duct. Lines F & G on this graph 8.3 illustrate this more clearly; the inner plume being shifted by some 15 cm on average.

The width of plume and its' displacement from the injection point is constant along the bed except at the inlet end; where, because there is less upstream space available more smoke flows in the downstream direction.

Duct End Partially Blocked

Graphs 8.4 to 8.6 present the experimental measurements and derived quantities for this case.

Graph 8.4. Experimental Measurements of the Smoke Plume with Smoke Injected at the Bed Base. Average Velocity in the Duct Before the Bed = 27.5 ms^{-1} Duct End Partially Blocked.

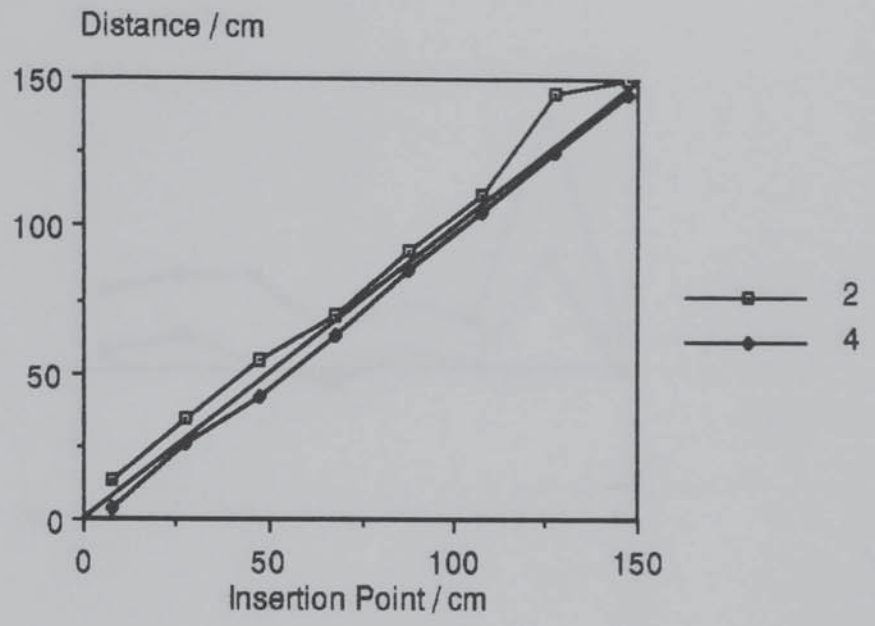

Graph 8.5. Derived Quantities from Measurements of the Smoke Plume with Smoke Injected at the Bed Base. Average Velocity in the Duct Before the Bed = 27.5 ms^{-1}. Duct End Partially Blocked.

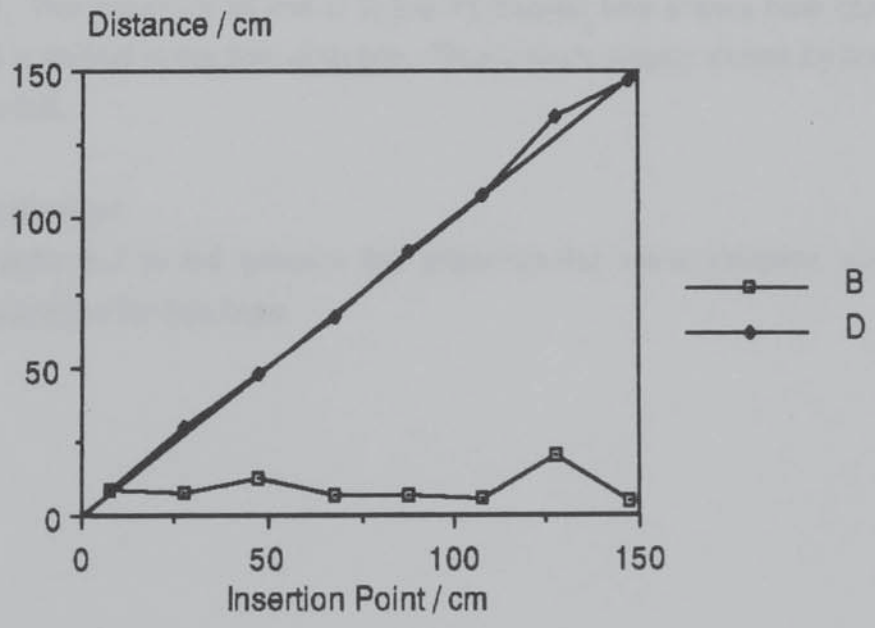

Graph 8.6. Derived Quantities from Measuremets of the Smoke Plume with Smoke Injected at the Bed Base. Average Velocity in the Duct Before the Bed = 27.5 ms^{-1}. Duct End Partially Blocked.

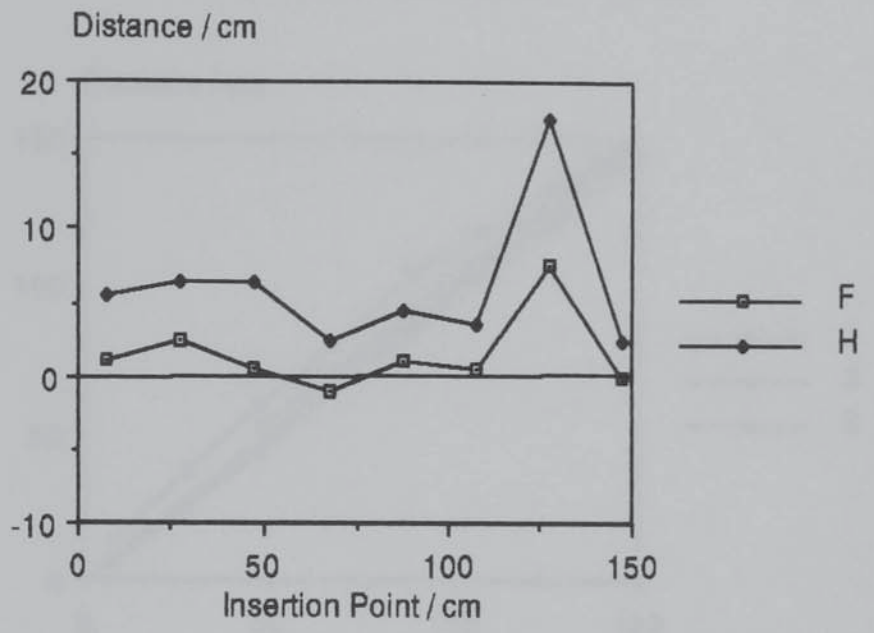

Graph 8.4 shows that there is no less dense outer plume. This is due to the lower horizontal component of velocity in the bed since more gas leaves through the bed than in the duct open case. It also shows the constant width of the plume, which is more clearly indicated by line B of graph 8.5. The proximity of line D to the 45 degree line shows how little the plume is shifted in the flow direction. This is more clearly shown by line F of graph 8.6.

Duct End Blocked.

Graphs 8.7 to 8.9 present the experimental measurements and derived quantities for this case.

Graph 8.7. Experimental Measurements of the Smoke Plume with Smoke Injected at the Bed Base. Average Velocity in the Duct Before the Bed = 27.3 ms^{-1}. Duct End Wholly Blocked (at the end of the bed).

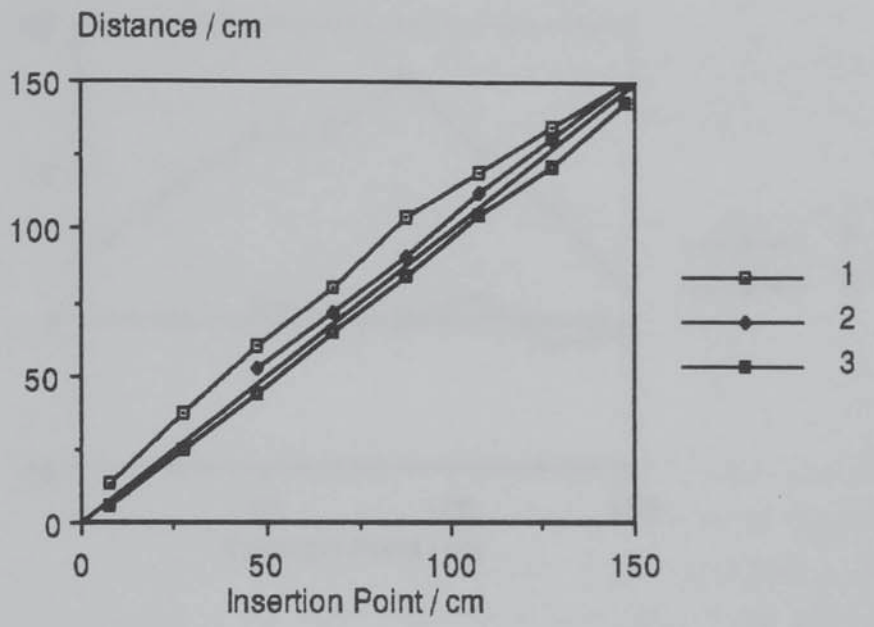

Graph 8.8. Derived Quantities from Measurements of the Smoke Plume with Smoke Injected at the Bed Base. Average Velocity in the Duct Before the Bed = 27.3 ms^{-1}. Duct End Wholly Blocked (at the end of the bed).

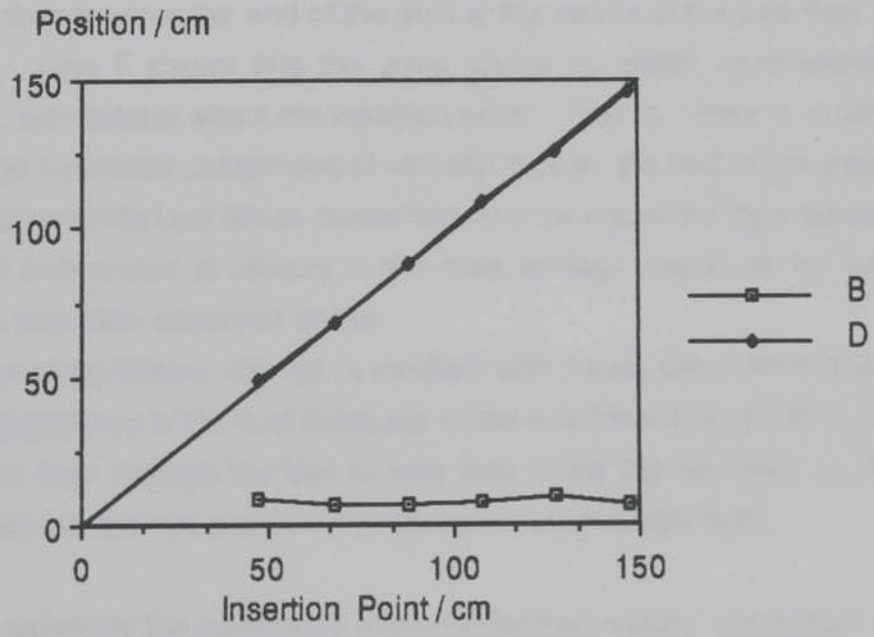

Graph 8.9. Derived Quantities from Measurements of the Smoke Plume with Smoke Injected at the Bed Base. Average Velocity in the Duct Before the Bed = 27.3 ms^{-1}. Duct End Wholly Blocked (at the end of the bed).

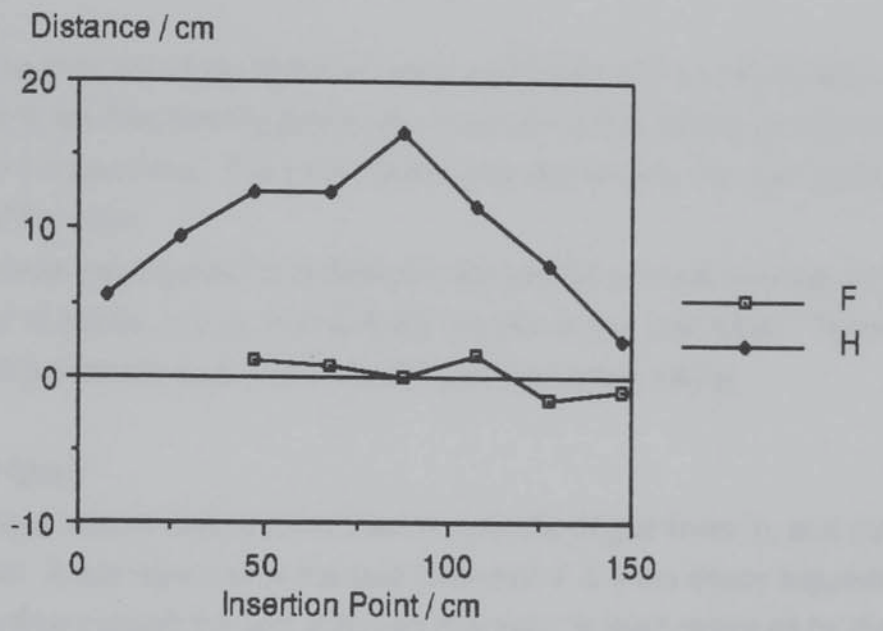

In this case the less dense, downstream plume is again observed although this only appears above the last two thirds of the bed. (Lines 1 & 2 of graph 8.7).

Line B of graph 8.8 shows the constancy of width of the denser, inner plume. Line H of graph 8.9 indicates that the plume as a whole is shifted further towards the end of the duct at the centre of the bed than at the ends. Line F shows that the inner plume is, within experimental accuracy, symmetrical about the insertion point. That is, there is a very much lower horizontal component of velocity through the bed in this case. The existence of the less dense plume can then be explained by a greater horizontal component of velocity in the high voidage region at the bed base than has been observed above.

The observations can be reconciled with those above as follows: the higher pressure in the duct (because all the gas flows through the bed) causes the flow through the bed to vary less along the bed than in the other cases (i.e. to have a smaller horizontal velocity component).

In summary the magnitude of the horizontal velocity component in and below the bed determines the flow patterns observed. This component of velocity is greatest when the duct end is open and smallest

when it is blocked. The significant effect of the bed base and support; and in particular, the region of higher voidage at the bed boundary is apparent.

8.2.3. Smoke Injected into the Duct Below The Bed.

A second set of experiments were performed where the smoke is injected into the free flowing gas in the duct, the probe being positioned parallel to the bed base. The smoke was observed leaving the bed and at the end of the duct.

Smoke was injected at positions 0, 55, and 95 cm from the inlet end of the bed at points 0.2, 2, 4, 6, 8 & 9.8 cm below the bed base. These results are presented as tables 8.2 to 8.4 and discussed below.

Duct End Open.

These results clearly show that the majority of gas flows in, and out of, the duct. A thin layer below the bed (between 2 & 4 cm deep) supplies the gas to flow through the bed although this layer is itself renewed by the gas in the remainder of the duct. The form and size of the plumes observed in this part of the study are consistent with those discussed above.

Duct End Partially Blocked.

A similar picture emerges as for the duct open case although the 'layer' supplying gas to the bed is wider since more gas leaves through the bed. In addition it can be seen that this layer gets thinner along the bed as would be expected. This implies the existence of a streamline as illustrated in figure 8.4 which is such that the gas above the streamline leaves through the bed and that below through the duct (ignoring re-circulation and turbulence effects).

Table 8.2. Results for Smoke Injected into the Duct. Duct End Open. Average Velocity in the Duct Before the Bed 27.3 ms^{-1}.

Injection Position cm	Injection Point Below Bed Base cm	Smoke Plume Boundary Position cm 1	2	3	4	Plume Width cm Inner	Total	Smoke Flow Through Duct Outlet
0	0.2	123	40	0		40	123	none
	2.0		119	73		48	48	none
	4.0							all
	6.0							all
	8.0							all
	9.8							all
55	0.2	130	98	67	55	31	75	none
	2.0		135	91		44	44	none
	4.0							all
	6.0							all
	8.0							all
	9.8							all
95	0.2		129	97		32	32	none
	2.0	150	128	112	104	16	46	some
	4.0							all
	6.0							all
	8.0							all
	9.8							all

Table 8.3. Results for Smoke Injected Into The Duct. Duct End Partially Blocked. Average Velocity in the Duct Before the Bed 27.3 ms^{-1}.

Injection Position cm	Injection Point Below Bed Base cm	Smoke Plume Boundary Position cm 1	2	3	4	Plume Width cm Inner	Total	Smoke Flow Through Duct Outlet
0	0.2	55	17	0		17	55	none
	2.0	128	109	73	46	36	62	none
	4.0		137	95		42	42	some
	6.0		150	110		40	40	some
	8.0							all
	9.8							all
55	0.2		86	58		28	28	none
	2.0	145	104	90		14	55	none
	4.0		150	117		33	33	some
	6.0		150	125		25	25	some
	8.0							all
	9.8							all
95	0.2		109	97		12	12	none
	2.0		150	124		26	26	some
	4.0							all
	6.0							all
	8.0							all
	9.8							all

Table 8.4. Results for Smoke Injected Into The Duct. Duct End Wholly Blocked (at the end of the bed). Average Velocity in the Duct Before the Bed 27.3 ms^{-1}.

Injection Position cm	Injection Point Below Bed Base cm	Smoke Plume Boundary Position cm 1	2	3	4	Plume Width cm Inner	Total	Smoke Flow Through Duct Outlet
0	0.2		4	0		4	4	-
	2.0		68	18		50	50	-
	4.0		103	42		61	61	-
	6.0		128	78		50	50	-
	8.0	137	119	111	103	8	34	-
	9.8	150	134	122	115	12	35	-
55	0.2	72	66	55		11	17	-
	2.0		91	71		20	20	-
	4.0		120	86		34	34	-
	6.0		128	94		34	34	-
	8.0		143	106		37	37	-
	9.8		150	115		35	35	-
95	0.2	107	102	95		7	12	-
	2.0	150	125	107		18	43	-
	4.0		150	110		40	40	-
	6.0		150	112		38	38	-
	8.0		150	115		35	35	-
	9.8		150	121		29	29	-

Figure 8.4. A Streamline that Divides the Flow in the Duct.

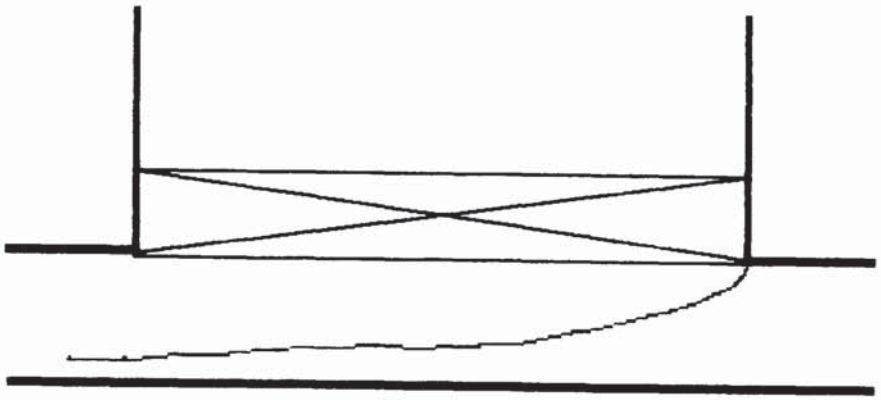

The smoke plumes described in table 8.3 can be seen to become broader and then narrower along the bed as would be expected from the discussion above concerning renewal of the layer of gas that supplies the bed (not to be confused with a boundary layer at the bed base which these results do not show) and, a consideration of the vectorial Ergun Equation. This observation and the results also suggest that more gas leaves the bed in the central part than at the duct inlet and outlet ends.

Duct End Blocked.

Referring to table 8.4, it can be seen that the plumes are narrower when the smoke is injected at 55 cm and, to a lesser extent at 95 cm, than at 0 cm. This suggests that more gas leaves the bed in the middle and at the duct outlet end than at the inlet end. It can also be seen that the widest plumes are obtained when the smoke is injected in the middle of the duct because the gas flows fastest here. When smoke is injected at 95 cm recirculation is observed above the bed close to the (outlet) end wall.

8.2.4. The Separating Streamline.

Smoke injected at certain points in the duct leaves through both the bed and the duct end. These points must lie on the 'separating streamline' discussed above. There is actually a vertical range (of about 1.5 cm.) over which this occurs due to turbulence. However, taking the centre of this range the position of the streamline can be experimentally identified.

The streamline will have the form shown in figure 8.5 for the duct open case, figure 8.6 for the duct partially blocked and figure 8.7 for the duct wholly blocked.

Figure 8.5. The Separating Streamline for the Duct Outlet Open (schematic).

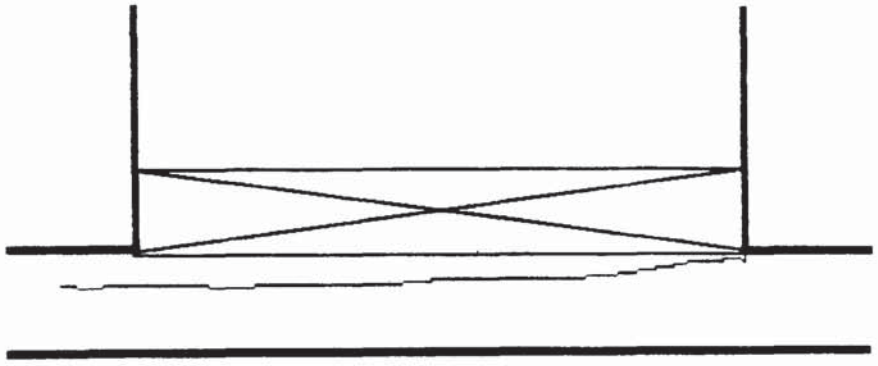

Figure 8.6. The Separating Streamline for the Duct Outlet Partially Blocked (schematic).

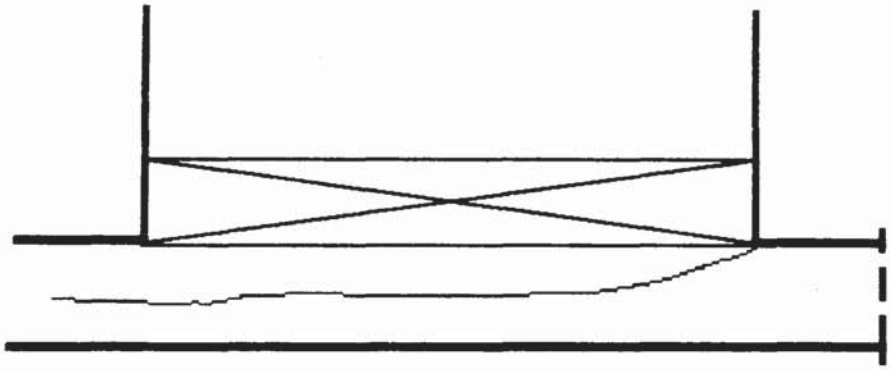

Figure 8.7. The Separating Streamline for the Duct Outlet Wholly Blocked (schematic).

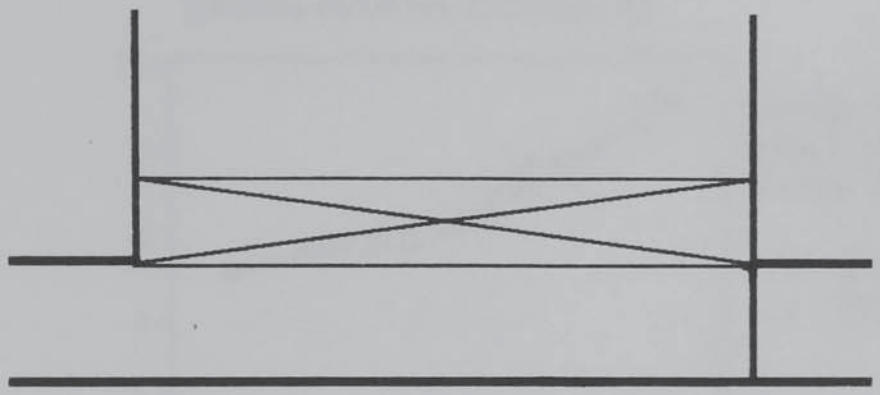

The streamlines for two flowrates (at velocities in the duct before the bed of approximately 21.0 and 33.5 ms^{-1}) and the two relevant duct end conditions (open & partially blocked) for 10 cm deep ducts and 5 or 10 cm deep beds are presented as graphs 8.10,11,12 & 13.

Graph 8.10. The Separating Streamline. Duct End Open. Bed Height 10 cm.

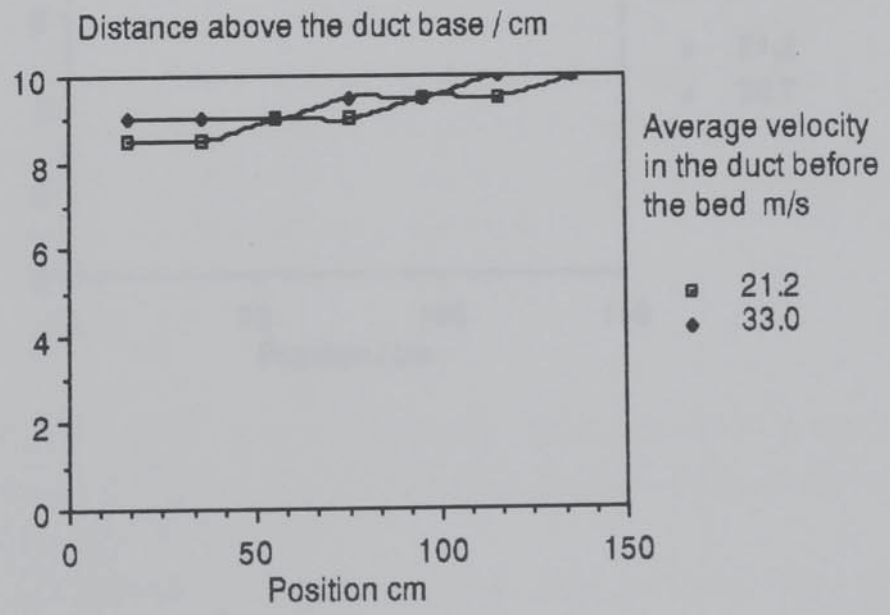

Graph 8.11. The Separating Streamline. Duct End Partially Blocked. Bed Height 10 cm.

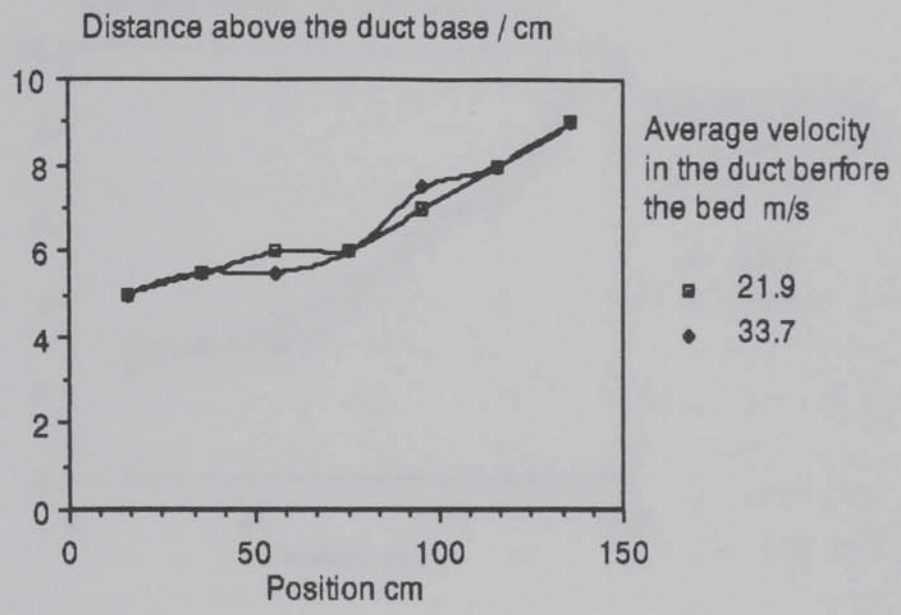

Graph 8.12. The Separating Streamline. Duct End Open. Bed Height 5 cm.

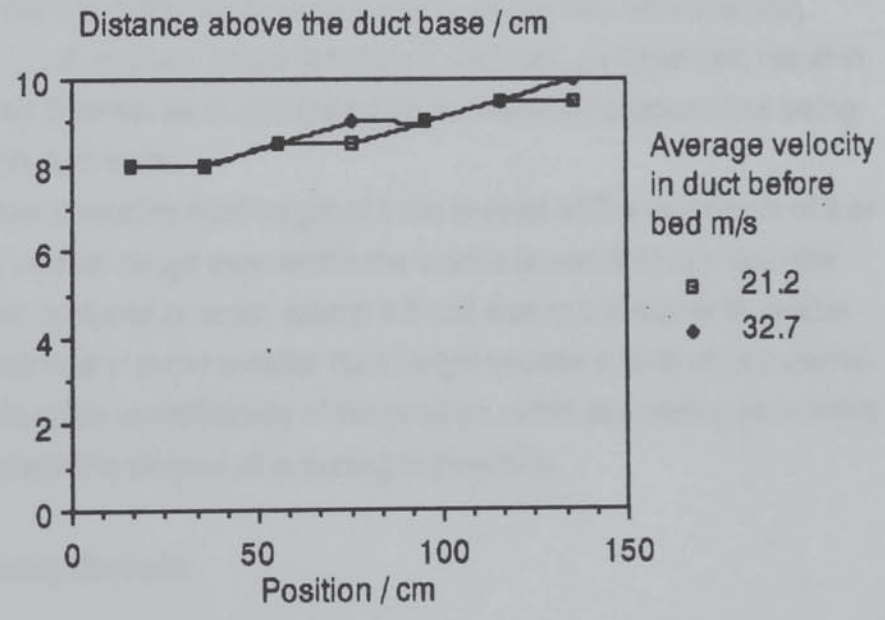

Graph 8.13. The Separating Streamline. Duct End Partially Open. Bed Height 5 cm.

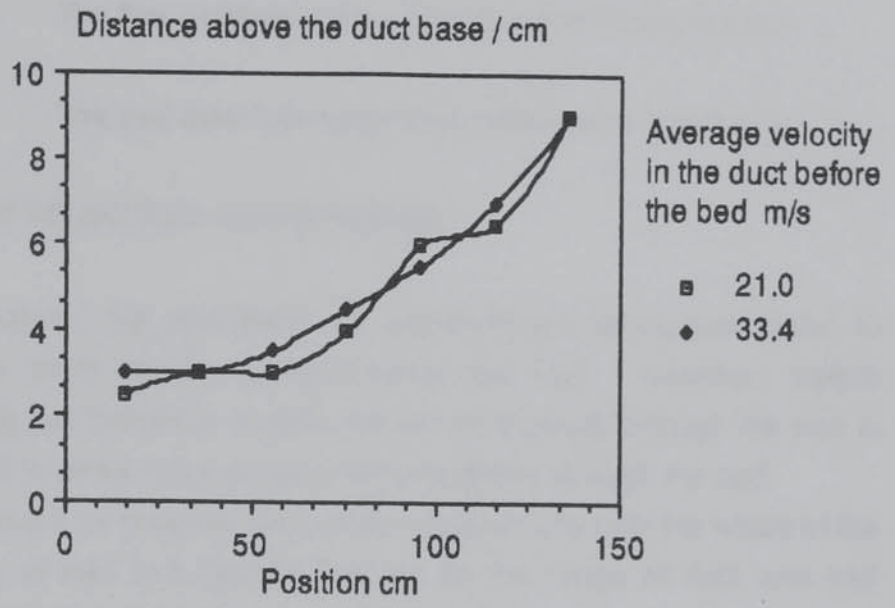

These graphs show that;

i. The streamline location is independant of flowrate (and imply that the flow patterns in the apparatus do not vary with flowrate).

ii. A shallow (lower resistance) bed will, as expected, result in a higher bed flowrate as is evidenced by the separating streamline being closer to the duct base.

When a smaller duct height of 5 cm is used with a bed depth of 5 or 10 cm, the vertical range over which the smoke leaves through both the bed and the duct end is larger (about 2.5 cm) due to the higher flowrates which, combined with the smaller duct height causes a level of turbulence which renders the identification of the position of the separating streamline with an acceptable degree of accuracy impossible.

8.2.5. Closing Remarks.

This study of the fluid dynamic behaviour at a packed bed/free fluid boundary using the flow visualisation technique of smoke tracing, allows a number of conclusions to be drawn:

i. Fluid flows through the bed horizontally as well as vertically.

ii. A streamline exists which divides the flow in the duct such that all the gas leaving the bed is above this streamline and the remainder

(that leaves through the duct outlet) below. This new concept is of use in considering and interpreting the remaining experimental results and will aid the development of the computer model of this apparatus.

iii. The flow patterns in the apparatus are independant of flowrate.

iv. The bed base has a significant effect on flow patterns.

8.3. POINT VELOCITIES ABOVE THE BED.

Section 7.3.2 discussed the measurement techniques used to obtain the point velocity profiles above the bed. However, before considering the individual profiles the overall flowrate through the bed is considered in terms of the average velocity of flow through the bed.

Graph 8.14 presents such an average velocity over the whole of the (centreline of the) bed against flowrate for the range of duct and bed heights, flowrates and duct end conditions used.

Graph 8.14. Average Velocity above (the centreline of) the Bed against flowrate for Various Duct and Bed Heights and Duct End Conditions.

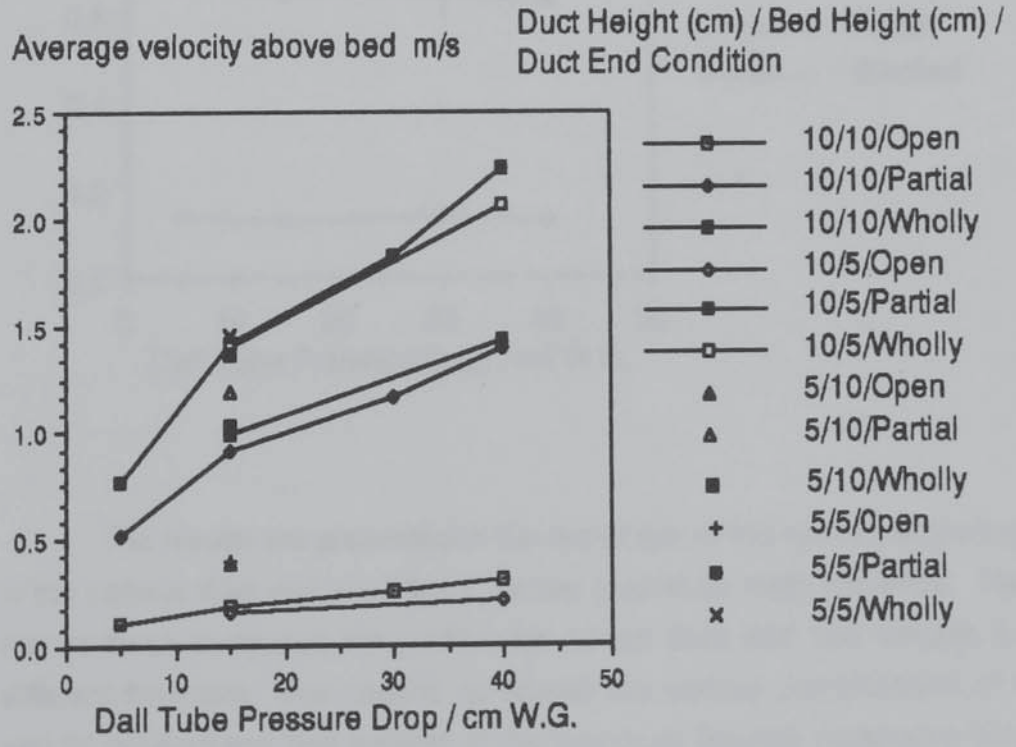

It can be seen that flow through the bed increases with flow into the apparatus and, as expected, that higher flowrates through the bed are observed as the duct end is blocked. Graph 8.15 shows the ratio of flow leaving through the bed to that entering (i.e. a 'diversion ratio'). This is constant with flowrate for all duct end conditions and confirms that the overall flowrate through the bed is not a function of the flowrate entering the apparatus. However, this does not imply that the point velocity distribution is independant of flowrate or duct end condition.

Graph 8.15. The Ratio of Flow Leaving Through the Bed to that Entering The Apparatus Against Flowrate. All Duct End Conditions and Bed and Duct Heights.

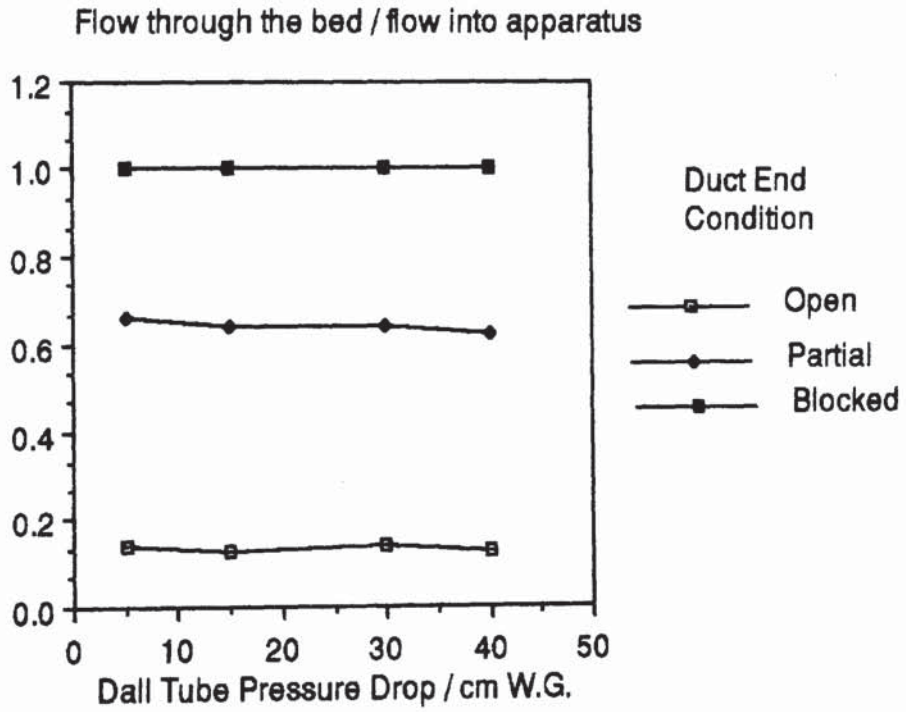

The results are presented in the remainder of this section according to the various duct end conditions; as two graphs for each condition. The first of these compares the profiles for 10 cm duct and bed heights for different flowrates. The second compares the various combinations of 5 and 10 cm duct end bed heights at the maximum flowrate obtainable from the fan for the given duct height.

8.3.1. Duct End Open.

On graph 8.16 the vertical lines show the positions of the bed support support wires (described in section 7.3.1). The graph shows that the bed support wires have a significant effect on the velocity profiles above the bed to the extent that the underlying profile cannot be readily determined. It is however clear that the velocity decreases after the inlet end wall and decreases before increasing at the outlet end wall. This is due to the higher voidage (and lower resistance) in these regions.

It can be seen that at the very beginning and end of the bed high velocities are encountered, these briefly decrease towards the middle where much higher velocities are encountered. Within this central area three clear peaks are apparent. These cannot be due to either bed base unevenness or, 'natural' maldistribution. These may be due to the bed support wires (the positions of which are marked on fthe graph with chain lines) which intrude into the duct very slightly and will also cause an area of localised, higher voidage. The bed support itself is flat and level. This explanation is unconvincing but, the best available. In chapter 10 further evidence is provided to support this conclusion. If the bed support wires were removed either a far narrower rig would have to be used (in which case two-dimensional flow could not be assumed) or, a far more substantial bed base would be required which would obscure the true behaviour of the bed base far more than the existing arrangement.

The profiles are, within experimental accuracy, similar in form for the various flowrates showing that the flow patterns in the apparatus are independant of the flowrate.

Graph 8.17 examines the effects of varying the duct and bed heights shows that other bed/duct height combination profiles are not effected to the same degree by the support wires. It can be concluded that more gas leaves through the central parts of the bed than at the ends.

Graph 8.16. Point Velocities Above the Bed with Position Along The Bed. Duct and Bed Height 10 cm. Various Flowrates. Duct End Open.

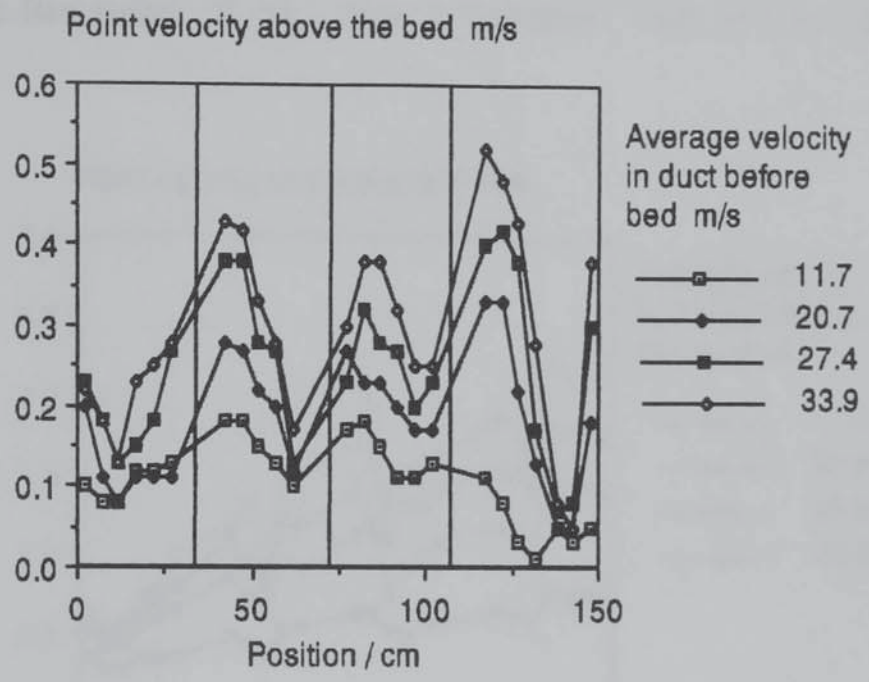

Graph 8.17. Point Velocities Above the Bed with Position Along the Bed. Various Duct and Bed Heights and Flowrates. Duct End Open.

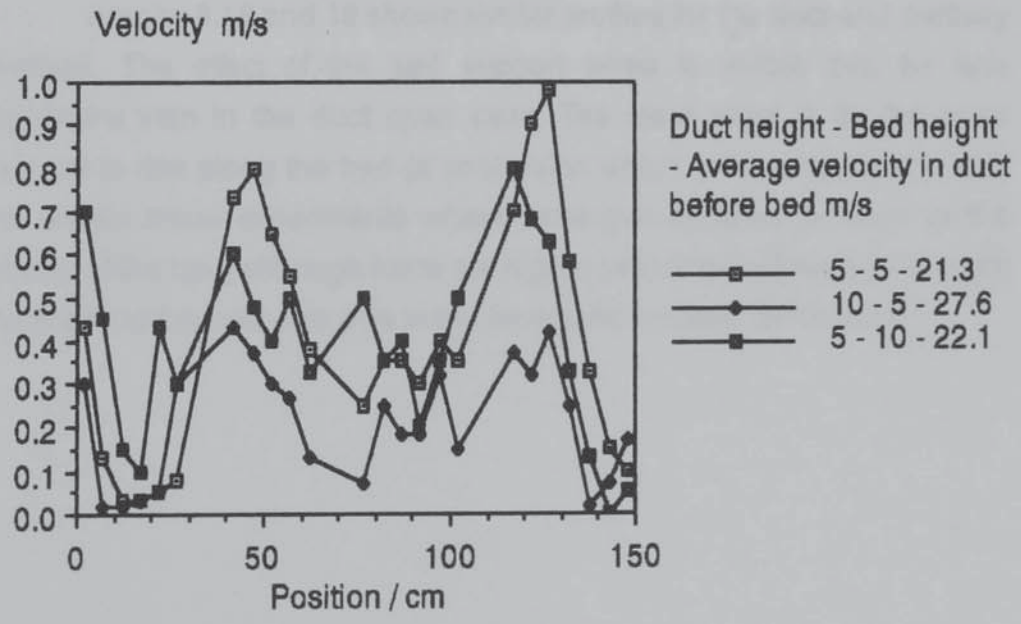

8.3.2. Duct End Partially Blocked.

Graph 8.18. Point Velocities Above the Bed with Position Along The Bed. Duct and Bed Height 10 cm. Various Flowrates. Duct End Partially Blocked.

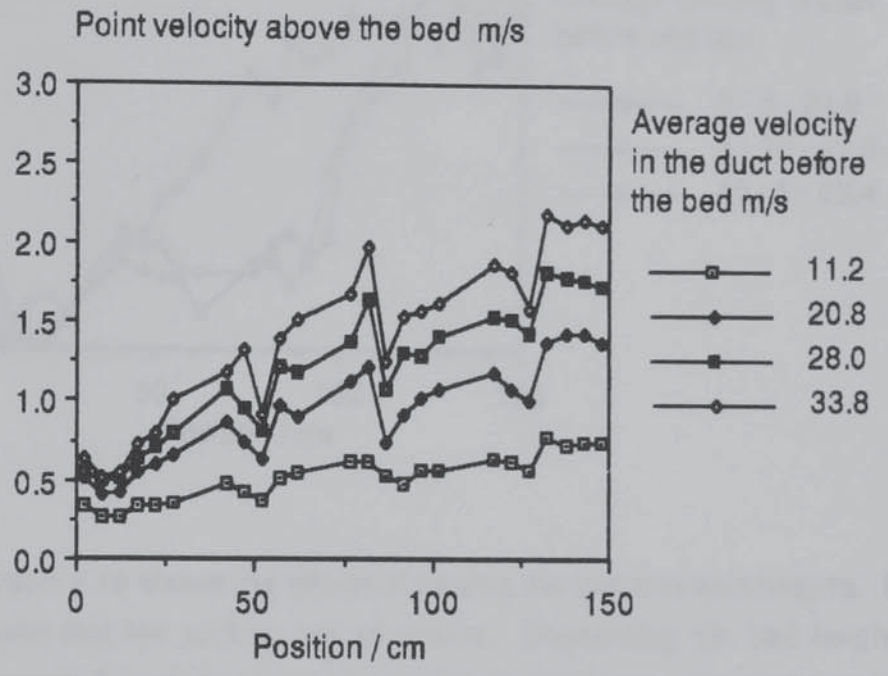

Graphs 8.18 and 19 shows similar profiles for the duct end partially blocked. The effect of the bed support wires is visible but, far less significant than in the duct open case. The clear trend is for the point velocity to rise along the bed (a conclusion which is in contradiction with the smoke tracer experiments where more gas appears to leave in the middle of the bed) although there are higher velocities followed by a slight decrease at the inlet end; due to the increased voidage at this point.

Graph 8.19. Point Velocities Above the Bed with Position Along the Bed. Various Duct and Bed Heights and Flowrates. Duct End Partially Blocked.

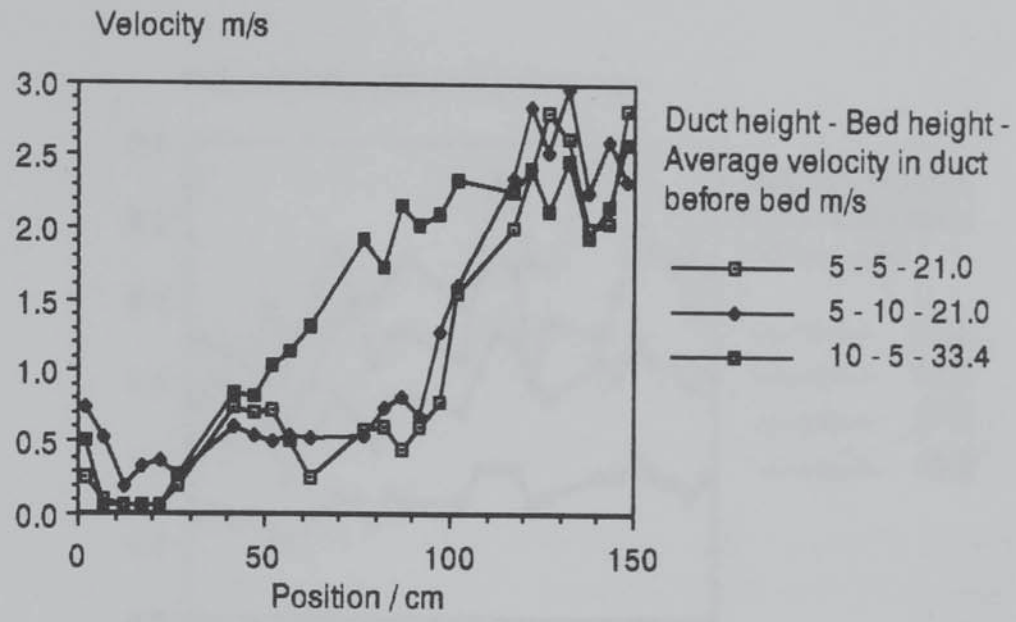

Graph 8.19 shows the effects of varying the bed and duct heights. It can be seen that the profiles are all similar. Decreasing the bed height causes greater flow through the bed whereas decreasing the duct height causes proprtionately more flow to leave through the duct outlet end of the bed (and less through the duct inlet end).

8.3.3. Duct End Wholly Blocked.

These are presented as graphs 8.20 and 8.21; it can be seen that a higher degree of 'natural' maldistribution is observed due to the higher flowrates (the position of the anenometer is not adjusted with flowrate). The effects of the support wires and higher voidage areas at the walls are not apparent. The point velocity above the bed increases with position along it

Graph 8.20. Point Velocities Above the Bed with Position Along The Bed. Duct and Bed Height 10 cm. Various Flowrates. Duct End Wholly Blocked (at the end of the bed).

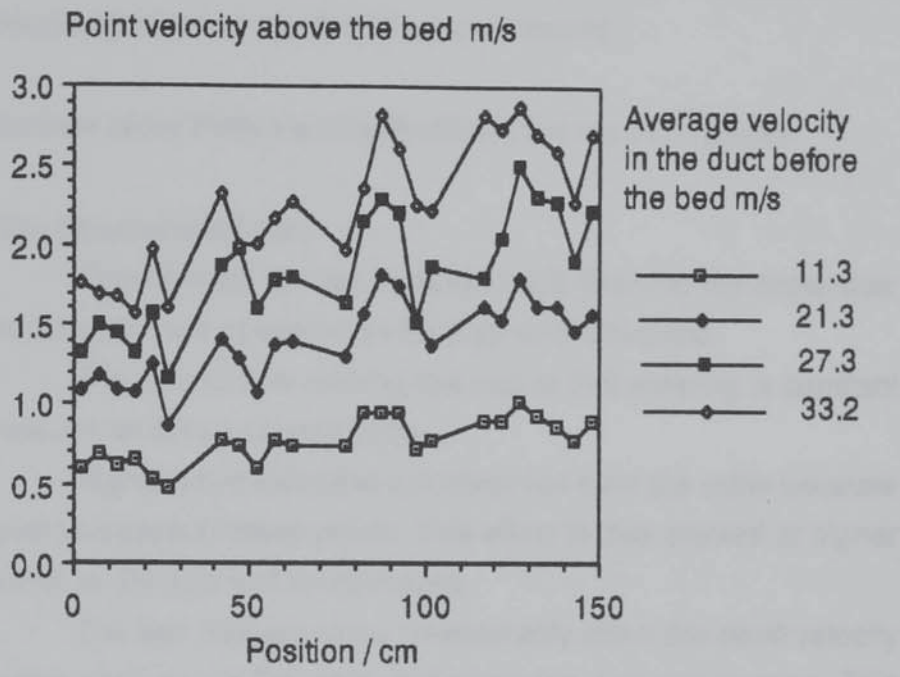

Graph 8.21. Point Velocities Above the Bed with Position Along the Bed. Duct and Bed Height 10 cm. Various Flowrates. Duct End Wholly Blocked (at the end of the bed).

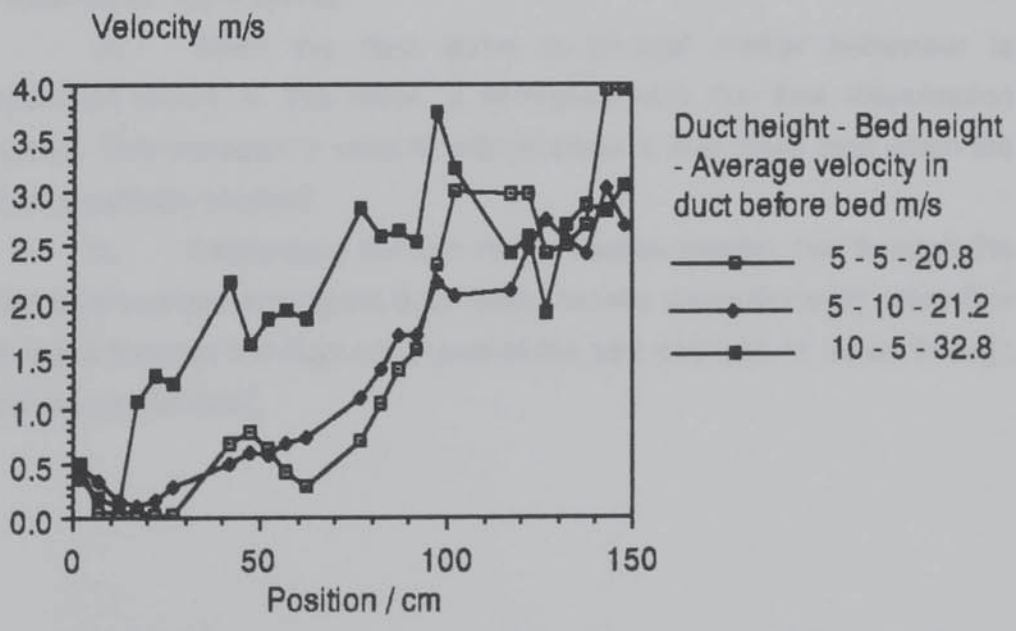

confirming the results of the smoke visualisation experiments, and agreeing with the partially blocked outlet results. However, the increase in velocity with position is steeper when the duct is partially blocked than when it is wholly blocked due to the lower horizontal components of velocity encountered when the duct is wholly blocked.

8.3.4. Overview of the Point Velocity Profile Above the Bed Results.

It can be concluded that:

i. Flow through the bed increases with flow into the apparatus; higher bed flowrates are observed as the duct end is blocked.

ii. The ratio of flow leaving the bed to that entering is constant with flowrate, for all duct end conditions.

iii. Higher point velocities are observed near the walls because of the higher voidages at these points. This effect is less marked at higher flowrates and as the duct end is obstructed.

iv. The bed support wires considerably affect the point velocity profiles, particularly at low flowrates and when the duct end is open. This explanation is not attractive, but the best available.

v. When the duct outlet is open point velocity is highest in the middle of the bed.

vii. When the duct outlet is partially blocked the point velocity rises along the bed. This conclusion contradicts those from the flow visualisation experiments.

viii. When the duct outlet is blocked similar behaviour is observed which, in this case, is consistent with the flow visualisation results. This increase in velocity with position is less steep than when the duct is partially blocked.

ix. Decreasing the bed height causes greater flow through the bed whereas decreasing the duct height causes proportionately more flow to leave through the duct outlet end of the bed and less to leave through the duct outlet itself.

8.4. DUCT PRESSURES AND VELOCITY PROFILES.

These measurements constitute the majority of experimental data obtained on this rig. In order to keep this section to a reasonable length much of the data is not presented and only the results from the maximum flowrates are considered. Results for bed and duct heights of 5 and 10 cm are presented. Initially the various components of pressure are considered along the length of the base of the bed (obtained using the pitot tube). Velocities derived from dynamic pressure measurements are also presented. These results are presented for the various duct end conditions. Finally, velocity profiles in the duct are presented.

8.4.1 Duct End Open.

Graphs 8.22 to 25 show static and total pressures measured with the pitot tube at the bed base. The static pressure is very small (due to the low bed resistance) and the total pressure is composed almost wholly of dynamic pressure. Both pressures show a drop at the beginning of the bed (where the area for flow increases) followed by a steady decrease along the bed, the total pressure then increases after the end of the bed. The results for the smaller duct heights are of a lower quality than those for the higher ducts because the pitot tube is larger with respect to the duct height. The effects of changing the bed and duct heights are as described above.

Graphs 8.26 to 29 show velocity at the same point (determined from dynamic pressure), it can be seen that this data displays the same trends as total pressure: dropping at the beginning of the bed (due to the increase in flow area) but, rising in the duct after the end of the bed as the developed velocity profile reasserts itself.

A less clear and consistent picture emerges in the duct end open case than in the partially and wholly blocked cases (below) because of the lower duct pressures and the predominance of flow through the duct (rather than through both the duct and the bed).

Graph 8.22. Static and Total Pressures Near the Bed Base. Duct End Open. Bed Height = 10 cm. Duct Height = 10 cm. Average Velocity the in Duct Before the Bed 33.9 ms^{-1}.

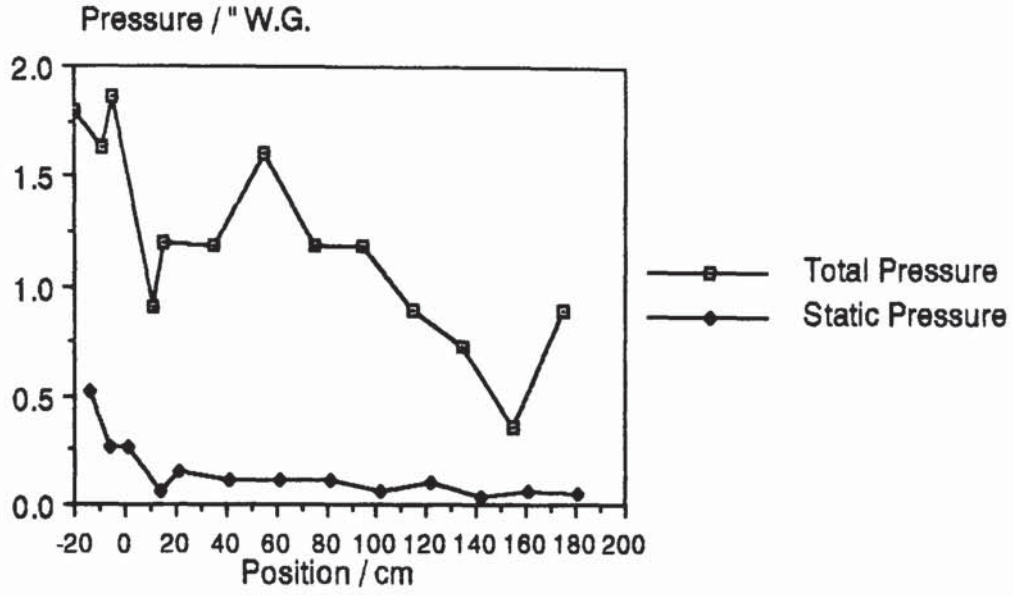

Graph 8.23. Static and Total Pressures Near the Bed Base. Duct End Open. Bed Height = 5 cm. Duct Height = 10 cm. Average Velocity in the Duct Before the Bed 33.4 ms^{-1}.

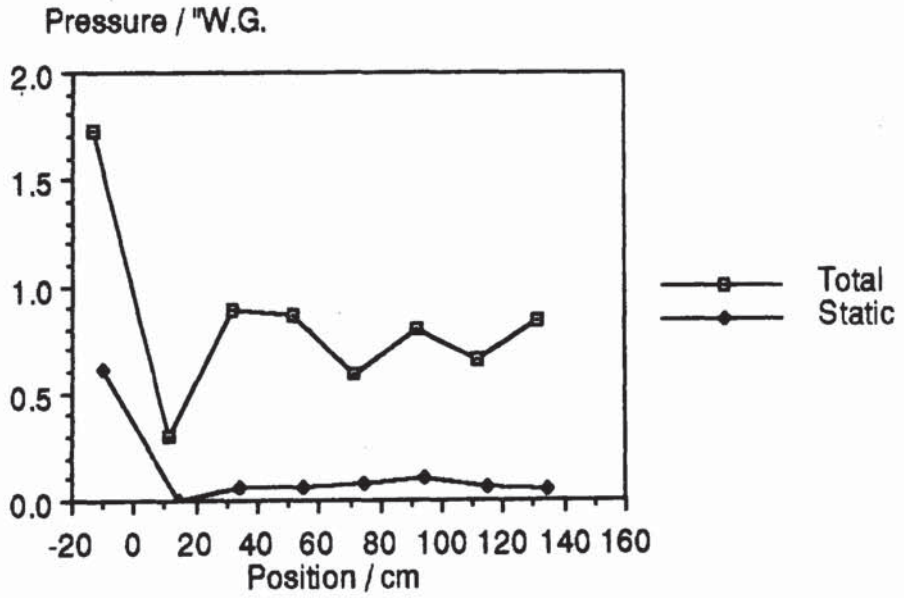

Graph 8.24. Static and Total Pressures Near the Bed Base. Duct End Open. Bed Height = 5 cm. Duct Height = 5 cm. Average Velocity in the Duct Before the Bed 41.7 ms^{-1}.

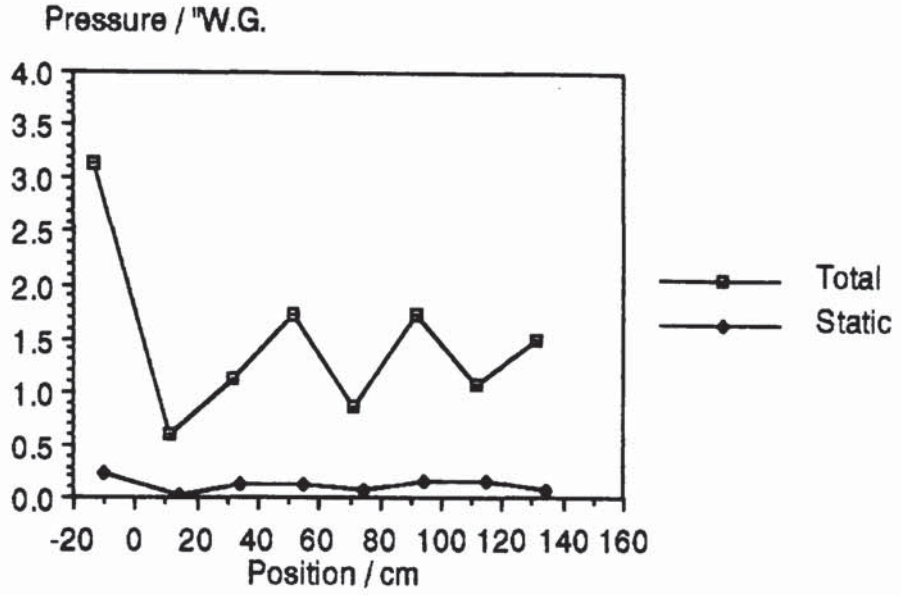

Graph 8.25. Static and Total Pressures Near the Bed Base. Duct End Open. Bed Height = 10 cm. Duct Height = 5 cm. Average Velocity in the Duct Before the Bed 41.6 ms^{-1}.

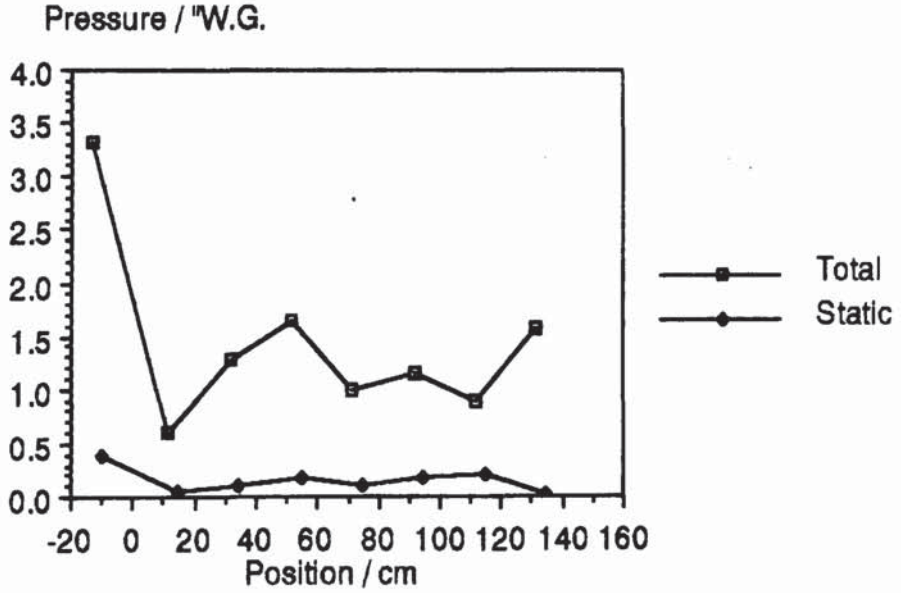

Graph 8.26. Horizontal Velocities (from dynamic pressure measurements) Near the Bed Base. Duct End Open. Bed Height = 10 cm. Duct Height = 10 cm. Average Velocity in the Duct Before the Bed 33.9 ms^{-1}.

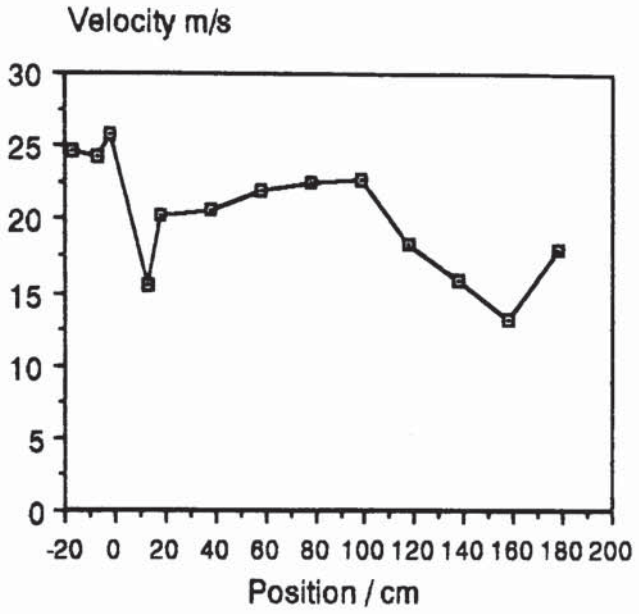

Graph 8.27. Horizontal Velocities (from dynamic pressure measurements) Near the Bed Base. Duct End Open. Bed Height = 5 cm. Duct Height = 10 cm. Average Velocity in the Duct Before the Bed 33.4 ms^{-1}.

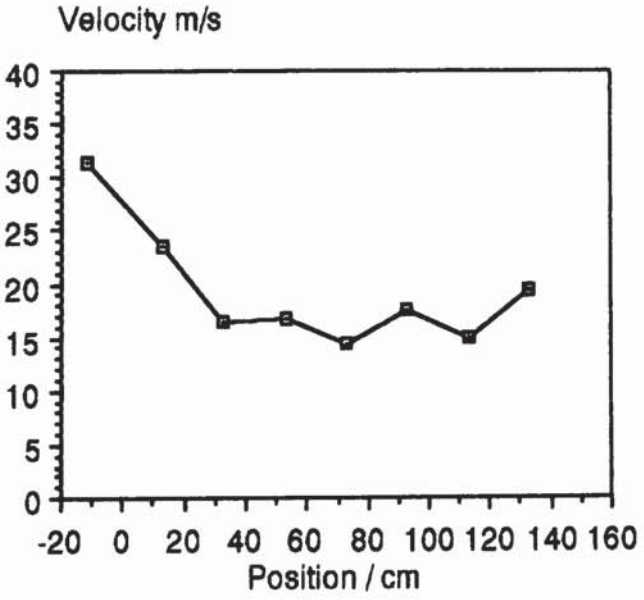

Graph 8.28. Horizontal Velocities (from dynamic pressure measurements) Near the Bed Base. Duct End Open. Bed Height = 5 cm. Duct Height = 5 cm. Average Velocity in the Duct Before the Bed 41.7 ms^{-1}.

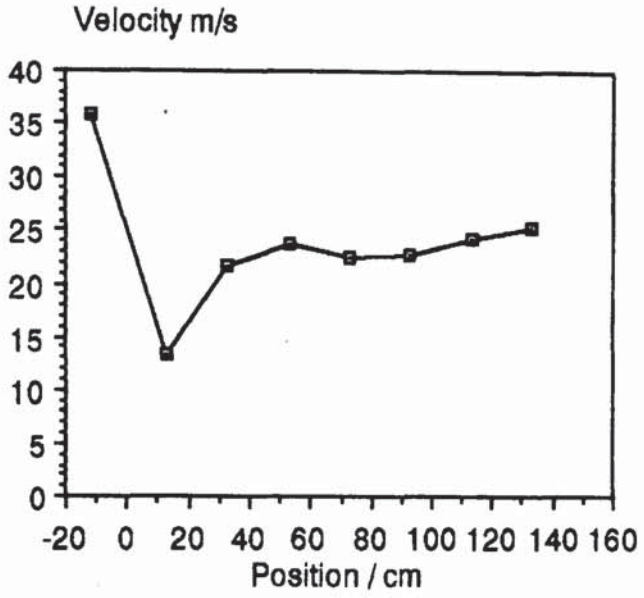

Graph 8.29. Horizontal Velocities (from dynamic pressure measurements) Near the Bed Base. Duct End Open. Bed Height = 10 cm. Duct Height = 5 cm. Average Velocity in the Duct Before the Bed 41.6 ms^{-1}.

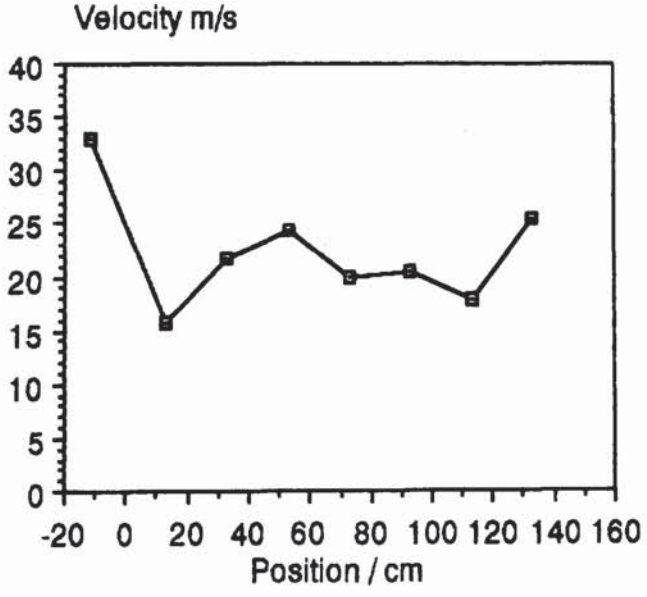

8.4.2. Duct End Partially Blocked.

Graphs 8.30 to 33 show the total and static pressure profiles at the bed base obtained using the pitot tube. The total pressure decreases at the inlet end of the bed and rises to a higher value over the first half of the bed which is then maintained (10 cm beds), with the lower duct heights the total pressure rises consistently towards the (outlet) end of the bed. Static pressure rises from the beginning of the bed to the end. Although with the smaller duct the increase is less pronounced and occurs nearer the outlet end of the bed.

Graphs 8.34 to 8.37 show velocity near the bed base which drops initially. The subsequent behaviour is less clear: for the larger bed and duct heights velocity decreases along the bed, for the lower heights it increases slightly.

Graph 8.30. Static and Total Pressures Near the Bed Base. Duct End Partially Blocked. Bed Height = 10 cm. Duct Height = 10 cm. Average Velocity in the Duct Before the Bed 33.7 ms^{-1}.

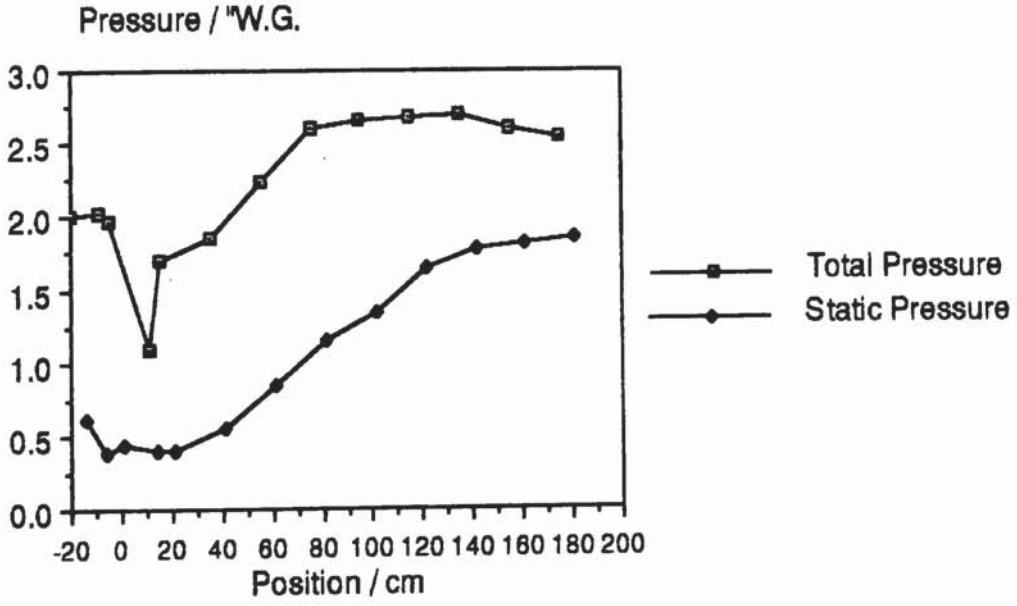

Graph 8.31. Static and Total Pressures Near the Bed Base. Duct End Partially Blocked. Bed Height = 5 cm. Duct Height = 10 cm. Average Velocity in the Duct Before the Bed 33.6 ms^{-1}.

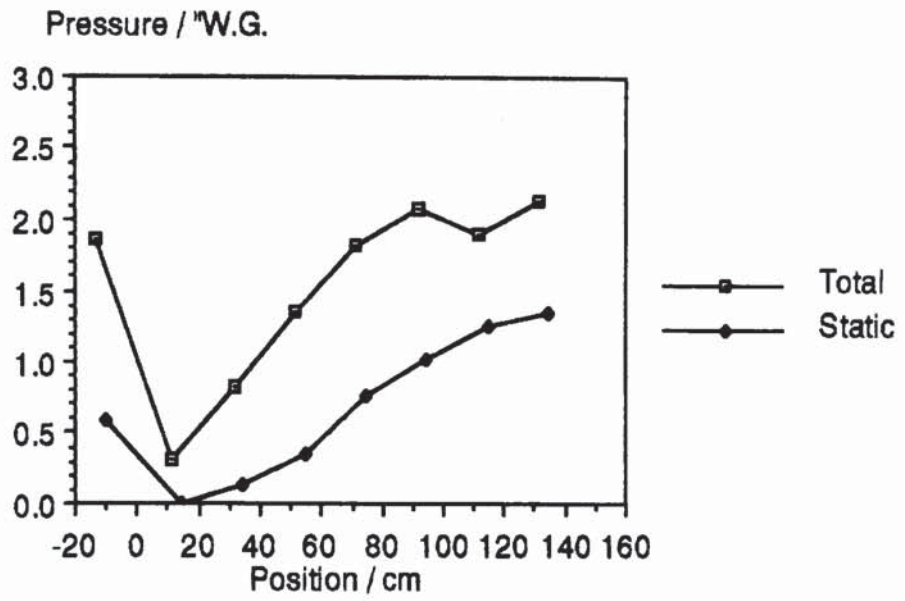

Graph 8.32. Static and Total Pressures Near the Bed Base. Duct End Partially Blocked. Bed Height = 5 cm. Duct Height = 5 cm. Average Velocity in the Duct Before the Bed 41.7 ms^{-1}.

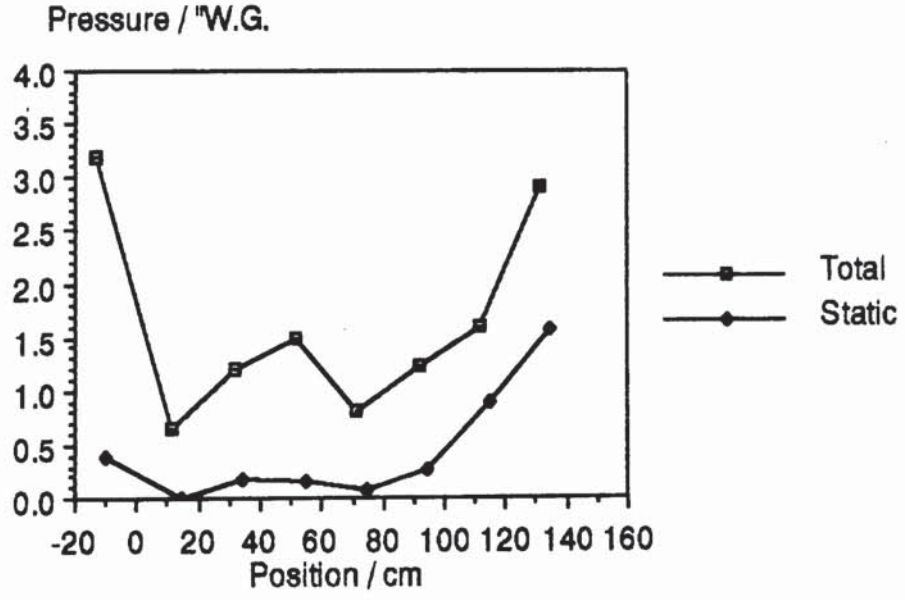

Graph 8.33. Static and Total Pressures Near the Bed Base. Duct End Partially Blocked. Bed Height = 10cm. Duct Height = 5 cm. Average Velocity in the Duct Before the Bed 41.8 ms^{-1}.

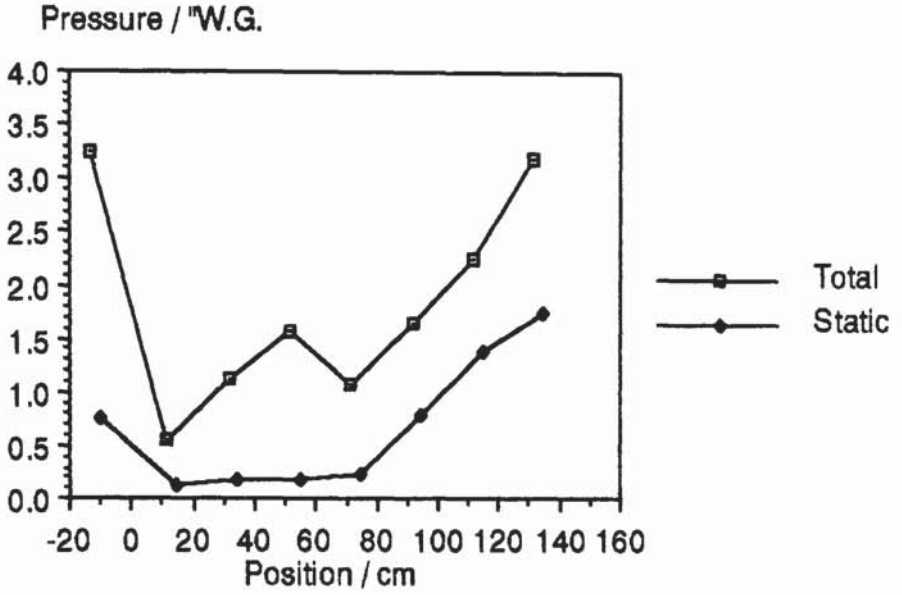

Graph 8.34. Horizontal Velocities (from dynamic pressure measurements) Near the Bed Base. Duct End Partially Blocked. Bed Height = 10 cm. Duct Height = 10 cm. Average Velocity in the Duct Before theBed 33.9 ms^{-1}.

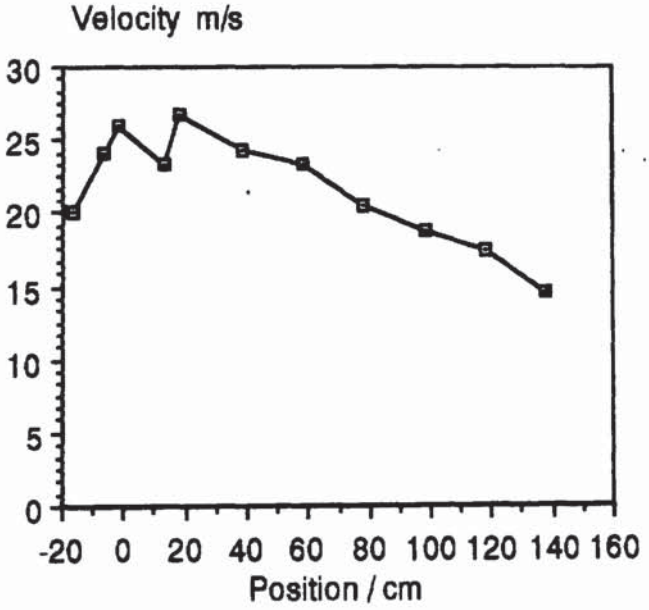

Graph 8.35. Horizontal Velocities (from dynamic pressure measurements) Near the Bed Base. Duct End Parttially Blocked. Bed Height = 5 cm. Duct Height = 10 cm. Average Velocity in the Duct Before the Bed 33.4 ms^{-1}.

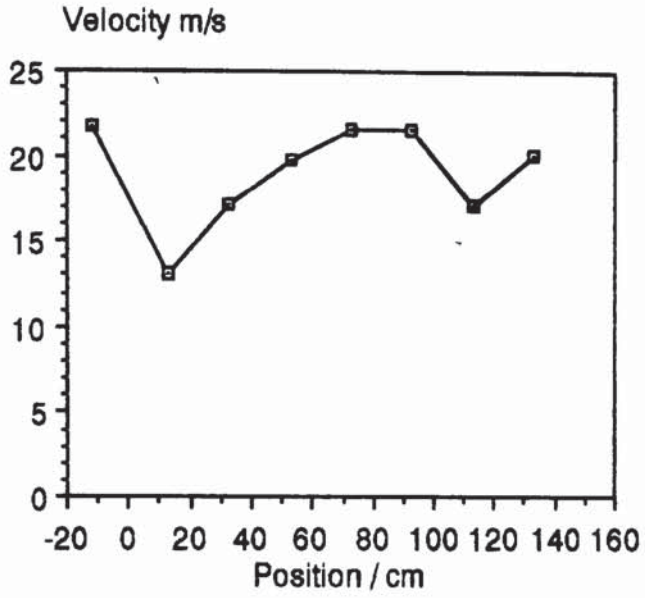

Graph 8.36. Horizontal Velocities (from dynamic pressure measurements) Near the Bed Base. Duct End Partially Blocked. Bed Height = 5 cm. Duct Height = 5 cm. Average Velocity in the Duct Before the Bed 41.6 ms^{-1}.

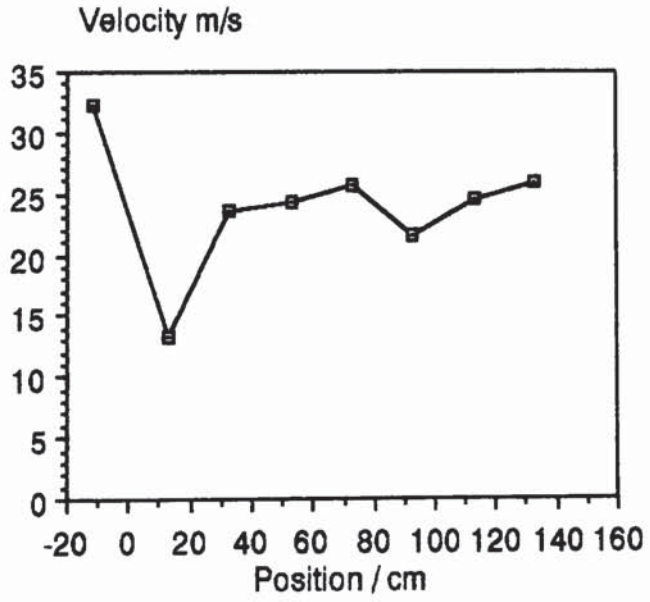

Graph 8.37. Horizontal Velocities (from dynamic pressure measurements) Near the Bed Base. Duct End Partially Blocked. Bed Height = 10 cm. Duct Height = 5 cm. Average Velocity in the Duct Before the Bed 41.7 ms^{-1}.

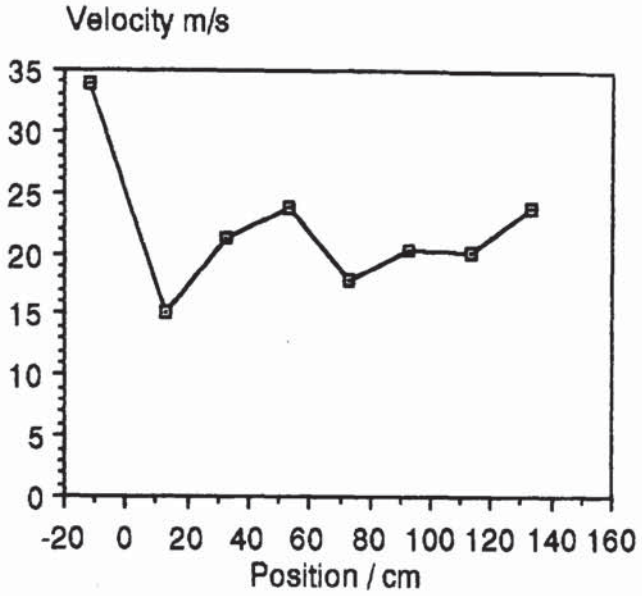

8.4.3. Duct End Blocked.

Graphs 8.38 to 41 show total and static pressures measured with the pitot tube at the bed base. Total pressure is approximately constant along the bed base for the 10 cm high duct ignoring the inlet effect; the shallower duct is associated with an increase in static pressure along the length of the bed due to pressure recovery against the end of the duct. The increase in static pressure is accompanied by a drop in velocities (determined from dynamic pressure) (see graphs 8.42 to 45).

Graph 8.38. Static and Total Pressures Near the Bed Base. Duct End Blocked. Bed Height = 10 cm. Duct Height = 10 cm. Average Velocity in the Duct Before the Bed 33.8 ms^{-1}.

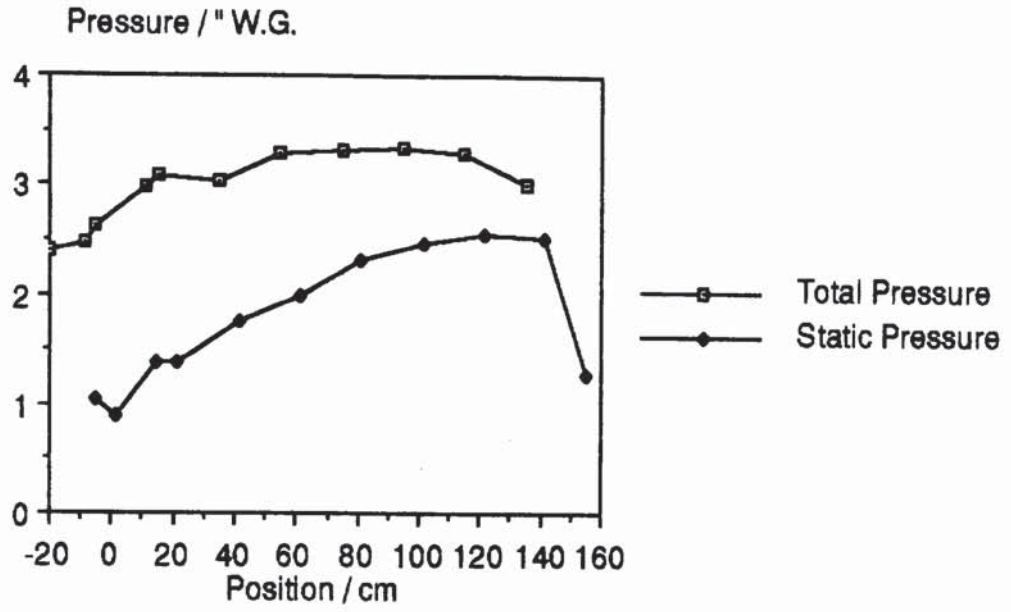

Graph 8.39. Static and Total Pressures Near the Bed Base. Duct End Blocked. Bed Height = 5 cm. Duct Height = 10 cm. Average Velocity in the Duct Before the Bed 33.3 ms^{-1}.

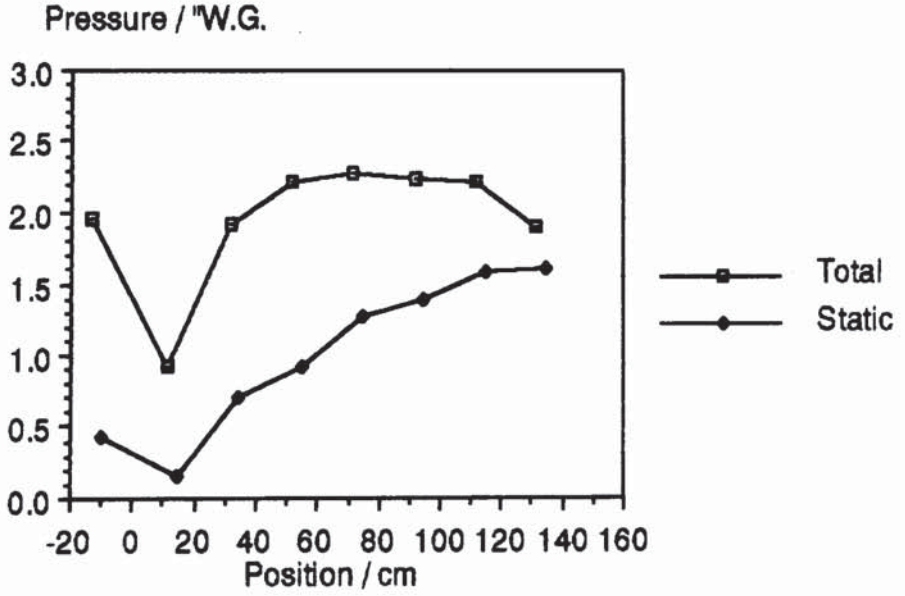

Graph 8.40. Static and Total Pressures Near the Bed Base. Duct End Blocked. Bed Height = 5 cm. Duct Height = 5 cm. Average Velocity in the Duct Before the Bed 41.8 ms^{-1}.

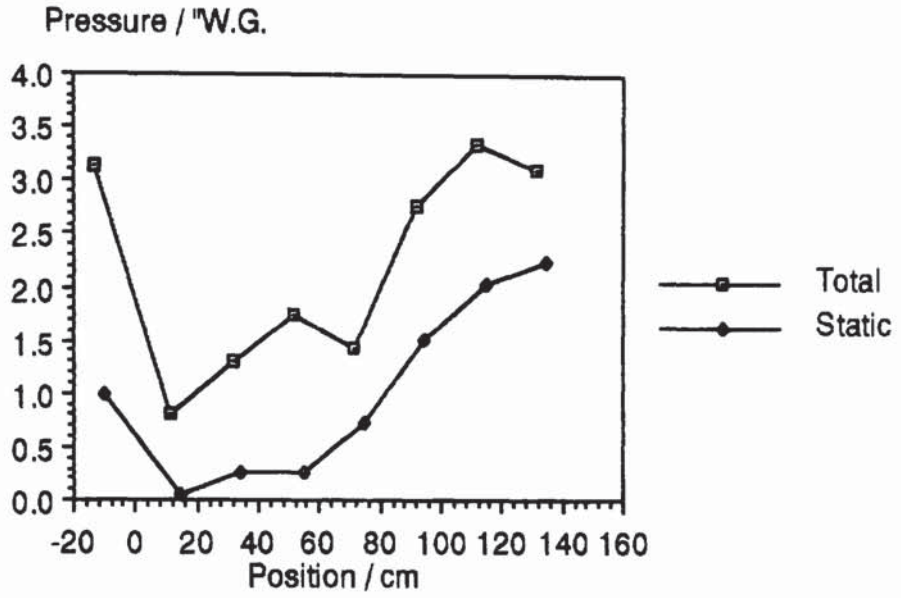

Graph 8.41. Static and Total Pressures Near the Bed Base. Duct End Blocked. Bed Height = 10 cm. Duct Height = 5 cm. Average Velocity in the Duct Before the Bed 15.0 ms^{-1}.

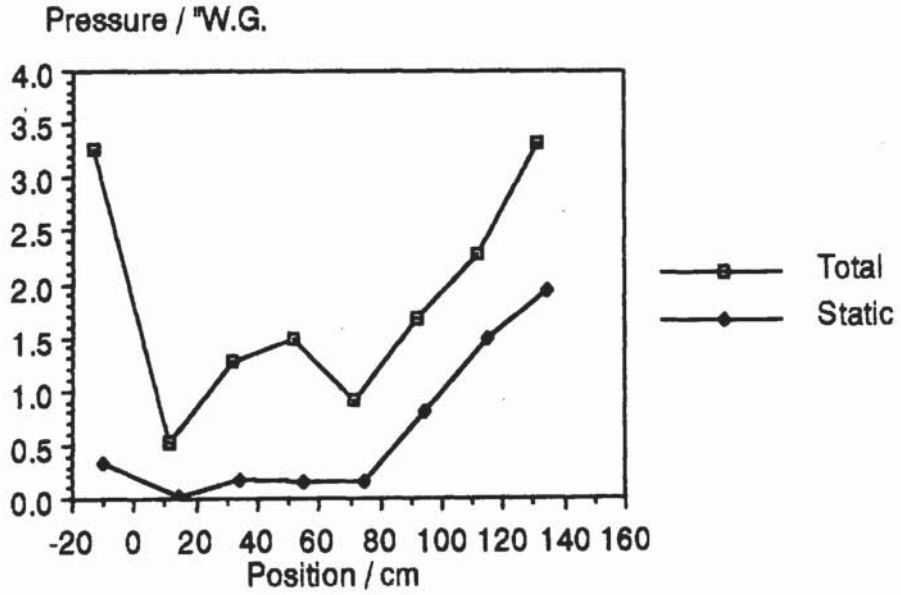

Graph 8.42. Horizontal Velocities (from dynamic pressure measurements) Near the Bed Base. Duct End Blocked. Bed Height = 10 cm. Duct Height = 10 cm. Average Velocity in the Duct Before the Bed 33.4ms^{-1}.

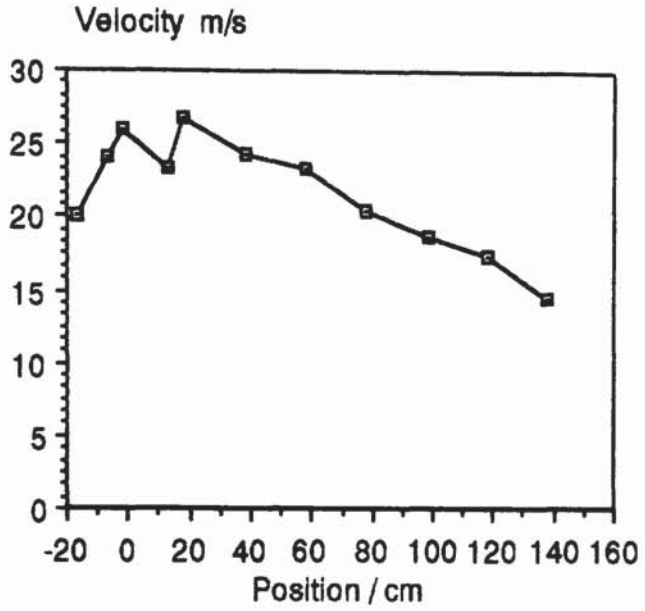

Graph 8.43. Horizontal Velocities (from dynamic pressure measurements) Near the Bed Base. Duct End Blocked. Bed Height = 5 cm. Duct Height = 10 cm. Average Velocity in the Duct Before the Bed 33.3ms^{-1}.

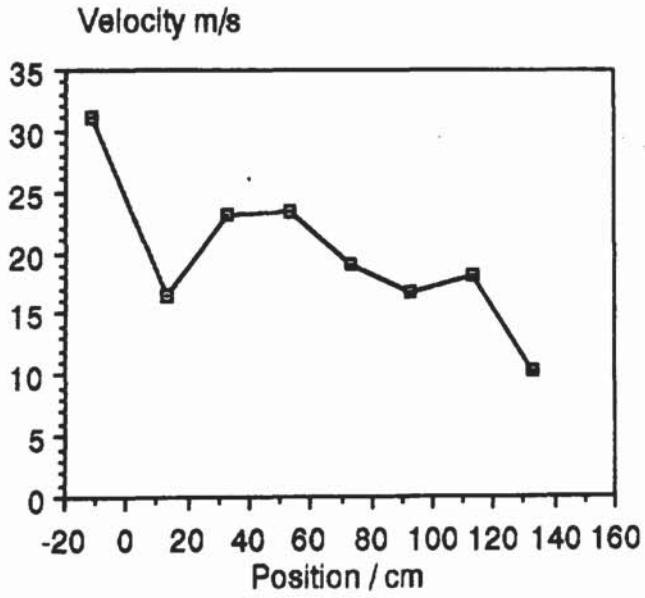

Graph 8.44. Horizontal Velocities (from dynamic pressure measurements) Near the Bed Base. Duct End Blocked. Bed Height = 5 cm. Duct Height = 5 cm. Average Velocity in the Duct Before the Bed 41.8 ms^{-1}.

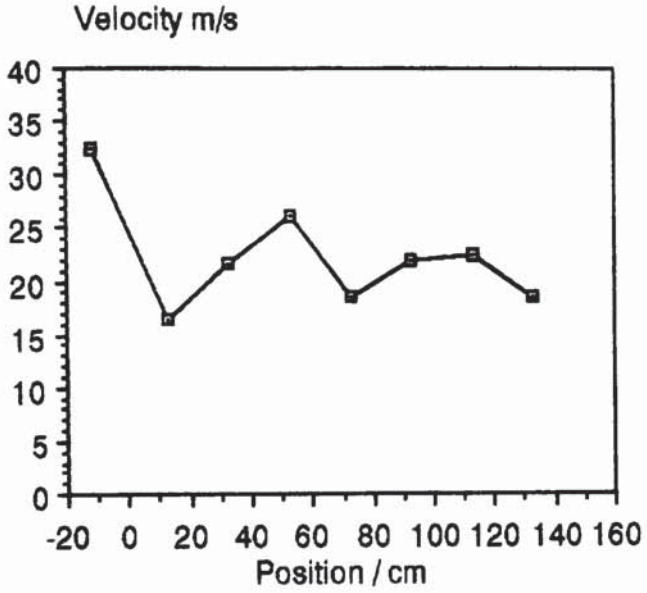

Graph 8.45. Horizontal Velocities (from dynamic pressure measurements) Near the Bed Base. Duct End Blocked. Bed Height = 10 cm. Duct Height = 5 cm. Average Velocity in the Duct Before the Bed 41.9 ms^{-1}.

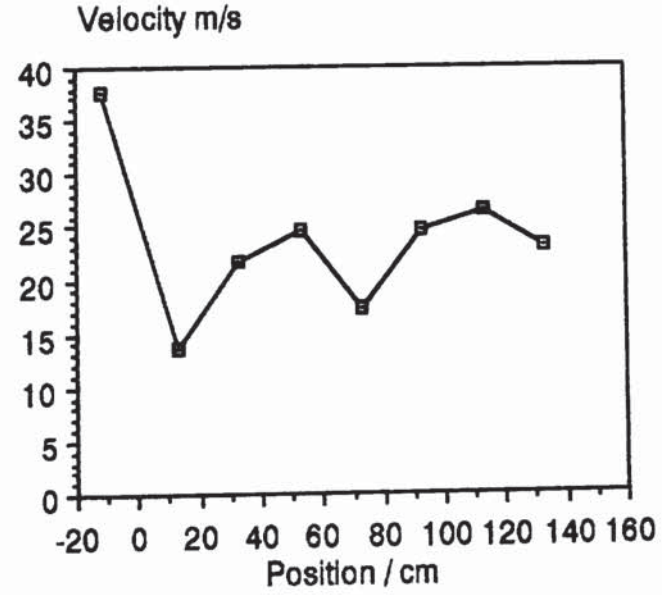

The pressures and velocities discussed above are higher in the duct blocked case than the partially blocked case which are in turn higher than in the duct open case. The results for the duct wholly and partially blocked are similar and different to those for the duct end open suggesting that different mechanisms operate in the two cases.

8.4.4. Duct Velocity Profiles.

Graphs 8.46 to 51 show velocity profiles in the duct. The velocity profiles should be considered in conjunction with the streamlines presented in section 8.2.

For the duct open case the velocity profiles can be seen to retain the same form in the lower 60% of the duct. In the upper part of the duct the gas can be seen decelerating as some of it flows into the bed.

When the duct is partially blocked the velocity can be seen to decrease along the duct and the profile changes because the velocity at the base of the duct decreases faster than that at the bed base. This suggests that gas flows from the lower part of the duct to the upper part (where the flowrate remains higher) before leaving through the bed. The gas at the bottom of the duct is then 'entrained' with that flowing in the upper part, a different mechanism to that occuring when the duct is open (the effect is not due to wall friction at the duct base).

The duct outlet blocked case is similar to the partially blocked case, but, the profiles are not as flat as all the gas leaves through the bed. The profiles are more evenly spaced than the partially blocked case and change shape more smoothly but the mechanism is the same.

The profiles for the different bed heights are identical in form for the various duct end conditions. The shallower, lower resistance bed however allows a greater flow through the bed (when the duct end is not blocked) and hence the profiles are spread more and the gas at the bed base flows at higher velocities. Recirculation at the duct end (at the bottom of the duct) is also observed when the duct end is wholly blocked.

Graph 8.46. Duct Velocity Profiles. Duct End Open. Duct Height 10 cm. Bed Height 10 cm. Average Velocity in the Duct Before the Bed Approximately 33.5 ms^{-1}.

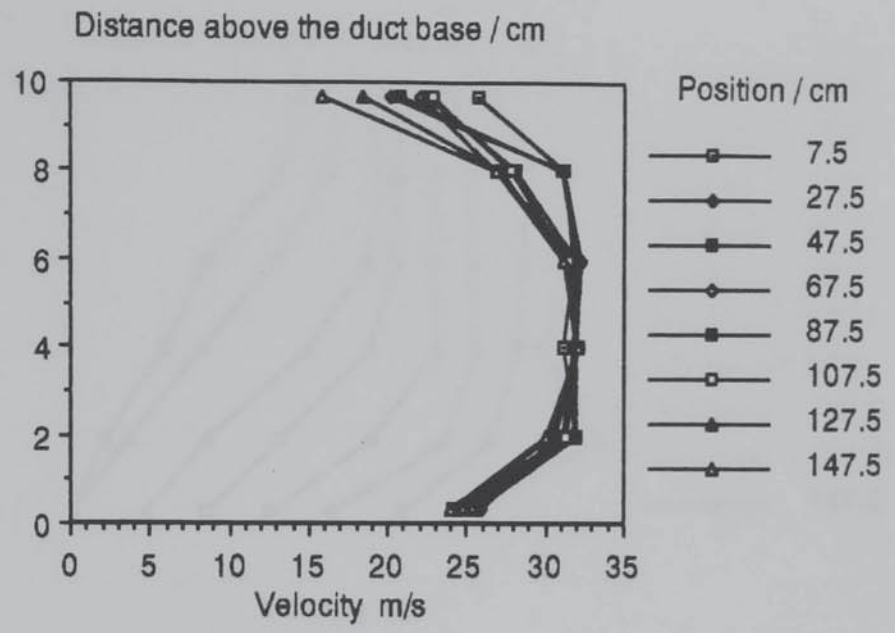

Graph 8.47. Duct Velocity Profiles. Duct End Partially Blocked. Duct Height 10 cm. Bed Height 10 cm. Average Velocity in the Duct Before the Bed Approximately 33.5 ms^{-1}.

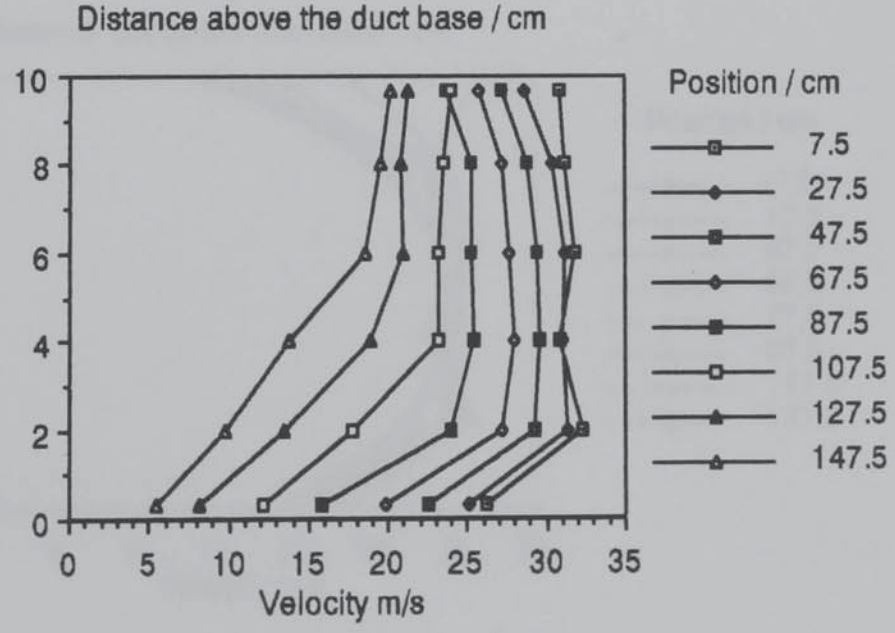

Graph 8.48. Duct Velocity Profiles. Duct End Wholly Blocked. Duct Height 10 cm. Bed Height 10 cm. Average Velocity in the Duct Before the Bed Approximately 33.5 ms^{-1}.

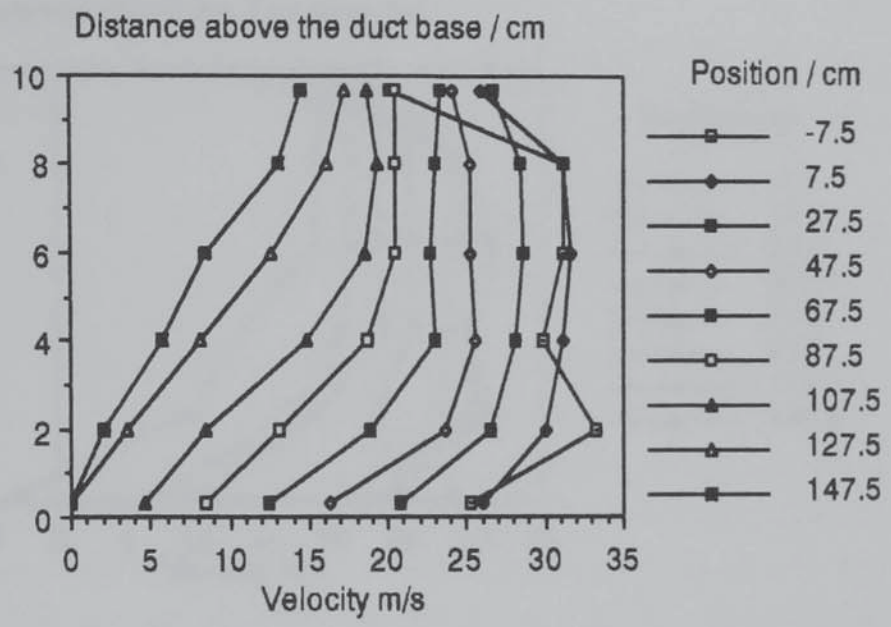

Graph 8.49. Duct Velocity Profiles. Duct End Open. Duct Height 10 cm. Bed Height 5 cm. Average Velocity in the Duct Before the Bed Approximately 33.7 ms^{-1}.

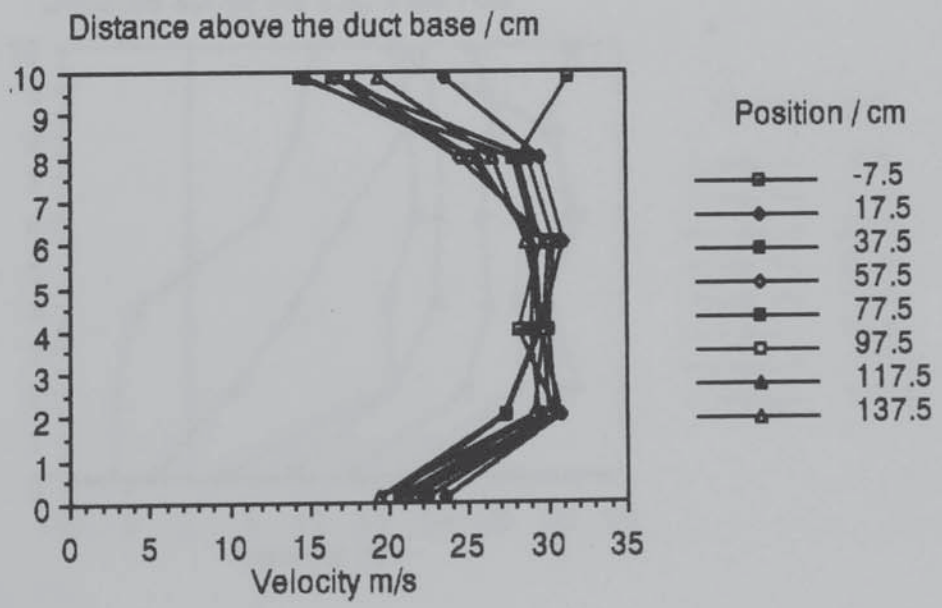

Graph 8.50. Duct Velocity Profiles. Duct End Partially Blocked. Duct Height 10 cm. Bed Height 5 cm. Average Velocity in the Duct Before the Bed Approximately 33.7 ms^{-1}.

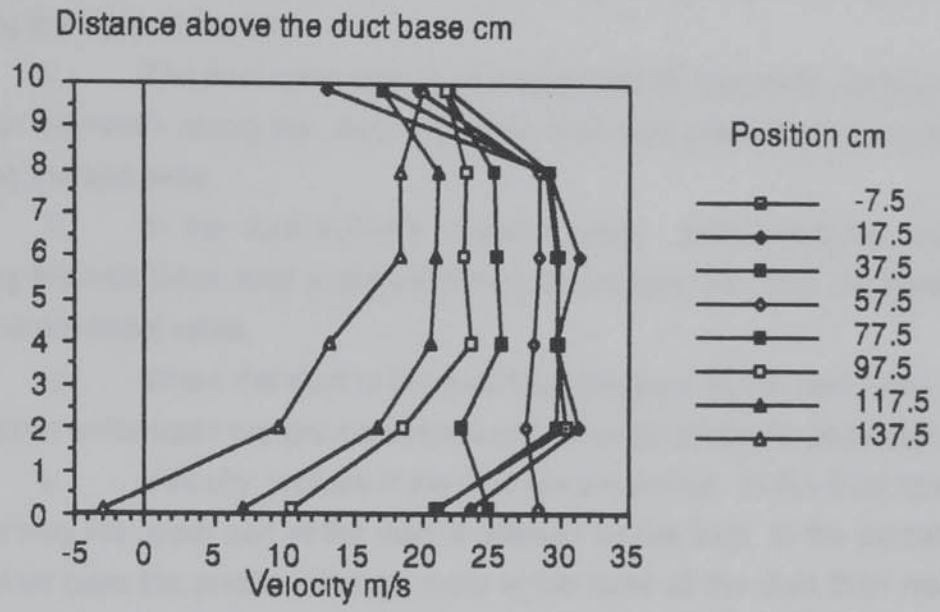

Graph 8.51. Duct Velocity Profiles. Duct End Wholly Blocked. Duct Height 10 cm. Bed Height 5 cm. Average Velocity in the Duct Before the Bed Approximately 33.7 ms^{-1}.

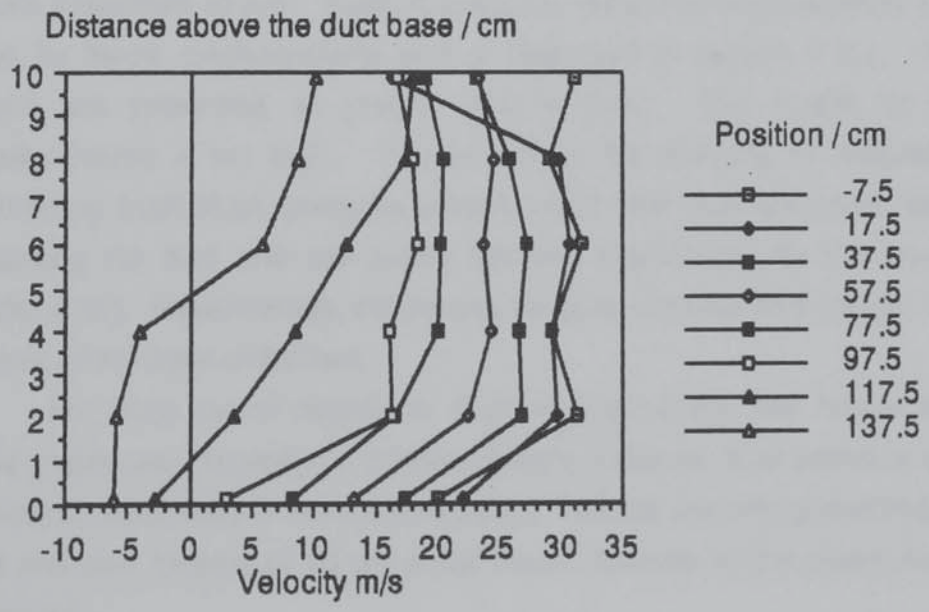

8.4.5. Concluding Remarks.

It can be concluded that;

i. The total pressure - and its components - are not constant along the base of the bed.

ii. The duct open case is characterised by low static pressures which decrease along the duct. Dynamic and total pressures decrease along the bed base.

iii. In the duct partially blocked case; static pressure rises along the bed base, total pressure initially decreases and then increases above the initial value.

iv. When the duct is blocked total pressure at the bed base is constant while static pressure inceases and dynamic pressure decreases.

v. Velocity profiles in the duct are presented. In the duct open case only the upper part of the duct is affected by the bed. In the partially blocked case the profiles change more at the base of the duct than near the bed base but are otherwise as expected. Similar behaviour is observed in the duct end blocked case.

8.5. PRESSURES AT THE BED BASE.

The effect of the bed base is obviously critical in explaining the results presented above. Special pressure measurement hardware was used for these measurements and is described in section 7.4.1. The results are presented as graphs 8.52 to 8.60. The quality of the measurements is not high. This is due to the difficulty in accurately positioning such small pressure probes which are also disturbed when repacking the bed and are easily blocked (particularly by the smoke machine oil). Nevertheless, the probes do give considerable insight into the role of the base of the bed.

For each set of conditions (duct end condition, bed height etc.) three graphs are presented in triplets of static pressure, total pressure and velocity on both sides of the support mesh. Results are only presented for duct and bed heights of 10 cm since these illustrate all the phenomena observed.

8.5.1. Duct Open.

Graph 8.52. Needle Tube Static Pressures. Duct End Open. Bed Height 10 cm. Duct Height 10 cm. Average Velocity in the Duct Before the Bed 33.8 ms^{-1}.

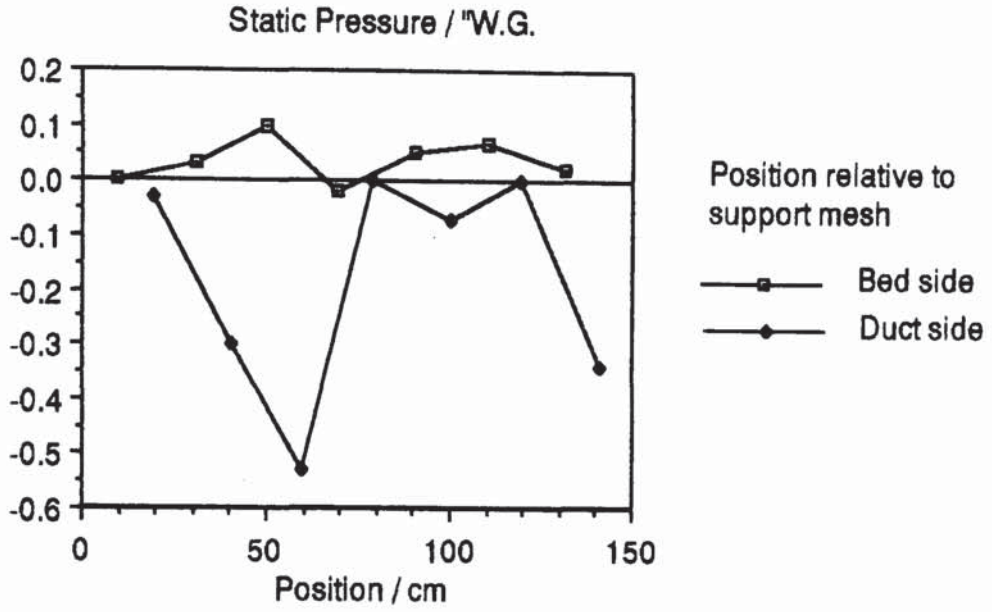

Graph 8.53. Needle Tube Total Pressures. Duct End Open. Bed Height 10 cm. Duct Height 10 cm. Average Velocity in Duct Before Bed 33.8 ms^{-1}.

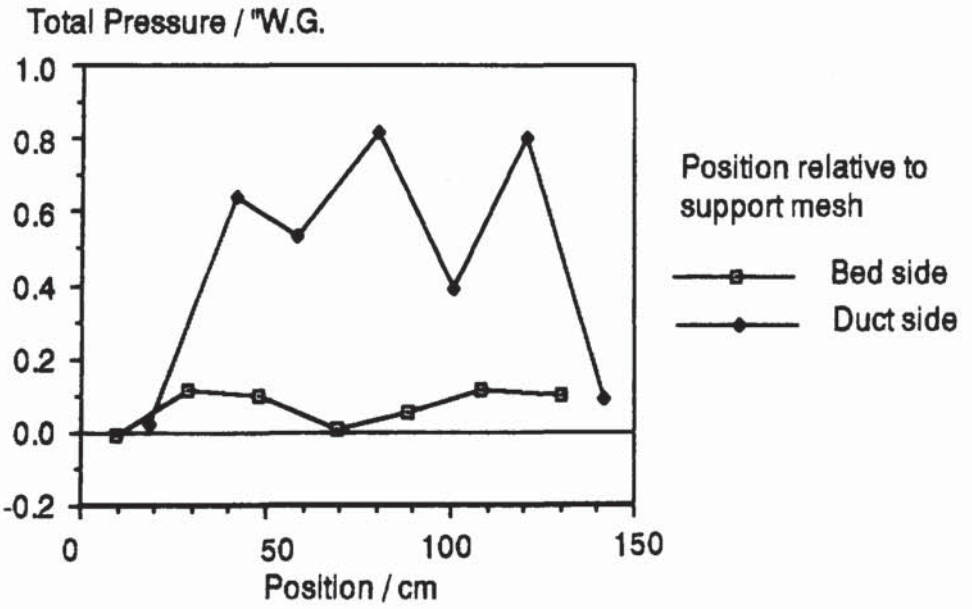

Graph 8.54. Needle Tube Velocities. Duct End Open. Bed Height 10 cm. Duct Height 10 cm. Average Velocity in Duct Before Bed 33.8 ms^{-1}.

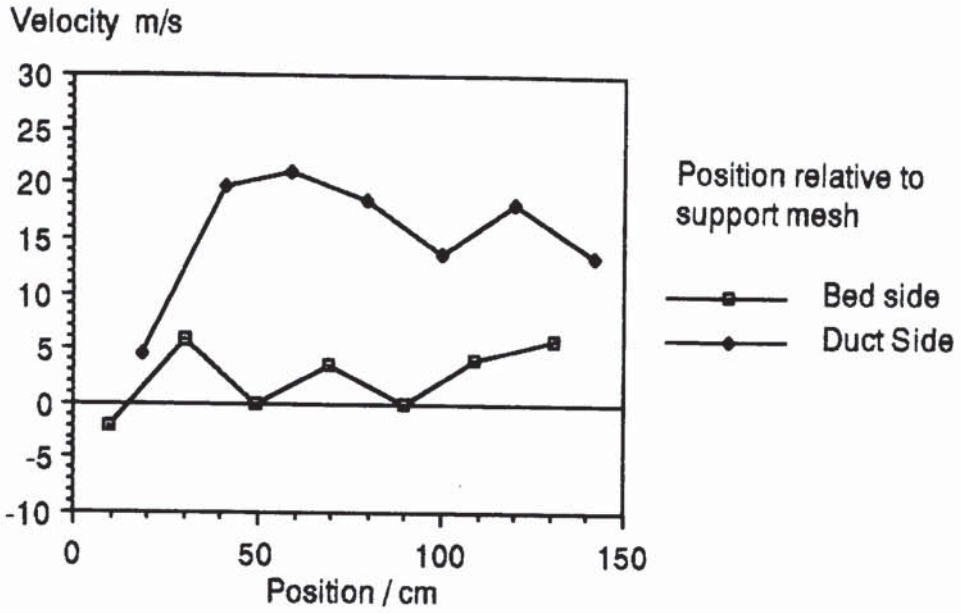

Many of the graphs presented must be considered in the light of the resolution of the micromanometer which is 0.01" W.G. Some negative pressures are observed which must be due to measurement inaccuracies.

The static pressure profiles particularly suffer from this limitation and are therefore not consistent. Nevertheless they show that the effect of the bed support is clearly critical.

The total pressures are highest in the middle of the bed on the duct side. On the bed side these pressures are very low and vary little along the base of the bed. This illustrates the effect of the bed support.

The velocities are much higher on the bed side of the support and suggest that the support is responsible for the conversion of much of the horizontal momentum to vertical momentum. With the deeper duct velocity increases along the bed base whereas with the shallower duct it increases towards the middle of the bed and then decreases on the duct side. On the bed side they vary less. This observation is consistent with the greater effect of pressure recovery against the end wall of the bed in the lower duct height cases. The effect of changes in bed height are as explained in the previous section.

8.5.2. Duct Partially Blocked.

In this case the resolution of the micromanometer is less significant due to the higher pressures encountered.

Static pressures increase along the bed and are higher on the bed side of the support than the duct side; showing the high frictional resistance of the support.

Total pressure follows the same trend but is higher on the duct side of the support confirming the comment made above.

Velocities on the duct side increase at the beginning of the bed and then remain approximately constant. On the bed side velocities are lower and are approximately constant if end effects are ignored.

Graph 8.55. Needle Tube Static Pressures. Duct End Partially Blocked. Bed Height 10 cm. Duct Height 10 cm. Average Velocity in the Duct Before the Bed 33.2 ms^{-1}.

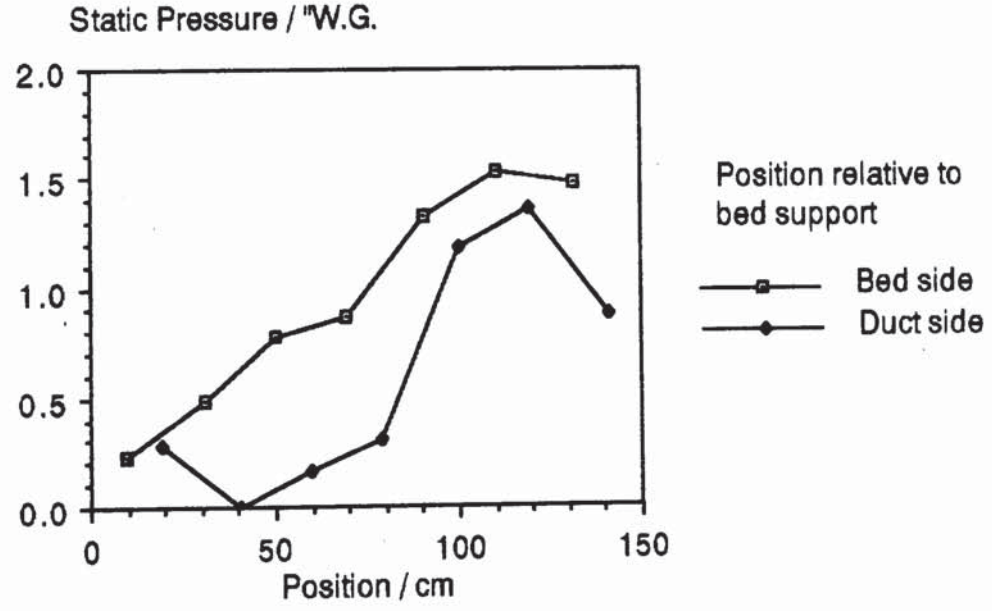

Graph 8.56. Needle Tube Total Pressures. Duct End Partially Blocked. Bed Height 10 cm. Duct Height 10 cm. Average Velocity in the Duct Before the Bed 33.2 ms^{-1}.

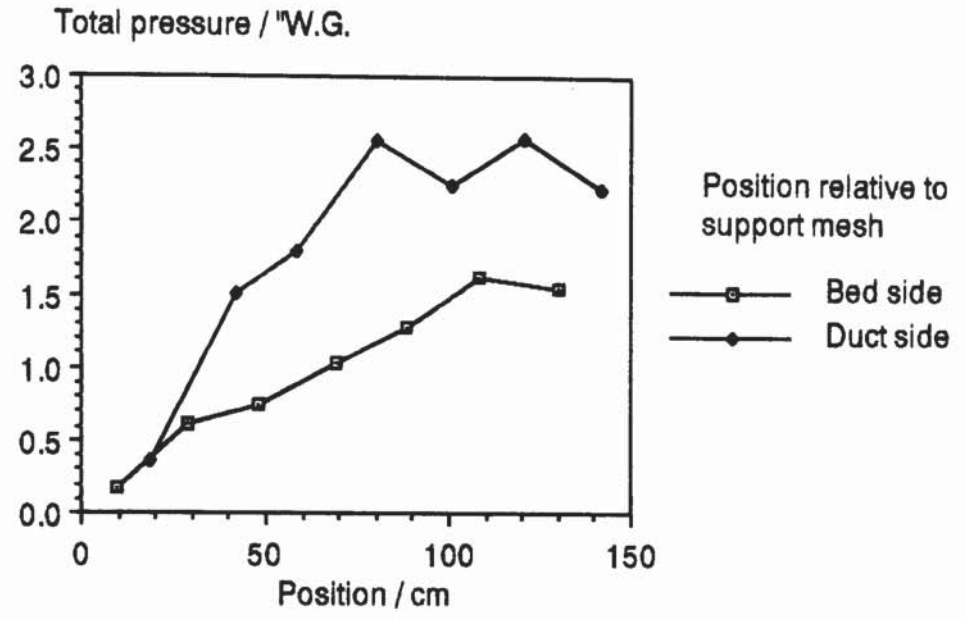

Graph 8.57. Needle Tube Velocities. Duct End Partially Blocked. Bed Height 10 cm. Duct Height 10 cm. Average Velocity in the Duct Before the Bed 33.2 ms^{-1}.

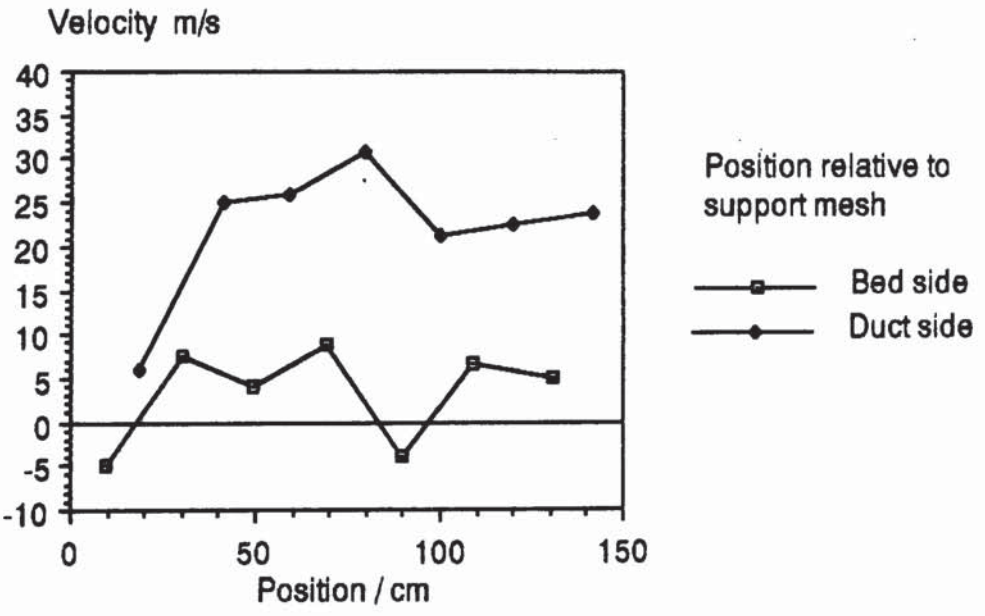

8.5.3. Duct Wholly Blocked.

The static pressures on the bed side increase along the bed and are higher than those on the duct side which also increase although to a lesser extent and, nearer the outlet end.

The total pressures on the duct side of the support increase along the bed at higher duct heights; at lower duct heights they also decrease towards the outlet end of the bed. On the duct side total pressures are lower and increase along the length of the bed.

These results are similar to those when the duct outlet is partially blocked and are explained by the same mechanisms; this is particularly true of the velocities.

Graph 8.58. Needle Tube Static Pressures. Duct End Wholly Blocked. Bed Height 10 cm. Duct Height 10 cm. Average Velocity in the Duct Before the Bed 33.5 ms^{-1}.

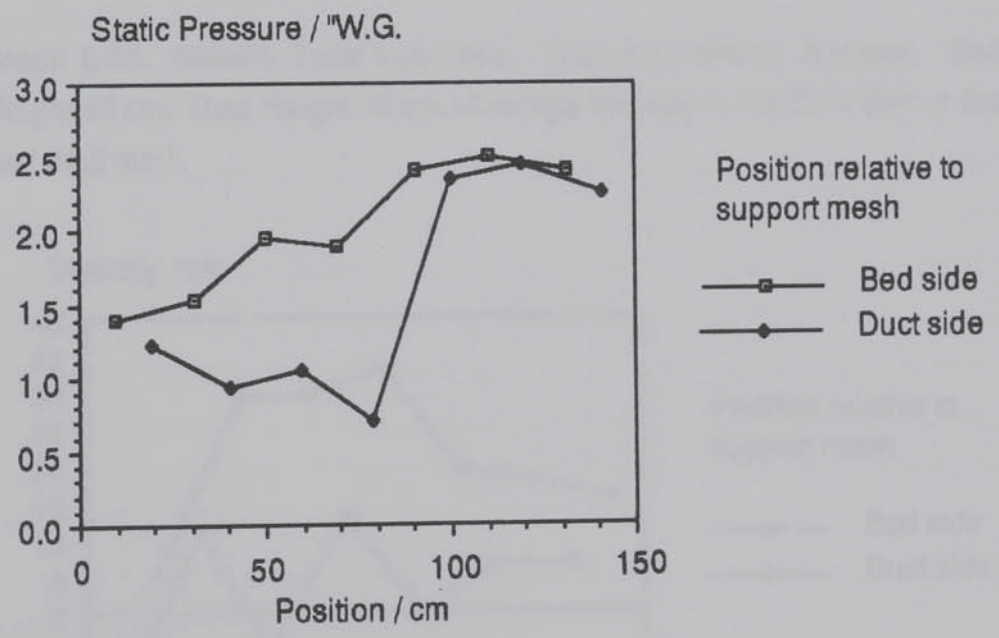

Graph 8.59. Needle Tube Total Pressures. Duct End Wholly Blocked. Bed Height 10 cm. Duct Height 10 cm. Average Velocity in the Duct Before the Bed 33.5 ms^{-1}.

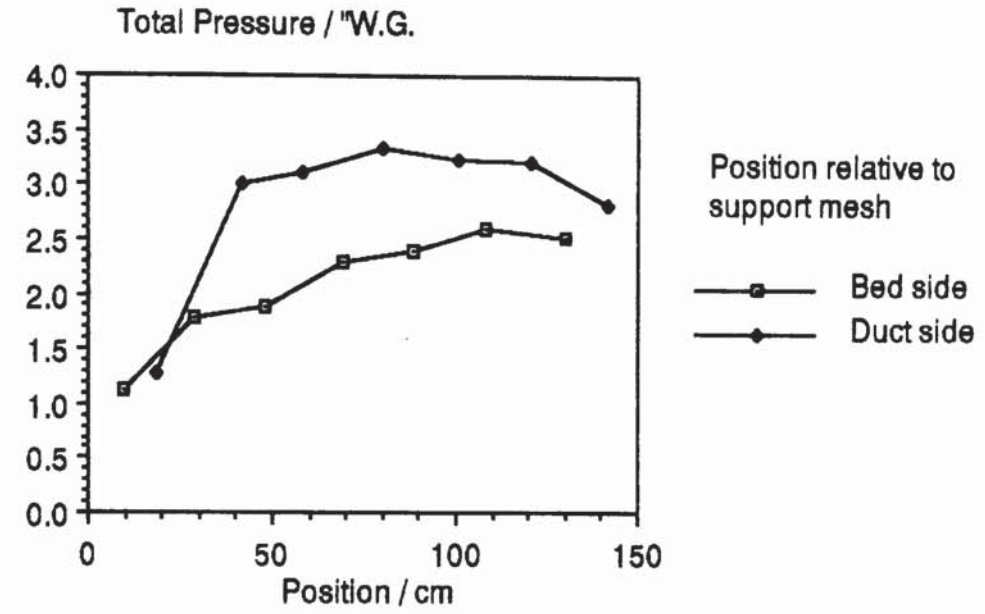

Graph 8.60. Needle Tube Velocities. Duct End Wholly Blocked. Bed Height 10 cm. Duct Height 10 cm. Average Velocity in the Duct Before the Bed 33.5 ms^{-1}.

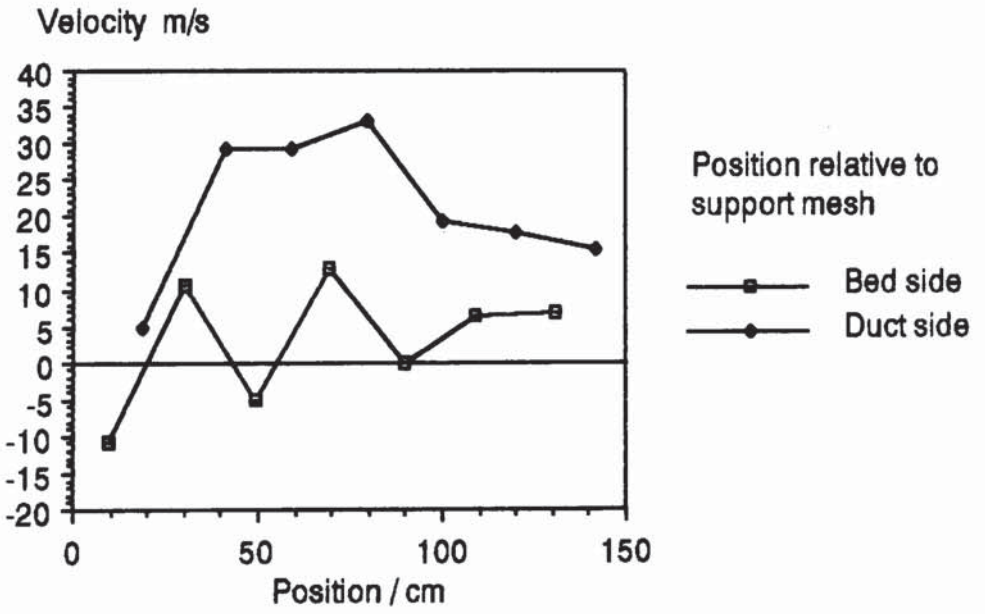

8.5.4. Overview.

The poor quality of much of these results is evident and has been explained. Nevertheless clear trends in pressure and velocity have been identified and are further discussed in section 8.8

The effect of the bed support mesh has been shown to be very significant and can be expected to dominate much of the underlying fluid behaviour. The bed support has two interrelated main effects:

i. Frictional.

ii. Conversion of the horizontal momentum/component of velocity to the vertical.

The effects of changing bed and duct heights are as previously discussed and the mechanisms are the same.

8.6. STATIC PRESSURES IN THE BED.

Having examined in detail the fluid mechanic behaviour of the bed base and support; measurements are presented in this section of static pressure in the bed. These static pressures were measured using the specially constructed static pressure tube (described in section 7.4.1) and the micromanometer (see section 6.5.1).

As discussed in section 7.4.1, the use of such a staic pressure tube disturbs the bed and, particularly, causes a localised area of higher voidage around the probe. Thus, the precise measurements obtained cannot be viewed as definitive; however, the measurements will permit qualitative discussion of static pressure in the bed. Results are presented for duct outlet open, partially blocked and wholly blocked at the maximum flowrate (as has already been shown flow patterns do not vary over the range of flowrates).

These measurements were made for the three duct end conditions and combinations of 5 and 10 cm height ducts and beds.

Some comments apply to all the data presented in this section;

i. Static pressures increase with flowrate, as expected

ii. Static pressures decrease as the gas travels through the bed.

iii. Higher Static pressures in the bed are associated with greater bed and lower duct heights as is to be expected.

8.6.1. Duct Open.

The static pressure profiles are presented as graphs 8.61 to 63. The three graphs all show the same basic phenomena. The static pressure in the bed rises and falls off towards the middle of the bed where it is uniform before rising and falling again towards the end of the bed. These results are in direct contrast to the results presented above.

The negative pressures at the end of the bed (graph 8.88) are more interesting and suggest recirculation through the bed which has not been observed with the anenometer or the flow visualisation although they are comparable to the needle tube static pressures.

Graph 8.61. Bed Static Pressure Profiles. Duct Open. 10 cm Bed Duct Heights. Average Velocity in the Duct Before the Bed 33.3 ms^{-1}.

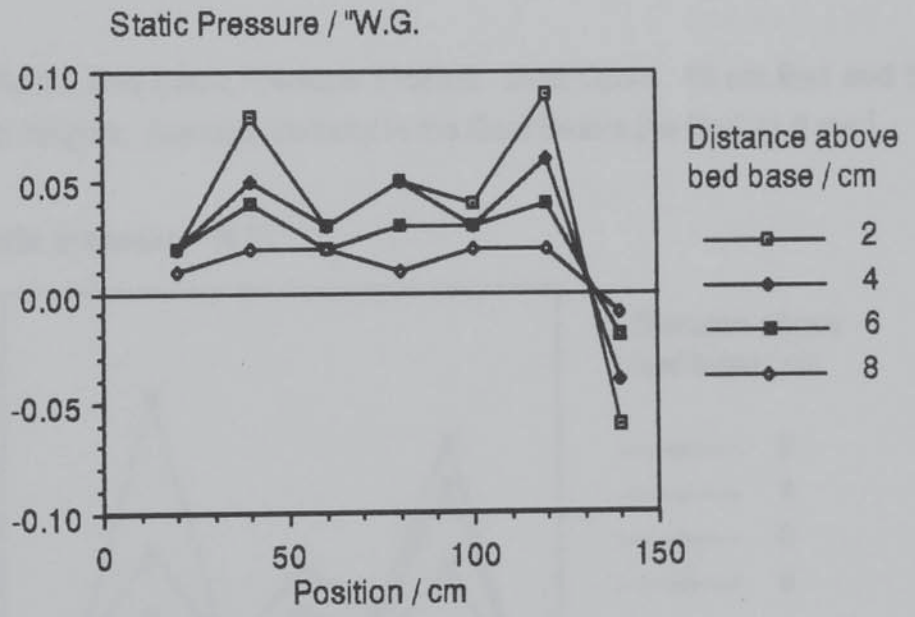

Graph 8.62. Bed Static Pressure Profiles. Duct Open. 5 cm Bed and 10 cm Duct Heights. Average Velocity in the Duct Before the Bed 33.5 ms^{-1}.

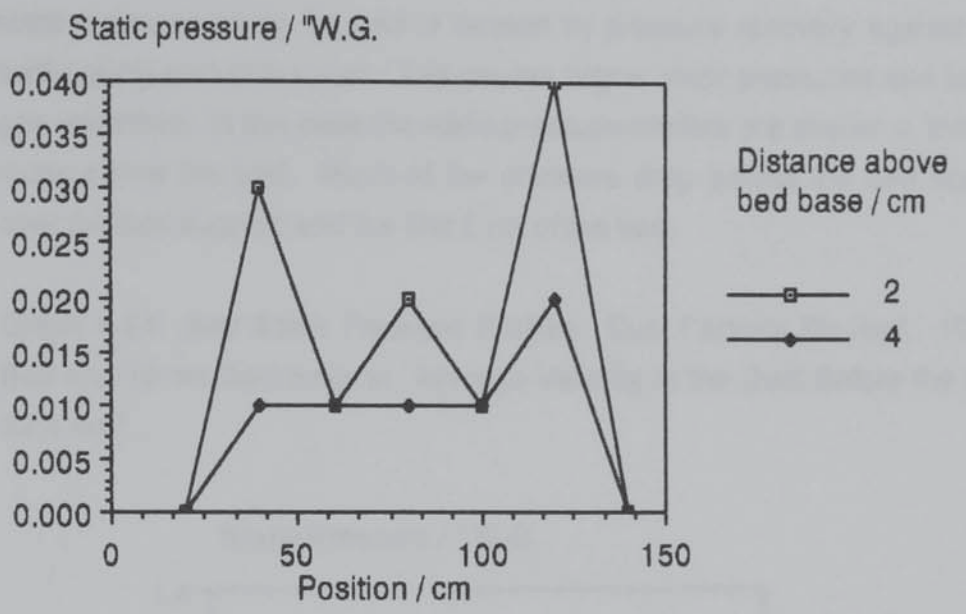

Graph 8.63. Bed Static Pressure Profiles. Duct Open. 10 cm Bed and 5 cm Duct heights. Average Velocity in the Duct Before the Bed 41.6 ms^{-1}.

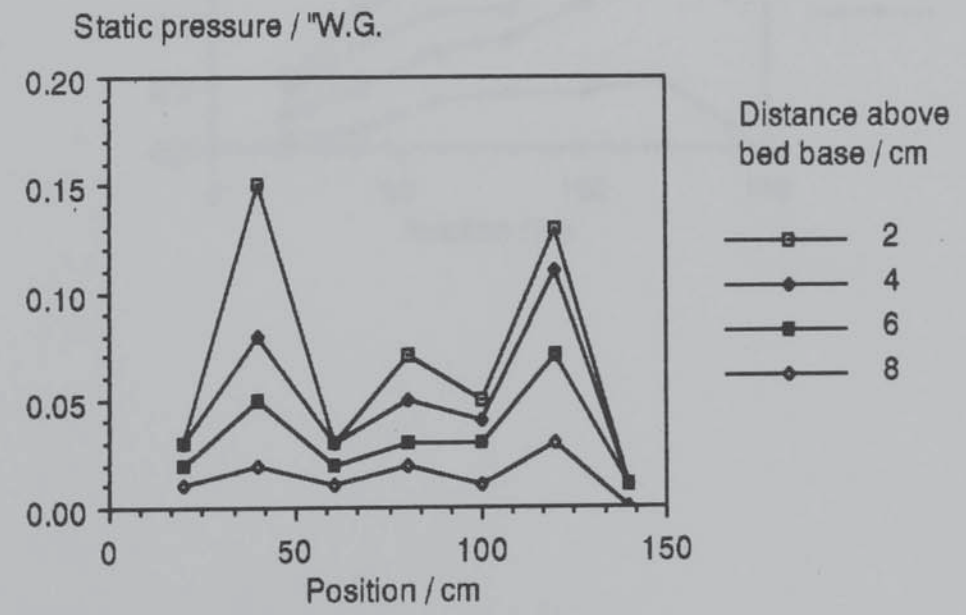

8.6.2. Duct Partially Blocked.

These results are presented as graphs 8.64 to 66. The increase in static pressure along the bed is caused by pressure recovery against the baffle at the end of the duct. This causes higher static pressures and lower gas velocities. In this case the static pressure profiles are similar in form to those below the bed. Much of the pressure drop across the bed occurs over the bed support and the first 2 cm of the bed.

Graph 8.64. Bed Static Pressure Profiles. Duct Partially Blocked. 10 cm Bed and 10 cm Duct heights. Average Velocity in the Duct Before the Bed 33.4 ms^{-1}.

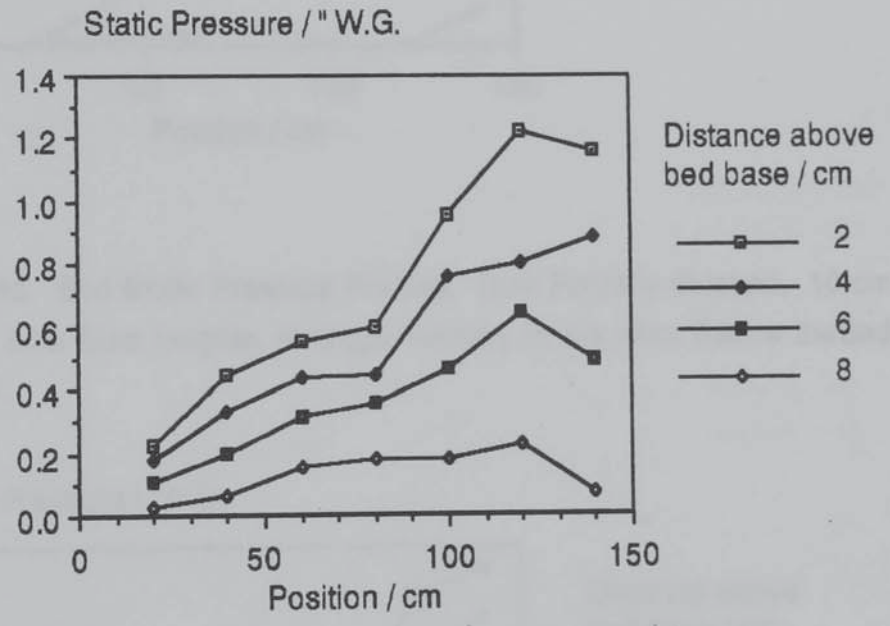

Graph 8.65. Bed Static Pressure Profiles. Duct Partially Blocked. 5 cm Bed and 10 cm Duct heights. Average Velocity in the Duct Before the Bed 33.7 ms^{-1}.

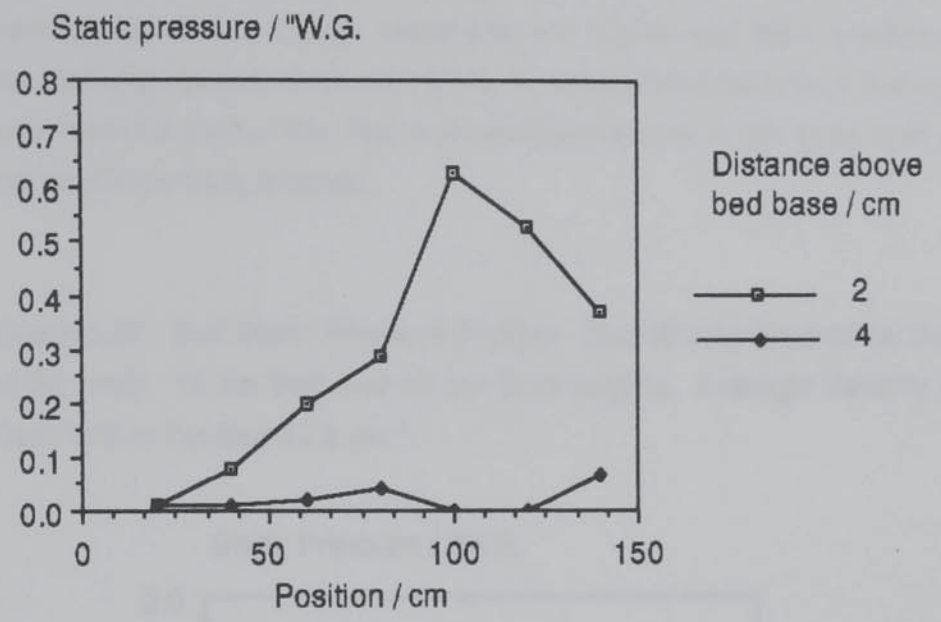

Graph 8.66. Bed Static Pressure Profiles. Duct Partially Blocked. 10 cm Bed and 5cm Duct heights. Average Velocity in the Duct Before theBed 41.7 ms^{-1}.

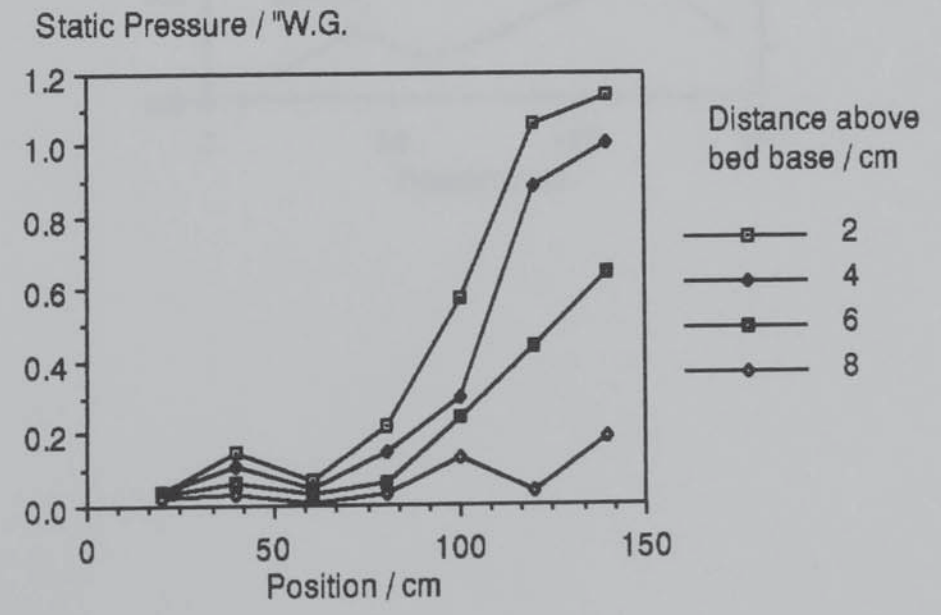

8.6.3. Duct Wholly Blocked.

Graphs 8.67 to 69 show the results when the duct outlet is blocked. Essentially these graphs show the same trends as those for the duct partially blocked, although pressures are higher and the increase along the bed less marked because of this. The pressure drop across the support and the initial part of the bed is proportionally less in this case than when the duct is partially blocked.

Graph 8.67. Bed Static Pressure Profiles. Duct Wholly Blocked (at the end of the bed). 10 cm Bed and 10 cm Duct heights. Average Velocity in the Duct Before the Bed 33.6 ms^{-1}.

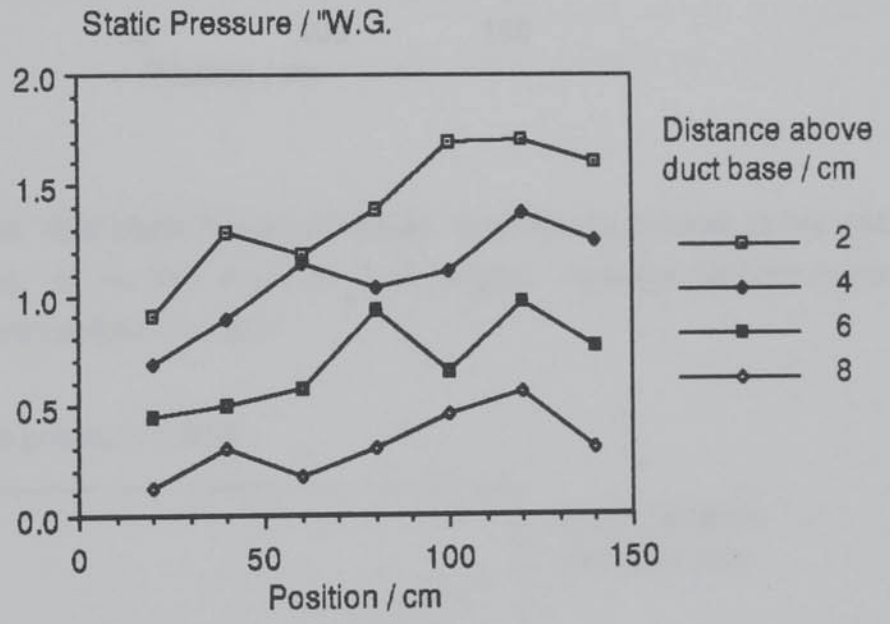

Graph 8.68. Bed Static Pressure Profiles. Duct Wholly Blocked (at the end of the bed). 5 cm Bed and 10 cm Duct heights. Average Velocity in the Duct Before the Bed 33.8 ms^{-1}.

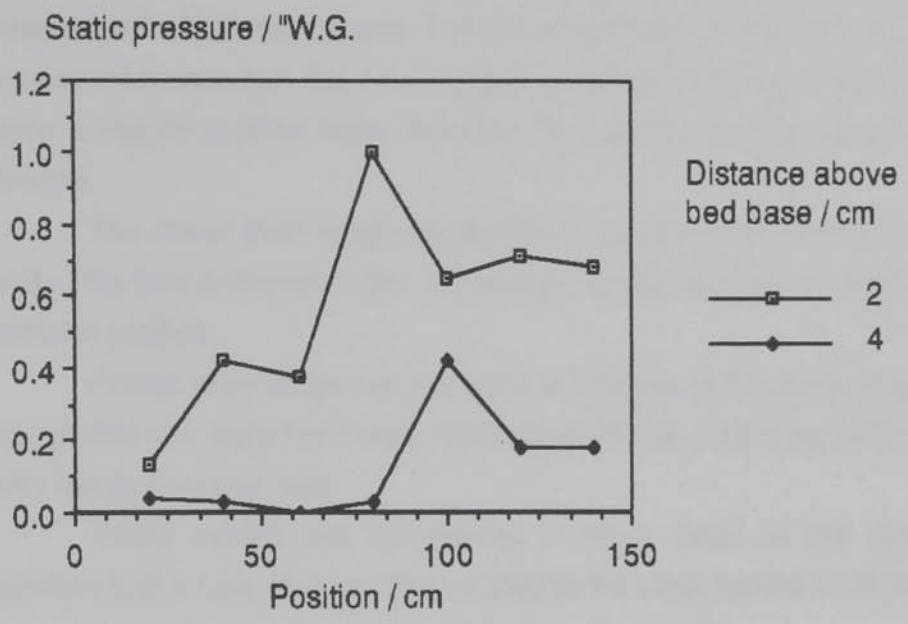

Graph 8.69. Bed Static Pressure Profiles. Duct Wholly Blocked (at the end of the bed). 10 cm Bed and 5cm Duct heights. Average Velocity in the Duct Before the Bed 41.8 ms^{-1}.

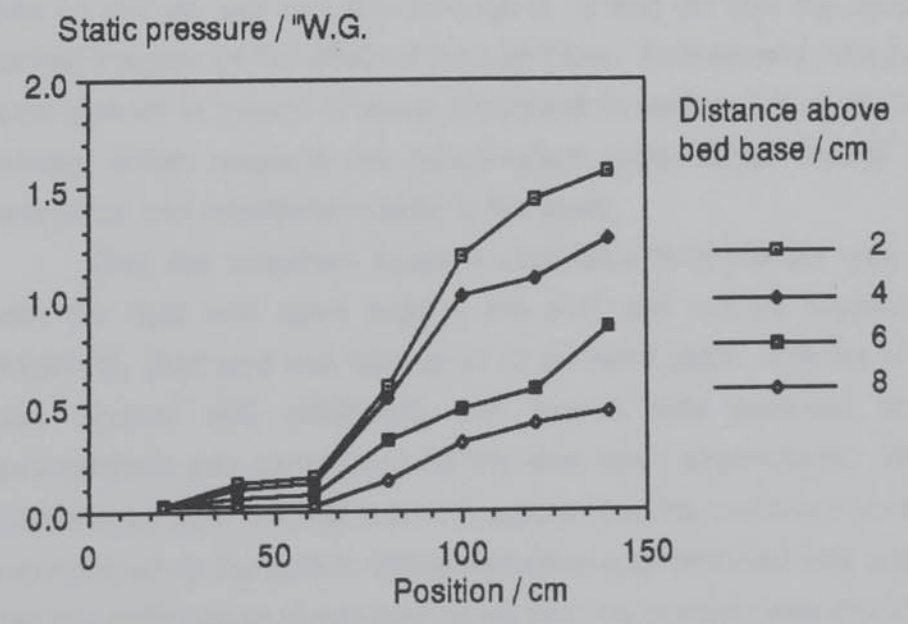

8.6.4. Overall Comments.

The effects of the lower duct height are to increase static pressures and produce a similar profile to those observed at higher flowrates with the deeper bed. This implies that it is the magnitude of the velocity (i.e. the amount of momentum the flowing gas contains) that determines the bed static pressure profiles rather than the (volumetric / mass) quantity of gas flowing.

The lower duct height gives rise to higher static pressures at the end of the bed and lower ones at the beginning thus accentuating the form of these profiles.

Furthermore when the duct end is blocked at the lower duct height the profiles are more like those obtained when the duct is partially blocked with the deeper bed duct.

These results are considered in more detail in the discussion (section 8.8) where they are also related to the other results obtained.

8.7. BLOCKED BED OUTLET RESULTS.

The reason for performing this subset of the experimental study was to examine the effect on conditions in the duct of blocking the top of the bed so that no gas can flow through it. It was felt that this would yield further insights on the effect of the bed base. Furthermore, this particular arrangement is similar to those discussed in section 2.5 of the literature survey; which presents the independant experimental results of most relevance and greatest similarity to this study.

Only the maximum flowrate obtainable from the fan was studied, with the duct end open (clearly the duct can not be blocked in this situation). Duct and bed heights of 10 cm were used. The top of the bed was blocked with cardboard and sealed with electrical tape; this arrangement was satisfactory for the duct open experiments. When the duct was partially blocked the air pressure lifted the cardboard and weights were placed on the board. However before sufficient load was applied the bed supports began to sag and hence this line of attack was abandoned.

The results for this case (maximum flowrate, duct end open, bed outlet blocked) are presented with those for the case when the bed outlet is not blocked (which are discussed in more detail above).

Graph 8.70. Static Pressures (obtained with the pitot tube) Below the Bed Base with the Bed Outlet Blocked and Open. Duct End Open. Average Velocity in the Duct Before the Bed Approximately 33.5 ms^{-1}. Duct and Bed Heights 10 cm.

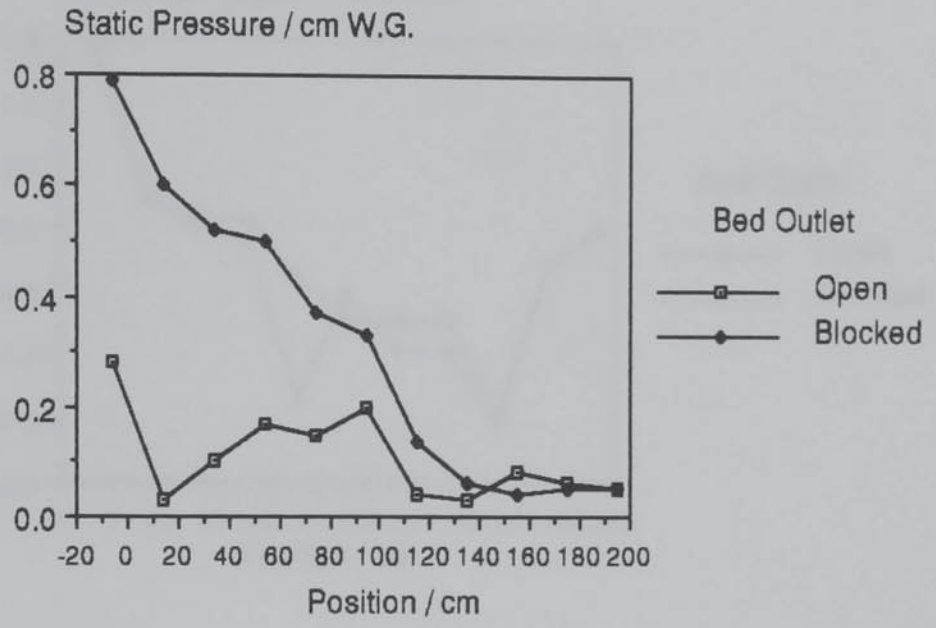

Graph 8.71. Total Pressure (measured with the pitot tube) Below the Bed Base with the Bed Outlet Blocked and Open. Duct End Open. Average Velocity in the Duct Before the Bed Approximately 33.5 ms^{-1}. Duct and Bed Heights 10 cm.

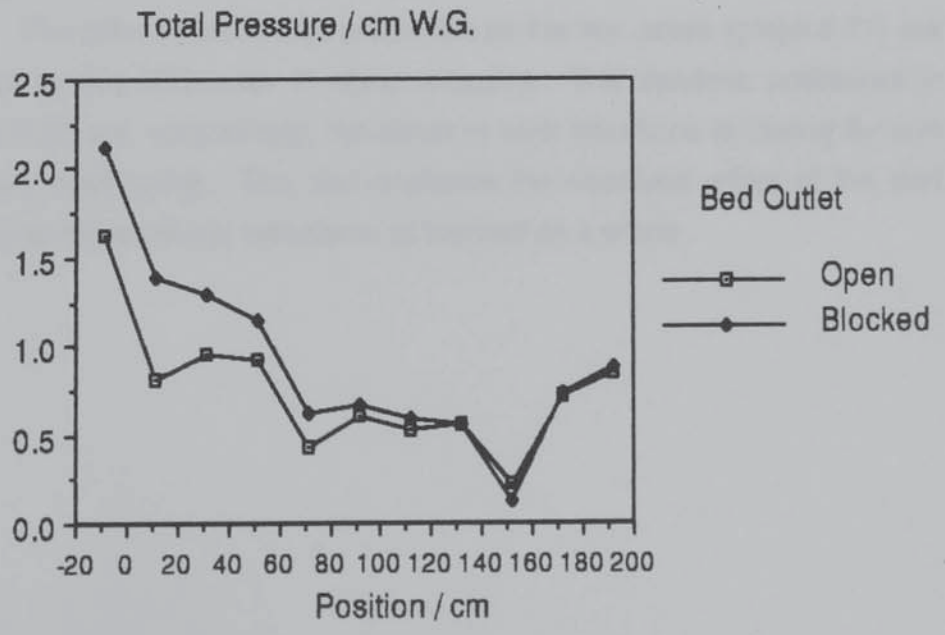

Graph 8.72. Dynamic Pressure (measured with the pitot tube) Below the Bed Base with the Bed Outlet Blocked and Open. Duct End Open. Average Velocity in the Duct Before the Bed Approximately 33.5 ms^{-1}. Duct and Bed Heights 10 cm.

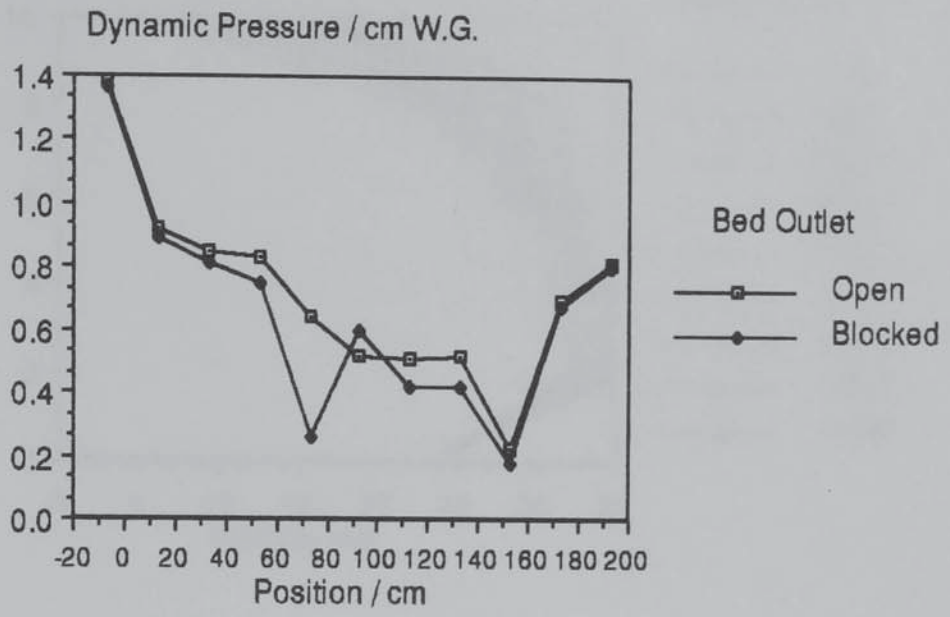

Graph 8.70 shows static pressure, this is higher nearer the duct inlet when the bed outlet is blocked and falls along the bed until the static pressure is the same in both cases. This is because, when the bed is blocked, at the inlet end of the bed there is a higher overall resistance to flow along the channel (nearer the bed,with the bed outlet blocked) than through the bed in the bed open case.

The differences in total pressures for the two cases (graph 8.71) are caused by this difference in static pressure. The dynamic pressures in graph 8.72 are, surprisingly, the same in both situations (allowing for one incorrect data point). This demonstrates the dominant effect of the bed base over the frictional resistance of the bed as a whole.

Graph 8.73. Horizontal Velocity Profiles in the Duct when the Bed Outlet is Blocked. Duct End Open. Average Velocity in the Duct Before the Bed 33.6 ms^{-1}. Bed and Duct Heights 10 cm.

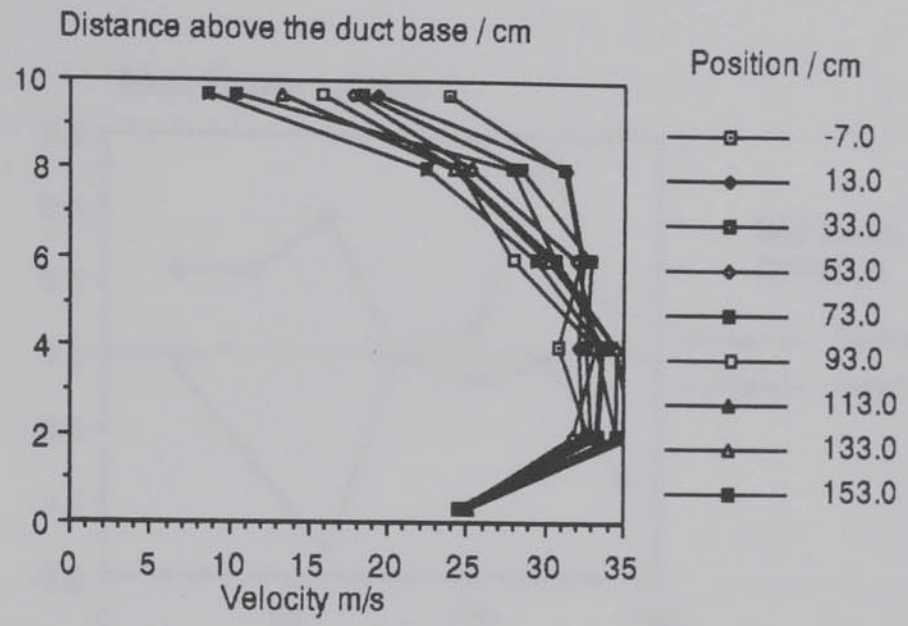

Graph 8.73 presents the duct velocity profiles when the bed outlet is blocked, when compared to the profiles in the normal case (graph 8.46) it is apparent that lower flows are observed in the top half of the duct (nearer the bed base) and higher flows in the lower half when the bed outlet is blocked. Since the gas cannot leave through the bed, the flow in the bed is now mainly horizontal and the bed resistance is therefore higher so velocities in, and near to the bed fall. Continuity then causes velocities to rise in the other, lower part of the duct.

Pressures at the bed base were also measured using the needle probes and are presented as graphs 8.74 to 8.79. The hollow square symbols are the results for the bed blocked case and the solid diamond symbols are those for the bed open.

Graph 8.74. Needle Tube Static Pressures on the Duct Side of the Bed Support Mesh with the Bed Outlet Blocked and Open. Duct End Open. Average Velocity in the Duct Before the Bed Approximately 33.5 ms^{-1}. Duct and Bed Heights 10 cm.

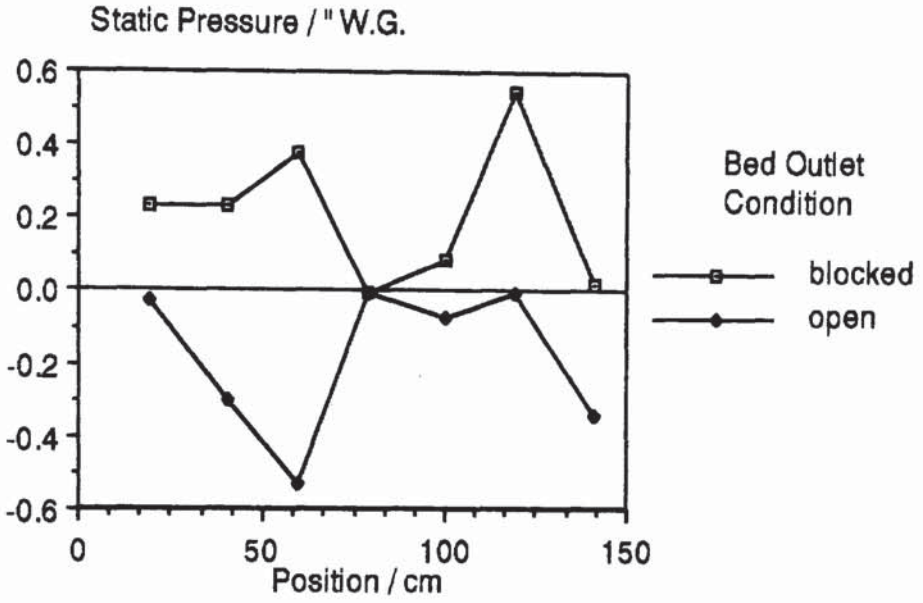

Graph 8.75. Needle Tube Static Pressures on the Bed Side of the Bed Support Mesh with the Bed Outlet Blocked and Open. Duct End Open. Average Velocity in the Duct Before the Bed Approximately 33.5 ms^{-1}. Duct and Bed Heights 10 cm.

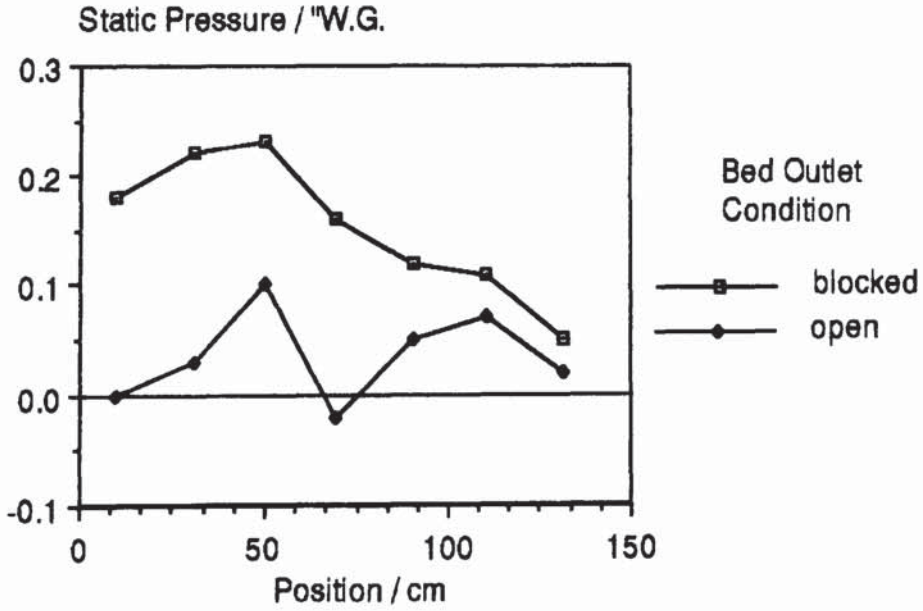

Graphs 8.74 and 75 show static pressure either side of the bed support. In the bed blocked case these pressures are higher than in the bed open case as discussed above; in particular, negative pressures are not observed. The trends in static pressure along the bed base are somewhat different when the bed is blocked than when it is open. On the bed side of the support mesh static pressures are higher initially when the bed is blocked and fall to the same value, as discussed above for the pitot measurements.

Graphs 8.76 and 77 compare total pressures for the same situations: the differences between the two situations being due to differences in static pressure discussed above as well as differences in dynamic pressure. Velocities at the bed base (calculated from dynamic pressures) are presented in graphs 8.78 and 79.

Graph 8.76. Needle Tube Total Pressures on the Duct Side of the Bed Support Mesh with the Bed Outlet Blocked and Open. Duct End Open. Average Velocity in the Duct Before the Bed Approximately 33.5 ms^{-1}. Duct and Bed Heights 10 cm.

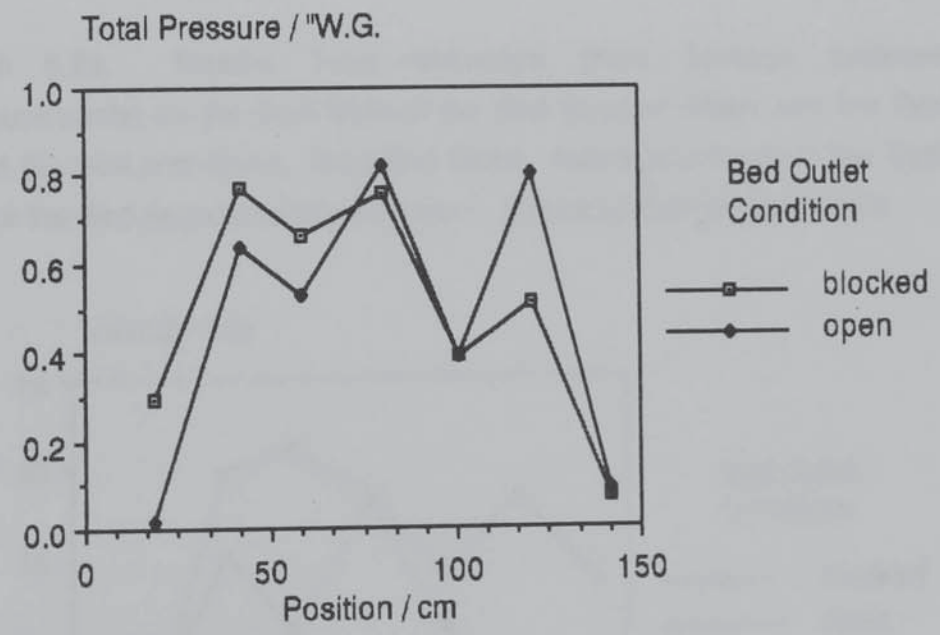

Graph 8.77. Needle Tube Total Pressures on the Bed Side of the Bed Support Mesh with the Bed Outlet Blocked and Open. Duct End Open. Average Velocity in the Duct Before the Bed Approximately 33.5 ms^{-1}. Duct and Bed Heights 10 cm.

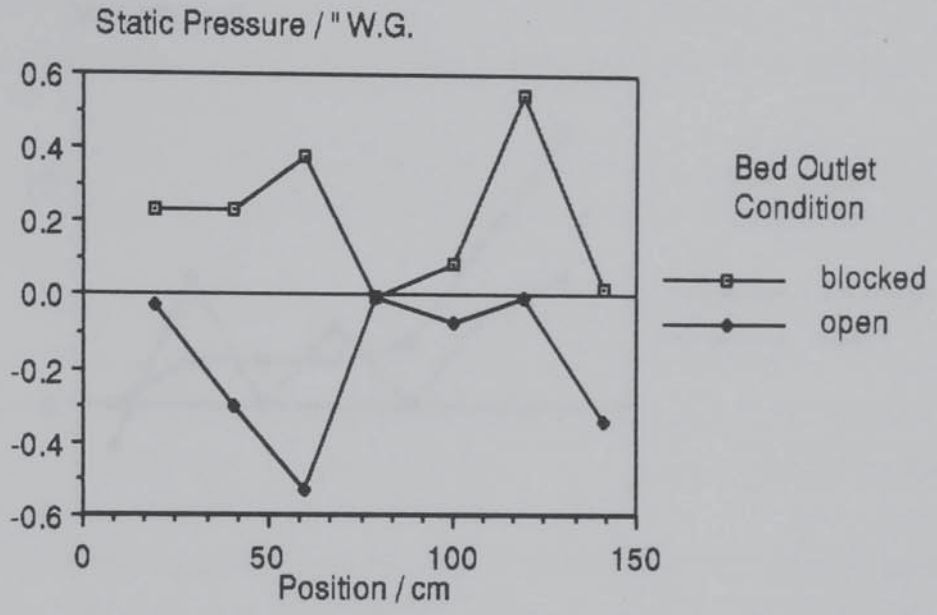

Graph 8.78. Needle Tube Velocities (from dynamic pressure measurements) on the Duct Side of the Bed Support Mesh with the Bed Outlet Blocked and Open. Duct End Open. Average Velocity in the Duct Before the Bed Approximately 33.5 ms^{-1}. Duct and Bed Heights 10 cm.

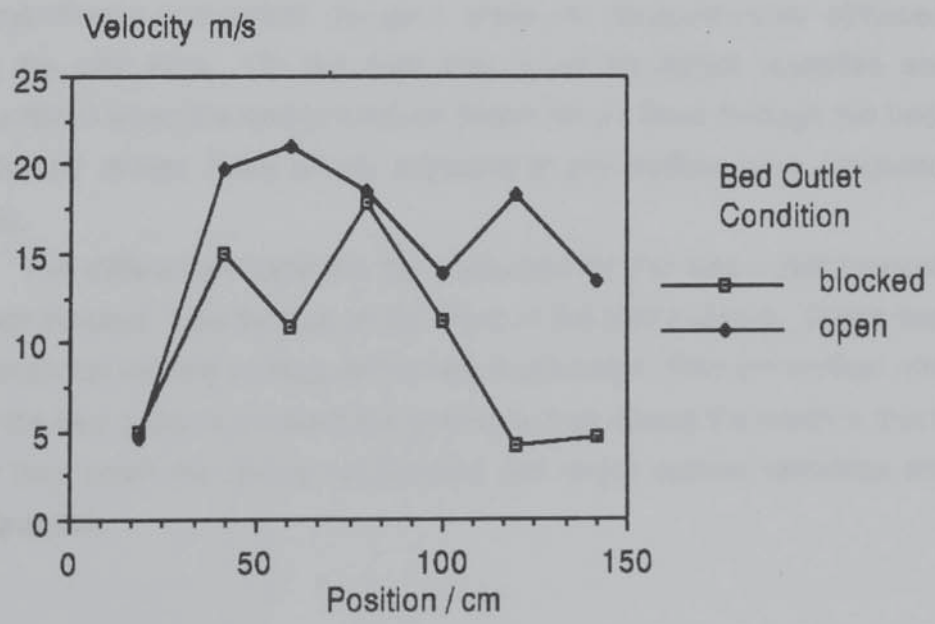

Graph 8.79. Needle Tube Velocities (from dynamic pressure measuremets) on the Bed Side of the Bed Support Mesh with the Bed Outlet Blocked and Open. Duct End Open. Average Velocity in the Duct Before the Bed Approximately 33.5 ms^{-1}. Duct and Bed Heights 10 cm.

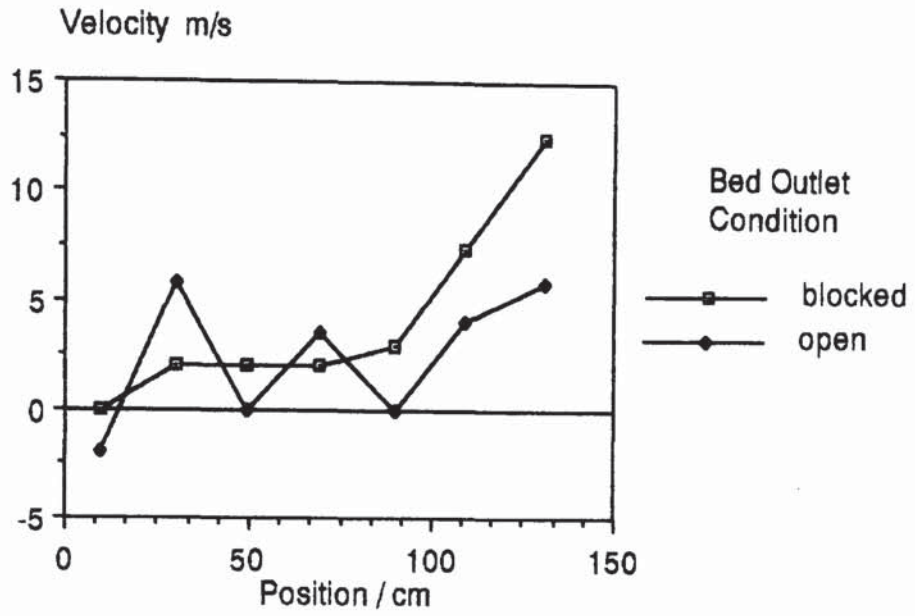

On the bed side of the mesh the velocity rises slowly along the first two thirds of the bed and more quickly along the last third. This may be due to air flowing into the (blocked) bed along the initial two thirds of its length and then out of the bed and into the duct for the last third. Since the inflow area is double that of the outflow area, outflow velocities are higher - this hypothesis contradicts dynamic pressure measurements obtained using the pitot tube. On the duct side, lower horizontal velocities are encountered when the bed is blocked (since no air flows through the bed, but, the air moves more slowly adjacent to the outflow area proposed above).

The differences between the pressures for the bed outlet blocked and not blocked is partly due to the effect of the bed support. Given that the horizontal velocity component is very much larger than the vertical one when the bed outlet is blocked; the pressure drop across the mesh is much larger than when the bed is not blocked and larger vertical velocities are encountered.

8.8. DISCUSSION.

The results presented in this chapter have allowed the identification of a number of significant aspects of the flow in packed beds. The arrangement of the apparatus used has been shown to be appropriate. In particular the facility for controlling the relative amounts of gas flowing through the bed and the duct outlet has allowed a detailed examination of the effects of the bed base.

The new concept of a 'separating streamline' in the free space below a shallow packed bed has been proposed and experimentally confirmed.

The need for a vectorial form of equation to describe flow in packed beds (since such flow is not unidirectional) has been confirmed. This is particularly apparent from the static pressure profiles measured in the bed. The experiments have also demonstrated that a 'no-slip' assumption for the velocity at the bed base is not correct.

Over the range of flowrates used it has been shown that the flow patterns in the apparatus are the same. This is somewhat surprising when the form of the Ergun Equation is considered; given that, because the flow is maldistributed in the bed,both low and high velocities are encountered .

The significant effect of increased voidage at the end walls has been shown. In a similar fashion, the limitations of using wires to support the bed have been shown.

The effect of changes in bed and duct height have been examined and are shown to act in opposition; thus following the principles of similarity.

Velocities leaving the bed and the components of pressures at its base can be related as follows:

i. Duct Open. Velocity above the bed is roughly inversely proportional to static and dynamic pressures below it.

ii. Duct Partially Blocked. Velocity above the bed is proportional to static pressure below it and inversely proportional to the dynamic pressure at the bed base.

iii. Duct Blocked. The same relationships are observed in this case as when the duct is partially blocked.

These relationships are only approximate and, ignore end effects. These conclusions for the duct open case differ from those for the other

cases and so they cannot be used to discriminate between contradictory flow visualisation results and duct measurements.

Measurements of pressure (and velocity) at the bed base (by pitot and needle tubes) must be considered in the light of Graph 8.80.

Graph 8.80. The Effect of Yaw Angle on Differential Pressure Output from a Pitot Tube (adapted from B.S.I (1977)).

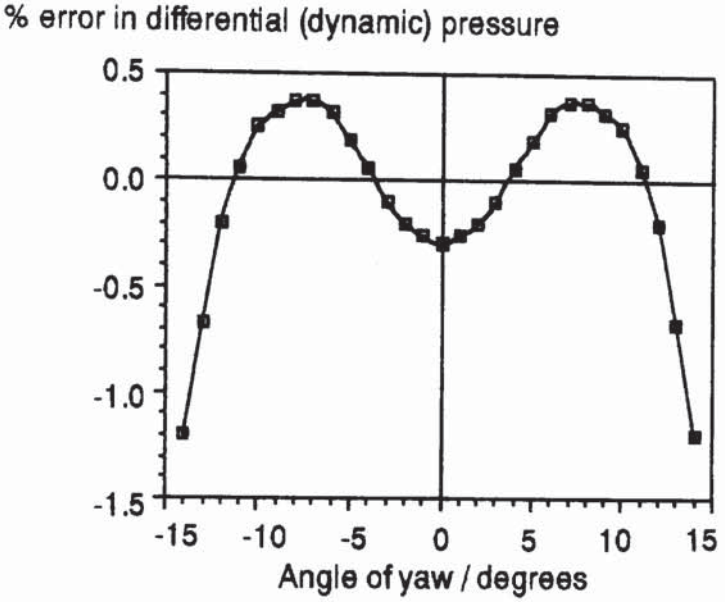

This graph shows the effect of aligning a pitot tube out of parallel with the flow direction and will clearly apply to many of the measurements presented above, as well as to the needle tube measurements; particularly near the end of the bed and when the duct outlet is obstructed. An improved approach to the collection of experimental measurements from this apparatus would be to use Laser Doppler Velocimetry; such measurements would be of particular use in developing and validating the C.F.D. model presented in the subsequent chapter.

No consistent, unified mechanism has been identified that explains the observations made in this chapter. Nor has it been possible to show that the duct end open results relate to small sections of the bed and duct when the latter is obstructed at its outlet. Nevertheless, the following behaviour has been identified.

i. Duct End Open. This case is characterised by low static pressures that decrease along the duct. Dynamic and total pressures decrease along the bed base.

ii. Duct End Partially Blocked. Static pressure rises along the bed base, while dynamic pressure decreases.

iii. Duct End Wholly Blocked. Total pressure at the bed base is constant, static pressure increases and dynamic pressure decreases.

iv. When the duct outlet is obstructed pressure recovery against the end plate in the duct is clearly significant and is shown by the increase in static pressures in the duct along the length of the bed. This pressure recovery is as described by the Bernouilli Equation.

The needle tubes used to measure pressure at the bed base have shown the dominant effect of the bed support both in overall frictional terms and in terms of converting the horizontal component of velocity to the vertical. This dominant effect of the bed base has justified the flexible, adaptable design of the bed support attachment.

8.9. CONCLUSIONS.

1. This chapter has presented and discussed an extensive set of experimental results for the two dimensional, shallow packed bed apparatus described in Chapter 7.

2. Unfortunately, no consistent explanation of the mechanisms invloved has been developed; this suggests that specific experiments must be performed to identify the precise nature of maldistributed gas flows in 'at risk' items of process equipment in packed beds. This, in turn, shows the potential usefulness of the C.F.D. modelling approach used in this work (and particularly that presented in the next chapter). Certain dominant effects have been identified:

i. When the duct outlet is open static pressure decreases along the duct ; when it is closed static pressure recovery against the end wall.

ii. Dynamic pressure decreases along the bed base (as does velocity).

iii. When the duct outlet is open velocity leaving the bed is roughly inversely proportional to static and dynamic pressure at the bed base.

iv. When the duct outlet is partially or wholly blocked velocity above the bed is proportional to static pressure and inversely proportional to the dynamic pressure.

v. The flow pattern in the apparatus does not depend on the gas flowrate.

3. The need for a vectorial decription of flow in the bed and, and a 'slip' velocity at its' base have been shown.

4. The critical effects of the bed support and flow in the base of the bed have been shown.

CHAPTER 9

A COMPUTER MODEL OF THE TWO DIMENSIONAL EXPERIMENT

9.1. INTRODUCTION.

As discussed in Chapter 3, a computer model of fluid flow in process equipment that contains packed beds is required so that such equipment can be reliably designed and particularly, so that gas distribution problems in packed beds can be avoided or overcome.

This chapter presents further developments of the models described in Chapters 4 and 5 (where the domain of study is wholly packed) by modelling the two dimensional experimental investigation of maldistributed gas flow in and outside a packed bed presented in Chapters 7 and 8. The results from the model are compared to these experimental results. The comparison reveals the need for an improved description of the bed base region. Two such improvements are introduced into the model and are as follows:

i. The representation of the variation in voidage within the bed near its' base.

ii. A boundary condition for the bed base. This involves applying the logarithmic law for velocity (near a wall) to the bed base without restricting the velocity to zero at the base. This boundary condition is implemented within a turbulence model.

These refinements greatly improve the predictive performance of the model.

Initially, however, a satisfactory, converged solution to the model was not obtained. The behaviour of the model is considered in detail and the reasons for the difficulties encountered in obtaining a solution identified. The algorithm presented in Chapter 4 is then modified; as a result of which satisfactory, converged solutions are obtained. This part of the work also reveals a significant limitation in the 'staggered grid' approach used in PHOENICS (described above in section 4.3.4).

9.2. THE COMPUTER MODEL.

The PHOENICS model is based on the realisation of a two dimensional Ergun Equation in the Ground Routine. In addition the k-ε turbulence model is applied to the domain in order to realistically include the effects of turbulence on the fluid flow.

9.2.1. Assumptions and Simplifications.

As with any engineering model, when a C.F.D. model is created assumptions are made which can be classified as belonging to one of two groups.

i. Justifiable assumptions, which can be shown to be reasonable and have a negligible effect on the results from the model.

ii. Simplifying assumptions, whose omission make the modelling task more straightforward in the initial stages. These assumptions may or may not effect the results from the model but this cannot be determined until the assumption is removed.

The justifiable assumptions are as follows:-

i. The bed is homogenous; it is not practically possible to model all the individual packing pieces.

ii. That the vectorial Ergun Equation satisfactorily predicts the pressure drop and flow pattern in a packed bed. This has been verified for situations where the domain of interest is wholly packed in Chapter 5.

iii. The gas is not compressible (i.e. it is of constant density). Ali (1984) indicates that in packed beds, when the Mach Number is less than 0.1 (as in the experiments modelled here) compressibility effects are not significant. If air is considered as obeying the ideal gas law, comparing the density of air at the maximum and minimum pressures encountered experimentally gives a density variation of 1.2% which can be ignored. This assumption considerably minimises the computational effort required to obtain a solution to the model as density is not considered as a variable.

The simplifying assumptions are as follows:

i. The bed voidage is constant.

ii. The bed support wires have no effect on the flow pattern.

iii. The wall friction in the bed can be ignored .

iv. The fluid flow in the bed does not require a turbulence model (see section 9.2.4).

v. The bed base is fully described by the Ergun Equation for the bed as a whole in addition to the full equations of motion used.

vi. The bed support mesh does not effect the flow (that is, it can be ignored)

These simplifying assumptions are discussed in greater detail below.

9.2.2. Grid Description.

For PHOENICS to solve the equations that describe the fluid flow of interest, a grid is required over which these equations can be solved. The grid used in these models is presented in this section.

The experiment is two dimensional and a grid has been created in the y-z plane to represent the apparatus. The reason for the selection of the y-z plane is discussed in section 9.2.4 below. This section explains how the grid is specified.

Two grids are required: one for the duct end open and partially blocked cases and the other for the duct end blocked case. The latter is a staightforward simplification of the former which is presented first. The Q1 files for these cases are presented as Appendices 5 and 6. Since the geometry of the apparatus is simple and orthogonal a straightforward cartesian grid can be used and body fitted co-ordinates are not required.

The apparatus is shown in figure 9.1 which also shows the location of the inlet and outlets and the subdivision of the domain into sections. As can be seen in the figure these sections are selected so that the domain is logically subdivided into areas which will require different fluid mechanic description (blocked areas, open areas, packed areas etc.). The grid is coded so that NYn and NZn which represent the number of cells in each direction and section can be independently varied. Each of the variables describing the number of cells in these sections have counterparts that define the length of each section (named LYn and LZn). The two sets of variables are defined in table 9.1.

Figure 9.1. The Division of the Apparatus into Sub-Domains for the Grid Specification and, the Positions of Inlet and Outlets.

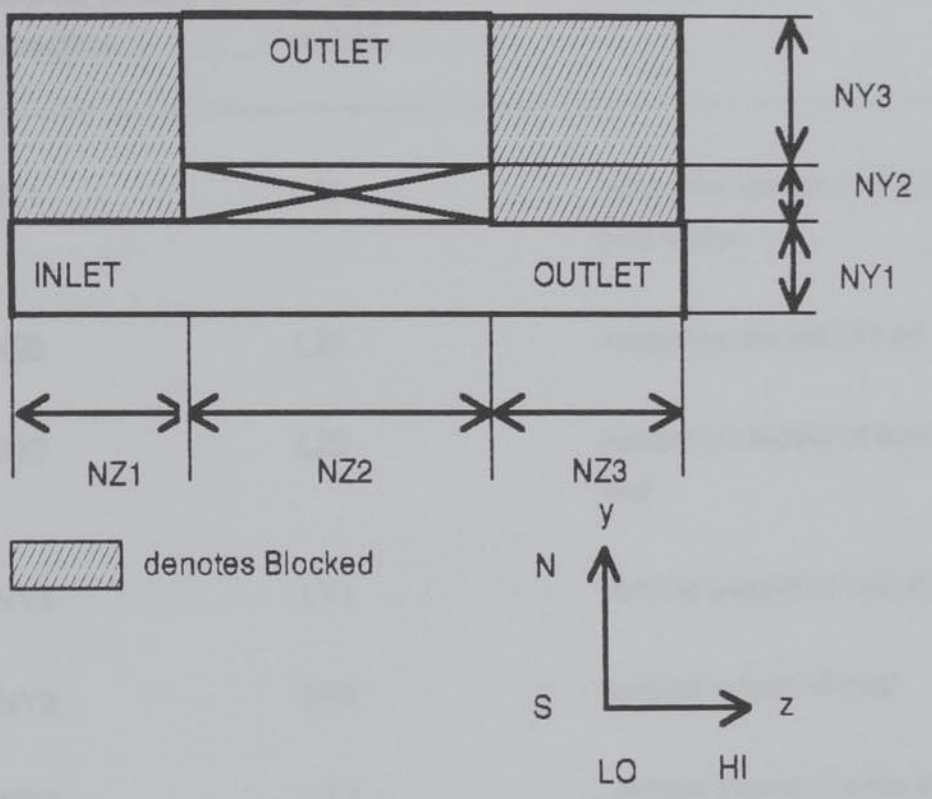

The length variables are set to the physical dimensions of the apparatus except that the vertical distance above the bed (LY3) is set to the distance between the bed base and the outlet (= 0.7m) less the bed height as shown in equation 9.1;

$$LY3 = 0.7 - LY2 \qquad \text{Equation 9.1}$$

thus when the bed height is adjusted the outlet plane remains correctly positioned.

A similair manipulation is performed for the horizontal distance between the beginning of the bed and the outlet (=2.01m). The length of the bed can then be varied without incorrectly moving the position of the duct outlet, as shown in equation 9.2;

$$LZ3 = 2.01 - LZ2 \qquad \text{Equation 9.2}$$

Table 9.1. Grid Definition Variables.

Number of cells in section.	Length of section.	Description.
NZ1	LZ1	horizontal aspect of inlet duct before bed
NZ2	LZ2	horizontal aspect of bed
NZ3	LZ3	horizontal aspect of duct after bed
NY1	LY1	vertical aspect of inlet duct
NY2	LY2	vertical aspect of bed
NY3	LY3	vertical aspect of area above bed

In addition thin cells are included at the walls and bed base/ free fluid boundaries. The thickness of these cells is defined by the variable TTC in the Q1 file. Such thin cells are provided;

i. At the walls; so that large variations in velocity between adjacent cells are avoided; thus easing the progress towards a converged solution.

ii. At the bed base/ free fluid interface to minimise the effect of averaging two cell velocities to obtain a nodal cell value (see section 4.4.5)

The grid is defined in the Q1 file using the "method of pairs" (Rosten and Spalding (1987 a & b)) (the same method described in section 5.4.3 of chapter 5). In brief, each section of the grid is defined by the number of cells and section length; within this PHOENICS automatically determines the discretisation of the domain.

As indicated above, the grid for the duct end blocked (at the end of the bed) is a simplification of the case discussed above. This is clearly

illustrated by comparing the schematic view of the apparatus in this model presented as figure 9.2 with figure 9.1. The grid defining commands in the duct open Q1 file for the third Z section of the grid (i.e. those commands using NZ3 & LZ3) are simply deleted. It is also necessary to remove the coding for the duct end outlet and the blocked region above this end of the duct which are discussed in the following section.

Figure 9.2. The Division of the Apparatus into Sub-Domains for the Grid Specification and the Positions of Inlet and Outlets for the Duct End Wholly Blocked Case.

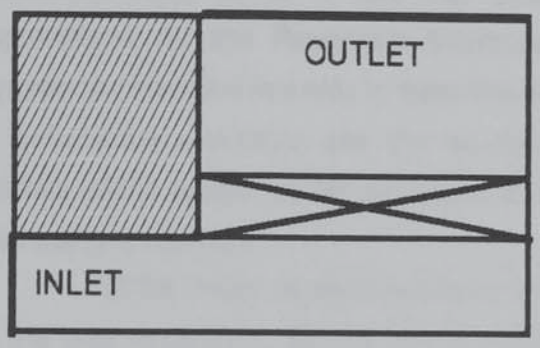

9.2.3. The PHOENICS Code for the Model.

THE Q1 FILES.

These are attached as Appendices 5 (duct end open) and 6 (duct end blocked). With the exception of the grid definition commands (discussed in the previous section) and the application of the turbulence model (discussed in the subsequent section); the commands and techniques used are the same as those used in the Q1 files described in chapter 5 to which the reader is referred.

THE GROUND FILE.

The GROUND File which describes the packed bed using the vectorial Ergun Equation is attached as Appendix 7. This is fundamentally the same as the GROUND coding discussed in Chapter 4 being based on the same algorithm. However, since the model is two dimensional only a two dimensional GROUND is required. The y-z plane is chosen although the x-z plane would be equally appropriate. It is important to use the z direction since, as has been shown, the slab-wise solution is performed in

this direction and its use will therefore promote and accelerate convergence.

9.2.4. The Turbulence Model.

In Chapter 4 the equations solved by PHOENICS were presented and discussed. The equations of motion used in PHOENICS strictly only describe laminar flows. They cannot describe the multiple, instantaneous fluctuations in flow quantities encountered in turbulent flows. The current state of knowledge of turbulence is such that these fluctuations cannot be described fully, since it has not been possible to obtain rigorous expressions for the Reynold's Stresses that must be included in the equations of motion in order to describe such flows. The best descriptions of turbulence available are the so-called Turbulence Models. These models while based, as far as possible, on the physics of turbulence are also partly empirical.

Of the many models available the k,ε model is generally regarded as the best (Spalding (1980)), and is available in the PHOENICS package (Rosten & Spalding (1987 a & b)). The variables k (the kinetic energy of turbulence) and ε (the dissipation rate of the kinetic energy of turbulence) are determined from the components of velocity. The two quantites are then used to determine a turbulent viscosity which is then applied to the equations of motion proper.

The subject of turbulence and its modelling is vast and extremely complex. It is therefore not possible to provide a full and detailed explanation of the various models or even the k-ε model used here. The reader is referred to the standard texts (such as Hinze (1975) and Davies (1972)) and the references cited above.

Appendices 5 and 6 present the Q1 files for the model and include the various commands necessary to describe the turbulent nature of the flow using the k, ε turbulence model. The turbulence model is also used in the prescription of wall friction. Essentially, the empirically based logarithmic law for velocity is imposed near to the walls. Its formulation is such that it makes use of the k and ε quantities in determining the effects of wall friction.

A brief explanation of the commands that describe the turbulence and wall friction (in the Q1 files presented as Appendices 5 and 6) follows, under the relevant group headings.

Group 1. Preliminaries.

The variables TKEIN & EPSIN are declared.

Group 7. Variables Stored, Solved and Named.

Instructions are issued to solve for k (KE) and ε (EP) and store the turbulent viscosity (ENUT).

Group 9. Properties of the Medium.

ENUT is set to equal to GRND3 which instructs the package to determine the turbulent viscosity from the Prandtl - Kolmogorov formula which is:

$$\mu_T = c_1 l k^{0.5} \qquad \text{Equation 9.3}$$

where; c_1 = a constant

l = the mixing length scale

k = the kinetic energy of turbulence.

EL1 the mixing length scale is set equal to GRND4 and so is derived from the turbulent kinetic energy and its dissipation rate, thus.

$$l = \frac{c_2 k^{1.5}}{\varepsilon} \qquad \text{Equation 9.4}$$

where c_2 = a constant.

The values of the constants C_1 and C_2 are built into PHOENICS and are such that they give the best empirical fit to a large, varied set of empirical data. This does not, of course, imply that they will give the most realistic description of a given situation.

Group 11. Initialisation of Variable and Porosity Fields.

The quantites TKEIN and EPSIN which describe the sources of k and ε at the inlet are determined using the appropriate equations and constants. Initial estimates of half the inflow values are then made throughout the domain using the FIINIT command. This will assist convergence.

Group 13.

PATCH and COVAL commands are used to determine the sources of k and ε using the appropriate formulae by setting the coefficients and values equal to GRND4. Hence, the patch names begin

with KESO (k ε source). The patches used in this way are shown in figure 9.3.

Figure 9.3. The Patches Use for the Turbulence Model Sources.

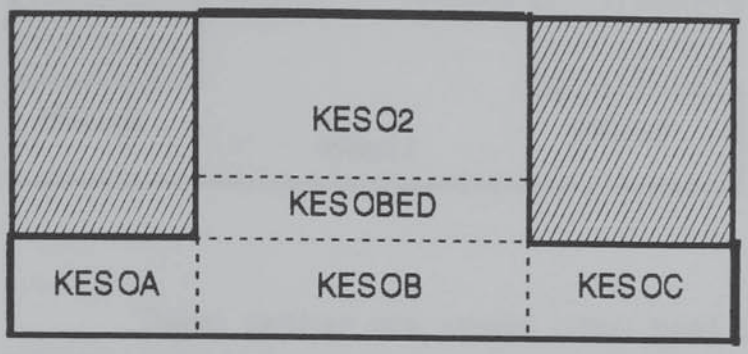

A number of patches are required (rather than just one which covers the whole domain) because:

i. The prescription of sources of turbulence quantites in blocked areas is meaningless.

ii. The treatment of turbulence in the bed is different from that outside the bed (in the free fluid), as is now discussed.

The constants (f_1 and f_2) in the Ergun Equation that allow for the effects of tortuosity and constriction are determined experimentally and therefore include the effects of turbulence. The simultaneous application of a turbulence model would therefore invalidate these constants and so, a turbulence model is not applied in the bed. Hence, the patch 'KESOBED' (see figure 9.3) is 'SKIP'ed, and souces of k and ε are not computed in the bed and so the turbulence model is not applied. In turn, the turbulent viscosity in the bed is not determined and must therefore be prescribed. This is done using the BETUVI (bed turbulent viscosity)patch and coval where the turbulent viscosity is set equal to the laminar viscosity divided by 100, as explained in Chapter 5.

Wall friction is applied in Group 13 in conjunction with the turbulence model. The patch names all begin with WALL- and their positions are shown in figure 9.4.

Figure 9.4. The Position of the Wall Friction Patches.

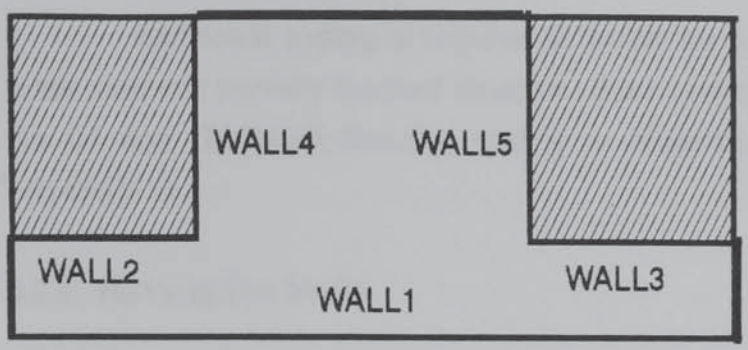

These patches use special patch types of the form SWALL, NWALL which imply that the specified coefficient is multiplied by the reference kinematic viscosity times the fluid density divided by the distance of the grid node from the specified face. That is, frictional wall effects are represented by sources on the velocity equations (and reduce with distance from the wall).

Thus COVALs are applied for the velocity component parallel to the wall with the value of the velocity set to zero. The coefficient is set to GRND2 which gives the logarithmic law for wall friction. Similarly COVALs are required for K and ε where the coefficients and values are set to GRND2 to include this wall boundary condition.

Group 17. Under-Relaxation Devices.

Relaxation is provided for k and ε; in addition, the setting of KELIN = 1 specifies the type of linearisation used for the source terms of the turbulence parameters k and ε. The settings of this variable will not effect the final solution but, can considerably alter the rate at which it is achieved. The setting used is such that it anticipates the effects of walls (where production and dissipation of turbulence are approximately equal).

Group 19. Data Communicated by SATELLITE to GROUND.

USEGRX = T instructs the package to use Ground Example 2 which contains the necessary formulae for the description of turbulence and wall friction described above.

GENK = T causes the inclusion of all spatial derivatives of velocity in the generation function for the source of K.

9.2.5. The Perforated Plate.

Additional coding is required to model the perforated plate used in the duct end partially blocked situation. Such coding will appear in both the Q1 and GROUND files.The coding is presented and explained in Appendix 11.

9.2.6. Running The Model.

The model is run on the same computer system and in the same way as the models described in Chapter 5. The reader is referred to section 5.3.3 for full details of the procedure.

9.3. A STRATEGY FOR EVALUATING THE MODEL.

When a converged and stable solution of the model has been obtained it must be compared to the experimental results presented in Chapter 8. This section presents a stategy for making such a comparison (which was concieved before the model was created) and should be considered in conjunction with the following sections which present results from the model presented above, and subsequent refinements to it.

i. The results from the model should, of course, first be checked for conservation and to ensure that the overall flow patterns are reasonable (by using the PHOTON graphics package of PHOENICS). The results can then be compared to the experimental results in the following order:

ii. The model should predict the velocity profile leaving the bed (i.e. at a given height above it) with due allowance made for the randomn nature of the real bed as against the homogenous nature in the model.

iii. The model should predict the velocity profiles in the duct below the bed and, in particular, their changing form along the duct.

iv. The model should predict the static pressure profiles at various depths in the bed.

v. The model should predict the static pressures in the duct and, particularly at the bed base; at various positions along the duct.

vi. The model should predict the horizontal components of fluid velocity at the bed base.

(vii. For the duct end open and partially blocked cases. The model should accurately predict the 'diversion' ratio of the gas in the apparatus (i.e. the amount leaving through the bed to that leaving through the duct end)) .

The comparisons are listed in an order which indicates which tests are more or less likely to be satisfied. The earlier (lower number) tests are expected to be the 'easier' ones. The judgement of a comparisons 'difficulty' reflects both the quality and precision of the specific experimental measurements concerned as well as the computational effort and subsequent data manipulation required.

These comparisons are based on velocity and static pressure readings only as these are the quantities determined by PHOENICS. As discussed in Chapter 7 velocity is directly related to dynamic pressure. Total pressure is the sum of static and dynamic pressures and hence these comparisons cover the complete spectrum of fluid behaviour.

Initially it is recommended that only the duct end open and closed results are modelled because the correlation used to model the perforated plate will introduce an additional empiricism (see section 9.2.5 above). Initial comparisons should be confined to one flowrate, one duct height and one bed height. A flowrate equivalent to an inlet velocity of 21.1 ms^{-1} and duct and bed heights of 10 cm are recommended since most data is available for this case. If and as the model is further developed other flowrates and duct and bed heights can be modelled as can the duct end partially blocked results.

The comparisons will inevitably reveal limitations of the model; however it is first necessary to obtain converged, stable solutions from the model.

9.4. OBTAINING A SOLUTION FROM THE BASIC MODEL.

9.4.1. Towards a Satisfactory Solution.

When the model discussed above, using the GROUND file presented as Appendix 7 and either of the Q1 files presented as Appendices 5 and 6, was initially run, convergence was not achieved. This was characterised by an initial decrease in the residuals which then levelled out to a constant (and too high) level. The solution field,

particularly at the bed base, fluctuated strongly despite the contancy of the residuals.

Careful checks were made of the coding which was found to be 'as intended'. Further investigations were made, as follows:

i. The variables were very heavily relaxed individually; thus effectively freezing them. The solution procedure was otherwise allowed to proceed unaltered. Divergence resulted, and it became apparent that this was due to the heavy coupling of the velocity components.

ii. Various physically limiting cases were then examined. If the coding describing the bed is deactivated a sensible, converged solution is obtained. Similarly, previous work in this study (chapter 5) has shown that the formulation describing the bed functions correctly when the domain is wholly packed. This suggests that it is the effect of the bed base (as described) that causes the convergence problems. A model was written that describes a bed with free (unpacked) spaces above and below it and through which gas flows axially, as shown in figure 9.5. A converged solution from this model could be obtained, albeit with some difficulty. The pressure drop results from this model compared well with those calculated from the basic Ergun Equation. This suggests that it is the changes in direction of the gas flow at the bed base that causes the convergence problems.

Figure 9.5. The Axial Flow Test Case.

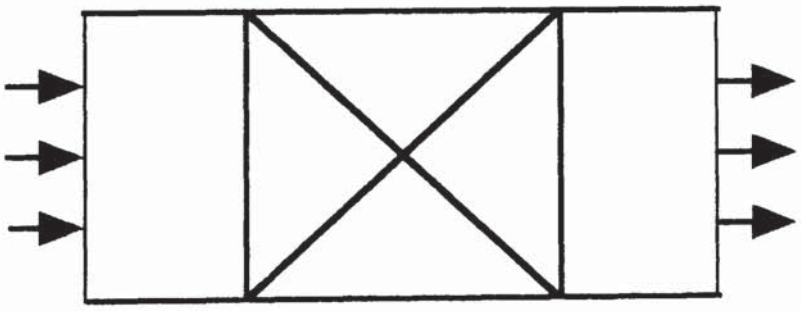

Contours of constant velocity in the original model (the two-dimensional, shallow packed bed model) are presented as figure 9.6.

Figure 9.6. Modelled Contours of Constant Velocity Component in the Two-Dimensional Apparatus, Duct End Open, Bed and Duct heights 10 cm, Flowrate Equivalent to a Dall Tube Pressure Drop of 15 cm W.G.

a. The Horizontal (z) Component of Velocity (ms^{-1})

b. The Vertical (y) Component of Velocity (ms^{-1})

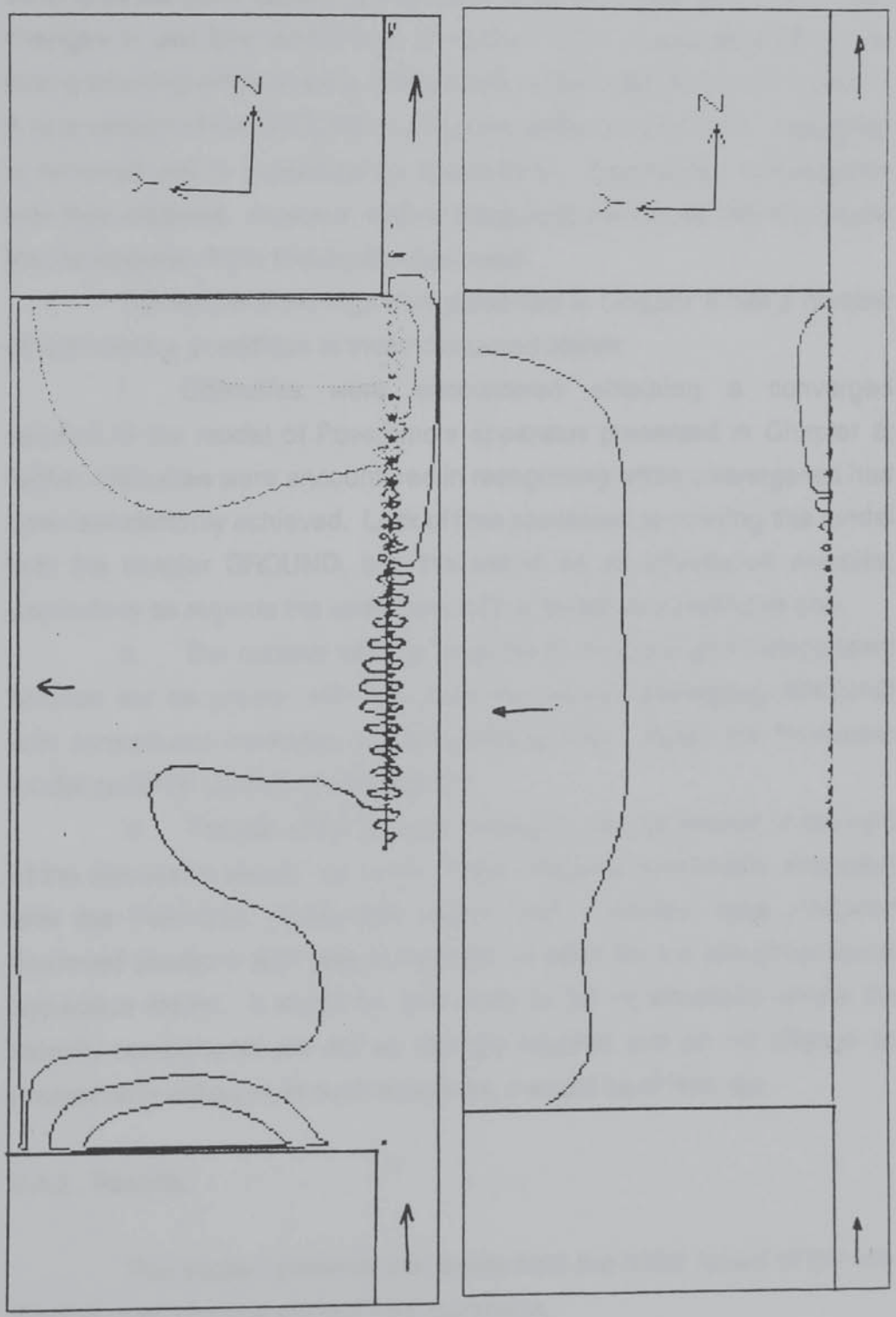

It is clear that a wavy velocity field of the type described in Chapter 4 is occuring at the bed base. This suggests that the approach used to minimise the effect of the staggered grid arrangement on the final solution is actually nullifying the effect of the staggered grid arrangement at this point. This occurs at the bed base because the Ergun Equation dominates the other aspects of fluid behaviour and because of the sudden changes in gas flow direction at this point. This is exacerbated by the strong coupling of the velocity components in the vectorial Ergun Equation. A new version of the GROUND coding was written in which this 'averaging' is removed and is presented as Appendix 8. Satisfactory convergence was then obtained. However, before presenting the results from the model the impications of this finding are discussed.

The failure of the algorithm presented in Chapter 4 has a number of implications in addition to those discussed above:

i. Difficulties were encountered obtaining a converged solution to the model of Poveromo's apparatus presented in Chapter 5; further difficulties were encountered in recognising when convergence had been satisfactorily achieved. Lack of time prevented re-running this model with the simpler GROUND, but, this would be an informative exercise; particularly as regards the usefulness of the model as a predictive one.

ii. The number of cells required to obtain a grid independent solution will be greater with the basic (no velocity averaging) GROUND with consequent increases in computational time. Again the Poveromo model could be used to investigate this.

iii. The use of the velocity averaging may be viewed, in the light of the discussion above, as naive. It was however reasonably succesfull with the Poveromo model and would, had it worked, have produced improved solutions with less computational effort for the two-dimensional apparatus model. It would be less likely to fail in situations where the velocity components are not so strongly coupled and do not change so dramatically although, in such situations, it would be of less use.

9.4.2. Results.

This section presents the results from the initial model of the two-dimensional, shallow packed bed apparatus.

Graph 9.1. Experimental and Computed (Basic Model) Duct Velocity Profiles at a position of 18 cm for 10 cm Duct and Bed Heights, Duct End Open, Average Velocity in the Duct before the Bed 21.1 ms^{-1}.

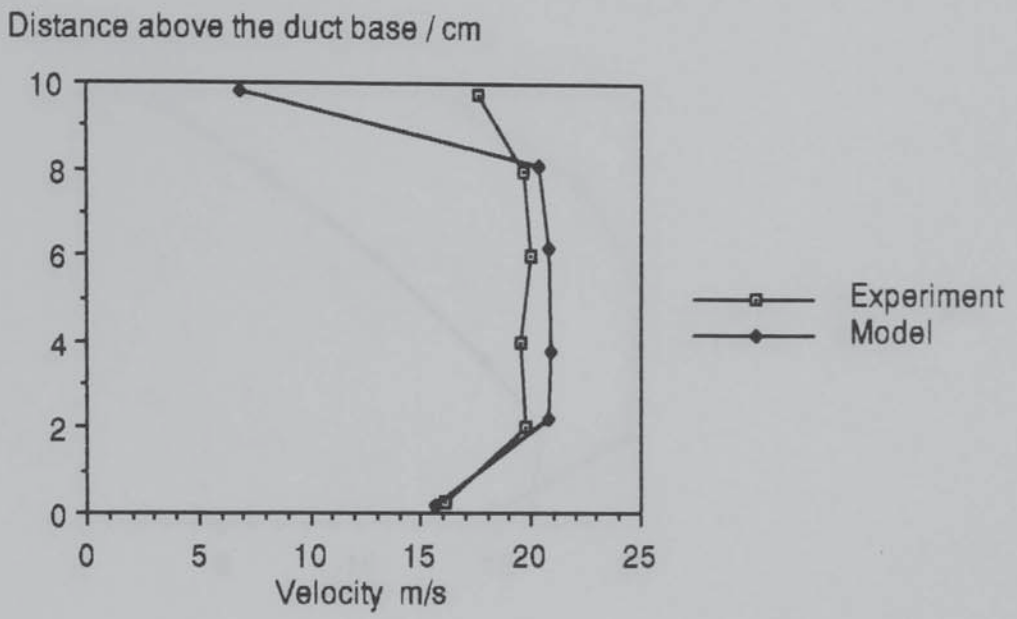

Graph 9.2. Experimental and Computed (Basic Model) Duct Velocity Profiles at a position of 58 cm for 10 cm Duct and Bed Heights, Duct End Open, Average Velocity in the Duct before the Bed 21.1 ms^{-1}.

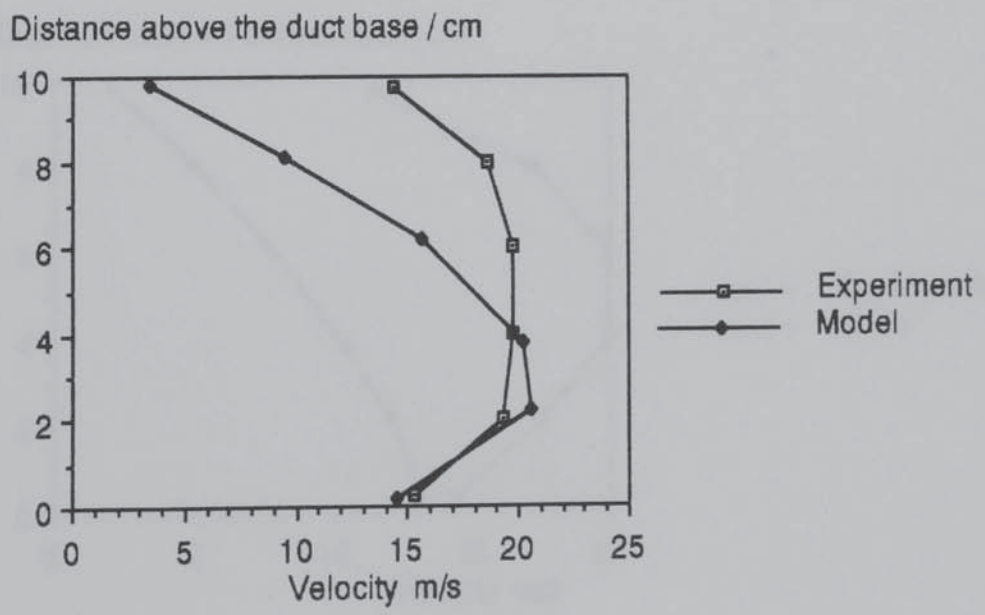

Graph 9.3. Experimental and Computed (Basic Model) Duct Velocity Profiles at a position of 98 cm for 10 cm Duct and Bed Heights, Duct End Open, Average Velocity in the Duct before the Bed 21.1 ms^{-1}.

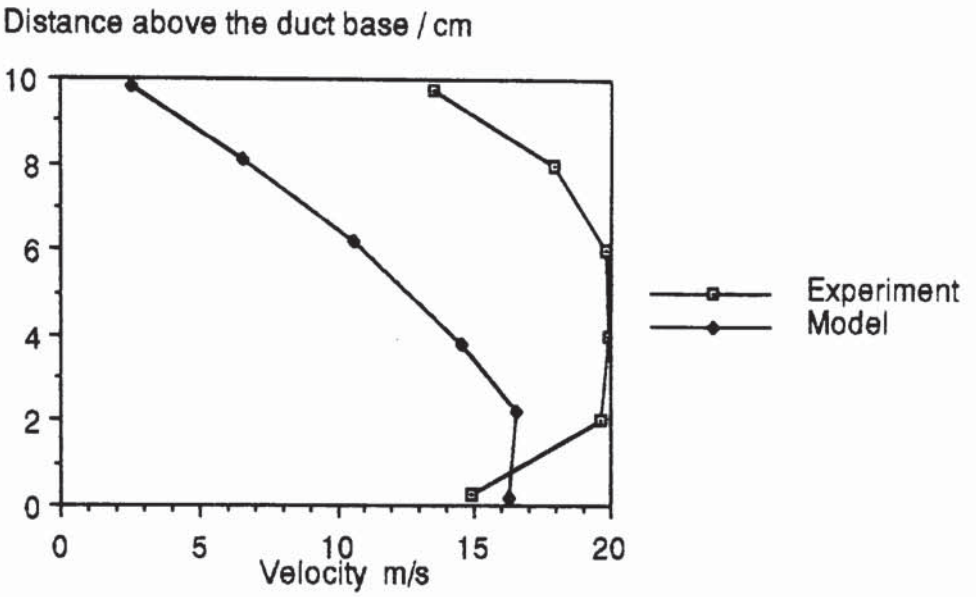

Graph 9.4. Experimental and Computed (Basic Model) Duct Velocity Profiles at a position of 138 cm for 10 cm Duct and Bed Heights, Duct End Open, Average Velocity in the Duct before the Bed 21.1 ms^{-1}.

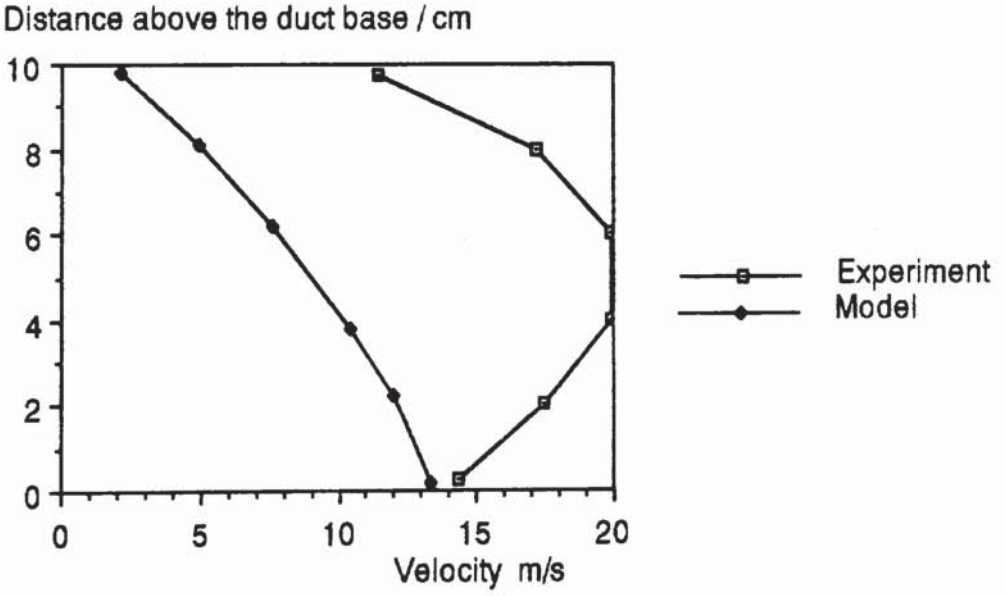

Graph 9.5. Experimental and Computed (Basic Model) Horizontal Velocities at the Bed Base for 10 cm Duct and Bed Heights, Duct End Open, Average Velocity in the Duct before the Bed 21.1 ms^{-1}.

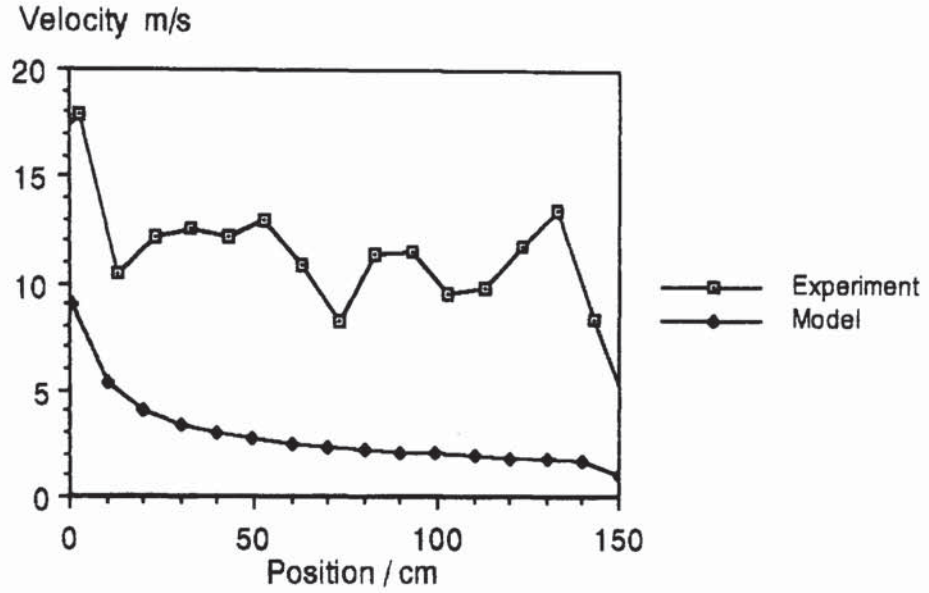

Graph 9.6. Experimental and Computed (Basic Model) Static Pressures at the Bed Base for 10 cm Duct and Bed Heights, Duct End Open, Average Velocity in the Duct before the Bed 21.1 ms^{-1}.

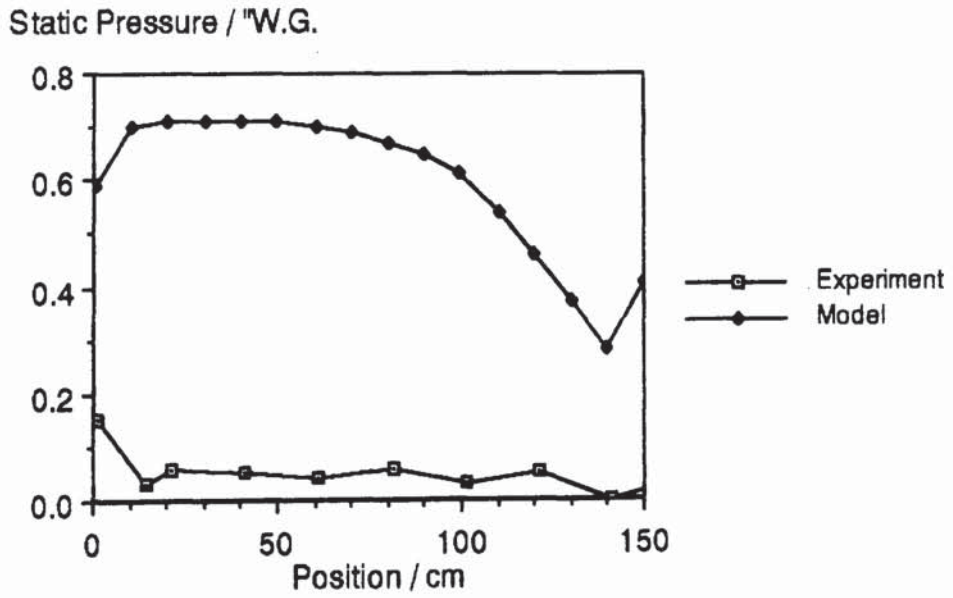

Graph 9.7. Experimental and Computed (Basic Model) Velocities 10 cm above the bed for 10 cm Duct and Bed Heights, Duct End Open, Average Velocity in the Duct before the Bed 21.1 ms^{-1}.

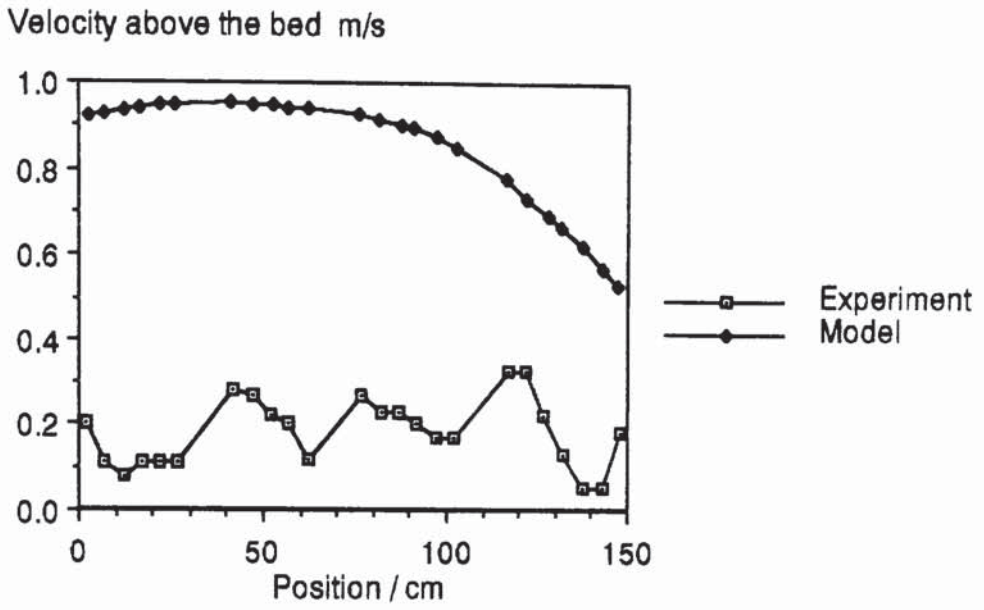

Graph 9.8. Experimental and Computed (Basic Model) Duct Velocity Profiles at a position of 18 cm for 10 cm Duct and Bed Heights, Duct End Blocked, Average Velocity in the Duct before the Bed 21.1 ms^{-1}.

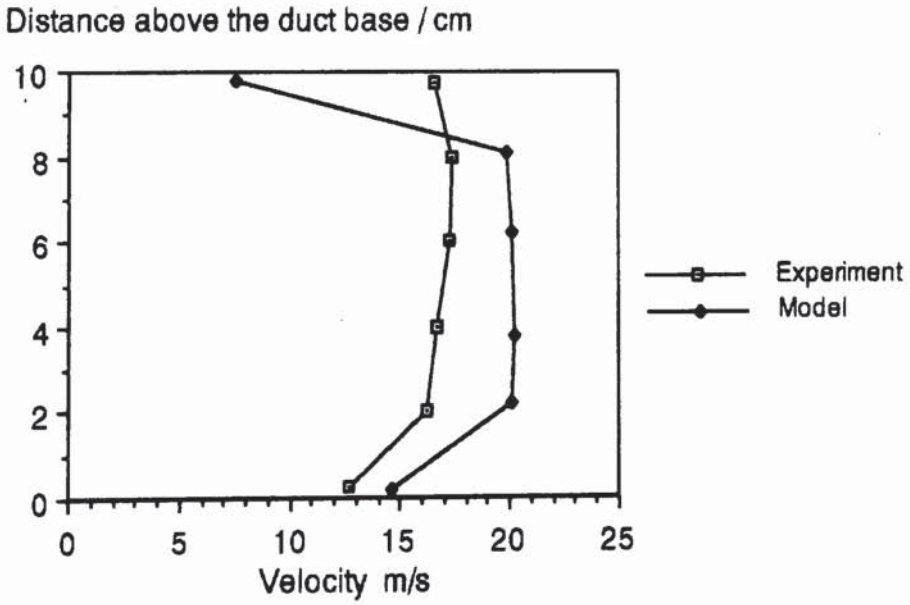

Graph 9.9. Experimental and Computed (Basic Model) Duct Velocity Profiles at a position of 58 cm for 10 cm Duct and Bed Heights, Duct End Blocked, Average Velocity in the Duct before the Bed 21.1 ms^{-1}.

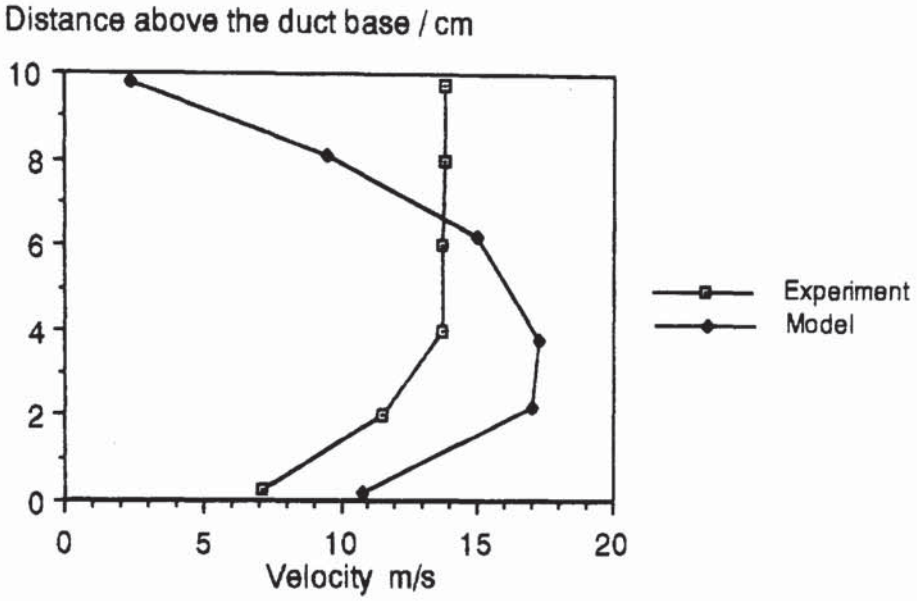

Graph 9.10. Experimental and Computed (Basic Model) Duct Velocity Profiles at a position of 98 cm for 10 cm Duct and Bed Heights, Duct End Blocked, Average Velocity in the Duct before the Bed 21.1 ms^{-1}.

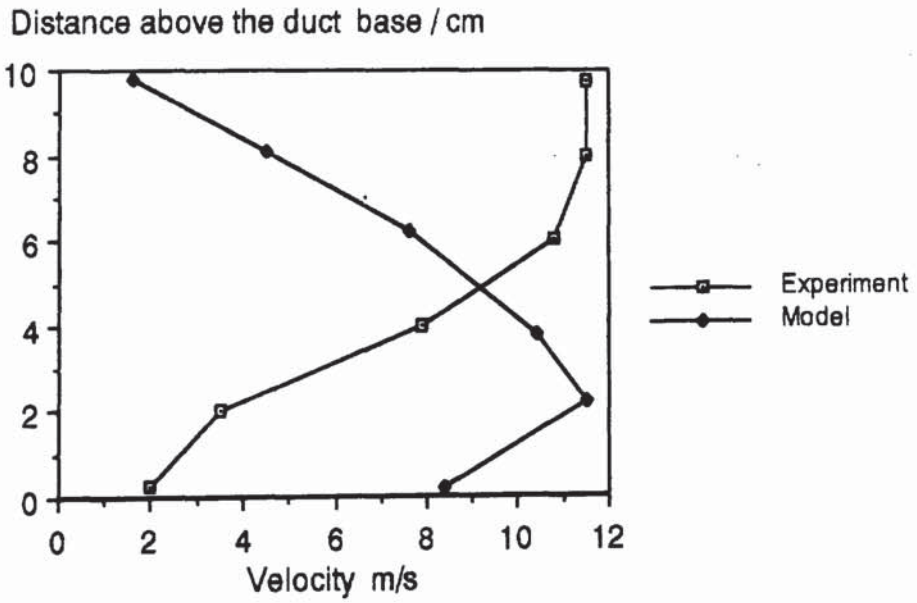

Graph 9.11. Experimental and Computed (Basic Model) Duct Velocity Profiles at a position of 138 cm for 10 cm Duct and Bed Heights, Duct End Blocked, Average Velocity in the Duct before the Bed 21.1 ms^{-1}

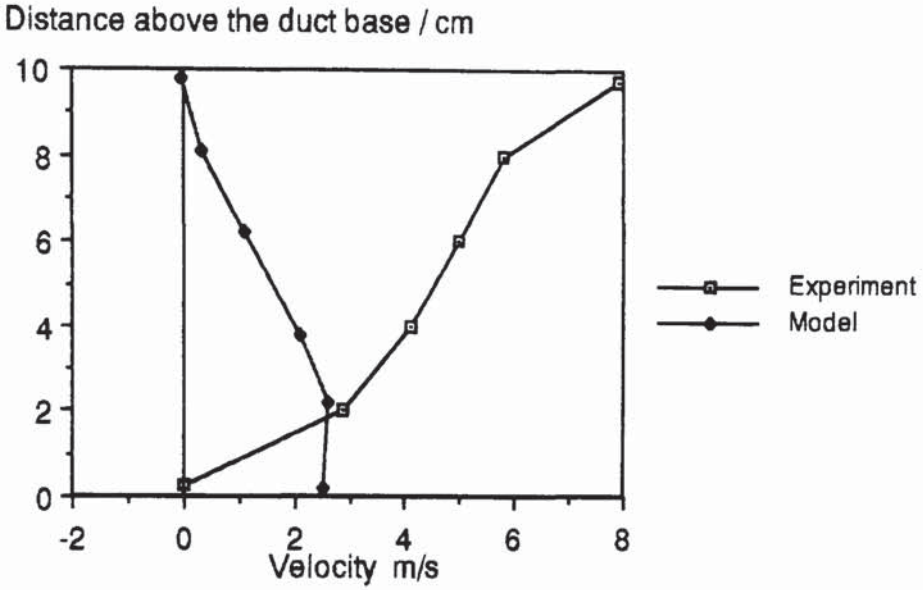

Graph 9.12. Experimental and Computed (Basic Model) Velocities at the Bed Base for 10 cm Duct and Bed Heights, Duct End Blocked, Average Velocity in the Duct before the Bed 21.1 ms^{-1}.

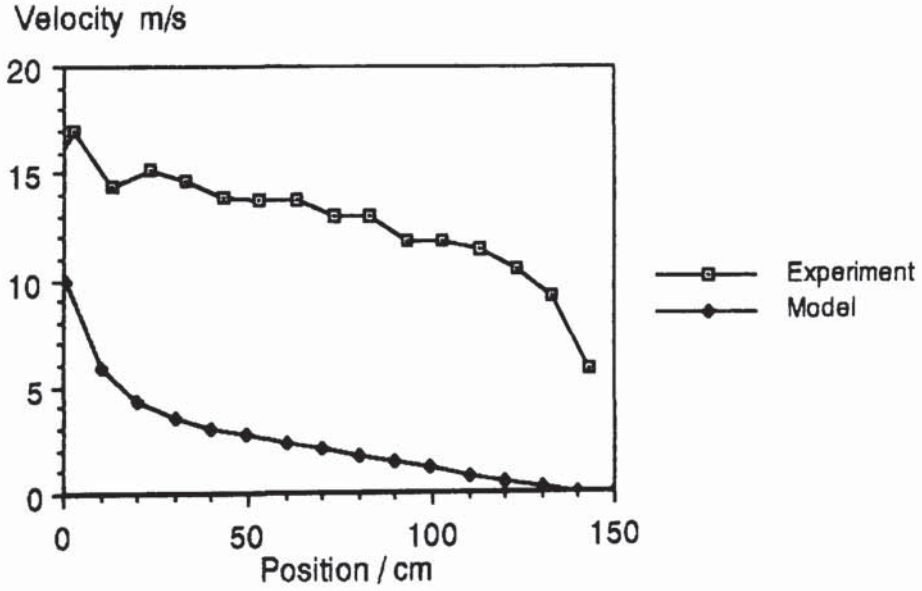

Graph 9.13. Experimental and Computed (Basic Model) Static Pressures at the Bed Base for 10 cm Duct and Bed Heights, Duct End Blocked, Average Velocity in the Duct before the Bed 21.1 ms^{-1}.

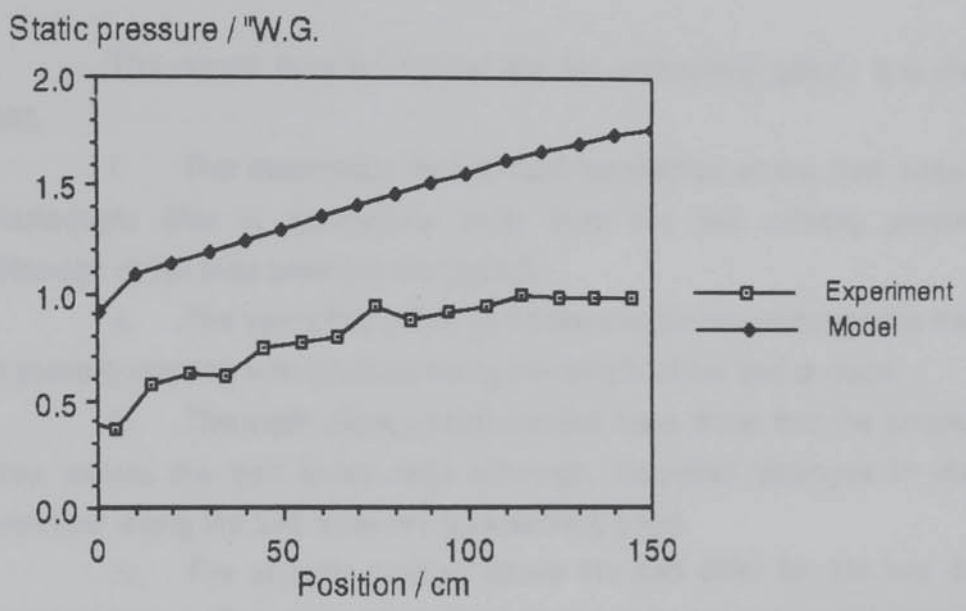

Graph 9.14. Experimental and Computed (Basic Model) Velocities 10 cm above the bed for 10 cm Duct and Bed Heights, Duct End Blocked, Average Velocity in the Duct before the Bed 21.1 ms^{-1}.

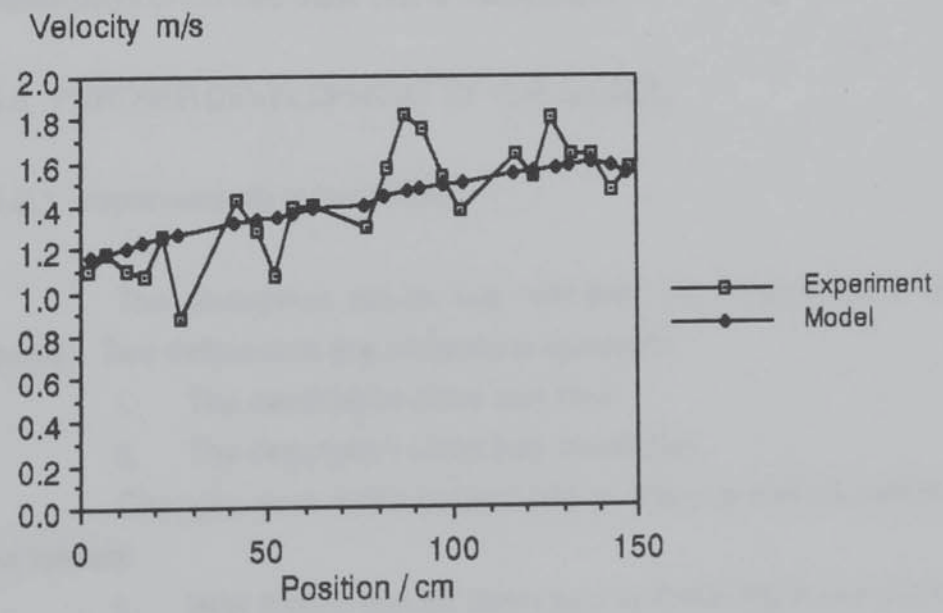

A grid independent solution is obtained with a 116 x 96 grid (duct end open) or a 96 x 96 grid (duct end blocked). Results are presented below for the basic cases identified in 9.3 for the initial comparison.

9.4.3. Discussion of Results.

The results from this model are not particularly good. It is clear that:

i. The description of the fluid mechanics at the bed base is inadequate (this is particularly clear from the the velocity profiles). Although at the duct base it is very good.

ii. The velocities at the bed base are too low although the trend in these quantities with position along the length of the bed is good.

iii. The static pressures at the bed base show that the pressure drop across the bed is too high although, modelled changes in static pressure along the bed base are qualitatively good.

iv. The velocity profiles above the bed differ for the two duct end conditions. The duct end blocked case results are very good because all the gas flows through the bed (that is the results are constrained by the mass balance), the results indicate that horizontal voidage variations are not significant. The duct end open results are much worse suggesting, in contrast to the static pressure results that the modelled bed resistance is too low. This can be resolved by recognising that it is probably the description of the bed base that is inadequate.

9.5. FURTHER DEVELOPMENT OF THE MODEL.

9.5.1. Improvements to the Model.

The discussion above has indicated the weakest parts of the model. Two deficiences are particularly apparent:

i. The description of the bed base

ii. The description of the bed resistance.

Changes were made to the model to overcome these deficiences as follows:

i. Wall friction can be described in PHOENICS (as discussed in section 9.2.4) by setting the velocity at the wall and parallel to it, to zero and introducing a logarithmic velocity profile through the turbulence model

(that is, by the appropriate setting of the coefficients and values in the COVAL statement for the wall PATCH). This is achieved since the turbulence model determines the turbulent viscosity used by the equations of motion. Clearly, the velocity at the base of the bed (the bed 'wall') is not zero but, the effects of the wall on local turbulence and hence flow patterns can still be included in the model. The additions to the relevant Q1 files are presented as Appendix 10. The coefficients on the turbulence quantities are set so that the local values of K and ε are given by the VALUE. The setting of the values to GRND2 gives:

$$k_{wall} = \frac{f_\phi |u_{\parallel wall}|^2}{\sqrt{c_\mu c_D}}$$

Equation 9.5.

$$\varepsilon_{wall} = \sqrt{k} / c_D \partial$$

Equation 9.6.

where $c_\mu c_D = 0.09$, ∂ is the distance of the grid node from the wall and f_ϕ is a generalised friction factor which for $N_{Re} > 132.5$ is given;

$$f_\phi = \left[\frac{0.0435}{\ln (1.01 + 9 N_{Re} \sqrt{f_\phi})} \right]^2$$

Equation 9.7.

and;

$$|u_{\parallel wall}| = \left[\left\{ \frac{v_e + v_w}{2} \right\}^2 + v_h \right]^{1/2}$$

Equation 9.8.

(for this geometry only). This is known as the Bed Wall Friction Model (B.W.F. Model).

ii. The inclusion of an approximation of the vertical voidage fluctuations in the bed. (As has been shown above the horizontal fluctuations are not significant). The GROUND coding for this is presented as Appendix 9, and is specific to a bed 10 cm deep and represented by 32 cells. The results of Benanti & Brosilov (1962) where used to determine the voidage for a given cell. This data is then placed in a string which is in turn used to obtain strings of Ergun Equation constants. The relevant constant is then used for each cell. This is known as the Voidage Variation Model (V.V. Model).

The two improvements are also applied simultaneously to produce a third model, the Combined Model.

9.5.2. Results from the Improved Models.

Graph 9.15. Experimental and Computed (B.W.F., V.V. and Combined Models) Duct Velocity Profiles at a position of 18 cm for 10 cm Duct and Bed Heights, Duct End Open, Average Velocity in the Duct before the Bed 21.1 ms^{-1}.

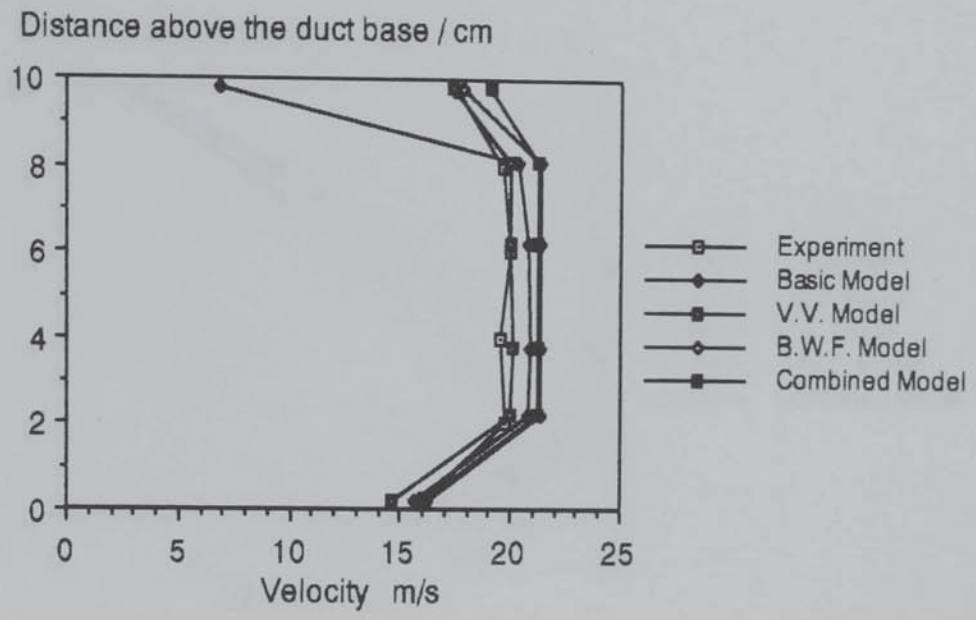

Graph 9.16. Experimental and Computed (B.W.F., V.V. and Combined Models) Duct Velocity Profiles at a position of 58 cm for 10 cm Duct and Bed Heights, Duct End Open, Average Velocity in the Duct before the Bed 21.1 ms^{-1}.

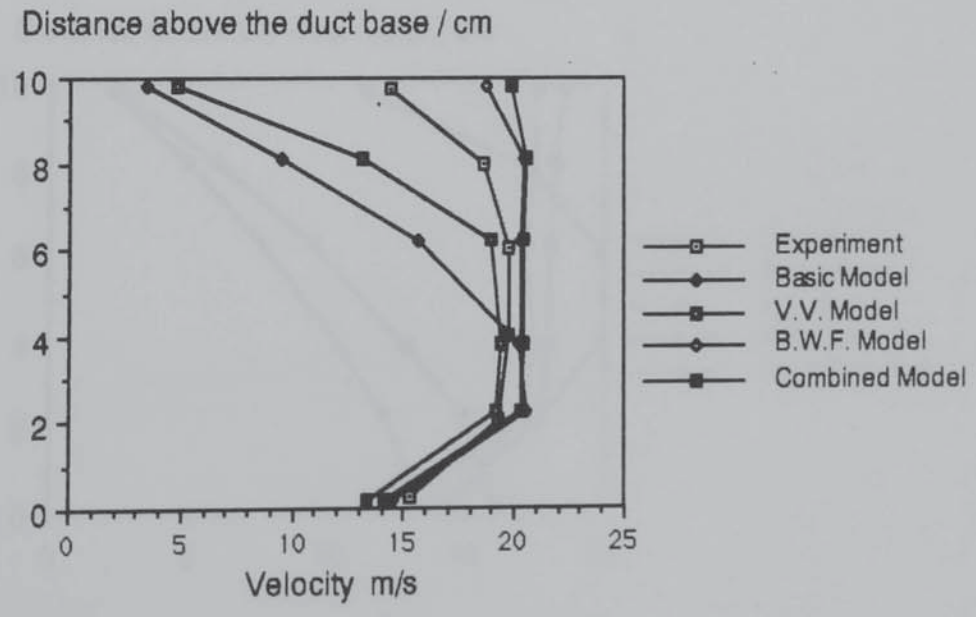

Graph 9.17. Experimental and Computed (B.W.F., V.V. and Combined Models) Duct Velocity Profiles at a position of 98 cm for 10 cm Duct and Bed Heights, Duct End Open, Average Velocity in the Duct before the Bed 21.1 ms^{-1}.

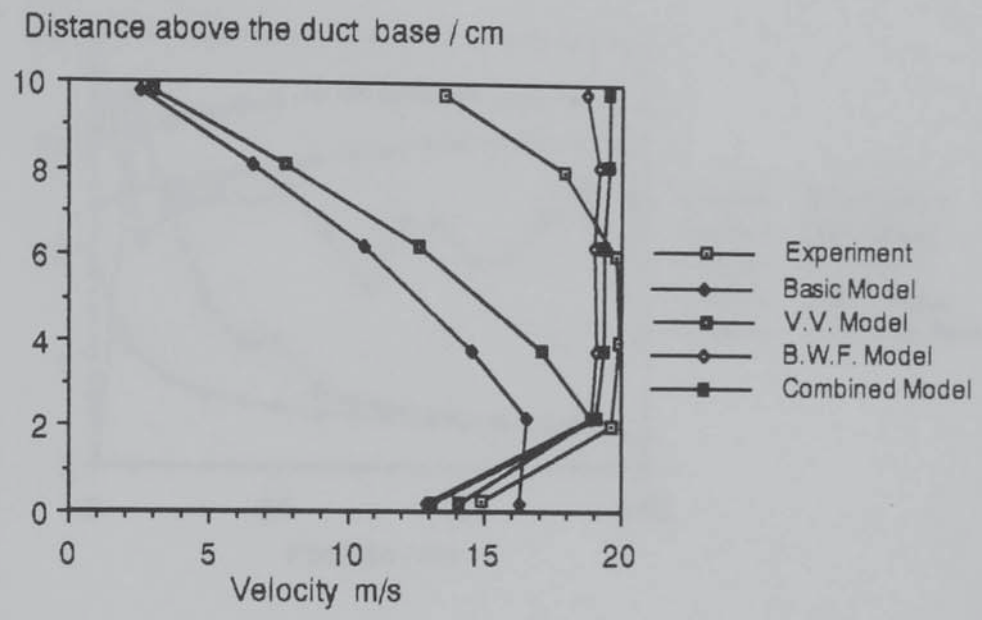

Graph 9.18. Experimental and Computed (B.W.F., V.V. and Combined Models) Duct Velocity Profiles at a position of 138 cm for 10 cm Duct and Bed Heights, Duct End Open, Average Velocity in the Duct before the Bed 21.1 ms^{-1}.

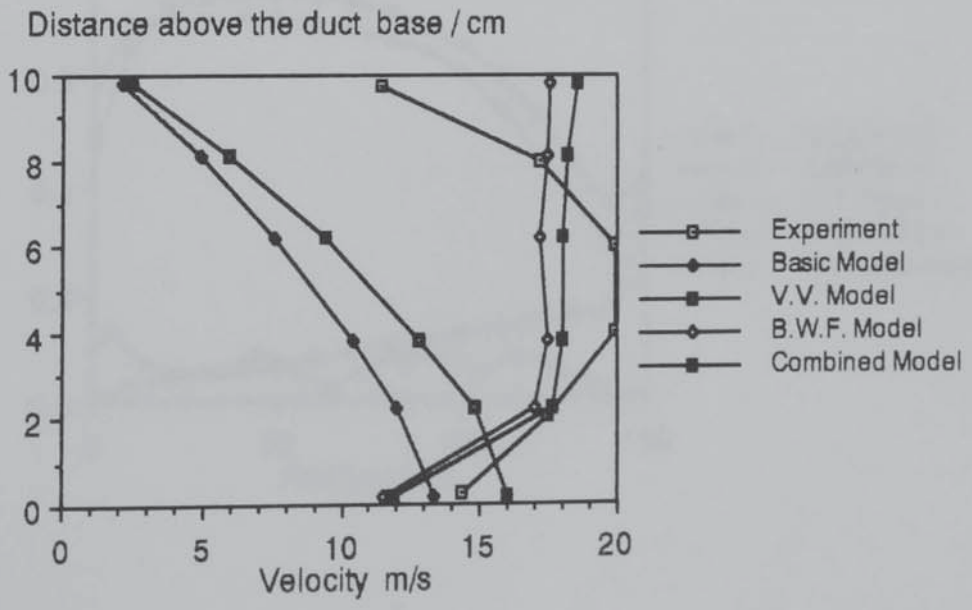

Graph 9.19. Experimental and Computed (B.W.F., V.V. and Combined Models) Velocities at the Bed Base for 10 cm Duct and Bed Heights, Duct End Open, Average Velocity in the Duct before the Bed 21.1 ms^{-1}.

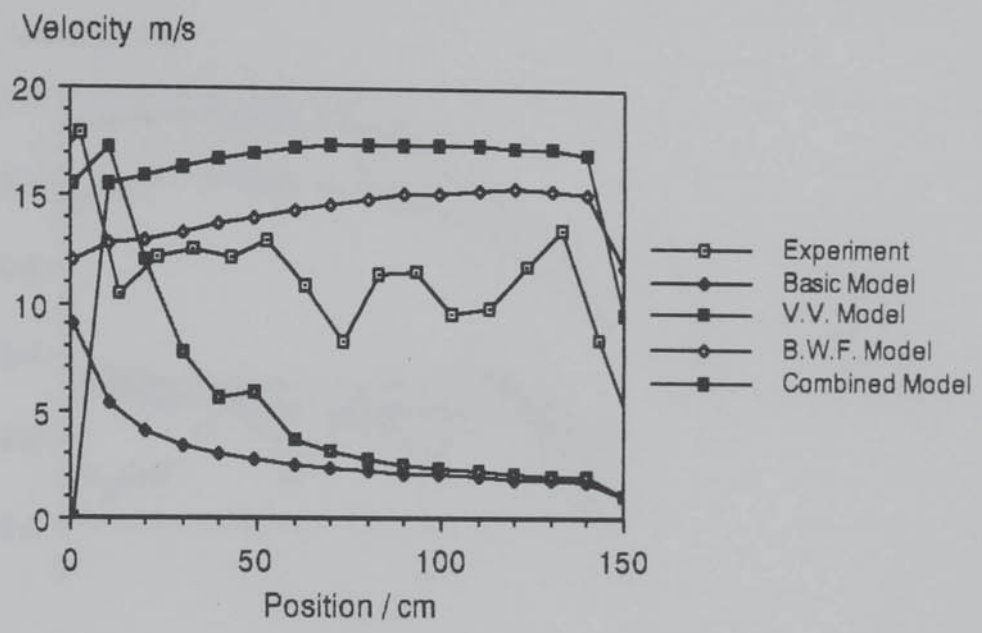

Graph 9.20. Experimental and Computed (B.W.F., V.V. and Combined Models) Static Pressures at the Bed Base for 10 cm Duct and Bed Heights, Duct End Open, Average Velocity in the Duct before the Bed 21.1 ms^{-1}.

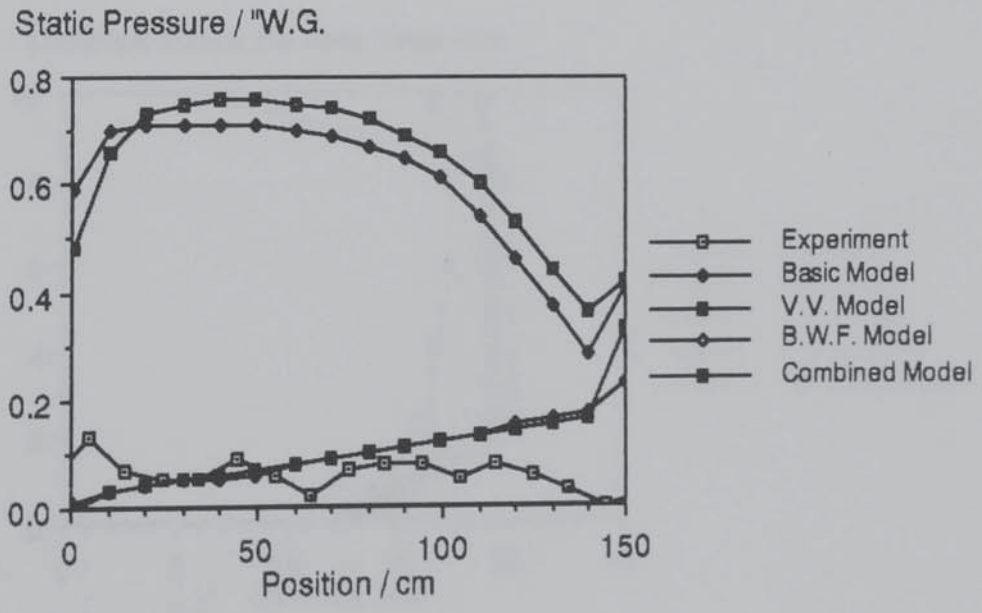

Graph 9.21. Experimental and Computed (B.W.F., V.V. and Combined Models) Velocities 10 cm above the bed for 10 cm Duct and Bed Heights, Duct End Open, Average Velocity in the Duct before the Bed 21.1 ms^{-1}.

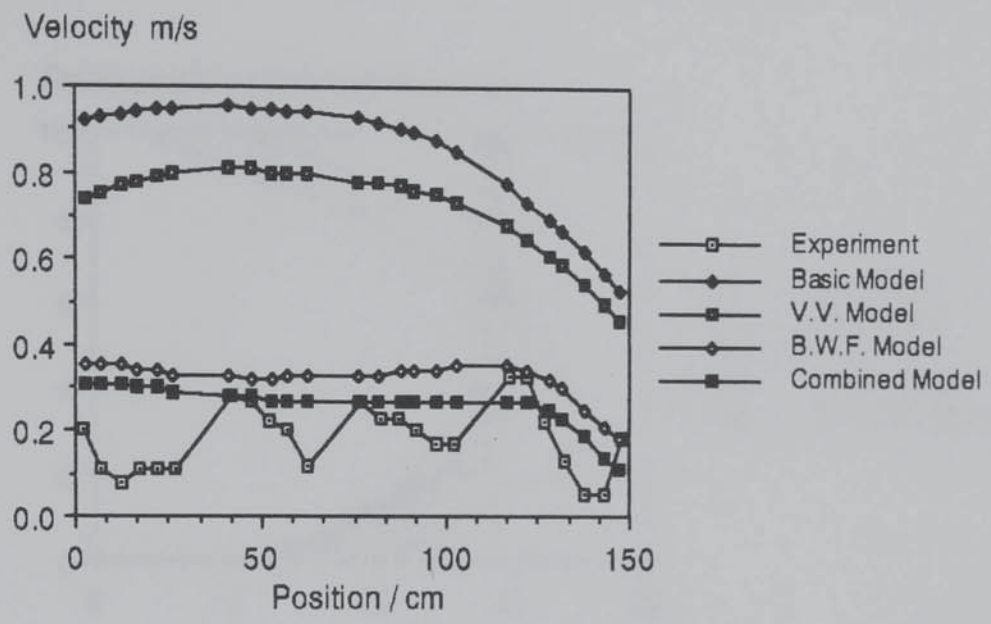

Graph 9.22. Experimental and Computed (B.W.F., V.V. and Combined Models) Duct Velocity Profiles at a position of 18 cm for 10 cm Duct and Bed Heights, Duct End Blocked, Average Velocity in the Duct before the Bed 21.1 ms^{-1}.

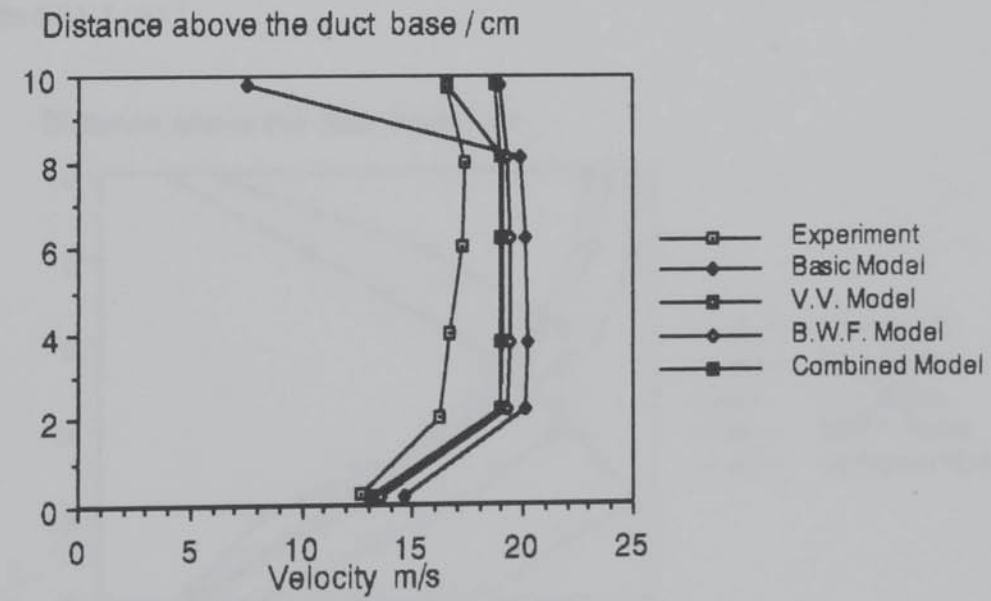

Graph 9.23. Experimental and Computed (B.W.F., V.V. and Combined Models) Duct Velocity Profiles at a position of 58 cm for 10 cm Duct and Bed Heights, Duct End Blocked, Average Velocity in the Duct before the Bed 21.1 ms^{-1}.

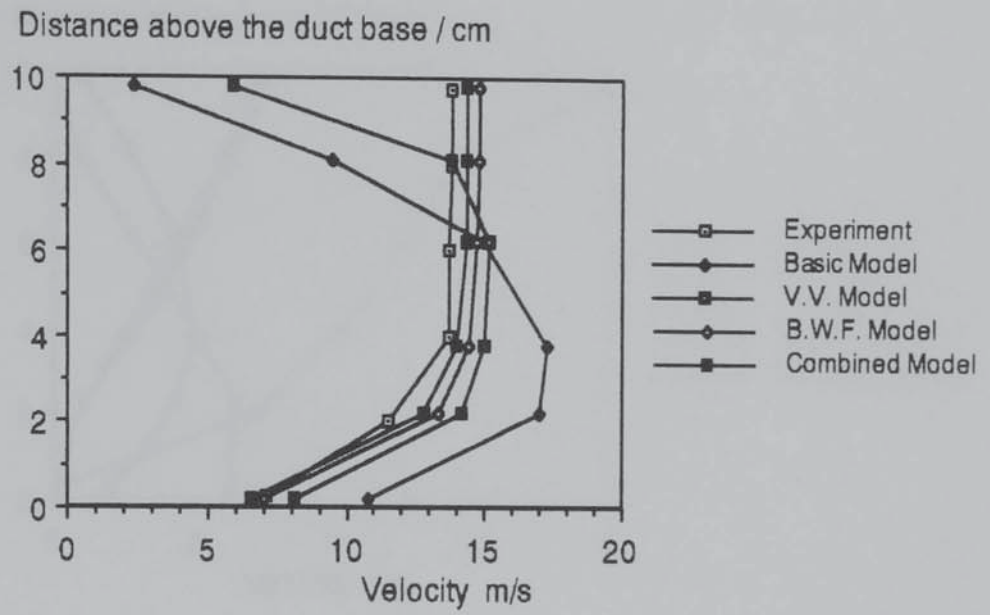

Graph 9.24. Experimental and Computed (B.W.F., V.V. and Combined Models) Duct Velocity Profiles at a position of 98 cm for 10 cm Duct and Bed Heights, Duct End Blocked, Average Velocity in the Duct before the Bed 21.1 ms^{-1}.

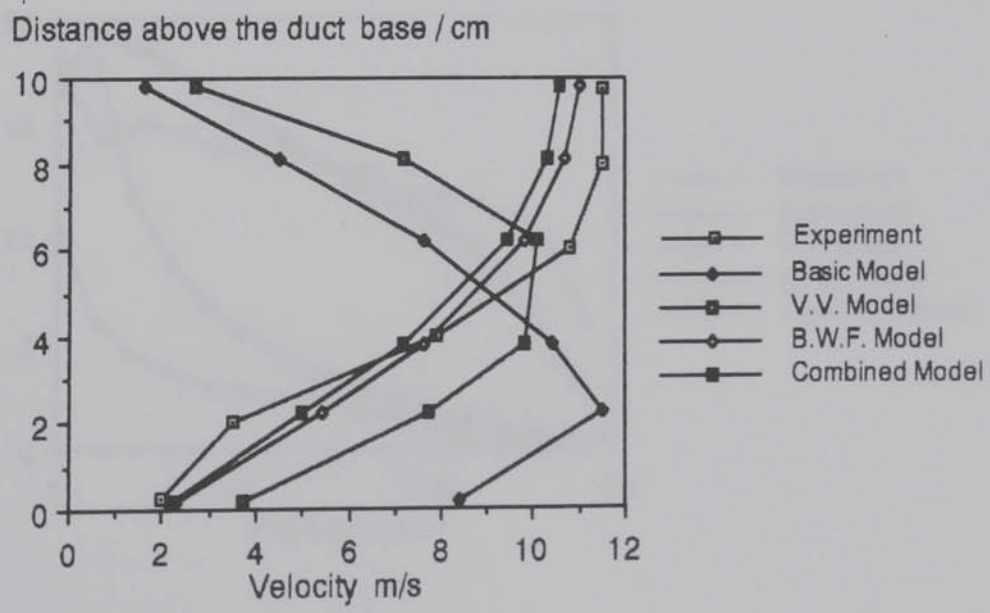

Graph 9.25. Experimental and Computed (B.W.F., V.V. and Combined Models) Duct Velocity Profiles at a position of 138 cm for 10 cm Duct and Bed Heights, Duct End Blocked, Average Velocity in the Duct before the Bed 21.1 ms^{-1}.

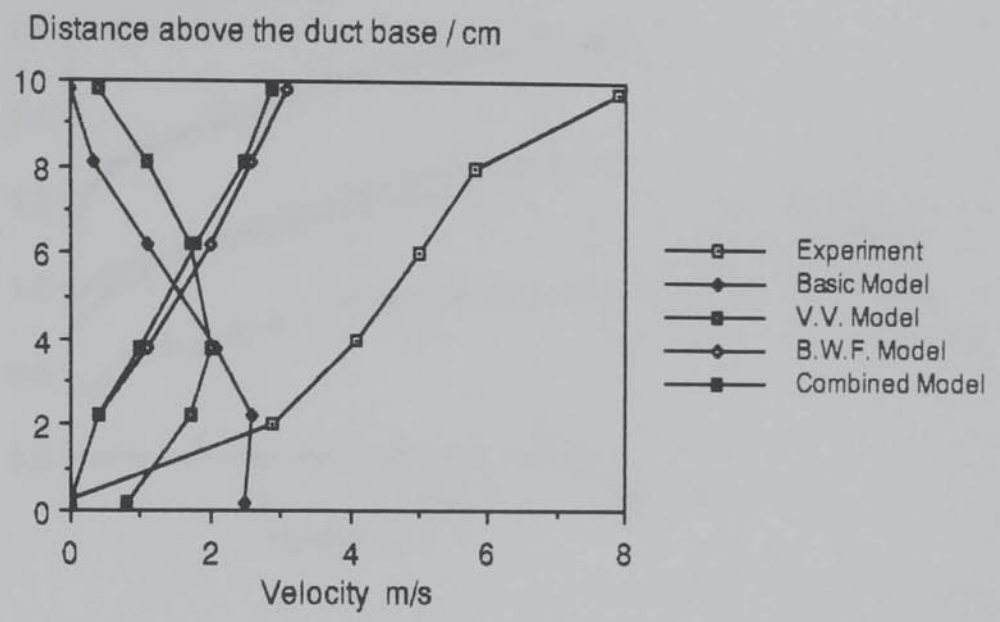

Graph 9.26. Experimental and Computed (B.W.F., V.V. and Combined Models) Velocities at the Bed Base for 10 cm Duct and Bed Heights, Duct End Blocked, Average Velocity in the Duct before the Bed 21.1 ms^{-1}.

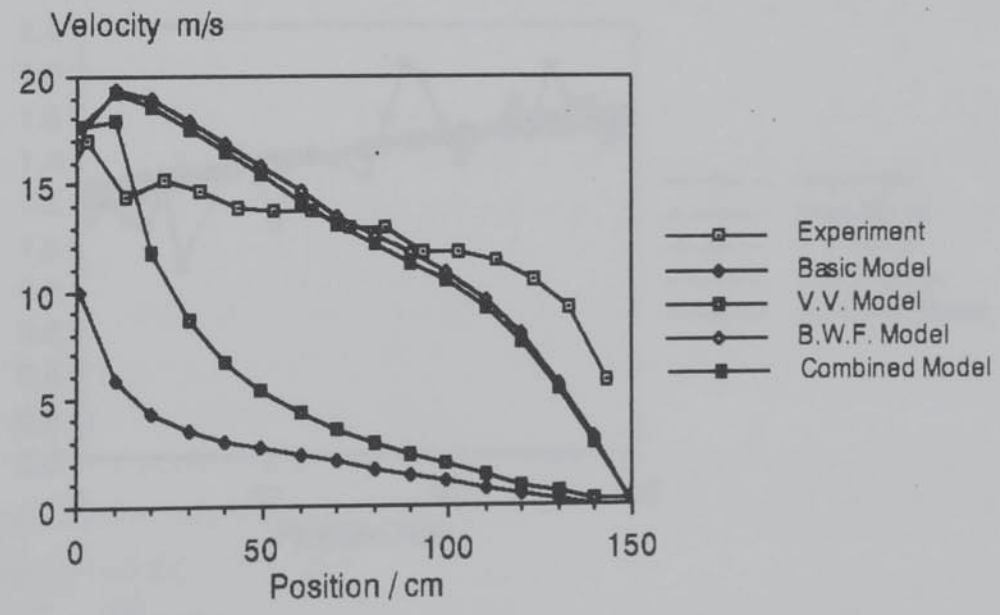

Graph 9.27. Experimental and Computed (B.W.F., V.V. and Combined Models) Static Pressures at the Bed Base for 10 cm Duct and Bed Heights, Duct End Blocked, Average Velocity in the Duct before the Bed 21.1 ms^{-1}.

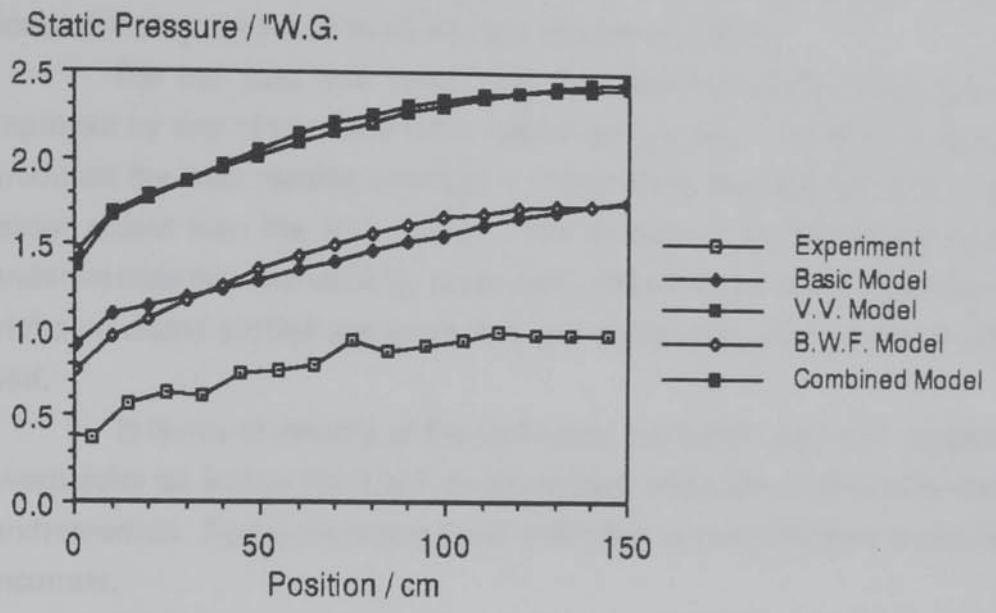

Graph 9.28. Experimental and Computed (B.W.F., V.V. and Combined Models) Velocities 10 cm above the bed for 10 cm Duct and Bed Heights, Duct End Blocked, Average Velocity in the Duct before the Bed 21.1 ms^{-1}.

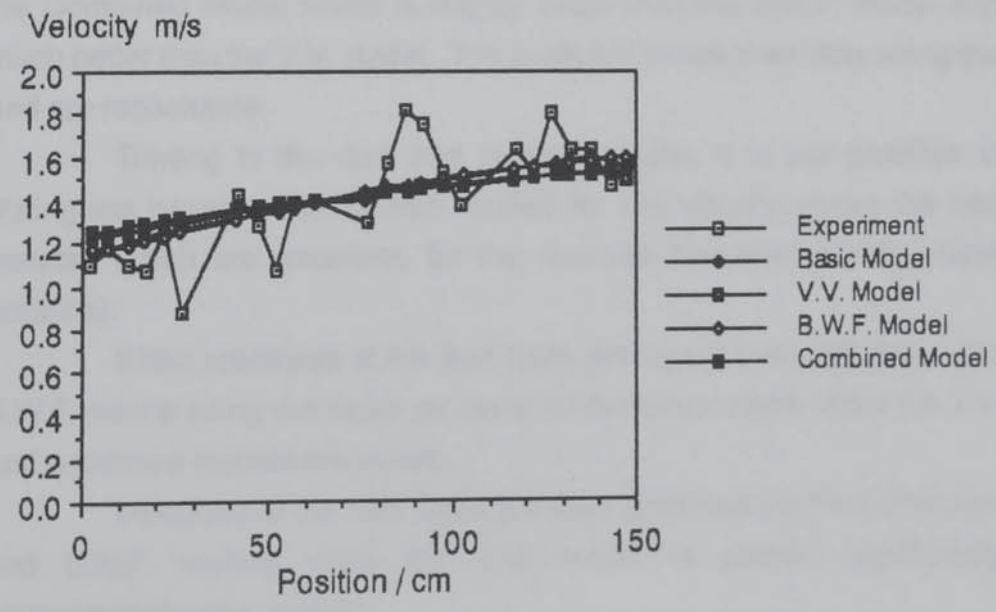

The same situations were modelled as for the basic model, whose results are presented in section 9.4. The results for the three developments of the initial model and the relevant experimental ones are presented together to ease comparison and reduce the length of this document as graphs 9.15 to 28 and are discussed below.

For the duct end open, the duct velocity profiles are much improved by any of the three more advanced models. The B.W.F. model produces the best results; although it overpredicts the duct flowrate to a lesser extent than the V.V. model. The combined model interestingly underpredicts the duct velocity, particularly near the bed base. The forms of the predicted profiles are good, but, get worse along the length of the bed.

In terms of velocity at the bed base, the B.W.F. and V.V. models overpredict (as before the B.W.F. model is best) while, the combined model underpredicts. Furthermore, the trend predicted by the combined model is incorrect.

The static pressures at the bed base predicted by the V.V. model are very much larger than the experimental measurements and similar to those predicted by the basic model. The B.W.F. and Combined Models are much better but, are not good; particularly since they predict an increase in static pressure along the bed as against the measured decrease.

The point velocity above the bed profiles are best predicted by the Combined model which is slightly better than the B.W.F. model and much better than the V.V. model. The predicted trends in velocity along the bed are reasonable.

Turning to the duct end blocked results, it is not possible to distinguish between the various models for the velocity above the bed results which are excellent; for the reasons discussed above (mass balance).

Static pressures at the bed base are again overpredicted. The B.W.F. results being the same as those for the basic model while the V.V. and combined models are worse.

Velocities at the bed base are best predicted by the Combined and B.W.F. models while the V.V. model is poorer, significantly underpredicting the velocity.

The velocity profiles in the duct are best predicted by the Combined model and, to a lesser extent the B.W.F. model. The V.V. model is very poor in this respect.

9.5.3. Discussion.

The treatment of the bed base in the models can be summarised as follows. In the basic model the description is that of the equations of motion and the vectorial Ergun Equation, assuming that the bed is of constant voidage. The V.V. model includes the increase in voidage near the bed boundaries; hence, the bed resistance is lower and higher velocities in (and parallel to) the bed base are permitted. The B.W.F. model is more complex and permits a more rigorous description of turbulence at the bed base.

The more advanced models are a clear improvement to the basic version. It is surprising to note that the Combined Model is often worse than the simpler B.W.F. and V.V. models. This suggests that minor changes to these models when combined will improve the performance of the models significantly. Such changes would include a more accurate representation of the voidage variation in the bed, fine tuning of the turbulence model constants and a representation of the bed support mesh.

Such improvements could be, in part, directed by the consideration of results from models of other bed and duct heights etc.

Unfortunately, the models have not enabled any further interpretation of the experimental results but it is to be expected that improved versions will. Such models could then be extended to three dimensions and compared to results from the three-dimensional apparatus presented in the next chapter.

9.6. CONCLUSIONS.

i. The GROUND coding used previously cannot give a converged solution to models of the two-dimensional apparatus.

ii. A modified GROUND where cell velocities are not averaged gives a converged solution.

iii. The basic model does not predict the experiments well.

iv. More advanced models featuring the vertical variation of the voidage in the bed and a bed base 'wall friction' (and these combined) are better predictive tools.

v. Further improvements to the model have been suggested.

CHAPTER TEN

A THREE DIMENSIONAL INVESTIGATION OF PACKED BED FLUID MECHANICS

10.1. INTRODUCTION.

This chapter presents a further experimental investigation of the fluid mechanics of gas flow in an apparatus containing a shallow packed bed; in this investigation a three-dimensional flow is examined. The investigation thus extends the earlier, two-dimensional work and is a useful basis for extending the modelling work, as discussed in the previous chapter. As before, the duct outlet can be left open or obstructed allowing a full examination of the effects of the bed base.

In this preliminary study flow visualisation using smoke tracers is used. Measurements of point velocities leaving the bed, pressures in the duct and static pressures in the bed are made.

10.2. OBJECTIVES.

The objectives of this part of the work are as follows:

i. To obtain experimental pressure and velocity data of a three-dimensional flow in and around a packed bed in order to further our understanding of the mechanisms involved in these situations.

ii. To obtain data of a three-dimensional flow in a simple geometry which can be used to test and further develop C.F.D. models.

iii. To investigate wall effects in the situation where flow is NOT parallel to the walls.

iv. To gain further insight into the results of Ali (1984) on a 1.22m diameter packed bed with a tangential inlet below the bed.

The investigation may reveal the necessity for a more advanced design of apparatus and/or different measurement techniques in order to obtain data that is consistent with these objectives.

10.3. DESCRIPTION AND COMMISIONING OF APPARATUS.

10.3.1. Overview.

The packed bed section used in this part of the work was chosen to be curved. This shape will clearly produce a flow that is three-dimensional in nature; furthermore, this flow pattern will be significantly affected by the walls and thus satisfies objective iii. The shape is similair to that used by Ali (1984) (objective iv.) and the simple geometry can easily be described in PHOENICS without the additional complications involved in using Body Fitted Co-ordinates.

10.3.2. Description of the Bed Section.

This curved bed section is attached to the air supply equipment previously described, hence the duct below the bed is 10 cm in height and 25 cm in width. In order to most closely satisfy objective iv. (above) the outer radius of the bed is 0.60m and hence the inner radius is 0.35m. The equipment extends through 180 degrees, the maximum size possible given the volume of packing available (as before 12mm spheres are used) and using a 10 cm bed height.

The rig is made of 6mm thick grey 'Simona' P.V.C. and is shown in plate 10.1. A plan view of the apparatus is given as figure 10.1. Perspex was rejected as the material of contruction as it is too expensive and difficult to work with. The curved walls are made by heating and progressively bending flat P.V.C. sheet. Using this technique it proved impossible to obtain smooth walls of constant radius. The departure of the wall radii from the ideal are shown in graph 10.1, the angle being measured from the inlet to the outlet.

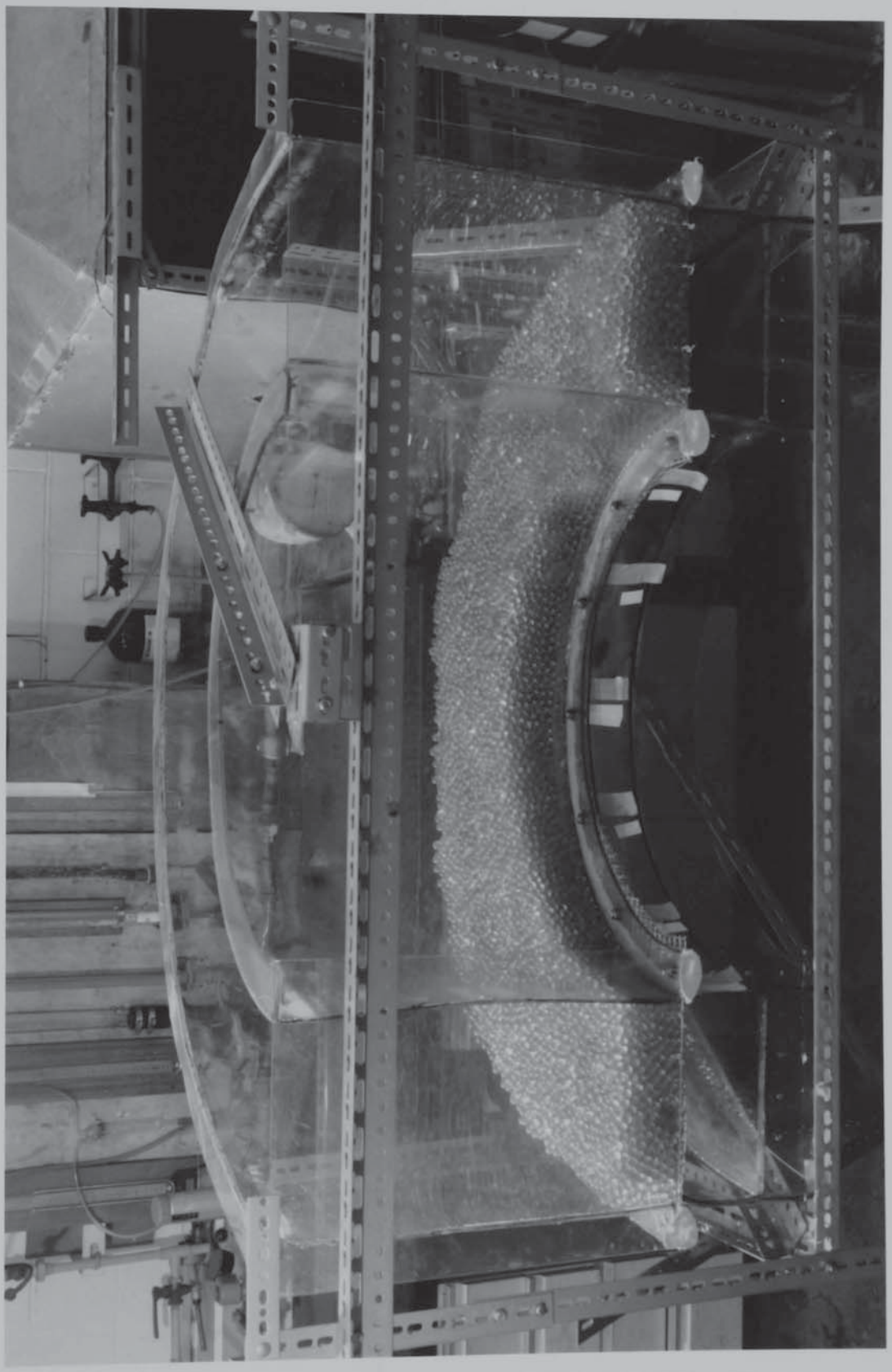

Plate 10.1. The Curved Bed Section.

Figure 10.1. A Plan View of the Curved Bed Section.

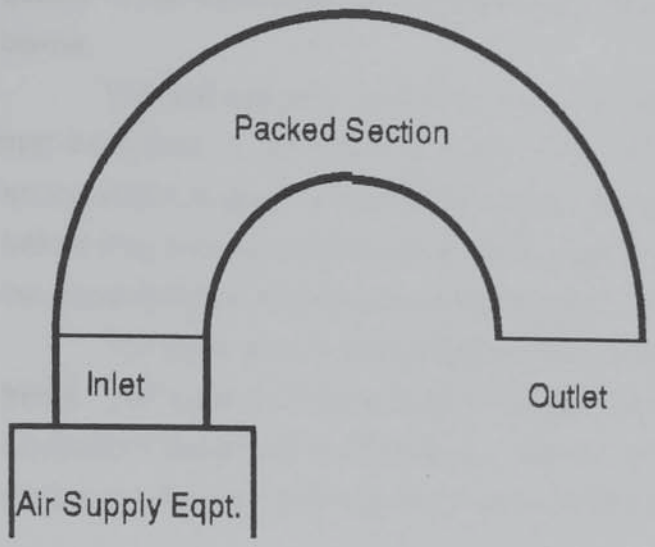

Graph 10.1. The Departure of The Wall Position From An Ideal Circle (Measured at the Bed Outlet Plane).

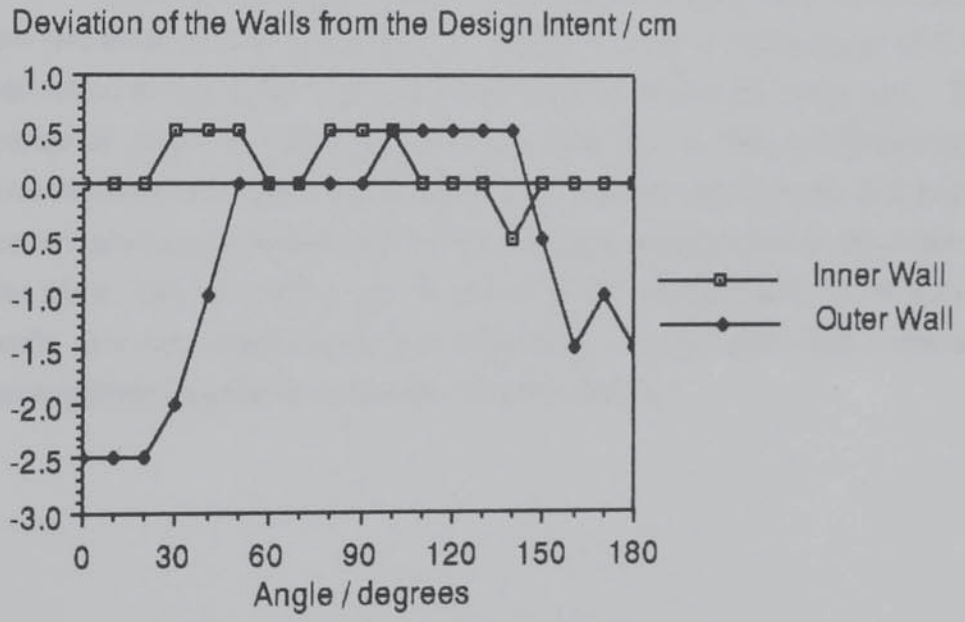

This deviation from the design condition will clearly reduce the quality of the experimental measurements; this point is discussed further below.

The bed support is made of two wire meshes and is the same as that described in 7.3.1 for the straight rig. A slightly different clamping arrangement is used; whereby the flanges are wider and packed with putty before they are clamped together. This, together with the different shape of the apparatus (i.e. curved) obviates the need for support wires.

The apparatus is supported at the correct height on a handy angle frame. The lower part of the duct is flanged and attached to the air supply equipment described in Chapter 6. The end walls of the upper part have slots cut in them so they can be bolted to distributor flanges.

10.3.3. Measurement Techniques.

Point Velocities Above the Bed.

These are measured in the same way as those above the bed in the two dimensional apparatus (i.e. each velocity is an average of three velocities at the given point, with the bed repacked for each set). The probe is positioned 20 cm above the bed (as in the two-dimensional investigation) on a traverse mechanism. This is shown in plate 10.2 and is essentially the same as that employed on the straight rig but, as shown in the plate, one end of the bar is bolted at the central point of the curved walls and can rotate above the apparatus. A protractor and cross-hair arrangement is used to accurately position the bar.

Plate 10.2. The Anenometer Traversing Mechanism.

Velocities are measured every 20 degrees around the apparatus from 10 degrees (at the inlet end) to 170 degrees. They are measured at positions between 2.5 cm and 22.5 cm from the inner wall on a 5 cm pitch. Where the apparatus is not of the correct width; the distance is nevertheless measured from the internal wall and so; for example, a reading at a position of 22.5 cm may not be 2.5 cm from the outer wall.

Duct Pressures and Velocities.

The traverses on which these are measured are shown in figure 10.2. It should be noted that the position given is that where the tube is inserted and therefore not where the actual measurement is made. Static pressures are measured using the pitot static tube, total pressure using a modified tube such that the pressure is measured at exactly the same point as the static pressure using the pitot static tube. The dynamic pressure (and hence the velocity) is found by difference. This method is more accurate than using a pitot tube and is necessitated by the three-dimensional nature of the flow. Measurements of total, static and dynamic pressure are made at angles of 0, 30, 60.....150 degrees; positions 2.5, 7.5, 12.5, 17.5 and 22.5 cm and vertical positions 0.2, 2.0, 4.0, 6.0, 8.0 and 9.8 cm (above the duct base). Holes are drilled in the inside wall of the apparatus to allow the insertion of the pressure tubes, these are taped over when not in use.

Figure 10.2. Details of the Traverses Used In the Collection of Duct Pressures.

PLAN

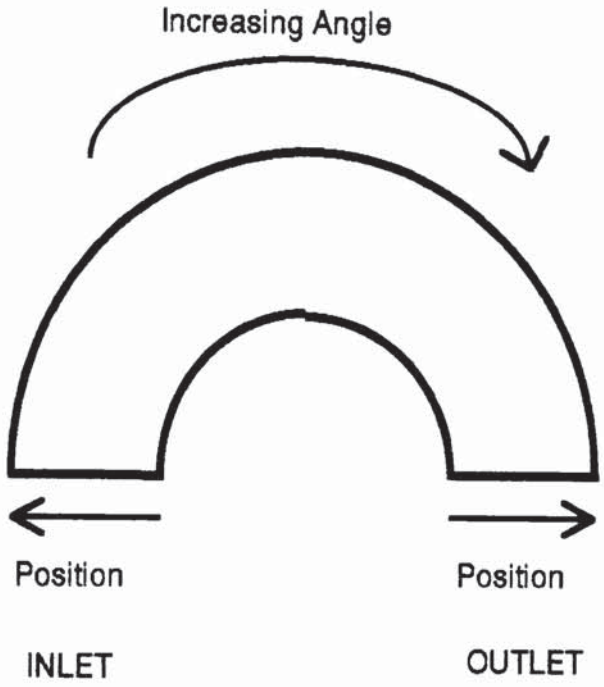

SECTION

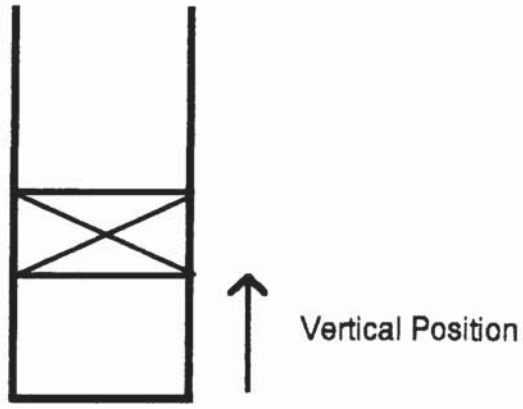

Bed Static Pressures.

These were obtained using the specially made pitot tube previously described. In addition to the limitations of this technique previously discussed additional problems are encountered using it in a three-

dimensional flow. The main problem is identifying the direction of flow so the hole on the side of the tube can be aligned correctly. This is less of a problem in the bed than outside of it. Nevertheless, if the probe is inserted into the bed and rotated the lowest reading can be taken as the static pressure. Typically this is when the probe is aligned so the static pressure hole is facing the outer curved wall. Bed static pressures were measured at angles of 10, 50, 90, 130, and 170 degrees; at positions 2.5, 12.5 and 22.5 cm and at distances of 2, 4, 6 and 8 cm above the bed base.

Needle pressures at the bed base were not determined. Before the experimental measurements are presented and discussed; the smoke visualisation results are considered.

10.4. FLOW VISUALISATION RESULTS.

These experiments were performed in the same way as those previously described on the straight rig. One flowrate only was studied (equivalent to an average velocity in the duct before the bed of approximately 21.0 ms^{-1}) with all three duct end conditions (open and partially & wholly blocked).

As before, the results are divided into two main parts: first, those where the probe is positioned vertically so its tip is adjacent to the bed support mesh; and secondly, those where the probe is positioned horizontally within the duct beneath the bed. The latter section reports attempts to identify a 'separating streamplane'.

The slight opacity and colouring of the P.V.C. used to construct the rig and the three-dimensional nature of the flow makes the collection and processing of information more difficult than was the case with the two-dimensional investigation.

10.4.1. Probe Positioned Vertically.

The primary data collected in this case is the boundary of the plume 10 cm above the bed base drawn on a scaled plan view of the rig. The shape and size of the plume immediately indicates the direction and approximate relative magnitude of the gas flow. Smoke was injected at intervals of 30 degrees and at positions 5, 10, 15 and 20 cm from the

inside wall. This gives 20 plume outlines for each flowrate and duct end condition.

In no cases was downflow of air through the bed observed (this was specifically looked for); although recirculation does occur in the duct. In these experiments it was not possible to distinguish between the various densities of smoke. Nor, were the 'dual plumes' observed in the straight rig encountered in these curved rig experiments.

Duct Blocked.

Figure 10.3 presents the smoke plume boundaries in this case. The upper part shows the plume when the smoke is injected at positions 10 & 20, the lower part is for smoke injected at positions 5 & 15 (cm from the inner wall).

A number of conclusions can be drawn:

i. The gas tends to flow in a straight line and is turned at the walls.

ii. Higher flowrates through the bed are observed near the walls. This is for two reasons: firstly because of the higher local voidage near the wall and secondly because as the gas flows into the wall some of its momentum is converted to static pressure which causes higher flowrates through the bed at this point.

iii. Lower flowrates through the bed are observed at higher angles (around the apparatus towards the outlet) and/or nearer the inner wall.

Figure 10.3. Smoke Plumes 10 cm Above the Bed In The Three-Dimensional Apparatus. Smoke Injected into the Bed Base (with the probe positioned vertically). Average Velocity in the Duct Before the Bed Approximately 21.0 ms^{-1}. Duct End Wholly Blocked.

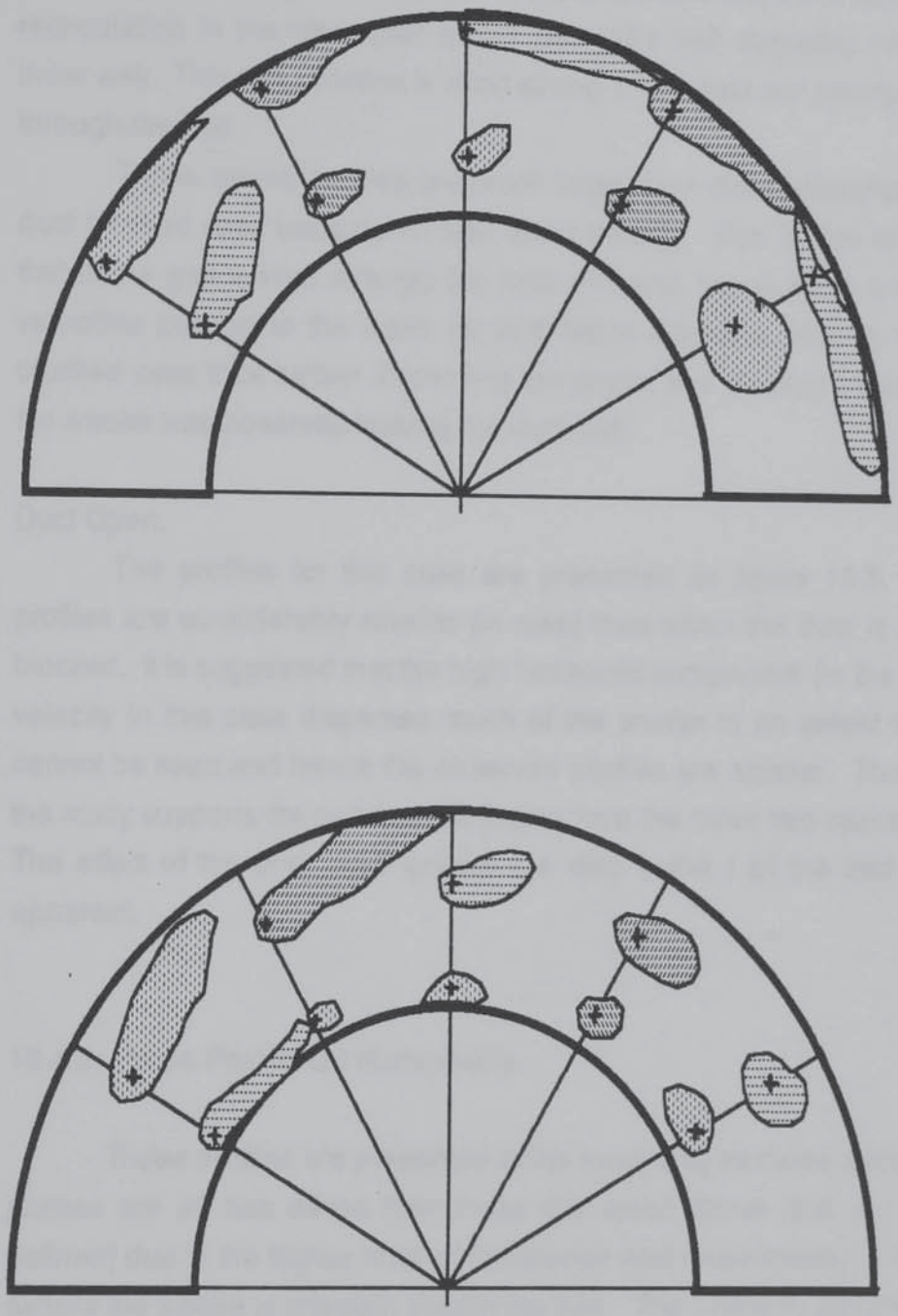

\+ denotes smoke injection point

Duct Partially Blocked.

The profiles are presented in figure 10.4 and support all the conclusions drawn from the duct blocked case. Particularly, the conclusion that the gas tends to flow in a direction tangential to the duct walls until these cause a change of direction. The profiles also show the existence of recirculation in the latter part of the bed (120-150 degrees) nearer the inner wall. This recirculation is most strong in the duct but clearly persists through the bed.

These smoke profiles are much larger than those observed in the duct blocked case because of their lower density. This is due to the fact that some gas leaves through the duct end and hence there are higher velocities parallel to the walls (in and below the bed) than in the duct blocked case thus further dispersing the plume and making it less dense. No smoke was observed leaving the duct end.

Duct Open.

The profiles for this case are presented as figure 10.5. These profiles are considerably smaller (in area) than when the duct is partially blocked. It is suggested that the high horizontal component (in the duct) of velocity in this case disperses much of the smoke to an extent where it cannot be seen and hence the observed profiles are smaller. This part of the study supports the conclusions drawn from the other two cases above. The effect of the end wall (above the duct outlet) of the bed is also apparent.

10.4.2. Probe Positioned Horizontally.

These profiles are presented in the same way as those above. The plumes are all less dense than those discussed above (but, still clearly defined) due to the higher level of turbulence and cross-mixing in the duct (where the smoke is injected) than in the bed. The injection point for each plume is described by three numbers which indicate, in order, the angle at which the smoke was injected, the radial position and the vertical position. This is as shown above in figure 10.2. Due to the large quantity of experimental data obtained, only selected plumes are presented. Nevertheless the plumes presented show the full range of behaviour observed.

Figure 10.4. Smoke Plumes 10 cm Above the Bed In The Three-Dimensional Apparatus. Smoke Injected into the Bed Base (with the probe positioned vertically). Average Velocity in the Duct Before the Bed Approximately 21.0 ms^{-1}. Duct End Partially Blocked.

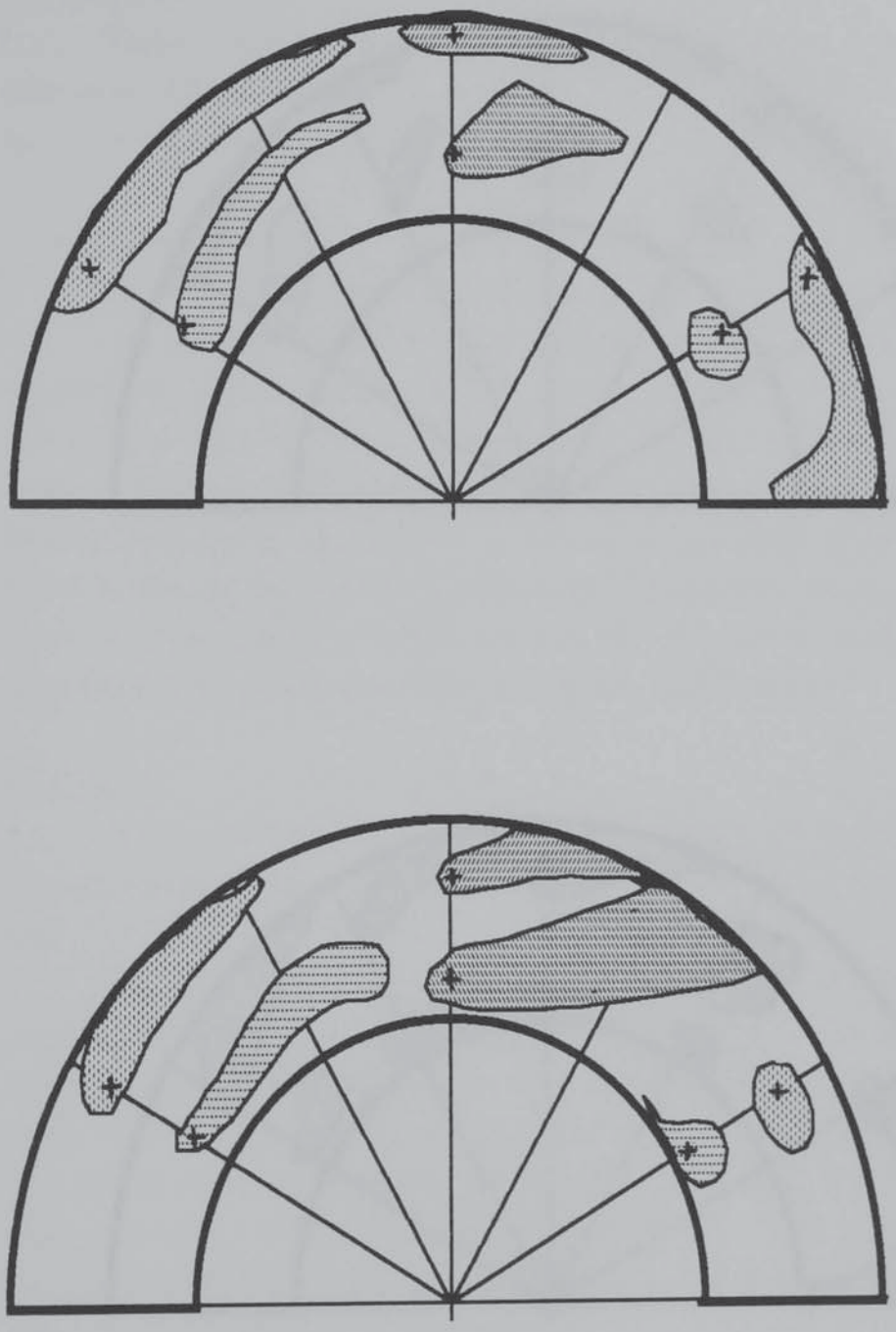

+ denotes smoke injection point

Figure 10.5. Smoke Plumes 10 cm Above the Bed In The Three-Dimensional Apparatus. Smoke Injected into the Bed Base (with the probe positioned vertically). Average Velocity in the Duct Before the Bed Approximately 21.0 ms^{-1}. Duct End Open.

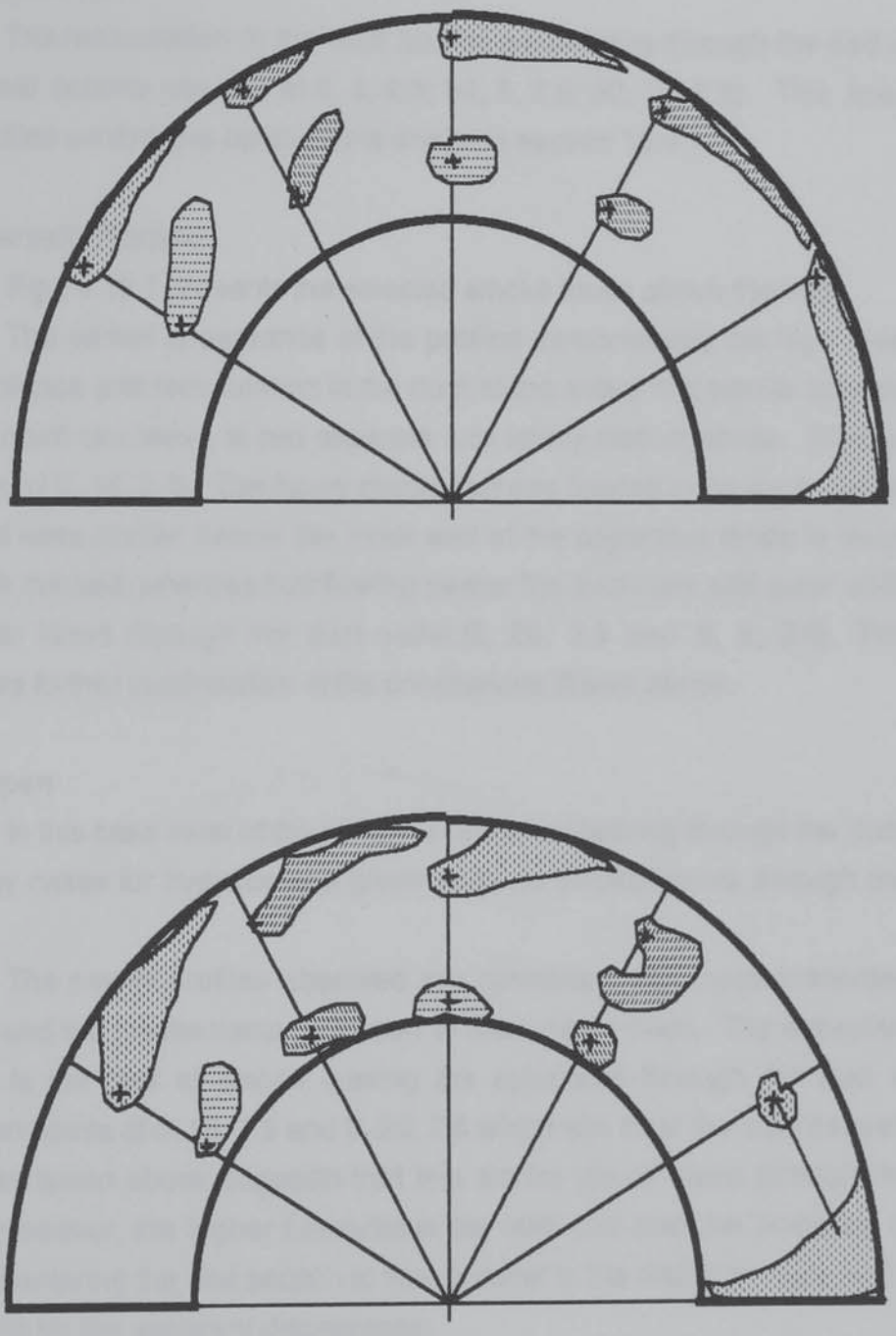

+ denotes smoke injection point

N.B. Smoke injected at 150 degrees, 5 & 10 cm left through the duct.

Duct Blocked.

The selected profiles for this case are presented as figure 10.6. It is immediately apparent that the closer the gas is injected to the bed base the nearer to the inlet it appears above the bed (smoke injected at 0, 5, 2.5 and 0, 5, 7.5). of 10.7.

The recirculation in the duct and its persistence through the bed is also clear (smoke injected at 0, 5, 2.5; 90, 5, 2.5; 90, 10, 2.5). This apart the profiles confirm the conclusions drawn in section 10.4.1.

Duct Partially Blocked.

Figure 10.7 presents the selected smoke those above the bed.

The varied appearance of the profiles demonstrates the high level of turbulence and recirculation in the duct; to the extent that smoke injected at one point can leave at two separate and totally distinct points. (Smoke injected at 0, 15, 2.5). The figure shows that gas flowing in the duct, nearer the bed base and/or nearer the inner wall of the apparatus tends to leave through the bed; whereas that flowing nearer the duct base and outer walls tends to leave through the duct outlet.(0, 20, 2.5 and 0, 5, 2.5). This provides further confirmation of the conclusions drawn above.

Duct Open

In this case most of the smoke is observed leaving through the duct; in many cases for injection at a given point no smoke leaves through the bed.

The smoke profiles observed are consistent with those presented above and the mechanisms proposed to account for them. The exception to this is the lack of smoke leaving the apparatus through the duct at injection points of 0, 15, 7.5 and 0, 20, 7.5 which are near the outside wall. The discussion above suggests that this smoke would leave through the duct. However, the higher flowrates at the inlet end and the tendency of the gas entering the bed section to flow parallel to the distributor side walls accounts for the apparent discrepancy.

Figure 10.6. Smoke Plumes 10 cm Above the Bed In the Three-Dimensional Apparatus. Smoke Injected Into the Duct (with the probe positioned horizontally). Average Velocity in the Duct Before the Bed Approximately 21.0 ms^{-1}. Duct End Wholly Blocked.

Smoke Injected at 0, 5, 2.5

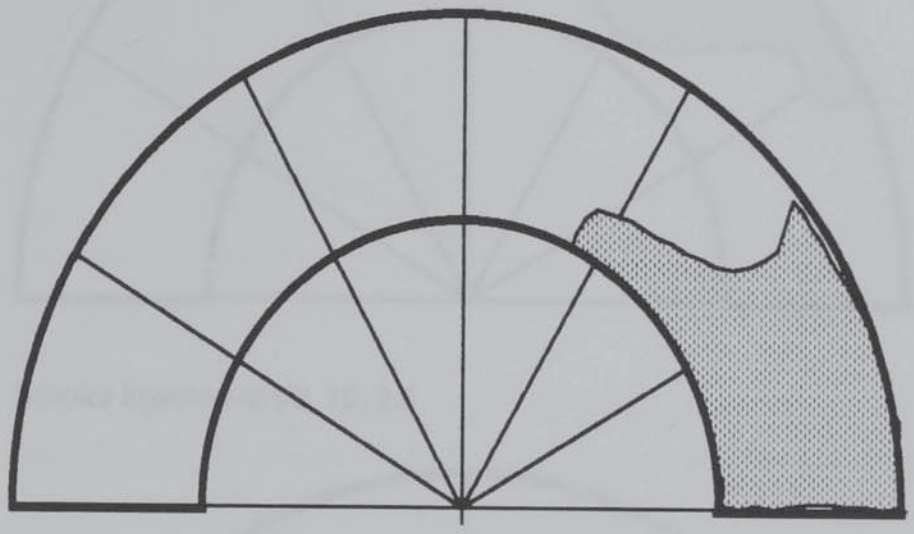

Smoke Injected at 0, 5, 7.5

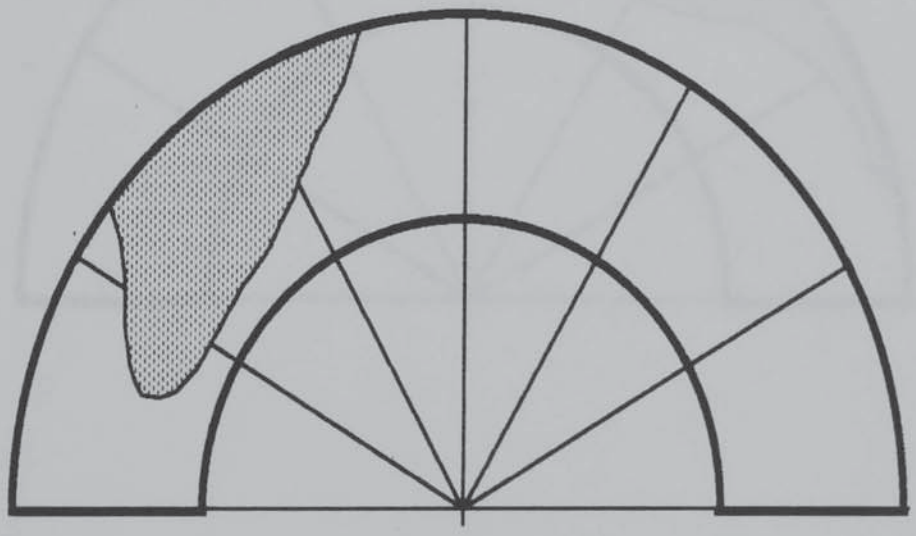

Smoke Injected at 90, 5, 2.5

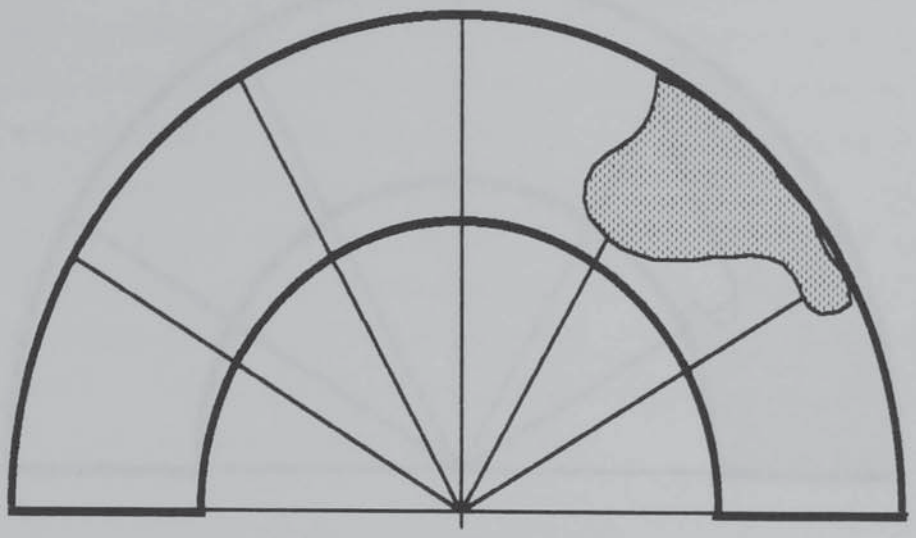

Smoke Injected at 90, 10, 2.5

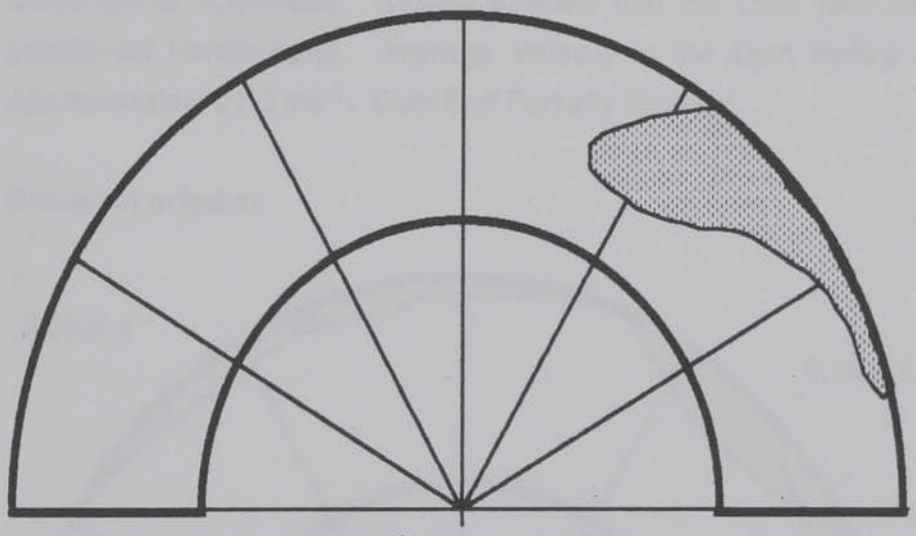

Smoke Injected at 90, 15, 2.5

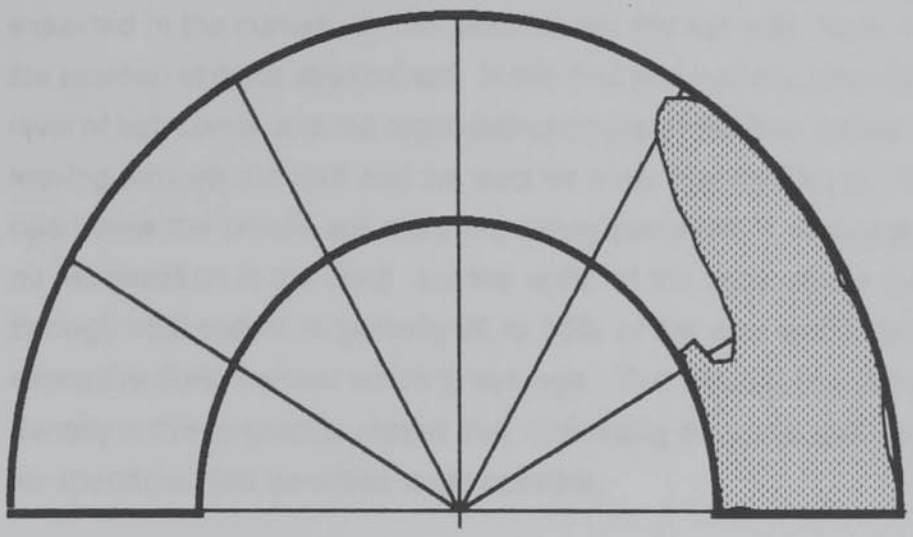

Figure 10.7. Smoke Plume 10 cm Above the Bed In the Three-Dimensional Apparatus. Smoke Injected Into the Duct (with the probe positioned horizontally). Average Velocity in the Duct Before the Bed Approximately 21.0 ms^{-1}. Duct End Partially Blocked.

Smoke Injected at:

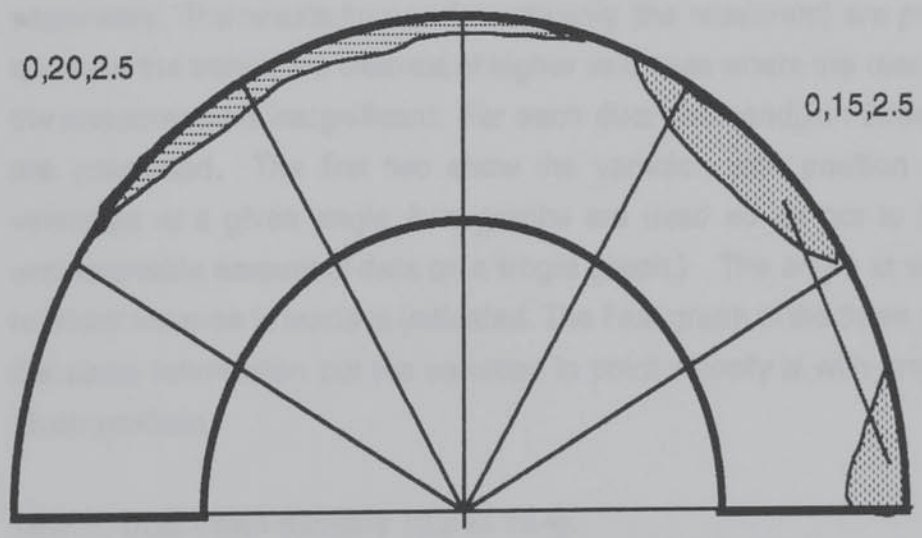

All Smoke Injected at 0, 5, 2.5 leaves through the duct outlet.

The existence of a separating streamline or streamplane (strictly a plane of streamlines) similar to that observed in the straight rig may be expected in the curved rig. An unsuccesful attempt was made to identify the position of these streamlines. In the duct end partially blocked case the level of turbulence and the recirculating nature of the flow results in smoke leaving through the bed and the duct for most injection points. In the duct open case the results are more promising (because, in this case, there is no recirculation in the duct) but the width of the zone where gas leaves through both outlets is typically 60 to 70% of the duct width, which is an excessive distance over which to average. The difficulty in judging smoke density in this apparatus means that minimising the zone width by looking for specific smoke densities is not possible.

10.5. POINT VELOCITIES ABOVE THE BED.

This data was collected as described in section 10.3.3. above, for flowrates equivalent to average velocities in the duct before the bed of approximately 11.5, 21.0 & 33.5 ms^{-1}

At the end of this section the results for the different duct end conditions and flowrates are compared and contrasted. However initially the point velocities for the various duct end conditions are presented separately. The results for one flowrate only (the maximum) are presented because the trends are clearest at higher velocities where the resolution of the anenometer is insignificant. For each duct end condition three graphs are presented. The first two show the variation with position of point velocities at a given angle (two graphs are used so as not to have an unreasonable amount of data on a single graph.) The angle at which the relevant traverse is made is indicated. The final graph of the three presents the same information but the variation in point velocity is with angle for a given position.

10.5.1. Duct Open (Graphs 10.2 to 10.4).

The profiles for a given angle show that velocity rises towards the outer wall that is, with position. This increase is approximately linear and is more marked towards the outlet end of the bed; there is also a trend for velocities at a given position to decrease with increasing angle (graph 10.4). The velocities at 170 degrees exhibit this trend particularly strongly

Graph 10.2. Point Velocities Above the Bed with Position (lower angles). Duct End Open. Average Velocity in the Duct Before the Bed 33.3 ms^{-1}.

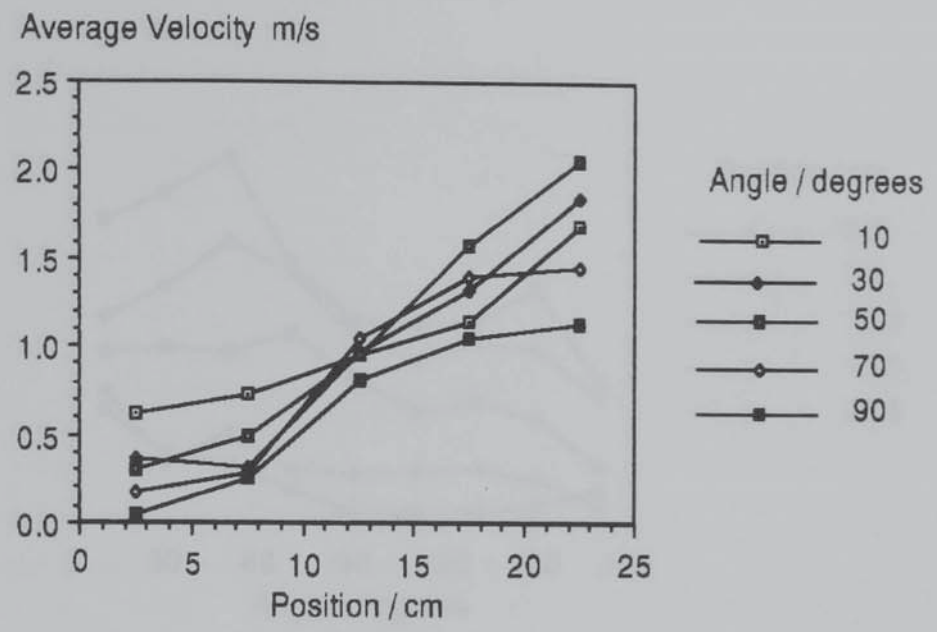

Graph 10.3. Point Velocities Above the Bed with Position (higher angles). Duct End Open. Average Velocity in the Duct Before the Bed 33.3 ms^{-1}.

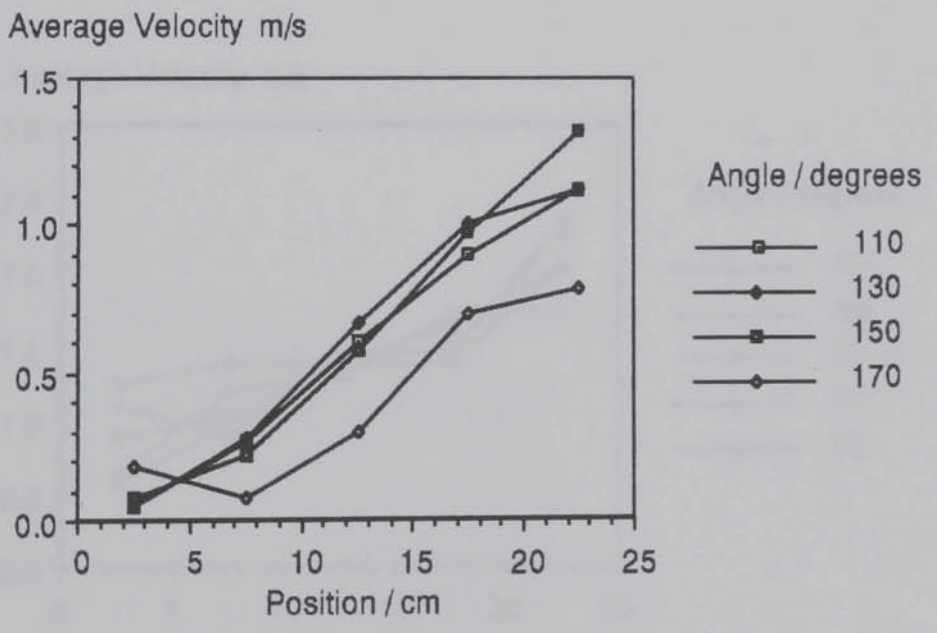

Graph 10.4. Point Velocities Above the Bed with Angle. Duct End Open. Average Velocity in the Duct Before the Bed Approximately 33.3 ms^{-1}.

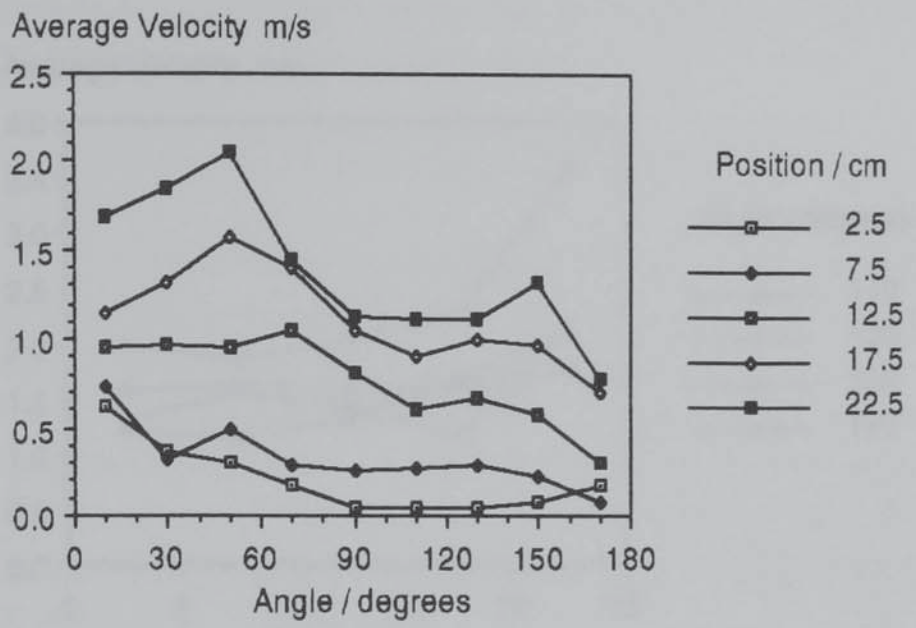

Graph 10.5. Point Velocities Above the Bed with Position (lower angles). Duct End Partially Blocked. Average Velocity in the Duct Before the Bed 33.6 ms^{-1}.

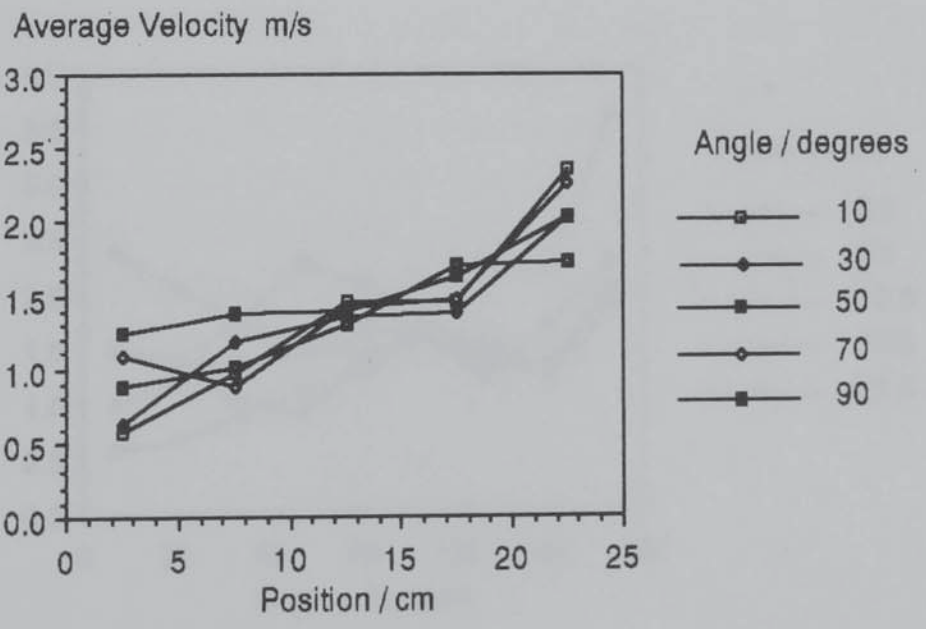

Graph 10.6. Point Velocities Above the Bed with Position (higher angles). Duct End Partially Blocked. Average Velocity in the Duct Before the Bed 33.6 ms^{-1}.

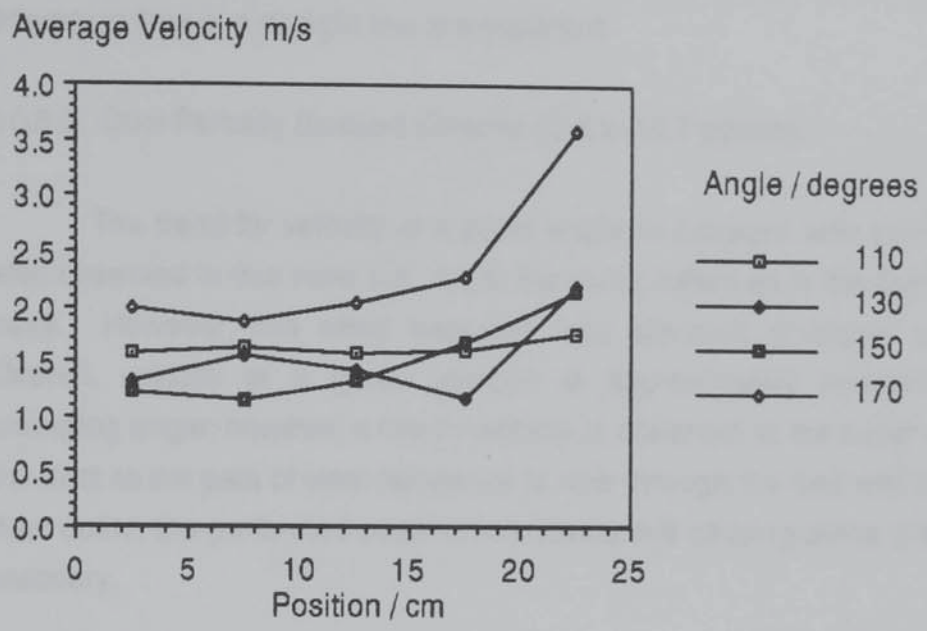

Graph 10.7. Point Velocities Above the Bed with Angle. Duct End Partially Blocked. Average Velocity in the Duct Before the Bed 33.6 ms^{-1}.

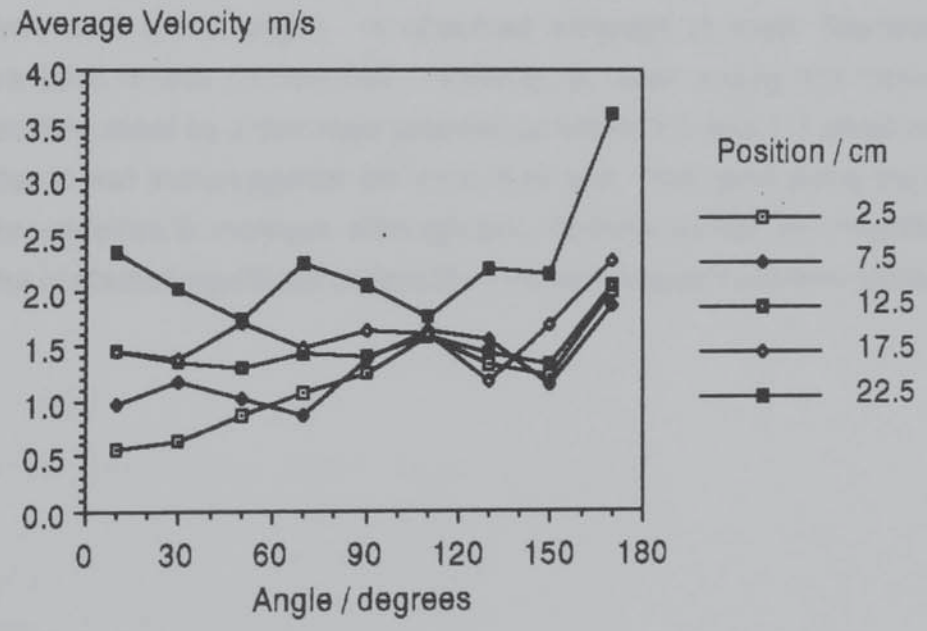

and are lower than those at 150 degrees; this is because, at this point, the lowest resistance path is to the duct outlet and not through the bed.

Again, the dual effect of the wall (higher bed voidage and conversion of momentum to static pressure) and the tendency of the fluid to attempt to flow in a straight line are apparent.

10.5.2. Duct Partially Blocked (Graphs 10.5 to 10.7 above).

The trend for velocity at a given angle to increase with position is also observed in this case but, not to the same extent as in the duct open case. However, this effect becomes less apparent at higher angles. Overall, velocity at a given position is approximately constant with changing angle; however a rise in velocity is observed at the outlet end of the duct as the path of least resistance is now through the bed and not the duct outlet, the perforated plate which covers this causing some pressure recovery.

10.5.3. Duct Blocked (Graphs 10.8 to 10.10).

The trends in this case are far less clear, particularly when the profiles for a given position and increasing angle are considered.

Generally however the increase with position (towards the outer wall at a given angle) is observed although at lower flowrates this variation is less pronounced. However, at lower angles this increase is accompanied by a decrease between positions 2.5 and 7.5 which may be due to wall friction against the inner duct wall. The trend along the bed is for velocities to increase although this increase should be considered in the context of significant variations in velocity between any two points.

Graph 10.8. Point Velocities Above the Bed with Position (lower angles). Duct End Blocked. Average Velocity in the Duct Before the Bed 33.5 ms^{-1}.

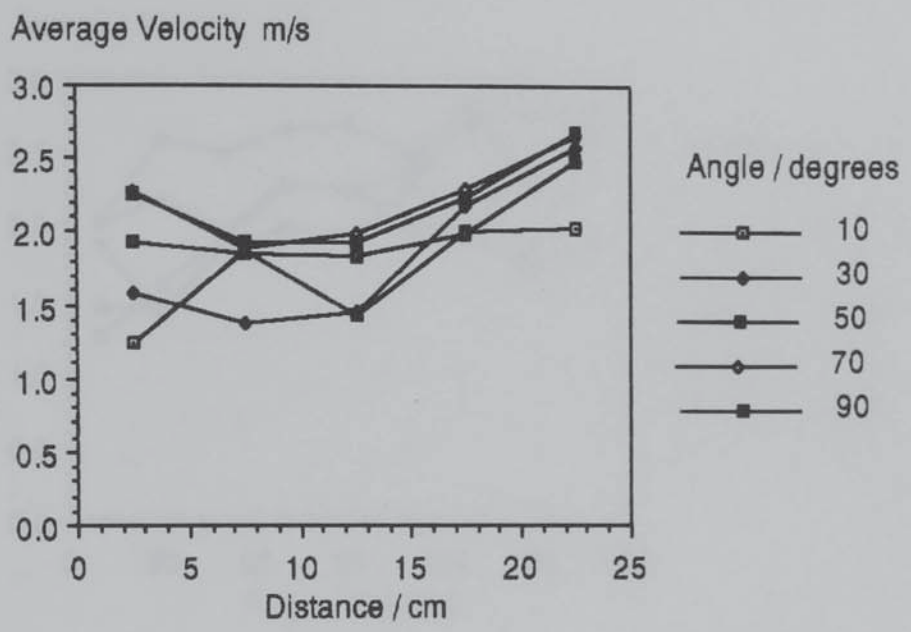

Graph 10.9. Point Velocities Above the Bed with Position (higher angles). Duct End Blocked. Average Velocity in the Duct Before the Bed 33.5 ms^{-1}.

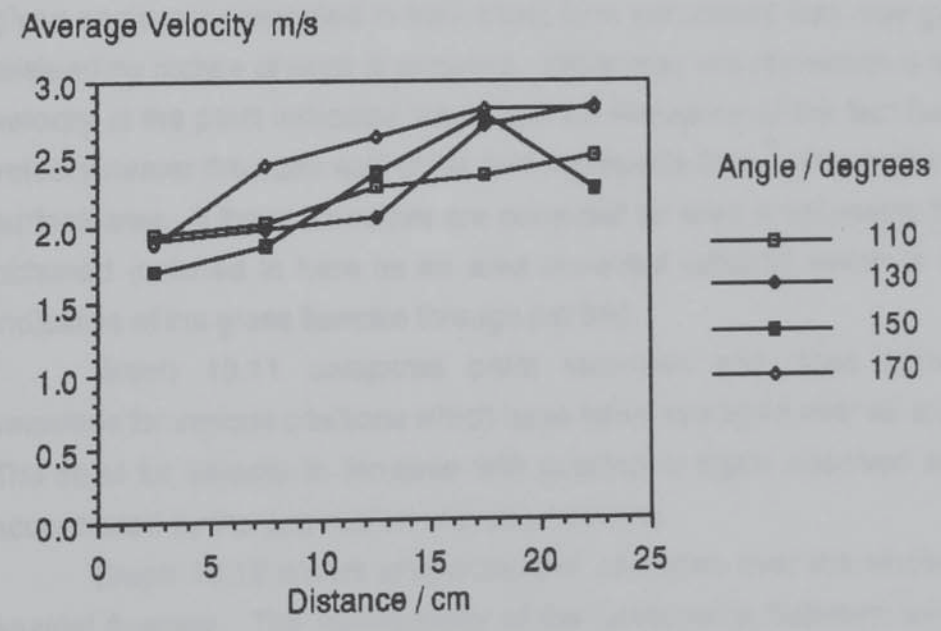

Graph 10.10. Point Velocities Above the Bed with Angles. Duct End Blocked. Average Velocity in the Duct Before the Bed 33.5 ms^{-1}.

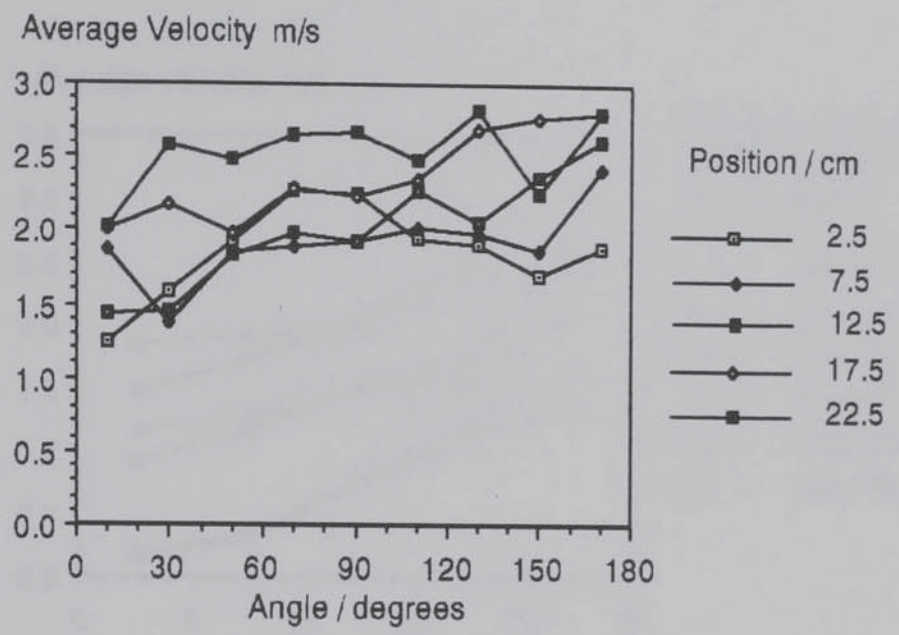

10.5.4. Different Duct End Conditions and Flowrates.

When profiles of point velocities for different positions but, at a given angle are presented in their basic form (as above) they may give a misleading picture of what is occuring. While they are representive of the velocity at the point indicated they make no allowance of the fact that the velocity nearer the outer wall of the bed represents flow over a higher bed surface area. If these velocities are corrected for area a volumetric flux is obtained (referred to here as an area corrected velocity) which is more indicative of the gross flowrate through the bed.

Graph 10.11 compares point velocities and area corrected velocities for various positions which have been averaged over all angles. The trend for velocity to increase with position is again observed and is accentuated by the application of area correction.

Graph 10.12 shows area corrected velocities over the whole bed against flowrate. The non-linearity of the relationship between average velocity (area corrected or not) and pressure drop is due to the non-linearity of the relationships between flowrate through and pressure drop across the Dall Tube.

Graph 10.11. The Effect of Area Correction on Point Velocities Above the Bed. Various Duct End Conditions. Average Velocity in the Duct Before the Bed Approximately 33.5 ms^{-1}.

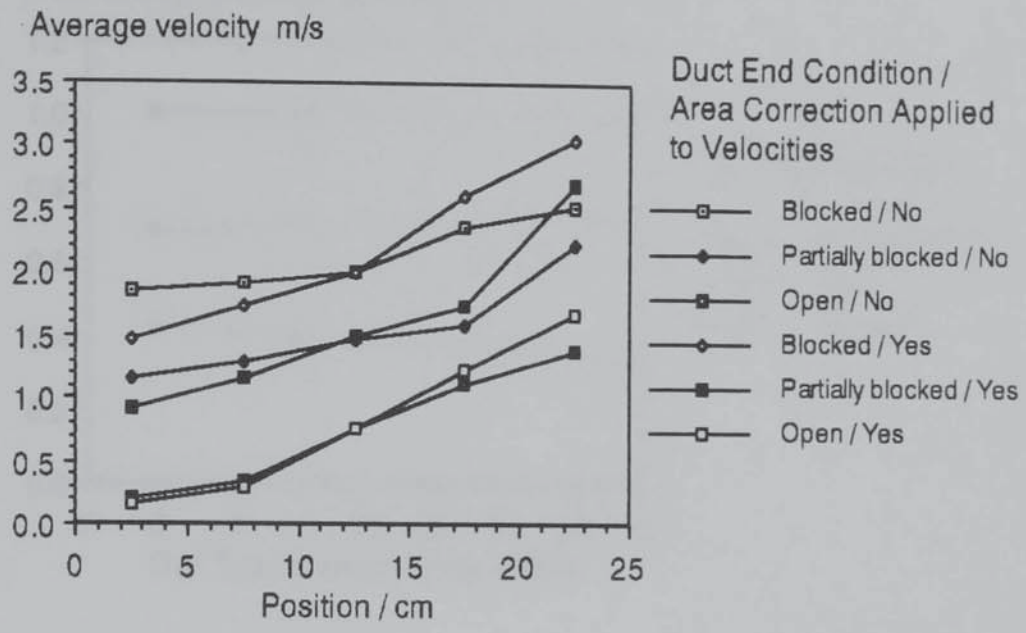

Graph 10.12. Average Area Corrected Velocity Above the Bed and Dall Tube Pressure Drop. Various Duct End Conditions.

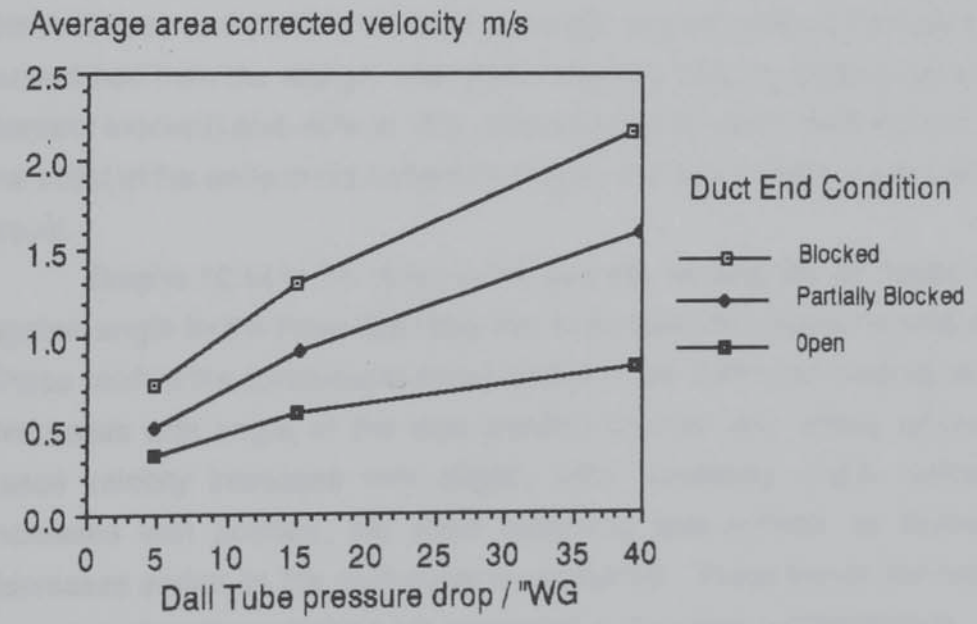

Graph 10.13. The Ratio of Flow Through the Bed to Flow into the Apparatus And Dall Tube Pressure Drop. Various Duct End Conditions.

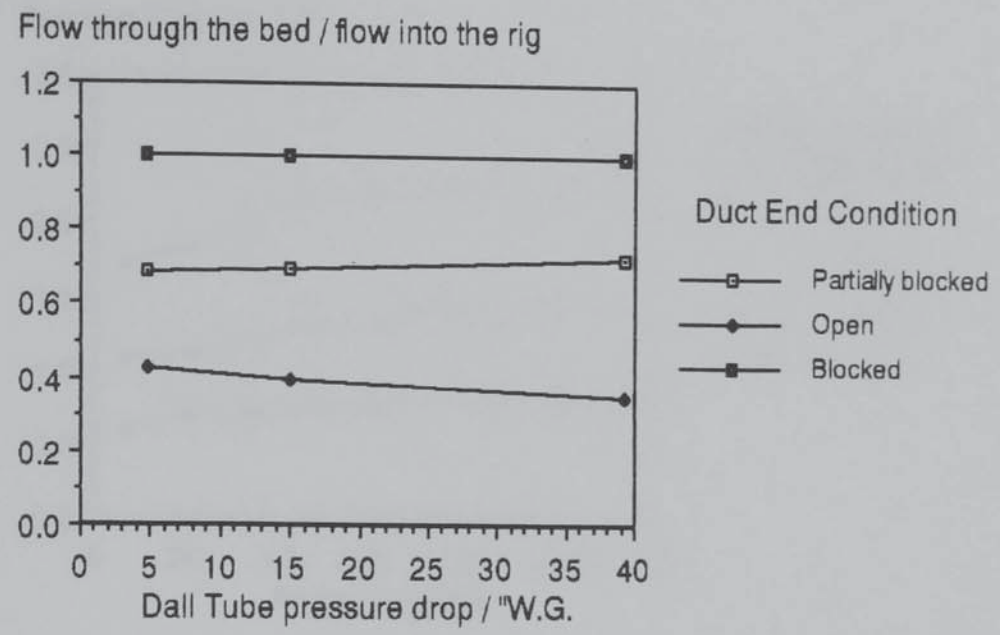

Graph 10.13 shows the ratio of the amount of air flowing through the bed to that entering the apparatus. Within experimental error this is constant with increasing flowrate although it does not alone imply that the variation in point velocities is the same. It is also interesting to note that for the duct open and partially blocked a greater proportion flows through the curved bed than the straight one (approximately 70% to 65% (duct end partially blocked) and 40% to 15% (duct end open)) which must be due to the effect of the walls in the curved bed case; the bed surface areas being equal.

Graphs 10.14 to 10.16 show the average velocity (for all positions) against angle for the three flowrates and three duct end conditions studied. These confirm the conclusions drawn above: in the duct open case velocity decreases with angle, in the duct partially blocked and wholly blocked cases velocity increases very slightly with increasing angle. Velocity increases with position, the effect becoming less marked as flowrate decreases and/or as the duct outlet is obstructed. These trends are more apparent when the velocities are presented in their area corrected form.

Graph 10.14. Position Averaged Velocity above the Bed and Angle Around the Bed at Various Flowrates. Duct End Blocked.

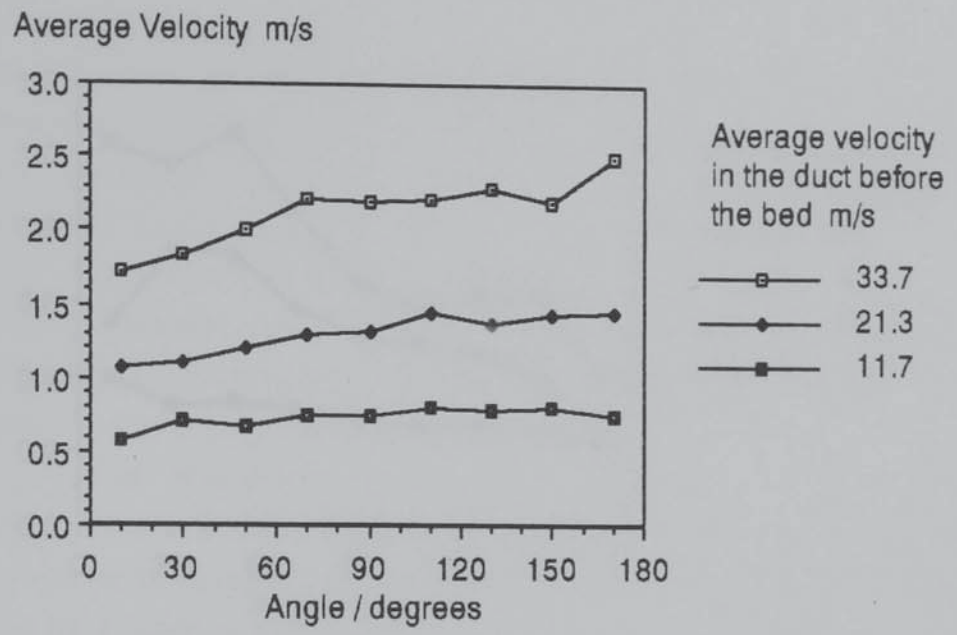

Graph 10.15. Position Averaged Velocity above the Bed and Angle Around the Bed at Various Flowrates. Duct End Partially Blocked.

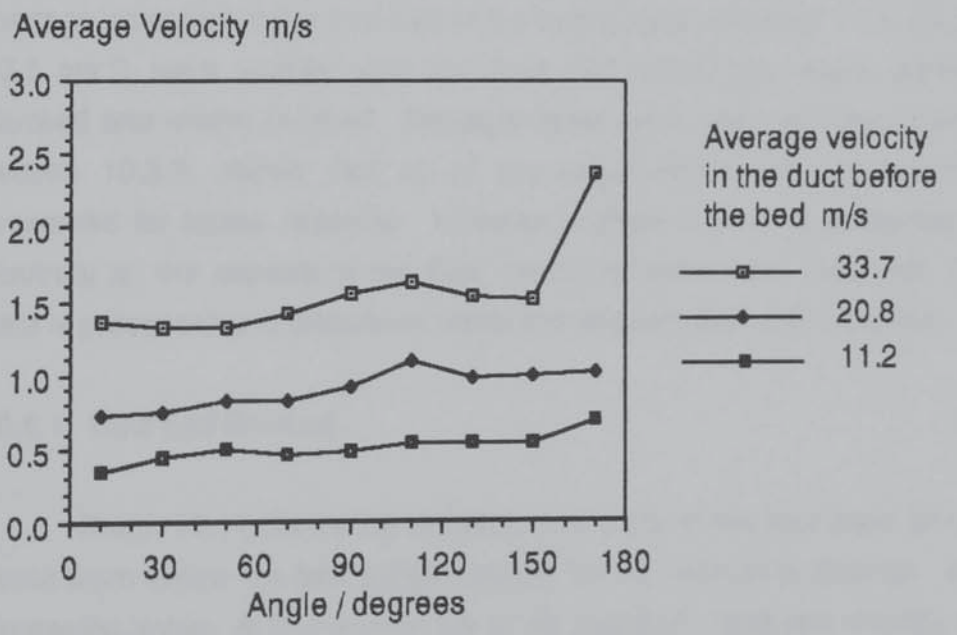

Graph 10.16. Position Averaged Velocity above the Bed and Angle Around the Bed at Various Flowrates. Duct End Open.

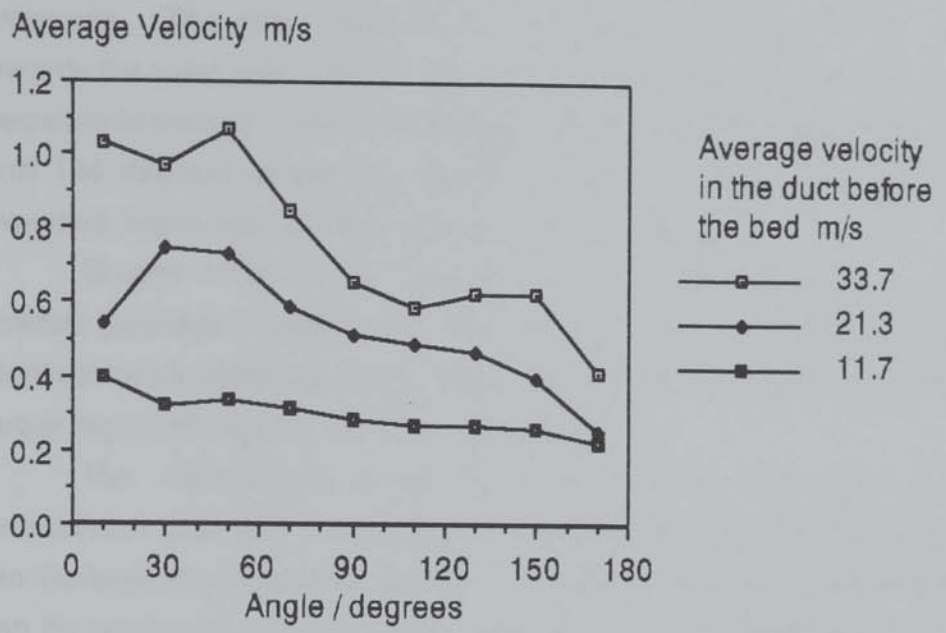

10.6. DUCT AND BASE OF BED RESULTS.

In this section total, static and dynamic pressures and velocities in the duct and at the bed base are presented. Three flowrates (equivalent to average velocities in the duct before the bed of approximately 11.5, 21.0 & 33.5 ms^{-1}) were studied with the duct end conditions: open, partially blocked and wholly blocked. Measurements were taken as described in section 10.3.3, above. Not all of the experimental data collected is presented for space reasons. However, sufficient data is presented to illustrate all the aspects of the fluid mechanic behaviour observed. The data is presented and discussed under the relevant duct end condition.

10.6.1. Duct End Blocked.

Graph 10.17 shows the variation in velocity at the bed base (strictly about 2mm below the bed support mesh) for the maximum flowrate with increasing angle. At low angles (up to 45 degrees) these are virtually the same with position (decreasing slightly towards the outer wall). Above 45 degrees they tend to remain approximately constant towards the outer wall. Towards the inner wall they decrease (with angle) to a minimum between 90 and 120 degrees. A 'negative' velocity (that is the direction of flow is reversed and towards the inlet) is observed at 90 degrees adjacent

to the inner wall showing the recirculation in the duct discussed above. This behaviour is consistent with the mechanisms proposed above.

Graphs 10.18 and 10.19 show similar profiles of total and static pressures. The total pressure is approximately constant with angle towards the outer wall. Nearer the inner wall it decreases because of the decrease in velocity. Graph 10.19 shows static pressures rising with angle until 150 degrees where they decrease slightly. Static pressure is, as expected, higher towards the outer wall of the apparatus.

Graphs 10.20 to 22 present the same information for a lower flowrate (average velocity in the duct before the bed 21.3 ms^{-1}) and show identical trends (although pressures and velocities are lower) except that a larger region of negative velocity is observed.

The inconsistent observations concerning the size of the recirculation area and the decrease in static pressure towards the duct end (an increase would be expected due to pressure recovery at the end wall) can be explained in part by a consideration of experimental error. The measurement of total pressure in a three-dimensional flow is straightforward; however, the measurement of static pressure is very difficult since it is difficult to determine the exact direction of flow at any one point. Hence the measured static pressure may include part of the total pressure. This observation and the preliminary nature of this investigation are the reasons why pressures (by the needle tubes) at the bed base are not determined. A better strategy but, one that is beyond the scope of this study, would be to use Laser Doppler Velocimetry to obtain precise velocity information in the duct. This could then be manipulated to obtain dynamic pressure which, when combined with conventially determined total pressures will give an exact and accurate indication of static pressure.

Graphs 10.23 to 10.25 compare dynamic, static and total pressures at the bed base at a given position with increasing angle. Towards the inner walls total pressure is proportional to dynamic prssure and static pressure increases with increasing angle. At the outer wall the components of pressure do not significantly change with angle.

Graphs 10.26 to 28 present velocity profiles in the duct. These are generally flat in a vertical direction but increase towards the outer wall and decrease towards the duct end. The recirculation at 90 degrees and near the inner wall, discussed above, is more clearly observed.

Graph 10.17. Velocity at the Bed Base with Angle for Various positions. Average Velocity in the Duct before the Bed 33.5 ms^{-1}. Duct End Blocked.

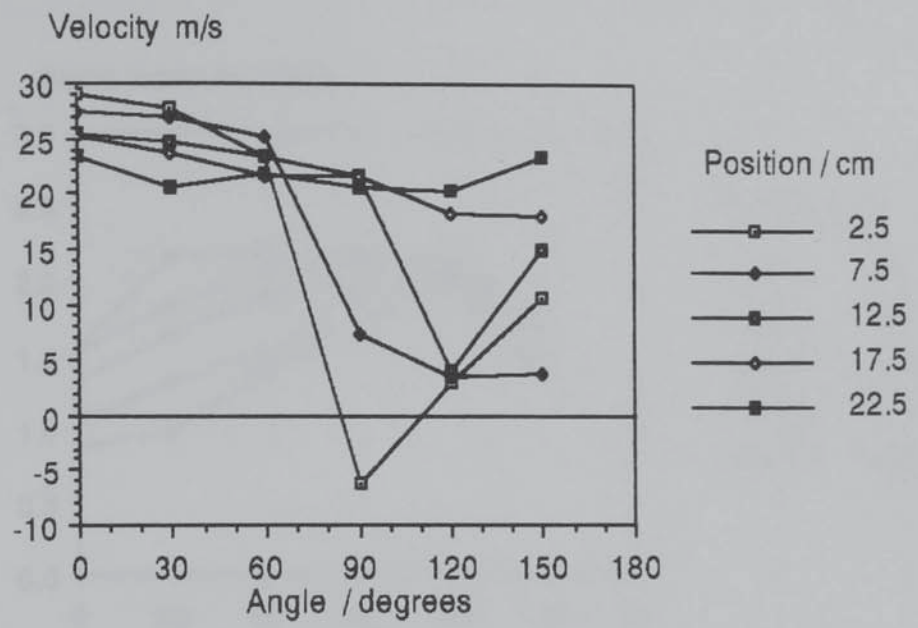

Graph 10.18. Total Pressure at the Bed Base with Angle for Various Positions. Average Velocity in the Duct before the Bed 33.5 ms^{-1}. Duct End Blocked.

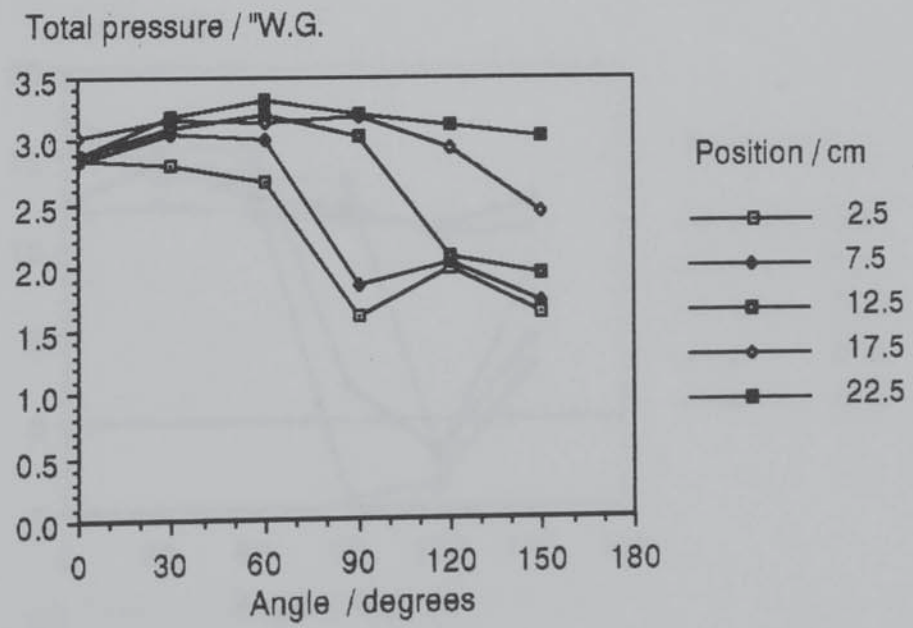

Graph 10.19. Static Pressure at the Bed Base with Angle for Various Positions. Average Velocity in the Duct before the Bed 33.5 ms^{-1}. Duct End Blocked.

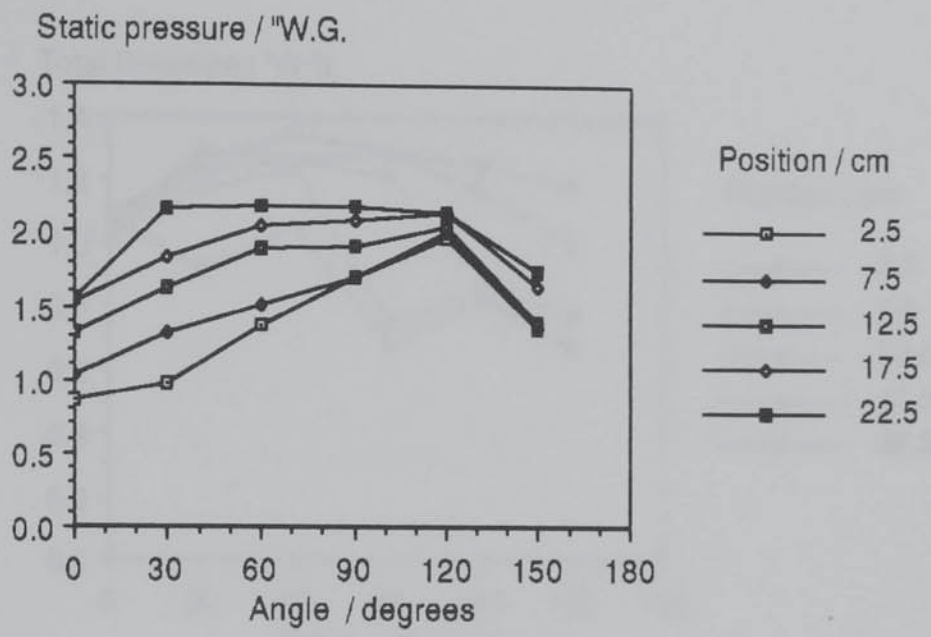

Graph 10.20. Velocity at the Bed Base with Angle for Various Positions. Average Velocity in the Duct before the Bed 21.3 ms^{-1}. Duct End Blocked.

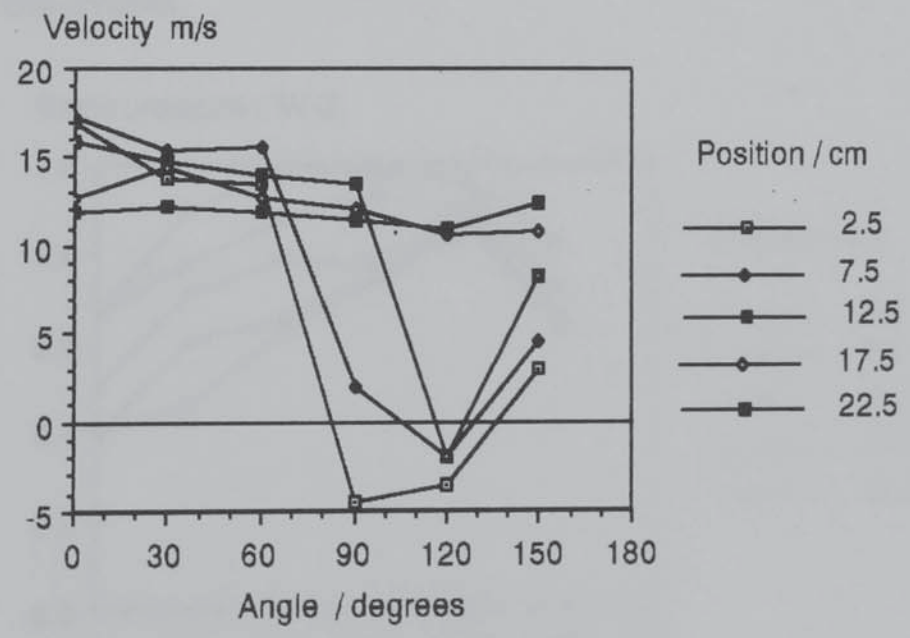

Graph 10.21. Total Pressure at the Bed Base with Angle for Various Positions. Average Velocity in the Duct before the Bed 21.3 ms^{-1}. Duct End Blocked.

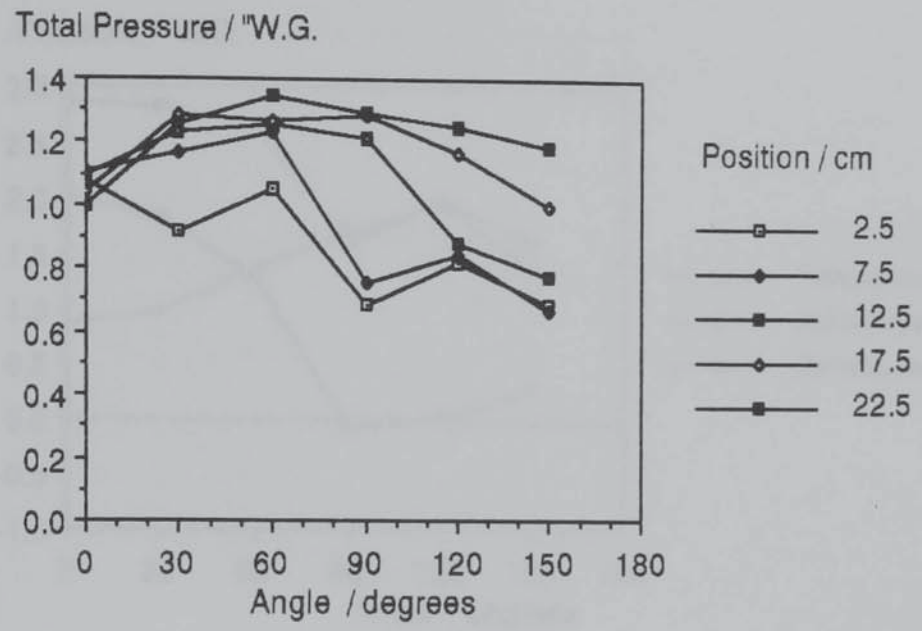

Graph 10.22. Static Pressure at the Bed Base with Angle for Various Positions. Average Velocity in the Duct before the Bed 21.3 ms^{-1}. Duct End Blocked.

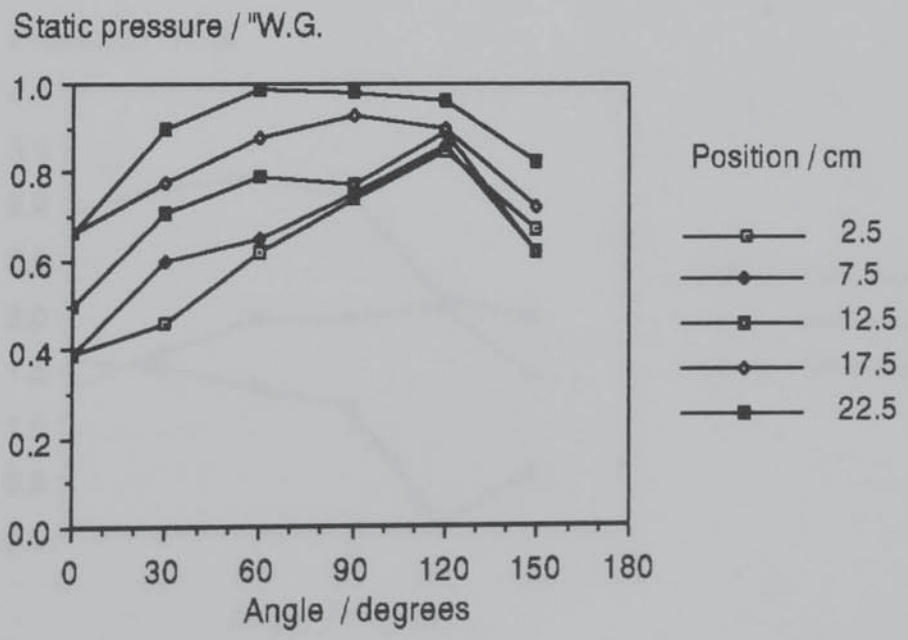

Graph 10.23. Dynamic, Total and Static Pressures at the Bed base with Angle at a Position of 2.5 cm. Average Velocity in the Duct before the Bed 33.5 ms^{-1}. Duct End Blocked.

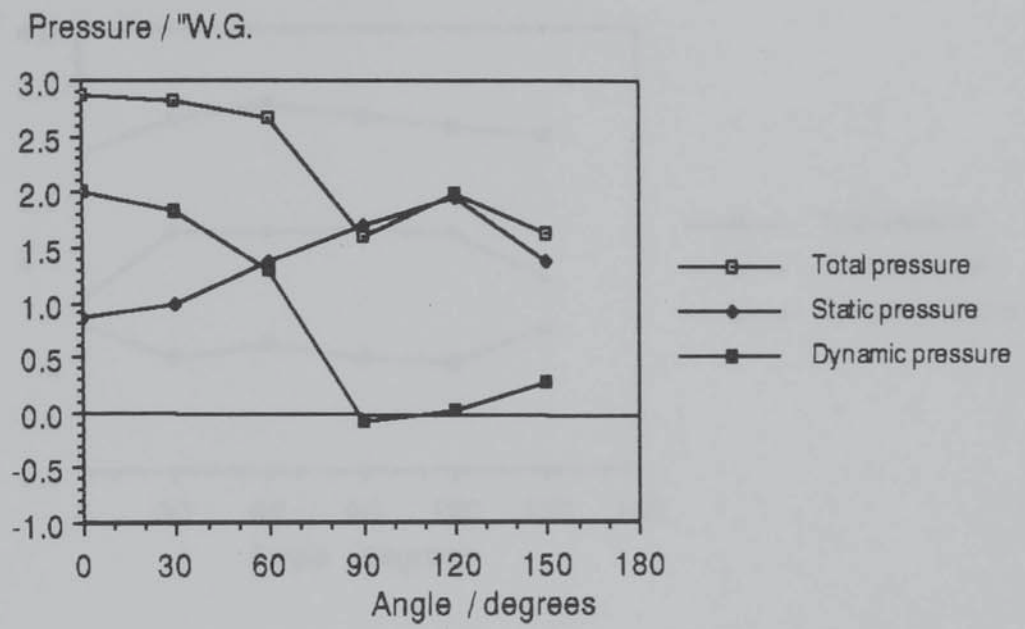

Graph 10.24. Dynamic, Total and Static Pressures at the Bed Base with Angle at a Position of 12.5 cm. Average Velocity in the Duct before the Bed 33.5 ms^{-1}. Duct End Blocked.

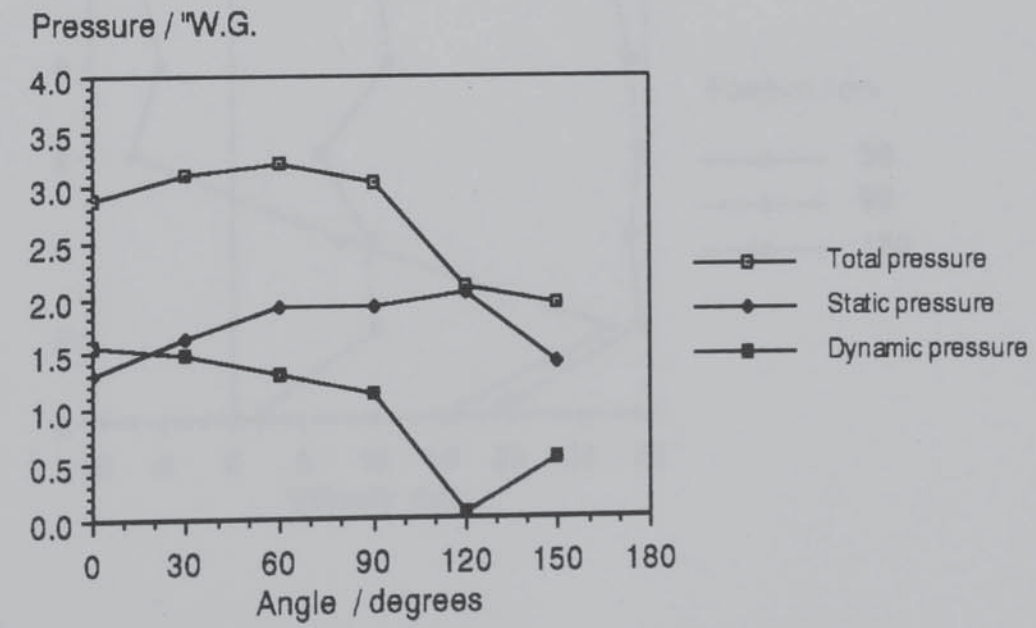

Graph 10.25. Dynamic, Total and Static Pressures at the Bed Base with Angle at a Position of 22.5 cm. Average Velocity in the Duct before the Bed 33.5 ms^{-1}. Duct End Blocked.

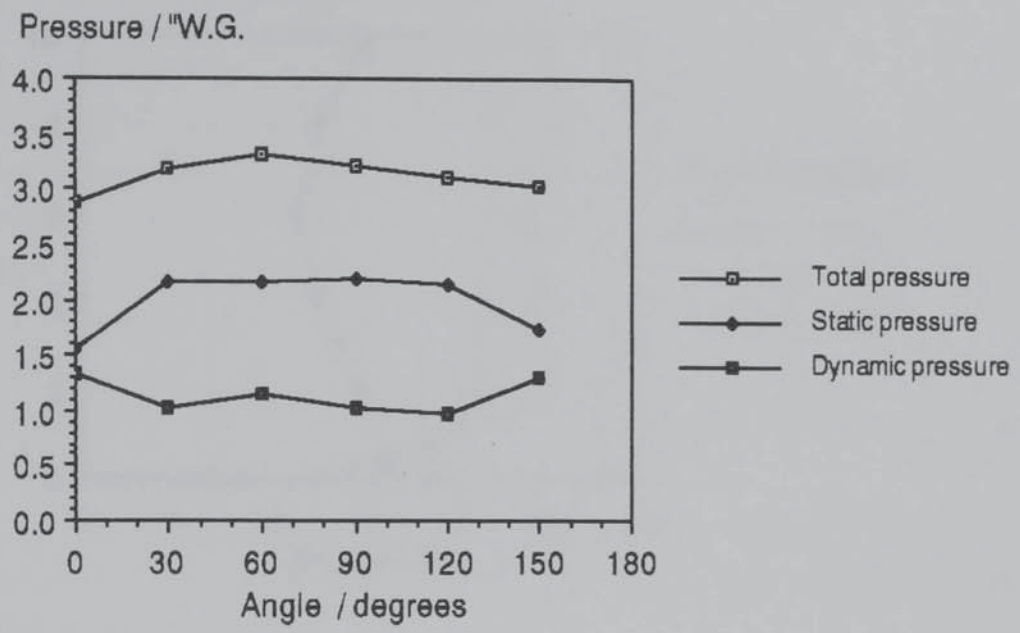

Graph 10.26. Duct Velocity Profiles with Angle at Position 2.5 cm. Average Velocity in the Duct before the Bed 33.5 ms^{-1}. Duct End Blocked.

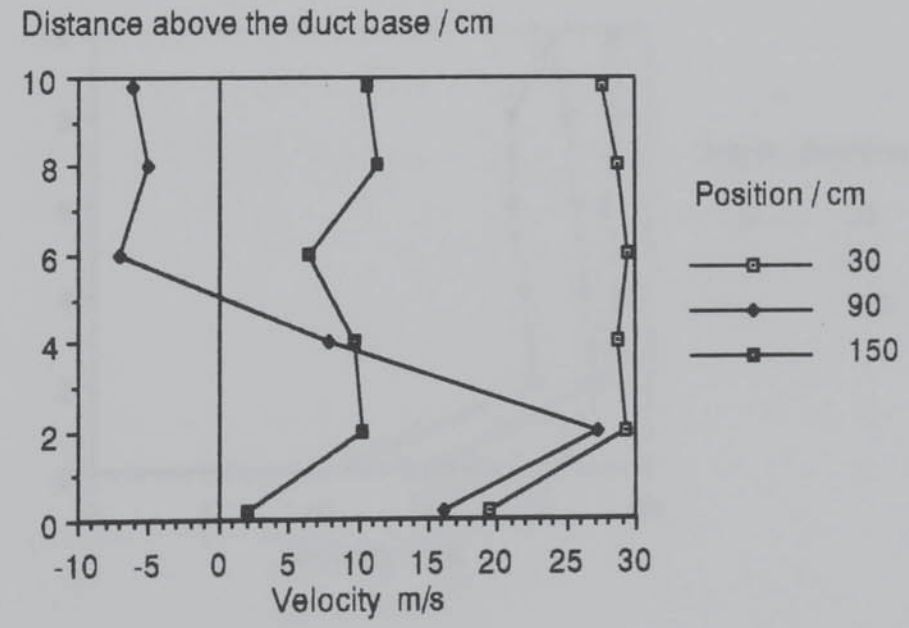

Graph 10.27. Duct Velocity Profiles with Angle at Position 12.5 cm. Average Velocity in the Duct before the Bed 33.5 ms^{-1}. Duct End Blocked.

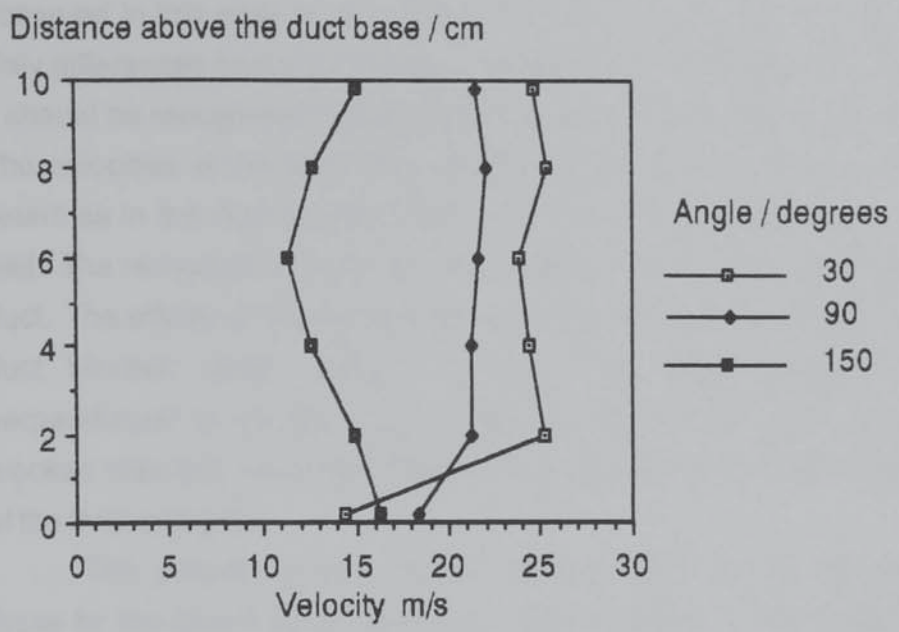

Graph 10.28. Duct Velocity Profiles with Angle at Position 22.5 cm. Average Velocity in the Duct before the Bed 33.5 ms^{-1}. Duct End Blocked.

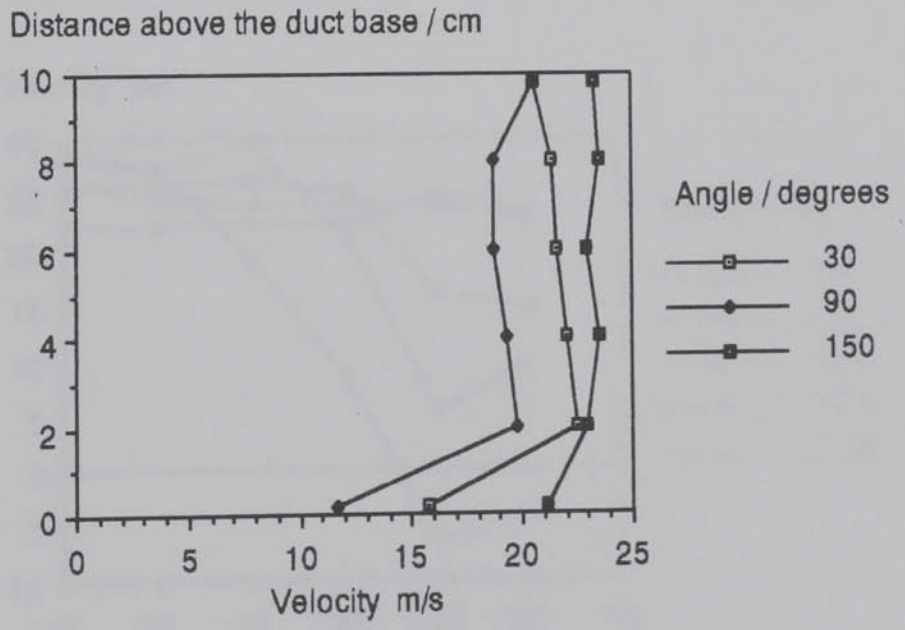

10.6.2. Duct End Partially Blocked.

These results are presented as graphs 10.29 to 37. The behaviour observed in this case is very similar to that in the duct end blocked case. Only differences from duct blocked behaviour are discussed here although it should be recognised that static and therefore total pressures are lower. The velocities at the bed base do not decrease with angle to the same extent as in the duct blocked case due to the lower flowrates through the bed. The recirculation in the duct is observed nearer the outlet end of the duct. The effects of changing flowrate in the duct are as described for the duct blocked case. Graphs 10.32 to 34 show pressure profiles perpendicular to the bed walls, these are similar to those in the duct blocked case but, here static pressure is (as expected) a lower proportion of the total pressure.

The vertical velocity profiles (graphs 10.35 to 37) are similar to those for the duct blocked case but, a larger region of recirculation in the duct is observed.

Graph 10.29. Velocity at the Bed Base with Angle for Various Positions. Average Velocity in the Duct before the Bed 33.6 ms^{-1}. Duct End Partially Blocked.

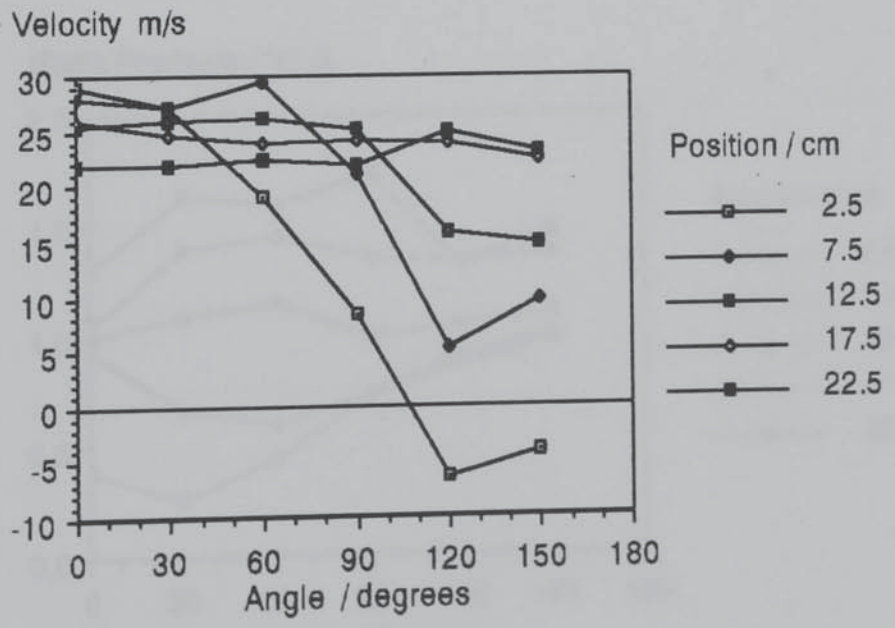

Graph 10.30. Total Pressure at the Bed Base with Angle for Various Positions. Average Velocity in the Duct before the Bed 33.6 ms^{-1}. Duct End Partially Blocked.

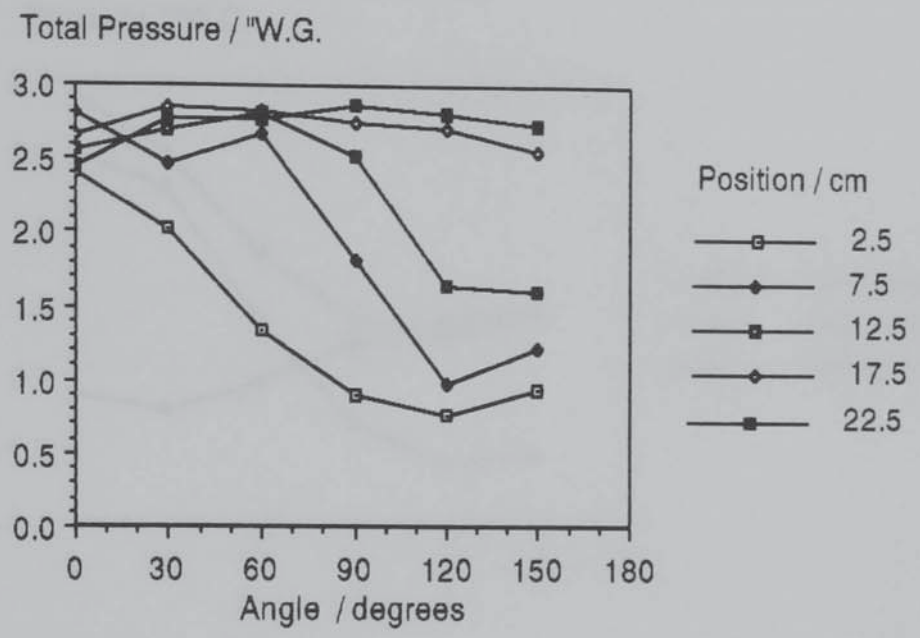

Graph 10.31. Static Pressure at the Bed Base with Angle for Various Positions. Average Velocity in the Duct before the Bed 33.6 ms^{-1}. Duct End Partially Blocked.

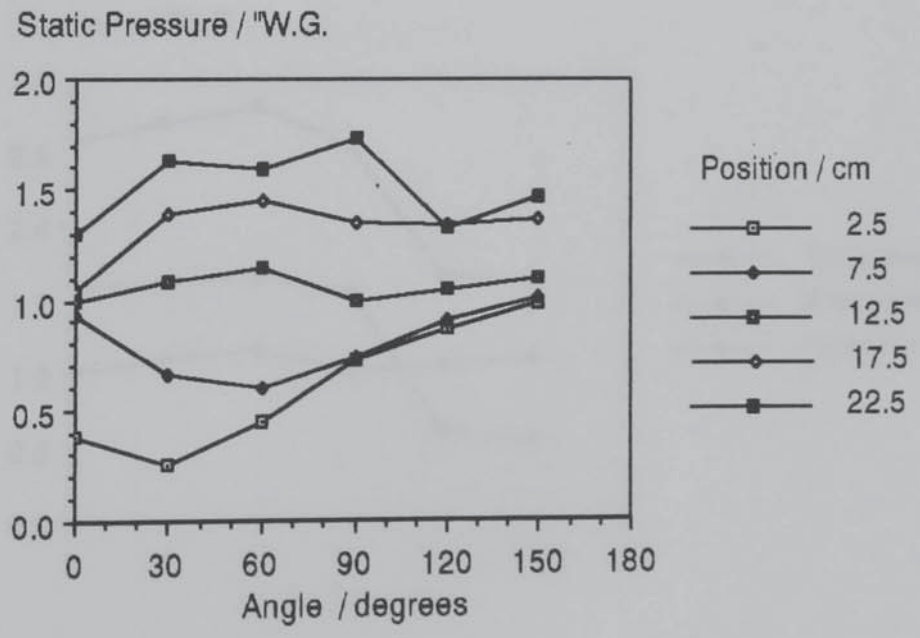

Graph 10.32. Dynamic, Total and Static Pressures at the Bed Base with Angle at a Position of 2.5 cm. Average Velocity in the Duct before the Bed 33.6 ms^{-1}. Duct End Partially Blocked.

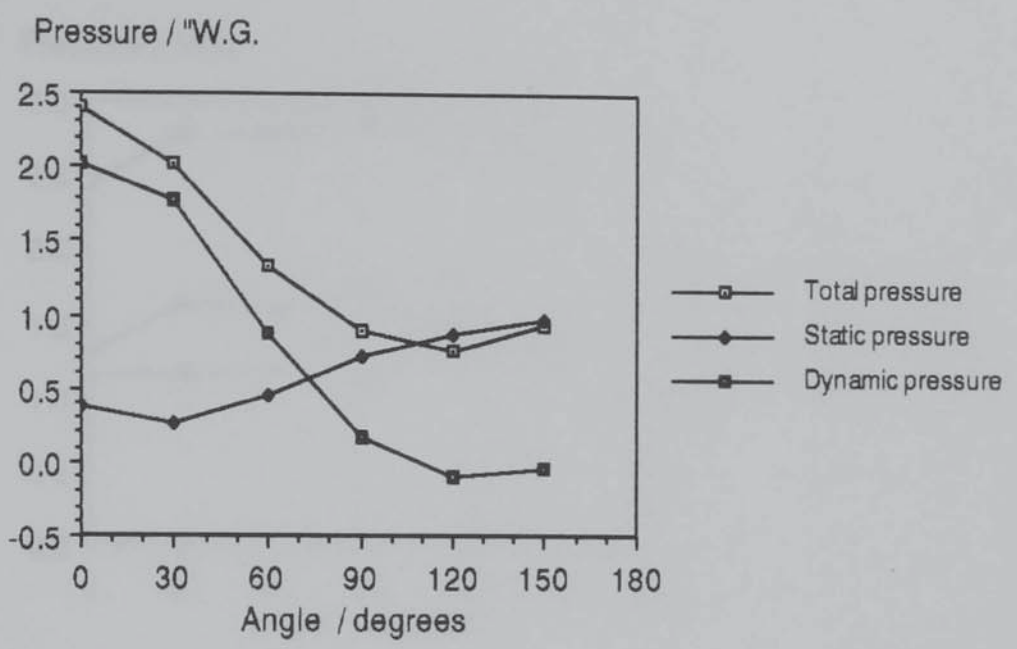

Graph 10.33. Dynamic, Total and Static Pressures at the Bed Base with Angle at a Position of 12.5 cm. Average Velocity in the Duct before the Bed 33.6 ms^{-1}. Duct End Partially Blocked.

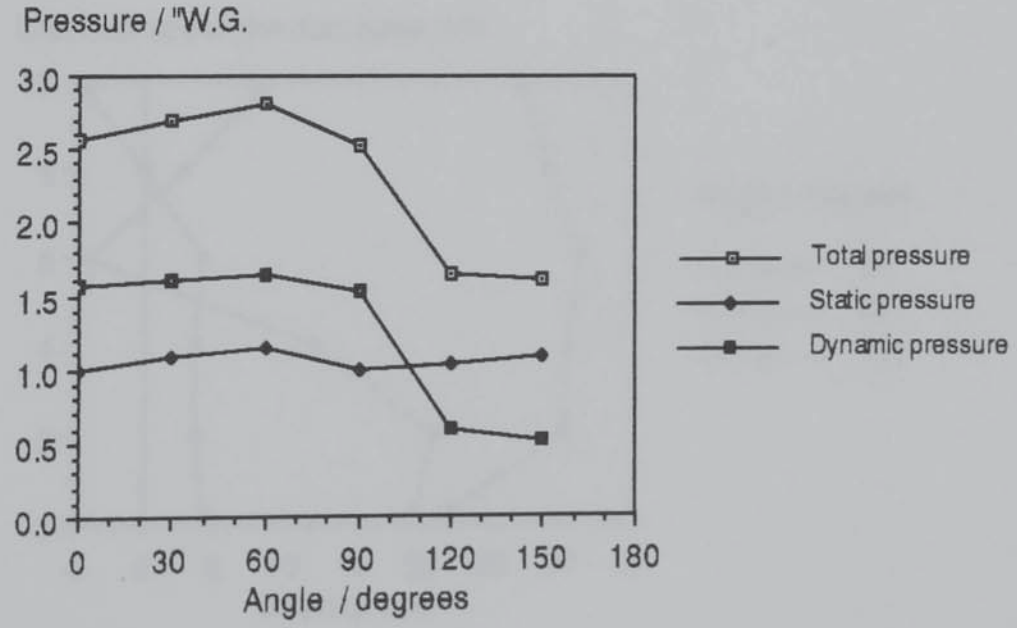

Graph 10.34. Dynamic, Total and Static Pressures at the Bed Base with Angle at a Position of 22.5 cm. Average Velocity in the Duct before the Bed 33.6 ms^{-1}. Duct End Partially Blocked.

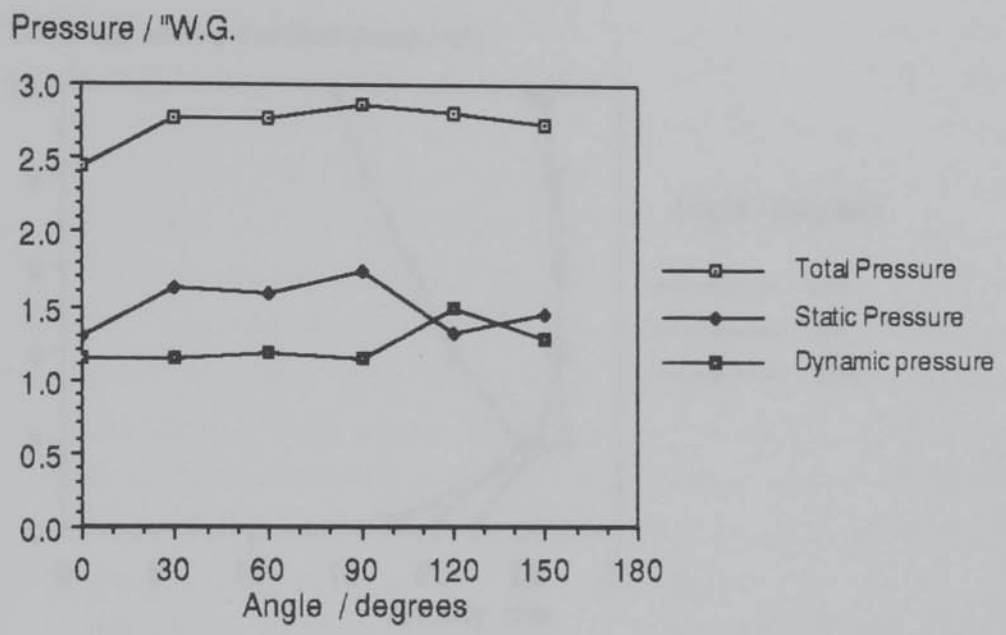

Graph 10.35. Duct Velocity Profiles with Angle at Position 2.5 cm. Average Velocity in the Duct before the Bed 33.6 ms^{-1}. Duct End Partially Blocked.

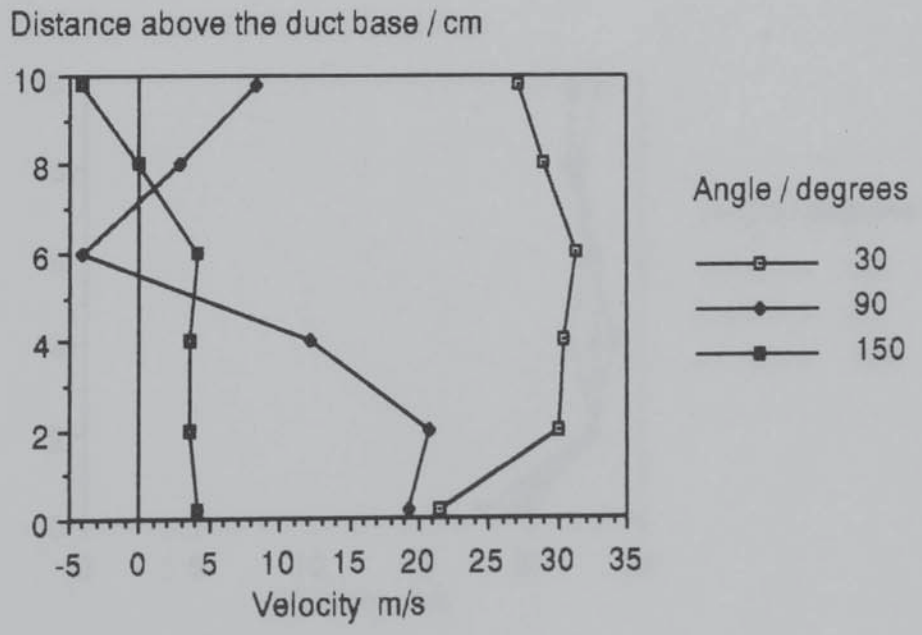

Graph 10.36. Duct Velocity Profiles with Angle at Position 12.5 cm. Average Velocity in the Duct before the Bed 33.6 ms^{-1}. Duct End Partially Blocked.

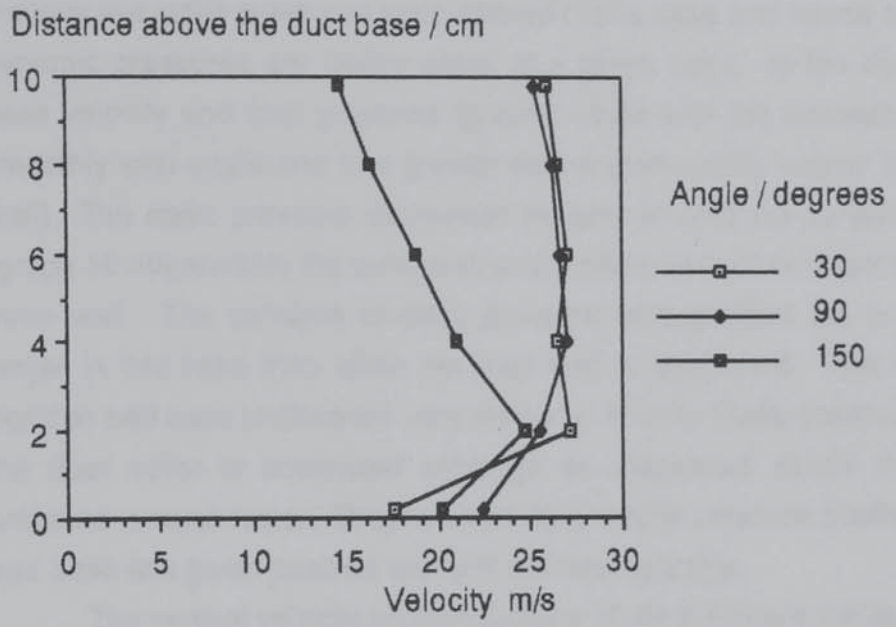

Graph 10.37. Duct Velocity Profiles with Angle at Position 22.5 cm. Average Velocity in the Duct before the Bed 33.6 ms^{-1}. Duct End Partially Blocked.

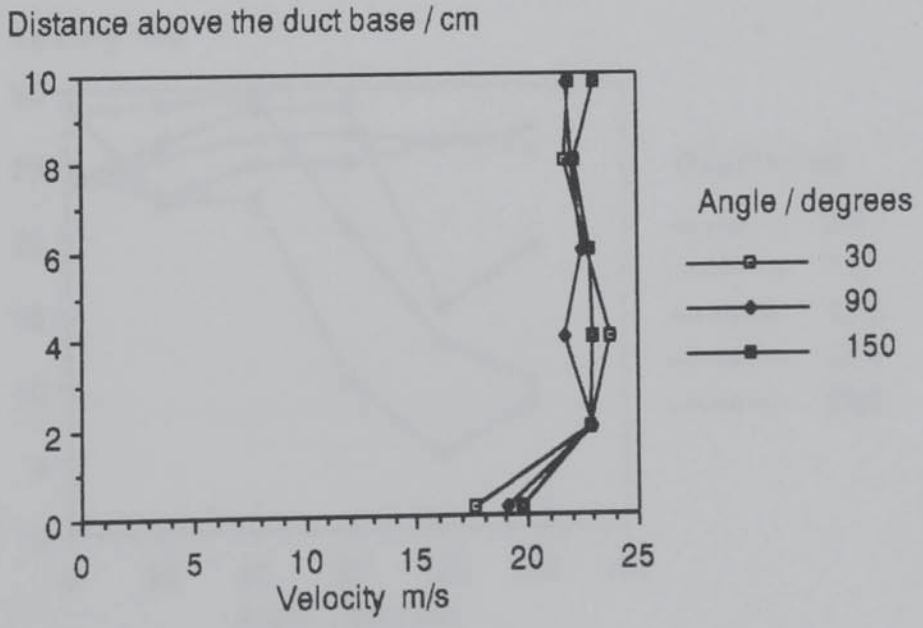

10.6.3. Duct End Open.

As in the straight rig experiments; duct open behaviour is different from that when the duct is wholly or partially blocked. This is mainly due to the very low static pressures encountered in this case and hence total and dynamic pressures are nearly equal at a given point. In the duct open case velocity and total pressure (graphs 10.38 and 39) decrease more smoothly with angle and to a greater extent (particularly nearer the inner wall). The static pressure decreases steadily around the curved section (graph 10.40) towards the outer wall and tends to remain constant near the inner wall. The variation of static pressure with position (as a ratio) is larger in this case than when the duct end is obstructed. The constant position bed base profiles are very similar in form to those observed when the duct outlet is obstructed although as discussed above the static pressure is much lower. Graphs 10.41 to 43 show pressure profiles at the bed base at a given position and with increasing angle.

The vertical velocity profiles (graphs 10.44 to 46) are similar in form to those in the duct end obstructed cases, although no re-circulation is observed.

Graph 10.38. Velocity at the Bed Base with Angle for Various Positions. Average Velocity in the Duct before the Bed 33.3 ms^{-1}. Duct End Open.

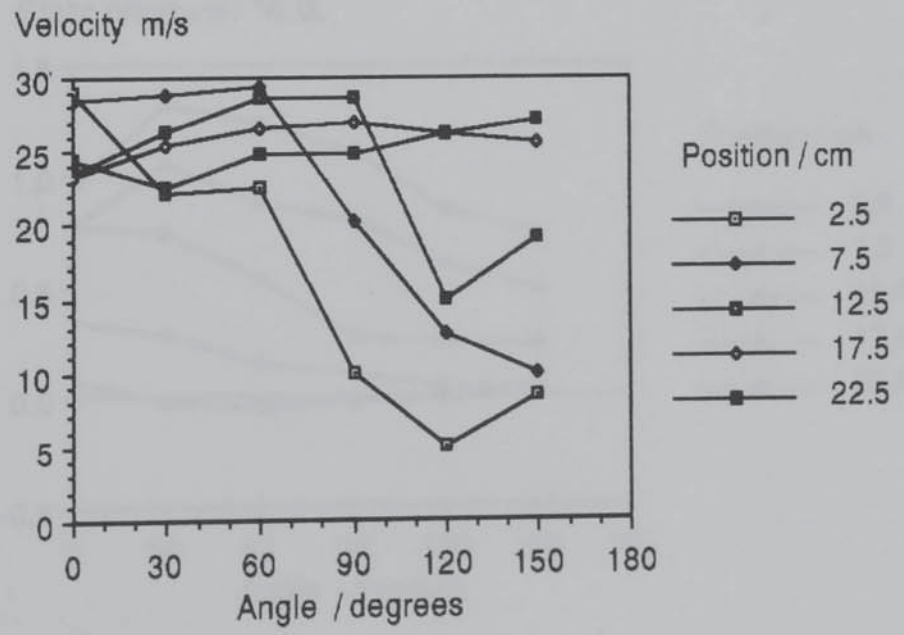

Graph 10.39. Total Pressure at the Bed Base with Angle for Various Positions. Average Velocity in the Duct before the Bed 33.3 ms^{-1}. Duct End Open.

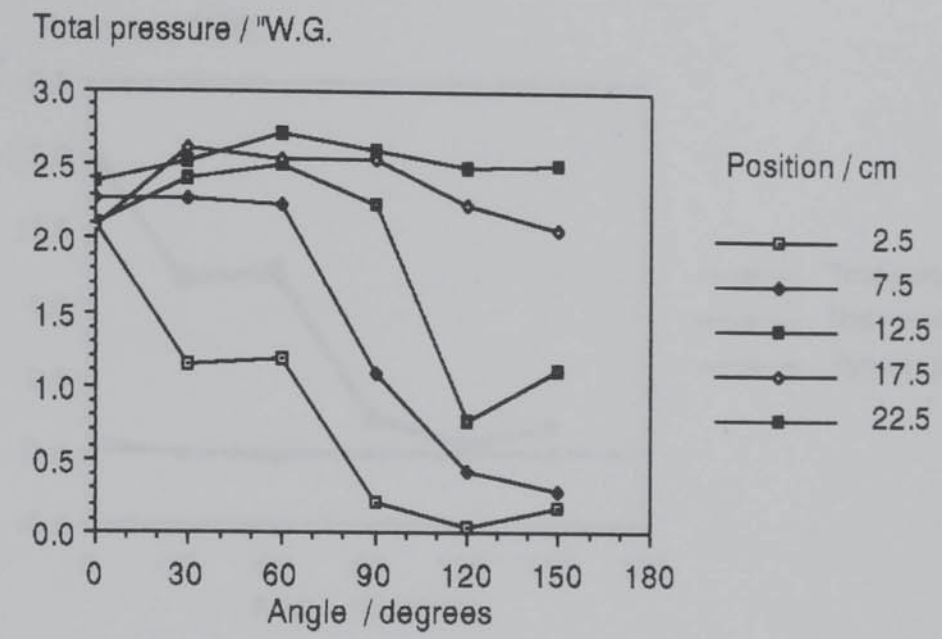

Graph 10.40. Static Pressure at the Bed Base with Angle for Various Positions. Average Velocity in the Duct before the Bed 33.3 ms^{-1}. Duct End Open.

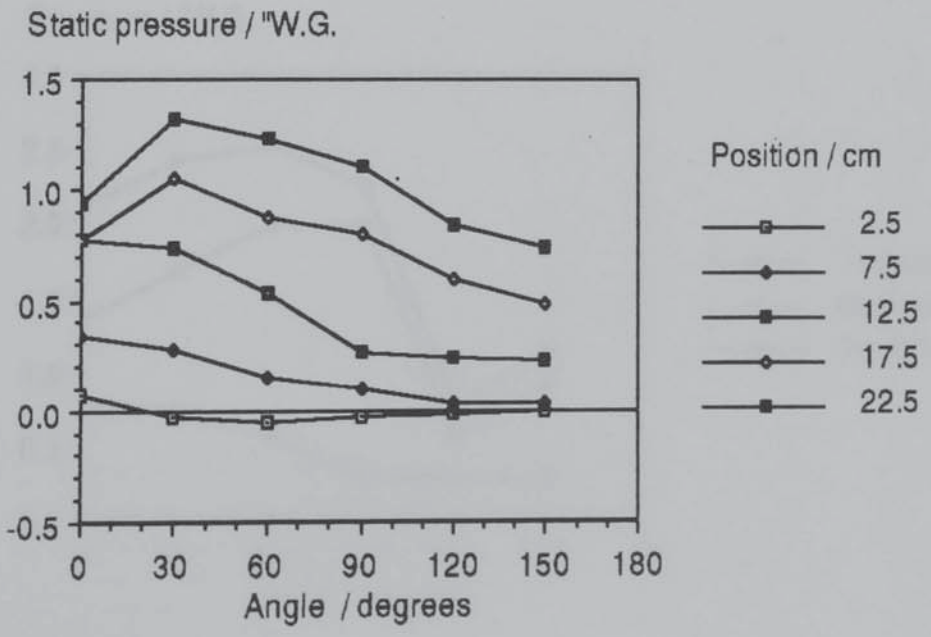

Graph 10.41. Dynamic, Total and Static Pressures at the Bed Base with Angle at a Position of 2.5 cm. Average Velocity in the Duct before the Bed 33.3 ms^{-1}. Duct End Open.

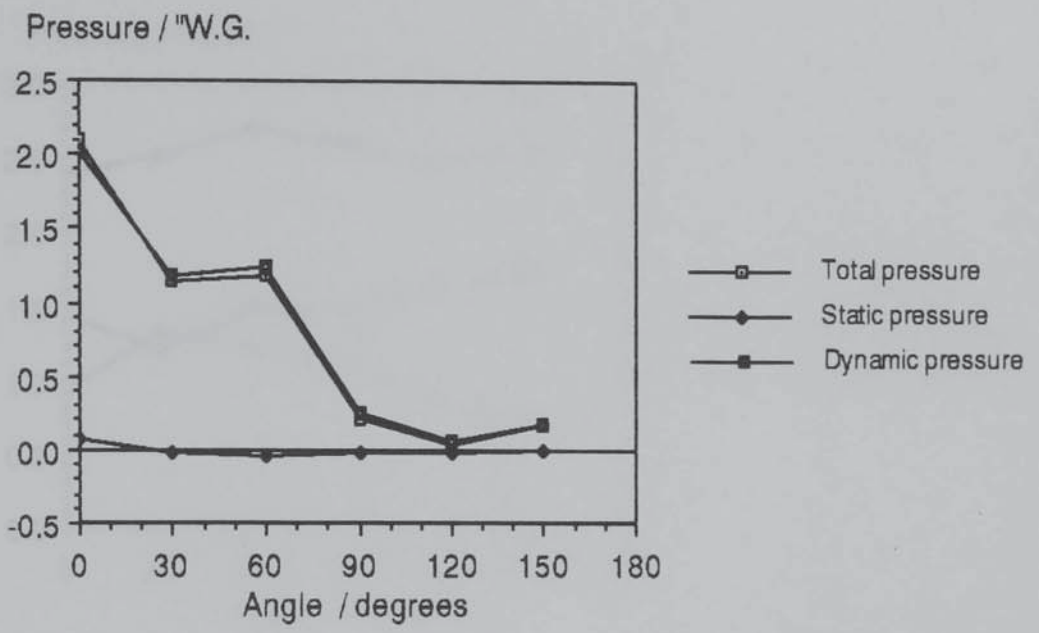

Graph 10.42. Dynamic, Total and Static Pressures at the Bed Base with Angle at a Position of 12.5 cm. Average Velocity in the Duct before the Bed 33.3 ms^{-1}. Duct End Open.

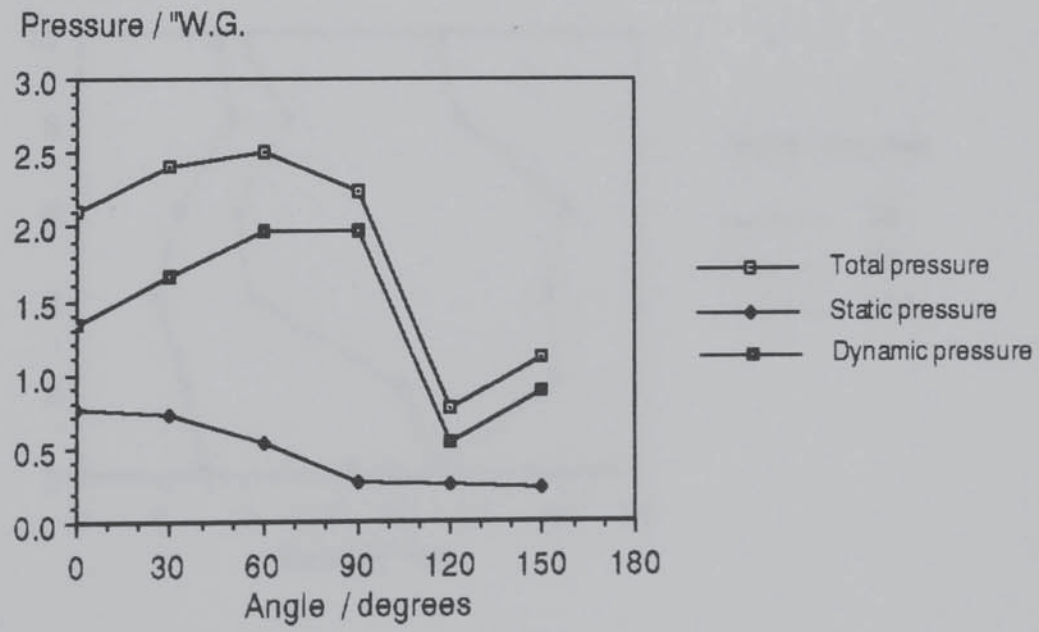

Graph 10.43. Dynamic, Total and Static Pressures at the Bed Base with Angle at a Position of 22.5 cm. Average Velocity in the Duct before the Bed 33.3 ms^{-1}. Duct End Open.

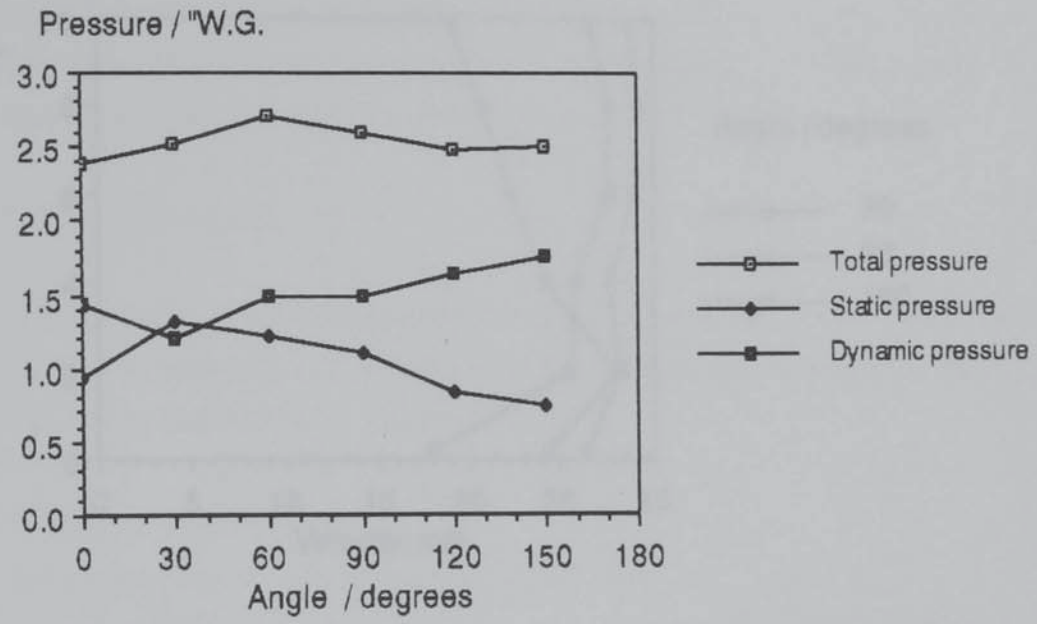

Graph 10.44. Duct Velocity Profiles with Angle at Position 2.5 cm. Average Velocity in the Duct before the Bed 33.3 ms^{-1}. Duct End Open.

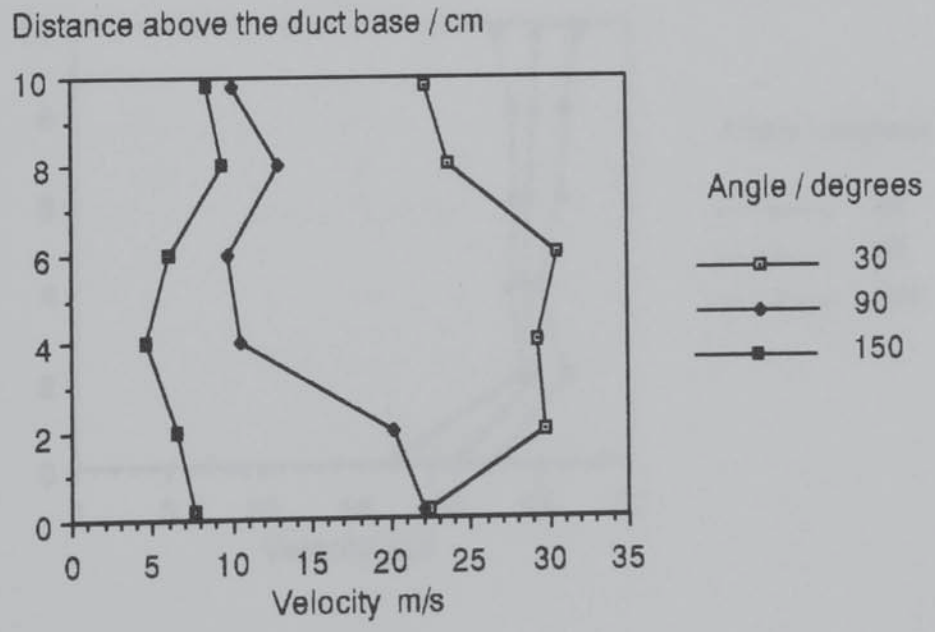

Graph 10.45. Duct Velocity Profiles with Angle at Position 12.5 cm. Average Velocity in the Duct before the Bed 33.3 ms^{-1}. Duct End Open.

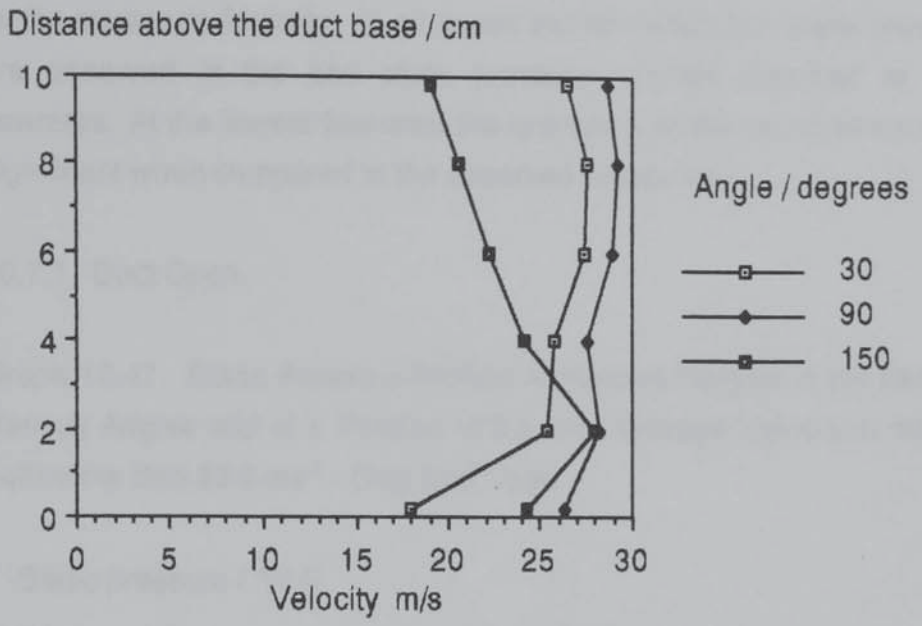

Graph 10.46. Duct Velocity Profiles with Angle at Position 22.5 cm. Average Velocity in the Duct before the Bed 33.3 ms^{-1}. Duct End Open.

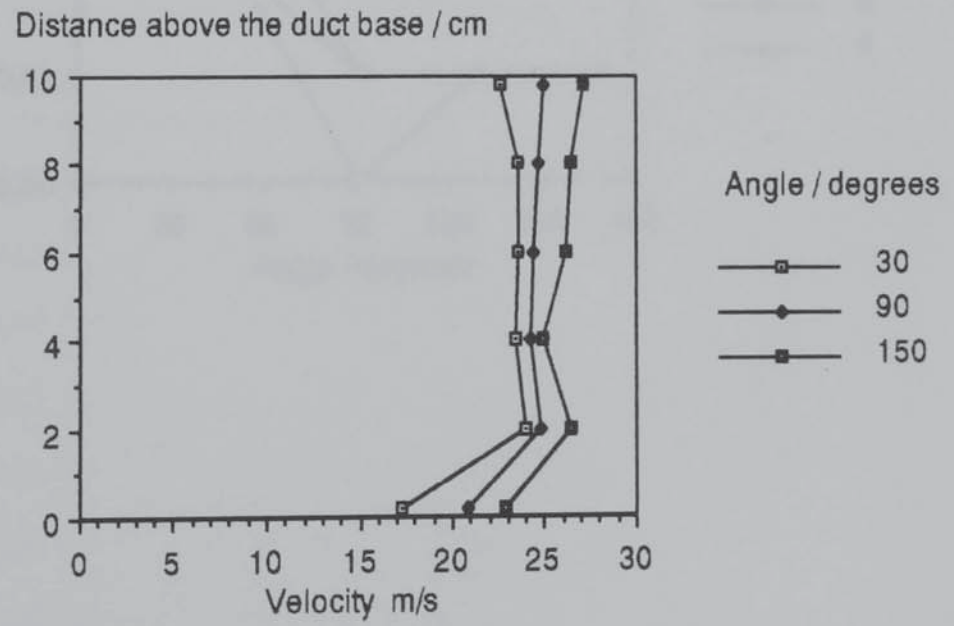

10.7. BED STATIC PRESSURES.

The results for the three duct end conditions are presented below for the maximum flowrate. In all cases similar trends but, lower pressures are observed in the bed static pressure profiles obtained at lower flowrates. At the lowest flowrates the resolution of the micromanometer is significant when compared to the observed pressures.

10.7.1. Duct Open.

Graph 10.47. Static Pressure Profiles at Various Heights in the Bed over Various Angles and at a Position of 2.5 cm. Average Velocity in the Duct before the Bed 33.3 ms^{-1}. Duct End Open.

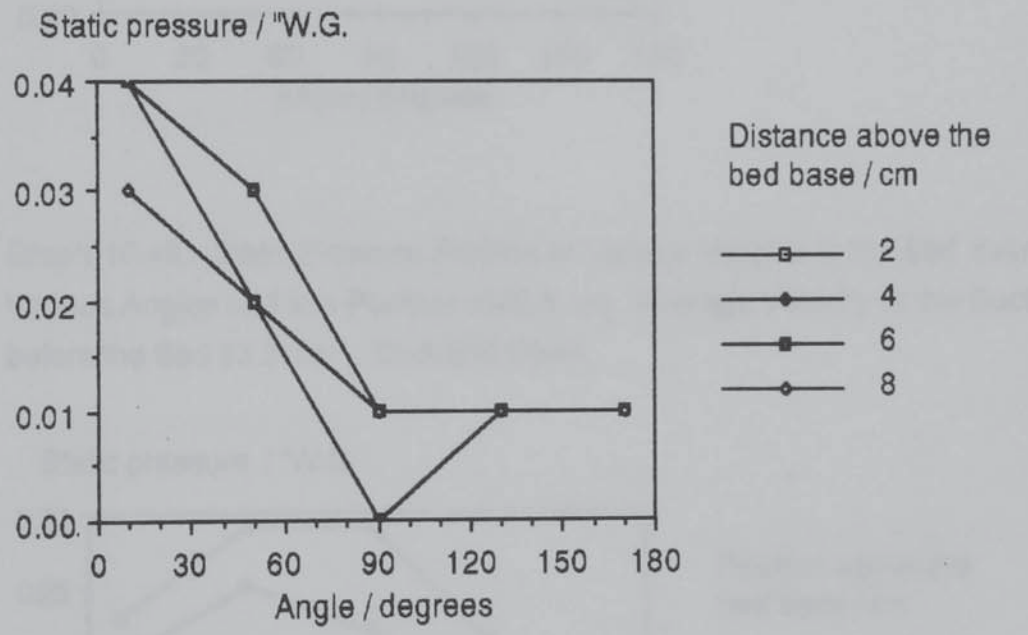

Graph 10.48. Static Pressure Profiles at Various Heights in the Bed over Various Angles and at a Position of 12.5 cm. Average Velocity in the Duct before the Bed 33.3 ms^{-1}. Duct End Open.

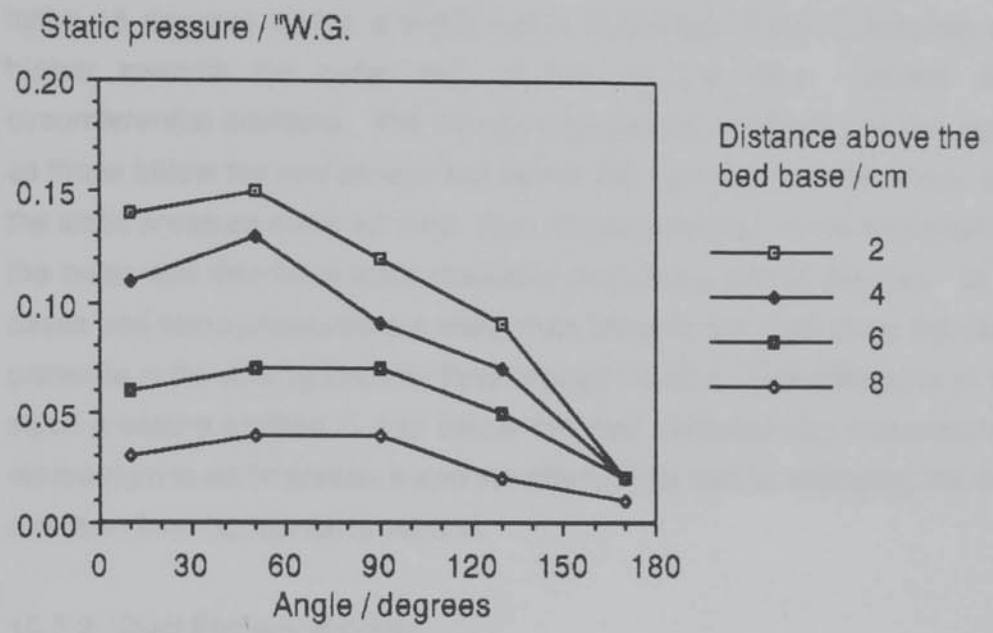

Graph 10.49. Static Pressure Profiles at Various Heights in the Bed over Various Angles and at a Position of 22.5 cm. Average Velocity in the Duct before the Bed 33.3 ms^{-1}. Duct End Open.

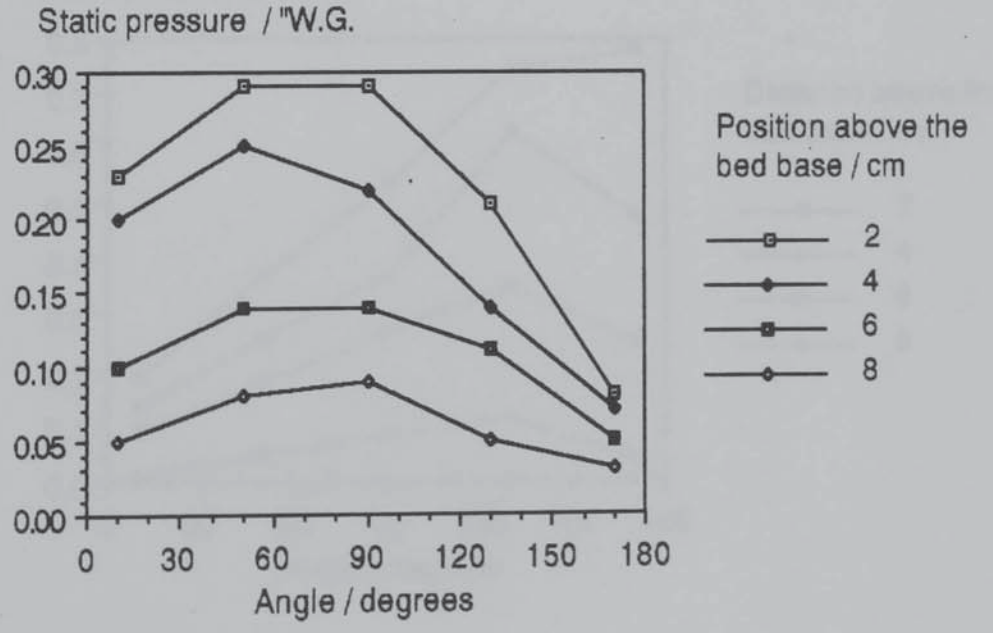

Graphs 10.47 to 49 present these results and can be compared to graphs 10.40 and 10.41 to 43 of the previous section which present static pressures in the duct.

Bed static pressures fall towards the duct outlet except over the initial 45 degrees where a slight rise is observed. Static pressures are higher towards the outer wall of the rig (i.e. they increase with circumferential position). The trends in bed static pressure are the same as those below the bed except that below the bed and near the inner wall the static pressure does not vary. Also, static pressures in the bed towards the outer wall decrease more markedly than those below the bed. In all cases bed static pressures are lower than those in the duct since the static pressure is the driving force for flow through the bed. The difference in the static pressure profiles in and below the bed indicates the conversion of momentum to static pressure and the effect of the bed in changing the flow direction from horizontal to vertical.

10.7.2. Duct Partially Blocked.

Graph 10.50. Static Pressure Profiles at Various Heights in the Bed over Various Angles and at a Position of 2.5 cm. Average Velocity in the Duct before the Bed 33.6 ms^{-1}. Duct End Partially Blocked.

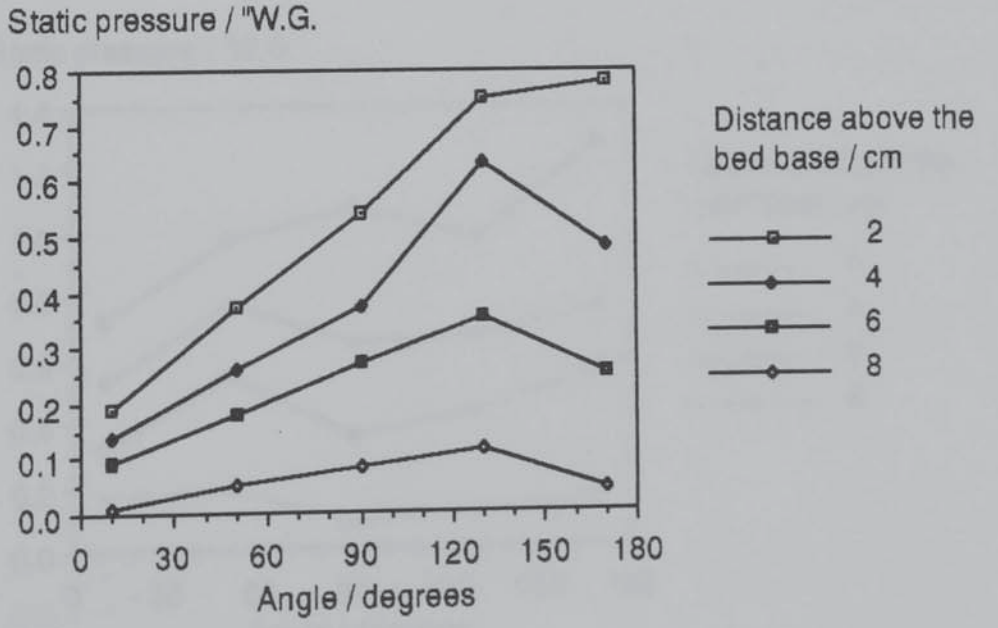

Graph 10.51. Static Pressure Profiles at Various Heights in the Bed over Various Angles and at a Position of 12.5 cm. Average Velocity in the Duct before the Bed 33.6 ms^{-1}. Duct End Partially Blocked.

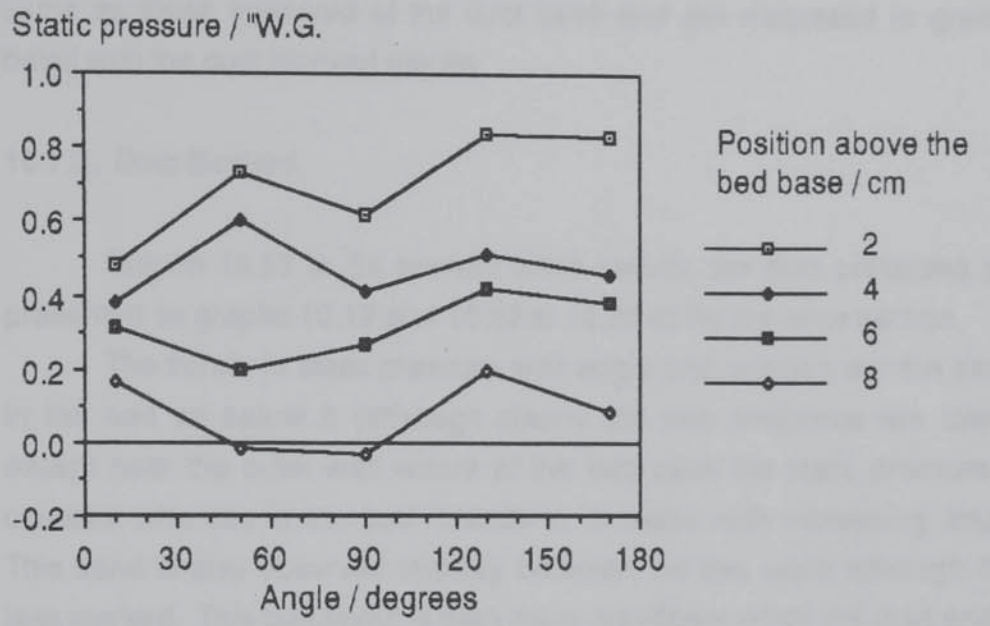

Graph 10.52. Static Pressure Profiles at Various Heights in the Bed over Various Angles and at a Position of 22.5 cm. Average Velocity in the Duct before the Bed 33.6 ms^{-1}. Duct End Partially Blocked.

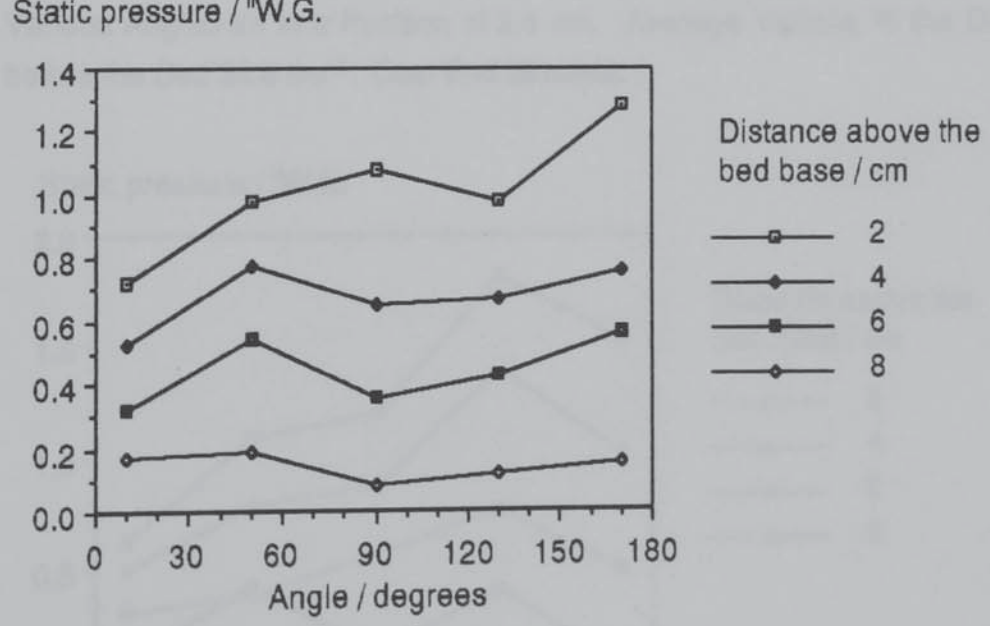

These results are presented as graphs 10.50 to 52 and can be compared to the duct static pressures in graphs 10.31 and 10.32 to 34 of the previous section. Static pressure increases with angle at the outer wall and is approximately constant nearer the inner wall. These trends are the same as those observed at the duct base and are discussed in greater detail with the duct blocked results.

10.7.3. Duct Blocked.

Graphs 10.53 to 55 present these results, the duct pressures are presented as graphs 10.19 and 10.23 to 10.25 of the previous section.

The trends in static pressure with angle and position are the same in the bed as below it (although clearly the bed pressures are lower) except near the outer wall where at the bed base the static pressure is constant whereas in the bed it tends to increase with increasing angle. This trend is also observed midway between the two walls although it is less marked. This behaviour is then more significant when the duct end is wholly blocked than when it is partially blocked and is due to the transformation of momentum to static pressure and the action of the bed in changing the direction of the gas flow.

Graph 10.53. Static Pressure Profiles at Various Heights in the Bed over Various Angles an at a Position of 2.5 cm. Average Velocity in the Duct before the Bed 33.5 ms^{-1}. Duct End Blocked.

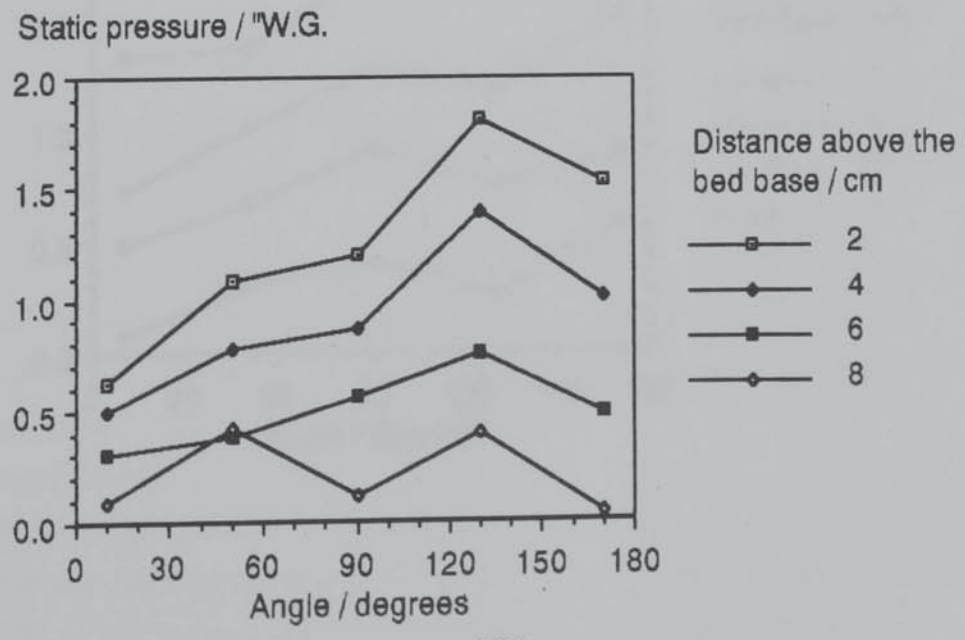

Graph 10.54. Static Pressure Profiles at Various Heights in the Bed over Various Angles an at a Position of 12.5 cm. Average Velocity in the Duct before the Bed 33.5 ms^{-1}. Duct End Blocked.

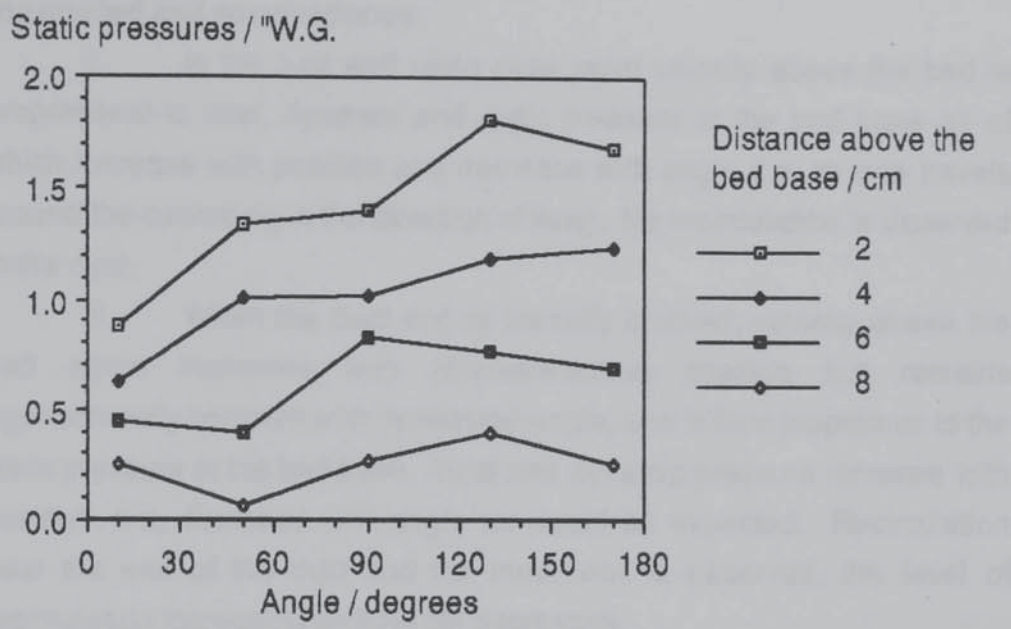

Graph 10.55. Static Pressure Profiles at Various Heights in the Bed over Various Angles an at a Position of 22.5 cm. Average Velocity in the Duct before the Bed 33.5 ms^{-1}. Duct End Blocked.

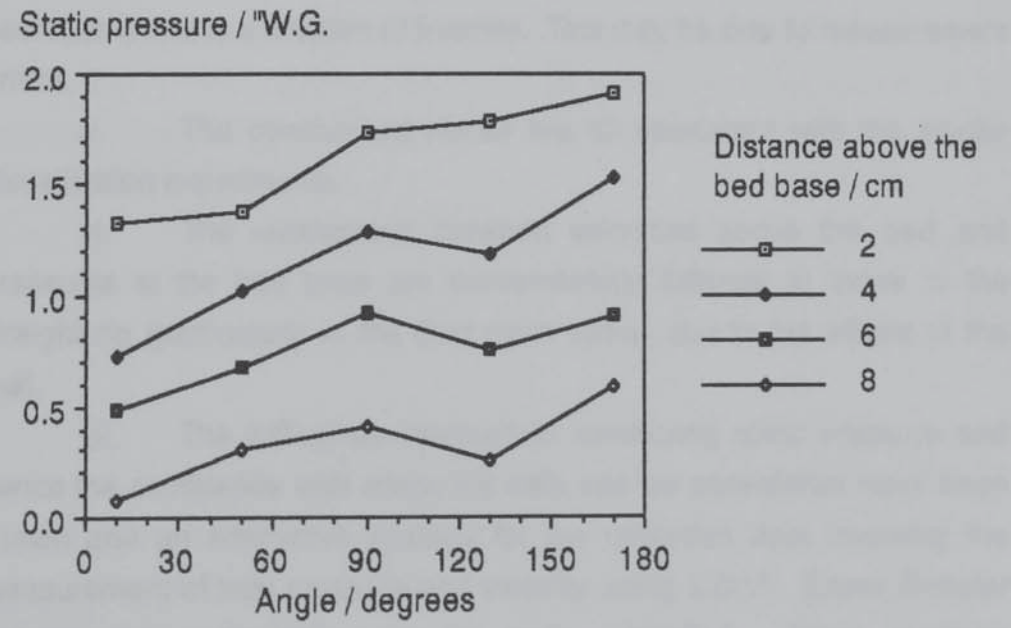

10.7. CONCLUSIONS.

i. An apparatus has been designed to satisfy the four objectives listed at the beginning of this chapter. This apparatus has been constructed and commissioned.

ii. In the duct end open case point velocity above the bed is proportional to total, dynamic and static pressure at the bed base all of which increase with position and decrease with angle (i.e. as one travels around the curved rig in the direction of flow). No recirculation is observed in the duct.

iii. When the duct end is partially blocked, velocity above the bed again increases with (circumferential) position but remains approximately constant with increasing angle, and is thus proprtional to the static pressure at the bed base. Total and dynamic pressure increase with position, but, decrease with angle as would be expected. Recirculation near the end of the duct and the inner wall is observed, the level of recirculation increasing as flowrate decreases.

iv. When the duct end is wholly blocked velocity above the bed increases with position and decreases with angle, and is therefore directly related to total pressure at the bed base. Whereas static pressure increases with angle and position and the variable nature of dynamic pressure measurements below the bed cannot be briefly summarized. Recirculation in the duct is again observed (and increases as flowrate decreases) and is a function of flowrate. This may be due to measurement errors.

v. The conclusions above are all consistent with the smoke visualisation experiments.

vi. The relationship between velocities above the bed and pressures at the bed base are fundamentally different to those in the straight rig (particularly in the duct open case), due to the effects of the wall.

vii. The difficulties involved in measuring static pressure and hence the confidence with which the data can be considered have been shown and an alternative strategy for the collection data involving the measurement of total pressure and velocity using L.D.V. (Laser Doppler Velocimetry), particularly near the walls, identified. Static pressure measurements in the bed are limited by the factors discussed in Chapter 8 and the additional difficulty of identifying the flow direction. The three-

dimensional nature of the flow described here (and in particular the high level of turbulence) considerably complicates the interpretation of experimental results.

viii. The features of the observed flows are explained by the following mechanisms:

1. The gas tends to flow as far as possible in a straight line when the duct end is obstructed, and in the duct open case parallel to tangents drawn at any point on the curved walls of the apparatus and hence higher flowrates are observed nearer the inlet and towards the outer wall.

2. At the walls (particularly the outer wall) momentum is converted to static pressure causing high flow below and through the bed.

3. The higher bed voidage at the walls results in higher flowrates through the bed in this area (particularly at the outer wall where there is a larger driving force (static pressure)).

4. Recirculation is observed when the duct end is obstructed due to the increased flow of gas at the outer wall. More recirculation is observed at lower flowrates. No recirculation is observed when the duct end is open because, in this case, the gas tends to flow parallel to the walls.

5. The absence of bed support wires results in smoother point velocity profiles above the bed. This confirms the conclusions drawn in chapter 8 concerning the two-dimensional apparatus where large variations in point velocity were attributed to the support wires.

ix. The complex nature of the flows examined would be an 'ultimate' test of models developed from the C.F.D. models described previously.

CHAPTER 11

DISCUSSION

It is well known that gas maldistribution may reduce the mass transfer efficiency of packed beds in process equipment, particularly when such beds have a low aspect ratio. Previous studies have experimentally examined maldistributed gas flows in packed beds although, significantly, gas distributor design and application is still largely empirical. Some progress had been made in modelling maldistributed gas flows.

11.1. MODELS OF GAS FLOW IN PACKED BEDS.

The vectorial form of the Ergun Equation has long been accepted as an excellent basis for models of gas flow in packed beds despite the lack of a rigorous derivation of its transient form. Where the formulation of models based on this equation is correct, this approach has been limited by the problem specific nature of the numerical models used. This work has recognised this limitation and has applied the vectorial Ergun Equation (as a coefficient in the velocity equations) within the Computational Fluid Dynamics PHOENICS. This approach is flexible and also allows the description of free fluid space (as discussed below) which previous models have not described.

This application of the vectorial Ergun Equation, which also allows the description of local resistance variations caused by changes in the local packing and fluid properties, has been verified by the comparison of modelled results with the independant experimental results of Poveromo (1975). The domain of study in this case is wholly packed and maldistributed flow is achieved by the assymetric injection of gas and/or spatial variations in bed resistance. This experimental situation is then a rigorous and comprehensive test of the model when the domain is wholly packed.

The main criticism of this modelling approach is that the full equations of motion are solved in the bed in addition to the Ergun Equation. The empirical constants contained in this equation will already include the effects described by the equations of motion. However, the bed resistance is likely to dominate other effects. An improved approach

might be to determine the empirical constants for the Ergun Equation when it is used in conjunction with the full equations of motion. This would be possible using the programs presented in this work.

This inaccuracy partly explains the imperfect agreement between the modelled and experimental results (Poveromo (1975)); also significant are experimental inaccuracies, convergence problems and the assumptions made in the model particularly those concerning the precise description of voidage in the bed.

Recently the FLUENT C.F.D. code (Creare Inc. (1990)) has provided a switch-on option that adequately describes the vectorial Ergun Equation (although it does not appear to allow for local variations in resistance). The work presented here provides support for this appliction of the vectorial Ergun Equation and, the usefulness of the approach work presented here is confirmed by the inclusion of the equation in FLUENT.

11.2. EXPERIMENTAL INVESTIGATIONS OF THE FLUID MECHANICS OF MALDISTRIBUTED GAS FLOWS IN SHALLOW PACKED BEDS.

Two novel experimental investigations of the fluid mechanics of maldistributed gas flow in shallow packed beds have been performed. The first of these examines two-dimensional flows in a straight apparatus and the second three-dimensional flows in a curved apparatus. Novel experimental techniques have been developed to measure pressure at the base of, and in the bed. These techniques have been found to be satisfactory in the two-dimensional experiment but of limited accuracy in the three-dimensional one, in the latter case a revised strategy for the measurement of flow quantities has been proposed. This involves the use of Laser Doppler Velocimetry and total pressure measurements.

Nevertheless, the three-dimensional experiment shows the effect of the vessel walls which act to convert velocity head to static head. This effect is so marked that in the curved apparatus the flow pattern is a function of flowrate whereas in the straight apparatus it is not.

Both experimental investigations were arranged so that the relative amount of gas passing through the bed to that leaving through the duct can be controlled. This is achieved by placing a solid or perforated plate over the duct outlet and allows a more rigorous examination of the effects of the bed base as well as changing static pressure levels in the apparatus.

In the two-dimensional apparatus flow visualisation has allowed the identification of a 'separating streamline' in the free fluid space below the bed. Further the maldistributed nature of the flow clearly demonstrates the need for a vectorial equation to describe the flow in such beds.

The effect of changes in the duct and bed height have been shown to act in opposition; following the principles of similarity. It is clear that the mechanisms are very different when the duct outlet is open to those when it is closed. The effect of the bed support has been shown by the novel bed support pressure probes.

The experimental results are discussed in full detail in Chapters 8 and 10. The two-dimensional experimental results have been used to improve and verify a computer model of gas flow in and around shallow packed beds. The exact mechanisms of flow around the bed base have not been completely explained but, the models discussed below (and improvements made to them) clarify the situation.

11.3. ADVANCED MODELS OF MALDISTRIBUTED GAS FLOWS.

The thesis has highlighted the limitations of previously published models of gas flow in packed beds. The use of the Vectorial Ergun Equation in PHOENICS has overcome many of these limitations, nevertheless it is clearly necessary to describe the flow outside as well as inside the bed.

This problem was addressed in Chapter 9, and was a significant reason in choosing to use a C.F.D. based model. The free fluid space is described by the full equations of motion and, a turbulence model. The turbulence model is not applied in the bed since the empirical constants in the Ergun Equation will already include its effect. A similar argument applies to the equations of motion (in the bed) but these cannot be 'switched off' in PHOENICS. Physically, the experimental situation described in Chapters 6,7 and 8 is realised in the model(two-dimensional flow in a shallow packed bed where bed base effects are particularly signficant).

PHOENICS employs a staggered grid for velocities, which are not solved for at the same points as the other dependant varibles. The implementation of the vectorial Ergun Equation in PHOENICS presented in Chapter 4 averaged two adjacent velocities , and then used this average value to determine the pressure at the relevant grid node. This approach

was satisfactory for models where the domain of study is wholly packed (section 11.1 above) but, does not yield converged solutions when free fluid space is also modelled. Instead, a wavy velocity field was produced in the bed base region. A staggered grid is employed in PHOENICS in order to avoid such wavy velocity fields. It was found that when the velocity averaging is removed satisfactory solutions are obtained. Clearly, the velocity averaging negates the application of the staggerd grid. In hindsight, this not surprising but nevertheless, a signifcant limitation to this approach has been revealed. It is interesting that the algorithms fail at the bed base, where the vectorial Ergun Equation interacts with the equations of motion and, the flow direction changes significantly.

Initially, the converged results from the model did not compare well with the experimental results. This is not due to experimental error and, Chapter 5 shows that the vectorial Ergun Equation and its implementation in PHOENICS are satisfactory. The experimental results have shown the significant effect of the bed base and the following improvements were therefore made to the model so that the bed base region is more fully described:

i. Inclusion of spatial voidage variations in the region adjacent to the bed wall (the V.V. Model).

ii. Applying the logarithmic resistance law (for wall friction) to the bed base outside the bed without restricting the velocity at the bed base (wall) to zero (the B.W.F. Model).

iii. Improvements i. & ii. applied simultaneously (the Combined Model).

These improvements vastly improve the predictive capabilities of the model relative to the experimental results. The results from the improved models are very similar and it appears that; with the inclusion of the bed support into the model, its extension to three dimensions, the use of new empirical constants in the Ergun Equation (as discussed above) and possibly the use of improved empirical constants in the turbulence model the model is likely to be a satisfactory predictive tool.

11.4. IMPLICATIONS FOR DISTIBUTOR AND PROCESS EQUIPMENT DESIGN.

The starting point for the work presented in this thesis was the recognition of the need for the development of new gas distributors and

rigorous design methods for them. There is clearly some way to go before this objective is realised. Nevertheless, some qualitative comments on the implications of this work on the design and operation of gas distributors and process equipment containing packed beds can be made.

The experimental and modelling studies have both shown the critical effect of the bed base region on the flow distribution in and through the packed bed. This effect is not simple and has yet to be fully described. Nevertheless, it is suggested that novel distributor designs should take advantage of the dominating nature of this effect. This suggestion could be realised in a number of ways.

One method would be to design the distributor so that it also acts as the bed support. Practically, such an arrangement might involve supporting the bed on a series of angled vanes. The actual angle and depth of individual vanes could be adjusted to achieve satisfactory gas distribution. This arrangement would be cheaper than existing designs both in capital cost and, its low pressure drop would result in savings in operating costs.

An alternative method would be to use shallow heights of different packings (both in shape and size) in different areas above a simple, regular bed support. These regions of varying resistance could be positioned so as to correct any gas maldistribution caused by the flow patterns outside the bed. In both of these examples a rigorous model of flow in and around a packed bed would be required for both development and design work.

The appreciation of the complex inter-relationships between a bed, its base and the surrounding free fluid space leads to the most significant implication of this work for the design of mass transfer equipment containing packed beds. This is that items of process equipment containing shallow packed beds should be designed as a whole unit; rather than as a bed design (height, diameter, packing type etc. dictated by mass transfer requirements), a containing column and finally a distributor to overcome flow pattern problems. Computational Fluid Dynamics codes incorporating the vectorial Ergun Equation provide a suitable design tool.

11.5. FUTURE WORK.

The work described here could usefully be followed by several further investigations:

i. The empirical constants in the vectorial Ergun Equation could be re-determined to permit the use of this equation with the full equations of motion and a turbulence model.

ii. A transient form of the vectorial Ergun Equation could be defined and would be of particular use in modelling cyclic applications such as adsorption.

iii. The use of shape factors with low voidage, open packings (e.g. Pall Rings) could be studied so that these commercial packings can be fully characterised.

iv. The two dimensional model of flow in, and around a packed bed presented here could be improved by the representation in the model of the bed support and, if necessary, by fine tuning of the empirical constants in the turbulence model.

v. This model could be extended to three spatial dimensions and verified by comparison with the results from the three dimensional apparatus. The model could then be adapted to describe transient flows.

vi. The model could then be used as a rigorous design tool for items of process equipment containing packed beds.

vii. Finally, novel distributors having the dual function of gas distribution and bed support could be developed; such distributors could be fully described by a C.F.D. based model.

CHAPTER 12

CONCLUSIONS

The main conclusions from the combined experimental and theoretical study presented in this thesis can be summarised as follows:

i. The vectorial Ergun Equation provides an excellent description of maldistributed gas flow in packed beds.

ii. A combined approach using the Computational Fluid Dynamics Code PHOENICS and the vectorial Ergun Equation to describe fluid flow in equipment containing packed beds has been presented.

iii. It has been found that this model gives results that agree well with independant experimental results for maldistributed gas flows in columns that are wholly packed.

iv. A novel two-dimensional experiment has been realised that investigates the fluid mechanics of maldistributed gas flow in shallow packed beds.

The detailed experimental conclusions from this investigation are presented in Chapter 8. In particular the critical effects of the bed base region and the bed support have been shown.

v. The vectorial Ergun Equation/ PHOENICS model has been extended to model this experimental investigation. The exact nature of the bed base is again shown to be important and the model has been improved by incorporating both the spatial variation in voidage in the bed (near the bed base) and, a novel base of bed boundary condition which is based on the logarithmic law for velocities near walls applied within the k-ε turbulence model.

vii. A novel, three-dimensional experimental study for maldistributed gas flows has been performed. This investigation has particularly highlighted the effect of:

a. The equipments walls (below the bed).

b. The effects of changes in gas flow direction below the bed.

Detailed conclusions are presented in Chapter 10.

vii. In practical terms the work presented here presents considerable progress towards the provision of a rigorous design tool for process equipment containing packed beds. The work has shown that a

combined vectorial Ergun Equation / C.F.D. model could form such a design tool since it would fully describe the vessel containing the packed bed (including the distribution device). However, the model requires some 'fine tuning' and extending to three spatial dimensions before it can be used in this way.

viii. Given the critical effect of the bed base and its' support on the flow pattern in process equipment containing packed beds; it is suggested that improved, novel gas distribution devices can be designed that would also function as the bed support.

REFERENCES

Ali Q.H., (1984), 'Gas Distribution in Shallow, Large Diameter Packed Beds', Ph.D. Thesis, University of Aston in Birmingham

Apte V.B., Wall T.F. & Truelove J.S., (1988), 'Gas Flows in Raceways formed by High Velocity Jets in a 2 Dimensional Packed Bed', Ch.E.R.D., 66(4),357

Aryan A.F., (1986) ,'The Fluid Mechanics of Maldistributed Gas Flows in Shallow Packed Beds', Final Year Experimental Project Report, Aston University

Bahnen R.H. & Stojanoff C.G., (1987), 'Velocity Fluctuations at the Walls of a Packed Bed of Spheres for Medium Reynolds Numbers', Trans. A.S.M.E. (J. Fluids Eng.), A109(3), 242

Bailey B.J., (1975), 'Fluid Flow in Perforated Pipes', J. Mech. Eng. Sci., 17(6), 338

Beavers G.S. & Joseph D.D., (1967), 'Boundary Conditions at a Naturally Permeable Wall', J. Fluid Mech., 30(1), 197

Beavers G.S., Sparrow E.M. & Magnuson R.A., (1970), 'Experiments on Coupled Parallel Flows in a Channel and Bounding Porous Medium', Trans. A.S.M.E. (J. Basic Eng.), D92(4), 843

Beavers G.S, Sparrow E.M. & Masha B.A., (1974), 'Boundary Condition at a Porous Surface which Bounds a Fluid Flow', A.I.Ch.E.J., 20(3), 596

Benenati R.F. & Brosilow C.B., (1962), 'Void Fraction Distribution in Beds Of Spheres', A.I.Ch.E.J., 8(3), 359

Bentham J., Cavill S. & Turner P., (1985), 'To Investigate the Maldistribution of Gas Flow Through a Packed Column', Final Year Experimental Project Report, Aston University

Berman A.S., (1953), 'Laminar Flows in Channels with Porous Walls', J. Appl. Phys., 24(9), 1232

Berman A.S., (1958), 'Laminar Flow in an Annulus With Porous Walls', J. Appl. Phys., 29(1), 71

Bird R.B., Stewart W.E. & Lightfoot E.N., (1960), 'Transport Phenomena', Wiley, New York

Blake F.E., (1922), Trans. A.I.Ch.E., 14, 415

Brady J.F., (1984), 'Flow development in a Porous Channel and Tube', Phys. Fluids, 27(5), 1061

Brinkman H.C., (1947), 'On the Permeability of Media Consisting of Closely Packed Porous Particles', App. Sci. Res. Sect. Al, 1 81-86

British Standards Institute, (1977), 'Measurement of Fluid Flow in Closed Conduits', Part 2, Section 2.1, BS 1042, B.S.I., London

Buchlin J.M., (1986), 'Prediction of Heat and Mass Transfer in Particulate Beds', in 'Introduction to the Numerical Solution of Industrial Flows', Von Karman Institute Lecture Series 9

Buchlin J.M., Reithmuller M. & Ginoux J.J., (1977), 'A Flourescence Method for the Measurement of the Local Voidage in Randomn Packed Beds', Chem. Eng. Sci., 32, 1116-1119

Burke S.P. & Plummer W.B., (1928), Ind. Eng. Chem., 20(11), 1196

Bushuev V.P., Kisarov V.M. & Fisher R.Y., (1982), 'Effect of the Non-Uniformity of Gas Distribution to the Height of Adsorbers on the Degree of Sorbent Layer Treatment', Prom. Sanit. Ochistka. Gazov., 1(14)

Calderbank P.H. & Pogorski L.A., (1957), 'Heat Transfer in Packed Beds', Trans. I.Chem.E., 35, 195

Chandrasekhara B.C. & Vortmeyer D., (1979), 'Flow Model for Velocity Distribution in Fixed Porous Beds Under isothermal Conditions', Warme-und. Stoff., 12, 105

Choudhary M., Propster M. & Szekely J., (1976), 'On the Importance of the Inertial Terms in the Modeling of Flow Maldistribution in Packed Beds', A.I.Ch.E.J., 22(3), 600

Choudhary M., Szekely J. & Weller S.M., (1976 a), 'The Effect of Flow Maldistribution on Conversion in a Catalytic Packed Bed Reactor Part One; Analysis', A.I.Ch.E.J., 22(6), 1021

Choudhary M., Szekely J. & Weller S.M., (1976 b), 'The Effect of Flow Maldistribution on Conversion in a Catalytic Packed Bed Reactor Part Two; Experimental Studies', A.I.Ch.E.J., 22(6), 1027

Coulson J.M., Richardson J.F., Backhurst J.R. & Harker J.H. (1978), 'Chemical Engineering', Vol. 2, 3rd Ed., Pergamon, Oxford

Cross M. & Gibson R.D., (1979), 'Gas Flow Through Multi-Layered Regions of Porous Media',Powd. Tech., 24, 167-178

Crawford C.W. & Plumb O.A., (1986), 'The Influence of Surface Roughness on Resistance to Flow through Packed Beds', Trans. A.S.M.E. (J. Fluids Eng.), 1108(4), 343

Creare Inc., (1990), ' The Fluent Users Manual', Vols 1 + 2, Hanover, New Hampshire.

Cross M. & Gibson R.D., (1979), 'Gas Flow Through Multi-Layered Regions of Porous Media', Pow. Tech., 24, 167

Daraktshiev R., (1984), 'On the Gas Distribution over the Cross-Section of a Packed Column', Chem. Eng. Process., 18, 317

Davies J.T., (1972), 'Turbulence Phenomena', Academic Press, New York.

Drahos J., Cermak J., Ziolkowska I. & Ziolkowski D., (1982), 'Statistical Analysis of Local Gas Velocities at the Exit from a Packed Bed', Chem. Eng. J. (Lausanne), 24(1), 71

Dybbs A. & Edwards R.V., (1984), 'A New Look at Porous Media Fluid Mechanics: Darcy to Turbulent', in 'Fundementals of Transport Phenomena in Porous Media', Martinus Nijhoff Publishers, Editor, J. Bear, NATO ASI. Ser. E. Applied Sciences No. 82, 201-256

Ergun S. & Orning A.A., (1949), 'Fluid Flow through Randomnly Packed Columns and Fluidised Beds', Ind. Eng. Chem., 41(6),1179

Ergun S., (1952), 'Fluid Flow through Packed Columns', Chem. Eng. Prog., 48(2), 89

Ergun S., (1953), 'Pressure Drop in Blast Furnace and in Cupola', Ind. Eng. Chem., 45(2), 477

Fahien R.W. & Stankovic I.M., (1979), 'An Equation for the Velocity Profile in Packed Columns', Chem. Engng. Sci., 34(11), 1350

Fenech K., Cross M. & Voller V., (1985), 'A Computational Framework for Modelling the Raceway of the Iron Blast Furnace', Thames Polytechnic, London, (CHAM ref. no. 85/32).

Forcheimer F., (1901), Deit .Ing., 45, 1782

Foscolo P.U., Gibilaro L.G. & Waldram S.P., (1983), 'A Unified Model for Particulate Expansion of Fluidised Beds and Flow in Fixed Porous Media', Chem. Engng. Sci., 38(8), 1251

Foumeny E.A. & Benhaya F., (1991), 'Computer Modelling of Non-Uniformities In Packed Bed Configurations', Proc. I.Chem.E. Research Event, 307-309, I.Chem.E., Rugby

Fukutake T. & Okabe K., (1976), 'Theoretical and Experimental Studies of the Scale-Up Conditions for Gas Flow in Packed Beds', Trans. Iron Steel Inst. Japan, 16, 189

Furnas C.C., (1929), 'The Flow of Gases Through Beds of Broken Solids', Bulletin # 307, U.S. Bureau of Mines

Gauvin W.H. & Katta S., (1973), 'Momentum Transfer Through Packed Beds of Various Particles in the Turbulent Flow Regime', A.I.Ch.E.J., 19(4),775

Gibilaro L.G., Di Felice R., Waldram S.P. & Foscolo P.U., (1985), 'Generalized Friction Factor and Drag Coefficient Correlations for Fluid-Particle Interactions', Chem. Engng. Sci., 40(10), 1817

Glynn D.R., Edwards J.P. & Parry J.D., (1988), 'Numerical Prediction of Flow Over an Idealised Car Body', 3rd International PHOENICS User Conference, Dubrovonik.

Govindaro V.M. & Froment G.F., (1986), 'Voidage Profiles in Packed Beds of Spheres', Chem. Engng. Sci., 41(3), 533

Griffiths N.B., (1986), 'Velocity Profiles in Packed Beds', Ph.D. Thesis, Cambridge University

Gunn D.J. & Malik A.A.,(1966), Trans. I.Chem.E., 44, T371

Gupte A.R., (1970), Dissertation, Karlsruhe

Haber S. & Mauri R., (1983), 'Boundary Conditions for Darcy Flow through Porous Media', Int. J. Multiphase Flow, 9(5), 561

Happel J. & Epstein N., (1954), Ind. Eng. Chem., 46(6), 1187

Hassan A.O., (1985), 'The Effect of Inlet Pipe to Tower Diameter Ratio and Packing Size on Gas Distribution Devices", M.Sc. Thesis, Aston University

Hendrie J.M., (1965), Ann. Rep. Nucl. Dept. Brookhaven Nat. Lab., B.N.L. 954 (S-68)

Hinze J.O., (1975), 'Turbulence' 2nd edn., McGran Hill, New York.

Hirata Y. & Ito R., (1981), 'Velocity Distribution and Prediction of Friction Factor and Pressure Gradient in a Turbulent Porous Tube Flow with Injection or Suction', J. Chem. Eng. Jap., 14(4), 277

Hirata Y., Komatsu S. & Ito R., (1982), 'Experimental Study of Flow Development in a Porous Tube with Injection or Suction', J. Chem. Eng. Jap., 15(6), 445

Hirata Y. & Ito R., (1982), 'Extension of the Mixing Length Theory to a Porous Tube Flow with Injection or Suction', J. Chem. Eng. Jap., 15(6), 452

Hong J.T., Tien C.L. & Kaviany M., (1985), 'Non-Darcian Effects on Vertical Plate Natural Convection in Porous Media with High Porosities', Int. J. Heat Mass Transfer, 28 (11), 2149-2157

Huber M. & Hiltbrunner R., (1966), 'Fullkorperrektifizierkolonnen mit Maldistribution', Chem. Engng. Sci., 21, 819

Hunt M.L. & Tien C.L., (1988), 'Non-Darcian Convection In Cylindrical Packed Beds', A.S.M.E.J. Heat Transfer, 110, 378 - 384

Hunt M.L. & Tien C.L., (1990), 'Non-Darcian Flow, Heat and Mass Transfer in Catalytic Packed Bed Reactors', Chem. Eng. Sci., 45(1),55-63

Jolls K.R. & Hanratty T.J., (1966), 'Transition to Turbulence for Flow through a Dumped Bed of Spheres', Chem. Engng. Sci., 21,1185

Kagan A.M., Gel'Perin I.I., Pushnov A.S., Kovaleva E.A., Khludeev I.K. & Shvedov Y.P., 'Influence of Gas Distribution Inhomogeneity on Adsorption Unit Efficiency', (1986), Khim. Prom. (Moscow), 18(9), 39

Kalthoff O. & Vortmeyer D., (1980), 'Ignition/Extinction Phenomena in a Wall Cooled Fixed Bed Reactor; Experiments and Model Calculations including Radial Porosity and Velocity Distributions', Chem. Engng. Sci., 35, 1637

Karabelas A.J., Wegner T.H. & Hanratty T.J., (1973), 'Flow Patterns in a Close Packed Cubic Array of Spheres near the Critical Reynolds Number', Chem. Engng. Sci., 28(3), 673

Kimura M., Nono K. & Kaneda T., (1955), Chem. Eng. (Japan), 19, 397

Kitaev B.I., Yaroshenko Y.G., Shvydkii V.S., Gordon Y.M., Scherbatskii V.B., Shklyar F.R. & Bokovikov B.A., (1975), 'Investigation of the Aerodynamics in Packed Metallurgical Furnaces with Tuyere Wind Entry', B.F.A. Symposium (ed. N. Standish), Wollongong, 68

Klapetzky J., (1970), 'An Experimental Investigation of Velocity Profiles for Laminar and Turbulent Pulsatile Flow in a Rigid Tube', M.Sc. Thesis, State University of New York, Buffalo

Kler S.C. & Lavin J.T., (1987), 'Computer Simulation of Gas Distribution in Large Shallow Packed Adsorbers', Gas Separation and Purification, 1, 55

Krebs C., (1983), 'Effect of Diffusion and Maldistribution of Gas Flow on the Separation Effect of Packed Columns', Chem. Ing. Tech., 55(4), 303

Kubo K., Aratani T., Mishima A. & Yano T., (1978), 'Photographic Observation of the Flow Pattern in Voids of Packed Beds of Spheres', J. Chem. Eng. Jap., 11(5), 405

Kuwabara M. & Muchi I., (1975 a), 'Theoretical Analysis of Blast Furnace Operation Based on Gas Flow Through Layered Ore & Coke Burdens', B.F.A. Symposium (ed. N. Standish), Wollongong, 61

Kuwabara M. & Muchi I., (1975 b), 'Mathematical Model of Blast Furnace with Horizontally Layered Burdens', Tetsu. To. Hagane., 61,301

Kuwabara M. & Muchi I., (1975 c), 'A Mathematical Model for Blast Furnace Operation with Inclined Layers of Burdens', Tetsu. To. Hagane., 61,787

Kyan C.P., Wassan D.T. & Kintner R.C., (1970), Ind. Eng. Chem. Fund., 9(4), 596

Lerou J.J. & Froment G.F., (1977), 'Velocity,Temperature and Conversion Profiles in Fixed Bed Catalytic Reactors', Chem. Engng. Sci., 32(8), 853

Lessner P. & Newman J., (1984), 'Hydrodynamics and Mass Transfer in a Porous-Wall Tube', J.Electrochem. Soc., 31(8), 1828

Liebson I., Kelly R.E., & Bullington L.A., (1957), 'How to Design Perforated Trays', Pet 36 (Feb), Ref 127

Lyderson A., (1949), Ph.D. Thesis, Trondheim University, Norway

MacDonald I.F., El-Sayed M.S., Mow K. & Dullien F.A.L., (1979), 'Flow through Porous Media - The Ergun Equation Revisited', Ind. Eng. Chem. Fund., 18(3), 199

MacIlwain C., (16 March 1989), 'Keeping Ahead of the Flow', The Engineer, 208, 36-7

McGreavy C., Kam E.K.T., Foumeny E.A., Guidom A. & Ikponmwosa A.N., (1984), 'A Study of Flow Patterns in Packed Beds', Paper 12-12, Int. Symp. on Applications of Laser Anenometry in Fluid Mechanics, Lisbon

Marivoet J., Teodoriou P. & Wajc S.J., (1974), 'Porosity,Velocity and Temperature Profiles in Cylindrical Packed Beds', Chem. Engng. Sci., 29(8), 1836

Martin H., (1978), 'Low Peclet Number Particle-to-Fluid Heat and Mass Transfer in Packed Beds', Chem. Engng. Sci. 33, 913-919.

Martin J.J., Monroe C. & Monra D.J., (1951), Chem. Eng. Prog., 47(2), 91

Merrick D., (1983), 'Mathematical Models of the Thermal Decomposition of Coal: 3 Density, Porosity and Contraction behaviour', Fuel, 62 547-552

Mickley H.S., Smith K.A. & Korchak E.I., (1965), 'Fluid Flow in Packed Beds', Chem. Engng. Sci., 20, 237

Molerus O. & Schweinzer J., (1989), 'Resistance of Particle Beds at Reynolds Numbers up to $N_{Re} = 10^4$', Chem. Engng. Sci., 44(5), 1071

Moore F. & Rukovena F., (1987), 'Liquid and Gas Distribution in Commercial Packed Towers', p. 11-15, C.P.P. Edn., Europe

Morales M., Spinn C.W. & Smith J.M., (1951), 'Velocities and Effective Thermal Conductivities in Packed Beds', Ind. Eng. Chem., 43(1), 225

Morcom A.R., (1946), Trans. I.Chem.E., 24, 30

Muir L.A. & Briens C.L., (1986), 'Low Pressure Drop Gas Distributors for Packed Distillation Columns', Can. J. Chem. Eng., 64(6), 1027

Mullin J.W., (1957), 'The Effect of Maldistribution on the Performance of Packed Columns', Industrial Chemist, 33(8), 408

Oman A.O. & Watson K.M., (1944), Natl. Petroleum News, 36, R795

Osinski E.J., Barr P.V. & Brimacombe J.K., (1989), 'Mathematical Model for Gas Flows through a Packed Bed in the Presence of Sources and Sinks', Can. J. Chem. Eng., 67, 722-730

Parnas R. & Cohen Y., (1987), 'Coupled Parallel Flows of Power Law Fluids in a Channel and a Bounding Porous Medium', Chem. Eng. Commun., 53, 3

Patanker S.V., (1980), 'Numerical Heat Transfer & Fluid Flow', Hemisphere, New York

Perry R.H. & Chilton C.H., (1984), 'The Chemical Engineer's Handbook', 6th Edn., McGraw Hill, New York

Pillai K.K., (1977), 'Voidage Variation at the Wall of a Packed Bed of Spheres', Chem. Engng. Sci., 32(1), 59

Poveromo J.J., (1975), 'Raceway and Channeling Phenomena in the Iron Blast Furnace', Ph.D. Thesis, State University of New York, Buffalo. (Microfilm Ref. No. 75-18830).

Poveromo J.J., Szekely J. & Propster M., (1975), 'Flow Maldistribution in the Iron Blast Furnace', B.F.A. Symposium (ed. N. Standish), Wollongong, 1

Price J., (1967), 'Velocity Distribution and Pressure Losses for Randomnly Packed Beds of Spheres', Report No. E178, Australian Atomic Energy Commission

Price J., (1968), 'The Distribution of Fluid Velocities for Randomnly Packed Beds of Spheres', Mech. Chem. Eng. Trans. Inst. Engrs. (Aust.), May, 7

Puncochar M., Drahos J. & Cermak J., 'The Limits of Applicability of Pressure Drop Correlations', Chem. Engng. Sci., 45(9), 2294-2298

Radestock V.J. & Jeschar R., (1970), 'Flow through the Charge in a Blast Furnace', Stahl. U. Eisen., 90(22), 1249

Richardson S., (1971), ' A Model of the Boundary Condition of a Porous Material. Part 2', J. Fluid. Mech., 49(2), 327

Ridgway K. & Tarbuck K.J., (1966), 'Radial Voidage Variation in Randomly Packed Beds of Spheres of Different Size', J. Pharm-Pharmac, 18, 168-175.

Roblee L.H.S., Baird R.M. & Tierney J.W., (1958), 'Radial Porosity Variations in Packed Beds', A.I.Ch.E.J., 4(4), 460

Ross S.M., (1983), 'Theoretical Model of the Boundary Condition at a Fluid-Porous Interface', A.I.Ch.E.J., 29(5), 840

Rosten H.I. & Spalding D.B., (1987 a), 'The PHOENICS Beginners Guide', TR/100, Revision 4, C.H.A.M., Wimbledon

Rosten H.I. & Spalding D.B., (1987 b), 'The PHOENICS Reference Manual', TR/200, Revision 6, C.H.A.M., Wimbledon

Rumpf H. & Gupte A.R., (1971), Chem. Ing. Tech., 43, 367

Saffman P.G., (1971), 'On the Boundary Condition at the Surface of a Porous Medium', Stud. Appl. Math., L(2), 93

Schertz W.W. & Bischoff K.B., (1967), 'Thermal and Material Transport in Nonisothermal Packed Beds', A.I.Ch.E.J., 15(4), 597

Schneider F.A. & Rippin D.W., (1988), 'Determination of the Local Distribution in Randomn Packed Beds of Complex Geometry', Ind. Eng. Chem. Res., 27, 1936-1941

Schwartz C.Z. & Smith J.H., (1953), 'Flow Distribution in Packed Beds', Ind. Eng. Chem., 45(6),1209

Senecal V.E., (1957), 'Fluid Distribution in Process Equipment', Ind. Eng. Chem., 49(6), 993

Shaffer M.R., (1956), M.Sc. Thesis, Purdue University, Lafayette

Sharatt P.N., (1990), 'Computational Fluid Dynamics and its Application in the Process Industries', Ch.E.R.D., 68(A1), 13-18

Shvydkii V.S., Gordon Ya.M., Yaroshenko Yu.G. & Shcherbatskii V.B., (1974), 'Gas Distribution Given by a Non-Linear Resistance Pattern in Shaft Furnaces', Steel in the U.S.S.R., 4(8), 622

Smith K.L. & Roper G.H., (1960), Austral. J. Chem. Engrs., 1(1), 5

Sorour M.M., Hassab M.A. & Estafanous S., (1987), 'Developing Laminar Flow in a Semi-Porous Two Dimensional Channel with Non-uniform Transpiration', Int. J. Heat & Fluid Flow, 8(1), 44

Spalding D.B., (1980), 'Turbulence Models: A Lecture Course', Report No. HTS/80/2, C.F.D.U., Imperial College, London

Spalding D.B., (1981), 'A General Purpose Computer Program for Multi-Dimensional One- and Two-Phase Flow', Mathematics & Computers in Simulation, Vol. XXIII, p. 267-276, North Holland Press

Speiser V., Muller J. & Barthel P., (1987), 'Contribution on the Constructive Formation of the Feeding-in of Gas or Steam Respectively into the Column Base', Chem. Techn., 39(10),428

Stanek V. & Szekely J., (1972), 'The Effect of Non-Uniform Porosity in Causing Flow Maldistribution in Isothermal Packed Beds', Can. J. Chem. Eng., 50(2),9

Stanek V. & Szekely J., (1973), 'Flow Maldistribution in Two Dimensional Packed Beds. Part 2: The Behaviour of Non-Isothermal Systems', Can. J. Chem. Eng., 51(2),22

Stanek V. & Szekely J., (1974), 'Three-Dimensional Flow of Fluids Through Non-Uniform Packed Beds', A.I.Ch.E.J., 20(5),974

Stephenson J.L. & Stewart W.E., (1986), 'Optical Measurements of Porosity and Fluid Motion in Packed Beds', Chem. Engng. Sci., 41(8), 2161

Stichlmair J. & Stemmer A., (1987), 'Influence of Maldistribution on Mass Transfer in Packed Columns', Paper No. 56, p. B213, I.Chem.E. Symp. Ser. No. 104

Susskind H. & Becker W., (1967), A.I.Ch.E.J., 13(6), 1155

Szekely J. & Poveromo J.J., (1975), 'Flow Maldistribution in Packed Beds: A Comparison of Measurements with Predictions', A.I.Ch.E.J., 21(4), 769

Szekely J., Propster M. & Choudhary M., (1975), 'A Note on the Kitaev et al. Formulation of the Gas Flow with Tuyere Wind Entry', B.F.A. Symposium (ed. N. Standish), Wollongong, 165

Szekely J. & Propster M., (1977), 'Resistance of Layer-Charged Blast Furnace Burdens to Gas Flow', Ironmaking & Steelmaking, 1, 15

Tayler C., (March 1989), 'C.F.D.: What it is, what it will do and what it will cost', The Engineer, 70(3), 43-47

Taylor G.I., (1971), 'A Model for the Boundary Condition of a Porous Material: Part One', J. Fluid. Mech., 49(2), 319

Thadani M.C. & Peebles F.N., (1966), 'Variation of Local Void Fraction in Randomnly Packed Beds of Equal Spheres', Ind. Eng. Chem. Proc. Des. Dev., 5(3), 265

Thomas C., (1962), Report No. 3302, Oak Ridge Nat. Lab., Tennessee

Tikhonova N.M., (1970), 'Distribution of Localized Gas Velocities in Equipment with Shallow Contact Zones', Khim. Prom. (Moscow), 46(1), 73

Van Der Hegge Zijnen B.G., (1953), 'Flow through Uniformly Tapped Pipes', Appl. Sci. Res., A3, 144

Van Der Merwe D.F. & Gauvin W.H., (1971 a), 'Pressure Drag Measurements for Turbulent Air Flow through a Packed Bed', A.I.Ch.E.J., 17(2), 402

Van Der Merwe D.F. & Gauvin W.H., (1971 b), 'Velocity and Turbulence Measurements of Air through a Packed Bed', A.I.Ch.E.J., 17(3), 519

Volkov S.A., Reznikov V.I., Khalilov K.F., Zel'Vensky V.Y. & Sakodynsky K.I., (1986), 'Non-Uniformity of Packed Beds and its Influence on Longitudinal Dispersion', Chem. Engng. Sci., 41(2), 389

Voller V.R., (1980), 'Mathematical Analysis of some Aspects of the Coking Process', Ph.D. Thesis, C.N.A.A./Sunderland Polytechnic

Voller V.R., Cross M. & Merrick D., (1983), 'Mathematical Models of the Thermal Decomposition of Coal Part 5; Distribution of Gas Flow in a Coke Oven Charge', Fuel, 62, 562-566

Vortmeyer D. & Schuster J., (1983), 'Evaluation of Steady Flow Profiles in Rectangular and Circular Packed Beds by a Variational Method', Chem. Engng. Sci., 38(10), 1691

Vortmeyer D. & Michael K., (1985), 'The Effect of Non-Uniform Flow Distribution on Concentration Profiles and Breakthrough Curves of Fixed Bed Adsorbers', Chem. Engng. Sci., 40(11), 2135

Weissberg H.L., (1955), 'Velocity & Pressure Distribution in Turbulent Pipe Flow with Uniform Wall Suction', Report No. K1187, Carbide & Carbon Chemical Co., Oak Ridge, Tennessee

Wentz C.A. & Thodos G., (1963), A.I.Ch.E.J., 9(1), 81

White F.M., (1962), 'Laminar Flow in a Uniformly Porous Tube', Trans. A.S.M.E. (J. Appl. Mech.), E29, 201

Yuan S.W., (1956), 'Further Investigation of Laminar Flow in Channels with Porous Walls', J. Appl. Phys., 27(3), 267

Yuan S.W. & Finkelstein A.B., (1956), 'Laminar Pipe Flow with Injection and Suction through a Porous Wall', Trans A.S.M.E., 78(5), 719

Zaytoun A.A., (1981), 'Gas Maldistribution in Shallow Large Diameter Packed Beds', M.Sc. Thesis, University of Aston in Birmingham

Zuiderweg F.J. & Hoek P.J., (1987), 'The Effect of Small Scale Liquid Distribution ('Natural Flow') on the Separating Efficiency of Randomn Packings', Paper No. 58, p. B247, I.Chem.E. Symp. Ser. No. 104

Zuiderweg F.J., Hoek P.J. & Lahm L. Jr., (1987), 'The Effect of Liquid Distribution and Redistribution on the Separating Efficiency of Packed Columns', Paper No. 14, p. A217, I.Chem.E. Symp. Ser. No. 104

APPENDIX ONE. THE GROUND CODING FOR THE VECTORIAL ERGUN EQUATION.

The contents of this Appendix are discussed in section 4.4.

```
\\\\\\\\\\\\\\\\\\\\\\\\\\\\\\\\\\\\\\\\\\\\\\\\\\\\\\\\\\\\\\\\\\\\\\\\\\\\
STANDARD PHOENICS CODE OMITTED
/////////////////////////////////////////////////////////////////////////
C
C 5    The numbers in the next two statements (which must be ident-
C      ical) indicate how much computer memory is to be set aside
C      for storing the main and auxiliary variables. The user may
C      alter them if he wishes, to accord with the number of
C      grid nodes and dependent variables he is concerned with.
       COMMON F(1000000)
       NFDIM=1000000

\\\\\\\\\\\\\\\\\\\\\\\\\\\\\\\\\\\\\\\\\\\\\\\\\\\\\\\\\\\\\\\\\\\\\\\\\\\\
STANDARD PHOENICS CODE OMITTED
/////////////////////////////////////////////////////////////////////////

C      User may here change message transmitted to logical unit
C      LUPR3
       CALL WRIT40('GROUND IS W-ERG-3D-GR4.FOR 3.7.89')

\\\\\\\\\\\\\\\\\\\\\\\\\\\\\\\\\\\\\\\\\\\\\\\\\\\\\\\\\\\\\\\\\\\\\\\\\\\\
STANDARD PHOENICS CODE OMITTED
/////////////////////////////////////////////////////////////////////////

C 1    Set dimensions of data-for-GROUND arrays here. WARNING: the
C      corresponding arrays in the MAIN program of the satellite
C      and EARTH must have the same dimensions.
       COMMON/LGRND/LG(20)/IGRND/IG(20)/RGRND/RG(100)
      */CGRND/CG(10)
       LOGICAL LG
       CHARACTER*4 CG
C  ==========================================================
   INTEGER NYD,NXD
C  These variables represent the number of cells in the X & Y
C  directions & must therefore equal NX & NY set in the Q1 File.
C  If they are changed then the PRINT statement at line 440
C  must also be changed.
   PARAMETER (NYD=10,NXD=10)
C
C 2  User dimensions own arrays here, for example:
C    DIMENSION UUH(10,10),UUC(10,10),UUX(10,10),UUZ(10)
C    The following arrays are used in the packed bed calculations.
C    Their meanings are as follows:
C     1. GX,GY & GZ are the velocities in the X,Y & Z directions
C        (i.e. equivalent to U1,V1 & W1 respectively in PHOENICS
C        nomenclature). It should be noted that the velocity as
```

```
C       given for a particular cell is strictly the velocity
C       leaving the cell through the relevant 'High' cell face.
C       The array GZLOW holds the values for the previous (i.e.
C       LOW) Z slab.
C     2. The G-AV arrays give an average velocity (of the 'High'
C       face velocity for the current cell and it's Lower
C       counterpart) for the cell node.
C     3. The array GCO holds the values of the coefficients
C       for the velocity component currently under consideration
C       It is these coefficients that describe the packed bed
C       (as a momentum sink).

      DIMENSION GX(NYD,NXD),GY(NYD,NXD),GZ(NYD,NXD)
      DIMENSION GXAV(NYD,NXD),GYAV(NYD,NXD),GZAV(NYD,NXD)
      DIMENSION GCO(NYD,NXD),GZLOW(NYD,NXD)
C     The following variables are the ERGUN Equation 'constants'
C     as set below. The variable GEVF has a special significance
C     which is explained below.
      REAL GEC11,GEC12,GEC1,GEC2,GEVF
C     ==================================================

\\\\\\\\\\\\\\\\\\\\\\\\\\\\\\\\\\\\\\\\\\\\\\\\\\\\\\\\\\\\\\\\\\\\\\\\\\\\
STANDARD PHOENICS CODE OMITTED
/////////////////////////////////////////////////////////////////////////

C
C--- GROUP 13. Boundary conditions and special sources
C
  13 CONTINUE
     GO TO (130,131,132,133,134,135,136,137,138,139,1310,
     11311,1312,1313,1314,1315,1316,1317,1318,1319,1320,1321),ISC
  130 CONTINUE
C------------------ SECTION  1 ------------ coefficient = GRND
C     ==================================================
C
C     GROUND CODING TO REPRESENT A PACKED BED BY THE
C     ERGUN EQUATION
C
C     This is coded as a coefficient on the velocity equations.
C     The variable names etc. are explained above, where they are
C     declared.
C
C     RETURN if not correct Patch (npatch).
      IF(NPATCH.NE.'BEDONE')RETURN
C     By-pass remainder of user inserted code if not correct
C     variable.
C      IF(INDVAR.EQ.U1 .OR. INDVAR.EQ.V1 .OR. INDVAR.EQ.W1) THEN
C     Determination of various constants (only necessary once).
      IF (IZ.EQ.IG(5) .AND. ISWEEP.EQ.1 .AND. INDVAR.EQ.U1) THEN
C       The Ergun Equation constants.
        GEC11=150.0*((1.0-RG(2))**2)*ENUL
        GEC12=(RG(2)**3)*((RG(1)*RG(3))**2)
        GEC1=GEC11/GEC12
```

```
      GEC2=(1.75*RHO1*(1-RG(2)))/((RG(2)**3)*RG(1)*RG(3))
C      The factor GEVF is used to give an average ('node') value
C      of the velocity by multiplying the High or Low value
C      when there is only one such value( i.e. at domain bound-
C      aries).
      GEVF=0.5
C      These are just reminders to the user - if they're ignored
C      the program may crash or give incorrect solutions.
C      Adjust in conjunction with Q1 file & lines 428-432 and
C      line 159.
      PRINT*,'Use this GROUND only when NX=',NXD
      PRINT*,'Use this GROUND only when NY=',NYD
      PRINT*,'Use this GROUND with VOLUME patch-types only'
    ENDIF
C   The velocity values are then collected (using the
C   PHOENICS GETYX subroutine) and placed in the GX,GY,GZ &
C   GZLOW arrays.
    CALL GETYX(U1,GX,NY,NX)
    CALL GETYX(V1,GY,NY,NX)
    CALL GETYX(W1,GZ,NY,NX)
    CALL GETYX(LOW(W1),GZLOW,NY,NX)
C
C   Where the edge of the bed and the edge of the integration
C   domain coincide there is only one value of velocity
C   associated with each cell,which is multiplied by the
C   factor GEVF to give an average velocity.
C   It is first necessary to determine whether the two
C   edges coincide; this is accomplished using an IF....
C   structure.If they coincide the manipulation described
C   above is performed and the integer variable indicating
C   the edge of the bed is altered so the remaining averaging
C   does not affect these edge cells.The integer variables are
C   also re-named:
C
C   Old Name:   New Name:   Edge of Bed Description:
C   IG(1)       JIG1        LOW X
C   IG(2)       JIG2        HIGH X
C   IG(3)       JIG3        LOW Y
C   IG(4)       JIG4        HIGH Y
C
C   Where the edges do not coincide (the ELSEIF) then JIGn
C   is equated to IG(n).
C
C   For the LOW X boundary:
    IF (IG(1) .EQ. 1) THEN
      DO 1322 J=IG(3),IG(4)
1322   GXAV(J,1)=GSF*GX(J,1)
      JIG1=IG(1)+1
    ELSE
      JIG1=IG(1)
    ENDIF
C
C   For the HIGH X boundary:
```

```
      IF (IG(2) .EQ. NX) THEN
        DO 1323 J=IG(3),IG(4)
 1323   GXAV(J,NX)=GSF*GX(J,NX)
        JIG2=IG(2)-1
      ELSE
        JIG2=IG(2)
      ENDIF
C
C     For the LOW Y boundary:
      IF (IG(3) .EQ. 1) THEN
        DO 1324 I=IG(1),IG(2)
 1324   GYAV(1,I)=GSF*GY(1,I)
        JIG3=IG(3)+1
      ELSE
        JIG3=IG(3)
      ENDIF
C
C     For the HIGH Y boundary:
      IF (IG(4) .EQ. NY) THEN
        DO 1325 I =IG(1),IG(2)
 1325   GYAV(NY,I)=GSF*GY(NY-1,1)
        JIG4=IG(4)-1
      ELSE
        JIG4=IG(4)
      ENDIF
C
C     The averaging for the X & Y velocities over the
C     rest of the domain is then performed.
      DO 9000 J=JIG3,JIG4
      DO 9000 I=JIG1,JIG2
        GXAV(J,I)=0.5*(GX(J,I)+GX(J,I-1))
        GYAV(J,I)=0.5*(GY(J,I)+GY(J-1,I))
 9000 CONTINUE
C
C     The averaging for the Z velocities is now performed.
C     Except where the bed edges coincide with the domain boundary
C     in the Z direction this is the average of the GZ & GZLOW
C     values.Where the low boundaries coincide the GZ values are
C     used (for high ones the GZLOW values are used), when
C     multiplied by GEVF.
      DO 9001 J=IG(3),IG(4)
      DO 9001 I=IG(1),IG(2)
        IF (IZ.NE.1 .AND. IZ.NE.NZ) THEN
          GZAV(J,I)=0.5*(GZ(J,I)+GZLOW(J,I))
        ELSEIF (IZ.EQ.1) THEN
          GZAV(J,I)=GZ(J,I)
        ELSE
          GZAV(J,I)=GZLOW(J,I)
        ENDIF
 9001 CONTINUE
C
C     The average velocities are then used to give the Magnitude of the
C     Velocity Vector for the cell, which when combined with the Ergun
```

```
C    Constants gives the coefficients (placed in the array GCO).
     DO 9002 J=1,NY
     DO 9002 I=1,NX
 9002 GCO(J,I)=GEC1+GEC2*(SQRT(GXAV(J,I)**2+
    *GYAV(J,I)**2+GZAV(J,I)**2))
C
C    The coefficients are finally placed at the appropriate point
C    in the  F-Array (where they available to the solver), using
C    the PHOENICS SETYX subroutine.
     CALL SETYX(CO,GCO,NY,NX)
     ENDIF
C    ==========================================================
```

\\

STANDARD PHOENICS CODE OMITTED

//

APPENDIX TWO. THE Q1 FILE FOR THE BASIC TEST MODEL.

The contents of this Appendix are discussed in section 5.3.2.

```
TALK=T;RUN( 1, 1);VDU=TTY
  GROUP 1. Run title and other preliminaries

  ************************************************************************

  Data for PACKED BED PRESSURE DROP CALCULATIONS
  using the ERGUN EQUATION.

  ------------------------------------------------------------------------
  Placed in the arrays IG(n) & RG(n) so it is available to both
  the SATELLITE and GROUND routines.

  Integer values:
  The low x bed boundary:
IG(1)=1
  The high x bed boundary:
IG(2)=NX
  The low y bed boundary:
IG(3)=1
  The high y bed boundary:
IG(4)=NY
  Thelow z bed boundary:
IG(5)=1
  The high z bed boundary:
IG(6)=NZ
  Real values:
  The particle/packing piece diameter (in metres):
RG(1)=0.01
  The bed porosity:
RG(2)=0.41
  The shape factor:
RG(3)=1.0
TEXT(ERGUN TEST ROUTINE)
REAL(WID,HT,WIN)
WID=1.0
HT=1.0
WIN=1.0
  GROUP 2. Transience; time-step specification
STEADY=T
  GROUP 3. X-direction grid specification
CARTES=T
GRDPWR(X,10,WID,1.0)
  GROUP 4. Y-direction grid specification
GRDPWR(Y,10,WID,1.0)
  GROUP 5. Z-direction grid specification
GRDPWR(Z,10,HT,1.0)
  GROUP 6. Body-fitted coordinates or grid distortion
```

```
  GROUP 7. Variables stored, solved & named
SOLUTN (U1,Y,Y,N,Y,N,N)
SOLUTN (V1,Y,Y,N,Y,N,N)
SOLUTN (W1,Y,Y,N,Y,N,N)
SOLUTN (P1,Y,Y,Y,N,N,N)
  GROUP 8. Terms (in differential equations) & devices
  GROUP 9. Properties of the medium (or media)
ENUL=1.8E-5
ENUT=1.8E-3
RHO1=1.2
  GROUP 10. Inter-phase-transfer processes and properties
  GROUP 11. Initialization of variable or porosity fields
  GROUP 12. Convection and diffusion adjustments
  GROUP 13. Boundary conditions and special sources
  INLET TO CUBE
PATCH (INLET,LOW,1,NX,1,NY,1,1,1,1)
COVAL (INLET,P1,FIXFLU,WIN*RHO1)
COVAL (INLET,W1,ONLYMS,WIN)
   OUTLET FROM CUBE
PATCH (OUTLET,HIGH,1,10,1,10,NZ,NZ,1,1)
COVAL (OUTLET,P1,FIXP,0.0)
  BED FRICTION (call to section 1 of group 13 of GROUND)
PATCH (BEDONE,VOLUME,IG(1),IG(2),IG(3),IG(4),IG(5),IG(6),1,1)
COVAL (BEDONE,U1,GRND,0.0)
COVAL (BEDONE,V1,GRND,0.0)
COVAL (BEDONE,W1,GRND,0.0)
  GROUP 14. Downstream pressure for PARAB=.TRUE.
  GROUP 15. Termination of sweeps
LSWEEP=40
  GROUP 16. Termination of iterations
  GROUP 17. Under-relaxation devices
RELAX (P1,LINRLX,0.5)
RELAX (U1,FALSDT,0.01)
RELAX (V1,FALSDT,0.01)
RELAX (W1,FALSDT,0.01)
  GROUP 18. Limits on variables or increments to them
  GROUP 19. Data communicated by satellite to GROUND
USEGRD=T
USEGRX=F
  GROUP 20. Preliminary print-out
  GROUP 21. Print-out of variables
OUTPUT (U1,Y,N,N,Y,N,Y)
OUTPUT (V1,Y,N,N,Y,N,Y)
OUTPUT (W1,Y,N,N,Y,N,Y)
OUTPUT (P1,Y,N,N,Y,N,Y)
  GROUP 22. Spot-value print-out
TSTSWP=5
  GROUP 23. Field print-out and plot control
NPRINT=LSWEEP
  GROUP 24. Dumps for restarts
STOP
```

APPENDIX THREE. THE Q1 FILE FOR THE POVEROMO (small column) MODEL.

The contents of this Appendix are discussed in section 5.4.3.

```
TALK=F;RUN( 1, 1);VDU=TTY
  GROUP 1. Run title and other preliminaries

TEXT(Poveromo Small Column Model 8/12/89)

  DECLARATION OF VARIABLES:
  =========================

  These are defined later in the code
REAL(POUT,W1IN1,V1IN2,V1IN3,V1IN4)
INTEGER(NCXIN,NCXBIN,NCXAIN,NCXTIN)
REAL(PI,ANGIN)
INTEGER(YNC1,YNC2,YNC2T,YNC3,YNC3T,YNC4)
INTEGER(ZNC1,ZNC2,ZNC2T,ZNC3,ZNC3T,ZNC4,ZNC4T,ZNC5,ZNC5T)
INTEGER(ZNC6,ZNC6T,ZNC7,ZNC7T,ZNC8,ZNC8T,ZNC9,ZNC9T)
INTEGER(ZNC10,ZNC10T,ZNC11)
REAL(TCT)

  SPECIFICATION OF FLOWRATES etc.
  ===============================

  The pressure at the outlet (Pa):
POUT=0.0
  The inlet velocities (ms-1):
  i) Inlet 1
W1IN1=0.0
  ii) Inlet 2
V1IN2=14.2
  iii) Inlet 3
V1IN3=0.0
  iv) Inlet 4
V1IN4=0.0

  X (Circumferential) CELL QUANTITY SPECIFICATION:
  ================================================

  The dimensions of the domain are fixed.

  The total no. of cells in the X direction:
NX=10
  The no.of cells for the inlets 2,3 & 4:
NCXIN=2
  The no. of cells before the inlet cells (lower X side):
NCXBIN=(NX-NCXIN)/2
  The no. of cels to the high side of the inlet:
NCXTIN=NCXBIN+NCXIN
  The no. of cells after the inlet cells (higher X side):
```

```
NCXAIN=NCXBIN

PI=3.141593
  The angle subtended by the inlet (in radians)
ANGIN=0.1956

  Y (Radial) CELL QUANTITY SPECIFICATION:
  ======================================

  The dimensions of the domain are fixed.
  Where variable names have the final letter 'T' this
  indicates the total number of cells below the higher
  boundary of the sub-domain.

  The no. of cells for inlet 1:
YNC1=2
  The no. of cells between the high side of inlet 1 & the low
  side of the boundary voidage region:
YNC2=3;YNC2T=YNC2+YNC1
  The no.of cells in the boundary voidage section (upper/lower
  core/annulus):
  NOTE: YNC3 must be an even number.
YNC3=2;YNC3T=YNC2T+YNC3
  The no. of cells between the higher side of the boundary
  voidage section and the vessel wall:
YNC4=4;NY=YNC3T+YNC4

  Z (Vertical) CELL QUANTITY SPECIFICATION:
  ======================================

  The dimensions of the domain are fixed.
  (except for the thickness of the thin cells at bed/free fluid
  boundaries (parallel flow cases) and at the top and bottom of the
  column).
  Where variable names have the final letter 'T' this
  indicates the total number of cells below the higher
  boundary of the sub-domain.

  The no. of cells in the distributor (parallel flow cases):
  (includes 1 thin cell at bed boundary & 1 at the column base)
ZNC1=4
  The no. of cells in the open space between the distributor &
  the bed base (parallel flow cases):
  (includes 2 thin cells at bed boundaries)
ZNC2=4;ZNC2T=ZNC2+ZNC1
  The no.of cells between the bed base (parallel flow cases) and
  the bottom of inlet 2:
  (includes 1 thin cell at bed boundary)
ZNC3=2;ZNC3T=ZNC3+ZNC2T
  The no. of cells for inlet 2:
ZNC4=3;ZNC4T=ZNC4+ZNC3T
  The no. of cells between inlet 2 & the bottom of the boundary
  voidage section (upper/lower core/annulus cases)
```

```
ZNC5=3;ZNC5T=ZNC5+ZNC4T
  The no. of cells between the bottom of the boundary voidage
  section (upper/lower core/annulus cases) and the bottom of
  inlet 3:
ZNC6=2;ZNC6T=ZNC6+ZNC5T
  The no. of cells between the bottom of inlet 3 and the top
  of the boundary voidage section(upper/lower core/
  annulus cases):
ZNC7=1;ZNC7T=ZNC7+ZNC6T
  The no of cells between the top of the boundary voidage section
  (upper/lower core/annulus cases) and the top of inlet 3:
ZNC8=1;ZNC8T=ZNC8+ZNC7T
  The no. of cells between the top of inlet 3 and the bottom of
  inlet 4:
ZNC9=4;ZNC9T=ZNC9+ZNC8T
  The no. of cells for inlet 4:
ZNC10=3;ZNC10T=ZNC10+ZNC9T
  The no.of cells between the top of inlet 4 and the outlet:
  (includes one thin cell at the top of the column)
ZNC11=5;NZ=ZNC11+ZNC10T

  The thickness of the thin ( < 2 mm ) cells at bed/free fluid
  boundaries (in metres):
TCT=0.0005
  GROUP 2. Transience; time-step specification
  GROUP 3. X-direction grid specification
CARTES=F
XULAST=1.0
XFRAC(1)=-NCXBIN;XFRAC(2)=(PI-ANGIN/2.)/NCXBIN
XFRAC(3)=NCXIN;XFRAC(4)=ANGIN/NCXIN
XFRAC(5)=NCXAIN;XFRAC(6)=(PI-ANGIN/2.)/NCXAIN
  GROUP 4. Y-direction grid specification
YVLAST=1.0
YFRAC(1)=-YNC1;YFRAC(2)=0.00635/YNC1
YFRAC(3)=YNC2;YFRAC(4)=0.01397/YNC2
YFRAC(5)=YNC3;YFRAC(6)=0.01016/YNC3
YFRAC(7)=YNC4-1;YFRAC(8)=(0.02032-TCT)/(YNC4-1)
YFRAC(9)=1;YFRAC(10)=TCT
  GROUP 5. Z-direction grid specification
ZWLAST=1.0
ZFRAC(1)=-1;ZFRAC(2)=TCT
ZFRAC(3)=(ZNC1-2);ZFRAC(4)=(0.0381-(2*TCT))/(ZNC1-2)
ZFRAC(5)=2;ZFRAC(6)=TCT
ZFRAC(7)=ZNC2-2;ZFRAC(8)=(0.0635-(2.0*TCT))/(ZNC2-2)
ZFRAC(9)=2;ZFRAC(10)=TCT
ZFRAC(11)=ZNC3-1;ZFRAC(12)=(0.00635-TCT)/(ZNC3-1)
ZFRAC(13)=ZNC4;ZFRAC(14)=0.0127/ZNC4
ZFRAC(15)=ZNC5;ZFRAC(16)=0.07747/ZNC5
ZFRAC(17)=ZNC6;ZFRAC(18)=0.00508/ZNC6
ZFRAC(19)=ZNC7;ZFRAC(20)=0.00508/ZNC7
ZFRAC(21)=ZNC8;ZFRAC(22)=0.00762/ZNC8
ZFRAC(23)=ZNC9;ZFRAC(24)=0.08255/ZNC9
ZFRAC(25)=ZNC10;ZFRAC(26)=0.0127/ZNC10
```

```
ZFRAC(27)=ZNC11;ZFRAC(28)=(0.09525-TCT)/(ZNC11-1)
ZFRAC(29)=1;ZFRAC(30)=TCT
   GROUP 6. Body-fitted coordinates or grid distortion
   GROUP 7. Variables stored, solved & named
SOLUTN(U1,Y,Y,N,Y,N,N)
SOLUTN(V1,Y,Y,N,Y,N,N)
SOLUTN(W1,Y,Y,N,Y,N,N)
SOLUTN(P1,Y,Y,Y,N,N,N)
   GROUP 8. Terms (in differential equations) & devices
   GROUP 9. Properties of the medium (or media)
ENUL=1.8E-5
ENUT=1.8E-3
RHO1=1.2
   GROUP 10. Inter-phase-transfer processes and properties
   GROUP 11. Initialization of variable or porosity fields
   BED VOIDAGE:
   ---------------------
   Due to programming limitations of PHOENICS version 1.4
   voidage is not coded in the Q1 file (although it is coded in
   GROUND). This will not affect the converged solution
   obtained for steady-state models.
   GROUP 12. Convection and diffusion adjustments
   GROUP 13. Boundary conditions and special sources
XCYCLE=T

   INLET(S):
   ------------
   Comment out those not required:
   i) Inlet 1
   PATCH(INLET1,LOW,1,NX,1,YNC1,1,1,1,1)
   COVAL(INLET1,W1,ONLYMS,W1IN1)
   COVAL(INLET1,P1,FIXFLU,W1IN1*RHO1)
   ii) Inlet 2
   PATCH(INLET2,NORTH,NCXBIN+1,NCXTIN,NY,NY,
ZNC3T,ZNC4T,1,1)
   COVAL(INLET2,V1,ONLYMS,V1IN2)
   COVAL(INLET2,P1,FIXFLU,V1IN2*RHO1)
   iii) Inlet 3
   PATCH(INLET3,NORTH,NCXBIN+1,NCXTIN,NY,NY,
ZNC6T,ZNC8T,1,1)
   COVAL(INLET3,V1,ONLYMS,V1IN3)
   COVAL(INLET3,P1,FIXFLU,V1IN3*RHO1)
   iv) Inlet 4
   PATCH(INLET4,NORTH,NCXBIN+1,NCXTIN,NY,NY,
ZNC9T,ZNC10T,1,1)
   COVAL(INLET4,V1,ONLYMS,V1IN4)
   COVAL(INLET4,P1,FIXFLU,V1IN4*RHO1)

   OUTLET:
   ------------
PATCH(OUTLET,HIGH,1,NX,1,NY,NZ,NZ,1,1)
COVAL(OUTLET,P1,FIXP,POUT)
```

BED FRICTION:

Call to Section 1 of Group 13 of GROUND.

```
PATCH(BEDONE,VOLUME,1,NX,1,NY,1,NZ,1,1)
COVAL(BEDONE,U1,GRND,0.0)
COVAL(BEDONE,V1,GRND,0.0)
COVAL(BEDONE,W1,GRND,0.0)
```

GROUP 14. Downstream pressure for PARAB=.TRUE.

GROUP 15. Termination of sweeps

```
LSWEEP=100
```

GROUP 16. Termination of iterations

GROUP 17. Under-relaxation devices

```
RELAX(U1,FALSDT,0.01)
RELAX(V1,FALSDT,0.01)
RELAX(W1,FALSDT,0.01)
RELAX(P1,LINRLX,0.5)
```

GROUP 18. Limits on variables or increments to them

GROUP 19. Data communicated by satellite to GROUND

```
USEGRX=F
USEGRD=T
```

SPECIFICATION OF PACKING PATTERN:

The following logical variables define the packing pattern used. The required pattern is selected by setting the relevant variable as TRUE; all other variables in this section must be set as FALSE.

i) Parallel Flow Arrangement:

```
LG(1)=F
```

ii) Higher Resistance Core Arrangement:

```
LG(2)=F
```

iii) Lower Higher Resistance Core Arrangement:

```
LG(3)=F
```

iv) Upper Higher Resistance Core Arrangement:

```
LG(4)=F
```

v) Higher Resistance Annulus Arrangement:

```
LG(5)=T
```

vi) Lower Higher resistance Annulus Arrangement:

```
LG(6)=F
```

vii) Upper Higher Resistance Annulus Arrangement:

```
LG(7)=F
```

TRANSMISSION OF GRID INFORMATION TO GROUND:

The settings in this section should not be altered.

```
IG(1)=ZNC1
IG(2)=ZNC2T
IG(3)=ZNC5T
IG(4)=ZNC6T
IG(5)=ZNC7T
```

```
IG(6)=ZNC8T
IG(7)=YNC2T
IG(8)=YNC3T
IG(9)=YNC3

  SPECIFICATION OF SPHERICAL PACKINGS USED:
  ------------------------------------------------------------------
  (by particle size and voidage)
  The settings in this section should not be altered.

  A) Parallel Flow Arrangements:
  i) The voidage of the distributor:
RG(1)=0.407
  ii) The particle diameter for the distributor:
RG(2)=0.006
  iii) The voidage of the bed:
RG(3)=0.407
  iv) The particle diameter for the bed:
RG(4)=0.003
  v) The `wall` voidage of the bed:
RG(5)=0.48

  B) Other Arrangements:
  (i.e. upper/lower/whole higher resistance cores/annuli)

  vi) The voidage of the lower resistance region:
RG(6)=0.407
  vii) The voidage of the higher resistance region:
RG(7)=0.407
  viii) The particle diameter for the lower resistance region:
RG(8)=0.003
  ix) The particle diameter for the higher resistance region:
RG(9)=0.001
  x) The 'wall' voidage for the lower resistance region:
RG(10)=0.48
  xi) The 'wall' voidage for the higher resistance region:
RG(11)=0.45
  xii) The voidage of the higher/lower resistance region
  interface (the `boundary' voidage):
RG(12)=0.327

  GROUP 20. Preliminary print-out
  GROUP 21. Print-out of variables
OUTPUT(U1,Y,N,N,Y,N,Y)
OUTPUT(V1,Y,N,N,Y,N,Y)
OUTPUT(W1,Y,N,N,Y,N,Y)
OUTPUT(P1,Y,N,N,Y,N,Y)
  GROUP 22. Spot-value print-out
TSTSWP=10
  GROUP 23. Field print-out and plot control
NPRINT=LSWEEP
  GROUP 24. Dumps for restarts
STOP
```

APPENDIX FOUR. THE GROUND CODING FOR THE POVEROMO (small column) MODEL.

The contents of this Appendix are discussed in section 5.3.2.

```
\\\\\\\\\\\\\\\\\\\\\\\\\\\\\\\\\\\\\\\\\\\\\\\\\\\\\\\\\\\\\\\\\\\\\\\\\\\\\\\\\\\
STANDARD PHOENICS CODE OMITTED
////////////////////////////////////////////////////////////////////////////////
C
C 5     The numbers in the next two statements (which must be ident-
C       ical) indicate how much computer memory is to be set aside
C       for storing the main and auxiliary variables. The user may
C       alter them if he wishes, to accord with the number of
C       grid nodes and dependent variables he is concerned with.
        COMMON F(1000000)
        NFDIM=1000000

\\\\\\\\\\\\\\\\\\\\\\\\\\\\\\\\\\\\\\\\\\\\\\\\\\\\\\\\\\\\\\\\\\\\\\\\\\\\\\\\\\\
STANDARD PHOENICS CODE OMITTED
////////////////////////////////////////////////////////////////////////////////

C       User may here change message transmitted to logical unit
C       LUPR3
        CALL WRIT40('GROUND IS POV-SC-ERG-3D-GR5.FOR 1.12.89')

\\\\\\\\\\\\\\\\\\\\\\\\\\\\\\\\\\\\\\\\\\\\\\\\\\\\\\\\\\\\\\\\\\\\\\\\\\\\\\\\\\\
STANDARD PHOENICS CODE OMITTED
////////////////////////////////////////////////////////////////////////////////

C 1     Set dimensions of data-for-GROUND arrays here. WARNING: the
C       corresponding arrays in the MAIN program of the satellite
C       and EARTH must have the same dimensions.
        COMMON/LGRND/LG(20)/IGRND/IG(20)/RGRND/RG(100)
       */CGRND/CG(10)
        LOGICAL LG
        CHARACTER*4 CG
C
================================================================
        INTEGER JMID,KLO,KHI,MARK
        INTEGER NYD,NXD,NZD
C       These variables represent the number of cells in the X & Y
C       directions & must therefore equal NX & NY set in the Q1 File.
C       If they are changed then the PRINT statement at line 440
C       must also be changed.
        PARAMETER (NYD=10,NXD=10,NZD=30)
C
C 2     User dimensions own arrays here, for example:
C       DIMENSION UUH(10,10),UUC(10,10),UUX(10,10),UUZ(10)
C       The following arrays are used in the packed bed calculations.
C       Their meanings are as follows:
C       1. GX,GY & GZ are the velocities in the X,Y & Z directions
```

```
C       (i.e. equivalent to U1,V1 & W1 respectively in PHOENICS
C       nomenclature). It should be noted that the velocity as
C       given for a particular cell is strictly the velocity
C       leaving the cell through the relevant 'High' cell face.
C       The array GZLOW holds the values for the previous (i.e.
C       LOW) Z slab.
C       2. The G-AV arrays give an average velocity (of the 'High'
C       face velocity for the current cell and it's Lower
C       counterpart) for the cell node.
C       3. The array GCO holds the values of the coefficients
C       for the velocity component currently under consideration
C       It is these coefficients that describe the packed bed
C       (as a momentum sink).
C       4. The GEC1 & GEC2 arrays hold the values of the Ergun
C       constants; thus allowing the representation of, for
C       example: porosity variations near walls, the use of
C       different packings etc.
C       Other variables used in the determination of these
C       constants are:
C       GEC11,GEC12
        DIMENSION GX(NYD,NXD),GY(NYD,NXD),GZ(NYD,NXD)
        DIMENSION GXAV(NYD,NXD),GYAV(NYD,NXD),GZAV(NYD,NXD)
        DIMENSION GEC1(NYD,NXD,NZD),GEC2(NYD,NXD,NZD)
        DIMENSION GZLOW(NYD,NXD),GCO(NYD,NXD)
C
=============================================================
C
        ZNC1=IG(1)
        ZNC2T=IG(2)
        ZNC5T=IG(3)
        ZNC6T=IG(4)
        ZNC7T=IG(5)
        ZNC8T=IG(6)
        YNC2T=IG(7)
        YNC3T=IG(8)
        YNC3=IG(9)
C 3     User places his data statements here, for example:
C       DATA NXDIM,NYDIM/10,10/
C
C
C 4     Insert own coding below as desired, guided by GREX examples.

\\\\\\\\\\\\\\\\\\\\\\\\\\\\\\\\\\\\\\\\\\\\\\\\\\\\\\\\\\\\\\\\\\\\\\\\\\\\\\\\
STANDARD PHOENICS CODE OMITTED
/////////////////////////////////////////////////////////////

C*************************************************************
C
C--- GROUP 13. Boundary conditions and special sources
C
  13  CONTINUE
      GO TO (130,131,132,133,134,135,136,137,138,139,1310,
      1311,1312,1313,1314,1315,1316,1317,1318,1319,1320,1321),ISC
```

```
 130  CONTINUE
C------------------ SECTION  1 ------------ coefficient = GRND
C
==========================================================
C
C       GROUND CODING TO REPRESENT A PACKED BED BY THE
C       ERGUN EQUATION
C       For POVEROMO (1975) Small Column Experiments.
C
C       This is coded as a coefficient on the velocity equations.
C       The variable names etc. are explained above, where they are
C       declared.
C
C       RETURN if not correct Patch (npatch).
        IF(NPATCH.NE.'BEDONE')RETURN
C       By-pass remainder of user inserted code if not correct
C       variable.
        IF(INDVAR.EQ.U1 .OR. INDVAR.EQ.V1 .OR. INDVAR.EQ.W1) THEN
C       Determination of various constants :
        IF (IZ.EQ.1 .AND. ISWEEP.EQ.1 .AND. INDVAR.EQ.U1) THEN
C       Warning messages so user checks that GROUND & Q1
C       Files are compatible:
        PRINT*,'Use this GROUND only when NX=',NXD
        PRINT*,'Use this GROUND only when NY=',NYD
        PRINT*,'Use this GROUND only when NZ=',NZD
        PRINT*,'Use this GROUND with VOLUME PATCH types only'
C       Check to ensure the user has chosen a realistic
C       bed configuration:
                MARK=0
         DO 1360 I=1,7
                        IF (LG(I)) THEN
                                MARK=MARK+1
                        ENDIF
 1360  CONTINUE
                IF (MARK.GT.1) THEN
                        PRINT*,'WARNING:You have specified 2 (or more)'
                        PRINT*,'mutually exclusive packing arrangements'
                        PRINT*,'Check coding of LG(i) variables in Q1'
                        ENDIF
                IF (MARK.LT.1) THEN
                        PRINT*,'WARNING:You have not specified which'
                        PRINT*,'packing arrangement you require.'
                        PRINT*,'Check coding of LG(i) variables in Q1'
                ENDIF
C       The Ergun Equation constants.
C       a.) For the PARALLEL FLOW case:
        IF ( LG(1) ) THEN
C           For the distributor:
           DO 1331 I=1,NX
           DO 1332 J=1,NY
           DO 1333 K=1,ZNC1
             GEC11=150.0*((1.0-RG(1))**2)*ENUL
             GEC12=(RG(1)**3)*(RG(2)**2)
```

```
          GEC1(J,I,K)=GEC11/GEC12
          GEC2(J,I,K)=(1.75*RHO1*(1-RG(1)))/((RG(1)**3)*RG(2))
1333      CONTINUE
         DO 1334 K=ZNC1,ZNC2T
C           For the empty space between distributor & bed:
          GEC1(J,I,K)=0.0
          GEC2(J,I,K)=0.0
1334      CONTINUE
1332      CONTINUE
         DO 1335 K=ZNC2T,NZ
         DO 1336 J=1,NY-1
C           For the bed:
          GEC11=150.0*((1.0-RG(3))**2)*ENUL
          GEC12=(RG(3)**3)*(RG(4)**2)
          GEC1(J,I,K)=GEC11/GEC12
          GEC2(J,I,K)=(1.75*RHO1*(1-RG(3)))/((RG(3)**3)*RG(4))
1336      CONTINUE
C         The wall voidage:
          GEC11=150.0*((1.0-RG(5))**2)*ENUL
          GEC12=(RG(5)**3)*(RG(4)**2)
          GEC1(NY,I,K)=GEC11/GEC12
          GEC2(NY,I,K)=(1.75*RHO1*(1-RG(5)))/((RG(5)**3)*RG(4))
1335      CONTINUE
1331      CONTINUE
      ENDIF
C                 b.) For HIGHER RESISTANCE CORES:
      IF (LG(2).OR.LG(3).OR.LG(4)) THEN
C           Initially set up bed as lower resistance
C             packing throughout:
         DO 1337 K=1,NZ
         DO 1338 I=1,NX
         DO 1339 J=1,NY-1
          GEC11=150.0*((1.0-RG(6))**2)*ENUL
          GEC12=(RG(6)**3)*(RG(8)**2)
          GEC1(J,I,K)=GEC11/GEC12
          GEC2(J,I,K)=(1.75*RHO1*(1-RG(6)))/((RG(6)**3)*RG(8))
1339      CONTINUE
C           Wall voidage
          GEC11=150.0*((1.0-RG(10))**2)*ENUL
          GEC12=(RG(10)**3)*(RG(8)**2)
          GEC1(NY,I,K)=GEC11/GEC12
          GEC2(NY,I,K)=(1.75*RHO1*(1-RG(10)))/((RG(10)**3)*RG(8))
1338      CONTINUE
1337      CONTINUE
          IF (LG(2)) THEN
C           For WHOLE HEIGHT CORES:
              KLO=1
              KHI=NZ
          ELSEIF (LG(3)) THEN
C           For LOWER CORES
              KLO=1
              KHI=ZNC7T
          ELSE
```

```
C            For UPPER CORES
                   KLO=ZNC8T
                   KHI=NZ
           ENDIF
             JMID=YNC2T+YNC3/2
           DO 1340 I=1,NX
             DO 1341 K=KLO,KHI
             DO 1342 J=1,YNC2T
C             For HIGHER RESISTANCE CORES (except boundary
C             voidage areas):
             GEC11=150.0*((1.0-RG(7))**2)*ENUL
             GEC12=(RG(7)**3)*(RG(9)**2)
             GEC1(J,I,K)=GEC11/GEC12
             GEC2(J,I,K)=(1.75*RHO1*(1-RG(7)))/((RG(7)**3)*RG(9))
 1342      CONTINUE
             DO 1343 J=YNC2T+1,JMID
C                   'Lower' vertical boundary voidage area:
             GEC11=150.0*((1.0-RG(12))**2)*ENUL
             GEC12=(RG(12)**3)*(RG(9)**2)
             GEC1(J,I,K)=GEC11/GEC12
             GEC2(J,I,K)=(1.75*RHO1*(1-RG(12)))/((RG
   *(12)**3)*RG(9))
 1343      CONTINUE
           DO 1344 J=JMID+1,YNC3T
C                   'Higher' vertical boundary voidage area:
             GEC11=150.0*((1.0-RG(12))**2)*ENUL
             GEC12=(RG(12)**3)*(RG(8)**2)
             GEC1(J,I,K)=GEC11/GEC12
             GEC2(J,I,K)=(1.75*RHO1*(1-RG(12)))/((RG
   *(12)**3)*RG(8))
 1344      CONTINUE
 1341      CONTINUE
 1340      CONTINUE
           IF (LG(3).OR.LG(4)) THEN
C          HORIZONTAL BOUNDARY VOIDAGE AREA (upper/lower
C          cores only):
             DO 1345 I=1,NX
             DO 1346 J=1,YNC3T
             DO 1347 K=ZNC5T+1,ZNC6T
               IF (LG(3)) THEN
C                     LOWER CORE BOUNDARY VOIDAGE AREA
C                     (LOW SECTION):
                 GEC11=150.0*((1.0-RG(12))**2)*ENUL
                 GEC12=(RG(12)**3)*(RG(9)**2)
                 GEC1(J,I,K)=GEC11/GEC12
                     GEC2(J,I,K)=(1.75*RHO1*(1-RG(12)))/
   *((RG(12)**3)*RG(9))
                  ELSE
C                     UPPER CORE BOUNDARY VOIDAGE AREA
C                     (LOW SECTION):
                 GEC11=150.0*((1.0-RG(12))**2)*ENUL
                 GEC12=(RG(12)**3)*(RG(8)**2)
                 GEC1(J,I,K)=GEC11/GEC12
```

```
                GEC2(J,I,K)=(1.75*RHO1*(1-RG(12)))/((RG
  *(12)**3)*RG(8))
                ENDIF
1347        CONTINUE
            DO 1348 K=ZNC6T+1,ZNC7T
              IF (LG(3)) THEN
C                 LOWER CORE BOUNDARY VOIDAGE AREA
C               (UPPER SECTION):
                GEC11=150.0*((1.0-RG(12))**2)*ENUL
                GEC12=(RG(12)**3)*(RG(8)**2)
                GEC1(J,I,K)=GEC11/GEC12
                GEC2(J,I,K)=(1.75*RHO1*(1-RG(12)))/((RG
  *(12)**3)*RG(8))
              ELSE
C               UPPER CORE BOUNDARY VOIDAGE AREA
C               (UPPER SECTION):
                GEC11=150.0*((1.0-RG(12))**2)*ENUL
                GEC12=(RG(12)**3)*(RG(9)**2)
                GEC1(J,I,K)=GEC11/GEC12
                GEC2(J,I,K)=(1.75*RHO1*(1-RG(12)))/((RG
  *(12)**3)*RG(9))
                ENDIF
1348        CONTINUE
1346        CONTINUE
1345        CONTINUE
          ENDIF
        ENDIF



C       C.) For HIGHER RESISTANCE ANNULI:
        IF (LG(5).OR.LG(6).OR.LG(7)) THEN
C       Initially set up the bed as higher resistance
C       packing throughout.
          DO 1367 K=1,NZ
          DO 1368 I=1,NX
          DO 1369 J=1,NY-1
           GEC11=150.0*((1.0-RG(7))**2)*ENUL
           GEC12=(RG(7)**3)*(RG(9)**2)
           GEC1(J,I,K)=GEC11/GEC12
           GEC2(J,I,K)=(1.75*RHO1*(1-RG(7)))/((RG(7)**3)*RG(9))
1369      CONTINUE
C         Wall voidage
          GEC11=150.0*((1.0-RG(11))**2)*ENUL
          GEC12=(RG(11)**3)*(RG(9)**2)
          GEC1(NY,I,K)=GEC11/GEC12
          GEC2(NY,I,K)=(1.75*RHO1*(1-RG(11)))/((RG(11)**3)*RG(9))
1368      CONTINUE
1367      CONTINUE
          IF (LG(5)) THEN
C               For WHOLE HEIGHT ANNULI:
            KLO=1
            KHI=NZ
```

```
          ELSEIF (LG(6)) THEN
C           For LOWER ANNULI:
            KLO=1
            KHI=ZNC7T
          ELSE
C             For UPPER ANNULI:
            KLO=ZNC8T
            KHI=NZ
          ENDIF
         DO 1350 I=1,NX
         DO 1351 K=KLO,KHI
         DO 1352 J=1,YNC3T
C           LOW RESISTANCE CORE
C           (except bed boundary voidage area)
            GEC11=150.0*((1.0-RG(6))**2)*ENUL
            GEC12=(RG(6)**3)*(RG(8)**2)
            GEC1(J,I,K)=GEC11/GEC12
            GEC2(J,I,K)=(1.75*RHO1*(1-RG(6)))/((RG(6)**3)*RG(8))
 1352   CONTINUE
        DO 1353 J=YNC2T+1,JMID
C           'LOWER' VERTICAL BOUNDARY VOIDAGE AREA:
            GEC11=150.0*((1.0-RG(12))**2)*ENUL
            GEC12=(RG(12)**3)*(RG(8)**2)
            GEC1(J,I,K)=GEC11/GEC12
            GEC2(J,I,K)=(1.75*RHO1*(1-RG(12)))/((RG
     *(12)*3)*RG(8))
 1353   CONTINUE
C         'HIGHER' VERTICAL BOUNDARY VOIDAGE AREA:
         DO 1354 J=JMID+1,YNC3T
            GEC11=150.0*((1.0-RG(12))**2)*ENUL
            GEC12=(RG(12)**3)*(RG(9)**2)
            GEC1(J,I,K)=GEC11/GEC12
            GEC2(J,I,K)=(1.75*RHO1*(1-RG(12)))/
   *((RG(12)**3)*RG(9))
 1354   CONTINUE
 1351   CONTINUE
 1350   CONTINUE
        IF (LG(6).OR.LG(7)) THEN
C         HORIZONTAL BOUNDARY VOIDAGE AREA:
C         (upper/lower annuli only):
           DO 1355 I=1,NX
           DO 1356 J=1,YNC3T
           DO 1357 K=ZNC5T+1,ZNC6T
              IF (LG(6)) THEN
C              LOWER ANNULI BOUNDARY VOIDAGE AREA
C              ('lower' section):
               GEC11=150.0*((1.0-RG(12))**2)*ENUL
               GEC12=(RG(12)**3)*(RG(8)**2)
               GEC1(J,I,K)=GEC11/GEC12
               GEC2(J,I,K)=(1.75*RHO1*(1-RG(12)))/((RG
   *(12)**3)*RG(8))
              ELSE
C              UPPER ANNULI BOUNDARY VOIDAGE AREA:
```

```
C               ('lower' section):
                  GEC11=150.0*((1.0-RG(12))**2)*ENUL
                  GEC12=(RG(12)**3)*(RG(9)**2)
                  GEC1(J,I,K)=GEC11/GEC12
                  GEC2(J,I,K)=(1.75*RHO1*(1-RG(12)))/((RG
   *(12)**3)*RG(9))
                ENDIF
 1357         CONTINUE
              DO 1358 K=ZNC6T+1,ZNC7T
                IF (LG(6)) THEN
C                LOWER ANNULI BOUNDARY VOIDAGE AREA
C                ('upper' section):
                  GEC11=150.0*((1.0-RG(12))**2)*ENUL
                  GEC12=(RG(12)**3)*(RG(9)**2)
                  GEC1(J,I,K)=GEC11/GEC12
                  GEC2(J,I,K)=(1.75*RHO1*(1-RG(12)))/((RG
   *(12)**3)*RG(9))
                ELSE
C                UPPER ANNULI BOUNDARY VOIDAGE AREA
C                ('upper' section):
                  GEC11=150.0*((1.0-RG(12))**2)*ENUL
                  GEC12=(RG(12)**3)*(RG(8)**2)
                  GEC1(J,I,K)=GEC11/GEC12
                  GEC2(J,I,K)=(1.75*RHO1*(1-RG(12)))/((RG
   *(12)**3)*RG(8))
                ENDIF
 1358         CONTINUE
 1356         CONTINUE
 1355         CONTINUE
            ENDIF
          ENDIF

C         The factor GSF is used to give an average ('node') value
C         of the velocity by multiplying the High or Low value
C         when there is only one such value( i.e. at domain bound-
C         aries).
          GSF=0.5
        ENDIF
C
C       The velocity values are then collected (using the
C       PHOENICS GETYX subroutine) and placed in the GX,GY,GZ &
C       GZLOW arrays.
        CALL GETYX(U1,GX,NY,NX)
        CALL GETYX(V1,GY,NY,NX)
        CALL GETYX(W1,GZ,NY,NX)
        CALL GETYX(LOW(W1),GZLOW,NY,NX)
C
C       Where the edge of the bed and the edge of the integration
C       domain coincide there is only one value of velocity
C       associated with each cell,which is multiplied by the
C       factor GEVF to give an average velocity.
C       It is first necessary to determine whether the two
C       edges coincide; this is accomplished using an IF....
```

```
C       structure.If they coincide the manipulation described
C       above is performed and the integer variable indicating
C       the edge of the bed is altered so the remaining averaging
C       does not affect these edge cells.The integer variables are
C       also re-named:
C
C       Old Name:   New Name:   Edge of Bed Description:
C       IG(1)       JIG1        LOW X
C       IG(2)       JIG2        HIGH X
C       IG(3)       JIG3        LOW Y
C       IG(4)       JIG4        HIGH Y
C
C       Where the edges do not coincide (the ELSEIF) then JIGn
C       is equated to IG(n).
C
C       For the LOW X boundary:
        IF (IG(1) .EQ. 1) THEN
          DO 1322 J=IG(3),IG(4)
1322       GXAV(J,1)=GSF*GX(J,1)
          JIG1=IG(1)+1
        ELSE
          JIG1=IG(1)
        ENDIF
C
C       For the HIGH X boundary:
        IF (IG(2) .EQ. NX) THEN
          DO 1323 J=IG(3),IG(4)
1323       GXAV(J,NX)=GSF*GX(J,NX)
          JIG2=IG(2)-1
        ELSE
          JIG2=IG(2)
        ENDIF
C
C       For the LOW Y boundary:
        IF (IG(3) .EQ. 1) THEN
          DO 1324 I=IG(1),IG(2)
1324       GYAV(1,I)=GSF*GY(1,I)
          JIG3=IG(3)+1
        ELSE
          JIG3=IG(3)
        ENDIF
C
C       For the HIGH Y boundary:
        IF (IG(4) .EQ. NY) THEN
          DO 1325 I =IG(1),IG(2)
1325       GYAV(NY,I)=GSF*GY(NY-1,1)
          JIG4=IG(4)-1
        ELSE
          JIG4=IG(4)
        ENDIF
C
C       The averaging for the X & Y velocities over the
C       rest of the domain is then performed.
```

```
      DO 9000 J=JIG3,JIG4
      DO 9000 I=JIG1,JIG2
        GXAV(J,I)=0.5*(GX(J,I)+GX(J,I-1))
        GYAV(J,I)=0.5*(GY(J,I)+GY(J-1,I))
 9000  CONTINUE
C
C     The averaging for the Z velocities is now performed.
C     Except where the bed edges coincide with the domain boundary
C     in the Z direction this is the average of the GZ & GZLOW
C     values.Where the low boundaries coincide the GZ values are
C     used (for high ones the GZLOW values are used), when
C     multiplied by GEVF.
      DO 9001 J=IG(3),IG(4)
      DO 9001 I=IG(1),IG(2)
       IF (IZ.NE.1 .AND. IZ.NE.NZ) THEN
        GZAV(J,I)=0.5*(GZ(J,I)+GZLOW(J,I))
       ELSEIF (IZ.EQ.1) THEN
        GZAV(J,I)=GZ(J,I)
       ELSE
        GZAV(J,I)=GZLOW(J,I)
       ENDIF
 9001  CONTINUE
C
C     The average velocities are then used to give the Magnitude of the
C     Velocity for the cell, which when combined with the Ergun
C     Constants gives the coefficients (placed in the array GCO).
      DO 9002 J=1,NY
      DO 9002 I=1,NX
      GV=(SQRT(GXAV(J,I)**2+GYAV(J,I)**2+GZAV(J,I)**2))
 9002  GCO(J,I)=GEC1(J,I,IZ)+GEC2(J,I,IZ)*GV
C
C    The coefficients are finally placed at the appropriate point
C    in the  F-Array (where they available to the solver), using
C    the PHOENICS SETYX subroutine.
     CALL SETYX(CO,GCO,NY,NX)
     ENDIF
C
=============================================================
 131  CONTINUE

\\\\\\\\\\\\\\\\\\\\\\\\\\\\\\\\\\\\\\\\\\\\\\\\\\\\\\\\\\\\\\\\\\\\\\\\\\\\\\\\
STANDARD PHOENICS CODE OMITTED
/////////////////////////////////////////////////////////////////////////////
```

APPENDIX FIVE. THE Q1 FILE FOR THE TWO-DIMENSIONAL APPARATUS WITH THE DUCT END OPEN.

The contents of this Appendix are discussed in section 9.2

```
 TALK=F;RUN( 1, 1);VDU=TTY
GROUP 1. Run title and other preliminaries
TEXT(2D app., duct open)
  Definition of variables for Z direction grid.
REAL(LZ,LZ1,LZ2,LZ3,LNZ1,LNZ2,LNZ3)
INTEGER(NZ1,NZ2,NZ3)
  Length & No. of cells from distributor to beginning
  of bed:
LZ1=0.285;NZ1=16
  Length & No. of cells for bed (0.5,1.0 or 1.5m):
LZ2=1.5;NZ2=80
  Length & No. of cells from end of bed to duct outlet:
LZ3=2.010-LZ2;NZ3=20
LZ=LZ1+LZ2+LZ3
NZ=NZ1+NZ2+NZ3
  Definition of variables for Y direction grid:
REAL(LY,LY1,LY2,LY3,LNY1,LNY2,LNY3)
INTEGER(NY1,NY2,NY3)
  Height & No. of cells for duct (0.02-0.1m):
LY1=0.1;NY1=32
  Height & No. of cells for bed ( < 0.7m):
LY2=0.1;NY2=32
  Height & No. of cells from top of bed to bed outlet:
LY3=0.7-LY2;NY3=32
LY=LY1+LY2+LY3
NY=NY1+NY2+NY3
  Thin (boundary) cell definition:
REAL(TTC)
TTC=0.0005
  Inlet velocity:
REAL(WIN)
WIN=21.10
  Outlet Pressures:
REAL(POUTBE,POUTDU)
POUTBE=0.0
POUTDU=0.0
  Turbulence Quantities:
REAL(TKEIN,EPSIN)

  ********************************************************

  Data for PACKED BED PRESSURE DROP CALCULATIONS
  using the ERGUN EQUATION.
```

Placed in arrays IG(n) & RG(n) so it is available to both

```
    the SATELLITE and GROUND routines.

    Integer values:
    The low y bed boundary:
 IG(1)=NY1+1
    The high y bed boundary:
 IG(2)=NY1+NY2
    The low z bed boundary:
 IG(3)=NZ1+1
    The high z bed boundary:
 IG(4)=NZ1+NZ2
    Real values:
    The particle/packing piece diameter (in metres):
 RG(1)=0.012
    The bed porosity:
 RG(2)=0.407
    The shape factor:
 RG(3)=1.0
    GROUP 2. Transience; time-step specification
 STEADY=T
    GROUP 3. X-direction grid specification
 CARTES=T
 GRDPWR(X,1,0.1,1.0)
    GROUP 4. Y-direction grid specification
 YVLAST=1.0
 YFRAC(1)=-1;YFRAC(2)=TTC
 YFRAC(3)=NY1-2;YFRAC(4)=(LY1-2*TTC)/(NY1-2)
 YFRAC(5)=1;YFRAC(6)=TTC
 LNY2=LY2/NY2
 YFRAC(7)=1;YFRAC(8)=TTC
 YFRAC(9)=NY2-2;YFRAC(10)=(LY2-2*TTC)/(NY2-2)
 YFRAC(11)=1;YFRAC(12)=TTC
 LNY3=LY3/NY3
 YFRAC(13)=NY3;YFRAC(14)=LNY3
    GROUP 5. Z-direction grid specification
 ZWLAST=1.0
 LNZ1=LZ1/NZ1
 ZFRAC(1)=-NZ1;ZFRAC(2)=LNZ1
 ZFRAC(3)=1;ZFRAC(4)=TTC
 ZFRAC(5)=NZ2-2;ZFRAC(6)=(LZ2-2*TTC)/(NZ2-2)
 ZFRAC(7)=1;ZFRAC(8)=TTC
 LNZ3=LZ3/NZ3
 ZFRAC(9)=NZ3;ZFRAC(10)=LNZ3
    GROUP 6. Body-fitted coordinates or grid distortion
    GROUP 7. Variables stored, solved & named
 SOLUTN(V1,Y,Y,N,Y,N,N)
 SOLUTN(W1,Y,Y,N,Y,N,N)
 SOLUTN(P1,Y,Y,Y,N,N,N)
 SOLVE(KE,EP)
 STORE(ENUT)
    GROUP 8. Terms (in differential equations) & devices
    GROUP 9. Properties of the medium (or media)
 ENUL=1.8E-5
```

```
ENUT=GRND3
EL1=GRND4
RHO1=1.18
  GROUP 10. Inter-phase-transfer processes and properties
  GROUP 11. Initialization of variable or porosity fields

  Blocked regions voidage:
CONPOR (0.0,VOLUME,1,1,NY1+1,NY,1,NZ1)
CONPOR (0.0,VOLUME,1,1,NY1+1,NY,NZ1+NZ2+1,NZ)

  Turbulence Quantities:
TKEIN=0.018*0.25*(WIN**2.0)
EPSIN=(TKEIN**1.5)*0.1643/2.0
FIINIT(KE)=TKEIN/2.0
FIINIT(EP)=EPSIN/2.0

  GROUP 12. Convection and diffusion adjustments
  GROUP 13. Boundary conditions and special sources
  INLET
PATCH (INLET,LOW,1,1,1,NY1,1,1,1,1)
COVAL (INLET,P1,FIXFLU,WIN*RHO1)
COVAL (INLET,W1,ONLYMS,WIN)
COVAL (INLET,KE,ONLYMS,TKEIN)
COVAL (INLET,EP,ONLYMS,EPSIN)
  OUTLET ABOVE BED
PATCH (OUT1,NORTH,1,1,NY,NY,NZ1+1,NZ1+NZ2,1,1)
COVAL (OUT1,P1,FIXP,POUTBE)
  OUTLET AT PIPE END
PATCH (OUT2,HIGH,1,1,1,NY1,NZ,NZ,1,1)
COVAL (OUT2,P1,FIXP,POUTDU)
  BED FRICTION (call to section 1 of group 13 of GROUND)
PATCH (BEDONE,VOLUME,1,1,IG(1),IG(2),IG(3),IG(4),1,1)
COVAL (BEDONE,V1,GRND,0.0)
COVAL (BEDONE,W1,GRND,0.0)
  WALL FRICTION:
PATCH (WALL1,SWALL,1,1,1,1,1,NZ,1,1)
COVAL (WALL1,W1,GRND2,0.0)
COVAL (WALL1,KE,GRND2,GRND2)
COVAL (WALL1,EP,GRND2,GRND2)
PATCH (WALL2,NWALL,1,1,NY1,NY1,1,NZ1,1,1)
COVAL (WALL2,W1,GRND2,0.0)
COVAL (WALL2,KE,GRND2,GRND2)
COVAL (WALL2,EP,GRND2,GRND2)
PATCH (WALL3,NWALL,1,1,NY1,NY1,NZ1+NZ2+1,NZ,1,1)
COVAL (WALL3,W1,GRND2,0.0)
COVAL (WALL3,KE,GRND2,GRND2)
COVAL (WALL3,EP,GRND2,GRND2)
PATCH (WALL4,HWALL,1,1,NY1+1,NY,NZ1,NZ1,1,1)
COVAL (WALL4,V1,GRND2,0.0)
COVAL (WALL4,KE,GRND2,GRND2)
COVAL (WALL4,EP,GRND2,GRND2)
PATCH (WALL5,HWALL,1,1,NY1+1,NY,NZ1+NZ2,NZ1+NZ2,1,1)
COVAL (WALL5,V1,GRND2,0.0)
```

```
COVAL (WALL5,KE,GRND2,GRND2)
COVAL (WALL5,EP,GRND2,GRND2)
  TURBULENCE QUANTITIES.
PATCH (KESOA,PHASEM,1,1,1,NY1,1,NZ1,1,1)
COVAL (KESOA,KE,GRND4,GRND4)
COVAL (KESOA,EP,GRND4,GRND4)
PATCH (KESOB,PHASEM,1,1,1,NY1,NZ1+1,NZ1+NZ2,1,1)
COVAL (KESOB,KE,GRND4,GRND4)
COVAL (KESOB,EP,GRND4,GRND4)
PATCH (KESOC,PHASEM,1,1,1,NY1,NZ1+NZ2+1,NZ,1,1)
COVAL (KESOC,KE,GRND4,GRND4)
COVAL (KESOC,EP,GRND4,GRND4)
PATCH (KESO2,PHASEM,1,1,NY1+1,NY,NZ1+1,NZ1+NZ2,1,1)
COVAL (KESO2,KE,GRND4,GRND4)
COVAL (KESO2,EP,GRND4,GRND4)
  BED TURBULENCE
PATCH (KESOBED, PHASEM, 1,1,IG(1),IG(2),IG(3),IG(4), 1,1)
KESOBED = SKIP
PATCH (BETUVI,VOLUME,1,1IG(1),IG(2),IG(3),IG(4),1,1)
COVAL (BETUVI,VOLUME,1,1IG(1),IG(2),IG(3),IG(4),1,1)
  GROUP 14. Downstream pressure for PARAB=.TRUE.
  GROUP 15. Termination of sweeps
LSWEEP=200
  GROUP 16. Termination of iterations
  GROUP 17. Under-relaxation devices
RELAX (P1,LINRLX,0.5)
RELAX (V1,FALSDT,0.001)
RELAX (W1,FALSDT,0.001)
RELAX (KE,FALSDT,0.05)
RELAX (EP,FALSDT,0.05)
KELIN=1
  GROUP 18. Limits on variables or increments to them
  GROUP 19. Data communicated by satellite to GROUND
GENK=T
USEGRX=T
USEGRD=T
  GROUP 20. Preliminary print-out
  GROUP 21. Print-out of variables
OUTPUT (V1,Y,N,N,Y,N,Y)
OUTPUT (W1,Y,N,N,Y,N,Y)
OUTPUT (P1,Y,N,N,Y,N,Y)
OUTPUT (ENUT,Y,N,N,Y,N,Y)
OUTPUT(KE,N,N,N,Y,N,N)
OUTPUT(EP,N,N,N,Y,N,N)
  GROUP 22. Spot-value print-out
IXMON=1
IYMON=NY/2
IZMON=NZ/2
TSTSWP=10
  GROUP 23. Field print-out and plot control
NPRINT=LSWEEP
  GROUP 24. Dumps for restarts
STOP
```

APPENDIX SIX. THE Q1 FILE FOR THE TWO-DIMENSIONAL APPARATUS WITH THE DUCT END BLOCKED.

The contents of this Appendix are discussed in section 9.2.

```
TALK=F;RUN( 1, 1);VDU=TTY
  GROUP 1. Run title and other preliminaries
TEXT(2d app., duct blocked)
  Definition of variables for Z direction grid.
REAL(LZ,LZ1,LZ2,LNZ1,LNZ2)
INTEGER(NZ1,NZ2)
  Length & No. of cells from distributor to beginning
   of bed:
LZ1=0.285;NZ1=16
  Length & No. of cells for bed (0.5,1.0 or 1.5m):
LZ2=1.5;NZ2=80
LZ=LZ1+LZ2
NZ=NZ1+NZ2
  Definition of variables for Y direction grid:
REAL(LY,LY1,LY2,LY3,LNY1,LNY2,LNY3)
INTEGER(NY1,NY2,NY3)
  Height & No. of cells for duct (0.02-0.1m):
LY1=0.1;NY1=32
  Height & No. of cells for bed ( < 0.7m):
LY2=0.1;NY2=32
  Height & No. of cells from top of bed to bed outlet:
LY3=0.7-LY2;NY3=32
LY=LY1+LY2+LY3
NY=NY1+NY2+NY3
  Thin (boundary) cell definition:
REAL(TTC)
TTC=0.0005
  Inlet velocity:
REAL(WIN)
WIN=21.10
  Outlet Pressures:
REAL(POUTBE)
POUTBE=0.0
  Turbulence Quantities:
REAL(TKEIN,EPSIN)


  **********************************************************

  Data for PACKED BED PRESSURE DROP CALCULATIONS
  using the ERGUN EQUATION.

  ----------------------------------------------------------
  Placed in arrays IG(n) & RG(n) so it is available to both
  the SATELLITE and GROUND routines.
```

```
   Integer values:
   The low y bed boundary:
IG(1)=NY1+1
   The high y bed boundary:
IG(2)=NY1+NY2
   The low z bed boundary:
IG(3)=NZ1+1
   The high z bed boundary:
IG(4)=NZ1+NZ2
   Real values:
   The particle/packing piece diameter (in metres):
RG(1)=0.012
   The bed porosity:
RG(2)=0.407
   The shape factor:
RG(3)=1.0
   GROUP 2. Transience; time-step specification
STEADY=T
   GROUP 3. X-direction grid specification
CARTES=T
GRDPWR(X,1,0.1,1.0)
   GROUP 4. Y-direction grid specification
YVLAST=1.0
YFRAC(1)=-1;YFRAC(2)=TTC
YFRAC(3)=NY1-2;YFRAC(4)=(LY1-2*TTC)/(NY1-2)
YFRAC(5)=1;YFRAC(6)=TTC
LNY2=LY2/NY2
YFRAC(7)=1;YFRAC(8)=TTC
YFRAC(9)=NY2-2;YFRAC(10)=(LY2-2*TTC)/(NY2-2)
YFRAC(11)=1;YFRAC(12)=TTC
LNY3=LY3/NY3
YFRAC(13)=NY3;YFRAC(14)=LNY3
   GROUP 5. Z-direction grid specification
ZWLAST=1.0
LNZ1=LZ1/NZ1
ZFRAC(1)=-NZ1;ZFRAC(2)=LNZ1
ZFRAC(3)=1;ZFRAC(4)=TTC
ZFRAC(5)=NZ2-2;ZFRAC(6)=(LZ2-2*TTC)/(NZ2-2)
ZFRAC(7)=1;ZFRAC(8)=TTC
   GROUP 6. Body-fitted coordinates or grid distortion
   GROUP 7. Variables stored, solved & named
SOLUTN(V1,Y,Y,N,Y,N,N)
SOLUTN(W1,Y,Y,N,Y,N,N)
SOLUTN(P1,Y,Y,Y,N,N,N)
SOLVE(KE,EP)
STORE(ENUT)
   GROUP 8. Terms (in differential equations) & devices
   GROUP 9. Properties of the medium (or media)
ENUL=1.8E-5
ENUT=GRND3
EL1=GRND4
RHO1=1.18
   GROUP 10. Inter-phase-transfer processes and properties
```

```
  GROUP 11. Initialization of variable or porosity fields

  Blocked regions voidage:
CONPOR (0.0,VOLUME,1,1,NY1+1,NY,1,NZ1)

  Turbulence Quantities:
TKEIN=0.018*0.25*(WIN**2.0)
EPSIN=(TKEIN**1.5)*0.1643/2.0
FIINIT(KE)=TKEIN/2.0
FIINIT(EP)=EPSIN/2.0
PATCH(BED1,VOLUME,1,1,IG(1),IG(2),IG(3),IG(4),1,1)
INIT(BED1,KE,0.0,0.0)
INIT(BED1,ENUT,0.0,1.8E-5)
INIT(BED1,EP,0.0,0.0)

  GROUP 12. Convection and diffusion adjustments
  GROUP 13. Boundary conditions and special sources
  INLET
PATCH (INLET,LOW,1,1,1,NY1,1,1,1,1)
COVAL (INLET,P1,FIXFLU,WIN*RHO1)
COVAL (INLET,W1,ONLYMS,WIN)
COVAL (INLET,KE,ONLYMS,TKEIN)
COVAL (INLET,EP,ONLYMS,EPSIN)
   OUTLET ABOVE BED
PATCH (OUT1,NORTH,1,1,NY,NY,NZ1+1,NZ1+NZ2,1,1)
COVAL (OUT1,P1,FIXP,POUTBE)
  BED FRICTION (call to section 1 of group 13 of GROUND)
PATCH (BEDONE,VOLUME,1,1,IG(1),IG(2),IG(3),IG(4),1,1)
COVAL (BEDONE,V1,GRND,0.0)
COVAL (BEDONE,W1,GRND,0.0)
  WALL FRICTION:
PATCH (WALL1,SWALL,1,1,1,1,1,NZ,1,1)
COVAL (WALL1,W1,GRND2,0.0)
COVAL (WALL1,KE,GRND2,GRND2)
COVAL (WALL1,EP,GRND2,GRND2)
PATCH (WALL2,NWALL,1,1,NY1,NY1,1,NZ1,1,1)
COVAL (WALL2,W1,GRND2,0.0)
COVAL (WALL2,KE,GRND2,GRND2)
COVAL (WALL2,EP,GRND2,GRND2)
PATCH (WALL4,HWALL,1,1,NY1+NY2+1,NY,NZ1,NZ1,1,1)
COVAL (WALL4,V1,GRND2,0.0)
COVAL (WALL4,KE,GRND2,GRND2)
COVAL (WALL4,EP,GRND2,GRND2)
PATCH (WALL5,HWALL,1,1,1,NY,NZ,NZ,1,1)
COVAL (WALL5,V1,GRND2,0.0)
COVAL (WALL5,KE,GRND2,GRND2)
COVAL (WALL5,EP,GRND2,GRND2)
  TURBULENCE QUANTITIES.
PATCH (KESOA,PHASEM,1,1,1,NY1,1,NZ1,1,1)
COVAL (KESOA,KE,GRND4,GRND4)
COVAL (KESOA,EP,GRND4,GRND4)
PATCH (KESOB,PHASEM,1,1,1,NY1,NZ1+1,NZ,1,1)
COVAL (KESOB,KE,GRND4,GRND4)
```

```
COVAL (KESOB,EP,GRND4,GRND4)
PATCH (KESO2,PHASEM,1,1,NY1+NY2+1,NY,NZ1+1,NZ,1,1)
COVAL (KESO2,KE,GRND4,GRND4)
COVAL (KESO2,EP,GRND4,GRND4)
  BED TURBULENCE.
PATCH (KESOBED,PHASEM,1,1,IG(1),IG(2),IG(3),IG(4),1,1)
KESOBED=SKIP
PATCH(BETUVI,VOLUME,1,1,IG(1),IG(2),IG(3),IG(4),1,1)
COVAL(BETUVI,ENUT,FIXVAL,1.8E-5)

  GROUP 14. Downstream pressure for PARAB=.TRUE.
  GROUP 15. Termination of sweeps
LSWEEP=200
  GROUP 16. Termination of iterations
  GROUP 17. Under-relaxation devices
RELAX (P1,LINRLX,0.5)
RELAX (V1,FALSDT,0.005)
RELAX (W1,FALSDT,0.005)
RELAX (KE,FALSDT,0.01)
RELAX (EP,FALSDT,0.01)
KELIN=1
  GROUP 18. Limits on variables or increments to them
  GROUP 19. Data communicated by satellite to GROUND
GENK=T
USEGRD=T
USEGRX=T
  GROUP 20. Preliminary print-out
  GROUP 21. Print-out of variables
OUTPUT (V1,Y,N,N,Y,N,Y)
OUTPUT (W1,Y,N,N,Y,N,Y)
OUTPUT (P1,Y,N,N,Y,N,Y)
OUTPUT (ENUT,Y,N,N,Y,N,Y)
OUTPUT(KE,N,N,N,Y,N,N)
OUTPUT(EP,N,N,N,Y,N,N)
  GROUP 22. Spot-value print-out
IXMON=1
IYMON=NY/2
IZMON=NZ/2
TSTSWP=10
  GROUP 23. Field print-out and plot control
NPRINT=LSWEEP
  GROUP 24. Dumps for restarts
STOP
```

APPENDIX SEVEN. THE VECTORIAL ERGUN EQUATION GROUND CODING FOR THE TWO-DIMENSIONAL APPARATUS MODEL.

The contents of this Appendix are discussed in section 9.2.

```
\\\\\\\\\\\\\\\\\\\\\\\\\\\\\\\\\\\\\\\\\\\\\\\\\\\\\\\\\\\\\\\\\\\\\\\\\\\\
STANDARD PHOENICS CODE OMITTED
/////////////////////////////////////////////////////////////////////////
```

```
C 5  The numbers in the next two statements (which must be ident-
C    ical) indicate how much computer memory is to be set aside
C    for storing the main and auxiliary variables. The user may
C    alter them if he wishes, to accord with the number of
C    grid nodes and dependent variables he is concerned with.
     COMMON F(1000000)
     NFDIM=1000000
```

```
\\\\\\\\\\\\\\\\\\\\\\\\\\\\\\\\\\\\\\\\\\\\\\\\\\\\\\\\\\\\\\\\\\\\\\\\\\\\
STANDARD PHOENICS CODE OMITTED
/////////////////////////////////////////////////////////////////////////
```

```
C    User may here change message transmitted to logical unit
C    LUPR3
     CALL WRIT40('GROUND IS W-ERG-2D-GR3.FOR 6.6.89')
```

```
\\\\\\\\\\\\\\\\\\\\\\\\\\\\\\\\\\\\\\\\\\\\\\\\\\\\\\\\\\\\\\\\\\\\\\\\\\\\
STANDARD PHOENICS CODE OMITTED
/////////////////////////////////////////////////////////////////////////
```

```
     INTEGER NYD
C    The variable represents the number of cells in the Y
C    direction & must therefore equal NY set in the Q1 File.
     PARAMETER (NYD=24)
C
C 2  User dimensions own arrays here, for example:
C    DIMENSION UUH(10,10),UUC(10,10),UUX(10,10),UUZ(10)
C    The following arrays are used in the packed bed calculations.
C    Their meanings are as follows:
C     1. GY & GZ are the velocities in the Y & Z directions
C        (i.e. equivalent to V1 & W1 respectively in PHOENICS
C        nomenclature). It should be noted that the velocity as
C        given for a particular cell is strictly the velocity
C        leaving the cell through the relevant 'High' cell face.
C        The array GZLOW holds the values for the previous (i.e.
C        LOW ) Z slab.
C     2. The G-AV arrays give an average velocity (of the 'High'
C        face velocity for the current cell and it's Lower
C        counterpart) for the cell node.
C     3. The array GCO holds the values of the coefficients
C        for the velocity component currently under consideration
```

```
C       It is these coefficients that describe the packed bed
C       (as a momentum sink).

      DIMENSION GY(NYD,1),GZ(NYD,1),GZLOW(NYD,1)
      DIMENSION GYAV(NYD,1),GZAV(NYD,1)
      DIMENSION GCO(NYD,1)
C     The following variables are the ERGUN Equation 'constants'
C     as set below. The variable GEVF has a special significance
C     which is explained below.
      REAL GEC11,GEC12,GEC1,GEC2,GEVF

\\\\\\\\\\\\\\\\\\\\\\\\\\\\\\\\\\\\\\\\\\\\\\\\\\\\\\\\\\\\\\\\\\\\\\\\\\\\
STANDARD PHOENICS CODE OMITTED
/////////////////////////////////////////////////////////////////////////

C
C--- GROUP 13. Boundary conditions and special sources
C
  13 CONTINUE
     GO TO (130,131,132,133,134,135,136,137,138,139,1310,
     11311,1312,1313,1314,1315,1316,1317,1318,1319,1320,1321),ISC
  130 CONTINUE
C------------------ SECTION  1 ------------ coefficient = GRND
C
=============================================================
C
C     GROUND CODING TO REPRESENT A PACKED BED BY THE
C     ERGUN EQUATION
C
C     This is coded as a coefficient on the velocity equations.
C     The variable names etc. are explained above, where they are
C     declared.
C
C     RETURN if not correct Patch (npatch).
      IF(NPATCH.NE.'BEDONE')RETURN
C     By-pass remainder of user inserted code if not correct
C     variable.
      IF(INDVAR.EQ.V1 .OR. INDVAR.EQ.W1) THEN
C     Determination of various constants (only necessary once).
      IF (IZ.EQ.IG(3) .AND. ISWEEP.EQ.1 .AND. INDVAR.EQ.V1)  THEN
C       The Ergun Equation constants.
        GEC11=150.0*((1.0-RG(2))**2)*ENUL
        GEC12=(RG(2)**3)*((RG(1)*RG(3))**2)
        GEC1=GEC11/GEC12
        GEC2=(1.75*RHO1*(1-RG(2)))/((RG(2)**3)*RG(1)*RG(3))
C       The factor GEVF is used to give an average ('node') value
C       of the velocity by multiplying the High or Low value
C       when there is only one such value( i.e. at domain bound-
C       aries).
        GEVF=0.5
C       The following are just reminders to the user - if they're ignored
C       the program may crash or give incorrect solutions.
C       Adjust in conjunction with Q1 file & lines 428-432 and
```

```
C       line 159 (and lines 466-510).
        PRINT*,'Use this GROUND only for 2D Y-Z models'
        PRINT*,'Use this GROUND only when NY=',NYD
        PRINT*,'Use this GROUND with VOLUME patch-types only'
      ENDIF
C
C     The velocity values are then collected (using the
C     PHOENICS GETYX subroutine) and placed in the GY,GZ &
C     GZLOW arrays.
      CALL GETYX(V1,GY,NY,1)
      CALL GETYX(W1,GZ,NY,1)
      CALL GETYX(LOW(W1),GZLOW,NY,1)
C
C     Where the edge of the bed and the edge of the integration
C     domain coincide there is only one value of velocity
C     associated with each cell,which is multiplied by the
C     factor GEVF to give an average velocity.
C     It is first necessary to determine whether the two
C     edges coincide; this is accomplished using an IF....
C     structure.If they coincide the manipulation described
C     above is performed and the integer variable indicating
C     the edge of the bed is altered so the remaining averaging
C     does not affect these edge cells.The integer variables are
C     also re-named:
C
C     Old Name:    New Name:    Edge of Bed Description:
C     IG(1)        JIG1         LOW Y
C     IG(2)        JIG2         HIGH Y
C
C     Where the edges do not coincide (the ELSEIF) then JIGn
C     is equated to IG(n).
C
C
C     For the LOW Y boundary:
      IF (IG(1) .EQ. 1) THEN
        GYAV(1,1)=GSF*GY(1,1)
        JIG1=IG(1)+1
      ELSE
        JIG1=IG(1)
      ENDIF
C
C     For the HIGH Y boundary:
      IF (IG(2) .EQ. NY) THEN
        GYAV(NY,1)=GSF*GY(NY-1,1)
        JIG2=IG(2)-1
      ELSE
        JIG2=IG(2)
      ENDIF
C
C     The averaging for the Y velocities over the
C     rest of the domain is then performed.
      DO 9000 J=JIG1,JIG2
        GYAV(J,1)=0.5*(GY(J,1)+GY(J-1,1))
```

```
 9000 CONTINUE
C
C    The averaging for the Z velocities is now performed.
C    Except where the bed edges coincide with the domain boundary
C    in the Z direction this is the average of the GZ & GZLOW
C    values.Where the low boundaries coincide the GZ values are
C    used (for high ones the GZLOW values are used), when
C    multiplied by GEVF.
     DO 9001 J=IG(1),IG(2)
      IF (IZ.NE.1 .AND. IZ.NE.NZ) THEN
       GZAV(J,1)=0.5*(GZ(J,1)+GZLOW(J,1))
      ELSEIF (IZ.EQ.1) THEN
       GZAV(J,1)=GEVF*GZ(J,1)
      ELSE
       GZAV(J,1)=GEVF*GZLOW(J,1)
      ENDIF
 9001 CONTINUE
C
C    The average velocities are then used to give the Magnitude of the
C    Velocity for the cell, which when combined with the Ergun
C    Constants gives the coefficients (placed in the array GCO).
     DO 9002 J=1,NY
 9002 GCO(J,1)=GEC1+GEC2*(SQRT(GYAV(J,1)**2+GZAV(J,1)**2))
C
C    The coefficients are finally placed at the appropriate point
C    in the  F-Array (where they available to the solver), using
C    the PHOENICS SETYX subroutine.
     CALL SETYX(CO,GCO,NY,1)
     ENDIF

\\\\\\\\\\\\\\\\\\\\\\\\\\\\\\\\\\\\\\\\\\\\\\\\\\\\\\\\\\\\\\\\\\\\\\\\\\\
STANDARD PHOENICS CODE OMITTED
////////////////////////////////////////////////////////////////////////
```

APPENDIX EIGHT. THE VECTORIAL ERGUN EQUATION GROUND CODING FOR THE TWO-DIMENSIONAL APPARATUS MODEL, WITHOUT VELOCITY AVERAGING.

The contents of this Appendix are discussed in section 9.4.1.

```
\\\\\\\\\\\\\\\\\\\\\\\\\\\\\\\\\\\\\\\\\\\\\\\\\\\\\\\\\\\\\\\\\\\\\\\\\\\\
STANDARD PHOENICS CODE OMITTED
/////////////////////////////////////////////////////////////////////////
```

```
C 5  The numbers in the next two statements (which must be ident-
C    ical) indicate how much computer memory is to be set aside
C    for storing the main and auxiliary variables. The user may
C    alter them if he wishes, to accord with the number of
C    grid nodes and dependent variables he is concerned with.
     COMMON F(1000000)
     NFDIM=1000000
```

```
\\\\\\\\\\\\\\\\\\\\\\\\\\\\\\\\\\\\\\\\\\\\\\\\\\\\\\\\\\\\\\\\\\\\\\\\\\\\
STANDARD PHOENICS CODE OMITTED
/////////////////////////////////////////////////////////////////////////
```

```
C    User may here change message transmitted to logical unit
C    LUPR3
     CALL WRIT40('GROUND IS W-ERG-2D-GR4na.FOR 6.6.89')
```

```
\\\\\\\\\\\\\\\\\\\\\\\\\\\\\\\\\\\\\\\\\\\\\\\\\\\\\\\\\\\\\\\\\\\\\\\\\\\\
STANDARD PHOENICS CODE OMITTED
/////////////////////////////////////////////////////////////////////////
```

```
     INTEGER NYD
C    The variable represents the number of cells in the Y
C    direction & must therefore equal NY set in the Q1 File.
     PARAMETER (NYD=24)
C
C 2  User dimensions own arrays here, for example:
C    DIMENSION UUH(10,10),UUC(10,10),UUX(10,10),UUZ(10)
C    The following arrays are used in the packed bed calculations.
C    Their meanings are as follows:
C     1. GY & GZ are the velocities in the Y & Z directions
C        (i.e. equivalent to V1 & W1 respectively in PHOENICS
C        nomenclature). It should be noted that the velocity as
C        given for a particular cell is strictly the velocity
C        leaving the cell through the relevant 'High' cell face.
C     2. The array GCO holds the values of the coefficients
C        for the velocity component currently under consideration
C        It is these coefficients that describe the packed bed
C        (as a momentum sink).

     DIMENSION GY(NYD,1),GZ(NYD,1),
```

```
      DIMENSION GCO(NYD,1)
C     The following variables are the ERGUN Equation 'constants'
C     as set below.
      REAL GEC11,GEC12,GEC1,GEC2

\\\\\\\\\\\\\\\\\\\\\\\\\\\\\\\\\\\\\\\\\\\\\\\\\\\\\\\\\\\\\\\\\\\\\\\\\\\
STANDARD PHOENICS CODE OMITTED
////////////////////////////////////////////////////////////////////////

C
C--- GROUP 13. Boundary conditions and special sources
C
  13 CONTINUE
     GO TO (130,131,132,133,134,135,136,137,138,139,1310,
    11311,1312,1313,1314,1315,1316,1317,1318,1319,1320,1321),ISC
 130 CONTINUE
C----------------- SECTION  1 ------------ coefficient = GRND
C
==========================================================
C
C     GROUND CODING TO REPRESENT A PACKED BED BY THE
C     ERGUN EQUATION
C
C     This is coded as a coefficient on the velocity equations.
C     The variable names etc. are explained above, where they are
C     declared.
C
C     RETURN if not correct Patch (npatch).
      IF(NPATCH.NE.'BEDONE')RETURN
C     By-pass remainder of user inserted code if not correct
C     variable.
      IF(INDVAR.EQ.V1 .OR. INDVAR.EQ.W1) THEN
C     Determination of various constants (only necessary once).
      IF (IZ.EQ.IG(3) .AND. ISWEEP.EQ.1 .AND. INDVAR.EQ.V1)  THEN
C       The Ergun Equation constants.
        GEC11=150.0*((1.0-RG(2))**2)*ENUL
        GEC12=(RG(2)**3)*((RG(1)*RG(3))**2)
        GEC1=GEC11/GEC12
        GEC2=(1.75*RHO1*(1-RG(2)))/((RG(2)**3)*RG(1)*RG(3))
C       The following are just reminders to the user - if they're ignored
C       the program may crash or give incorrect solutions.
C       Adjust in conjunction with Q1 file & lines 428-432 and
C       line 159 (and lines 466-510).
        PRINT*,'Use this GROUND only for 2D Y-Z models'
        PRINT*,'Use this GROUND only when NY=',NYD
        PRINT*,'Use this GROUND with VOLUME patch-types only'
      ENDIF
C
C     The velocity values are then collected (using the
C     PHOENICS GETYX subroutine) and placed in the GY&GZ
C     arrays.
      CALL GETYX(V1,GY,NY,1)
      CALL GETYX(W1,GZ,NY,1)
```

```
C
C    The velocities are then used to give the Magnitude of the
C    Velocity for the cell, which when combined with the Ergun
C    Constants gives the coefficients (placed in the array GCO).
     DO 9002 J=1,NY
 9002 GCO(J,1)=GEC1+GEC2*(SQRT(GY(J,1)**2+GZ(J,1)**2))
C
C    The coefficients are finally placed at the appropriate point
C    in the  F-Array (where they available to the solver), using
C    the PHOENICS SETYX subroutine.
     CALL SETYX(CO,GCO,NY,1)
      ENDIF

\\\\\\\\\\\\\\\\\\\\\\\\\\\\\\\\\\\\\\\\\\\\\\\\\\\\\\\\\\\\\\\\\\\\\\\\\\\\
STANDARD PHOENICS CODE OMITTED
/////////////////////////////////////////////////////////////////////////
```

APPENDIX NINE. THE VECTORIAL ERGUN EQUATION GROUND CODING FOR THE TWO-DIMENSIONAL APPARATUS MODEL, WITHOUT VELOCITY AVERAGING AND INCLUDING VOIDAGE VARIATIONS IN THE BED.

The contents of this Appendix are discussed in section 9.5.1.

```
\\\\\\\\\\\\\\\\\\\\\\\\\\\\\\\\\\\\\\\\\\\\\\\\\\\\\\\\\\\\\\\\\\\\\\\\\\\\
STANDARD PHOENICS CODE OMITTED
/////////////////////////////////////////////////////////////////////////
```

```
C 5  The numbers in the next two statements (which must be ident-
C    ical) indicate how much computer memory is to be set aside
C    for storing the main and auxiliary variables. The user may
C    alter them if he wishes, to accord with the number of
C    grid nodes and dependent variables he is concerned with.
     COMMON F(1000000)
     NFDIM=1000000
```

```
\\\\\\\\\\\\\\\\\\\\\\\\\\\\\\\\\\\\\\\\\\\\\\\\\\\\\\\\\\\\\\\\\\\\\\\\\\\\
STANDARD PHOENICS CODE OMITTED
/////////////////////////////////////////////////////////////////////////
```

```
C    User may here change message transmitted to logical unit
C    LUPR3
     CALL WRIT40('GROUND IS W-ERG-2D-GR5naev(2D).FOR 6.6.89')
================================================================
     INTEGER NYD
C    The variable represents the number of cells in the Y
C    direction & must therefore equal NY set in the Q1 File.
     PARAMETER (NYD=96)
C
C 2  User dimensions own arrays here, for example:
C    DIMENSION UUH(10,10),UUC(10,10),UUX(10,10),UUZ(10)
C    The following arrays are used in the packed bed calculations.
C    Their meanings are as follows:
C     1. GY & GZ are the velocities in the Y & Z directions
C        (i.e. equivalent to V1 & W1 respectively in PHOENICS
C        nomenclature). It should be noted that the velocity as
C        given for a particular cell is strictly the velocity
C        leaving the cell through the relevant 'High' cell face.
C
C     2. The array GCO holds the values of the coefficients
C        for the velocity component currently under consideration
C        It is these coefficients that describe the packed bed
C        (as a momentum sink).

     DIMENSION GY(NYD,1),GZ(NYD,1)
     DIMENSION GCO(NYD,1)
```

```
C    The following array variables contain the ERGUN Equation 'constants'
C    as set below.
     REAL GEC11,GEC12
     DIMENSION GEC1(33:64),GEC2(33:64),GVOID(33:64)
     DATA GVOID/0.91,0.55,0.23,0.36,0.50,0.32,0.37,0.44,0.33,0.39,0.40
    *,0.33,0.41,0.40,0.37,0.39,0.39,0.37,0.40,0.41,0.33,0.40,0.39,0.33
    *,0.44,0.37,0.32,0.50,0.36,0.23,0.55,0.91/

\\\\\\\\\\\\\\\\\\\\\\\\\\\\\\\\\\\\\\\\\\\\\\\\\\\\\\\\\\\\\\\\\\\\\\\\\\\
STANDARD PHOENICS CODE OMITTED
////////////////////////////////////////////////////////////////////////


C
C--- GROUP 13. Boundary conditions and special sources
C
  13 CONTINUE
     GO TO (130,131,132,133,134,135,136,137,138,139,1310,
    11311,1312,1313,1314,1315,1316,1317,1318,1319,1320,1321),ISC
 130 CONTINUE
C------------------ SECTION  1 ------------ coefficient = GRND
C
==========================================================
C
C    GROUND CODING TO REPRESENT A PACKED BED BY THE
C    ERGUN EQUATION
C
C    This is coded as a coefficient on the velocity equations.
C    The variable names etc. are explained above, where they are
C    declared.
C
C    RETURN if not correct Patch (npatch).
     IF(NPATCH.NE.'BEDONE')RETURN
C    By-pass remainder of user inserted code if not correct
C    variable.
     IF(INDVAR.EQ.V1 .OR. INDVAR.EQ.W1) THEN
C    Determination of various constants (only necessary once).
     IF (IZ.EQ.IG(3) .AND. ISWEEP.EQ.1 .AND. INDVAR.EQ.V1)  THEN
C       The Ergun Equation constants.
        DO 8999 J=33,64
        GEC11=150.0*((1.0-GVOID(J))**2)*ENUL
        GEC12=(GVOID(J)**3)*((RG(1)*RG(3))**2)
        GEC1(J)=GEC11/GEC12
        GEC2(J)=(1.75*RHO1*(1-GVOID(J)))/((GVOID(J)**3)*RG(1)*RG(3))
        PRINT*,J,GVOID(J),GEC1(J),GEC2(J)
 8999    CONTINUE
C       The following are just reminders to the user - if they are ignored
C       the program may crash or give incorrect solutions.
C       Adjust in conjunction with Q1 file & lines 428-432 and
C       line 159 (and lines 466-510).
        PRINT*,'Use this GROUND only for 2D Y-Z models'
        PRINT*,'Use this GROUND only when NY=',NYD
        PRINT*,'use this GROUND only when NY1=NY2=32'
```

```
        PRINT*,'This GROUND includes voldage variation for spheres'
        PRINT*,'Use this GROUND with VOLUME patch-types only'
      ENDIF
C
C     The velocity values are then collected (using the
C     PHOENICS GETYX subroutine) and placed in the GY&GZ
C     arrays.
      CALL GETYX(V1,GY,NY,1)
      CALL GETYX(W1,GZ,NY,1)

C     The velocities are then used to give the Magnitude of the
C     Velocity for the cell, which when combined with the Ergun
C     Constants gives the coefficients (placed in the array GCO).
      DO 9002 J=1,NY
 9002 GCO(J,1)=GEC1(J)+GEC2(J)*(SQRT(GY(J,1)**2+GZ(J,1)**2))
C
C     The coefficients are finally placed at the appropriate point
C     in the  F-Array (where they available to the solver), using
C     the PHOENICS SETYX subroutine.
      CALL SETYX(CO,GCO,NY,1)
       ENDIF
C
```

==========

\\\

STANDARD PHOENICS CODE OMITTED

//

APPENDIX 10. ADDITIONS TO THE Q1 FILES TO INCLUDE THE NOVEL PRESCRIPTION OF THE BASE OF BED BOUNDARY CONDITION.

The contents of this Appendix are discussed in section 9.5.1.

This appendix presents changes to the Duct End Open Q1 file presented as Appendix 5 and to the Duct End Blocked Q1 file presented as Appendix 6 to include this base of bed boundary condition.

>>>>>>>>> Add to Group 13

```
  Wall Friction at Bed Base
PATCH (WALL6,NWALL,1,1,NY1,NY1,NZ1+1,NZ1+NZ2,1,1)
COVAL (WALL6,KE,GRND2,GRND2)
COVAL (WALL6,EP,GRND2,GRND2)
```

APPENDIX 11. THEORY AND ADDITIONS TO THE Q1 & GROUND FILES TO INCLUDE THE PERFORATED PLATE AT THE DUCT OUTLET.

The contents of this Appendix are discussed in section 9.2.5.

This appendix presents changes to the Duct End Open Q1 file presented as Appendix 5 and GROUND file presented as Appendix 8, to include the perforated plate at the duct outlet.

A11.1. THEORY.

It will be recalled that a perforated plate was used to partially block the duct outlet. Liebson et al. (1957) present a correlation for the pressure drop across perforated plates, as follows:

$$(-\Delta P) = c\,(v_h / c_o)^2 \rho_G \qquad \text{Equation A11.1.}$$

where; C = a constant = 0.5003

ρ_G = gas density

v_h = the hole velocity

C_o = the orifice coefficient.

The orifice coefficient is a function of plate thickness, hole diameter and percent free area and for this plate equals 0.89 (Liebson et al. (1957)). Substituing this and the density of air into equation A 11.1 and re-arranging gives:

$$(-\Delta P) = 0.757\,(v_h)^2 \qquad \text{Equation A11.2}$$

Adjusting the hole velocity to the superficial velocity (V_s) gives:

$$(-\Delta P) = 2.857\,(v_s)^2 \qquad \text{Equation A11.3}$$

This equation can now be converted to a coefficient and applied in the same way as the vectorial Ergun Equation. To be applied as a coefficient the pressure drop must be in the form of a pressure drop per distance. Taking this as th thickness of the plate (0.006 m) (and therefore recognising that a VOLUME patch type is required whose width (in the flow direction) will equal the plate thickness) and furthermore recognising that the appropriate velocity is the z-direction one (W1 in PHOENICS) gives:

$$C_{W1} = \frac{(-\Delta P)}{L\ W1} = \frac{2.857\ W1^2}{0.006\ W1} = 476.16\ W1 \qquad \text{Equation A11.4.}$$

The Q1 and GROUND coding to implement this coefficient is presented below; and is the same, in principle, as that for the vectorial Ergun Equation described in Chapter 4.

This coding was tested by writing a simple Q1 file of flow in a two-dimensional duct with the perforated plate positioned in the centre. The agreement between the pressure drop given by the model and that calculated, by hand, from the expression of Liebson et al. (1957) was excellent; being comparable to the round-off / convergence tolerance of the C.F.D. model and the supposed accuracy of the experimental

measurements used to determine the orifice coefficients. this does not, of course, validate either the expression or the orifice coefficient used.

A 11.2. CHANGES TO THE Q1 FILE.

```
>>>>>>>>> Add to Group 1.
REAL (TPP)
   Thickness of Perforated Plate
TPP = 0.006

>>>>>>>>> Delete from Group 5.
LNZ3 = LZ3/NZ3
>>>>>>>>> Add to Group 5.
LNZ3 = LZ3/(NZ3 - 1)
ZFRAC(11)=1;ZFRAC(12)=LPP

>>>>>>>>> Add to Group 13.
   Perforated Plate at Duct Outlet
   (call to section 2 of Group 13 of Ground).
PATCH (PLATE1,VOLUME,1,1,1,NY1,NZ,NZ,1,1)
COVAL (PLATE1,W1,GRND1,0.0)
```

A 11.3. ADDITIONS TO THE GROUND FILE.

```
>>>>>>>>> Insert at the top of the GROUND subroutine
>>>>>>>>> (variable declarations)
    PARAMETER (NY1 = 16)
    DIMENSION GZPL (NY1,1), GCOPL(NY1,1)

>>>>>>>>> Insert at section 2 of Group 13 (before RETURN).
    IF (NPATCH.NE'PLATE1') RETURN
    IF (INDVAR.NE.W1) RETURN
    IF (ISWEEP.EQ.1) THEN
       PRINT*,'Perforated Plate at Duct Outlet Routine called'
       PRINT*,'Use this GROUND only for Perforated Plate no. 1'
       PRINT*,'Use this GROUND only when NY1=',NY1
    ENDIF
    CALL GETYX (W1,GZPL,NY1,1)
    DO 9003 I=1,NY1
9003  GCOPL(I,1) = 476.16 *GZPL(I,1)
    CALL SETYX (W1,GCOPL,NY1,1)
```

APPENDIX 12. DETAILS OF THE COMPUTER SOFTWARE AND HARDWARE USED FOR THE C.F.D. MODELLING WORK.

The contents of this Appendix are discussed in section 4.3.7.

A 12.1. C.F.D. PACKAGE.

Version 1.4 of the PHOENICS package was used. It is supplied by:

C.H.A.M. Ltd.,
Bakery House,
40, High St.,
Wimbledon.
SW19 5AU

The manuals (Rosten & Spalding (1987 a & b)) used were document revisions 04 (TR/100) and 06 (TR/200).

A 12.2. OTHER SOFTWARE.

The Operating System used was VAX VMS version 5.3 - 1. PHOENICS is based on the FORTRAN language; VMS version 5.4 was used.

A 12.3. HARDWARE.

The computational work was performed on two clustered DEC VAX 8650 machines. A TEKTRONICS 4107 gra[phics terminal was used, graphical output being produced on a DIGITAL LCG01.